IAEA TECDOC SERIES

IAEA-TECDOC-1941

IAEA-TECDOC-1941

Assessment of Radioactive Contamination in Urban Areas

Report of Working Group 9
Urban Areas
of EMRAS II Topical Heading
Approaches for Assessing Emergency Situations

Environmental Modelling for
Radiation Safety (EMRAS II) Programme

IAEA
International Atomic Energy Agency

IAEA SAFETY STANDARDS AND RELATED PUBLICATIONS

IAEA SAFETY STANDARDS

Under the terms of Article III of its Statute, the IAEA is authorized to establish or adopt standards of safety for protection of health and minimization of danger to life and property, and to provide for the application of these standards.

The publications by means of which the IAEA establishes standards are issued in the **IAEA Safety Standards Series**. This series covers nuclear safety, radiation safety, transport safety and waste safety. The publication categories in the series are **Safety Fundamentals**, **Safety Requirements** and **Safety Guides**.

Information on the IAEA's safety standards programme is available on the IAEA Internet site

http://www-ns.iaea.org/standards/

The site provides the texts in English of published and draft safety standards. The texts of safety standards issued in Arabic, Chinese, French, Russian and Spanish, the IAEA Safety Glossary and a status report for safety standards under development are also available. For further information, please contact the IAEA at: Vienna International Centre, PO Box 100, 1400 Vienna, Austria.

All users of IAEA safety standards are invited to inform the IAEA of experience in their use (e.g. as a basis for national regulations, for safety reviews and for training courses) for the purpose of ensuring that they continue to meet users' needs. Information may be provided via the IAEA Internet site or by post, as above, or by email to Official.Mail@iaea.org.

RELATED PUBLICATIONS

The IAEA provides for the application of the standards and, under the terms of Articles III and VIII.C of its Statute, makes available and fosters the exchange of information relating to peaceful nuclear activities and serves as an intermediary among its Member States for this purpose.

Reports on safety in nuclear activities are issued as **Safety Reports**, which provide practical examples and detailed methods that can be used in support of the safety standards.

Other safety related IAEA publications are issued as **Emergency Preparedness and Response** publications, **Radiological Assessment Reports**, the International Nuclear Safety Group's **INSAG Reports**, **Technical Reports** and **TECDOCs**. The IAEA also issues reports on radiological accidents, training manuals and practical manuals, and other special safety related publications.

Security related publications are issued in the **IAEA Nuclear Security Series**.

The **IAEA Nuclear Energy Series** comprises informational publications to encourage and assist research on, and the development and practical application of, nuclear energy for peaceful purposes. It includes reports and guides on the status of and advances in technology, and on experience, good practices and practical examples in the areas of nuclear power, the nuclear fuel cycle, radioactive waste management and decommissioning.

ASSESSMENT OF RADIOACTIVE CONTAMINATION IN URBAN AREAS

The following States are Members of the International Atomic Energy Agency:

AFGHANISTAN
ALBANIA
ALGERIA
ANGOLA
ANTIGUA AND BARBUDA
ARGENTINA
ARMENIA
AUSTRALIA
AUSTRIA
AZERBAIJAN
BAHAMAS
BAHRAIN
BANGLADESH
BARBADOS
BELARUS
BELGIUM
BELIZE
BENIN
BOLIVIA, PLURINATIONAL STATE OF
BOSNIA AND HERZEGOVINA
BOTSWANA
BRAZIL
BRUNEI DARUSSALAM
BULGARIA
BURKINA FASO
BURUNDI
CAMBODIA
CAMEROON
CANADA
CENTRAL AFRICAN REPUBLIC
CHAD
CHILE
CHINA
COLOMBIA
COMOROS
CONGO
COSTA RICA
CÔTE D'IVOIRE
CROATIA
CUBA
CYPRUS
CZECH REPUBLIC
DEMOCRATIC REPUBLIC OF THE CONGO
DENMARK
DJIBOUTI
DOMINICA
DOMINICAN REPUBLIC
ECUADOR
EGYPT
EL SALVADOR
ERITREA
ESTONIA
ESWATINI
ETHIOPIA
FIJI
FINLAND
FRANCE
GABON
GEORGIA
GERMANY
GHANA
GREECE
GRENADA
GUATEMALA
GUYANA
HAITI
HOLY SEE
HONDURAS
HUNGARY
ICELAND
INDIA
INDONESIA
IRAN, ISLAMIC REPUBLIC OF
IRAQ
IRELAND
ISRAEL
ITALY
JAMAICA
JAPAN
JORDAN
KAZAKHSTAN
KENYA
KOREA, REPUBLIC OF
KUWAIT
KYRGYZSTAN
LAO PEOPLE'S DEMOCRATIC REPUBLIC
LATVIA
LEBANON
LESOTHO
LIBERIA
LIBYA
LIECHTENSTEIN
LITHUANIA
LUXEMBOURG
MADAGASCAR
MALAWI
MALAYSIA
MALI
MALTA
MARSHALL ISLANDS
MAURITANIA
MAURITIUS
MEXICO
MONACO
MONGOLIA
MONTENEGRO
MOROCCO
MOZAMBIQUE
MYANMAR
NAMIBIA
NEPAL
NETHERLANDS
NEW ZEALAND
NICARAGUA
NIGER
NIGERIA
NORTH MACEDONIA
NORWAY
OMAN
PAKISTAN
PALAU
PANAMA
PAPUA NEW GUINEA
PARAGUAY
PERU
PHILIPPINES
POLAND
PORTUGAL
QATAR
REPUBLIC OF MOLDOVA
ROMANIA
RUSSIAN FEDERATION
RWANDA
SAINT LUCIA
SAINT VINCENT AND THE GRENADINES
SAN MARINO
SAUDI ARABIA
SENEGAL
SERBIA
SEYCHELLES
SIERRA LEONE
SINGAPORE
SLOVAKIA
SLOVENIA
SOUTH AFRICA
SPAIN
SRI LANKA
SUDAN
SWEDEN
SWITZERLAND
SYRIAN ARAB REPUBLIC
TAJIKISTAN
THAILAND
TOGO
TRINIDAD AND TOBAGO
TUNISIA
TURKEY
TURKMENISTAN
UGANDA
UKRAINE
UNITED ARAB EMIRATES
UNITED KINGDOM OF GREAT BRITAIN AND NORTHERN IRELAND
UNITED REPUBLIC OF TANZANIA
UNITED STATES OF AMERICA
URUGUAY
UZBEKISTAN
VANUATU
VENEZUELA, BOLIVARIAN REPUBLIC OF
VIET NAM
YEMEN
ZAMBIA
ZIMBABWE

The Agency's Statute was approved on 23 October 1956 by the Conference on the Statute of the IAEA held at United Nations Headquarters, New York; it entered into force on 29 July 1957. The Headquarters of the Agency are situated in Vienna. Its principal objective is "to accelerate and enlarge the contribution of atomic energy to peace, health and prosperity throughout the world''.

IAEA-TECDOC-1941

ASSESSMENT OF RADIOACTIVE CONTAMINATION IN URBAN AREAS

REPORT OF WORKING GROUP 9 URBAN AREAS OF EMRAS II TOPICAL HEADING APPROACHES FOR ASSESSING EMERGENCY SITUATIONS

ENVIRONMENTAL MODELLING FOR RADIATION SAFETY (EMRAS II) PROGRAMME

INTERNATIONAL ATOMIC ENERGY AGENCY
VIENNA, 2021

COPYRIGHT NOTICE

All IAEA scientific and technical publications are protected by the terms of the Universal Copyright Convention as adopted in 1952 (Berne) and as revised in 1972 (Paris). The copyright has since been extended by the World Intellectual Property Organization (Geneva) to include electronic and virtual intellectual property. Permission to use whole or parts of texts contained in IAEA publications in printed or electronic form must be obtained and is usually subject to royalty agreements. Proposals for non-commercial reproductions and translations are welcomed and considered on a case-by-case basis. Enquiries should be addressed to the IAEA Publishing Section at:

Marketing and Sales Unit, Publishing Section
International Atomic Energy Agency
Vienna International Centre
PO Box 100
1400 Vienna, Austria
fax: +43 1 26007 22529
tel.: +43 1 2600 22417
email: sales.publications@iaea.org
www.iaea.org/publications

For further information on this publication, please contact:

Waste and Environmental Safety Section
International Atomic Energy Agency
Vienna International Centre
PO Box 100
1400 Vienna, Austria
Email: Official.Mail@iaea.org

© IAEA, 2021
Printed by the IAEA in Austria
February 2021

IAEA Library Cataloguing in Publication Data

Names: International Atomic Energy Agency.
Title: Assessment of radioactive contamination in urban areas / International Atomic Energy Agency.
Description: Vienna : International Atomic Energy Agency, 2021. | Series: IAEA TECDOC series, ISSN 1011–4289 ; no. 1941 | Includes bibliographical references.
Identifiers: IAEAL 21-01383 | ISBN978-92-0-134221-8 (paperback : alk. paper) |
ISBN 978-92-0-134121-1 (pdf)
Subjects: LCSH: Radioactive contamination. | Radiation — Safety measures. | Radiation — Measurement. | Environmental impact analysis. | Metropolitan areas.

FOREWORD

Radiological environmental impact assessment models are used to assess the expected radiological impacts of facilities and activities on the environment for the purposes of protecting the public and the environment against radiation risks. This includes estimation of actual and potential releases of radionuclides to the environment. Such models are essential tools for use in regulatory control of planned discharges to the environment; evaluation of doses in existing exposure situations, including predicting the effectiveness of countermeasures (protective actions, including remedial actions); and planning of measures to be taken in the event of accidental or intentional releases. They are also used for predicting the impact of releases which may occur far into the future, for example from underground radioactive waste disposal facilities. It is important to verify, to the extent possible, the reliability of the predictions of such models by a comparison with measured values in the environment or with predictions of other models.

To address these needs, the IAEA has established a number of international model validation and data compilation programmes, which have been running since the 1980s. These programmes have contributed to a general improvement in models, in the sharing of data and in the capabilities of modellers in Member States. For example, the IAEA's Environmental Modelling for Radiation Safety II (EMRAS II) programme ran from 2009 to 2011. EMRAS II focused on the improvement of environmental transfer models and the development of reference approaches to estimate the radiological impacts on humans, as well as on flora and fauna, arising from radionuclides in the environment.

Different aspects were addressed by nine working groups covering three themes: reference approaches for human dose assessment, reference approaches for biota dose assessment and approaches for assessing emergency situations. This publication describes the work of the Urban Areas Working Group (Working Group 9), established to discuss and document international modelling tools for use in urban settings in the event of accidental or intentional releases.

The objective of Working Group 9 was to test and improve the predictive ability of models used for the assessment of radioactive contamination in urban settings, including dispersion and deposition events; short and long term contaminant redistribution following deposition events; and the effectiveness of potential countermeasures (protective actions, including remedial actions) for reducing human exposures and corresponding external and internal doses.

The IAEA wishes to express its gratitude to all those who participated in the work of the EMRAS II programme and gratefully acknowledges the valuable contribution of K. Thiessen (United States of America), the leader of Working Group 9. The IAEA officers responsible for this publication were T. Yankovich and J. Brown of the Division of Radiation, Transport and Waste Safety.

EDITORIAL NOTE

This publication has been prepared from the original material as submitted by the contributors and has not been edited by the editorial staff of the IAEA. The views expressed remain the responsibility of the contributors and do not necessarily represent the views of the IAEA or its Member States.

Neither the IAEA nor its Member States assume any responsibility for consequences which may arise from the use of this publication. This publication does not address questions of responsibility, legal or otherwise, for acts or omissions on the part of any person.

The use of particular designations of countries or territories does not imply any judgement by the publisher, the IAEA, as to the legal status of such countries or territories, of their authorities and institutions or of the delimitation of their boundaries.

The mention of names of specific companies or products (whether or not indicated as registered) does not imply any intention to infringe proprietary rights, nor should it be construed as an endorsement or recommendation on the part of the IAEA.

The authors are responsible for having obtained the necessary permission for the IAEA to reproduce, translate or use material from sources already protected by copyrights.

The IAEA has no responsibility for the persistence or accuracy of URLs for external or third party Internet web sites referred to in this publication and does not guarantee that any content on such web sites is, or will remain, accurate or appropriate.

CONTENTS

SUMMARY

Radiological environmental impact assessment (REIA) models are important tools to ensure protection of the public and the environment for use in the regulatory control of planned discharges to the environment, evaluation of doses in existing exposure situations including predicting the effectiveness of countermeasures (protective actions, including remedial actions) and also in planning of measures to be taken in the event of accidental or intentional releases. The International Atomic Energy Agency's (IAEA's) Environmental Modelling for Radiation Safety II (EMRAS II) programme, which ran from 2009 to 2011, contained a theme on 'Approaches for Assessing Emergency Situations'. The Urban Areas Working Group (hereinafter called 'WG9') was later established to discuss and document international modelling tools for use in in urban settings in the event of accidental or intentional releases within this theme.

The objective of WG9 was to test and improve the predictive ability of models used for the assessment of radioactive contamination in urban settings, including dispersion and deposition events, short and long term contaminant redistribution following deposition events, and the effectiveness of potential countermeasures (protective actions, including remedial actions) or for reducing human exposures and corresponding external and internal doses. WG9 has built on the work done by the Urban Remediation Working Group of the earlier EMRAS I programme, which ran from 2003 to 2007. WG9 developed three exercises, which were designed to facilitate intercomparison of the predictions of models used for the assessment of radiological impacts in urban areas. Reasons for similarities and differences amongst model predictions were discussed in terms of the modelling approaches, the processes included in the models, assumptions, and parameter values used in the models by different participants. Areas in which models or the selection of parameter values could be improved were identified where possible. Some of the results have previously been reported elsewhere.

The first modelling exercise was a short range atmospheric dispersion exercise (hereinafter called the 'short range exercise'), based on data from several field tests performed by the National Radiation Protection Institute (SÚRO) on a test area belonging to the National Institute for Nuclear, Chemical and Biological Protection (SÚJCHBO) in Kamenná, near Prague in the Czech Republic. During the exercise, model predictions were compared with measurements of surface contamination, time integrated activity concentrations in air, and dose rates, up to 50 m downwind. Intercomparisons of model predictions were used for distances of up to 2000 m downwind and for additional modelling endpoints.

In these field tests, a short lived radionuclide (^{99m}Tc) in liquid form was released by detonation of a small amount of explosive in an open field (flat terrain) and in an open field with some simulated structures, which presented 'obstacles' to air flow. Measurements made included dose rates, surface contamination, activity concentrations in air, particle size distributions, time distributions of dust particles in air, and thermocamera snapshots. The test area was selected due to its stable wind direction under typical meteorological conditions.

Four individual field tests were considered in the modelling exercise. Participants were asked to submit predictions for surface contamination and dose rates as a function of distance, and activity concentrations in air as a function of height and distance from the detonation site. Participants were provided with all available measurements for the first two tests, to allow for calibration of models, if desired. For the third and fourth tests, participants were asked to submit model predictions before having access to measurements of the modelling endpoints.

Eight participants submitted calculations for the short range exercise. The models represented three main types of computational approaches to modelling atmospheric dispersion and had been developed for a variety of purposes. Results were generally closer to each other and to measured values under stable wind conditions and when downwind obstacles were not present.

The second modelling exercise was a mid-range atmospheric dispersion intercomparison exercise (hereinafter called the 'mid-range exercise'), based on a hypothetical accident at a nuclear power plant that resulted in deposition in urban areas up to 70 km downwind of the release. The scenario assumed a 1 hour release from a rupture of a steam generator tube, based on an accident scenario developed by the Institut de Radioprotection et de Sûreté Nucléaire (IRSN), and used actual geographic and meteorological information for a nuclear power plant in central Spain. The exercise considered two sets of atmospheric stability conditions, stable (Class E) and neutral (Class D), and used wind fields of 10 m above the ground. The radionuclides were assumed to be released in a gaseous form, at a release height of 50 m. Only dry deposition was considered. Although a variety of radionuclides would be released under such conditions, for modelling purposes, only ^{137}Cs and ^{131}I were considered. Time dependent release rates were provided to participants.

Participants were asked to carry out a simulation for a 10 hour period and to provide estimates of deposited activity at the end of the period, time integrated activity concentrations in air, and time dependent activity concentrations in air at selected locations. This was a model intercomparison exercise for all endpoints.

Five participants submitted calculations for the mid-range exercise. The models represented two main types of computational approaches to modelling atmospheric dispersion; one type used time dependent input information, while the other type used the total releases as input. The models used a variety of values for some parameters. The meteorological conditions that were assumed were important in determining whether the predicted plume intersected or bypassed the major city in the test region. Although the predicted paths of the plumes varied amongst the model predictions, the predicted times to arrival of the plume at specific locations (i.e. the time available to implement evacuation in case of a real situation) was more consistent.

The third modelling exercise (hereinafter called the 'countermeasures exercise') focused on prediction of contaminant transport within an urban area and the effects of implementing various countermeasures. This exercise started with an assumed concentration of either ^{60}Co or ^{239}Pu in air, in parts of a city (Seoul, Republic of Korea) for which detailed geographic and building information was available. Participants were asked to predict deposition for several kinds of initial weather conditions (dry, light rain, and heavy rain), for different seasons (summer and winter), and for both a business area (with buildings and paved areas) and a park area. Additional endpoints for model intercomparison included contamination densities as a function of time, dose rates, doses for specified individuals (defined for this exercise in terms of location and exposure characteristics), and the effectiveness of selected countermeasures, in terms of dose reduction.

Five participants submitted calculations for the countermeasures exercise. Three models used the activity concentration in air as a starting point, which was provided in the exercise scenario description. The other two models used the deposition on a lawn, as predicted by the METRO-K model for a given set of conditions. Most participants focused on external doses for ^{60}Co and internal doses for ^{239}Pu. Predicted initial contamination densities amongst models were generally similar but predicted rates of decrease of contamination densities varied amongst models. Predicted contamination densities and subsequent endpoints were highly dependent on

weather conditions at the time of deposition (especially wet versus dry conditions) but were not greatly dependent on seasonality. Important differences in the surfaces contributing to external dose rates were noted between the business area and the park area. In general, the predicted effectiveness of remediation of a given surface, in terms of reduction in external dose, depended on the predicted contribution of that surface to the external dose rate and dose. The predicted effectiveness in reducing internal doses depended on whether a model considered only inhalation doses from the initial plume or only inhalation doses from resuspension of contaminated material.

Predicted contamination densities and subsequent modelling endpoints in this exercise were highly dependent on weather conditions at the time of deposition (especially wet versus dry conditions) but were not greatly dependent on seasonality (summer versus winter). As anticipated, differences in the surfaces contributing to external dose rates were predicted between the business area (Region 1) and the park area (Region 2) between the five models used in the exercise, which subsequently influenced the external and inhalation doses that were predicted.

In general, the predicted effectiveness of countermeasures, in terms of reduction in cumulative external dose, depended on the predicted contribution of a given surface to external dose rates and the cumulative external dose. The exercise showed that countermeasures can potentially be useful in reducing inhalation doses, particularly for radionuclides, such as ^{239}Pu, that can give rise to high inhalation doses.

For each of the test exercises, WG9 has explained the similarities and differences amongst model predictions, and between model predictions and measurements (where applicable). Differences in model results reflect differences in model purpose, interests of assessors, types of dispersion modelling used, components included in the models, interpretation of input information, assumptions and selection of parameter values. To understand the similarities and differences in results, it is necessary to understand the individual modelling approaches and the effects of the different assumptions made and parameter values used on the model results. Comparing and discussing predictions from several models provides an opportunity to better understand the models and their results and to provide an overall improvement in models used for assessing exposures in urban areas. The range of results for each of the exercises indicate the level of uncertainty in model predictions that can be expected.

1. INTRODUCTION

1.1. BACKGROUND

Radiological environmental impact assessment (REIA) models are important tools to ensure protection of the public and the environment for use in evaluation of doses in existing exposure situations, predicting the effectiveness of countermeasures (protective actions, including remedial actions), and also in planning of measures to be taken in the event of accidental or intentional releases.

The IAEA established a programme on Environmental Modelling for RAdiation Safety (EMRAS II), which ran from 2009 to 2011 [1.1–1.6]. EMRAS II focused on the improvement of environmental transfer models and the development of reference approaches to estimate the radiological impacts on humans, as well as on flora and fauna, arising from radionuclides in the environment.

The programme comprised three themes, each containing three working groups (WGs). Theme 1 covered 'Reference Approaches for Human Dose Assessment' and included: WG1 (the 'Routine Releases' WG) on 'Reference Methodologies for 'Controlling Discharges' of Routine Releases'; WG2 (the 'NORM and Legacy Sites WG') on 'Reference Approaches to Modelling for Management and Remediation at NORM and Legacy Sites'; and WG3 (the 'Waste Disposal' WG) on 'Reference Models for Waste Disposal'.

Theme 2 covered 'Reference Approaches for Biota Dose Assessment' and included: WG4 (the 'Biota Modelling' WG) on 'Biota Modelling'; WG5 (the 'Handbook for Wildlife' WG) to develop a 'Wildlife Transfer Coefficient Handbook'; and WG6 (the 'Dose-Effect Relationships' WG) on 'Biota Dose Effects Modelling'.

Theme 3 covered 'Approaches for Assessing Emergency Situations' and included: WG7 (the 'Tritium' WG) on 'Tritium Accidents'; WG8 on 'Environmental Sensitivity'; and WG9 (the 'Urban Areas[1]' WG) on Radioactive Contamination in 'Urban Areas'.

The activities and the results achieved by the working groups are described in individual IAEA Technical Documents (TECDOCs). This publication presents the work of WG9 under Theme 3, which covered the dispersion and retention of radionuclides in urban environments following accidental releases of radionuclides.

WG9 has built on the work done by the previous WG on 'Remediation Assessment for Urban Areas Contaminated with Dispersed Radionuclides', which ran as part of the earlier EMRAS programme [1.1–1.10]. The primary objective of WG9 was to test and improve the predictive ability of models used for the assessment of radioactive contamination in urban settings.

The primary objective of WG9 was to test and improve the prediction of:

(a) Contamination densities and activity concentrations in air following an atmospheric dispersion and deposition event;
(b) Short and long term contaminant redistribution following deposition events;

[1] An urban area, or built-up area, is a human settlement with a high population density and infrastructure of buildings, such as towns and cities.

(c) Changes in radionuclide activity concentrations or dose rates as a function of location and time;
(d) The most important contributors (e.g. surfaces or exposure pathways) to human exposure at an urban location following a deposition event affecting an urban area;
(e) Effectiveness of various potential countermeasures[2] (protective actions[3], including remedial actions[4]) for reducing radionuclide activity concentrations, dose rates and corresponding external and internal doses [1.12].

Specific objectives included the development of three modelling exercises under different types of conditions for which a number of models were tested and compared. Analysis of the outcomes of the modelling exercises included comparison of approaches, models, and modelling results for the three scenarios that were covered in the exercises.

1.2. OBJECTIVES

The objective of this publication is to provide States with a technical description of the work undertaken by the EMRAS II WG9 to test and improve the predictive ability of models used for the assessment of radioactive contamination in urban and inhabited areas. This includes assessment of dispersion and deposition events, short and long term contaminant redistribution following deposition events, and the effectiveness of potential countermeasures (protective actions, including remedial actions) for reducing human exposures and corresponding external and internal doses.

This TECDOC describes each of the modelling exercises conducted by WG9, the models used in the exercises, the approaches, assumptions, and parameter values that were selected and used by individual participants, and the results of each exercise. The TECDOC is intended to provide information about the performance of various models in various contexts, both for assessing the radiological impact under a given set of conditions and for evaluating proposed countermeasures that could be undertaken in the event of accidental or intentional releases. For the purposes of the exercises described in this publication, different models were generally used for assessing the radiological impact of a release (e.g. to predict dispersion and deposition from an event) and for evaluating the effect of countermeasures (i.e. to predict the reduction in dose rate or dose expected for a given countermeasure).

This publication provides States with technical information that can be used by their national authorities to develop and improve their modelling capability for REIA for facilities and activities, in order to support them in meeting the respective requirements of IAEA Safety Standards Series No. GSR Part 3, Radiation Protection and Safety of Radiation Sources: International Basic Safety Standards [1.13]. Further, the TECDOC supports the implementation of the following IAEA Safety Standards Series publications, which provide recommendations on how to meet the requirements of GSR Part 3 with respect to REIA. use for evaluation of

[2] A countermeasure is defined as “an action aimed at alleviating the radiological consequences of an accident. Countermeasures are forms of intervention” and “may be protective actions or remedial actions” [1.11].
[3] A countermeasure is defined as “an action aimed at alleviating the radiological consequences of an accident. Countermeasures are forms of intervention” and “may be protective actions or remedial actions” [1.11].
[4] A remedial action is defined as “the removal of a source or the reduction of its magnitude (in terms of activity or amount) for the purposes of preventing or reducing exposures that might otherwise occur in an emergency or in an existing exposure situation. Remedial actions could also be termed protective actions, but protective actions are not necessarily remedial actions” [1.11].

doses in existing exposure situations and prediction of the effectiveness of countermeasures (protective actions, including remedial actions):

- No. GSG-10, Prospective Radiological Environmental Impact Assessment for Facilities and Activities [1.14][5];
- No. GSG-8, Radiation Protection of the Public and the Environment [1.15];
- No. GSG-15, Remediation Strategy and Process for Areas Affected by Past Activities or Events [1.16].

1.3. SCOPE

The scope of this publication is REIA models and tools that can be used in the assessment of the expected radiological impacts of facilities and activities on the environment for the purposes of protecting the public and the environment against radiation risks. These models and tools are applied specifically to urban and inhabited areas for use in emergency exposure situations.

The scope of this TECDOC covers three modelling exercises conducted by WG9: a short range atmospheric dispersion exercise (distances <2 km), a mid-range atmospheric dispersion exercise (distances up to about 70 km), and an exercise dealing with contaminant transport and effectiveness of countermeasures. The short range atmospheric dispersion exercise was based on field tests involving dispersion of a radionuclide by a small amount of explosive. This exercise involved a comparison of model predictions with measurements, as well as an intercomparison of model predictions. The mid-range atmospheric dispersion exercise was based on a hypothetical release from a nuclear power plant, resulting in deposition in downwind urban areas and involved an intercomparison of model predictions. For both of these exercises, participants were asked to predict the downwind surface contamination densities and radionuclide concentrations in air. The third exercise began with a unit concentration of radionuclide in air, and participants were asked to predict the deposition under various weather conditions, the changes in surface contamination densities and dose rates over time, and doses (external and internal) for specified persons (defined for this exercise in terms of location and exposure characteristics). This exercise also included prediction of the effects of various countermeasures in terms of their short or long term effect on external and internal (inhalation) dose rates and doses. Each modelling exercise and a detailed description of the exercise scenario is described in the report. Details of the models used by participants in each exercise are given. The results of the exercises, including the model predictions and an intercomparison between the models are presented and discussed, with conclusions drawn, where appropriate. Some of the results have previously been reported elsewhere [1.12, 1.17–1.19].

The technical information provided in this publication allows national authorities to evaluate the available models, assist them in developing models and approaches for REIA and test their models using case studies.

[5] GSG-10 [1.14] is focused on planned exposure situations. An ‘environmental impact assessment’ refers to “a procedure within a governmental decision making process for identifying, describing and assessing prospectively the effects and the risk of effects of a particular proposed activity or facility on aspects of environmental significance” [1.14]. Remediation, which is defined as “Any measures that may be carried out to reduce the radiation exposure due to existing contamination of land areas through actions applied to the contamination itself (the source) or to the exposure pathways to humans [1.16], is a planned activity.

1.4. STRUCTURE OF THE REPORT

Section 1 provides a brief description of the background of WG9, its objectives, and the scope of its activities. Sections 2 to 4 describe the three modelling exercises that were run (Exercises 1, 2 and 3, respectively), including the scenario descriptions, the models used in each exercise, the modelling results, and a discussion of the differences between models and, as applicable, between modelled and measured values. Specifically, Section 2 covers the short range atmospheric dispersion exercise, Section 3 the mid-range atmospheric dispersion exercise, and Section 4 describes the contaminant transport and countermeasures exercise.

Appendix I provides the scenario descriptions and documentation for the short range atmospheric dispersion exercise, and Appendix II describes each of the models run for this scenario.

Appendix III provides the scenario descriptions and documentation for the mid-range atmospheric dispersion exercise, and Appendix IV describes each of the models run for this scenario.

Appendix V provides the scenario descriptions and documentation for the contaminant transport and countermeasures exercise, and Appendix VI describes each of the models run for this scenario. Appendix VII provides tables of the model predictions for the contaminant transport and countermeasures exercise for each of the models tested. These tabulated results were used to produce the results shown in Section 4 and can be used for further evaluation of the model results in the future.

Annex I provides an example of the estimation of a source term from source activity measurements based on the modelling scenario in Section 2.

1.5. REFERENCES SECTION 1

[1.1] INTERNATIONAL ATOMIC ENERGY AGENCY, Environmental Modelling for Radiation Safety (EMRAS). A Summary Report of the Results of the EMRAS Programme (2003–2007), IAEA-TECDOC-1678, IAEA, Vienna (2012).

[1.2] INTERNATIONAL ATOMIC ENERGY AGENCY, Environmental Sensitivity in Nuclear Emergencies in Rural and Semi-natural Environments, Report of Working Group 8, Environmental Sensitivity of EMRAS II Topical Heading Approaches for Assessing Emergency Situations, Environmental Modelling for Radiation Safety (EMRAS II) Programme, IAEA-TECDOC-1719, IAEA, Vienna (2013).

[1.3] INTERNATIONAL ATOMIC ENERGY AGENCY, Modelling of Biota Dose Effects, Report of Working Group 6 Biota Dose Effects Modelling of EMRAS II Topical Heading Reference Approaches for Biota Dose Assessment, Environmental Modelling for Radiation Safety (EMRAS II) Programme, IAEA-TECDOC-1737, IAEA, Vienna (2014).

[1.4] INTERNATIONAL ATOMIC ENERGY AGENCY, Transfer of Tritium in the Environment after Accidental Releases from Nuclear Facilities, Report of Working Group 7 Tritium Accidents of EMRAS II Topical Heading Approaches for Assessing Emergency Situations, Environmental Modelling

for Radiation Safety (EMRAS II) Programme, IAEA-TECDOC-1738, IAEA, Vienna (2014).

[1.5] INTERNATIONAL ATOMIC ENERGY AGENCY, Environmental Change in Post-closure Safety Assessment of Solid Radioactive Waste Repositories, Report of Working Group 3 Reference Models for Waste Disposal of EMRAS II Topical Heading Reference Approaches for Human Dose Assessment, Environmental Modelling for Radiation Safety (EMRAS II) Programme, IAEA-TECDOC-1799, IAEA, Vienna (2016).

[1.6] INTERNATIONAL ATOMIC ENERGY AGENCY, Performance of Models in Radiological Impact Assessment for Normal Operation, Report of Working Group 1 Reference Methodologies for Controlling Discharges of Routine Releases of EMRAS II Topical Heading Reference Approaches for Human Dose Assessment, Environmental Modelling for Radiation Safety (EMRAS II) Programme, IAEA-TECDOC-1808, IAEA, Vienna (2017).

[1.7] THIESSEN, K.M., BATANDJIEVA, B., ANDERSSON, K.G., ARKHIPOV, A., CHARNOCK, T.W., GALLAY, F., GASCHAK, S., GOLIKOV, V., HWANG, W.T., KAISER, J.C., KAMBOJ, S., STEINER, M., TOMÁS, J., TRIFUNOVIC, D., YU, C., ZELMER, R., ZLOBENKO, B., Improvement of modelling capabilities for assessing urban contamination: The EMRAS Urban Remediation Working Group, Applied Radiation and Isotopes **66** (2008) 1741.

[1.8] THIESSEN, K.M., ARKHIPOV, A., BATANDJIEVA, B., CHARNOCK, T.W., GASCHAK, S., GOLIKOV, V., HWANG, W.T., TOMÁS, J., ZLOBENKO, B., Modelling of a large-scale urban contamination situation and remediation alternatives, Journal of Environmental Radioactivity **100** (2009) 413.

[1.9] THIESSEN, K.M., ANDERSSON, K.G., BATANDJIEVA, B., CHENG, J.-J., HWANG, W.T., KAISER, J.C., KAMBOJ, S., STEINER, M., TOMÁS, J., TRIFUNOVIC, D., YU, C., Modelling the long-term consequences of a hypothetical dispersal of radioactivity in an urban area including remediation alternatives, Journal of Environmental Radioactivity **100** (2009) 445.

[1.10] THIESSEN, K.M., ANDERSSON, K.G., CHARNOCK, T.W., GALLAY, F., Modelling remediation options for urban contamination situations, Journal of Environmental Radioactivity **100** (2009) 564.

[1.11] INTERNATIONAL ATOMIC ENERGY AGENCY, IAEA Safety Glossary: Terminology Used in Nuclear Safety and Radiation Protection: 2018 Edition, IAEA, Vienna (2019).

[1.12] THIESSEN, K.M., ANDERSSON, K.G., BERKOVSKYY, V., CHARNOCK, T.W., CHOUHAN, S.L., De WITH, G., ĎÚRAN, J., FUKA, V., HELEBRANT, J., HŮLKA, J., HWANG, W.T., KUČA, P., MANCINI, F., NAVARRO, E., PERIÁÑEZ, R., PROUZA, Z., SDOUZ, G., TOMÁS, J., TRIFUNOVIĆ, D., URSO, L., WALTER H., Assessing emergency situations and their aftermath in urban areas: The EMRAS II Urban Areas Working Group, Radioprotection **46** (2011) S601.

[1.13] EUROPEAN COMMISSION, FOOD AND AGRICULTURE ORGANIZATION OF THE UNITED NATIONS, INTERNATIONAL ATOMIC ENERGY AGENCY, INTERNATIONAL LABOUR ORGANIZATION, OECD NUCLEAR ENERGY AGENCY, PAN

AMERICAN HEALTH ORGANIZATION, UNITED NATIONS ENVIRONMENT PROGRAMME, WORLD HEALTH ORGANIZATION, Radiation Protection and Safety of Radiation Sources: International Basic Safety Standards, IAEA Safety Standards Series No. GSR Part 3, IAEA, Vienna (2014).

[1.14] INTERNATIONAL ATOMIC ENERGY AGENCY, UNITED NATIONS ENVIRONMENT PROGRAMME, Prospective Radiological Environmental Impact Assessment for Facilities and Activities, IAEA Safety Standards Series No. GSG-10, IAEA, Vienna (2018).

[1.15] INTERNATIONAL ATOMIC ENERGY AGENCY, UNITED NATIONS ENVIRONMENT PROGRAMME, Radiation Protection of the Public and the Environment, IAEA Safety Standards Series No. GSG-8, IAEA, Vienna (2018).

[1.16] FOOD AND AGRICULTURE ORGANIZATION OF THE UNITED NATIONS, INTERNATIONAL ATOMIC ENERGY AGENCY, UNITED NATIONS DEVELOPMENT PROGRAMME, UNITED NATIONS ENVIRONMENT PROGRAMME, UNITED NATIONS OFFICE FOR THE COORDINATION OF HUMANITARIAN AFFAIRS, Remediation Strategy and Process for Areas Affected by Past Activities or Events, IAEA Safety Standards Series No. GSG-15, IAEA, Vienna (in publication).

[1.17] THIESSEN, K.M., CHARNOCK, T.W., CHOUHAN, S.L., HWANG, W.T., KAMBOJ, S., TOMÁS, J., YU, C., "Modelling the effectiveness of remediation efforts in contaminated urban areas: An EMRAS II Urban Areas Working Group exercise", Proc. of 41st Annual Conference on Waste Management, WM2015, Phoenix, AZ (2015) paper #15631.

[1.18] PERIÁÑEZ, R., THIESSEN, K.M., CHOUHAN, S.L., MANCINI, F., NAVARRO, E., SDOUZ, G., TRIFUNOVIĆ, D., Mid-range atmospheric dispersion modelling. Intercomparison of simple models in EMRAS-2 project, Journal of Environmental Radioactivity **162–163** (2016) 225.

[1.19] PROUZA, Z., BECKOVA, V., CESPIROVA, I., HELEBRANT, J., HULKA, J., KUCA, P., MICHALEK, V., RULIK, P., SKRKAL, J., HOVORKA, J., Field tests using radioactive matter, Radiation Protection Dosimetry **139** (2010) 519.

2. SHORT RANGE ATMOSPHERIC DISPERSION EXERCISE

2.1. OVERVIEW

The objective of the short range atmospheric dispersion exercise was to test the models against measurements made during a short range atmospheric field test. The participants of the exercise were tasked to predict the dispersion and deposition of a radionuclide over a short range (50 m) following a small explosion, given relevant meteorological data and other site specific or test specific information [2.1]. The exercise was based on experimental data from a series of four field tests performed between 2007 and 2009 by the National Radiation Protection Institute (SÚRO) in the Czech Republic. Each field test involved the dispersal of a short lived radionuclide (^{99m}Tc) with a small amount of explosive [2.2].

During each field test, ^{99m}Tc in liquid form was spread by detonation of a small amount of explosive under different spatial arrangements, including in an open field with and without simulated structures to provide potential obstacles to air flow. The measurements performed included dose rates, surface contamination of ground and structures, activity concentrations in air, particle size distribution, time distribution of dust particles in air, and thermocamera snapshots to record changes in infrared radiation. Videos of the explosions from several vantage points were also recorded. The test area was selected for its stable wind direction under typical meteorological conditions.

The experimental conditions for the four field tests (explosion events) are summarized in Section 2.2, and full details for all four events are provided in Appendix I. Input information for each event includes the amount of radioactivity involved, the arrangement of the various detectors in the vicinity of the explosion, meteorological information, and particle size information. For Tests 1 and 2, all available data were provided to the participants to be used for model calibration if desired (Appendix I). These data included measurements of surface contamination, dose rates, and time integrated activity concentrations in air. Tests 3 and 4 were conducted as blind model tests, and only the input information was provided to participants during the exercise. Comparisons were made with measurements only after the modelling results were submitted by the participants.

Endpoints to be modelled for Tests 3 and 4 were:

(1) Surface contamination (Bq/m^2) as a function of distance from the detonation site;
(2) Dose rates (mGy/h at 1 m height) as a function of distance from the detonation site;
(3) Time integrated activity concentrations[6] in air (Bq · min · m^{-3}) as a function of height and distance along the centre line of the plume; and
(4) Estimated percentile contamination zones (50%, 75% and 95%) for each explosion event.

As described in Section 2.5, most of the attention was focused on predictions of the surface contamination (deposition) resulting from each field test. In addition to the modelling exercise described in this publication, this set of information can also be used for validation of location

[6] Time-integrated activity concentrations refer to the product of the time-dependent activity concentrations (Bq/m^3) × time (min). These are calculated for short time steps, and then added together.

factors[7], data assimilation[8] to improve initial modelling results, and estimation of a source term based on measurements (an example of estimation of a source term is described in Annex I).

2.2. SUMMARY OF INITIAL CONDITIONS FOR THE FIELD TESTS

Table 2.1 summarizes the conditions for the four field tests included in this exercise. Table 2.2 provides a summary of the meteorological data for Tests 1 to 4. More detailed meteorological data were provided in electronic form (Appendix I). Meteorological data were measured at a height of 2 m. The indicated wind direction is the direction the wind is blowing from.

For Test 4, two simulated structures were erected in the grid area, as depicted in Fig. I.4 of Appendix I. The larger obstacle was located directly on the centreline of the grid and had dimensions of 11 m × 2.5 m × 6 m (length, width, height). The smaller obstacle was located to one side of the grid centreline and had dimensions of 3 m × 3 m × 1.5 m (length, width, height).

2.3. MODELS USED IN THE EXERCISE

Table 2.3 provides a summary of the models and parameter values used by participants in the short range atmospheric dispersion exercise. The models represented three main types of computational approaches to modelling atmospheric dispersion (Gaussian, Lagrangian, and computational fluid dynamics (CFD)) and were developed for a variety of purposes. Eight participants provided model predictions for the short range exercise, using seven models (Table 2.3). Two participants used the HotSpot 2.07.1 model, and one participant provided two sets of predictions using the same model (CLMM) with different sizes for the model domain (the distance or area for which model predictions were made). All participants provided predictions for both Test 3 and Test 4; most participants also ran calculations for Tests 1 and 2. Information on the use of the data generated during Tests 1 and 2 by participants for calibration purposes is indicated in Table 2.3. The HotSpot 2.07.1 model provided predictions along the plume centreline; the remaining six models provided predictions corresponding to the test grid. More information about the individual models and how they were used in this exercise is provided in Appendix II.

[7] A location factor is the ratio of the exposure rate determined or estimated for a location of interest and a reference exposure rate [2.3, 2.4]; the location factor accounts for the geometry at the location, e.g. the presence and configuration of buildings and trees and any protection from exposure at the location of interest compared to the reference location.

[8] Data assimilation techniques combine measurements with model results to improve the predictive power of assessment models [2.3].

TABLE 2.1. SUMMARY INFORMATION FOR THE FIELD TESTS

Test No.	Date	Explosion time[a]	Time of measurement of Tc-99m activity[a]	Activity of Tc-99m (MBq)	Amount of liquid containing the activity	Amount and type of explosive used[b]
Test 1	6 December 2007	12:45	10:20	780	1.5 L	Permon 10T, 350 g
Test 2	15 May 2008	11:30	10:10	1058	6 mL	Permon 10T, 350 g
Test 3	5 May 2009	12:22	12:22	1222	6 mL	Permon 10T, 350 g
Test 4	14 July 2009	12:42	11:00	1088	6 mL	Permon 10T, 350 g

[a] 24 hour system (12:00 = noon).

[b] Descriptions of the explosives were provided separately.

TABLE 2.2. SUMMARY OF WEATHER CONDITIONS DURING THE FIELD TESTS[a]

Experiment	Test 1	Test 2	Test 3	Test 4
Date	6 December 2007	15 May 2008	5 May 2009	14 July 2009
Temperature (°C)	6.9–7.1	22.2–22.4	10.1–10.7	25.4–25.6
Relative air humidity (%)	85–87	41–47	48–54	56–61
Condensation point (°C)	4.7–5.1	8.4–10.6	0.3–1.3	16.1–17.4
Wind speed (km/h)	7.9–16.2	1.2–5.4	3.2–7.9	0–1.4
Gust wind speed (km/h)	–	–	4.7–16.2	0–3.2
Wind direction	225–202.5	–	247.5–292.5	135–315
Air pressure (hPa)	1011.1–1011.2	1009.1–1009.2	1021.3–1021.5	1012.6–1012.8

[a] More detailed meteorological data were provided in electronic form (Appendix I). Measurements were taken at 2 m height. The indicated wind direction is the direction wind is blowing from.

TABLE 2.3. COMPARISON OF MODELS AND SELECTED PARAMETERS USED IN THE SHORT RANGE ATMOSPHERIC DISPERSION EXERCISE

Model name	**ADDAM/CSA-ERM**	**HotSpot 2.07.1 (HPA)**	**HotSpot 2.07.1 (HR)**
Participant and country	S.L. Chouhan Canada	T. Charnock United Kingdom	D. Trifunović Croatia
Type of model	Gaussian	Gaussian	Gaussian
Purpose of model	ADDAM: Safety assessment for accidents; CSA-ERM, research tool	Emergency response	Emergency response
Domain size	ADDAM: Plume centreline from 100 m; CSA-ERM, 5 m grid	Plume centreline only	Plume centreline only
Calibration	Tests 1 and 2	Test 2	Test 2
Stability classes	Test 3: Class C Test 4: Class A	Test 3: Class D Test 4: Class C	Test 2: Class B Test 3: Class D Test 4: Class C
Wind speed (m/s)	Test 3: 2.7 Test 4: `0.726	Test 3: 1.5 Test 4: 0.4	Test 2: 0.6 Test 3: 1.3 Test 4: 0.1
Wind conditions (transient or steady-state)	Not provided	Not provided	Not provided
Dry deposition velocity (m/s)	1×10^{-1}	1×10^{-4} (for respirable fraction[a]) 4×10^{-1} (for non-respirable fraction)	8×10^{-4} (for respirable fraction)
Source term partitioning	Not provided	Source partitioned uniformly up to a height of 5 m	h1, 0.04 (ground level) h2, 0.16 (0.2 × cloud top) h3, 0.25 (0.4 × cloud top) h4, 0.35 (0.6 × cloud top) h5, 0.20 (0.8 × cloud top)
Column dimensions	Height = 12.9 m Effective release height = 6.45 m (Tests 3 and 4)	Column height constrained to 13 m	Cloud top = 76 $(w)^{0.25}$ where w = pounds of high explosive; cloud radius = 0.20 × cloud top Test 2: Cloud top = 5 m Test 3: Cloud top = 13 m Test 4: Cloud top = 13 m
Surface roughness	Grass terrain; roughness length, 0.4 m	Model options are ‘standard’ or ‘urban’; ‘standard’ was used	Not provided
Particle size distribution (% of activity per particle size intervals)	Not provided	Respirable fraction, 0.999 Non-respirable fraction, 0.001	Respirable fraction, 0.99
Time to set up and run	Not provided	Not provided	Not provided
Time to process results	Not provided	Not provided	Not provided

TABLE 2.3. COMPARISON OF MODELS AND SELECTED PARAMETERS USED IN THE SHORT RANGE ATMOSPHERIC DISPERSION EXERCISE (cont.)

Model name	**RDD_MMC**	**USev**	**LASAIR**
Participant and country	J. Ďúran Slovakia	R. Periáñez Spain	H. Walter Germany
Type of model	Lagrangian	Lagrangian (5000 particles each for liquid and gas)	Lagrangian (60 000 particles)
Purpose of model	Not provided	Research model	Decision support
Domain size	Not provided	2000 m downwind, 100 m upwind	40 × 40 km²
Calibration	Not provided	Tests 1 and 2	None
Stability classes	Test 1: Class C Test 2: Class A Test 3: Class B Test 4: Class A	Not applicable[b]	Test 1: Class D Test 2: Class B–C Test 3: Class D Test 4: Class C
Wind speed (m/s)	Test 1: 4.00 Test 2: 0.59 Test 3: 1.30 Test 4: 0.20	Time dependent measurements	Test 1: 0–6.3 Test 2: 0.28–1.85 Test 3: 0.9–7.2 Test 4: 0–4.9
Wind conditions (transient or steady state)	Not provided	Transient	Transient
Dry deposition velocity (m/s)	0.2 µm, 5.0×10^{-3} 1.0 µm, 1.5×10^{-4} 8.0 µm, 1.0×10^{-3} 20.0 µm, 8.0×10^{-3}	Not applicable	<0.39 µm, 5×10^{-5} 0.39–1.3 µm, 1.5×10^{-4} 1.3–10.2 µm, 1×10^{-3} >10.2 µm, 8×10^{-3}
Source term partitioning	Not provided	Partitioning between liquid and gas particles	Uniformly distributed within initial cloud
Column dimensions	Test 2: Volume 1 (20%), 13 m × 6 m × 2 m; Volume 2 (80%), 4 m × 2 m × 3 m	(1) 7 m × 7 m, with effective height ± 6 m (2) as for HotSpot 2.07.01 (HR)	Test 1: ht 7 m, base 3 m Test 2: ht 5 m, base 2 m Test 3: ht 13 m, base 5 m Test 4: ht 13 m, base 5 m
Surface roughness	Not provided	Not applicable	Test ground, 0.1 m vicinity 1.0 m obstacle (Test 4), 1.5 m
Particle size distribution (% of activity per particle size intervals)	0.2 µm, 20% 1.0 µm, 15% 8.0 µm, 50% 20.0 µm, 15%	Not applicable	0–2.5 µm, 40% 2.5–10 µm, 40% 10–50 µm, 10% ≥50 µm, 10%
Time to set up and run	Not provided	<5 min	<5 min
Time to process results	Not provided	<5 min	<10 min

TABLE 2.3. COMPARISON OF MODELS AND SELECTED PARAMETERS USED IN THE SHORT RANGE ATMOSPHERIC DISPERSION EXERCISE (cont.)

Model name	**CFD**	**CLMM**
Participant and country	G. de With Netherlands	V. Fuka Czech Republic
Type of model	Computational fluid dynamics	Atmospheric computational fluid dynamics
Purpose of model	Commercial software	Research model
Domain size	1000 m × 100 m × 2000 m	Up to 50 m; up to 2000 m (separate calculations)
Calibration	Test 2	Not provided
Stability classes	Not applicable	Not applicable
Wind speed (m/s)	Test 1: 4.0 Test 2: 1.5 Test 3: 3.0 Test 4: 0.3	Test 1: 3.8 Test 2: 0.77 Test 3: 2.3 Test 4: 0.4
Wind conditions (transient or steady state)	Steady state	Not provided
Dry deposition velocity (m/s)	0.2 µm, 5.0×10^{-5} 1.0 µm, 1.5×10^{-4} 8.0 µm, 1.0×10^{-3} 20.0 µm, 8.0×10^{-3}	Not applicable
Source term partitioning	Not provided	As for HotSpot 2.07.1 (HR)
Column dimensions	12 m × 7 m × 7 m	As for HotSpot 2.07.1 (HR)
Surface roughness	Aerodynamic roughness length (y_0) 0.03 m	Ground surface, 3 mm
Particle size distribution (% of activity per particle size intervals)	2×10^{-5} m: 10% 8×10^{-6} m: 46.6% 1×10^{-6} m: 15.0% 2×10^{-7} m: 28.4%	0.2 µm: 39.6% 1 µm: 11.8% 8 µm: 37.8% 20 µm: 10.8%
Time to set up and run	10 h	Not provided
Time to process results	120 h	Not provided

[a] The respirable fraction is the fraction of aerosolized material that is respirable, generally considered as having an Activity Median Aerodynamic Diameter (AMAD) ≤10 µm; the non-respirable fraction is the fraction of aerosolized material that has an AMAD >10 µm. In HotSpot, the respirable fraction is assumed to have an AMAD of 1 µm [2.5].

[b] 'Not applicable' indicates that the model does not necessitate or does not use the specified information.

2.4. METEOROLOGICAL CONDITIONS DURING THE FIELD TESTS

For the simulation of the atmospheric dispersion in this exercise, several types of dispersion models were applied (Table 2.3). The meteorological input data need to be handled appropriately for the given type of model. In particular, the Gaussian type can use only averaged data, whereas the Lagrangian models can use data sets with a time resolution of down to 1 minute (transient wind conditions). Wind speed and especially wind direction are the most important parameters with respect to the accuracy of model predictions when compared with measured data. In particular, rapid changes in wind direction can cause errors within a simulation when only averaged input data are used.

Figures 2.1 and 2.2 depict the 1 minute averaged wind speed and wind direction for Tests 3 and 4, respectively. For Test 3, the wind direction after the explosion was quite stable, whereas the wind speed varied from approximately 1 to 3.5 m/s. Therefore, the plume from the explosion travelled more or less in a straight line. However, for Test 4, the wind speed shortly after the explosion was very slow (0–1 m/s, then 0–2 m/s), with periods of no wind, whereas the wind

direction after the explosion varied considerably. Therefore, the plume did not travel in the anticipated direction, and the complex meteorological conditions made the dispersion modelling more difficult. In addition, Test 4 included two simulated structures in the grid area, which provided potential obstacles to the wind flow and may have affected the plume behaviour. Low wind speed conditions are usually very difficult to handle for simulation models, as they have been validated according to dispersion experiments during which higher wind speeds occurred. In general, no dispersion model is available that is able to handle wind speeds of below 0.5 m/s, so some meteorological conditions that occurred during these experiments have to be examined very carefully, recognizing that the results of the dispersion models include a high uncertainty.

In addition, the measurements of the wind speed and direction for Tests 1 to 4 were taken from devices at a height of 2 m, in contrast to the standard 10 m height. Data taken at a height of 2 m do not, in general, reflect actual air mass movements, as at this height the topography (e.g. concrete, meadow, trees) has a large influence on the air movement at such a height.

2.5. ANALYSIS OF MODELLING RESULTS

Tests 1 and 2 were used as experimental trials and for calibration at the discretion of each participant. In general, calibration usually involves adjustment of parameter values or of a modelling approach, in order to achieve better correspondence between model predictions and relevant measurements. Details of model calibration are not discussed in this publication but are provided by some participants in Appendix IV.

As described above, the modelling endpoints requested for this exercise included deposition (surface contamination, Bq/m^2), dose rates (mGy/h), time integrated activity concentrations in air ($Bq \cdot min \cdot m^{-3}$), and estimated percentile contamination zones. In practice, predictions for deposition were provided by all eight participants, while the remaining endpoints were of less apparent interest and were addressed by fewer participants. Thus, this analysis of modelling results has focused primarily on deposition. Measurements of deposition (surface contamination) are available for the test grid (approximately 50 m × 40 m) and include all activity deposited in the grid area as the plume passed over the test site, effectively corresponding to the deposition resulting from a time integrated activity concentration in air over the test site. Section 2.5.1 describes the initial analysis of the modelling results, which led to the need for improved methods to compare complex modelling results. Sections 2.5.2 to 2.5.6 provide more detailed comparisons of the modelling results.

2.5.1. Initial analysis of modelling results

Predicted and measured values for the deposition of ^{99m}Tc, the test radionuclide, along the centreline of the test grid are shown in Figs 2.3 and 2.4 for Tests 3 and 4, respectively. The test grid was used as the basis for measurement locations (locations of the sample collectors) and for locations of model predictions. Measurements were available out to 50 m from the dispersion point (the detonation site or origin of the explosion; see Appendix I for details), whereas model predictions extended out to 2000 m in some cases. Therefore, at distances of greater than 50 m from the dispersion point, only model intercomparisons were possible. The figures show both the first 50 m (top panel in each figure) and the first 500 m (bottom panel in each figure). In Test 3, the plume from the explosion went more or less down the centreline of the grid. However, in Test 4, there was an unexpected change in wind conditions at the time of the explosion, and the plume did not go directly down the grid centreline as planned. The simulated structures in the grid area during Test 4 may also have influenced the movement of the plume.

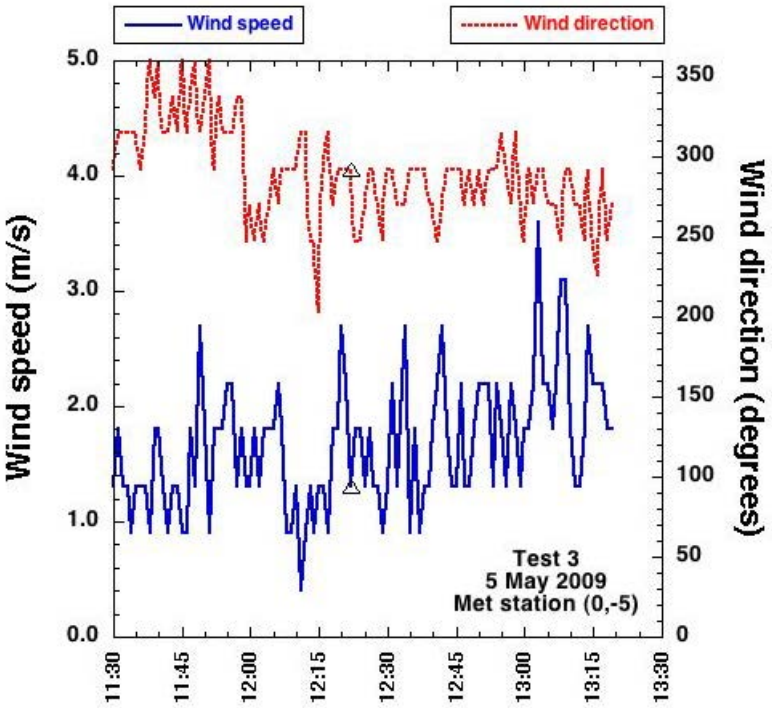

FIG. 2.1. Wind speed and wind direction (1 minute averages) for Test 3 (5 May 2009). The triangles indicate the time of the explosion.

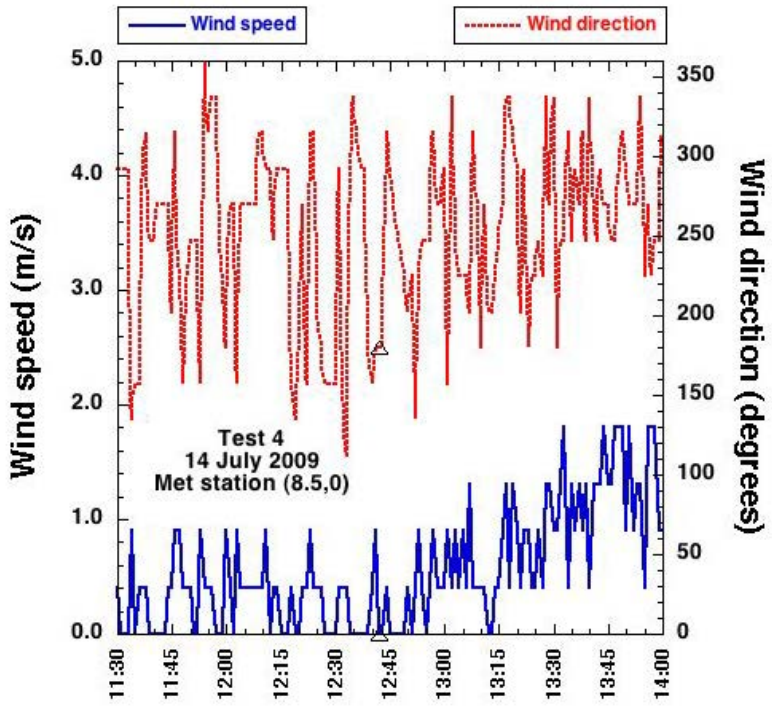

FIG. 2.2. Wind speed and wind direction (1 minute averages) for Test 4 (14 July 2009). The triangles indicate the time of the explosion.

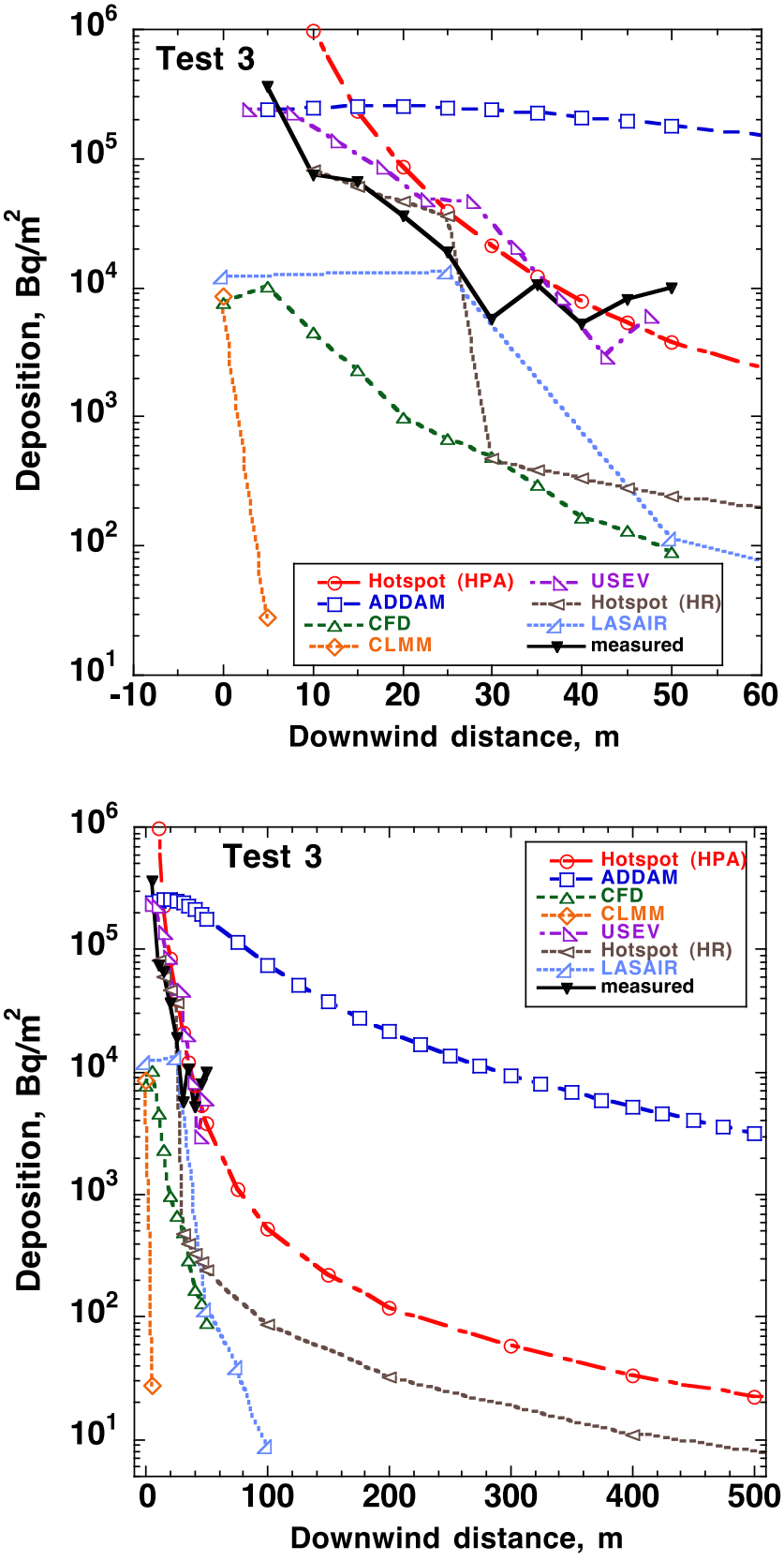

FIG. 2.3. Comparison of predicted and measured deposition along the grid centre line for Test 3, shown for the domain of the measurements (50 m, top) and for 500 m (bottom).

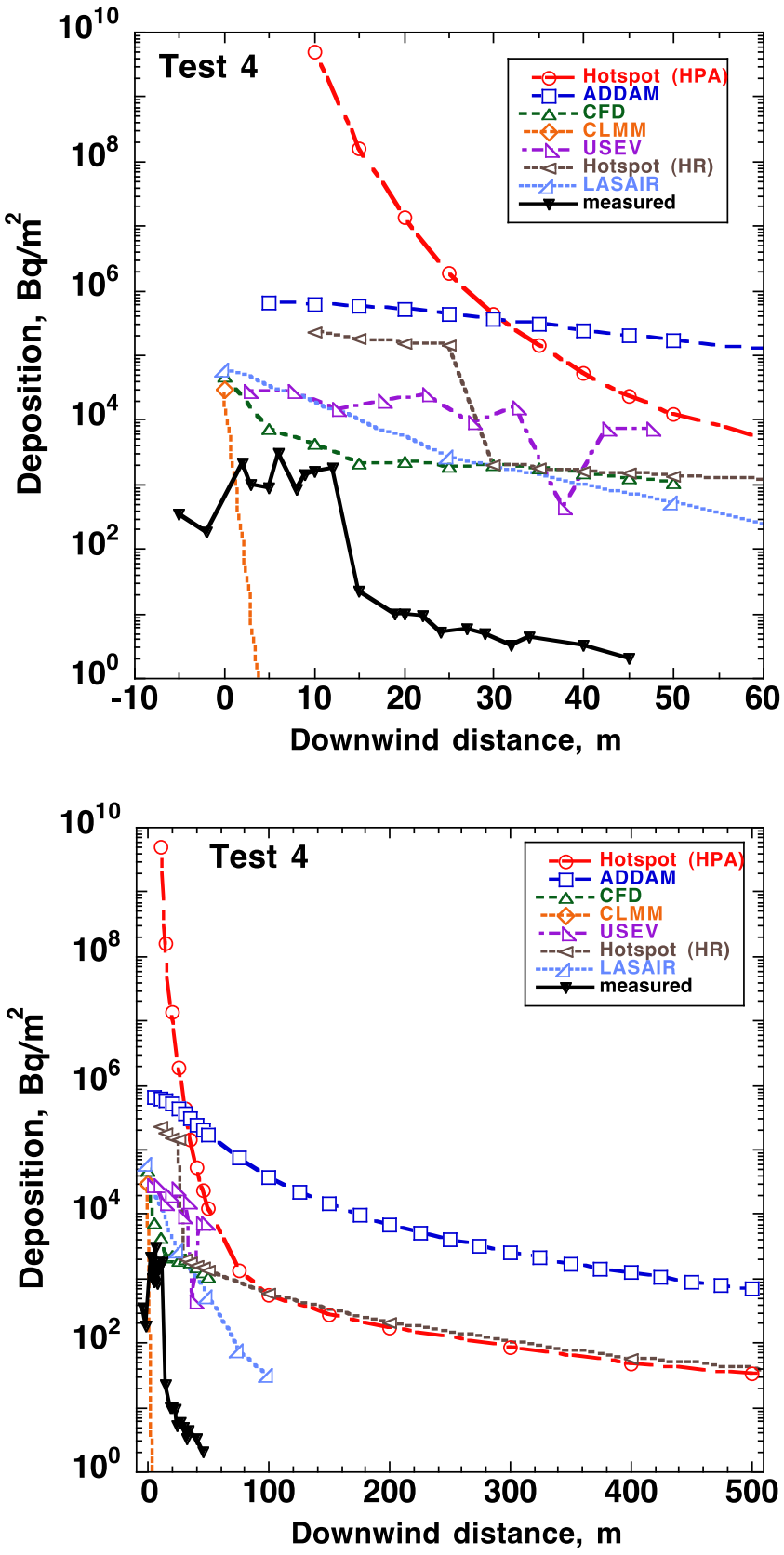

FIG. 2.4. Comparison of predicted and measured deposition along the grid centre line for Test 4, shown for the domain of the measurements (50 m, top) and for 500 m (bottom).

Differences amongst model predictions, and between predictions and measurements, are more apparent when only the first 50 m are considered. It is important to note that the centreline of the test grid and the centreline of the real or modelled plumes do not necessarily correspond; this was addressed in later analyses of the modelling results (Sections 2.5.2 to 2.5.6). While HotSpot 2.07.1 (used by two participants) provides predictions only down a plume centreline without indicating a direction, most models provided predictions according to the layout of the test grid. Thus, if a plume went at an angle from the grid centreline, deposition along the grid centreline (measured or modelled) did not reflect the deposition along the centreline of the plume.

The predicted zones of contamination (the area expected to contain 50%, 75%, or 95% of the deposited contamination) were summarized for several models in terms of either the radius or the area of the zone (Table 2.4); results from the LASAIR model depended on the grid size used and the resulting resolution of the calculations. The predicted percentage of initial activity deposited in the modelling domain (the area included in the model predictions) was 4.7% for CFD, and 12.4 to 22.3% for LASAIR (the only models for which this was reported), depending on the test.

Predicted shapes and locations of the plume (e.g. direction of the plume centreline in comparison with the test grid) varied amongst models, as did the predicted deposition amounts. Even when two participants used the same model (HotSpot 2.07.1 in Figs 2.3 and 2.4), the results differed substantially (Sections 2.5.3 to 2.5.5). The differences amongst predictions could have been due to the type of model used and how the wind conditions were handled. As shown in Table 2.3, participants chose different stability classes for the same test conditions (Stability Classes B, C, or D for Test 3; Stability Classes A or C for Test 4). Wind speeds varied from 1.3 to 2.7 m/s for Test 3 and from 0.1 to 0.7 m/s for Test 4 for participants using a single value for a given test (Table 2.3); two models (LASAIR and University of Seville) used time dependent wind speeds. The assumed dimensions of the initial cloud and partitioning of the source term in the cloud varied amongst participants. Dry deposition velocities varied from 1.5×10^{-5} to 1×10^{-1} m/s, with some participants using a single value for all particle sizes and others using different values for different particle sizes (Table 2.3).

Following this initial analysis of model predictions and measurements, it became apparent that a better method of analysis would be useful, specifically, a method that would account for different directions or locations of the predicted and measured deposition patterns. This improved analysis is described in Sections 2.5.2 to 2.5.6.

2.5.2. Development of grids, contour plots, and profiles for model outputs

Further analysis of the modelling results was focused on comparisons of the predicted and measured deposition (surface contamination, Bq/m^2) within the grid area (the area with measurements), using an approach developed for this exercise. Although some model predictions extended to distances greater than 50 m, there are no measured values at those distances for comparison. Measurement points used during Tests 3 and 4 are shown in Appendix I. All sets of model predictions were first represented in the same Cartesian coordinate system as the measurements, in terms of predicted deposition at the same points for which measured deposition was available, designating the dispersion point (origin of the explosion) at grid coordinates (0,0). Comparisons were then made of the measured and predicted maximum activity concentrations within the grid area and of the total measured or predicted activity within the grid area (Section 2.5.3). Deposition profiles were defined in terms of profiles from the dispersion point through the point with the maximum measured or predicted deposition (Section 2.5.4), and from the dispersion point through the cloud axis, defined as the approximate centre of the measured or predicted plume (Section 2.5.5). Figure 2.5 provides a schematic illustration of these two profiles.

TABLE 2.4. PREDICTED RADIUS OR AREA OF ZONES OF 50%, 75%, AND 95% CONTAMINATION FOR TESTS 3 AND 4

Model	Scale	Contamination zone		
		50%	75%	95%
Test 3			*Radius (m)*	
CFD		31.7	75	132.7
USEV		277	511	812
			Area (ha)	
CLMM		4	14.2	30.6
ADDAM		3.26	57.1	2630
LASAIR	1:10 000	1.0625	6.8125	64.625
	1:25 000	2	12.25	159
	1:50 000	4	23	405
	1:100 000	12	36	624
	1:200 000	32	64	880
Test 4			*Radius (m)*	
CFD		3.7	7.3	20
USEV		111	189	348
			Area (ha)	
CLMM		3.36	12.5	30.9
ADDAM		0.193	2.43	263
LASAIR	1:10 000	0.1875	0.4375	4.8125
	1:25 000	0.5	1	7.25
	1:50 000	2	4	13
	1:100 000	8	16	32
	1:200 000	32	48	96

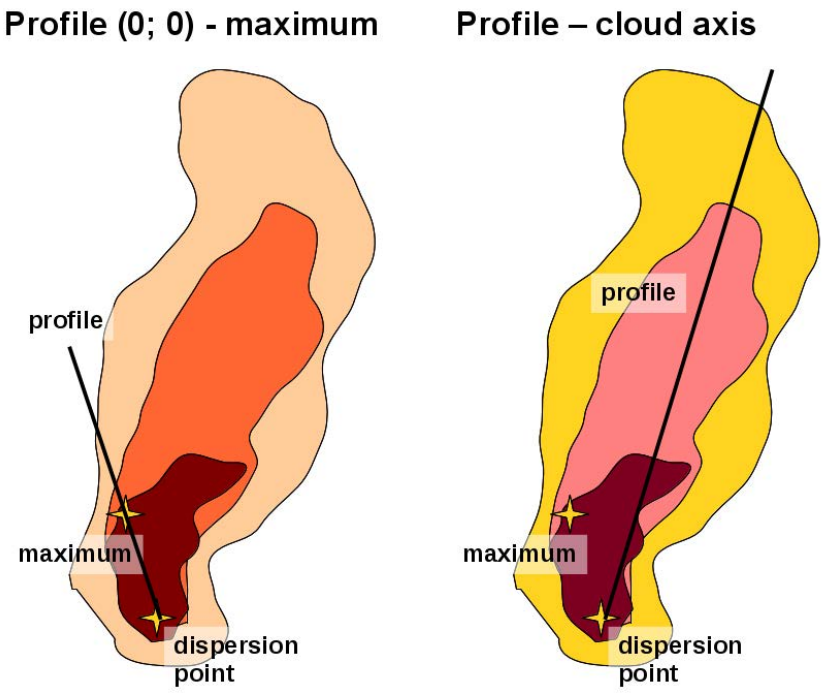

FIG. 2.5. Schematic diagram showing the profile through the point of maximum deposition (left) or through the cloud axis (right). For any given set of activity concentrations, the point of maximum measured or predicted deposition is not necessarily along the cloud axis. The dispersion point is the origin of the radiative release (0,0).

To better characterize the measured or predicted deposition, not only at the measurement points, but in the entire grid area, values of activity concentrations were first calculated from measurements using a Multilevel B-Spline interpolation methodology [2.6] with SAGA GIS[9] software. Each set of model predictions was similarly interpolated using the same methodology and settings as for the measured data and using the same set of grid coordinates as for the measurements. Negative values produced by the calculations were replaced with zeros. Section 2.5.3 discusses the predictions of the total activity deposited in the grid area and of the maximum deposited activity.

Figures 2.6 to 2.11 show the predicted and measured deposition by model type (computational fluid dynamics (CFD) models, Gaussian models, and Lagrangian models) for Tests 3 and 4, in terms of contour plots of the measured or predicted activity concentrations (deposition, Bq/m^2). These plots of the normalized data sets show the predictions and measurements in the same coordinate system and with the same color scale. The plots thus permit a visual comparison of the two dimensional predicted or measured surface contamination. For Test 3, the measurements show deposition largely to the grid north. In contrast, the models predicted the primary deposition in a range from northwest to northeast. For Test 4, the measurements show deposition largely to the grid northwest, then to the southwest. Model predictions included a range from northwest to west, southwest, and south. For Test 4, the measurements indicate that the plume was not stable in direction during the deposition event, and the models did not fully reproduce this effect.

For the contour maps and for the comparisons of profiles (Sections 2.5.4 and 2.5.5), each set of measured or predicted activity concentrations was normalized to the maximum value in the set, i.e. rescaled to a range of 0 to 1, using the following formula:

$$e_{i,normalized} = \frac{e_i - e_{min}}{e_{max} - e_{min}} \quad (2.1)$$

where:

$e_{i,normalized}$ is the normalized value of the activity concentration at a given point i;
e_i is the measured or predicted value of the activity concentration at a given point i;
e_{min} is the minimum value of the set of measured or predicted activity concentrations; and
e_{max} is the maximum value of the set of measured or predicted activity concentrations.

The maximum and minimum values were acquired for each of two ‘profiles’ for each set of measurements or model predictions, as follows:

(1) A line from the dispersion point to the point with the maximum activity concentration (measured or modelled; see Fig. 2.5, left panel); and
(2) A line from the dispersion point along the axis (centreline) of the cloud (measured or modelled), as determined manually from the contour plot (Fig. 2.5, right panel).

The normalization was performed independently for each set of measurements or predictions; thus, the maximum value for a given set of normalized activity concentrations is 1 and the minimum value is 0.

[9] http://www.saga-gis.org/

Profiles of the measurements and of each set of model predictions were developed for each of the two descriptions above (from the dispersion point to the point of maximum activity concentration, and from the dispersion point through the cloud axis), according to the following steps:

(1) A profile line *X* was defined from –65 to +65 m, in a shape file format, with the centre at coordinates (0,0).
(2) The profile line was converted to points in SAGA GIS.
(3) The maximum value and its coordinates were acquired for each set of measurements or model outputs (for the first profile), or the cloud axis was manually defined (or provided by the participant) for the measurements or model outputs (for the second profile).
(4) The rotation angle was calculated for each profile; this is a simple calculation using goniometry[10].
(5) The line of the profile was rotated using the measured angle in SAGA GIS (module Transform Shapes).
(6) Coordinates were added to the line.
(7) Measurements or model predictions from the grid were added to profile points using the Nearest Neighbor method.
(8) The predicted values were processed using the software LibreOffice Calc[11] and Scidavis/QTIplot[12].

Two profile integrals were calculated for Tests 3 and 4 (Sections 2.5.4 and 2.5.5):

(1) A profile integral describing the predicted pattern of deposition along a line from the dispersion point through the point of maximum deposited activity; and
(2) A profile integral describing the predicted pattern of deposition from the dispersion point along the cloud axis (plume centreline).

The rectangle method was used to calculate these integrals. The distance range for the calculation was set as wide as possible in order to include values for all models. For the first profile, the distance ranged from approximately –10 m to 24 m for Test 3 and from approximately –10 m to 17 m for Test 4. For the second profile, the distance ranged from approximately –10 m to 21 m for Test 3 and from approximately –10 m to 15 m for Test 4. The x-axis variable for the profile integrals was in units of m (distance from the dispersion point), and the y-axis variable for the profile integrals was in units of Bq/m^2 (deposited activity per unit ground area, at a distance of *x* m). The profile was assumed to have a width of 0.01 m (1 cm); thus, the profile integral has units of Bq (total activity under the profile).

2.5.3. Maximum activity and total activity in the grid area

Tables 2.5 and 2.6 summarize the maximum deposited activity (Bq/m^2, along with the coordinates for the location) and the total activity deposited in the grid area (MBq), before normalization, for the measurements and for each set of model predictions, for Tests 3 and 4, respectively.

[10] Goniometry is the measurement of angles.
[11] https://www.libreoffice.org/discover/calc/
[12] http://www-mdp.eng.cam.ac.uk/web/CD/engapps/scidavis/scidavis.pdf

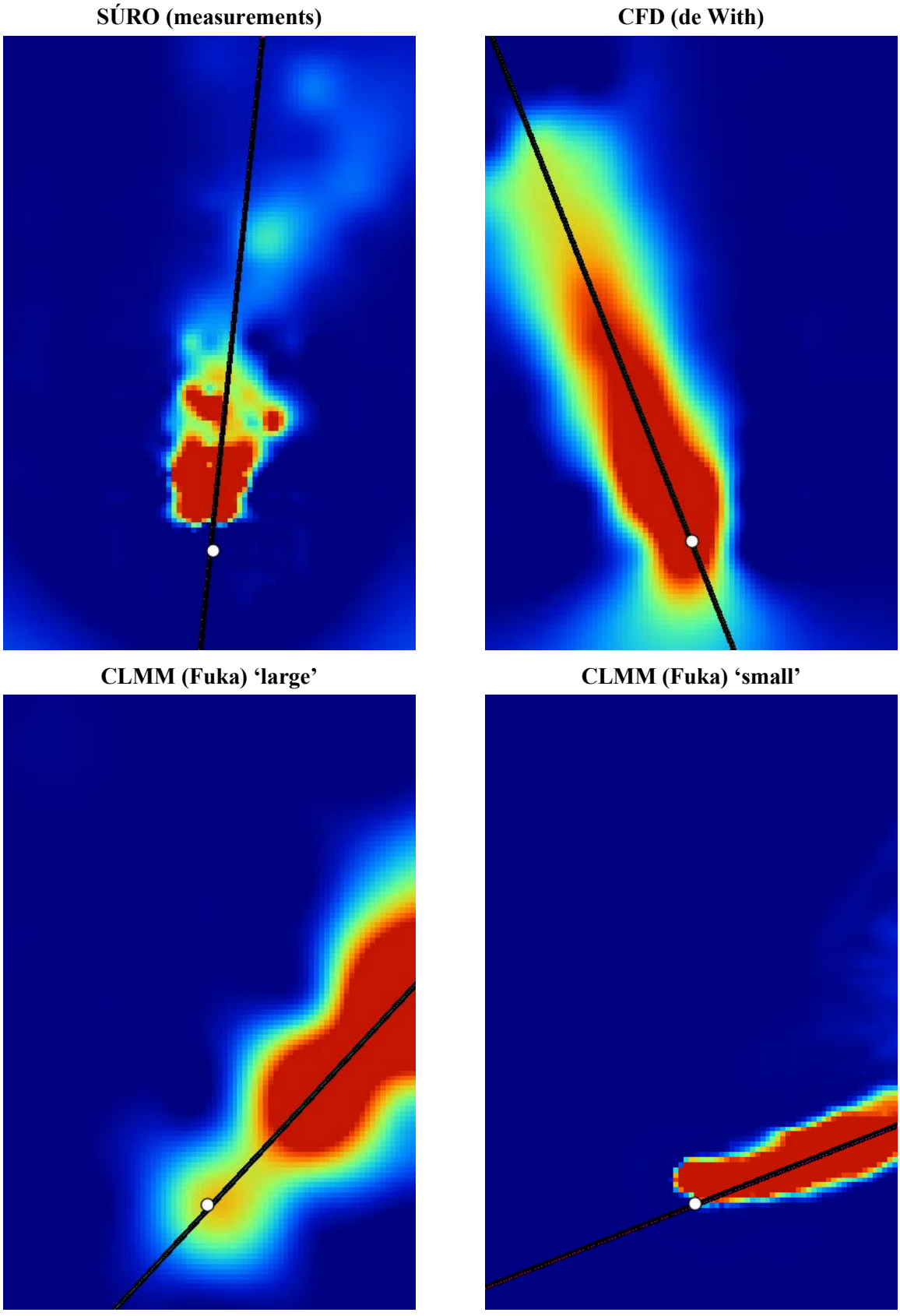

FIG. 2.6. Contour maps of the predicted deposition from computational fluid dynamics models (CFD, CLMM) in comparison with the measurements (SÚRO) for Test 3. The white dot indicates the dispersion point, and the black line indicates the cloud axis.

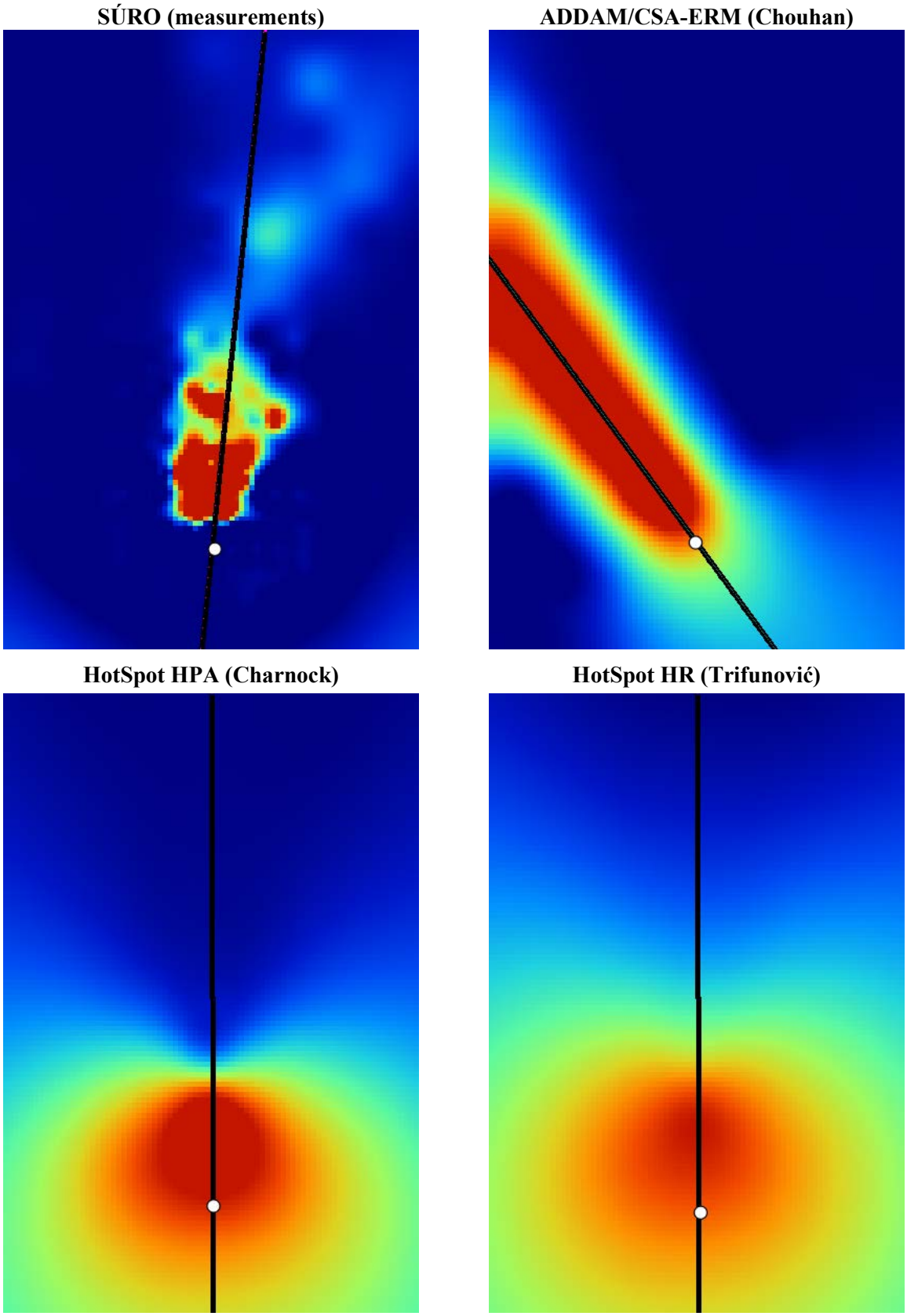

FIG. 2.7. Contour maps of the predicted deposition from Gaussian models (ADDAM/CSA-ERM, Hotspot HPA, Hotspot HR) in comparison with the measurements (SÚRO) for Test 3. The white dot indicates the dispersion point, and the black line indicates the cloud axis.

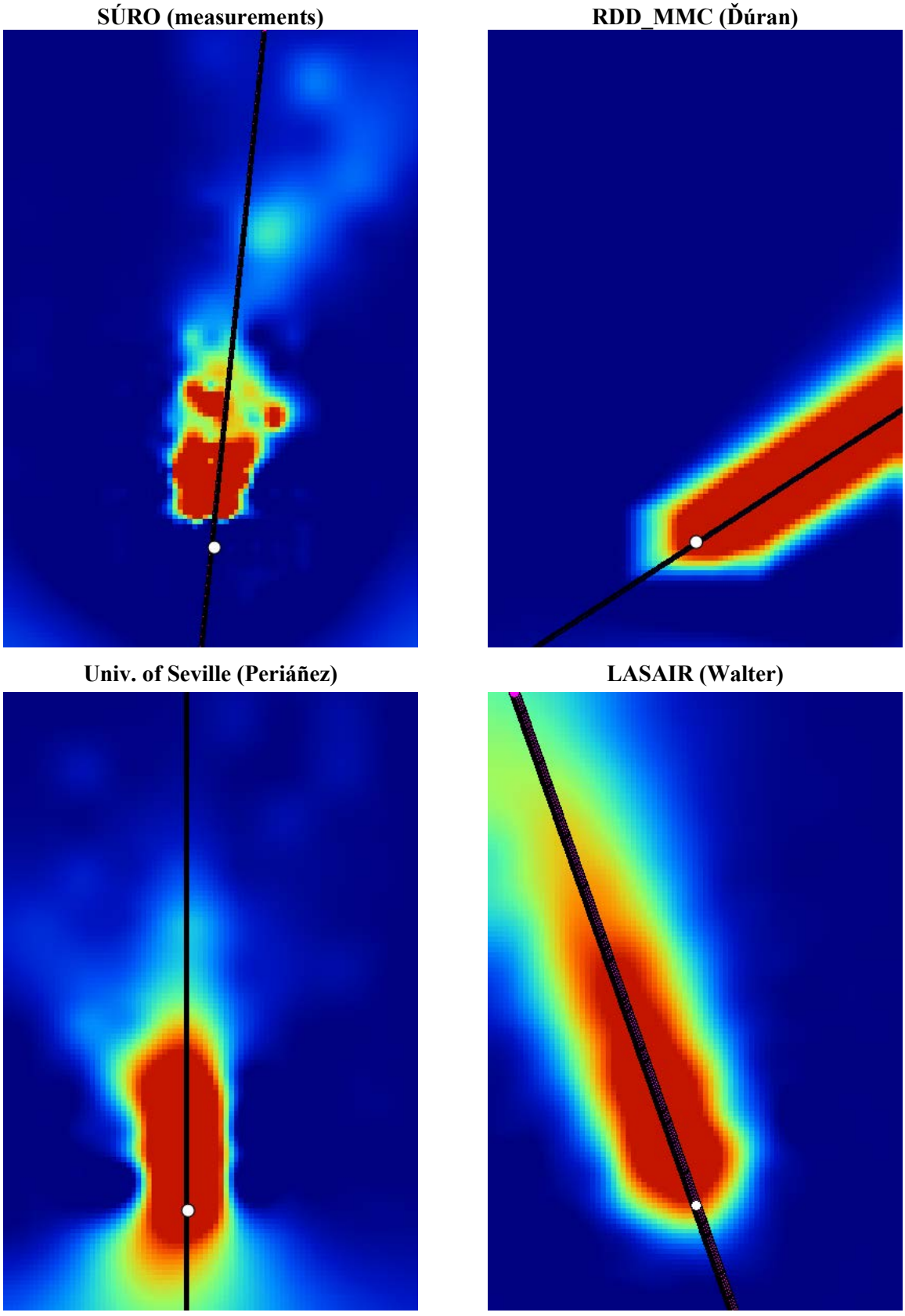

FIG. 2.8. Contour maps of the predicted deposition from Lagrangian models (RDD_MMC, University of Seville, LASAIR) in comparison with the measurements (SÚRO) for Test 3. The white dot indicates the dispersion point, and the black line indicates the cloud axis.

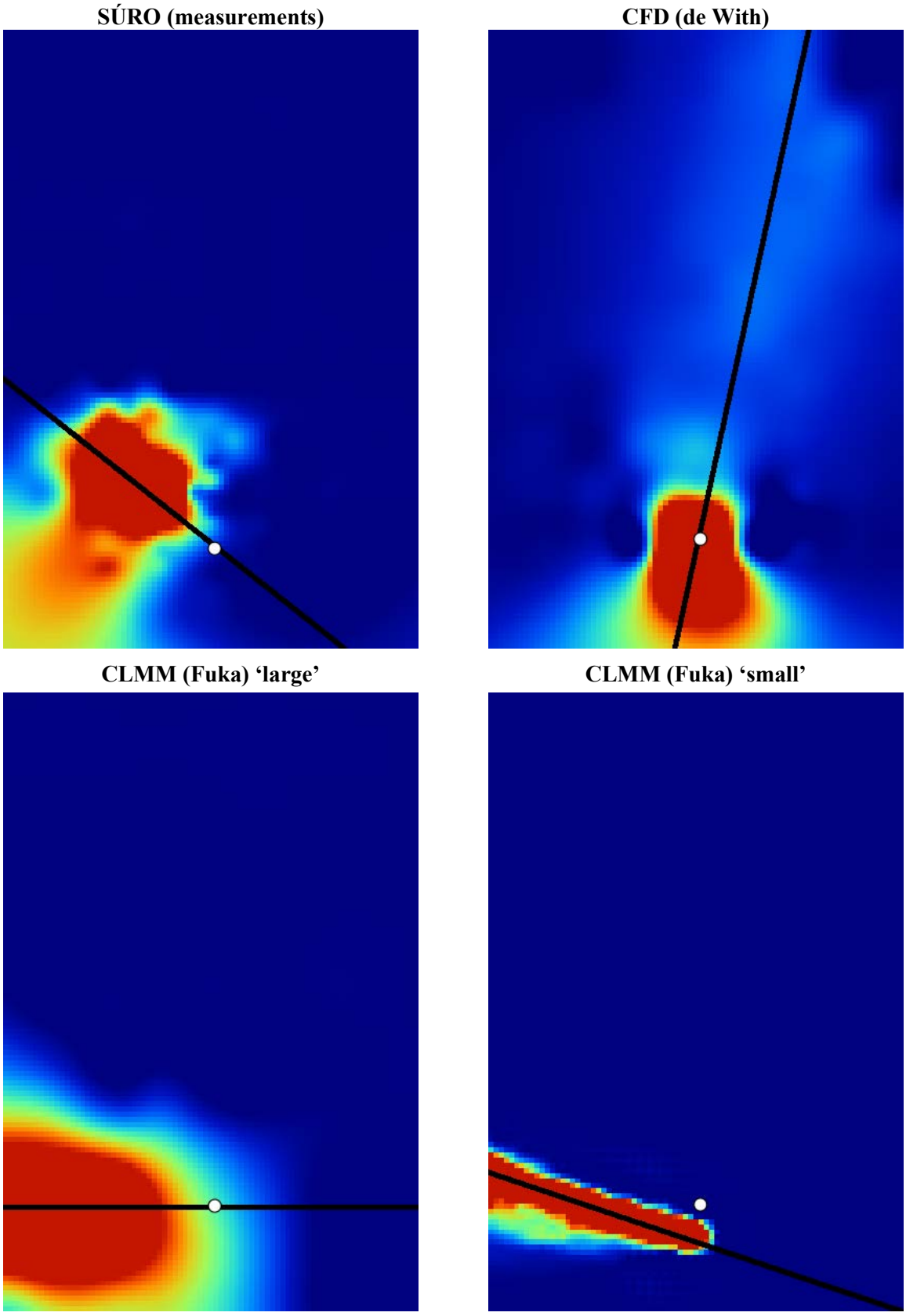

FIG. 2.9. Contour maps of the predicted deposition from computational fluid dynamics models (CFD, CLMM) in comparison with the measurements (SÚRO) for Test 4. The white dot indicates the dispersion point, and the black line indicates the cloud axis.

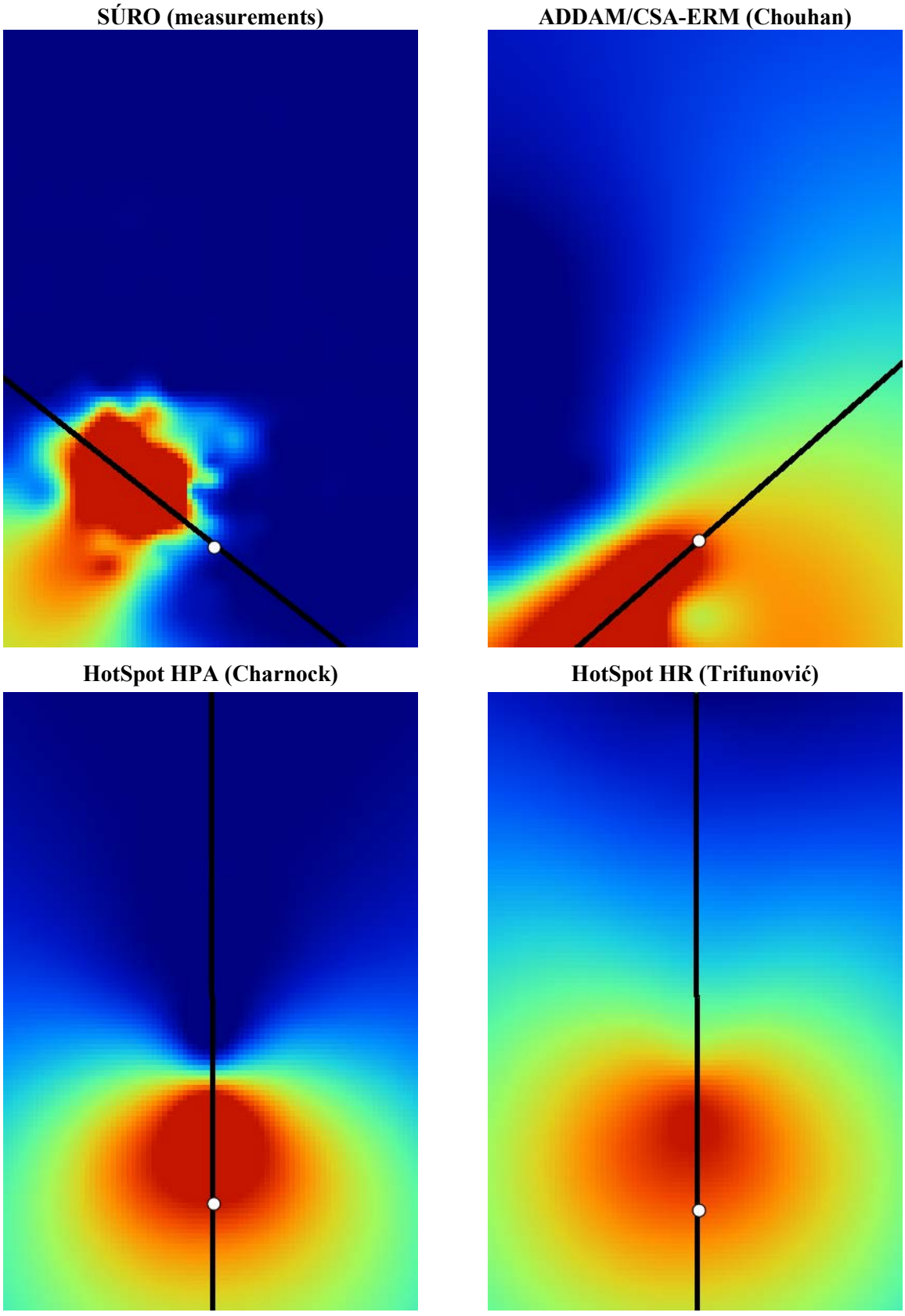

FIG. 2.10. Contour maps of the predicted deposition from Gaussian models (ADDAM/CSA-ERM, Hotspot HPA, Hotspot HR) in comparison with the measurements (SÚRO) for Test 4. The white dot indicates the dispersion point, and the black line indicates the cloud axis.

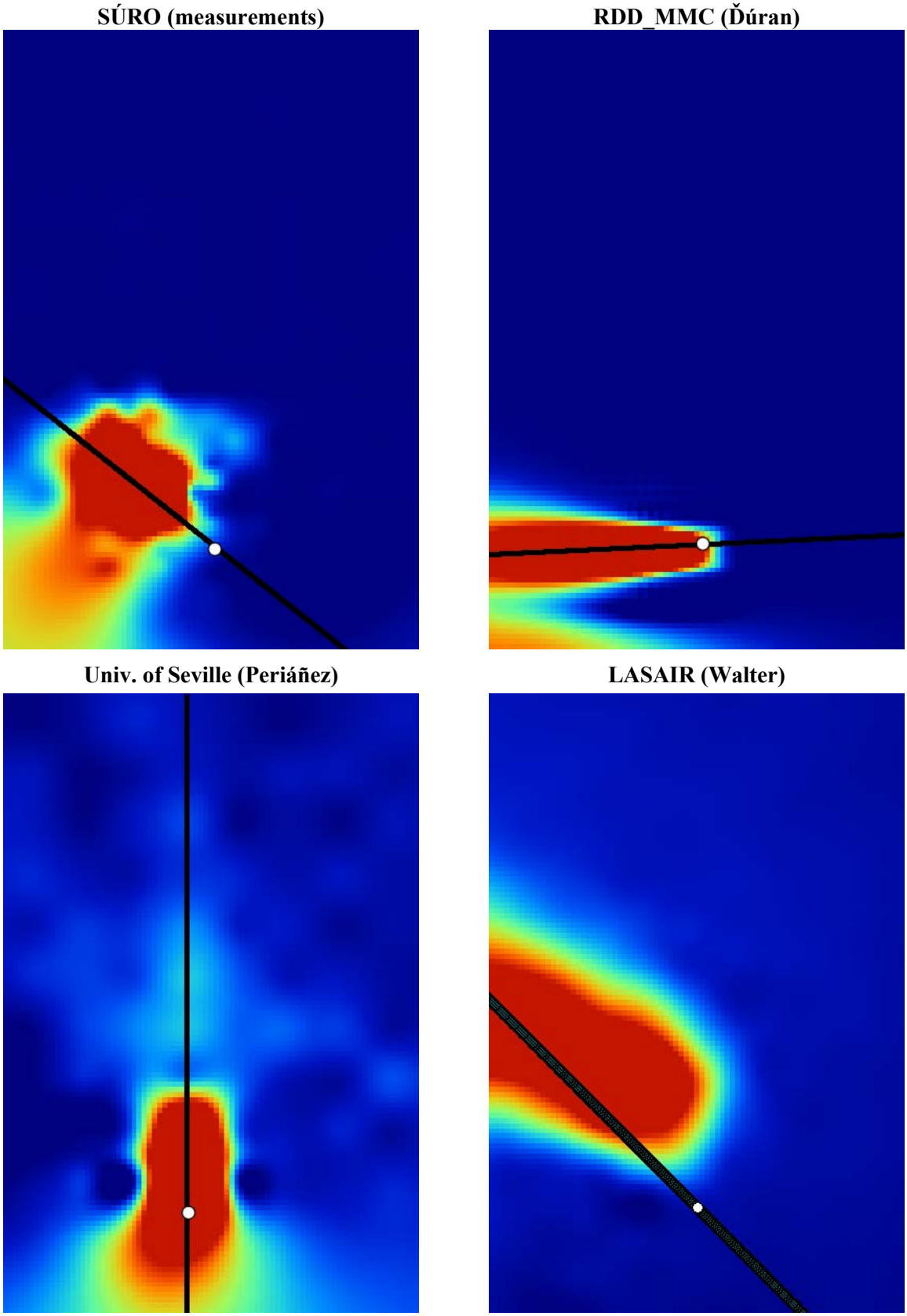

FIG. 2.11. Contour maps of the predicted deposition from Lagrangian models (RDD_MMC, University of Seville, LASAIR) in comparison with the measurements (SÚRO) for Test 4. The white dot indicates the dispersion point, and the black line indicates the cloud axis.

TABLE 2.5. PREDICTED AND MEASURED MAXIMUM VALUES OF DEPOSITED ACTIVITY AND TOTAL ACTIVITY DEPOSITED WITHIN THE GRID AREA[a] FOR TEST 3

Model	Coordinates[b]		Maximum deposited activity (Bq/m^2)	Total activity deposited within the grid area (MBq)
	X	Y		
Measurements (SÚRO)	0	4.0	1.4×10^6	36
Model Predictions:				
CFD (de With)	-1.0	5.0	1.1×10^4	3.1
CLMM (Fuka) – 'large'	10.5	10.5	7.9×10^3	1.8
CLMM (Fuka) – 'small'	1.0	2.5	4.9×10^4	1.9
ADDAM/CSA-ERM (Chouhan)	-12.5	16.5	2.5×10^5	120
HotSpot 2.07.1 (HPA) (Charnock)	0	8.0	1.0×10^6	730
HotSpot 2.07.1 (HR) (Trifunović)	0	8.0	1.3×10^3	1.8
RDD_MMC (Ďúran)	5.5	3.5	1.4×10^5	23
University of Seville (Periáñez)	-2.5	2.5	4.7×10^5	85
LASAIR (Walter)	-2.5	6.5	1.2×10^5	52

[a] The total dispersed activity for Test 3 was 1222 MBq.

[b] Coordinates for the locations of the maximum predicted and measured activities, assuming a dispersion point (origin of the explosion) at (0,0); distances are in m.

TABLE 2.6. PREDICTED AND MEASURED MAXIMUM VALUES OF DEPOSITED ACTIVITY AND TOTAL ACTIVITY DEPOSITED WITHIN THE GRID AREA FOR TEST 4

Model	Coordinates[b]		Maximum deposited activity (Bq/m^2)	Total activity deposited within the grid area (MBq)
	X	Y		
Measurements (SÚRO)	-6.0	5.0	1.9×10^4	2.3
Model Predictions:				
CFD (de With)	0.0	-0.5	4.6×10^4	5.8
CLMM (Fuka) – 'large'	-12.5	-1.0	3.4×10^4	8.6
CLMM (Fuka) – 'small'	-3.0	-2.0	1.8×10^5	7.4
ADDAM/CSA-ERM (Chouhan)	-4.5	-3.5	6.4×10^5	360
HotSpot 2.07.1 (HPA) (Charnock)	0	8.0	5.6×10^9	3.4×10^6
HotSpot 2.07.1 (HR) (Trifunović)	0	8.0	3.8×10^3	6.0
RDD_MMC (Ďúran)	-3.5	-0.5	1.2×10^6	83
University of Seville (Periáñez)	-2.5	2.5	5.7×10^5	94
LASAIR (Walter)	-6.0	12.5	2.4×10^5	79

[a] The total dispersed activity for Test 4 was 1088 MBq.

[b] Coordinates for the locations of the maximum predicted and measured activities, assuming a dispersion point (origin of the explosion) at (0,0); distances are in m.

2.5.3.1. Test 3

The total activity dispersed by Test 3 was 1222 MBq. Based on measurements, the total activity deposited within the grid area was 36 MBq, and the maximum deposited activity was 1.4 MBq/m^2, at a location 4 m directly down grid from the dispersion point (coordinates (0,0); Table 2.5). The predicted maximum deposited activity varied from 1.3 kBq/m^2 to 1.0 MBq/m^2, while the predicted total activity deposited within the grid area ranged from 1.8 to 730 MBq.

The plume from Test 3 went almost directly down the y-axis of the grid (Figs 2.6 to 2.8), and the point of measured maximum deposited activity was directly down the y-axis of the grid. Most of the predicted plumes were displaced to one side or the other of the y-axis (Figs 2.6 to 2.8), the main exception being generated by the University of Seville model (Fig. 2.8). The two sets of predictions that were generated using HotSpot 2.07.01 do not account for the direction of the plume; instead, the predictions are for the plume centreline, wherever it happens to be. Therefore, the predicted plumes in Fig. 2.7 appear to be directly down the y-axis. The points corresponding to the predicted maximum deposited activity are generally displaced slightly from the centrelines of the predicted plumes (Table 2.5), the exception being the HotSpot 2.07.01 predictions, which by definition are down the plume centreline. For the two sets of predictions using HotSpot 2.07.01, the location of the predicted maximum deposited activity is the same, but farther from the dispersion point than the measured maximum.

The predicted maximum deposited activity by HotSpot 2.07.01 (HPA) was quite close to the measured value, 1.0 MBq/m^2 versus 1.4 MBq/m^2. Four other predictions (ADDAM/CSA-ERM, RDD_MMC, University of Seville, and LASAIR) were within about a factor of 10 below the measured value. The lowest predicted value (1.3 kBq/m^2 by HotSpot 2.07.01 (HR)) was about 3 orders of magnitude below the measured value. HotSpot 2.07.01 (HPA) also gave the highest prediction for the total activity deposited within the grid area, about a factor of 20 higher than the measured value. HotSpot 2.07.01 (HR) and CLMM gave the lowest predictions for the total activity deposited within the grid area, about a factor of 20 below the measured value. Three models (RDD_MMC, University of Seville, and LASAIR) were within about a factor of 2 of the measured value of the total deposited activity in the grid area.

For Test 3, two participants using the same model (HotSpot 2.07.01) predicted the highest and lowest values for both the maximum deposited activity and the total activity deposited within the grid area. The two participants used different assumptions for the wind speed, dry deposition velocity, and partitioning of the source term, and these probably account for the differences in the results, which are discussed further in Section 2.5.3.2.

2.5.3.2. Test 4

The total activity dispersed by Test 4 was 1088 MBq. Based on measurements, the total activity deposited within the grid area was 2.3 MBq, and the maximum deposited activity was 19 kBq/m^2, at a point 5 m down the y-axis but displaced 6 m to one side of the y-axis (coordinates (–6,5); Table 2.6). The predicted maximum deposited activity varied from 3.8 kBq/m^2 to 5.6 GBq/m^2, while the predicted total activity deposited within the grid area ranged from 5.8 Bq to 3.4 MBq.

The lower values for Test 4 than Test 3, with similar total dispersed activities, reflects the deviation of the plume from the grid area in Test 4, due to unexpected changes in wind speed and direction at the time of the test. As shown in Figs 2.9 to 2.11, most of the model predictions also show a plume significantly displaced from the y-axis and even going backwards from the

intended direction (y-coordinate with a negative value). The one model that appears to have a plume down the y-axis also shows a strong component in the backwards direction (see contour maps for the University of Seville in Fig. 2.11 above). As for Test 3, the two predictions using HotSpot 2.07.01 do not account for the direction of the plume but show only the plume centreline.

All but one (HotSpot 2.07.01 (HR)) of the predicted values of maximum deposited activity were greater than the measured value, although predictions from two models (CFD and CLMM 'large') were within a factor of 3 of the measured value, and all but one (HotSpot 2.07.1 (HPA)) were within a factor of about 60 of the measured value. Although all predicted values of the total activity deposited within the grid area were greater than the measured value, predictions from several models (CFD, CLMM (both predictions), and HotSpot 2.07.01 (HR)) were within a factor of 4 of the measured value, and three others (RDD_MMC, University of Seville, and LASAIR) were within a factor of about 40 of the measured value. Thus, even with the unexpected movement of the plume, most participants were within a factor of about 40 or better of the measured total deposited activity within the grid area.

For Test 4 as with Test 3, two participants using the same model (HotSpot 2.07.01) predicted the highest and lowest values for both the maximum deposited activity and the total activity deposited within the grid area. The two participants used different assumptions for the wind speed, dry deposition velocity, and partitioning of the source term, and these probably account for the differences in the results. In particular, for HotSpot 2.07.01 (HPA), the high dry deposition velocity associated with the largest particles (non-respirable fraction, >10 μm) and the assumption of uniform partitioning of the source term within the cloud (as opposed to much smaller fractions associated with the lowest part of the cloud for HotSpot 2.07.01 (HR)), may have contributed to a much higher prediction of near in deposited activity for HotSpot 2.07.01 (HPA). ADDAM/CSA-ERM also used a high value for the dry deposition velocity, which probably explains why this model gave the second highest predictions for total activity deposited within the grid area for both Test 3 and Test 4.

2.5.4. Profiles from the dispersion point to the maximum activity

Tables 2.7 and 2.8 provide the predicted and measured profile integrals (profiles of deposited activity) along the line from the dispersion point through the maximum deposited activity for each model for Tests 3 and 4, respectively. Figures 2.12 (Test 3) and 2.13 (Test 4) show the normalized profiles of the predicted deposition in comparison with the measurements, from the dispersion point through the maximum value, by type of model (CFD models, Gaussian models, and Lagrangian models). Only the range from the dispersion point (0,0) to the maximum was plotted. The stepped shape of the graphed lines is caused by differences in resolution between the calculated profile and the grid. All profiles were checked to be sure that they crossed the maximum value of the input grid (the maximum value predicted by the model). The profile integrals (Figs 2.12 and 2.13) do not show differences in the predicted direction from the dispersion point (Figs 2.6 to 2.11).

TABLE 2.7. PROFILE INTEGRALS OF DEPOSITION FOR TEST 3

Model	Profile through maximum		Profile through cloud axis	
	Normalized values (unitless)	Measured or predicted values (Bq)	Normalized values (unitless)	Measured or predicted values (Bq)
Measurements (SÚRO)	0.03	4.32×10^4	0.03	4.03×10^4
CFD (de With)	0.14	1.98×10^3	0.17	2.10×10^3
CLMM (Fuka) – 'large'	0.18	1.15×10^3	0.16	1.02×10^3
CLMM (Fuka) – 'small'	0.02	1.22×10^3	0.11	3.61×10^3
ADDAM/CSA-ERM (Chouhan)	0.23	6.68×10^4	0.21	6.11×10^4
Hotspot 2.07.1 (HPA) (Charnock)	0.25	2.06×10^5	0.19	2.05×10^5
Hotspot 2.07.1 (HR) (Trifunović)	0.27	3.68×10^2	0.21	3.54×10^2
RDD_MMC (Ďúran)	0.22	3.20×10^4	0.21	2.97×10^4
University of Seville (Periáñez)	0.15	8.28×10^4	0.14	8.12×10^4
LASAIR (Walter)	0.21	2.54×10^4	0.19	2.36×10^4

TABLE 2.8. PROFILE INTEGRALS OF DEPOSITION FOR TEST 4

Model	Profile through maximum		Profile through cloud axis	
	Normalized values (unitless)	Measured or predicted values (Bq)	Normalized values (unitless)	Measured or predicted values (Bq)
Measurements (SÚRO)	0.09	1.71×10^3	0.09	1.62×10^3
CFD (de With)	0.09	4.30×10^3	0.08	4.22×10^3
CLMM (Fuka) – 'large'	0.14	4.75×10^3	0.12	4.23×10^3
CLMM (Fuka) – 'small'	0.03	5.24×10^3	0.11	1.90×10^4
ADDAM/CSA-ERM (Chouhan)	0.15	1.30×10^5	0.14	1.22×10^5
Hotspot 2.07.1 (HPA) (Charnock)	0.18	9.97×10^8	0.17	9.97×10^8
Hotspot 2.07.1 (HR) (Trifunović)	0.16	9.06×10^2	0.14	8.64×10^2
RDD_MMC (Ďúran)	0.12	1.44×10^5	0.12	1.38×10^5
University of Seville (Periáñez)	0.11	6.82×10^4	0.11	6.73×10^4
LASAIR (Walter)	0.09	2.28×10^4	0.08	1.51×10^4

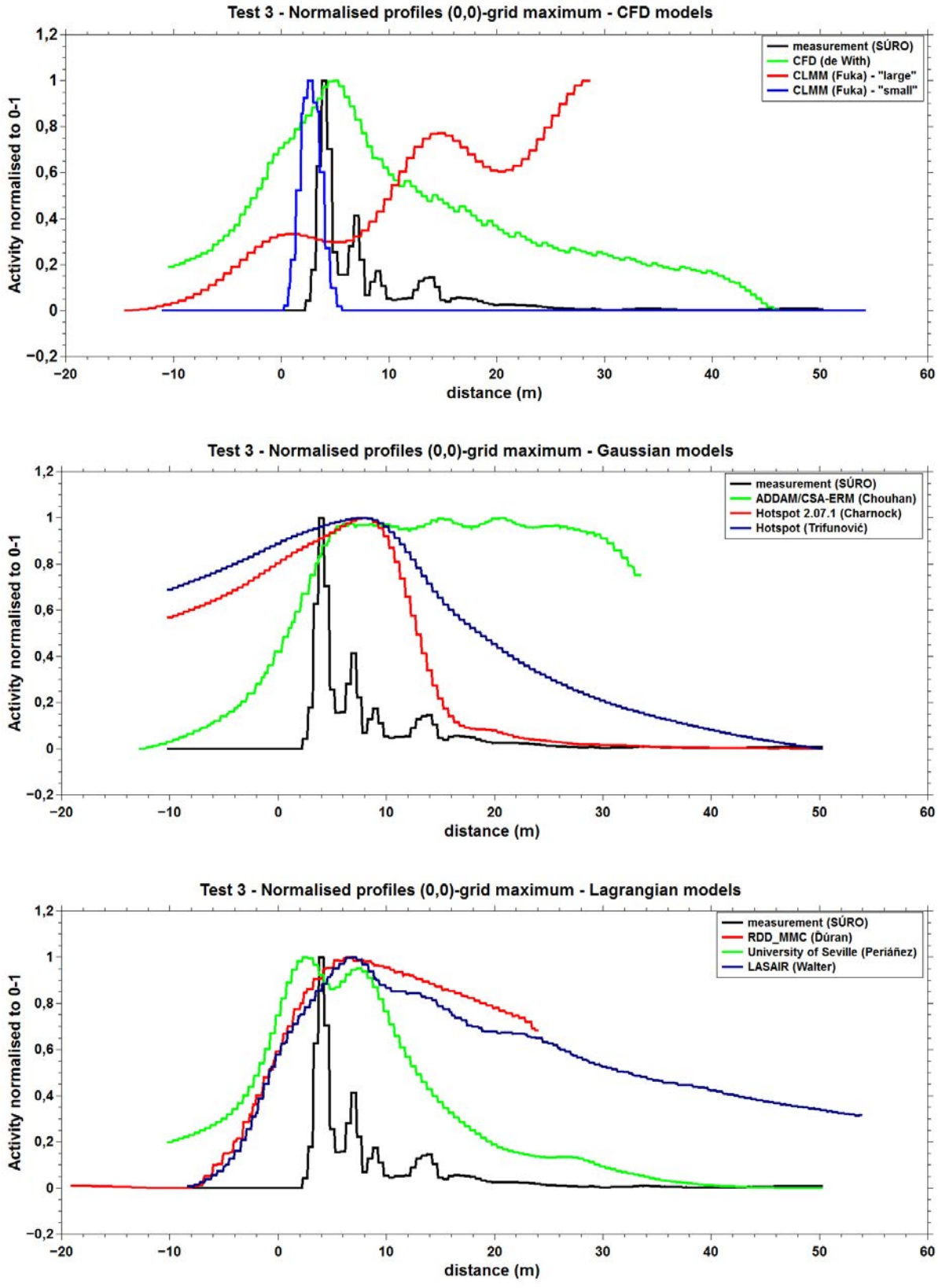

FIG. 2.12. Normalized profiles of the predicted deposition in comparison with the measurements for Test 3, by type of model: computational fluid dynamics (CFD; top), Gaussian (centre), or Lagrangian (bottom).

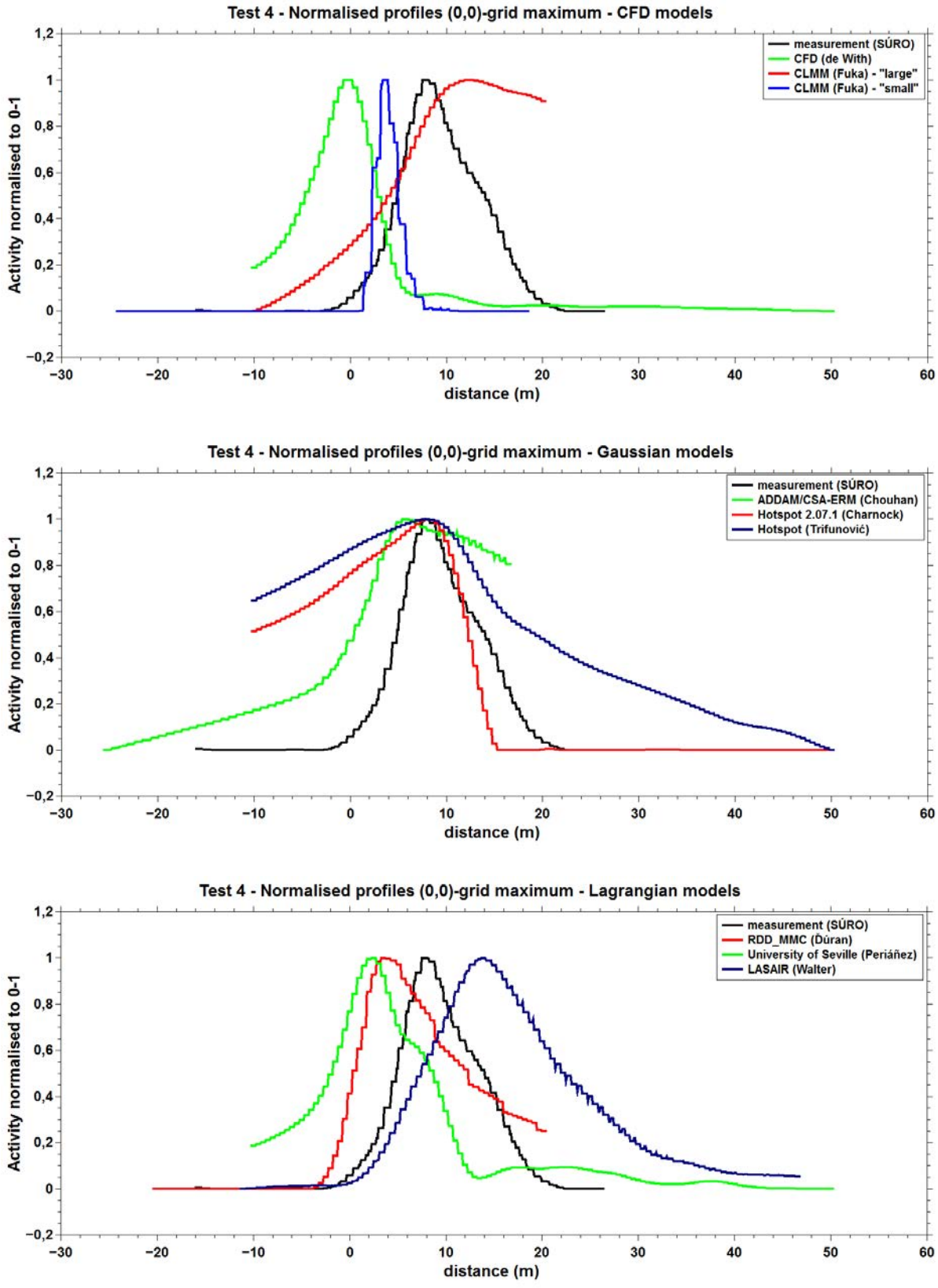

FIG. 2.13. Normalized profiles of the predicted deposition in comparison with the measurements for Test 4, by type of model: computational fluid dynamics (CFD; top), Gaussian (centre), or Lagrangian (bottom).

2.5.4.1. Test 3

For Test 3, predicted profile integrals from the dispersion point through the maximum value ranged from 370 Bq to 210 kBq, a range of about a factor of 600 (Table 2.7). The measured profile integral was 43 kBq, within the range of the predicted values, which varied from a factor of 120 below the measured value to a factor of 5 above the measured value. Four of the models (LASAIR, RDD_MMC, ADDAM/CSA-ERM, and University of Seville) were within a factor of 2 of the measurements. The HotSpot 2.07.01 model, with two different users, gave the lowest and highest values for the profile integral, but the highest (HotSpot 2.07.01 (HPA)) was still within a factor of 5 of the measured value.

Two of the three computational fluid dynamics models (CFD and CLMM 'small') had their peak values very close to the location of the measured peak (Fig. 2.12, top), while the third (CLMM 'large') gave a different profile. The two sets of predictions with HotSpot 2.07.1 gave similar profiles (Fig. 2.12, centre), while the third Gaussian model (ADDAM/CSA-ERM) had a similar peak but a different shape to the profile beyond the peak; all three of the Gaussian models showed a peak a few meters beyond the peak of the measurements. The Lagrangian models (Fig. 2.12, bottom) also gave peaks near the measured peak, with one slightly closer in (University of Seville) and two farther out (RDD_MMC and LASAIR). The measurements showed several smaller peaks beyond the maximum peak; a few of the models (University of Seville, LASAIR, ADDAM/CSA-ERM) predicted secondary peaks but did not reproduce the shape. CLMM 'large' gave higher predictions at longer distances, the reverse of the measured profile.

2.5.4.2. Test 4

For Test 4, predicted profile integrals from the dispersion point through the maximum value ranged from 910 Bq to 1 GBq, a range of about a factor of 10^6 (Table 2.8). The measured profile integral was 1.7 kBq, within the range of the predicted values, which varied from a factor of 2 below the measured value to a factor of 6×10^5 above the measured value. Four of the models (Hotspot 2.07.1 (HR), CFD, CLMM 'large', and CLMM 'small') were within a factor of 3 of the measured value. Again, the HotSpot 2.07.01 model gave the lowest and highest predicted values for the profile integral, but in this case, the lowest (HotSpot 2.07.1 (HR)) was within a factor of 2 of the measured value.

In general, the predicted profile integrals had similar shapes to the measured profile integral (Fig. 2.13). The three Gaussian models (Fig. 2.13, centre) all gave peaks close to the measured peak, although the shapes of the predictions were generally broader. Of the computational fluid dynamics models (Fig. 2.13, top), two (CLMM 'large' and 'small') had peaks beyond the measured peak and the third (CFD) had its peak closer to the dispersion point (coordinates (0,0)). Two of the Lagrangian models (RDD_MMC and University of Seville) gave predicted peaks closer to the dispersion point than the measured peak, while the third (LASAIR) predicted a peak beyond the measured peak. Test 4 involved some unexpected wind directions, as described earlier, which complicated the modelling.

2.5.5. Profiles along the cloud axis

Tables 2.7 and 2.8 provide the predicted and measured profile integrals (profiles of deposited activity) along the cloud axis for each model for Tests 3 and 4, respectively. Figures 2.14 (Test 3) and 2.15 (Test 4) show the normalized profiles along the cloud axis of the predicted deposition in comparison with the measurements, by type of model (computational fluid dynamics models, Gaussian models, and Lagrangian models). As with the profiles through the

maximum predicted deposition, the stepped shape of the graphed lines is caused by differences in resolution between the calculated profile and the grid. The profile integrals in Figs 2.14 and 2.15 do not show differences in predicted direction from the dispersion point (Figs 2.6 to 2.11).

2.5.5.1. Test 3

For Test 3, predicted profile integrals from the dispersion point along the cloud axis ranged from 3.5×10^2 Bq to 2.1×10^5 Bq, a range of about a factor of 600 (Table 2.7). The measured profile integral along the cloud axis (4.0×10^4 Bq) was slightly lower than the measured profile integral through the maximum measured activity (4.3×10^4 Bq; Table 2.7). The measured profile integral along the cloud axis was within the range of the predicted values, which varied from a factor of 110 below the measured value to a factor of 5 above the measured value. Four of the predictions (LASAIR, RDD_MMC, ADDAM/CSA-ERM, and University of Seville) were within a factor of 2 of the measured value. As with the profiles through the maximum values, HotSpot 2.07.1 gave both the lowest and highest values, with the highest (HotSpot 2.07.1 (HPA)) being about a factor of 5 greater than the measured value. In general, the profile through the cloud axis for each model was similar in value to the profile through the predicted maximum deposition for the same model (Table 2.7), with the greatest difference being a factor of about 3 (CLMM 'small'). This means that the predicted maximum value was close to the cloud axis for any given model.

In general, the predicted profile integrals through the cloud axis (Fig. 2.14) had different shapes than the measured profile integral, with the predicted profiles having broader peaks, and in most cases, not showing the secondary peaks. CLMM 'small', University of Seville, and to a lesser extent ADDAM/CSA-ERM did predict secondary peaks, with CLMM 'small' being most similar in shape to the measured profile. CLMM 'large' again had the more distant peak larger than the first peak, in contrast to the other models.

2.5.5.2. Test 4

For Test 4, predicted profile integrals from the dispersion point along the cloud axis ranged from 8.6×10^2 Bq to 1.0×10^9 Bq, a range of about a factor of 10^6 (Table 2.8). The measured profile integral (1.6×10^3 Bq) was slightly lower than the measured profile integral through the cloud axis (1.7×10^3; Table 2.8). The measured profile integral along the cloud axis was within the range of the predicted values, which varied from a factor of 2 below the measured value to a factor of 6×10^5 above the measured value. Three of the predictions (HotSpot 2.07.1 (HR), CFD, and CLMM 'large') were within a factor of 3 of the measured value. As with the profiles through the maximum values, HotSpot 2.07.1 gave both the lowest and highest values of the profile integral, with the lowest (HotSpot 2.07.1 (HR)) being within a factor of 2 of the measured value. In general, the profile through the cloud axis for each model was similar in value to the profile through the predicted maximum deposition for the same model (Table 2.8), with the greatest difference being a factor of about 4 (CLMM 'small'). This means that the predicted maximum value was close to the cloud axis for any given model.

In contrast to Test 3, most of the predicted profile integrals through the cloud axis for Test 4 (Fig. 2.15) had similar shapes to the measured profile integral, with the predicted profiles differing with respect to where the peaks were located. The Gaussian models (ADDAM/CSA-ERM, HotSpot 2.07.1 (HPA), and HotSpot 2.07.1 (HR)) came closest to the predictions in terms of the location of the predicted peak of the profile integral.

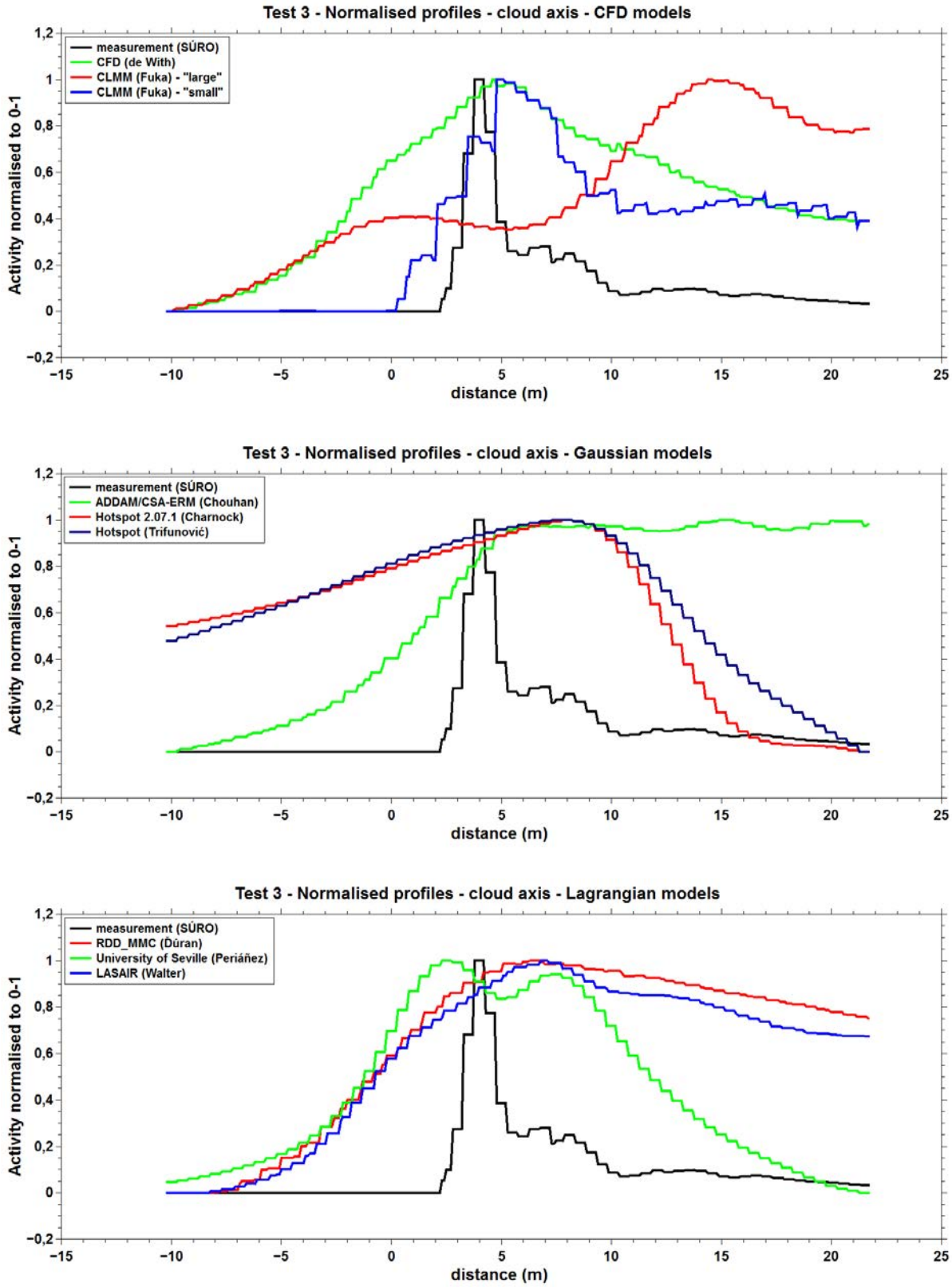

FIG. 2.14. Normalized profiles of the predicted deposition along the cloud axis, in comparison with the measurements for Test 3, by type of model: computational fluid dynamics (CFD; top), Gaussian (centre), or Lagrangian (bottom).

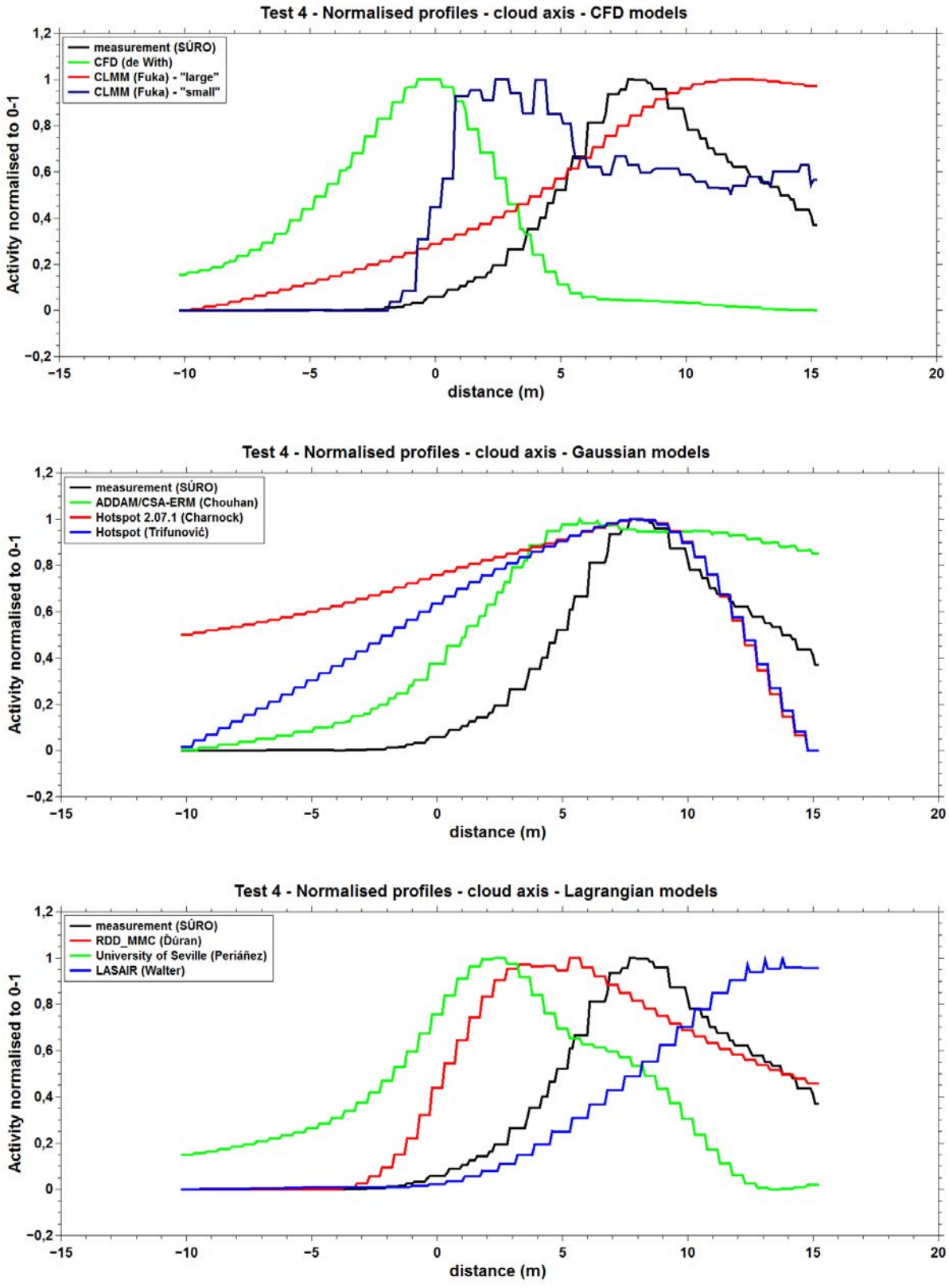

FIG. 2.15. Normalized profiles of the predicted deposition along the cloud axis, in comparison with the measurements for Test 4, by type of model: computational fluid dynamics (CFD; top), Gaussian (centre), or Lagrangian (bottom).

2.6. CONCLUSIONS FROM THE SHORT RANGE ATMOSPHERIC DISPERSION EXERCISE

The field tests for this exercise were challenging for the participants to model, as they involved prediction of spatially varying activity concentrations for time dependent wind conditions. The explosion itself was not modelled directly; instead, participants started with the initial cloud or plume, but differed in their characterization of the initial cloud (e.g. in terms of cloud height, partitioning of the source term within the cloud). A suggested set of default cloud dimensions and partitioning of the source term was developed by the participants, although some participants chose to use different assumptions (Table 2.3).

As seen in the contour plots, the predicted direction of the plume varied considerably amongst participants for each test (Figs 2.6 to 2.11). The predicted amounts of deposited activity (the maximum amounts, the total amounts in the grid area, and the profiles of deposited activity) also varied widely, as discussed in the previous sections. Still, for each test, some model predictions were close to the measurements, especially for the integrated endpoints, such as the total activity within the grid area and the profiles of deposited activity. However, for each test, it was different sets of model predictions that were close to the measurements. Therefore, the results indicate that it is not the case that a model with accurate predictions for one test had accurate predictions for another test, or vice versa. Nor do the results indicate that better predictions for Test 4 than for Test 3 can be attributed to refinement of the models between the two tests, as participants submitted results for both tests at the same time and did not have access to measurements for either test until later.

For the models considered, the location of the maximum predicted activity concentration was generally close to the predicted cloud axis, resulting in profile integrals through the predicted maximum that were quite close in value to the profile integrals through the predicted cloud axis. Even given the difficulty of characterizing some time dependent plumes by one axis, it is to be expected that the maximum point concentration would usually be close to the predicted cloud axis.

The choice of a value for the dry deposition velocity (for the models that used that parameter) may explain some, but not necessarily all, of the highest values for the predictions. It is interesting that the two users of the same model (HotSpot 2.07.1) produced the lowest and highest values for the predictions, likely because of different choices of values that were made for the dry deposition velocity, as well as other differences in model implementation by the two participants (e.g. wind speeds, source term partitioning).

Some models were intended for domain or grid sizes larger than those used in the experiment (i.e. lower resolution in the model predictions), and some models were intended for smaller grid sizes (i.e. higher resolutions) than used in the experiment. The resolution of key site specific conditions and factors, such as the spatial extent of contamination, local meteorological conditions that can affect contaminant dispersion and other factors relative to the model grid size can affect model predictability. For example, in cases where grid sizes are large relative to the spatial extent of contamination, radiological impacts at a local level may be underestimated, whereas in cases where the grid size is too small compared to the experimental area, model predictions may be quite ‘noisy’, making it more difficult to discern radiological impacts of interest. There were also important differences amongst model predictions in the wind speeds used (both differences in selected values for the wind speeds, and whether the model used average wind speeds or time dependent information). Additional work with these experiments (Tests 3 and 4, plus additional tests) has continued during the IAEA’s MODARIA (Modelling and Data for Radiological Impacts Assessments) Programme.

2.7. REFERENCES TO SECTION 2

[2.1] THIESSEN, K.M., ANDERSSON, K.G., BERKOVSKYY, V., CHARNOCK, T.W., CHOUHAN, S.L., De WITH, G., ĎÚRAN, J., FUKA, V., HELEBRANT, J., HŮLKA, J., HWANG, W.T., KUČA, P., MANCINI, F., NAVARRO, E., PERIÁÑEZ, R., PROUZA, Z., SDOUZ, G., TOMÁS, J., TRIFUNOVIĆ, D., URSO, L., WALTER H., Assessing emergency situations and their aftermath in urban areas: The EMRAS II Urban Areas Working Group, Radioprotection **46** (2011) S601.

[2.2] PROUZA, Z., BECKOVA, V., CESPIROVA, I., HELEBRANT, J., HULKA, J., KUCA, P., MICHALEK, V., RULIK, P., SKRKAL, J., HOVORKA, J., Field tests using radioactive matter, Radiation Protection Dosimetry **139** (2010) 519.

[2.3] INTERNATIONAL ATOMIC ENERGY AGENCY, Environmental Modelling for Radiation Safety (EMRAS). A Summary Report of the Results of the EMRAS Programme (2003–2007), IAEA-TECDOC-1678, IAEA, Vienna (2012).

[2.4] MECKBACH, R., JACOB, P., Gamma exposures due to radionuclides deposited in urban environments. Part II: Location factors for different deposition patterns, Radiation Protection Dosimetry **25** (1988) 181.

[2.5] HOMANN, S.G., HotSpot Health Physics Codes Version 2.07 User's Guide, Rep. LLNL-TM-411345, Lawrence Livermore National Laboratory, CA (2009).

[2.6] LEE, S., WOLBERG, G., SHIN, S.Y., Scattered data interpolation with multilevel B-splines, IEEE Transactions on Visualization and Computer Graphics **3** (1997) 228.

3. MID-RANGE ATMOSPHERIC DISPERSION EXERCISE

3.1. OVERVIEW

The mid-range atmospheric dispersion scenario was based on a hypothetical release of radioactivity from a nuclear power plant (NPP) [3.1, 3.2] (see Appendix III). The scenario was developed with the objective of providing an opportunity to test model predictions for a mid-range dispersion event, including the dispersion of radioactivity from an NPP and the resulting deposition in urban areas. The exercise was based on real geographic information. Using this scenario, the effects of different meteorological conditions on dispersion and deposition were studied.

Input information for the scenario included a description of the hypothetical accident, the amounts and types of radioactivity involved, meteorological information, the locations of the cities of interest, the locations for modelling endpoints, and information on the terrain and topography. Modelling endpoints for intercomparison amongst participants were the deposition on the ground (i.e. a reference lawn surface), time integrated activity concentrations in air, a contour map of deposition, and a time series for contamination at selected locations. A full description of the scenario is provided in Appendix III.

The exercise was based on the Trillo NPP, which is located in the central part of Spain, approximately 70 km from the Madrid metropolitan area and 46 km from Guadalajara, a smaller town in central Spain located between the Trillo NPP and Madrid [3.2]. The Trillo NPP started operation in 1987 and is a pressurized water reactor (PWR), which operates at a power of 1043 MW. Reactor cooling is carried out through two cooling towers.

Specified meteorological conditions representative of a worst case scenario were used for the exercise. Participants were provided with simulated wind fields at 10 m above the ground (Appendix III), and two sets of conditions were considered: one which assumed a stable atmosphere (Class E); and one which assumed neutral atmospheric stability (Class D). This approach allowed the assessment of the effects of stability conditions on radionuclide dispersion. The same geostrophic wind direction was considered for both cases. However, stable stratification and neutral conditions are found at low wind speeds; therefore, wind speeds of 3.0 m/s and 6.0 m/s were assumed for the stable and neutral conditions, respectively.

The same hypothetical accident was considered for both sets of meteorological conditions. Two radionuclides with different half-lives were considered in the scenario: ^{137}Cs and ^{131}I, the latter of which was assumed to be released only in the molecular form (i.e. as I_2). These radionuclides were assumed to be released in a gaseous form, and only dry deposition was considered.

The hypothetical accident involved a steam generator tube rupture. The scenario was developed by the Institut de Radioprotection et de Sûreté Nucléaire (IRSN) of France. The release duration was assumed to be 1 hour, and the release rate varied with time for both radionuclides. Release data for the 1 hour period were provided to the participants. An effective release height of 50 m was assumed.

Participants were requested to simulate the plume behavior for a 10 hour period and to provide contour maps of:

(1) Deposited activity on the ground; and
(2) Time integrated activity concentrations in air at ground level, at the end of the simulation.

Participants were also requested to provide a time series of activity concentrations in air at four selected locations.

3.2. MODELS USED IN THE EXERCISE

Table 3.1 summarizes the five models used in the mid-range atmospheric dispersion exercise (see also Ref. [3.2]). Additional information about individual models and how they were used in this exercise is provided in Appendix IV. The models have been developed to meet several different purposes (e.g. emergency assessment and research) and include two major types of modelling approaches (Gaussian and Lagrangian). One model (HotSpot 2.07.1) provided results in terms of downwind distance along the centreline of the plume; the other four models provided results that accounted for the local geography. The range of the model predictions generated using the RASCAL model was less than the distance to Madrid. Four models (ADDAM, RASCAL, University of Seville (Usev), and HotSpot 2.07.1) were used to generate results for both sets of atmospheric conditions, whereas the fifth (JRODOS) was used only for stable conditions. One model (Usev) used time dependent source term information in 1 minute increments, three models (ADDAM, RASCAL, and HotSpot 2.07.1) considered the entire release within a single 1 hour time step, and one model (JRODOS) considered the release in two half-hour time steps. Different approaches were used to handle the information on wind speed and direction, and different values were selected for the dry deposition velocities (Table 3.1).

3.3. RESULTS OF MODEL INTERCOMPARISON EXERCISE

The model endpoints listed in Section 3.1 (and discussed in detail below) were predicted by five participants in this model intercomparison exercise (see also Ref. [3.2]). Not all participants submitted predictions for each endpoint.

3.3.1. Contour maps

All five participants provided contour maps of predicted deposition of ^{137}Cs (Figs 3.1 to 3.5), and three participants (Usev, ADDAM, JRODOS) provided contour maps of time integrated radionuclide activity concentrations in air (not shown in main text but provided in Appendix IV). Two sets of predictions (Usev and ADDAM, Figs 3.1 and 3.2) clearly showed the effect of different sets of meteorological conditions: the predicted plumes intersected Madrid under stable conditions, whereas under neutral stability, the plume bypassed Madrid. The JRODOS plume under stable conditions also intersected Madrid (Fig. 3.3). Predictions made using RASCAL did not reach as far as Madrid, but the plots suggest that the plume would have intersected Madrid under stable conditions and would have bypassed Madrid under neutral stability (Fig. 3.4). HotSpot 2.07.1 provided results only in terms of the plume centre line, without accounting for the local geography; the results showed higher deposition farther downwind under stable conditions (Fig. 3.5).

TABLE 3.1. SUMMARY OF MODELS USED FOR THE MID-RANGE SCENARIO

Parameter	Model name				
	ADDAM	**RASCAL 3.0.3**	**University of Seville**	**JRODOS**	**HotSpot 2.07.1**
Participant and country	S.L. Chouhan Canada	F. Mancini Italy	R. Periáñez Spain	G. Sdouz Austria	D. Trifunović Croatia
Purpose of model	Safety assessment for accidents	Radiological emergency assessment	Research	Nuclear emergency preparedness	Radiological emergency assessment
Type of model	Gaussian plume	Gaussian plume and Lagrangian puff	Lagrangian	Gaussian + simplified puff	Gaussian
Number of particles	Not applicable[a]	Not applicable	200 per time step	Not applicable	Not applicable
Processes included	Not provided	Not provided	Advection, turbulent diffusion, radioactive decay, deposition to ground	Not provided	Diffusion, depletion, ground deposition
Domain size/calculation range	16 sectors, user specified radius	≤50 miles (80 km)	<100 km	<100 km	>10 m, <100 km
Grid size	Radial distance	0.5 miles (0–10 miles) 1.25 miles (10–25 miles) 2.5 miles (25–50 miles)	No limitation	1.2 km	Not applicable
Release height	50 m	50 m	50 m	10 m	50 m
Receptor height	0 m	0 m	0 m	0 m	0 m
Stability class	E (stable), D (neutral)	E (stable), D (neutral)	E (stable), D (neutral)	E (stable)	E (stable), D (neutral)
Wind speed and direction	Wind vectors summed outside the code	Limited number of wind vectors used	As provided	From WINMOD data	Class E: 3.0 m s^{-1} Class D: 6.0 m s^{-1}
Air temperature	20°C	Not applicable	Not applicable	Not applicable	Not applicable
Dispersion parameters	Briggs	Pasquill-Gifford curves	Horizontal diffusivity, 60 m^2 s^{-1}; vertical diffusivity, 30 m^2 s^{-1}	High roughness, Karlesruhe-Jülich; moderate roughness, Mol	Pasquill-Gifford sigmas
Plume rise	Not applied	Not applied	Effective release height	Standard/Briggs	= effective release height
Depletion	Depletion factor governed by deposition velocity, downwind distance, and decay	Decay, wet deposition	Radioactive decay	Not provided	Depletion factor governed by deposition velocity and downwind distance, ground deposition (velocity)
Dry deposition velocity (m/s)	0.01 for Cs 0.008 for I	0.003 for Cs and I	Not applicable	Internally determined	0.0004 for Cs 0.0022 for I

TABLE 3.1. SUMMARY OF MODELS USED FOR THE MID-RANGE SCENARIO (cont.)

Parameter	Model name				
	ADDAM	**RASCAL 3.0.3**	**University of Seville**	**JRODOS**	**HotSpot 2.07.1**
Definition of deposition velocity	Ground level deposition velocity, uses ground level air concentration	Ground level deposition velocity, uses ground level air concentration	Not applicable	Not provided	Empirical data
Release time step	1 h	1 h	1 min	0.5 h	1 h
Calculation time step	One step, time integrated	15 min	10 s	1 h	One step, time integrated outside of the calculation
Simulation time	Not applicable	10 h	10 h	7 h (reached the end)	Not applicable
Rain intensity	No rain or fog	Not used	No rain	0.0 mm h^{-1}	Not applicable
Inversion layer height	1000 m for stable conditions; 1500 m for neutral conditions	1000 m for stable conditions; 1500 m for neutral conditions	1000 m for stable conditions; 1500 m for neutral conditions	Not provided	Not used
Terrain/topography	Flat, grass, roughness length = 0.4 m	Not used	As provided	Not applicable	Not applicable
Friction coefficient	Not applicable	Friction velocity (m/s); calculated from surface roughness, and Monin-Obukhov length	1.50×10^{-2}	Not provided	Not applicable
Rugosity	Roughness length = 0.4 m	Roughness length = 0.2 m	40 cm	Not provided	City terrain
Time to set up and run	1 day	Not provided	<5 min	Not provided	<5 min
Time to process results	1 day	Not provided	<5 min	Not provided	<5 min
Total source term	6.43×10^{11} Bq for Cs-137 3.69×10^{12} Bq for I-131	6.43×10^{11} Bq for Cs-137 3.69×10^{12} Bq for I-131	As provided	As provided	6.4×10^{11} Bq for Cs-137 3.7×10^{12} Bq for I-131
Height at which air concentration was used for calculating dry deposition	0 m (ground level)	Not provided	Not applicable	Not provided	Not applicable
Reference(s) for code (URL)	Not available to public	http://www.nrc.gov/reading-rm/doc-collections/nuregs/staff/sr1887/	None	Not provided	http://narac.llnl.gov/hotspot

[a] The model does not necessitate or does not use the specified information.

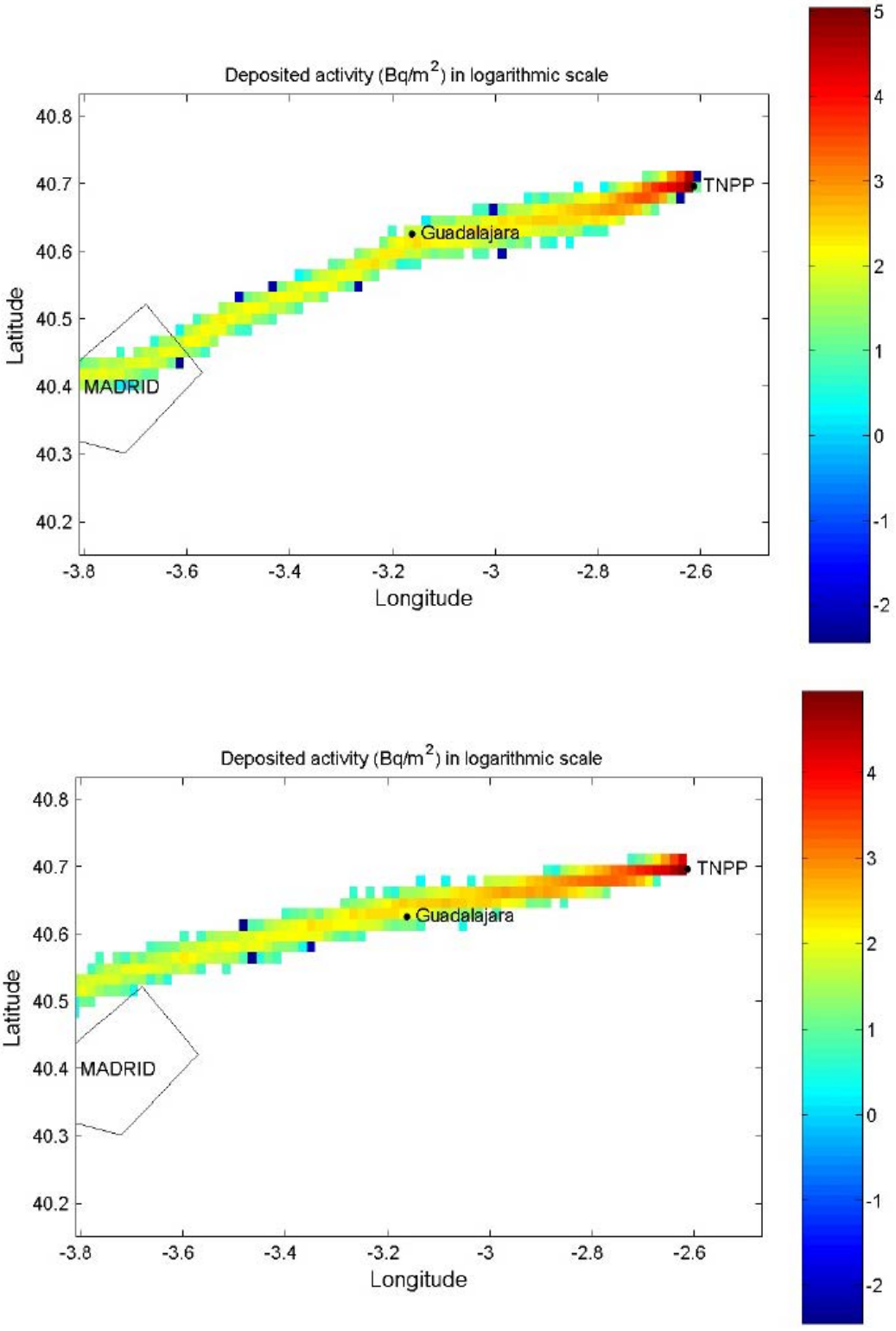

FIG. 3.1. Contour maps showing predictions using Usev, for ^{137}Cs deposition assuming stable conditions (top) and neutral stability (bottom). Reproduced courtesy of Elsevier [3.2].

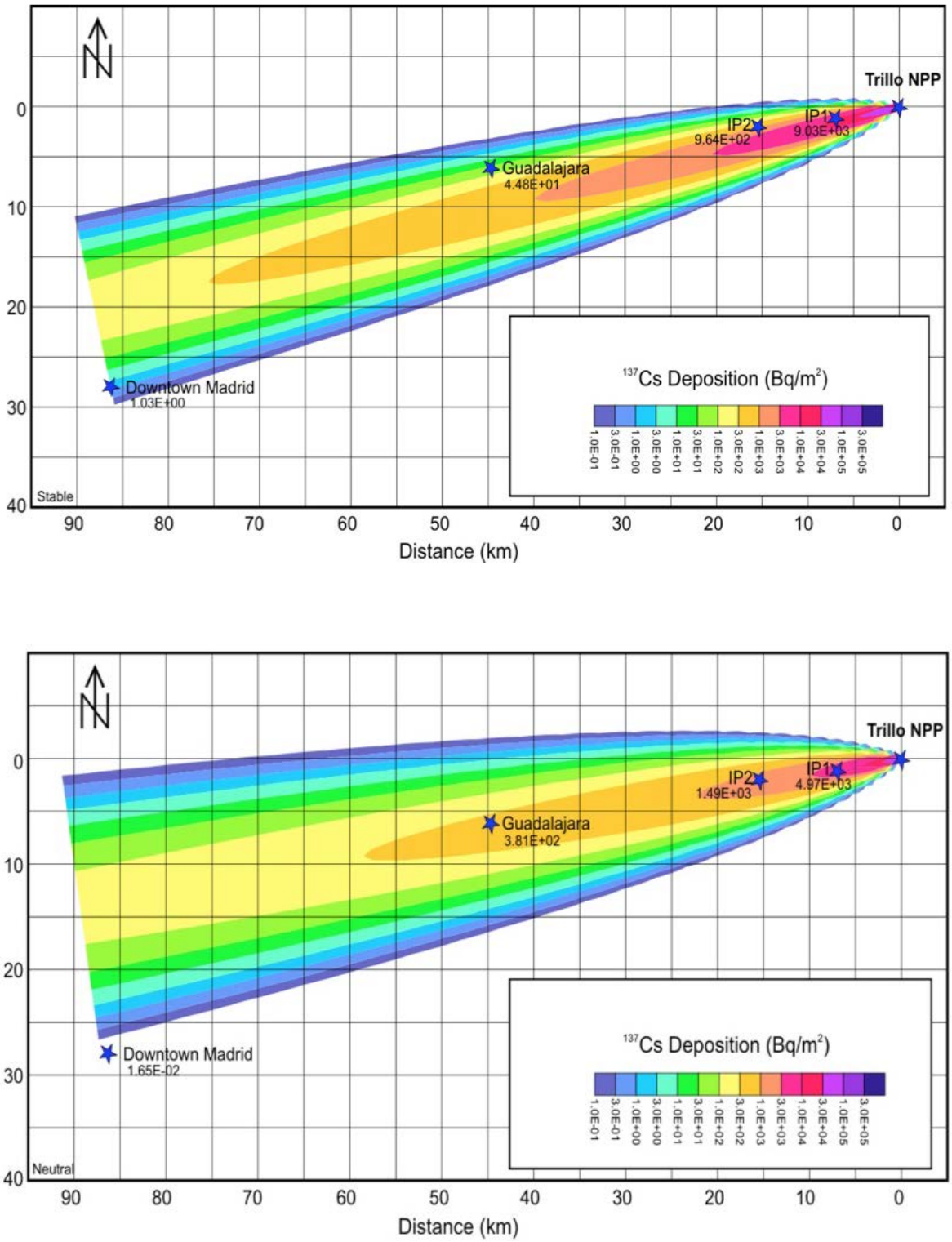

FIG. 3.2. Contour maps showing predictions using ADDAM, for ^{137}Cs deposition assuming stable conditions (top) and neutral stability (bottom). Reproduced courtesy of Elsevier [3.2].

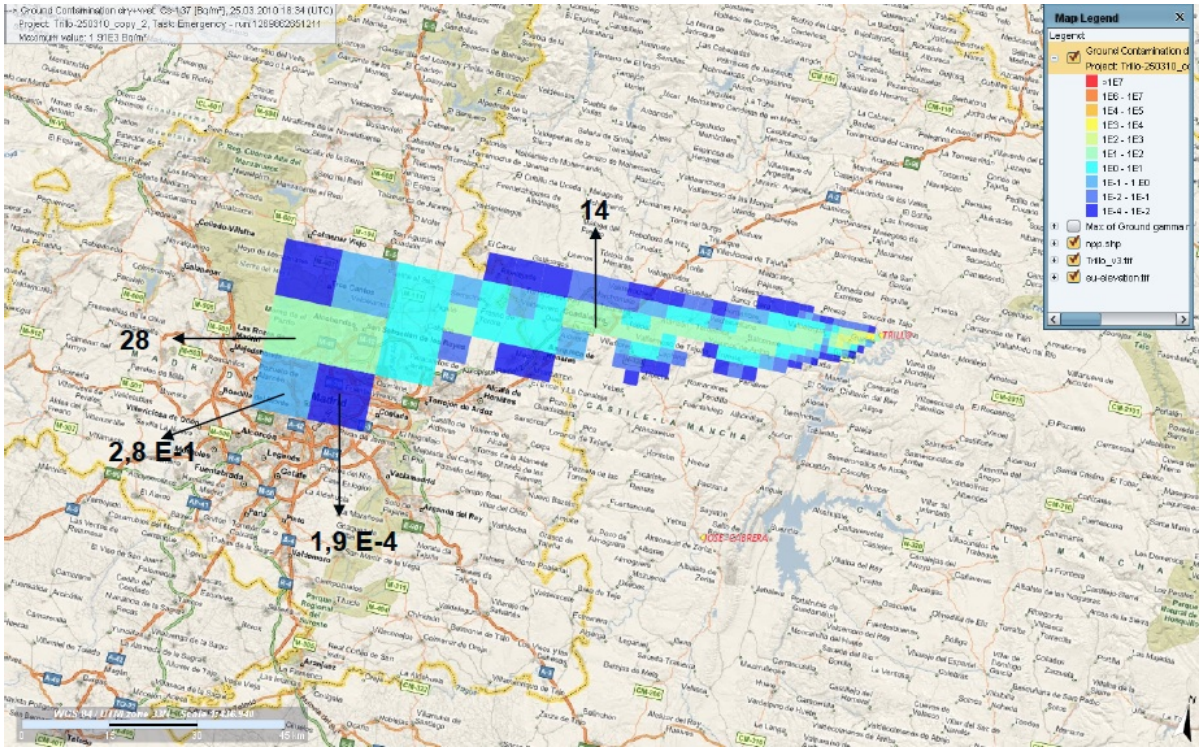

FIG. 3.3. Contour map showing predictions using JRODOS, for ^{137}Cs deposition assuming stable conditions. Reproduced courtesy of Elsevier [3.2].

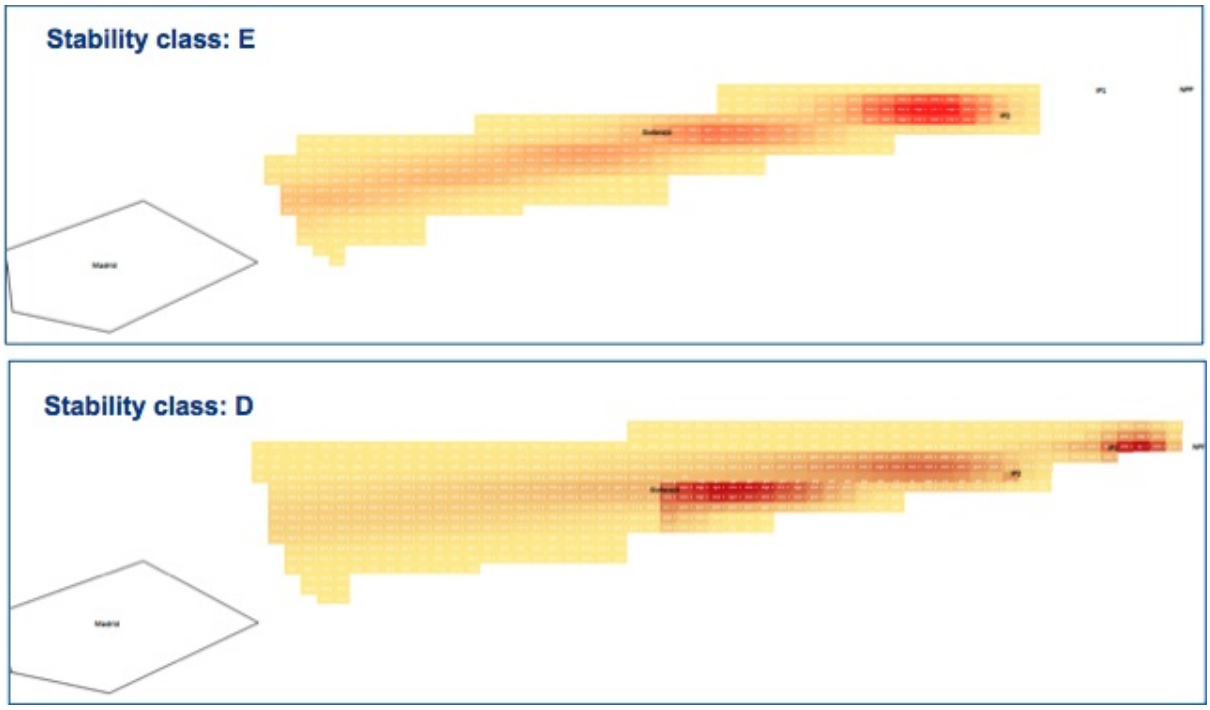

FIG. 3.4. Contour maps showing predictions using RASCAL, for ^{137}Cs deposition assuming stable conditions (top) and neutral stability (bottom). Reproduced courtesy of Elsevier [3.2].

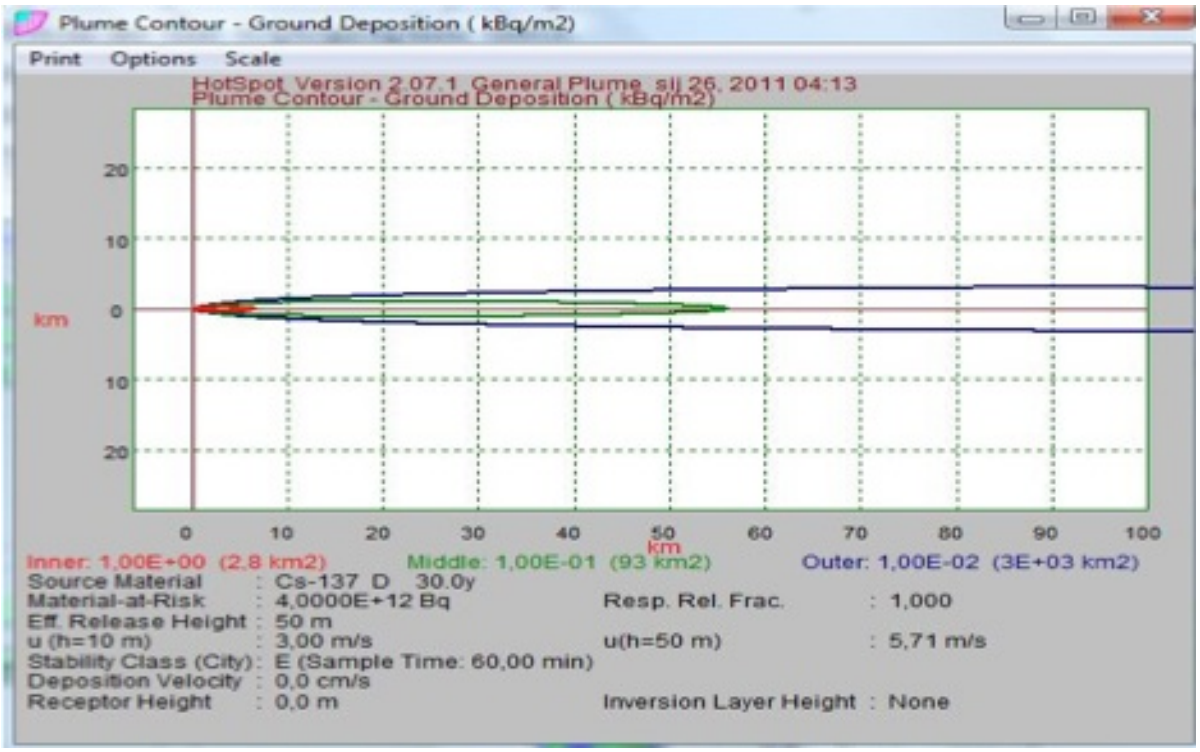

FIG. 3.5. Contour maps showing predictions using HotSpot 2.07.1, for ^{137}Cs deposition assuming stable conditions (top) and neutral stability (bottom). Reproduced courtesy of Elsevier [3.2].

3.3.2. Deposition

Predicted values for deposition of ^{137}Cs and ^{131}I at specified locations are provided in Tables 3.2 and 3.3 and are shown in Figs 3.6 and 3.7. As expected, based only on the distances, the highest deposition generally occurred at Intermediate Point 1 (IP-1), followed by IP-2, Guadalajara, and Madrid, respectively. Differences in predicted deposition between ^{137}Cs and ^{131}I are due to the different source terms, and, for some models, also to use of different deposition velocities for the two radionuclides.

Predicted values of the ^{137}Cs deposition in Madrid, under stable conditions (ADDAM, Usev, JRODOS, HotSpot 2.07.1), varied by a factor of 28. Under neutral stability, all models predicted values of 0 (Usev) or a factor of approximately 10–100 lower for Madrid than under stable conditions, consistent with predicting that the plume would bypass Madrid. Predicted values of the ^{131}I deposition in Madrid under stable conditions varied by a factor of approximately 60. As was the case for ^{137}Cs, predicted values for ^{131}I for Madrid under neutral stability were 0 or were a factor of approximately 10–100 lower than under stable conditions. The predicted deposition in Madrid is thus in agreement with the contour maps, which predicted that the plume would bypass Madrid under neutral stability.

All five models predicted deposition in Guadalajara under stable conditions within a factor of 12 for ^{137}Cs and within a factor of 24 for ^{131}I. Under neutral stability, predicted values were within a factor of 165 for ^{137}Cs and within a factor of 26 for ^{131}I, indicating more variability amongst the models under conditions of neutral stability. ADDAM and Usev predicted higher deposition in Guadalajara under neutral stability than under stable conditions, while HotSpot 2.07.1 and RASCAL predicted higher deposition in Guadalajara under stable conditions.

The plume predicted using RASCAL bypassed IP-1 (zero deposition) under stable conditions, whereas the plume predicted using Usev bypassed IP-2 under neutral stability conditions. ADDAM predicted deposition at both IP-1 and IP-2 under both stable conditions and neutral stability, with a decrease from IP-1 to IP-2 of about a factor of 9 under stable conditions and a factor of 3 under neutral stability.

3.3.3. Time integrated concentrations in air

Predicted values for time integrated ^{137}Cs and ^{131}I activity concentrations in air at the four specified locations (Guadalajara, downtown Madrid, and 2 intermediate points between Trillo NPP and Guadalajara) are provided in Tables 3.4 and 3.5 and are shown in Figs 3.8 and 3.9. As expected solely from the distances, the general tendency was for the highest radionuclide activity concentrations in air to occur at IP-1, followed by IP-2, Guadalajara, and Madrid, respectively. One exception occurred for the JRODOS predictions with slightly higher concentrations predicted for parts of Madrid than for Guadalajara. Also, the plume that was predicted using RASCAL bypassed IP-1 under stable conditions and predicted higher concentrations of ^{131}I in Guadalajara than in IP-2 under both sets of meteorological conditions. Predicted differences between ^{137}Cs and ^{131}I primarily reflected the different source terms of the two radionuclides. Five participants provided predictions for ^{131}I and four (ADDAM, Usev, JRODOS, and HotSpot 2.07.1) for ^{137}Cs.

TABLE 3.2. COMPARISON OF PREDICTIONS FOR DEPOSITION OF Cs-137 (Bq/m^2)

Model	Location			
	IP-1	IP-2	Guadalajara	Madrid
Stable conditions (Class E)				
ADDAM	9030	964	44.8	1.03
HotSpot 2.07.1	– [a]	– [a]	20	13
JRODOS	– [a]	– [a]	14	28
RASCAL	0	174	166	– [a]
USev	4348	233.5	56.86	10.14
Neutral stability (Class D)				
ADDAM	4970	1490	381	0.0165
HotSpot 2.07.1	– [a]	– [a]	2.3	1.4
RASCAL	267	69.8	122	– [a]
USev	7414	0	144.3	0

[a] Not reported.

TABLE 3.3. COMPARISON OF PREDICTIONS FOR DEPOSITION OF I-131 (Bq/m^2)

Model	Location			
	IP-1	IP-2	Guadalajara	Madrid
Stable conditions (Class E)				
ADDAM	43 800	4920	256	6.66
HotSpot 2.07.1	– [a]	– [a]	610	390
JRODOS	– [a]	– [a]	110	72
RASCAL	0	964	922	– [a]
USev	4312	149.7	38.98	11.45
Neutral stability (Class D)				
ADDAM	23 400	7120	1880	0.0837
HotSpot 2.07.1	– [a]	– [a]	71	45
RASCAL	1480	389	677	– [a]
USev	7395	0	146	0

[a] Not reported.

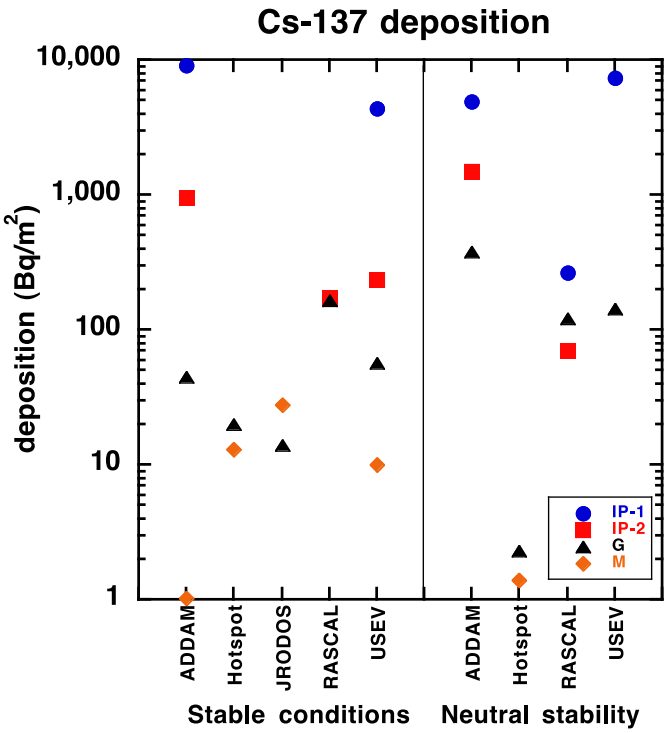

FIG. 3.6. Comparison of model predictions for deposition of ^{137}Cs at specified locations. IP-1 = Intermediate Point 1; IP-2 = Intermediate Point 2; G = Guadalajara; M = Madrid.

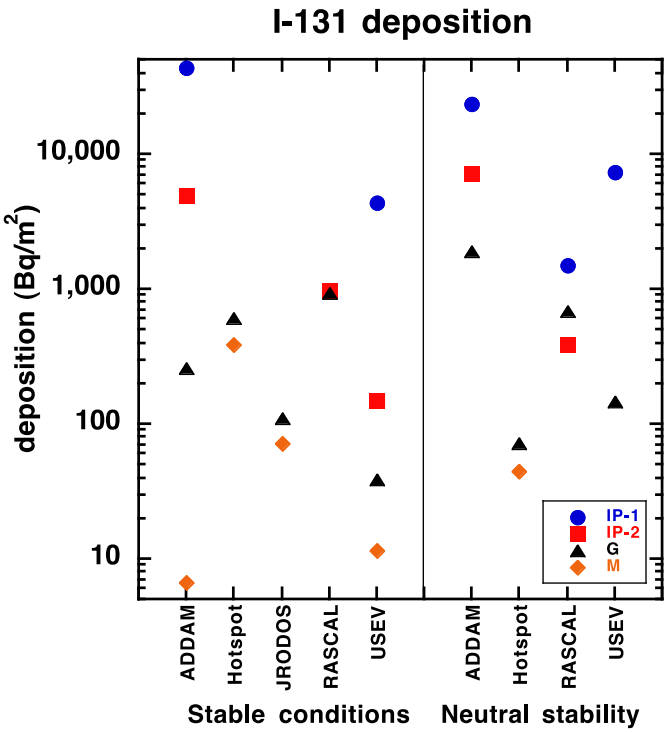

FIG. 3.7. Comparison of model predictions for deposition of ^{131}I at specified locations. IP-1 = Intermediate Point 1; IP-2 = Intermediate Point 2; G = Guadalajara; M = Madrid.

TABLE 3.4. COMPARISON OF PREDICTIONS FOR TIME INTEGRATED ACTIVITY CONCENTRATION OF Cs-137 IN AIR ($Bq \cdot min \cdot m^{-3}$)

Model	Location			
	IP-1	IP-2	Guadalajara	Madrid
Stable conditions (Class E)				
ADDAM	15 100	1610	74.7	1.72
HotSpot 2.07.1	– [a]	– [a]	817	517
JRODOS	– [a]	– [a]	417	823
USev	235	130	11.1	5.79
Neutral stability (Class D)				
ADDAM	8290	2480	635	0.0275
HotSpot 2.07.1	– [a]	– [a]	95	60
USev	394	0	12.5	0

[a] Not reported.

TABLE 3.5. COMPARISON OF PREDICTIONS FOR TIME INTEGRATED ACTIVITY CONCENTRATION OF I-131 IN AIR ($Bq \cdot min \cdot m^{-3}$)

Model	Location			
	IP-1	IP-2	Guadalajara	Madrid
Stable conditions (Class E)				
ADDAM	91 300	10 200	533	13.9
HotSpot 2.07.1	– [a]	– [a]	4500	3000
JRODOS	– [a]	– [a]	1830	2170
RASCAL	0	373 000	417 000	– [a]
USev	230	28.9	11.0	5.78
Neutral stability (Class D)				
ADDAM	48 800	14 800	3910	0.174
HotSpot 2.07.1	– [a]	– [a]	533	333
RASCAL	522 000	142 000	263 000	– [a]
USev	400	0	10.4	0

[a] Not reported.

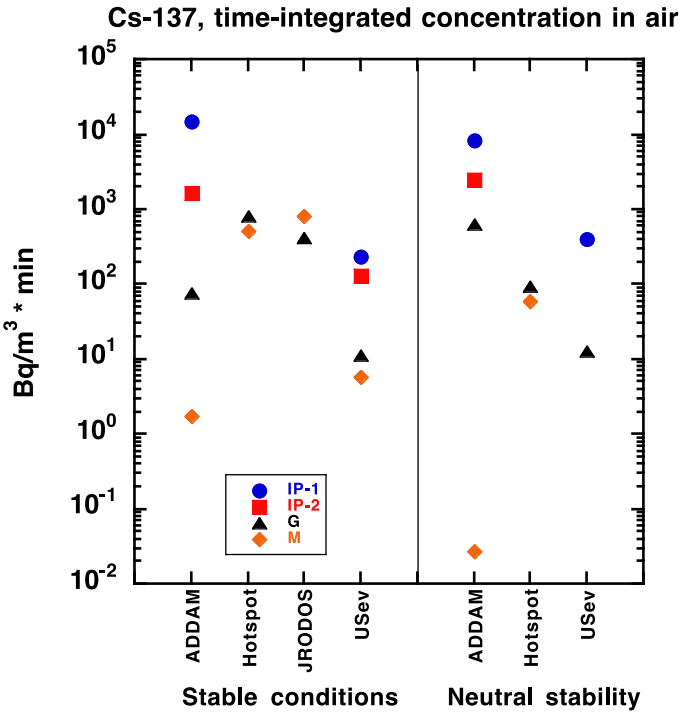

FIG. 3.8. Comparison of model predictions for time integrated concentration of ^{137}Cs in air at specified locations. IP-1 = Intermediate Point 1; IP-2 = Intermediate Point 2; G = Guadalajara; M = Madrid.

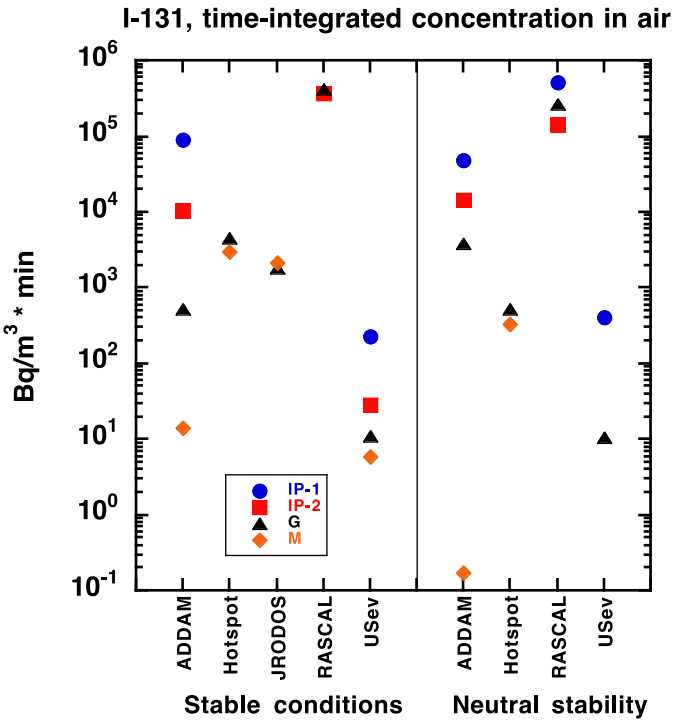

FIG. 3.9. Comparison of model predictions for time integrated concentration of ^{131}I in air at specified locations. IP-1 = Intermediate Point 1; IP-2 = Intermediate Point 2; G = Guadalajara; M = Madrid.

For Madrid, the results again showed a large decrease (by a factor of ~10 or more) between the values predicted under stable conditions relative to those predicted under neutral stability, consistent with the predicted plumes bypassing Madrid in the case of neutral stability. For Guadalajara, ADDAM predicted 7 to 9 fold higher air concentrations under neutral stability than under stable conditions, while HotSpot 2.07.1 and RASCAL predicted 8 to 9 fold and 1.5 fold higher activity concentrations, respectively, under stable compared to neutral stability conditions. Usev predicted similar concentrations under both sets of conditions. As with deposition, RASCAL predicted that the plume would bypass IP-1 under stable conditions.

3.3.4. Time to arrival of plume

Predicted values for the approximate time to arrival of the predicted plume at specific locations are provided in Table 3.6 and are shown in Fig. 3.10. For each combination of location and stability class, the predicted times to arrival varied by a factor of approximately 2 for those predicted plumes that reached the location. As described above, RASCAL predicted that the plume would bypass IP-1 under stable conditions, and USev predicted that the plume would bypass both IP-2 and Madrid under neutral stability. For each location, predicted times to arrival were shorter under neutral stability than under stable conditions. ADDAM predicted the longest times to arrival for a given location, whereas USev and RASCAL predicted the shortest times.

3.3.5. Time series of air concentrations

Predicted radionuclide activity concentrations in air as a function of time, for each location, are shown for four models (USev, ADDAM, JRODOS, and RASCAL) in Figs 3.11 to 3.14. The plots reflect the predicted times to arrival (Table 3.6), with earlier arrival of the plume under neutral stability than under stable conditions. USev and JRODOS predicted similar activity concentrations in air for ^{137}Cs and ^{131}I, whereas ADDAM predicted almost 10 fold higher activity concentrations of ^{131}I compared to ^{137}Cs. For USev and ADDAM, neutral stability was associated with slightly higher radionuclide activity concentrations than were predicted under stable conditions; for RASCAL, stable conditions resulted in slightly higher (3 fold) radionuclide activity concentrations compared to neutral stability conditions. The plots also reflect the USev predictions that the plume bypassed IP-2 and Madrid under neutral stability, and the RASCAL predictions that the plume bypassed IP-1 under stable conditions.

TABLE 3.6. COMPARISON OF PREDICTIONS FOR THE APPROXIMATE TIME TO ARRIVAL (min) OF THE PLUME

Model	Location			
	IP-1	IP-2	Guadalajara	Madrid
Stable conditions (Class E)				
ADDAM	67	150	417	850
JRODOS	– [a]	120	240	420
RASCAL	bypassed [b]	90	210	– [a]
USev	40	100	210	460
Neutral stability (Class D)				
ADDAM	33	83	233	483
RASCAL	15	60	150	– [a]
USev	20	bypassed [b]	130	bypassed [b]

[a] Not reported.

[b] Predicted plume did not pass over the location.

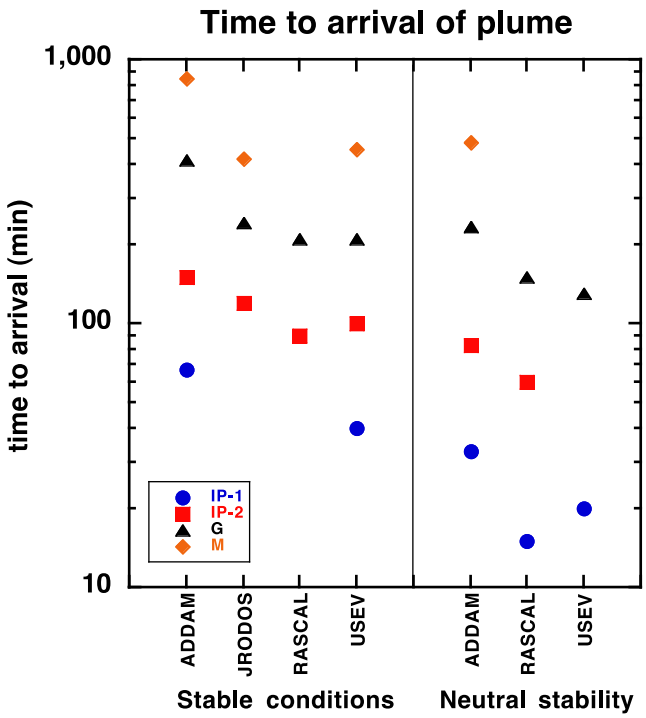

FIG. 3.10. Comparison of model predictions for the time to arrival of the plume at specified locations. Times are approximate. IP-1 = Intermediate Point 1; IP-2 = Intermediate Point 2; G = Guadalajara; M = Madrid.

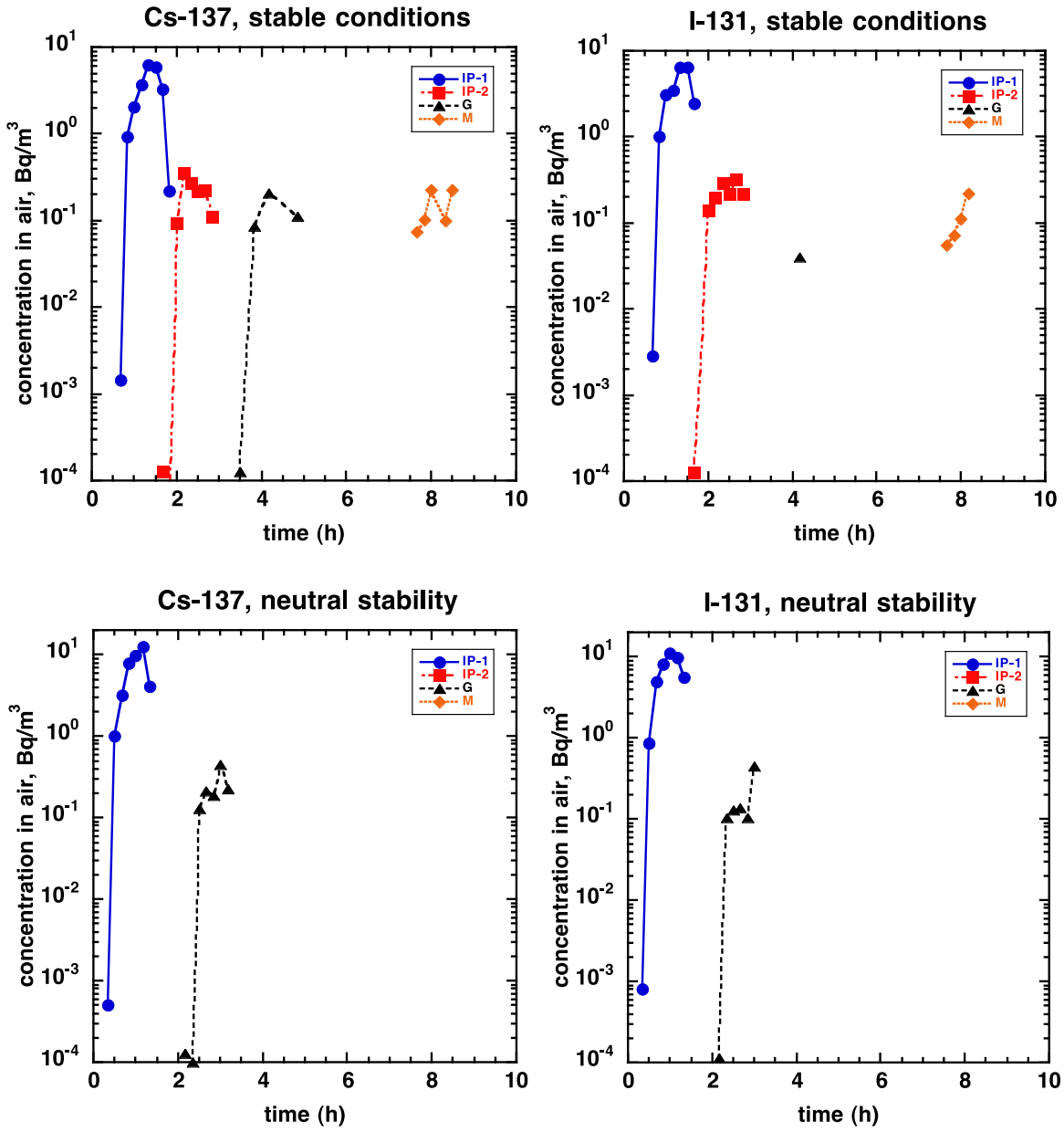

FIG. 3.11. Time series of radionuclide concentrations in air predicted by USev, assuming stable conditions (top) and neutral stability (bottom).

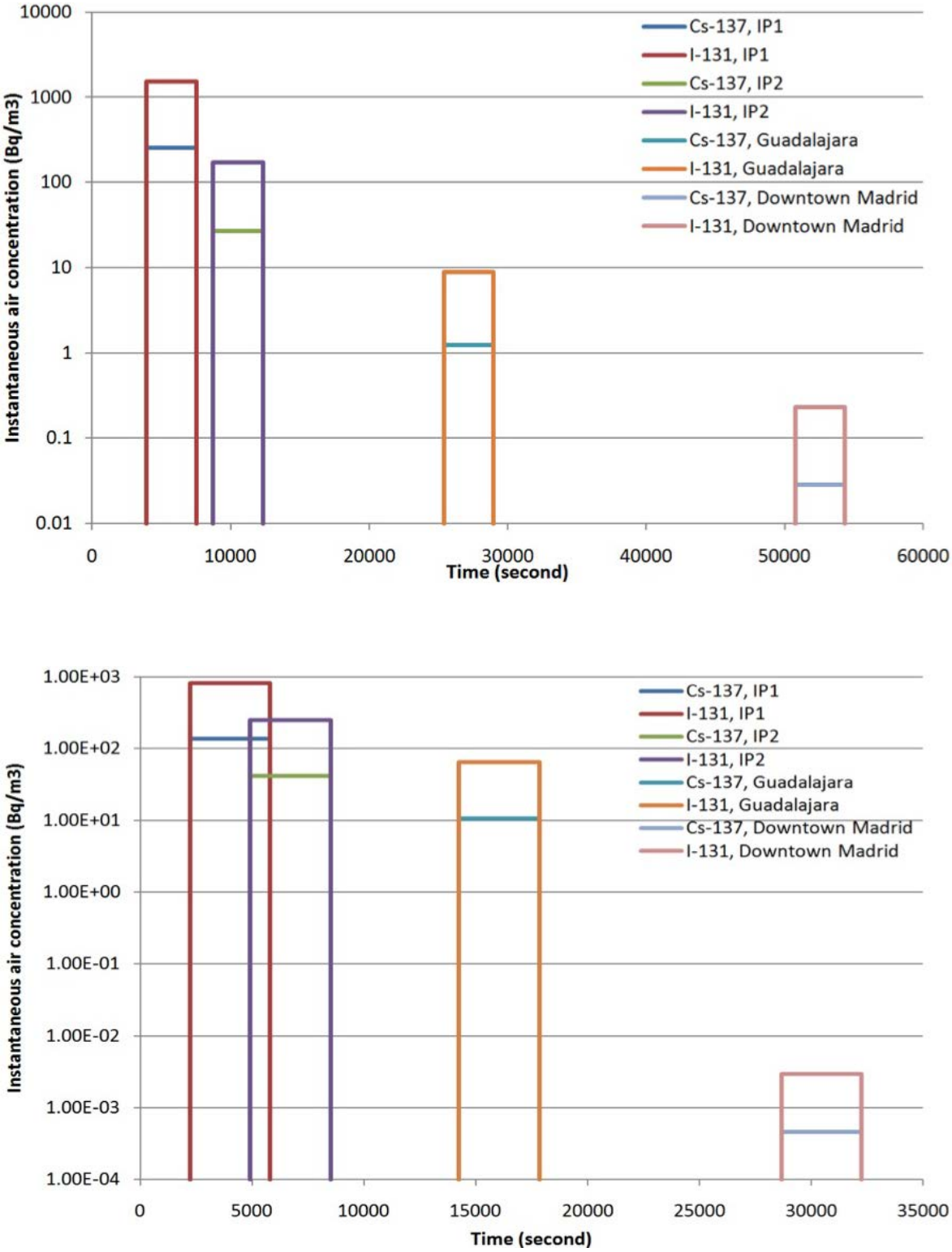

FIG. 3.12. Time series of radionuclide concentrations in air predicted by ADDAM, assuming stable conditions (top) and neutral stability (bottom).

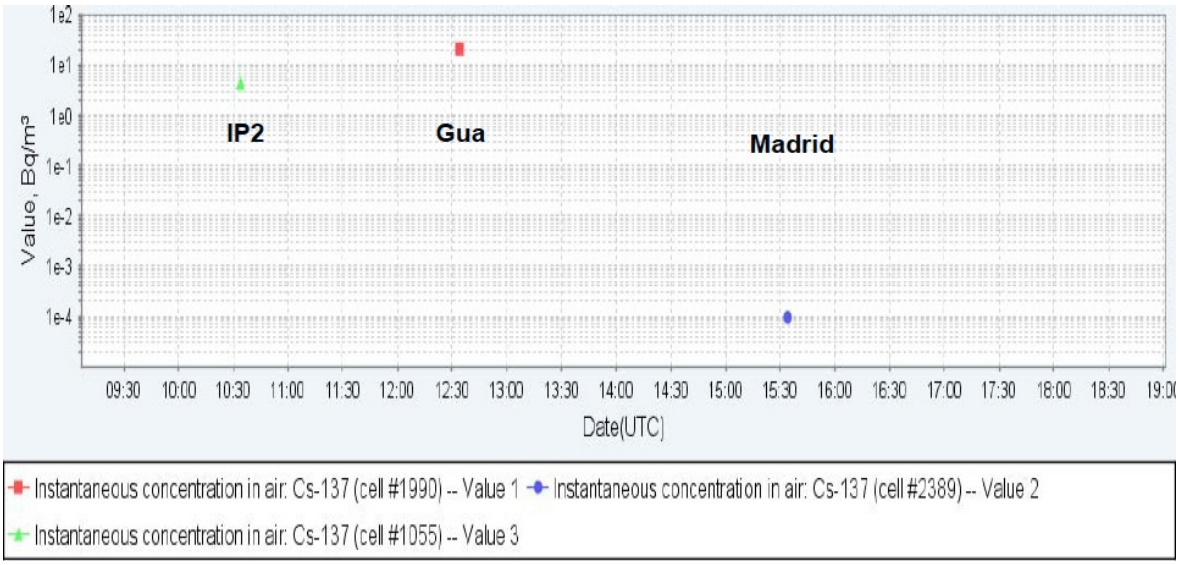

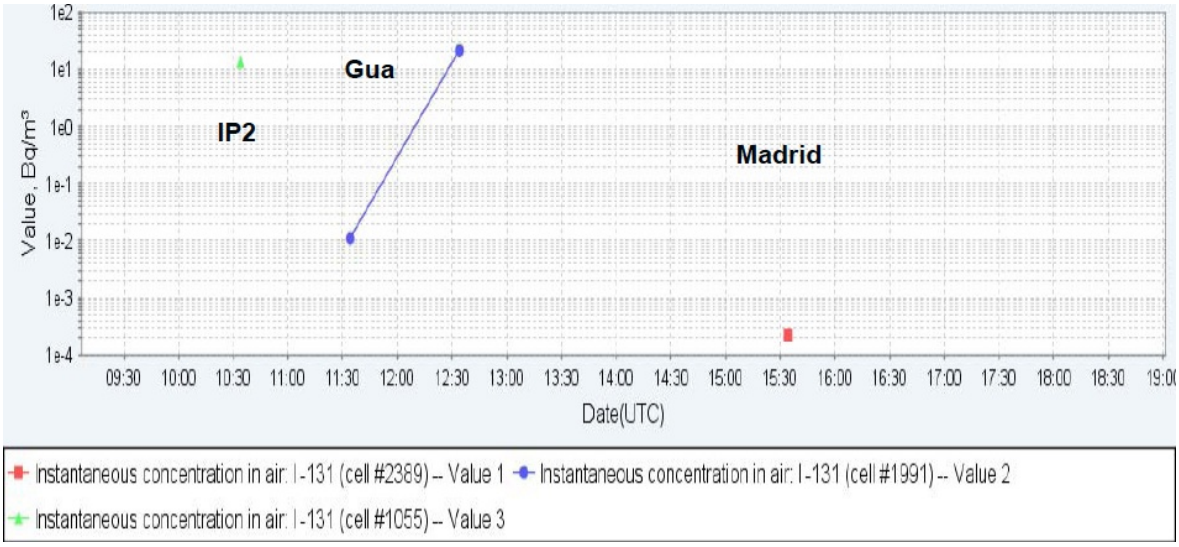

FIG. 3.13. Time series of radionuclide concentrations in air predicted by JRODOS, assuming stable conditions. The upper plot shows ^{137}Cs and the lower plot shows ^{131}I.

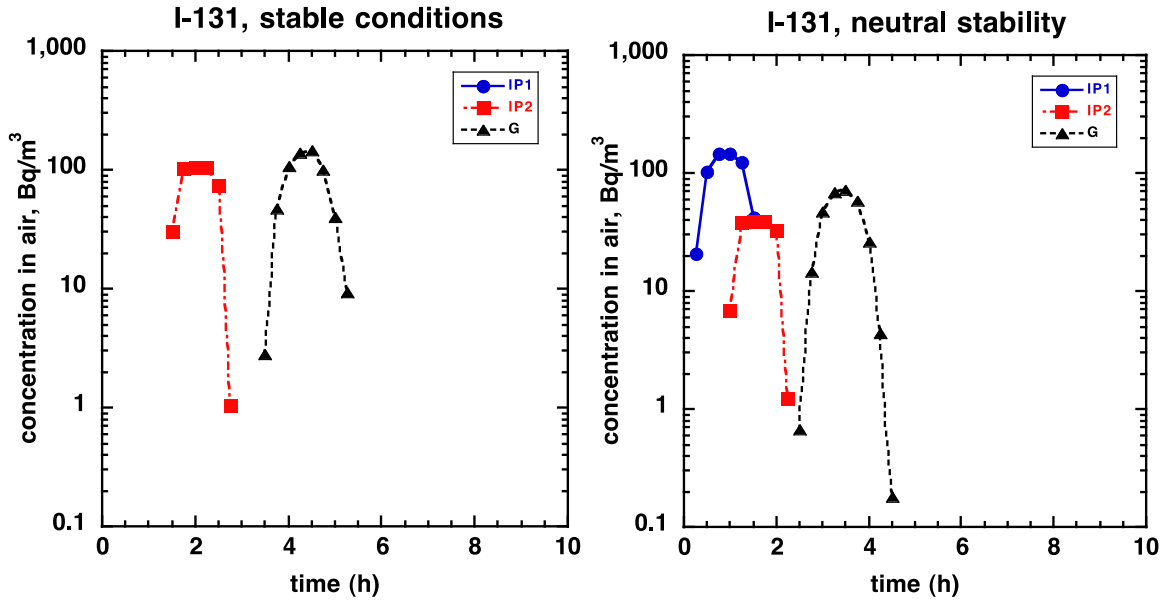

FIG. 3.14. Time series of ^{131}I concentrations in air predicted by RASCAL, assuming stable conditions (left) and neutral stability (right).

3.4. CONCLUSIONS FROM THE MID-RANGE ATMOSPHERIC DISPERSION EXERCISE

Participants in this test exercise were given the same input information, but there were some obvious differences in the model predictions [3.2]. As described above, participants varied in how they used the source term information (time dependent release or release all at once) and wind field data. Participants also differed in their choices of parameter values, for example deposition velocity.

Comparison of two sets of meteorological conditions within the exercise scenario demonstrated important differences in the behavior of the plume under neutral stability versus under stable conditions. The most important difference for this exercise was that the predicted plumes bypassed Madrid (the largest city in the test region) under conditions of neutral stability but intersected it under stable conditions. Predicted plumes reached the intermediate points for some participants and bypassed them for others. Even for a single stability class, the predicted path of a plume varied amongst participants.

Predicted deposition and activity concentrations in air varied more widely amongst models than did other endpoints. To some extent, this variability reflects the uncertainties present in atmospheric dispersion modelling generally and in selection of parameter values for this kind of exercise. For example, in three models the user had to select values for the deposition velocity (ADDAM, RASCAL, and HotSpot 2.07.1); the selected values ranged from 0.0004 to 0.003 m/s for ^{137}Cs and from 0.0022 to 0.008 m/s for ^{131}I (Table 3.1). Although uncertainties in individual model predictions were not reported, the results are indicative of the level of uncertainty that needs to be acknowledged in dealing with modelling results for assessment purposes.

The predicted times to arrival of the plume at specific locations were consistent amongst participants, usually varying by less than a factor of 2 amongst three (neutral stability) or four (stable conditions) sets of model predictions (Table 3.6). This can be an important endpoint in practice, in that it corresponds to the estimated time available to evacuate an area or get people to shelter. As also shown by these results, this endpoint depends on the meteorological conditions, with shorter times to arrival predicted for neutral stability and higher wind speeds.

3.5. REFERENCES TO SECTION 3

[3.1] THIESSEN, K.M., ANDERSSON, K.G., BERKOVSKYY, V., CHARNOCK, T.W., CHOUHAN, S.L., De WITH, G., ĎÚRAN, J., FUKA, V., HELEBRANT, J., HŮLKA, J., HWANG, W.T., KUČA, P., MANCINI, F., NAVARRO, E., PERIÁÑEZ, R., PROUZA, Z., SDOUZ, G., TOMÁS, J., TRIFUNOVIĆ, D., URSO, L., WALTER H., Assessing emergency situations and their aftermath in urban areas: The EMRAS II Urban Areas Working Group, Radioprotection **46** (2011) S601.

[3.2] PERIÁÑEZ, R., THIESSEN, K.M., CHOUHAN, S.L., MANCINI, F., NAVARRO, E., SDOUZ, G., TRIFUNOVIĆ, D., Mid-range atmospheric dispersion modelling. Intercomparison of simple models in EMRAS-2 project, Journal of Environmental Radioactivity **162-163** (2016) 225.

4. CONTAMINANT TRANSPORT AND COUNTERMEASURES EXERCISE

4.1. OVERVIEW

The contaminant transport and countermeasures exercise provided an opportunity to compare model predictions for contaminant transport and countermeasures[13] following a release of radioactivity [4.1, 4.2]. The scenario was based on a hypothetical deposition of radioactivity from airborne radioactivity with a defined concentration in air (1 $MBq \cdot d \cdot m^{-3}$ at ground level of ^{60}Co and ^{239}Pu, considered separately). It made use of detailed geographical information for an actual urban area in Seoul, Republic of Korea (see Appendix V, Figs V.2 to V.4)

Input information for the scenario included information about the radionuclides, the conditions of the initial deposition, meteorological information, locations for modelling endpoints, and descriptions of the countermeasures (protective actions, including remedial actions) to be modelled. Modelling endpoints for intercomparison between models included the deposition at specified outdoor locations, external dose rates at specified locations and times, contributions of radioactivity on relevant surfaces to external dose rate, external and internal doses for specified exposure scenarios, and effectiveness of countermeasures in terms of reduction in external and internal doses. A full description of the scenario is provided in Appendix V.

The impact of different seasons (summer or winter) and weather conditions (dry conditions, light rain, which is assumed to be 3 mm per day, or heavy rain, assumed to be 20 mm per day) at the time of the initial deposition was considered, and average weather conditions for the region were used for the longer term estimation of contaminant transport. Two areas of the city were selected for the modelling exercise (Appendix V, Figs V.2 to V.4):

(1) A business area (Region 1); and
(2) A park area near an apartment town (Region 2).

Several locations within each region (both indoor and outdoor for Region 1, outdoor for Region 2) were selected as test locations for which model calculations were to be made. The test locations are summarized in Table 4.1. Appendix V provides more detailed descriptions of the regions and test locations, along with corresponding climatological information and information on the population, building structures, and land use.

For each test location, participants were requested to calculate the external dose rates without any countermeasure (i.e. 'no countermeasure') and to predict the most important surfaces contributing to the external dose rate and the percentage contribution from each of them. In addition, participants were asked to predict annual and cumulative doses (up to five years) for each of the exposure scenarios. For ^{60}Co, predictions of external dose rates and doses were requested, and predictions of internal doses were optional; for ^{239}Pu, predictions of internal doses were requested, and predictions of external dose rates and doses were optional.

[13] A countermeasure is defined as "an action aimed at alleviating the radiological consequences of an accident." Countermeasures are forms of intervention and may be protective actions or remedial actions [4.3].

TABLE 4.1. TEST LOCATIONS FOR WHICH MODEL PREDICTIONS WERE MADE

Location		Region 1	Region 2
		Business Area	Park area near an apartment town
Indoors	1	Building 1: Ground floor	
	2	Building 1: 10th floor	
	3	Building 1: 24th floor (top floor)	
Outdoors	4	Outside Building 1 (pavement)	
	5		Centre of a park
	6		Parking lot at edge of park (pavement)

The participants were also asked to calculate external doses rates following implementation of several countermeasures, as well as the annual cumulative doses (up to five years) for each exposure scenario. The countermeasures and times of their implementation that were to be used in the modelling exercise are listed in Appendix V (Table V.5). The countermeasures were: temporary relocation of the population, removal of trees or leaves (depending on the time of year), cleaning roads (e.g. vacuuming, sweeping, washing, hosing), washing of roofs and exterior walls, and cutting of grass and removal of soil (5 cm depth) in the park area. Two combinations were also included:

(1) A combination of tree or leaf removal plus vacuuming or sweeping of roads; and
(2) A combination of temporary relocation of the population plus cleaning roads.

4.2. MODELS USED IN THE EXERCISE

Five EMRAS II WG9 participants contributed model predictions for the exercise. Four sets of model predictions were presented and discussed during the course of the EMRAS II programme (CPHR, ERMIN, METRO-K, RESRAD-RDD), and one additional set of predictions (CHERURB) was submitted later. Selected information about the models and their use in this exercise is summarized in Table 4.2; additional documentation is provided in Appendix VI. Three participants (METRO-K, CPHR and CHERURB) started with the activity concentration in air, as provided in the scenario description; two participants (ERMIN and RESRAD-RDD) used the deposition calculated by METRO-K as a start point. Two participants (METRO-K and ERMIN) provided predictions for both winter and summer starting conditions, whereas the other three participants (CHERURB, CPHR, RESRAD-RDD) provided predictions only for summer starting conditions. For internal doses from ^{239}Pu, two participants (CPHR and CHERURB) considered only inhalation of the initial plume (no contribution from resuspension), and three (METRO-K, ERMIN, and RESRAD-RDD) considered only resuspension (no contribution from the initial plume). Four participants (METRO-K, ERMIN, RESRAD-RDD and CPHR) provided information on which surfaces contributed most to predicted external dose rates from ^{60}Co and ^{239}Pu at a given location.

TABLE 4.2. SUMMARY OF MODELS USED FOR THE COUNTERMEASURES SCENARIO

Parameter	**Description**				
Model name:	**METRO-K**	**ERMIN**	**CPHR**	**CHERURB**	**RESRAD-RDD**
Participant and country	W.T. Hwang Republic of Korea	T. Charnock United Kingdom	J. Tomás Cuba	S.L. Chouhan Canada	C. Yu, S. Kamboj USA
Deposition	Dry deposition velocity by surface, (not radionuclide specific)	Started with deposition on a lawn (obtained from METRO-K); other surfaces relative to the lawn, wet or dry	Dry deposition velocity; radionuclide specific values	Dry deposition velocity by surface (due to limited data, Co-60 and Pu-239 values were assumed to be same as Ru-103)	Started with deposition on a lawn (obtained from METRO-K under three weather conditions); used initial partitioning relative to lawn to calculate initial concentration for different surfaces under dry or wet conditions
Wet deposition	From daily rainfall and washout ratio, with washoff and retention on surfaces in heavy rain	See above for deposition	Washout coefficient; lower deposition with rain due to washoff to drains	Washout ratio, with retained fraction (heavy rain > light rain), (due to limited data, Co-60 and Pu-239 values were assumed to be same as Ru-103)	Assumed under light rain and heavy rain weather conditions
Rainfall duration	At time of deposition; average weather conditions after that	At time of deposition; average weather conditions after that	First 2 weeks of the period	1 day only	At time of deposition
Weathering	Short term and long term removal rates (by surface)	Surface specific empirical weathering functions (short and long component for some surfaces), movement down soil column	Half-lives depending on surface	Short term and long term removal rates (all surfaces)	Short term and long term weathering half-lives, mobile and fixed fractions
Indoor contamination	Not included	Included, but only from initial penetration of airborne radionuclides into building	Indoor air but not surfaces; filtration factor	Calculated from outdoor air concentration, ventilation rate, filtering fraction, volume of the room, deposition within the room	Included; indoor floors and walls considered separately; partitioning factors to account for direct and indirect penetration
Indoor retention	Indoor contamination not included	Generic indoor surfaces, simple empirical retention function	Indoor surfaces not included	Weathering half-life of 2.5 months	Floors and walls; indoor weathering with specific half-lives; resuspension indoors

TABLE 4.2. SUMMARY OF MODELS USED FOR THE COUNTERMEASURES SCENARIO (cont.)

Parameter	**Description**				
Model name:	**METRO-K**	**ERMIN**	**CPHR**	**CHERURB**	**RESRAD-RDD**
Trees	Only deciduous for street trees, mixed (equal percentages of deciduous and coniferous) for park trees; date for leaf fall not specified	Two types (deciduous, coniferous); specified date for deciduous leaf fall, all at once; coniferous pine needle fall was continuous	Deciduous, no contamination after first leaf fall	One type (deciduous), with leaf fall; same model was used for winter and summer time contamination	Does not include trees
Seasonality	Only 5% of deposition on deciduous trees in winter compared to summer; same deposition on coniferous trees regardless of season; snow similar to rain	Presence or absence of leaves on trees (only difference)	Results only for summer	Results only for summer	Results only for summer
Surface roughness	Considered for realistic dose estimates (correction factor for external dose)	Not considered	Not considered	Included	Ground roughness correction factor = 1
Deposition to glass surfaces	Not distinguished from walls	Not distinguished from walls	Not distinguished from walls	Not distinguished from walls	Not distinguished from walls
Resuspension factor	Time dependent	Time dependent	Not used	Not used	Time dependent outdoors, fixed indoors; adjusted for conditions (weather, traffic)
Decontamination factors	IAEA-TECDOC-1678 [4.4]	European handbook [4.5]	IAEA-TECDOC-1678 [4.4]	From CHERURB documentation, which contains some fresh and some old decontamination PDFs; lower bounds from fresh and upper bounds from old values were used	Gallay [4.6]
Dose rate reduction factors	IAEA-TECDOC-1678 [4.4]	Not used	Not used	From CHERURB documentation [4.7]	Calculated from decontamination factors [4.8]
Internal dose (inhalation)	Resuspension only	Resuspension only	Plume only	Plume only	Resuspension only
Internal dose coefficients	ICRP (CD-ROM) [4.9]	ICRP (CD-ROM) [4.9]	IAEA GSR Part 3 [4.10]	CSA N288.1 [4.11]	ICRP 72 [4.12]

TABLE 4.2. SUMMARY OF MODELS USED FOR THE COUNTERMEASURES SCENARIO (cont.)

Parameter	**Description**				
Model name:	**METRO-K**	**ERMIN**	**CPHR**	**CHERURB**	**RESRAD-RDD**
Assumptions regarding inhalation classes	M type	ICRP recommended default absorption type assumed for each radionuclide [4.12]	Highest coefficient	CSA N288.1 [4.11]	Co-60, S type; Pu-239, F type (most restrictive dose conversion factors from ICRP 72 [4.12])
External dose coefficients	Modified Kerma from Refs [4.13, 4.14], geometry considerations	Dose library, taken from Refs [4.13, 4.15–4.16]	Federal Guidance Report No. 12 [4.16]	Kerma from Ref. [4.13], geometry considerations	Calculated using RESRAD-BUILD code and external dose coefficients from Federal Guidance Report No. 12 [4.16]
mGy to mSv	Outdoor: 0.8 mSv/mGy Indoor: 0.7 mSv/mGy	Conversion factor calculated from ICRP 74 [4.17] (radionuclide specific, not surface specific)	1 mSv/mGy	0.77 mSv/mGy for external dose for Co-60; Zero external dose from Pu-239	1 mSv/mGy for external dose

4.3. MODELLING RESULTS

The following Sections 4.3.1 to 4.3.6 describe the model predictions for each modelling endpoint, which were contamination densities, external dose rates, the surfaces contributing most to external dose rates, annual and cumulative external and internal doses, and the effectiveness of countermeasures. Table 4.3 summarizes the endpoints modelled by each participant. In general, comparisons have been made (as applicable) amongst locations, radionuclides, and initial conditions for each model. Comparisons have also been made (as applicable) between models, comparing results between radionuclides and initial conditions for each location. As described in Section 4.1 and as shown in Figs V.2 to V.4 (Appendix V), Locations 1 to 3 are indoors in Region 1 (a business area), Location 4 is outdoors in Region 1, and Locations 5 and 6 are outdoors in Region 2 (a park area). Locations 4 and 6 are both on pavements (see Table 4.1 for summary).

Appendix VII provides tables of model predictions for the 'no countermeasures' scenario (i.e. with no protective actions, including remedial actions implemented). Tables VII.1 to VII.5 provide the predicted contamination densities over time at outdoor locations for each participating model. Tables VII.6 to VII.10 provide the predicted external dose rates over time at both indoor and outdoor locations for each participating model. Tables VII.11 to VII.14 provide the percentage contributions to predicted external dose rate from the most important surfaces for each of the four models (METRO-K, ERMIN, CPHR, RESRAD-RDD) for which these predictions were produced. Tables VII.15 to VII.19 provide the predicted external doses (annual doses and cumulative doses) for Regions 1 and 2, corresponding to specified exposure scenarios, as described in Appendix V. Tables VII.20 to VII.24 provide the predicted internal doses (annual doses and cumulative doses) for Regions 1 and 2, corresponding to the same specified exposure scenarios. An annual dose is defined as the dose received during the year preceding the indicated 'time since event'. A cumulative dose is defined as the dose received from the time of the event to the indicated 'time since event'.

4.3.1. Contamination densities

Figures 4.1 to 4.8 show the model predictions for contamination density at the outdoor locations (Locations 4 (Region 1) and 5 and 6 (Region 2), as shown in Appendix V, Figs V.3 and V.4) for ^{60}Co for deposition in the summer. The tabulated results for ^{60}Co and ^{239}Pu, including the predicted contamination density for deposition in the winter, are given in Appendix VII (Tables VII.1 to V11.5). Figures 4.1 to 4.5 provide comparisons of the predictions made at all outdoor locations for each model separately. Figures 4.6 to 4.8 provide intercomparisons of all model predictions for ^{60}Co for each outdoor location and set of initial conditions (dry, light rain and heavy rain). Only two sets of model predictions (METRO-K and ERMIN) were submitted for deposition during the winter; there was no difference between predicted deposition during the summer and during the winter for either of these models, and therefore, the results are not shown (see Appendix VII, Tables VII.1 and VII.2 for tabulated results). For CPHR, predictions were submitted only for dry conditions and light rain. For CHERURB, predictions were submitted only for Locations 4 and 6 and the predicted contamination density was the same.

TABLE 4.3. SUMMARY OF ENDPOINTS MODELLED BY EACH PARTICIPANT

Modelling endpoint	Model				
	METRO-K	ERMIN	CPHR	RESRAD-RDD	CHERURB
Contamination density (outdoor locations only) Figs 4.1–4.5 (by model) Figs 4.6–4.8 (by location)	Summer and winter[a] Co-60 and Pu-239 dry, light rain, heavy rain Locations 4–6	Summer and winter[a] Co-60 and Pu-239 dry, light rain, heavy rain Locations 4–6	Summer Co-60 and Pu-239 dry, light rain Locations 4–6	Summer Co-60 and Pu-239 dry, light rain, heavy rain Locations 4–6	Summer Co-60 and Pu-239 dry, light rain, heavy rain Locations 4 and 6
External dose rates, Co-60 (indoor and outdoor locations) Figs 4.9–4.13 (by model) Figs 4.14–4.19 (by location)	Summer and winter dry, light rain, heavy rain Locations 1–6	Summer and winter dry, light rain, heavy rain Locations 1–6	Summer dry, light rain Locations 1–6	Summer dry, light rain, heavy rain Locations 1–6	Summer dry, light rain, heavy rain Locations 2, 4, 5
External dose rates, Pu-239 (indoor and outdoor locations) Appendix VII, Tables VII.6 to VII.10	Not done	Summer and winter dry, light rain, heavy rain Locations 1–6	Summer dry, light rain Locations 1–6	Summer dry, light rain, heavy rain Locations 1–6	Not done
Surfaces contributing to external dose rate (% contributions) (indoor and outdoor locations) Figs 4.20–4.21 (by location) Figs 4.22–4.26 (by model)	Summer and winter Co-60 dry, light rain, heavy rain Locations 1–6	Summer and winter Co-60 and Pu-239 dry, light rain, heavy rain Locations 1–6	Summer Co-60 and Pu-239 dry, light rain Locations 1–6	Summer Co-60 and Pu-239 dry, light rain, heavy rain Locations 1–6	Not done
External doses, Co-60 First year and first 5 years Fig. 4.27 (by region)	Summer and winter[a] dry, light rain, heavy rain Regions 1 and 2	Summer and winter[a] dry, light rain, heavy rain Regions 1 and 2	Summer dry Regions 1 and 2	Summer dry, light rain, heavy rain Regions 1 and 2	Summer dry, light rain, heavy rain Regions 1 and 2
Internal doses, Co-60 First year and first 5 years Fig. 4.28 (by region)	Summer and winter[a] dry, light rain, heavy rain Regions 1 and 2	Summer and winter[a] dry, light rain, heavy rain Regions 1 and 2	Summer dry Regions 1 and 2	Summer dry, light rain, heavy rain Regions 1 and 2	Summer dry, light rain, heavy rain Regions 1 and 2
Internal doses, Pu-239 First year and first 5 years Fig. 4.29 (by region)	Summer and winter[a] dry, light rain, heavy rain Regions 1 and 2	Summer and winter[a] dry, light rain, heavy rain Regions 1 and 2	Summer dry Regions 1 and 2	Summer dry, light rain, heavy rain Regions 1 and 2	Summer dry, light rain, heavy rain Regions 1 and 2
External doses, Pu-239 First year and first 5 years Appendix VII, Tables VII.15 to VII.19 (by region)	Not done	Summer and winter[a] dry, light rain, heavy rain Regions 1 and 2	Summer dry Regions 1 and 2	Summer dry, light rain, heavy rain Regions 1 and 2	Not done
Countermeasure effectiveness Co-60, external dose First year and first 5 years Tables 4.3–4.5	Summer and winter[a] dry, light rain, heavy rain Regions 1 and 2	Summer and winter[a] dry, light rain, heavy rain Regions 1 and 2	Summer dry Regions 1 and 2	Summer dry, light rain, heavy rain Regions 1 and 2	Summer dry, light rain, heavy rain Regions 1 and 2
Countermeasure effectiveness, Pu-239, internal dose First year and first 5 years Tables 4.6–4.8	Summer and winter[a] dry, light rain, heavy rain Regions 1 and 2	Summer and winter[a] dry, light rain, heavy rain Regions 1 and 2	Summer dry Regions 1 and 2	Summer dry, light rain, heavy rain Regions 1 and 2	Summer dry, light rain, heavy rain Regions 1 and 2

[a] Winter predictions are not shown for indicated endpoints.

Most models produced the same or similar predictions for Locations 4 and 6; however, the predictions differed for Location 5. Location 5 is on a dirt pathway in a park area, while Locations 4 and 6 are both on pavements (see Appendix V, Figs V.3 and V.4). ERMIN (Fig. 4.2) used different characterizations or descriptions for Locations 4 and 6 (a street near buildings for Location 4 and a car park for Location 6), resulting in differences between results for the two locations. In contrast, METRO-K (Fig. 4.1), RESRAD-RDD (Fig. 4.4), and CHERURB (Fig. 4.5) each used the same characterization for both paved locations, therefore giving the same results for both Locations4 and 6. CPHR (Fig. 4.3) produced similar results for all three locations under dry conditions and for Locations 4 and 6 under conditions of light rain. The predicted rate of decrease in contamination densities predicted using METRO-K, ERMIN, and RESRAD-RDD was smaller for Location 5 than for Locations 4 and 6, likely reflecting higher loss rates from the paved surfaces (or greater retention in the unpaved area).

METRO-K (Fig. 4.1), ERMIN (Fig. 4.2), and RESRAD-RDD (Fig. 4.4) all produced higher contamination density predictions for Location 5 than for Locations 4 and 6. The initial contamination densities between Location 5, and Locations 4 and 6, under dry conditions, differed by approximately a factor of 8 for METRO-K, and by approximately 3 fold for ERMIN and RESRAD-RDD. This difference decreased under wet conditions, with similar initial depositions at all three locations for a given model. CPHR (Fig. 4.3) showed a very steep loss of the initial contamination density at Location 5 (on dirt), compared to Locations 4 and 6 (on pavement), under light rain conditions, indicating different assumptions about initial loss rates on the two surfaces.

The predicted initial deposition did not depend on the specific radionuclide considered; for all models except for CPHR, the predicted initial contamination densities for ^{60}Co and ^{239}Pu did not differ; differences were less than a factor of 2 for CPHR. However, changes in contamination density over time did depend on the radionuclide being considered, with ^{60}Co generally showing a slightly faster loss rate (steeper slope) than ^{239}Pu, consistent with the shorter half-life of ^{60}Co and the higher mobility in the environment of ^{60}Co compared to ^{239}Pu. Predicted loss rates were similar for METRO-K, ERMIN, and RESRAD-RDD (Figs 4.6 to 4.8), especially for wet initial conditions. CHERURB showed the slowest loss rate for paved surfaces (Locations 4 and 6), indicating a different removal rate was used in CHERURB.

Under dry conditions, the initial contamination density predicted using four of the models (METRO-K, ERMIN, RESRAD-RDD, and CHERURB) was approximately 10 MBq/m^2 (ranging by about a factor of 4 from 7 MBq/m^2 to 30 MBq/m^2) for either radionuclide at Locations 4 and 6; an initial contamination density of approximately 50 MBq/m^2 was predicted at Location 5 by all models (Figs 4.6 to 4.8). Predicted initial contamination densities at all locations were about 2–3 GBq/m^2 for either radionuclide (^{60}Co or ^{239}Pu) for light rain and about 10 GBq/m^2 for either radionuclide for heavy rain. When comparing between models, the contamination densities predicted both during light and heavy rain varied by about a factor of 2. These predictions clearly showed the importance of initial weather conditions in determining the initial deposition of radionuclides.

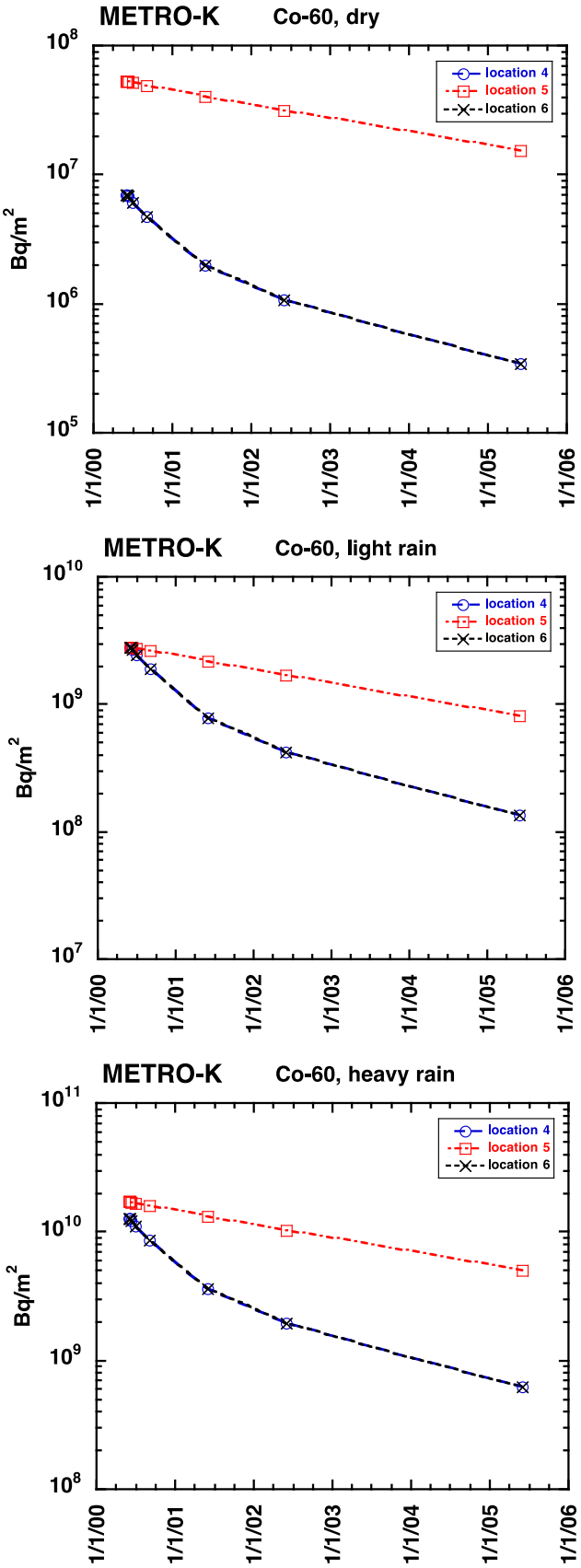

FIG. 4.1. Contamination densities (Bq/m^2) of ^{60}Co at three outdoor locations, as predicted by METRO-K for a summer release under different initial weather conditions as a function of time (1 day, 1 week, 1 month, 3 months, 1 year, 2 years, 5 years).

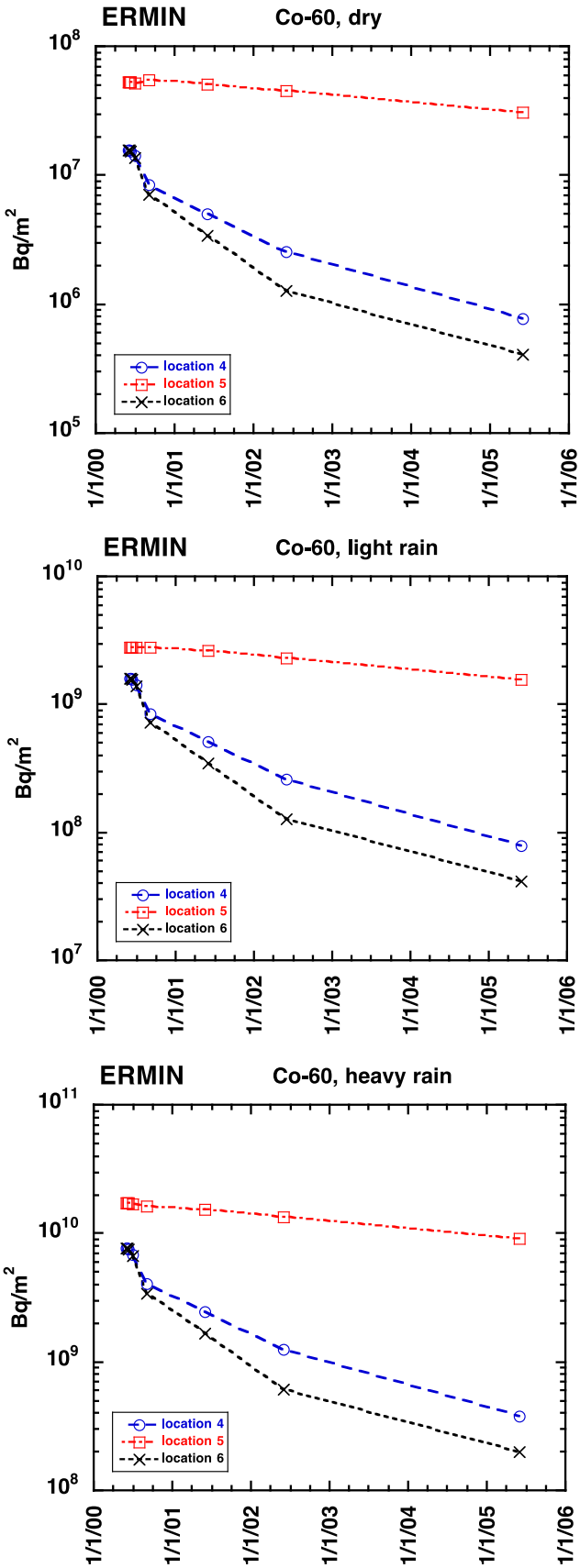

FIG. 4.2. Contamination densities (Bq/m^2) of ^{60}Co at three outdoor locations, as predicted by ERMIN for a summer release under different initial weather conditions as a function of time (1 day, 1 week, 1 month, 3 months, 1 year, 2 years, 5 years).

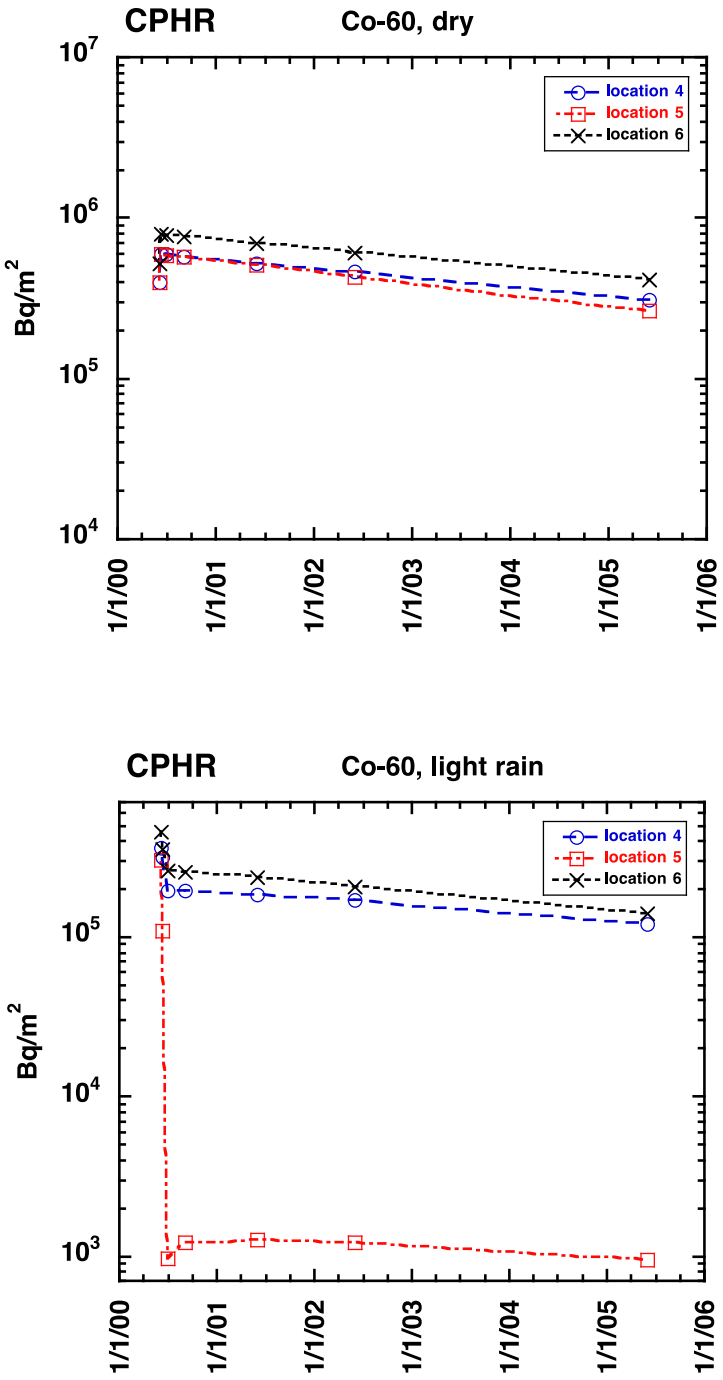

FIG. 4.3. Contamination densities (Bq/m^2) of ^{60}Co at three outdoor locations, as predicted by CPHR for a summer release under different initial weather conditions as a function of time (1 day, 1 week, 1 month, 3 months, 1 year, 2 years, 5 years).

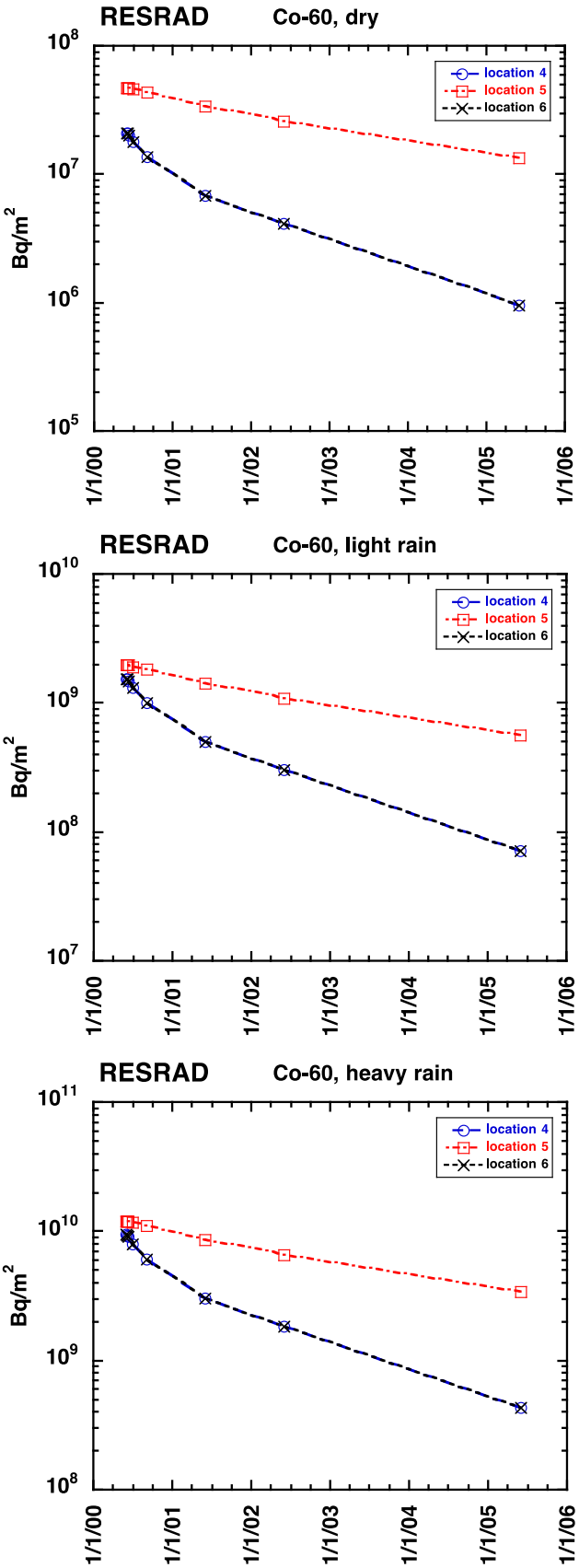

FIG. 4.4. Contamination densities (Bq/m^2) of ^{60}Co at three outdoor locations, as predicted by RESRAD-RDD for a summer release under different initial weather conditions as a function of time (1 day, 1 week, 1 month, 3 months, 1 year, 2 years, 5 years).

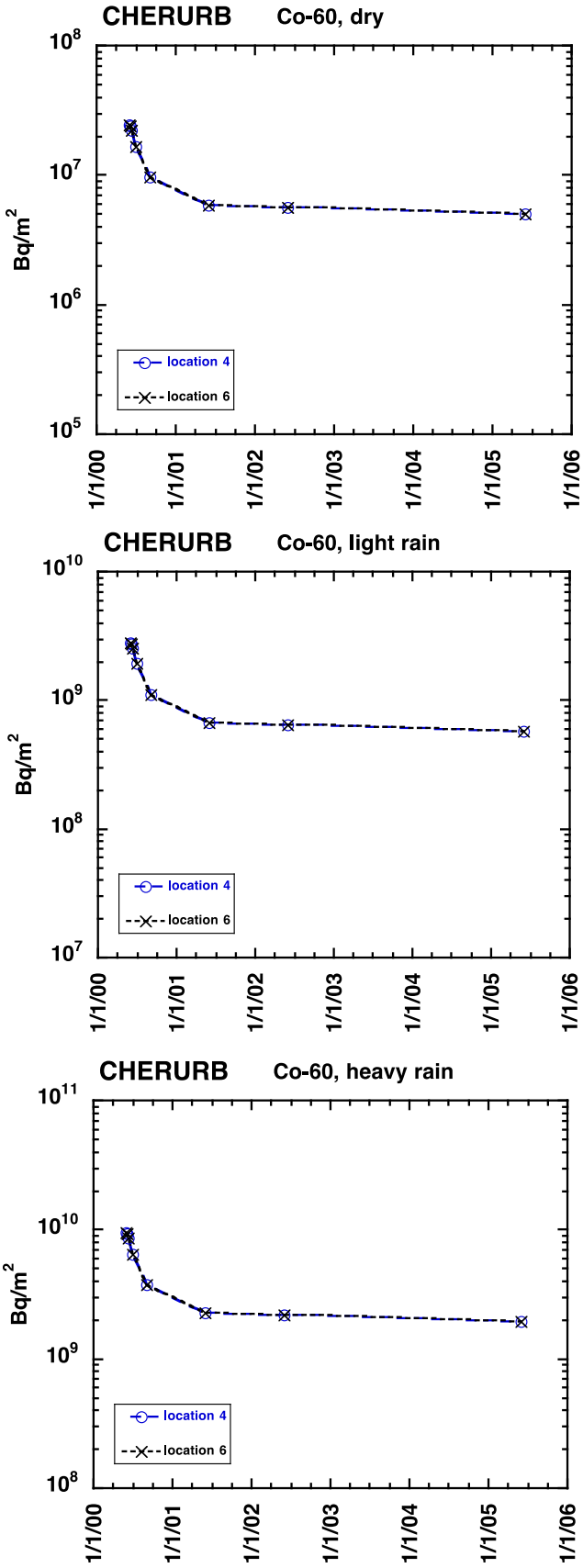

FIG. 4.5. Contamination densities (Bq/m^2) of ^{60}Co at two outdoor locations, as predicted by CHERURB for a summer release under different initial weather conditions as a function of time (1 day, 1 week, 1 month, 3 months, 1 year, 2 years, 5 years).

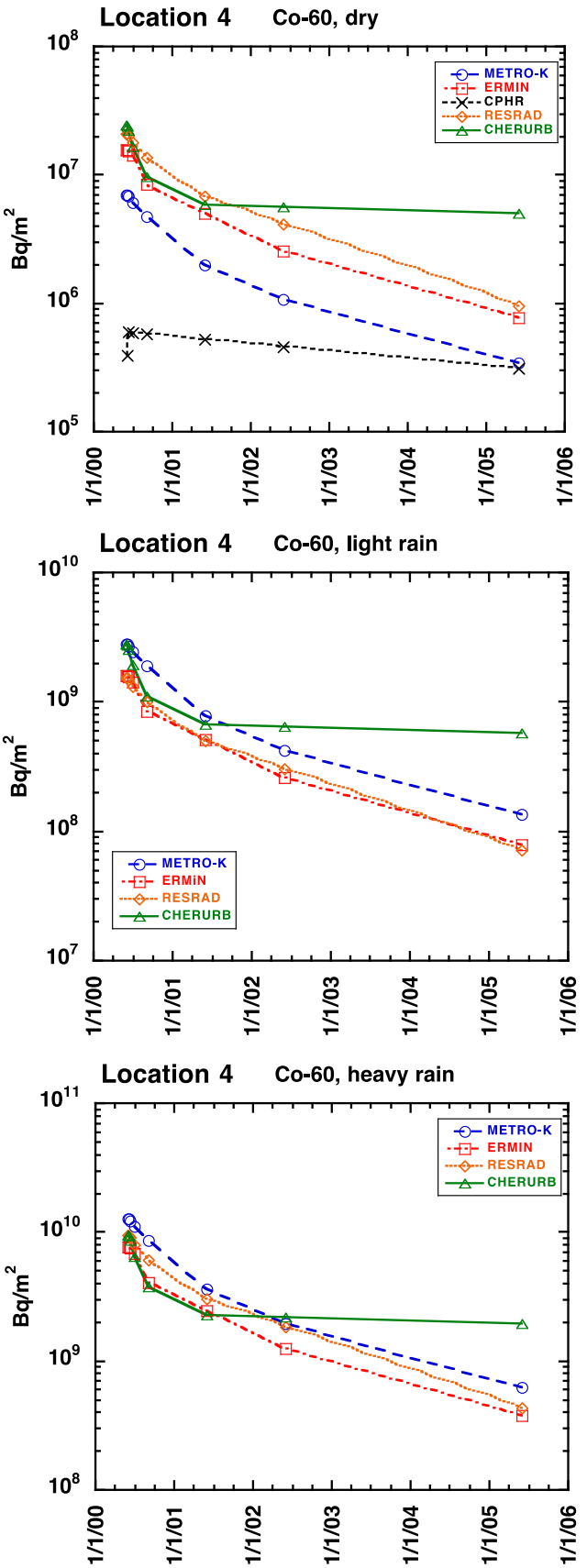

FIG. 4.6. Comparison of model predictions for the contamination density (Bq/m^2) of ^{60}Co at Location 4 under different initial weather conditions as a function of time (1 day, 1 week, 1 month, 3 months, 1 year, 2 years, 5 years).

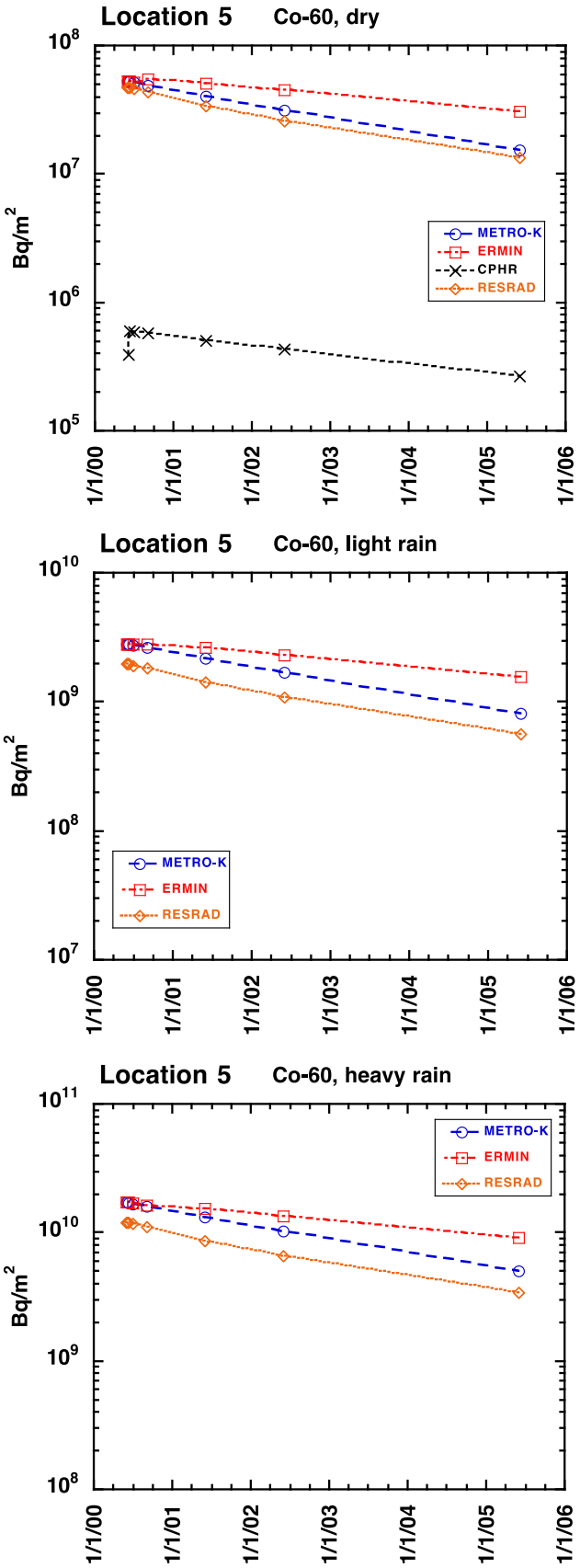

FIG. 4.7. Comparison of model predictions for the contamination density (Bq/m^2) of ^{60}Co at Location 5 under different initial weather as a function of time (1 day, 1 week, 1 month, 3 months, 1 year, 2 years, 5 years).

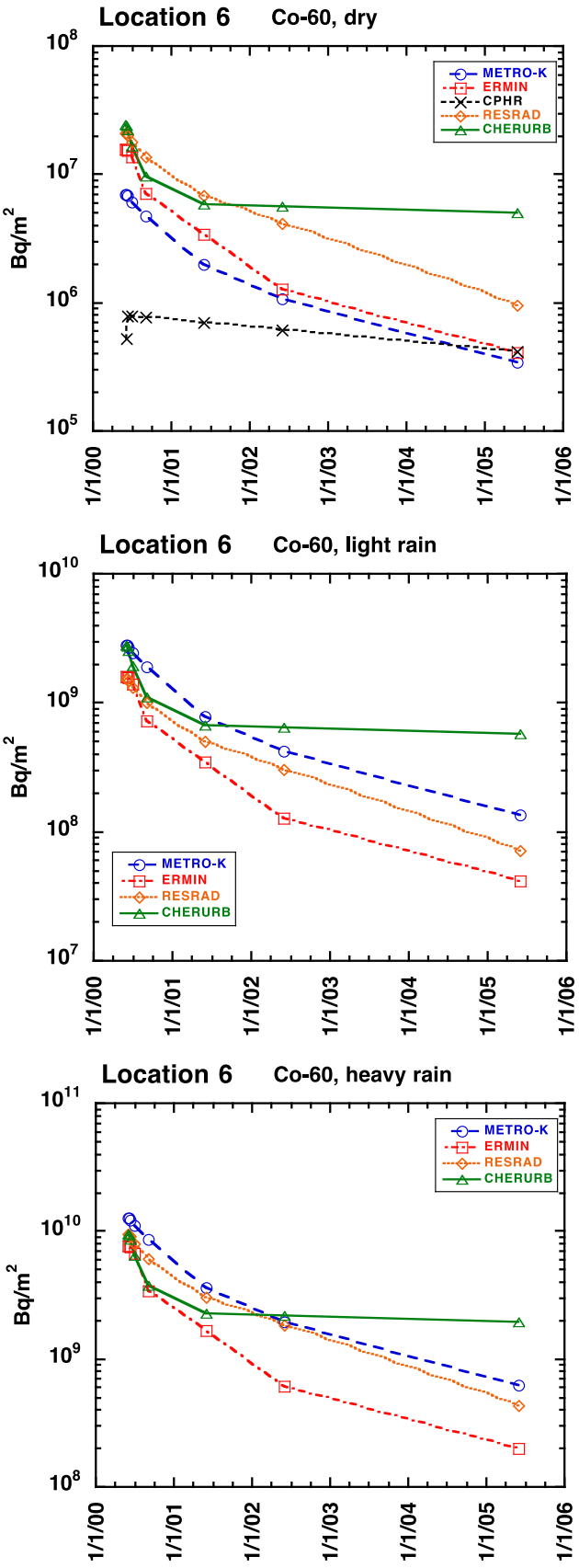

FIG. 4.8. Comparison of model predictions for the contamination density (Bq/m^2) of ^{60}Co at Location 6 under different initial weather conditions as a function of time (1 day, 1 week, 1 month, 3 months, 1 year, 2 years, 5 years).

4.3.2. External gamma dose rates (Cobalt-60)

Figures 4.9 to 4.13 show the predicted external gamma dose rates from ^{60}Co, by model, for both the indoor and outdoor locations (described in Table 4.1 and Appendix V, Figs V.2 to V.4). A comparison of the predictions by all models are also shown for each of the six locations (Figs 4.14 to 4.19). Predictions for all five models were provided for a summer release (Table 4.2); for a winter release, predictions were provided only for METRO-K and ERMIN; these results are tabulated in Appendix VII, Tables VII.6 and VII.7. For CPHR, predictions were submitted only for dry and light rain conditions. For CHERURB, predictions were submitted only for indoor Location 2 and for the outdoor locations (as described in Table 4.2).

4.3.2.1. Outside locations

The predictions for external gamma dose rates at outdoor locations reflected the results for contamination densities at those locations (Section 4.3.1).

Three models (METRO-K, ERMIN, RESRAD-RDD) each produced the same or similar predictions for Locations 4 and 6 (both in paved areas) and higher values for Location 5 (a dirt pathway in a park area) (see Figures 4.9, 4.10 and 4.12, respectively). Weather conditions (dry, light rain, heavy rain) at the time of deposition had a large influence on the predicted external gamma dose rates. For wet deposition (light rain or heavy rain conditions), initial values from these three models were similar for all three locations (around 10–30 mGy/h for light rain and 100 mGy/h for heavy rain), but dose rates decreased faster for the paved locations than for the location with the dirt pathway. The difference in dose rates between the paved and dirt locations was greater under dry conditions (initial values around 0.05–0.2 mGy/h for the paved locations and 0.4–0.5 mGy/h for Location 5). For both the METRO-K and ERMIN models, differences between a summer release and a winter release were small (see Appendix VII, Tables VII.6 and VII.7). These differences are due to there being no deposition onto leaves of trees during a winter release; however, the contribution of trees to dose rates is typically small for most locations considered in this scenario by the two models, and so the overall differences between a summer and winter release are also small.

Both CHERURB (especially for dry conditions) and CPHR showed an initial fast decrease in dose rate followed by a much slower decrease at later times. Predictions from CHERURB for Locations 4 and 5 were the same (Fig. 4.13). Predictions made using CPHR predicted higher dose rates at later times for Location 6 than for Locations 4 or 5 (Fig. 4.11).

Under dry conditions at the outdoor locations, predictions from CPHR for the early time period were within the range of the predictions from the other four models (Figs 4.17 to 4.19); however, after the initial time period, CPHR predictions were substantially lower than those of the other models. CHERURB predictions were consistent with those produced using the other three models (METRO-K, ERMIN, RESRAD-RDD) for Location 5 (Fig. 4.18), and were generally higher for Location 4, especially after the initial time point (Fig. 4.17).

4.3.2.2. Indoor locations

Predicted external dose rates at indoor locations were typically at least an order of magnitude lower than the external dose rates predicted by the same model for outdoor locations (Figs 4.9 to 4.13). In general, most models predicted the highest values for Location 3 (top floor of building 1; i.e. 24th floor), followed by Location 1 (ground floor), and Location 2 (10th floor), respectively (Figs 4.9 to 4.12). For heavy rain, METRO-K produced much higher values (by nearly two orders of magnitude) for Location 1 than for Locations 3 and 2 (Fig. 4.9).

RESRAD-RDD produced similar initial values for all three locations for a given set of initial conditions (Fig. 4.12), with a slightly lower loss rate for later time periods for Location 3.

The differences between Locations 1, 2 and 3 can be explained by their height within the building. Location 1 is at ground level and therefore outdoor ground level surfaces are contributing significantly to the dose rate. Location 3 is near to the roof of the building and so is exposed to radioactivity deposited on the roof. Location 2 is in the middle of the building, relatively far from both roofs and ground level outdoor surfaces. The main contributing surfaces at Location 2 are likely to be external walls of the building and adjacent buildings and indoor surfaces. METRO-K does not include indoor surface and hence the difference in dose rate between Location 2 and Locations 1 and 3 is around two orders of magnitude. The effect of the different surfaces contributing to dose rates at the different locations can be seen in the initial dose rates which are predicted to be in the range 0.003–0.08 mGy/h at Location 1, 0.00006–0.06 mGy/h at Location 2 and 0.003–0.06 mGy/h at Location 3.

In general, RESRAD-RDD produced the highest predictions for all three indoor locations and all three sets of initial weather conditions (Figs 4.14 to 4.16). CHERURB (Location 2 only) produced the next highest predictions for all weather conditions (Fig. 4.15). Under dry conditions, CPHR had the highest initial predicted values, but also had a very fast decrease in dose rate and generally low values over later time periods (Figs 4.14 to 4.16). As was the case for the outdoor locations, the METRO-K and ERMIN models predicted very similar dose rates for deposition occurring in winter and summer, except for the ground floor location (Location 1) under dry conditions for METRO-K, for which the initial predictions varied by about a factor of 4 (winter results shown in Appendix VII, Tables VII.6 and VII.7).

4.3.3. External gamma dose rates (Plutonium-239)

Predicted external gamma dose rates from ^{239}Pu were submitted for three models (ERMIN, CPHR, RESRAD-RDD). Predicted external dose rates from ^{239}Pu for a given model were four or more orders of magnitude lower than those predicted for ^{60}Co, with the lowest values for the indoor locations. Results for external gamma dose rates for ^{239}Pu are not discussed further in detail but the results are given in Appendix VII, Tables VII.7 to VII.9. Plutonium-239 is not an important contributor to external gamma dose, as demonstrated by the dose rates being at least four orders of magnitude lower than those for ^{60}Co.

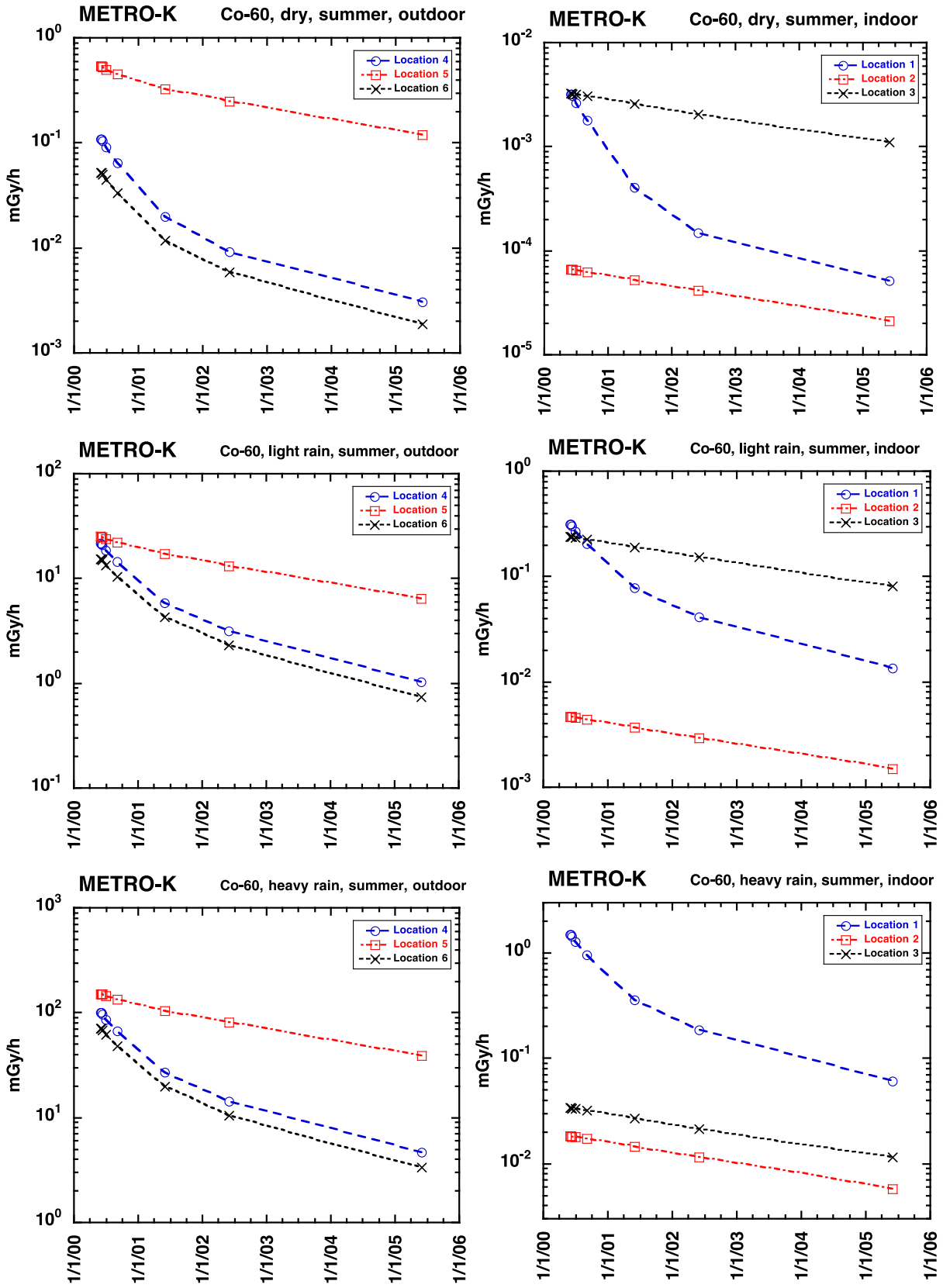

FIG. 4.9. Predictions from METRO-K for external dose rates from ^{60}Co at outdoor locations, for a summer release under different initial weather conditions as a function of time (1 day, 1 week, 1 month, 3 months, 1 year, 2 years, 5 years).

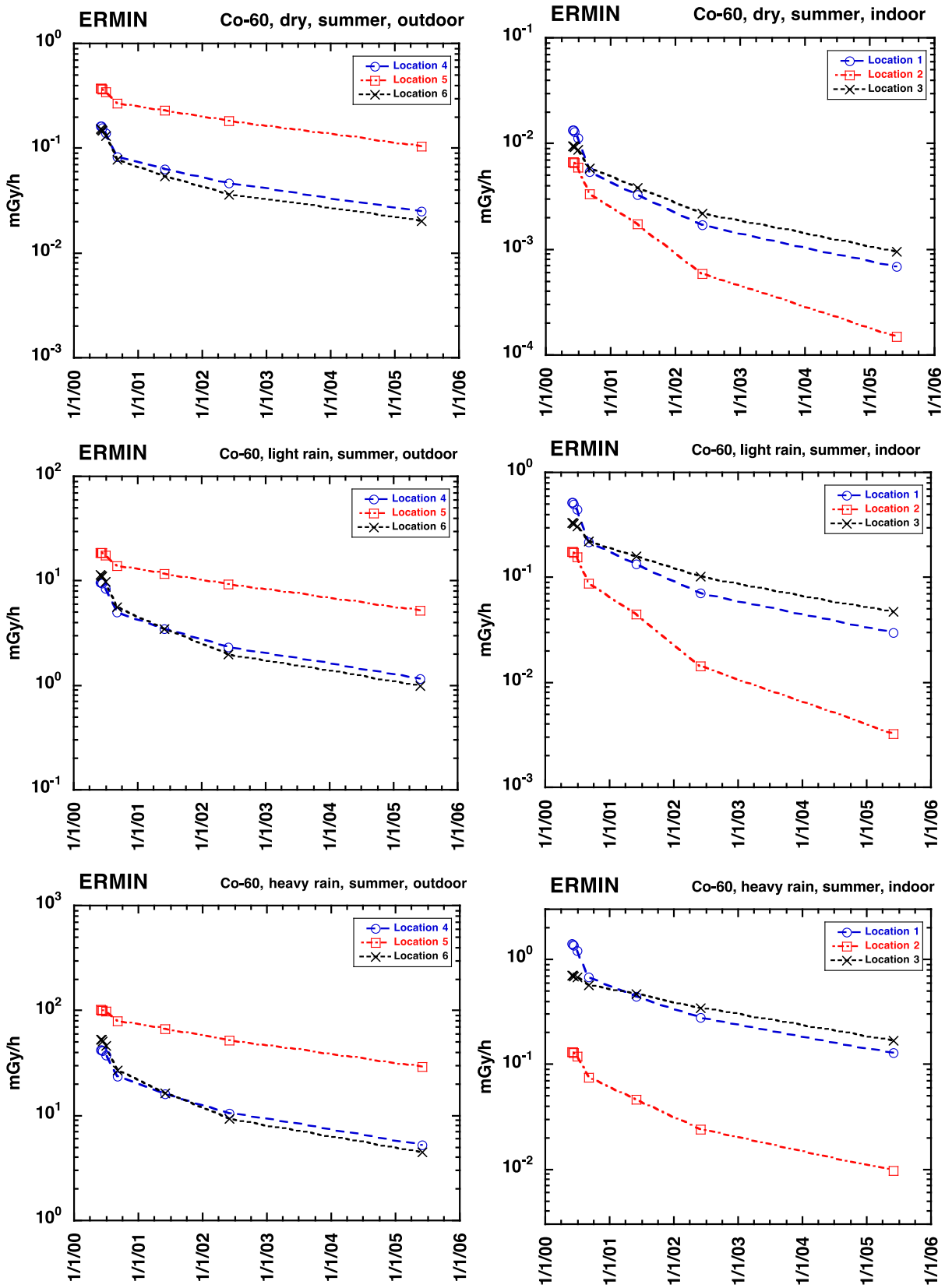

FIG. 4.10. Predictions from ERMIN for external dose rates from ^{60}Co at indoor locations, for a summer release under different initial weather conditions as a function of time (1 day, 1 week, 1 month, 3 months, 1 year, 2 years, 5 years).

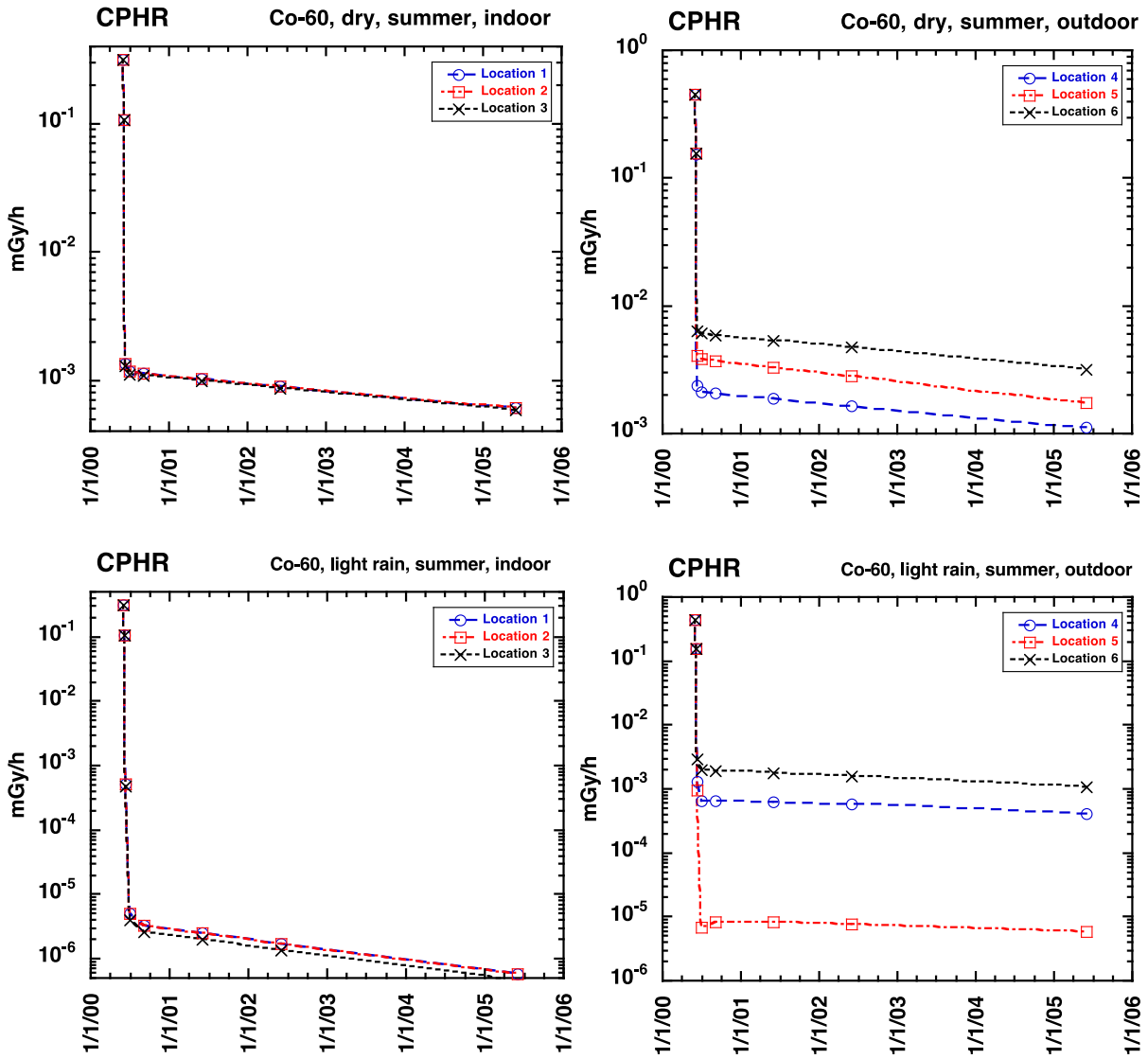

FIG. 4.11. Predictions from CPHR for external dose rates from ^{60}Co at indoor (left) and outdoor (right) locations, for a summer release under different initial weather conditions as a function of time (1 day, 1 week, 1 month, 3 months, 1 year, 2 years, 5 years).

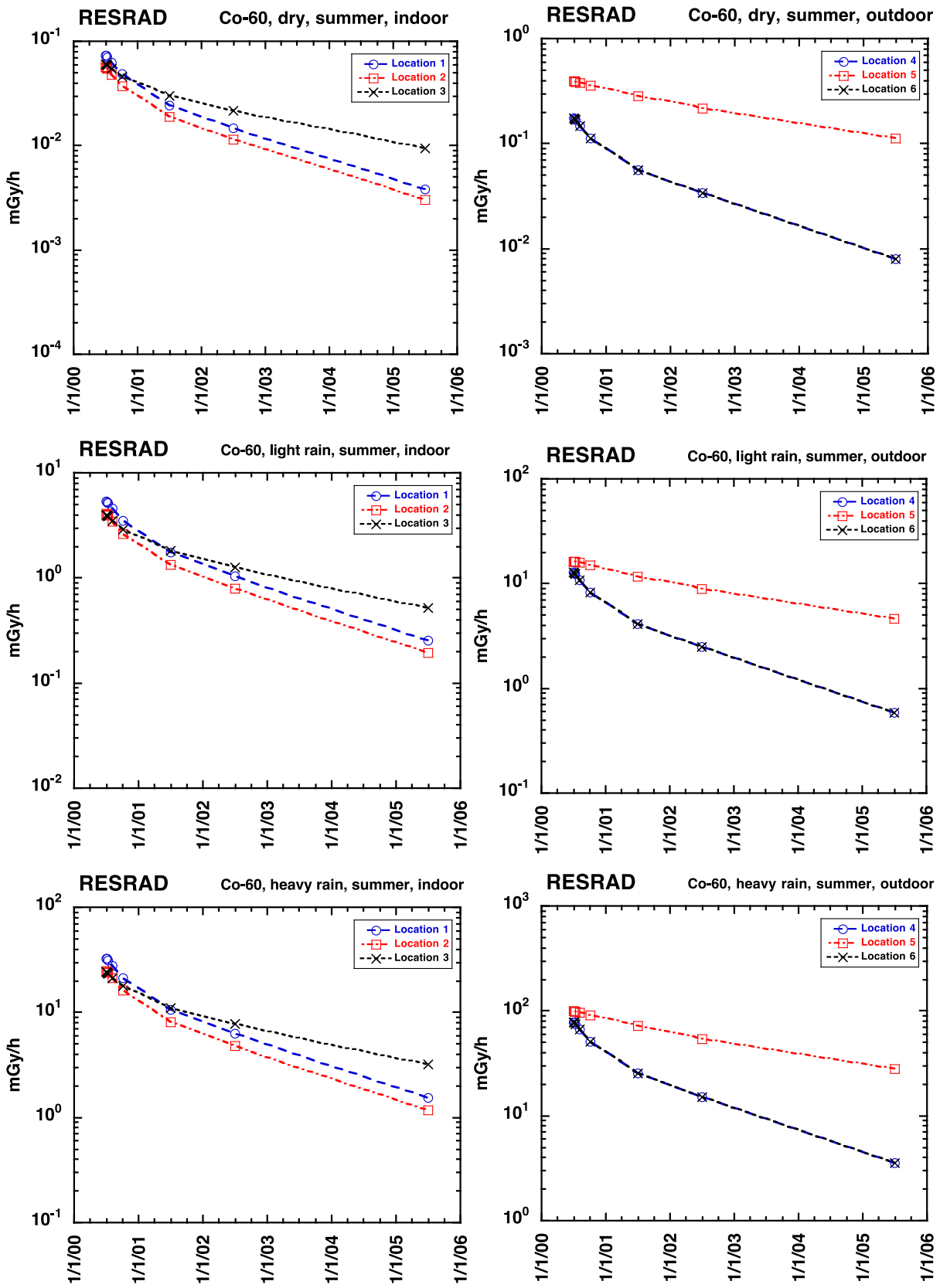

FIG. 4.12. Predictions from RESRAD-RDD for external dose rates from ^{60}Co at indoor (left) and outdoor (right) locations, for a summer release under different initial weather conditions as a function of time (1 day, 1 week, 1 month, 3 months, 1 year, 2 years, 5 years).

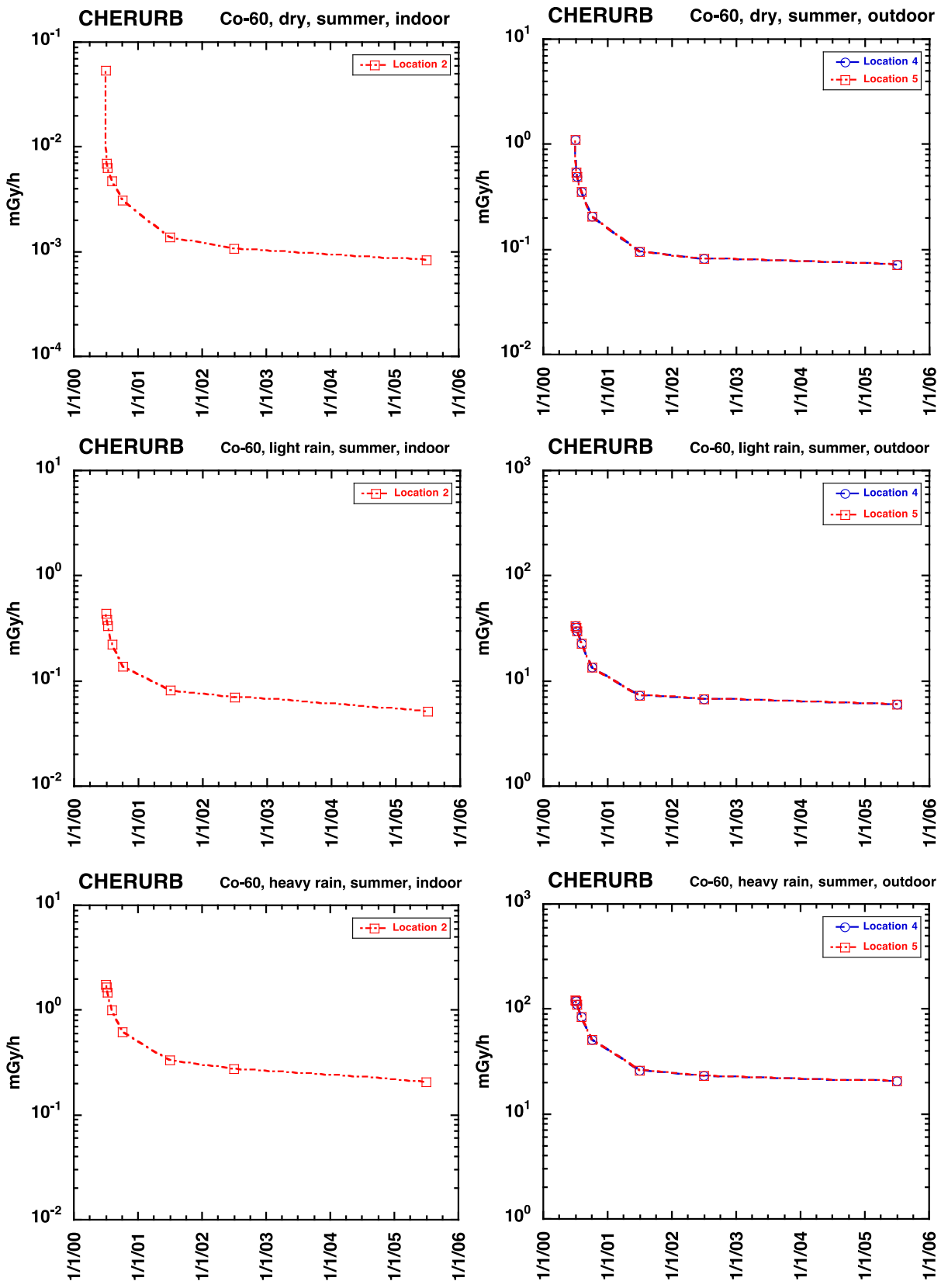

FIG. 4.13. Predictions from CHERURB for external dose rates from ^{60}Co at indoor (left) and outdoor (right) locations, for a summer release under different initial weather conditions as a function of time (1 day, 1 week, 1 month, 3 months, 1 year, 2 years, 5 years).

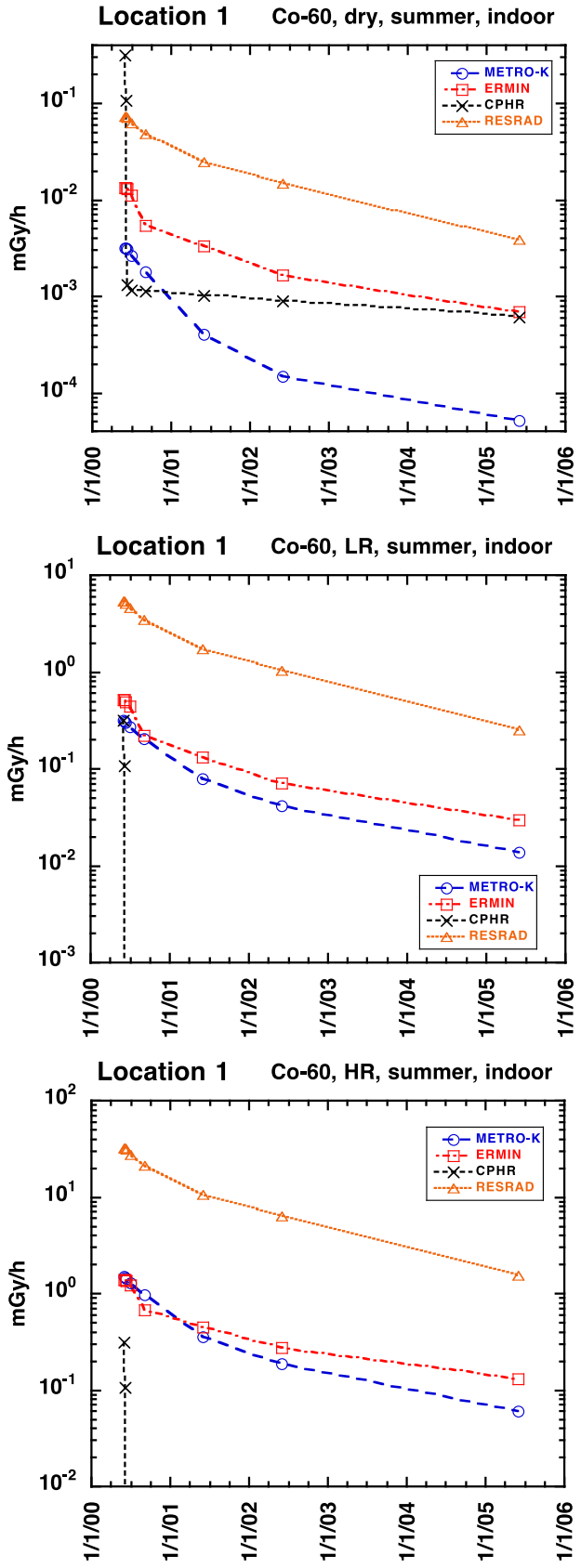

FIG. 4.14. Predictions from all models for external dose rates from ^{60}Co at Location 1 (ground floor of Building 1), for a summer release under different initial weather conditions. 'LR' indicates light rain conditions, and 'HR' indicates heavy rain conditions as a function of time (1 day, 1 week, 1 month, 3 months, 1 year, 2 years, 5 years).

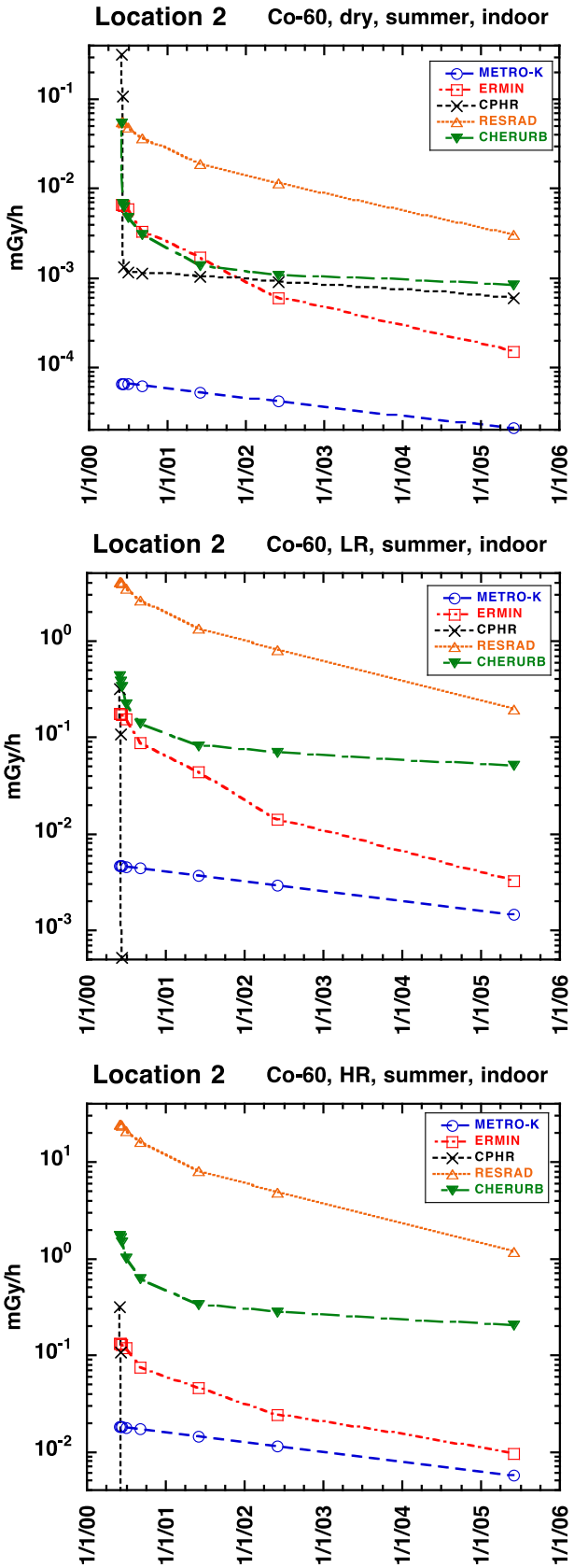

FIG. 4.15. Predictions from all models for external dose rates from ^{60}Co at Location 2 (10th floor of Building 1), for a summer release under different initial weather conditions. 'LR' indicates light rain conditions, and 'HR' indicates heavy rain conditions as a function of time (1 day, 1 week, 1 month, 3 months, 1 year, 2 years, 5 years).

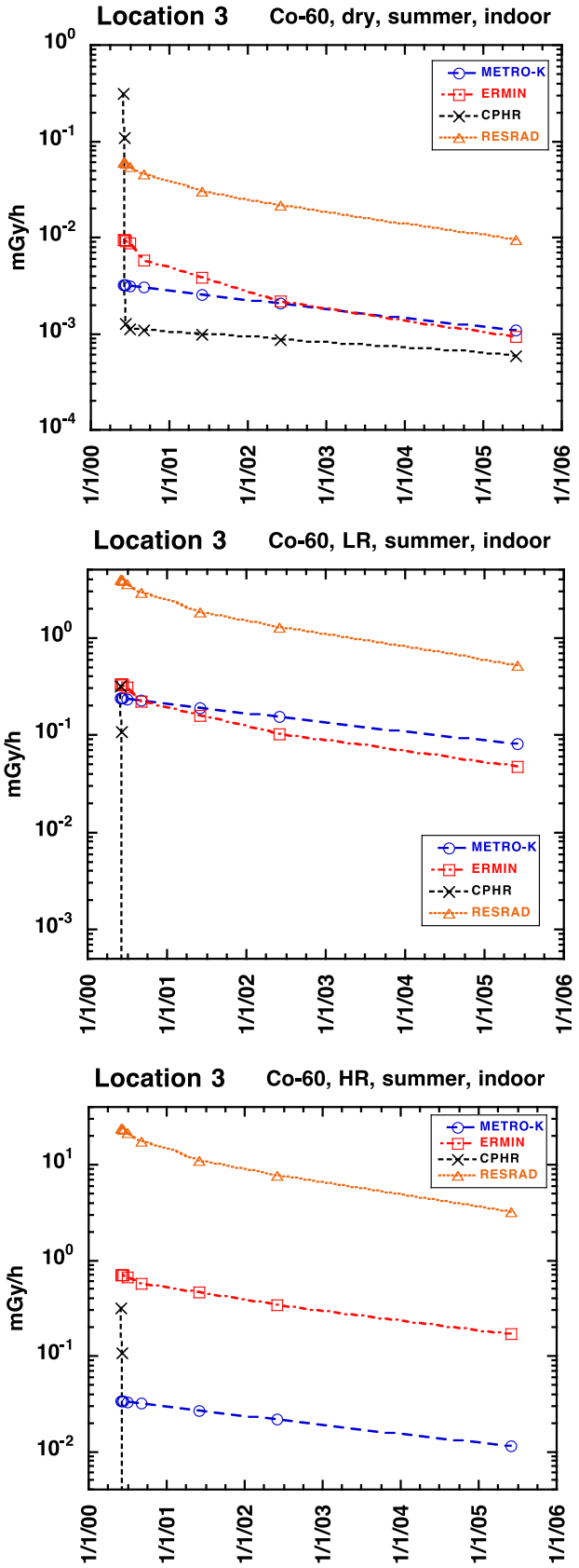

FIG. 4.16. Predictions from all models for external dose rates from ^{60}Co at Location 3 (top (24th) floor of Building 1), for a summer release under different initial weather conditions. 'LR' indicates light rain conditions, and 'HR' indicates heavy rain conditions as a function of time (1 day, 1 week, 1 month, 3 months, 1 year, 2 years, 5 years).

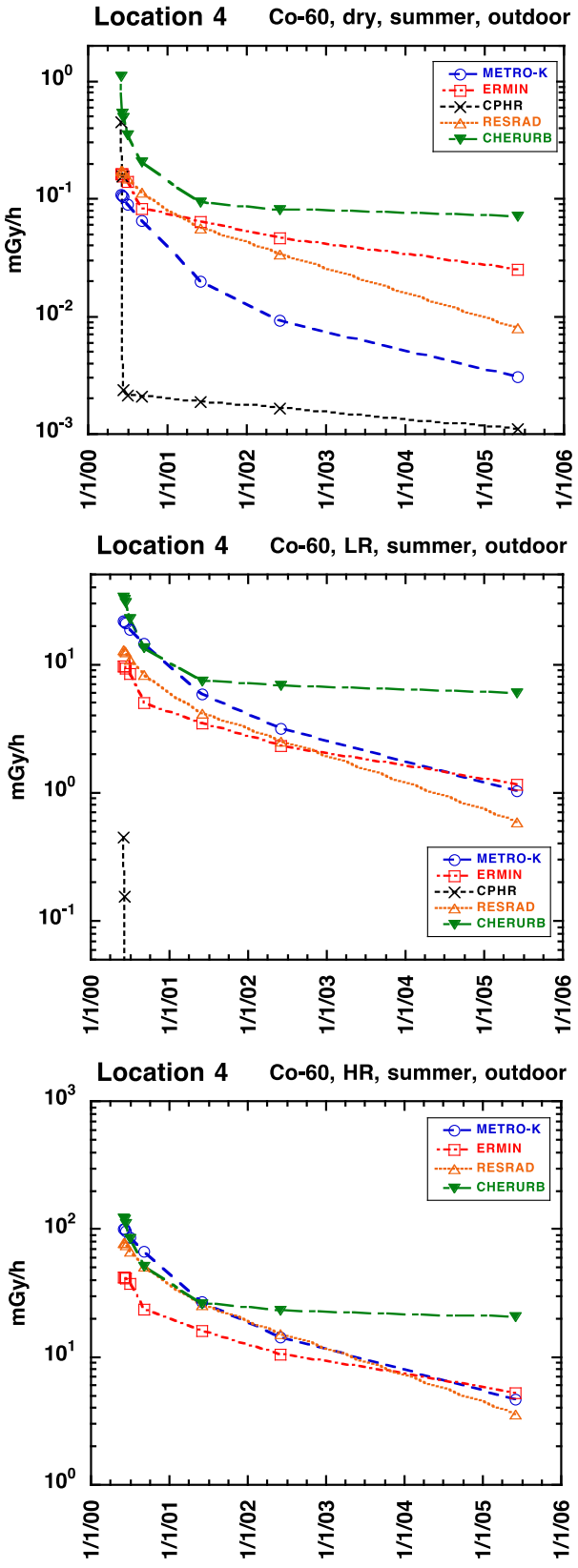

FIG. 4.17. Predictions from all models for external dose rates from ^{60}Co at Location 4 (right: paved area outside Building 1), for a summer release under different initial weather conditions. 'LR' indicates light rain conditions, and 'HR' indicates heavy rain conditions as a function of time (1 day, 1 week, 1 month, 3 months, 1 year, 2 years, 5 years).

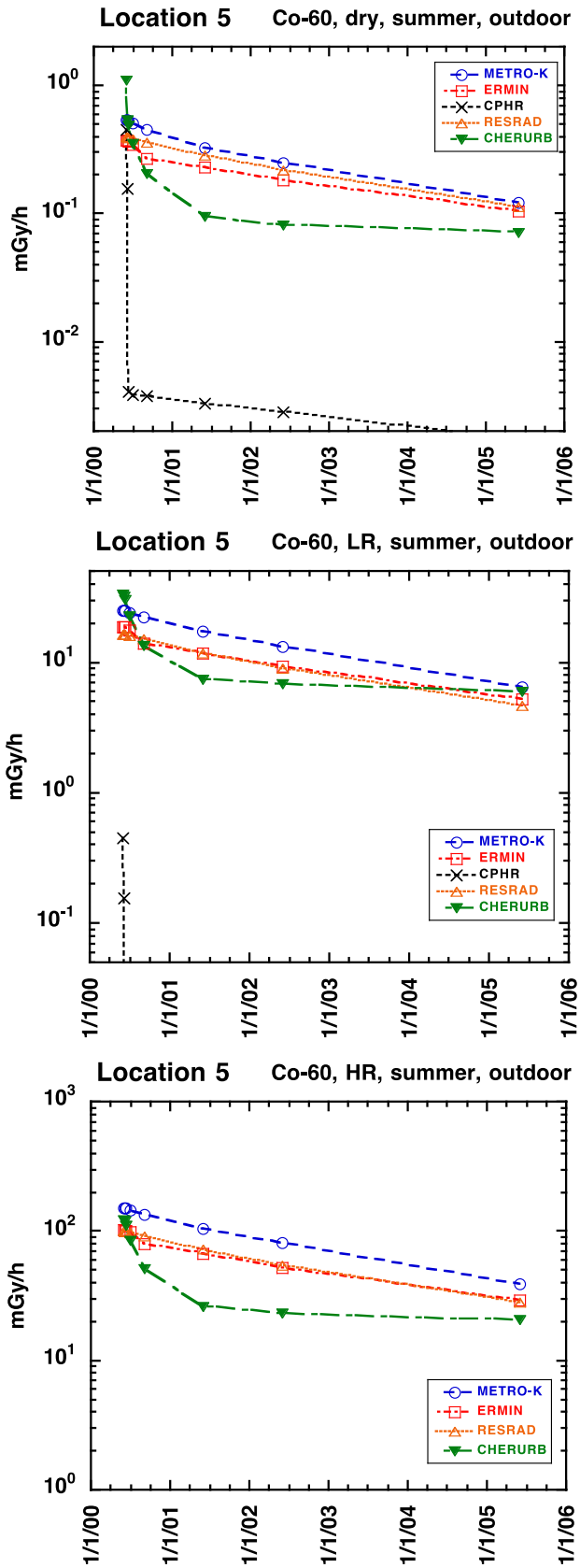

FIG. 4.18. Predictions from all models for external dose rates from ^{60}Co at Location 5 (dirt path in park area), for a summer release under different initial weather conditions. 'LR' indicates light rain conditions, and 'HR' indicates heavy rain conditions as a function of time (1 day, 1 week, 1 month, 3 months, 1 year, 2 years, 5 years).

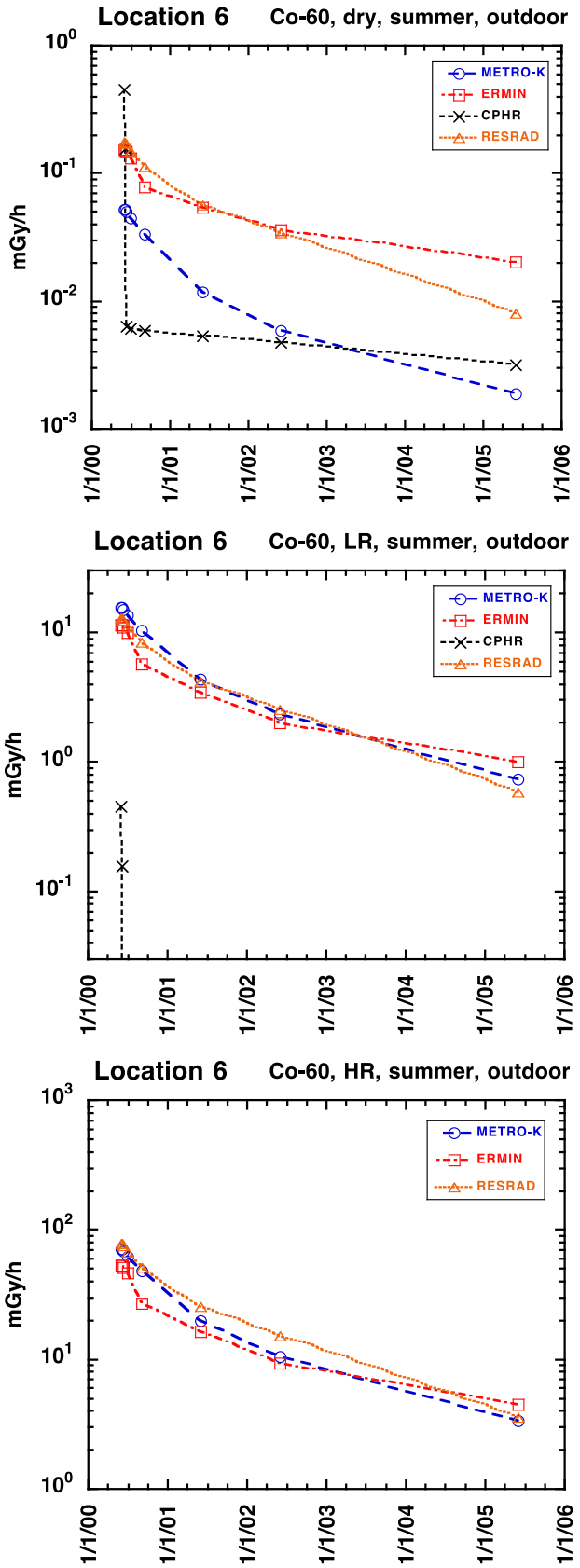

FIG. 4.19. Predictions from all models for external dose rates from ^{60}Co at Location 6 (right: paved parking lot), for a summer release under different initial weather conditions. 'LR' indicates light rain conditions, and 'HR' indicates heavy rain conditions as a function of time (1 day, 1 week, 1 month, 3 months, 1 year, 2 years, 5 years).

TABLE 4.4. SURFACES CONSIDERED IN THE MODELS

Surfaces	Model			
	ERMIN	METRO-K	RESRAD-RDD	CPHR
Outdoor surfaces				
Paved	×	×		×
Trees	×	×		×
Soil		×		×
Grass	×			
Roofs	×	×	×	×
External walls	×	×	×	×
Indoor surfaces				
Interior surfaces	×			
Interior walls			×	
Floors			×	

4.3.4. Surfaces contributing to external gamma dose rates

For the predictions of external dose rates described in Sections 4.3.2 and 4.3.3, predictions were also made for four models (METRO-K, ERMIN, CPHR, RESRAD-RDD) of the surfaces contributing the most to the predicted external dose rate at each location at three times following deposition. The percentage that each surface contributed to the predicted external dose rate at each location and time point for an initial deposition of ^{60}Co and ^{239}Pu in dry conditions was estimated. The predictions for ^{60}Co are shown in Figs 4.20 and 4.21 and a comparison is given between the four models. Figures 4.22 to 4.26 provide comparisons by location and initial weather conditions for ^{60}Co for each model. The initial time point 'Year 0' represents less than 1 day since the release. The time points 'Year 1' and 'Year 5' are one year and five years, respectively, following the release of the radionuclide. Participants were asked to provide the three most important surfaces contributing to external dose rate at each location. In some cases, more than three surfaces contributed; thus, the percentages do not always sum to 100%. In other cases, only one or two surfaces contributed to external dose rate. Tabulated results for an initial deposition of ^{239}Pu are given in Appendix VII, Tables VII.11 to VII.14; however, the model predictions for ^{239}Pu are discussed here to enable a direct comparison with those for ^{60}Co.

Different models included different specifications of surfaces; surfaces are designated in the figures as they were reported by the participants (soil and grass are considered together in the figures). The surfaces considered in each model are listed in Table 4.4. Understanding the variety of surfaces included by different models is important to understanding the model predictions of external dose rates (Sections 4.3.2 and 4.3.3) and external doses (Section 4.3.5), especially in terms of how the predicted external dose rates vary over time under different release conditions, by location, by isotope, and amongst models.

RESRAD-RDD also included two generic surfaces 'from outside' (for external dose rates at indoor locations), and 'infinite area' (for external dose rates at outdoor locations) representing all outdoor contributors to external dose rate (e.g. paved surfaces, soil, grass). CPHR also included the contribution from 'air' (the initial plume) at the initial time point (immediately after the release), for all locations.

4.3.4.1. Indoor locations (Locations 1–3)

For indoor locations (Fig. 4.20), the contributing surfaces were dependent on the location within the building. For Location 1 (ground floor), most models included contributions from outdoor surfaces (e.g. trees and pavement for METRO-K, trees, pavement, grass and external walls for ERMIN, and exterior walls and 'from outside', i.e. from outdoor surfaces, for RESRAD-RDD). Contributions from indoor surfaces were included as 'interior surfaces' by ERMIN and internal walls and floors by RESRAD-RDD, whereas CPHR and METRO-K do not include consideration of internal deposition. CPHR included the contribution from 'air' (the initial air contamination or plume) at the initial time point after the release, for all indoor locations; the predicted external dose rate from the plume was high enough that no other surfaces contributed at the initial time point (Fig. 4.20 and considered further in Section 4.3.5). For Location 2 (10^{th} floor), RESRAD-RDD showed a major contribution 'from outside' (66–78% of the predicted external dose rate from ^{60}Co and 27–29% of the predicted external dose rate from ^{239}Pu at this indoor location), while the other three models predicted that the major contribution to external dose rate at Location 2 was from external walls or interior surfaces (Fig. 4.20). For Location 3 (24^{th} or top floor), a major contribution to external dose rate from roofs was evident for all models, ranging from 17% to 98% of the predicted external dose rate from ^{60}Co and from 2% to 67% of the predicted external dose rate from ^{239}Pu, depending on the model and the time point. At this location, RESRAD-RDD still predicted a significant (14–48%) contribution to external dose rate 'from outside.'

For ^{60}Co at the ground floor location (Location 1), both METRO-K and ERMIN predicted an important contribution to the external dose rate from trees, representing 78% and 33% of the total external dose rate, respectively, at the initial time point (Fig. 4.20). For METRO-K, trees were the dominant surface initially contributing to the external dose rate (Year 0) (78%), less so (43%) at the time point Year 1 (1 year since the release), and not contributing at all (0%) at Year 5, while walls and paved surfaces became increasingly important over time (from 2% at Year 0 to 40% at Year 5 for walls and from 20% at Year 0 to 60% at Year 5 for paved surfaces; see Fig. 4.20). For ERMIN, trees were important contributors to external dose rate (33%) only at the initial time point (Year 0); however, grass became increasingly important over time, contributing 69% of the external dose rate at Year 5 (Fig. 4.20).

ERMIN also predicted a decrease over time in the importance of interior surfaces as contributors to external dose rate, with corresponding increases in the percent contribution to external dose rate by walls for all indoor locations; this was especially the case at Location 2, where interior surfaces contributed 93% of the external dose rate at Year 0, but only 2% at Year 5, while walls contributed 7% of the external dose rate at Year 0, but 98% at Year 5 (Fig. 4.20). Location 2 is on the 10^{th} floor of the building, which is too high for significant contributions to external dose rate from trees, grass, or paved surfaces (unlike Location 1, on the ground floor) (see Section 4.3.4.1), but also not having a significant contribution to external dose rate from the roof (unlike Location 3 on the top floor, for which the contribution from the roof was significant) (see Section 4.3.4.1). METRO-K predicted that walls were the only surface contributing to the external dose rate at Location 2 at all the time points.

For Location 3 (top floor, i.e. the 24^{th} floor), ERMIN and RESRAD-RDD both predicted higher contributions to external dose rates from roofs than from walls or interior surfaces (after the initial time point for ERMIN and at all time points for RESRAD-RDD), increasing from 31% at Year 0 to 87% at Year 5 for ERMIN and from 34% at Year 0 to 76% at Year 5 for RESRAD-RDD (Fig. 4.20). METRO-K predicted that roofs contributed 98% of the external dose rate at Location 3 at all the time points (Fig. 4.20). In general, surfaces that can act as

'sinks' for radioactivity (grass, walls, roofs) tended to contribute a greater percentage of the external dose rate at later time points than those surfaces presumed to have net losses of radioactive contamination over time (e.g. trees, interior surfaces).

For the three models that were used to predict external dose rates for ^{239}Pu (CPHR, ERMIN, RESRAD-RDD), the same surfaces were important contributors to external dose rate as for ^{60}Co, but the percentage contributions were different. In general, the nearer surfaces (e.g. 'interior', floors) were more important for ^{239}Pu than more distant surfaces (e.g. trees, grass, paved surfaces, 'from outside', roofs). For example, for ERMIN, 'interior' surfaces were predicted to contribute 41–46% of the external dose rate at Location 1 for ^{60}Co, whereas 87–88% of the external dose rate at Location 1 was predicted to be contributed by ^{239}Pu. For RESRAD-RDD, the predicted contribution 'from outside' at Location 1 was 73–83% of the external dose rate for ^{60}Co, but only 29–31% of the external dose rate for ^{239}Pu. For predictions generated using either ERMIN or RESRAD-RDD, contributions from trees, interior surfaces, and floors became less important over time, while contributions from walls and roofs became more important over time, depending on the location within the building.

4.3.4.2. Outdoor locations (Locations 4–6)

Results for Locations 4 and 6 tended to be similar for any given model (Fig. 4.21). These two locations were both outdoors with mostly paved surfaces; Location 4 was near buildings, while Location 6 was not, but the walls at Location 4 were a minor contributor to external dose rate (representing 2–19%, depending on the model, the time point, and the radionuclide). The results for three models (METRO-K, ERMIN, CPHR) included a significant contribution to the external dose rate from paved surfaces at both locations: 47–81% at Location 4 and 73–100% at Location 6 for ^{60}Co for METRO-K; 9–35% at Location 4 and 11–56% at Location 6 for ^{60}Co for ERMIN; 94% at both locations for both radionuclides for CPHR. METRO-K and ERMIN both predicted a contribution from trees at the initial time point, which decreased over time. For METRO-K predictions, the contributions to external dose rate from walls (Location 4) and pavement (Locations 4 and 6) increased over time. For ERMIN, the results showed a decrease in contribution over time from pavement and an increase over time from grass.

For Location 5 (the centre of a park area), the main contributors to external dose rate predicted by three models (METRO-K, ERMIN, CPHR) were grass and trees (Fig. 4.21). CPHR included the contribution from 'air' at the initial time point (immediately after the release), for all outdoor locations. The fourth model (RESRAD-RDD) was used to calculate the external dose rate for all outdoor locations in terms of an 'infinite area' and did not distinguish amongst individual surfaces or between ^{60}Co and ^{239}Pu. CPHR also predicted the same percentages for contributing surfaces for ^{60}Co and ^{239}Pu.

The predictions from ERMIN had the same percentages for contributing surfaces for ^{60}Co and ^{239}Pu at Locations 5 and 6 at the initial time point and predicted small differences (e.g. 0.96% for ^{60}Co versus 1.16% for ^{239}Pu at Location 5) at the later time points, due to the shorter half-life of ^{60}Co. At Location 4, where the building walls also contributed to external dose rates, there were small differences predicted between ^{60}Co and ^{239}Pu in terms of the percent contributions (e.g. 34.6% for ^{60}Co and 33.5% for ^{239}Pu for paved surfaces at the initial time point; see Fig. 4.21).

For METRO-K (Figs 4.22 and 4.23), trees were predicted to contribute a larger percentage of the external dose rate (e.g. 51% versus 5%) for a summer release than for a winter release, as well as under dry conditions relative to wet conditions (e.g. 51% versus 20%). In all cases in

which trees were a major contributor to external dose rate (Locations 1, 4, 5, and 6), the relative contribution to external dose rate decreased over time, with corresponding increases in the percent contributions from walls (Locations 1 and 4), soil (Location 5), or paved surfaces (Locations 1, 4, and 6). At Locations 2 (10^{th} floor inside the building) and 3 (top floor), no significant seasonal or weather related differences in contributing surfaces were apparent. At Location 2, the entire contribution to external dose rate was predicted to be from walls, while at Location 3, 97–98% of the external dose rate was predicted to be from roofs.

Results from the ERMIN model (Figs 4.24 and 4.25) also predicted a greater percent contribution to external dose rate from trees (Locations 1, 4, 5, and 6) for a summer release (20–40% under dry conditions) than for a winter release (5–13% under dry conditions), as well as under dry versus wet initial conditions (5–28% for a summer release under wet conditions and 1–6% for a winter release under wet conditions). Effects of season or initial weather conditions at indoor locations were less apparent for other surfaces. Differences in the importance of walls and 'interior' surfaces were seen for ^{60}Co versus ^{239}Pu at indoor locations; roofs were less important contributors to external dose rate for ^{239}Pu than for ^{60}Co. At the outdoor locations, the importance of grass surfaces increased over time, whereas the predicted contribution from paved surfaces decreased.

At indoor locations, RESRAD-RDD (Fig. 4.26) predicted a greater percent contribution to external dose rate from floors for ^{239}Pu (67–76% of the external dose) than for ^{60}Co (13–18% of the external dose rate), and a corresponding decrease in the fraction contributed 'from outside' or from roofs. Roofs became increasingly important contributors to external dose rate over time at Location 3 (the top floor of the building, i.e. the 24^{th} floor), and were slightly less important under wet release conditions than under dry conditions; for example, for a ^{60}Co release under dry conditions, a 34% contribution to external dose rate was initially predicted and 76% was predicted after five years, and 27.5% was predicted initially and 73% after five years for a release under wet conditions.

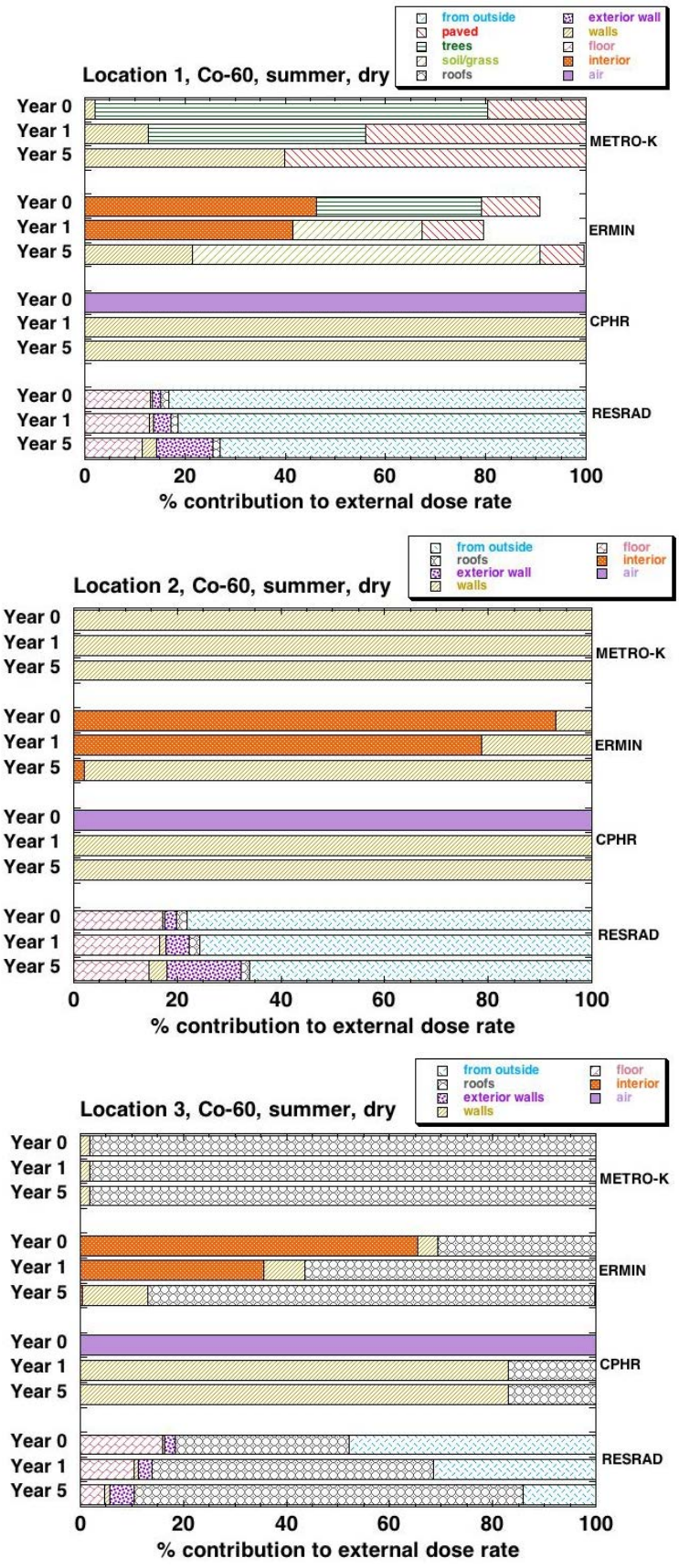

FIG. 4.20. Percent contributions to the predicted external dose rates from specified surfaces at indoor locations, shown separately for ^{60}Co, by model and time point, for a summer release in dry conditions.

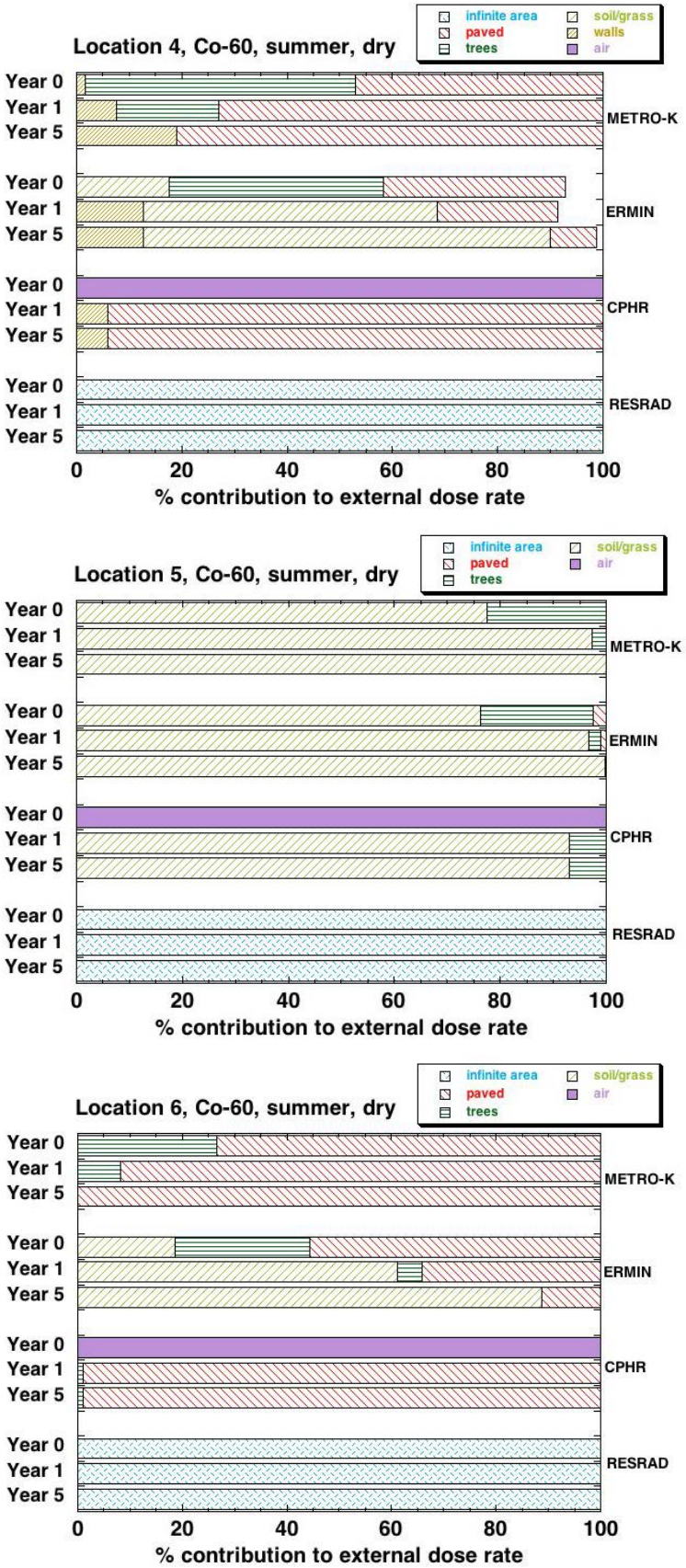

FIG. 4.21. Percent contributions to the predicted external dose rates from specified surfaces at outdoor locations, shown separately for ^{60}Co, by model and time point, for a summer release in dry conditions.

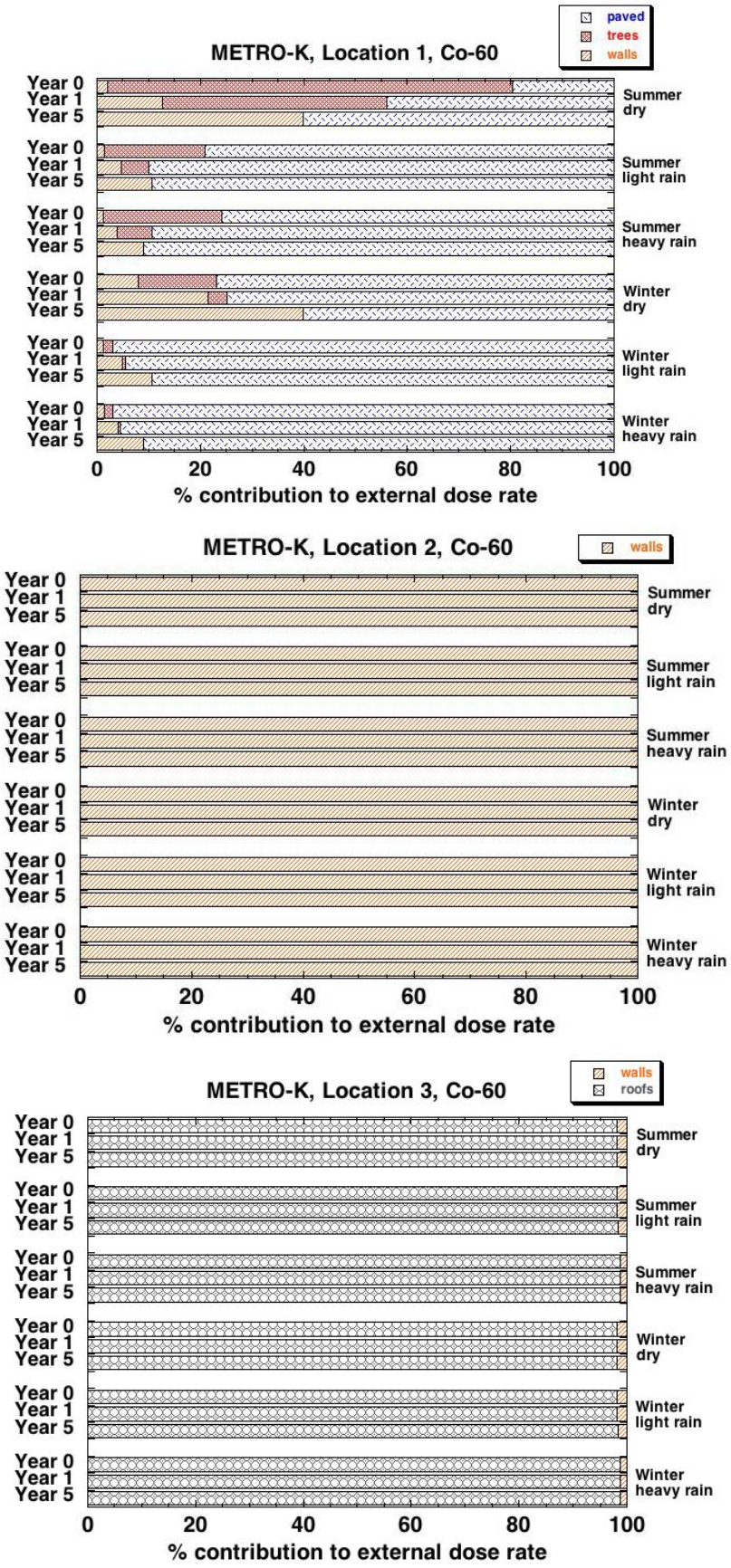

FIG. 4.22. Percent contributions to the predicted external dose rates from ^{60}Co from specified surfaces at indoor locations, shown for METRO-K, for the indicated time points and release conditions.

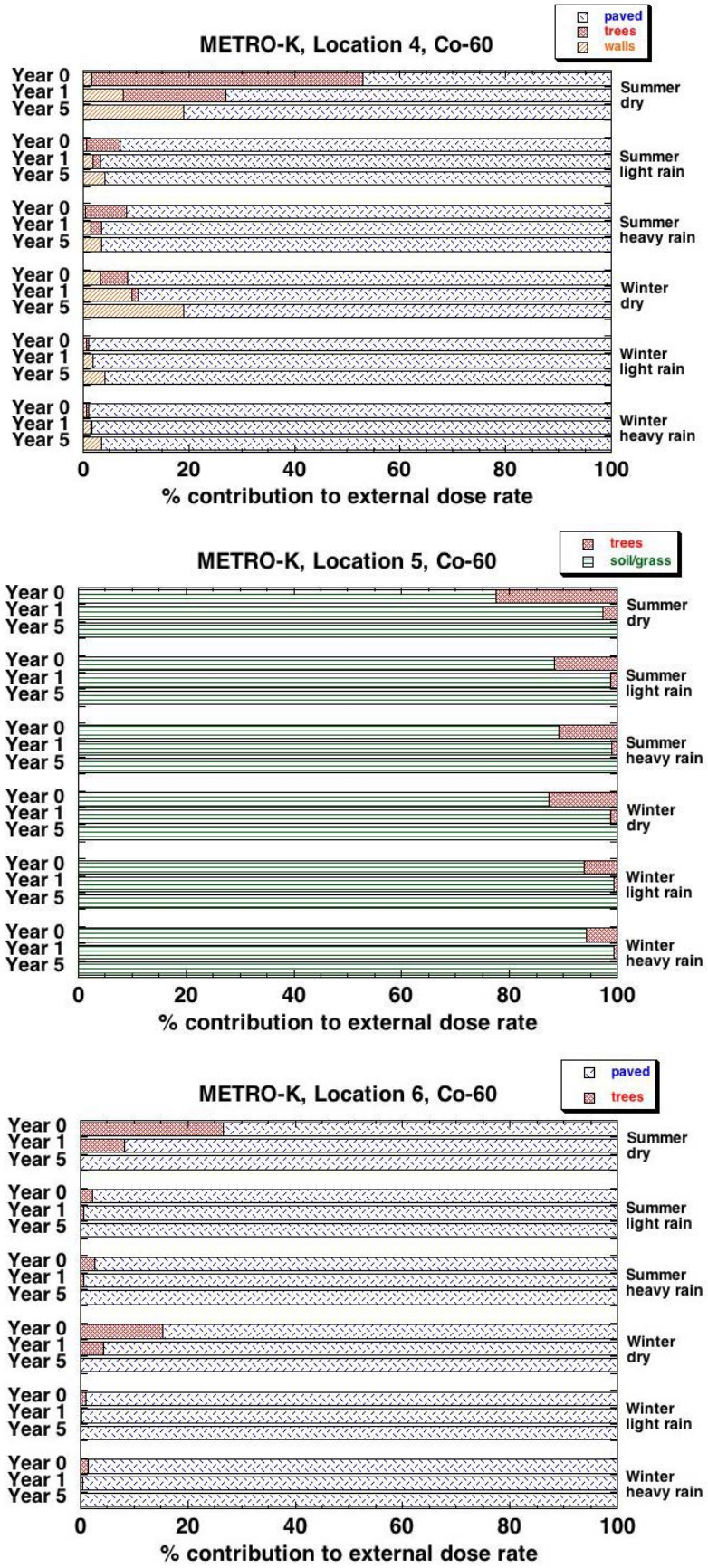

FIG. 4.23. Percent contributions to the predicted external dose rates from ^{60}Co from specified surfaces at outdoor locations, shown for METRO-K, for the indicated time points and release conditions.

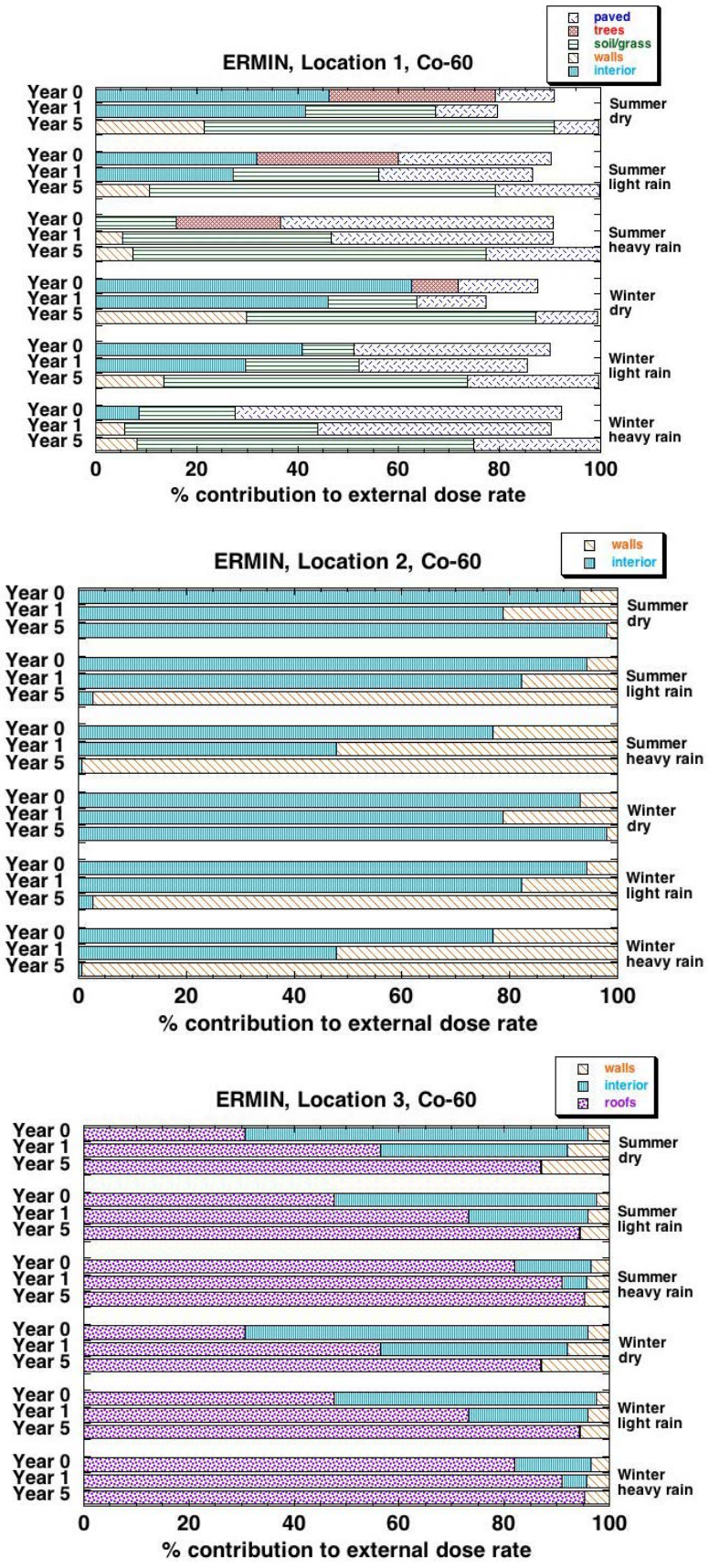

FIG. 4.24. Percent contributions to the predicted external dose rates from ^{60}Co from specified surfaces at indoor locations, shown for ERMIN, for the indicated time points and release conditions.

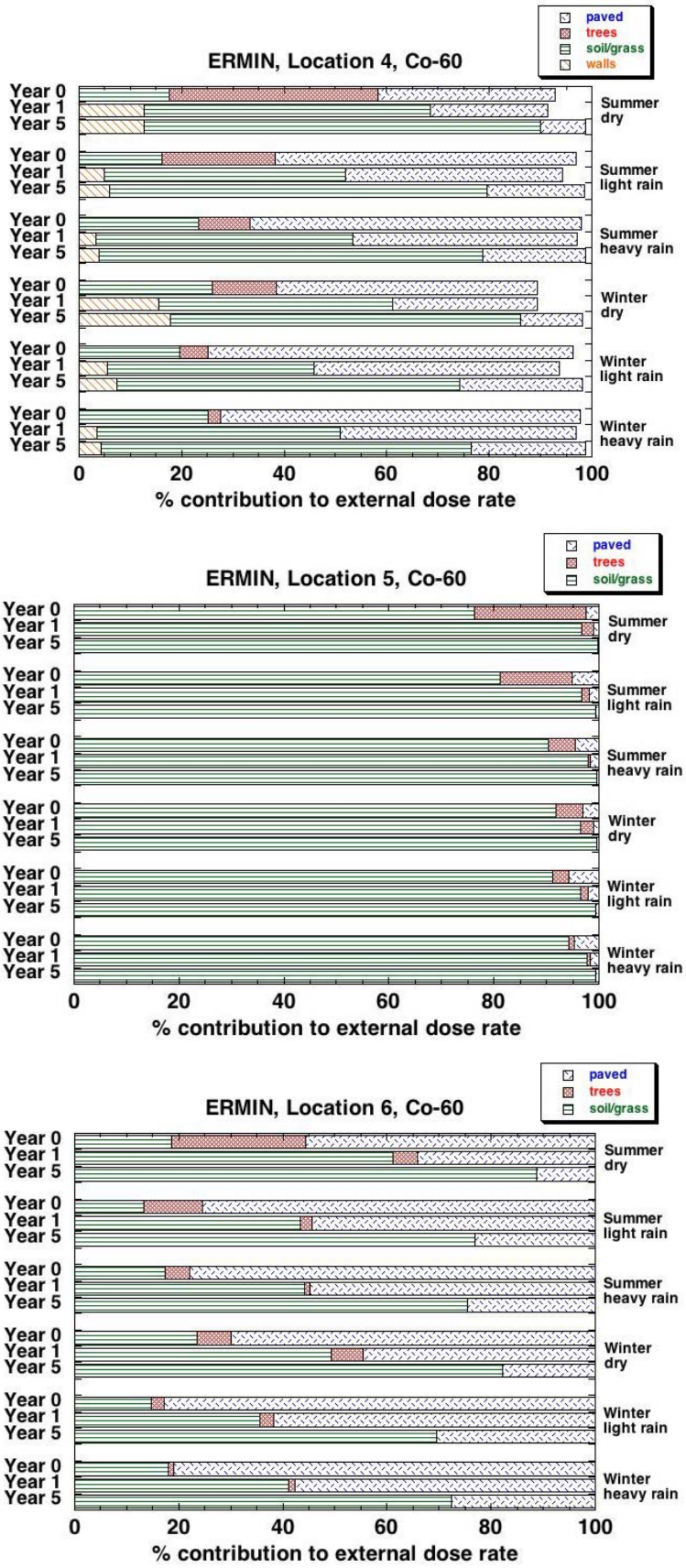

FIG. 4.25. Percent contributions to the predicted external dose rates from ^{60}Co from specified surfaces at outdoor locations, shown for ERMIN, for the indicated time points and release conditions.

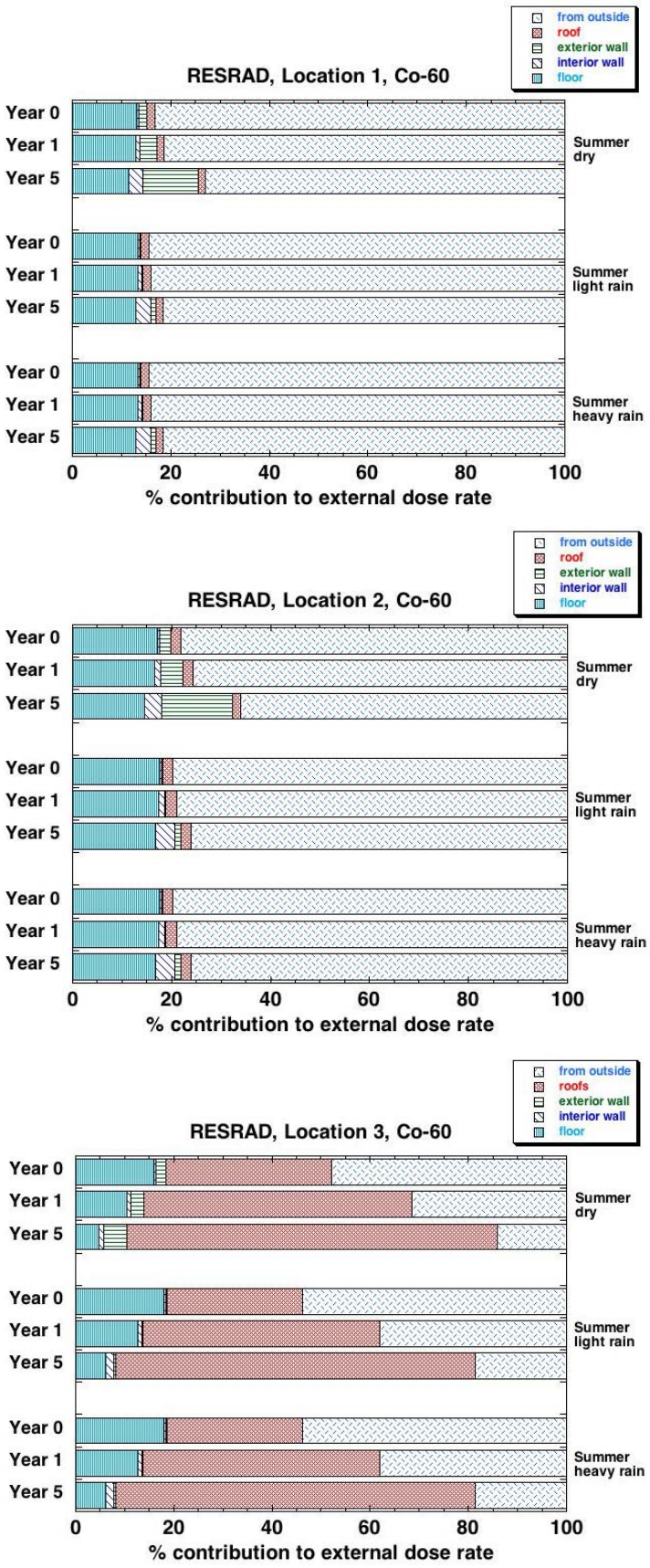

FIG. 4.26. Percent contributions to the predicted external dose rates from ^{60}Co from specified surfaces at indoor locations, shown for RESRAD-RDD, for the indicated time points and release conditions.

4.3.5. Doses

Annual and cumulative doses (up to five years) were predicted for each of two exposure scenarios, for the 'no countermeasures' scenario (without protective actions, including remedial actions). The exposure scenario in Region 1 (a business area) assumed an adult who was spending 40 hours per week indoors (at work) and 5 hours per week outside the building (lunch breaks). Specified inhalation rates were assumed to be 0.5 m^3/h indoors (sitting) and 1 m^3/h outdoors (standing or walking). The exposure scenario in Region 2 (a park area) assumed an adult exercising in the park for 3 hours per week (0.5 hours per day, 6 days per week). The specified inhalation rate was assumed to be 1.5 m^3/h (moderate exercise).

Predicted annual and cumulative doses are provided in Appendix VII (Tables VII.15 to VII.24) for external doses and inhalation doses. The discussion in this section is restricted to the cumulative doses, which depended primarily (and in some cases, totally) on the dose received during the first year. In other words, the annual doses after the first year were much smaller than the annual dose during the first year following the deposition event.

The main focus of the scenario, and hence, of this discussion, is external gamma doses from ^{60}Co and inhalation (internal) doses from ^{239}Pu. All participants also calculated inhalation doses from ^{60}Co, and three participants (ERMIN, CPHR, RESRAD-RDD) also calculated external doses from ^{239}Pu; these are discussed briefly in the following Sections 4.3.5.1 and 4.3.5.2.

4.3.5.1. External doses from Cobalt-60 and Plutonium-239

Predicted cumulative external doses from ^{60}Co after 1 year and 5 years post-deposition are shown in Fig. 4.27 for different initial weather conditions (dry, light rain (3 mm/d), or heavy rain (20 mm/d)), for a summer release. Tabulated results for ^{239}Pu for three models, ERMIN, CPHR and RESRAD-RDD are given in Appendix VII, Tables VII.16 to VII.18, respectively).

For ^{60}Co, consistent with the predictions for contamination densities and external dose rates, predicted cumulative external doses were higher under conditions of wet deposition than for dry deposition (heavy rain > light rain >> dry). Differences in cumulative external doses between summer and winter releases predicted by METRO-K and ERMIN were small or negligible (Tables VII.15 and VII.16). Predicted cumulative external doses for Region 2 (the park area) were very similar amongst four models (METRO-K, ERMIN, RESRAD-RDD and CHERURB), reflecting similar predicted radionuclide behavior at Location 5 (the centre of the park). Cumulative external doses predicted for Region 1 (the business area) showed more variability amongst models, reflecting the contribution from time spent indoors, as well as outdoors. This is because, in general, predicted external dose rates at indoor locations (Figs 4.14 to 4.16) varied more widely amongst models than did those at outdoor locations (Figs 4.17 to 4.19), reflecting differences amongst models in their treatment of surfaces contributing to external dose rates at indoor locations. For RESRAD-RDD, CPHR, and CHERURB, predicted cumulative external doses were higher in Region 1 than in Region 2, while for METRO-K and ERMIN, predicted cumulative external doses were higher in Region 2 than in Region 1.

As for predicted deposition and internal dose, predicted external doses for ^{239}Pu were higher for wet deposition than for dry deposition. Predictions made using ERMIN were higher in Region 2 than in Region 1, while those made using CPHR were higher in Region 1 and those made using RESRAD-RDD were similar for the two regions.

4.3.5.2. Internal doses from Cobalt-60 and Plutonium-239

Predicted cumulative inhalation doses from ^{60}Co (Fig. 4.28) and ^{239}Pu (Fig. 4.29) were predicted by all five models. The predicted cumulative internal doses from ^{239}Pu reflect either the inhalation dose from the initial plume (CPHR and CHERURB) or the inhalation dose from resuspension (METRO-K, ERMIN, and RESRAD-RDD). None of the models used in this exercise included both the initial plume and resuspension. This leads to very different predictions of inhalation doses across these two groups of models for this exercise.

For ^{60}Co, the predicted inhalation doses from resuspension were three to four orders of magnitude lower than the corresponding predicted external doses from ^{60}Co for METRO-K, ERMIN, and RESRAD-RDD. For CHERURB, predicted cumulative internal doses from ^{60}Co were approximately a factor of 2 to 4000 less than the corresponding predicted external doses. For CPHR, the predicted cumulative internal doses from ^{60}Co were a factor of 2.5 to 15 greater than the corresponding predicted external doses in Region 1 and a factor of 8 to 24 greater in Region 2. The CHERURB and CPHR models predict much higher inhalation doses than the other three models due to inclusion of inhalation from the initial plume, these inhalation doses being much higher than those from resuspension (see Fig. 4.28). ERMIN and RESRAD-RDD use a similar resuspension factor and the predicted doses were in general similar, reflecting the similar predicted deposition, particularly for dry deposition and deposition during light rain. The METRO-K model assumes a resuspension factor about a factor of 10 higher than ERMIN and RESRAD-RDD, which in general leads to higher inhalation doses being predicted compared to the other models. Consistent with the predicted deposition and predicted external doses, predicted inhalation doses from resuspension for ^{60}Co and ^{239}Pu (METRO-K, ERMIN, RESRAD-RDD) were higher under conditions of wet deposition than for dry deposition (heavy rain > light rain > dry). The predicted inhalation dose from the initial plume (CHERURB) did not vary with initial weather conditions for both ^{60}Co and ^{239}Pu.

Predictions of inhalation doses for ^{239}Pu made using CPHR and CHERURB indicate that tall the inhalation dose was received early on, i.e. from the initial plume, and the cumulative doses after 1 year or 5 years were the same. For the other three models that considered inhalation doses from resuspension, much or most of the cumulative inhalation dose was received during the first year, with only small additional contributions to the cumulative dose after the first year. For both CPHR and CHERURB, the predicted cumulative inhalation dose in Region 1 was higher than that in Region 2, substantially so for CPHR. Cumulative inhalation doses from resuspended materials that were predicted using ERMIN and RESRAD-RDD were higher in Region 1 than in Region 2 by about an order of magnitude. METRO-K predicted higher cumulative internal doses in Region 2 than in Region 1 by about an order of magnitude under dry initial conditions, but only slightly higher doses were predicted in Region 2 than in Region 1 under initial conditions of light or heavy rain.

Predicted cumulative inhalation doses from ^{239}Pu (see Appendix VII, Tables VII.16 to VII.18) were several orders of magnitude higher than the predicted cumulative external doses from ^{239}Pu, for any given model, consistent with the very low external dose coefficient for ^{239}Pu compared to the inhalation dose coefficient.

4.3.5.3. General comments

In general, the relative predicted external doses for a given model for the different locations and exposure scenarios were consistent with the predicted contamination densities and external dose rates. For example, higher predicted external doses under conditions of wet deposition versus dry deposition corresponded to higher predicted contamination densities under conditions of wet deposition versus dry deposition. Predicted inhalation doses from resuspension (METRO-K, ERMIN, RESRAD-RDD) were also consistent with predicted contamination densities, as resuspension is usually predicted as a function of the contaminated material on the soil or other exposed surfaces. Thus, inhalation doses that were predicted using these models were higher under conditions of wet deposition versus dry deposition.

Inhalation doses that had been predicted from the initial plume, without consideration of resuspension, were dependent only on the plume, and not on conditions of deposition (wet versus dry). Thus, predictions of internal dose from the plume (CHERURB) did not vary with initial weather conditions. The predicted inhalation doses by CHERURB and CPHR from the initial plume were much higher than those from resuspension predicted by METRO-K, ERMIN and RESRAD-RDD.

Comparisons of predicted external doses between Region 1 (the business area) and Region 2 (the park area) are complex functions of predicted external dose rates (dependent, in turn, on predicted contamination densities) from various surfaces, the importance of each surface to the total external dose rate at a location, and assumptions about time spent at a given location. There are not necessarily clear reasons for predicted external doses being higher in Region 1 than Region 2 for some models, or for the reverse being predicted for other models. For models predicting inhalation doses from resuspension (METRO-K, ERMIN, RESRAD-RDD), the same considerations would apply, as the resuspension depends on the predicted contamination densities at each location, as well as predicted changes in contamination densities and resuspension factors over time. For the models predicting inhalation doses only from the initial plume (CPHR and CHERURB), differences in predicted internal doses in the two regions are probably related to the assumptions about time spent at a given location.

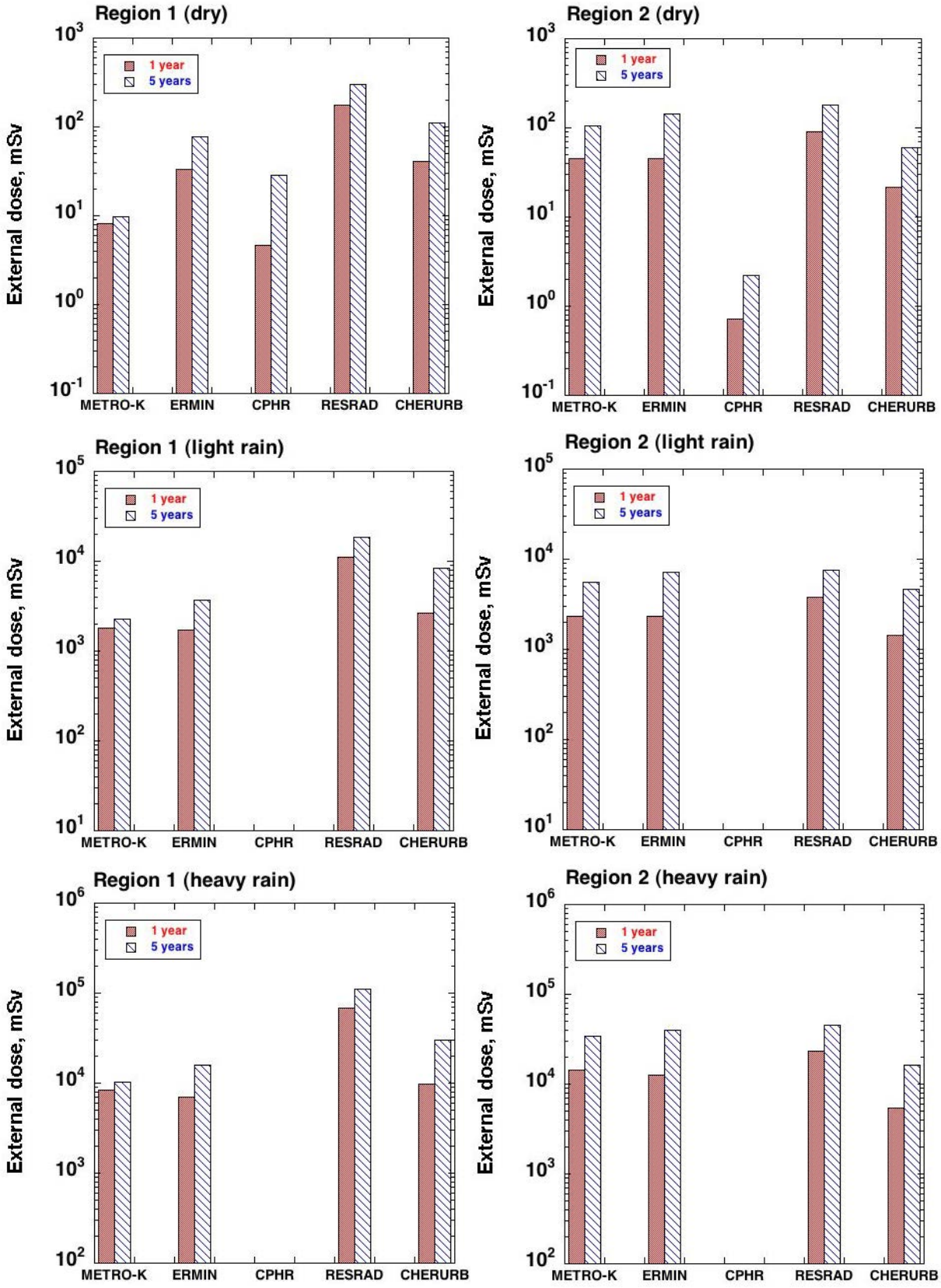

FIG. 4.27. Predicted cumulative external doses (mSv) from ^{60}Co during the first year and the first 5 years after the deposition event in Region 1 (left; business area) and Region 2 (right; park area). Predictions are shown for initial conditions in summer of dry weather (top), light rain (centre), and heavy rain (bottom).

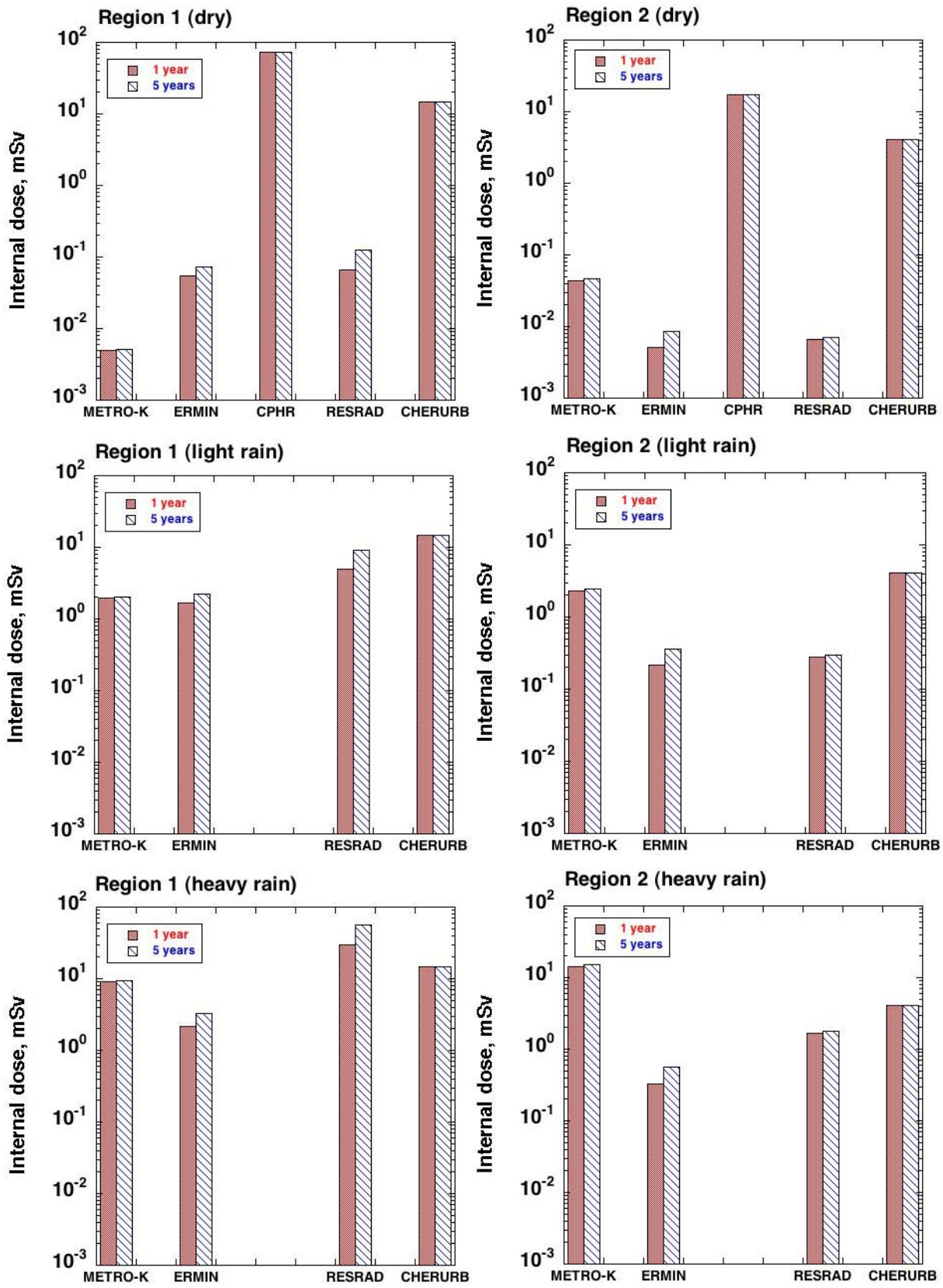

FIG. 4.28. Predicted cumulative inhalation doses (mSv) from ^{60}Co during the first year and the first 5 years after the deposition event in Region 1 (left; business area) and Region 2 (right; park area). Predictions are shown for initial conditions in summer of dry weather (top), light rain (centre), and heavy rain (bottom).

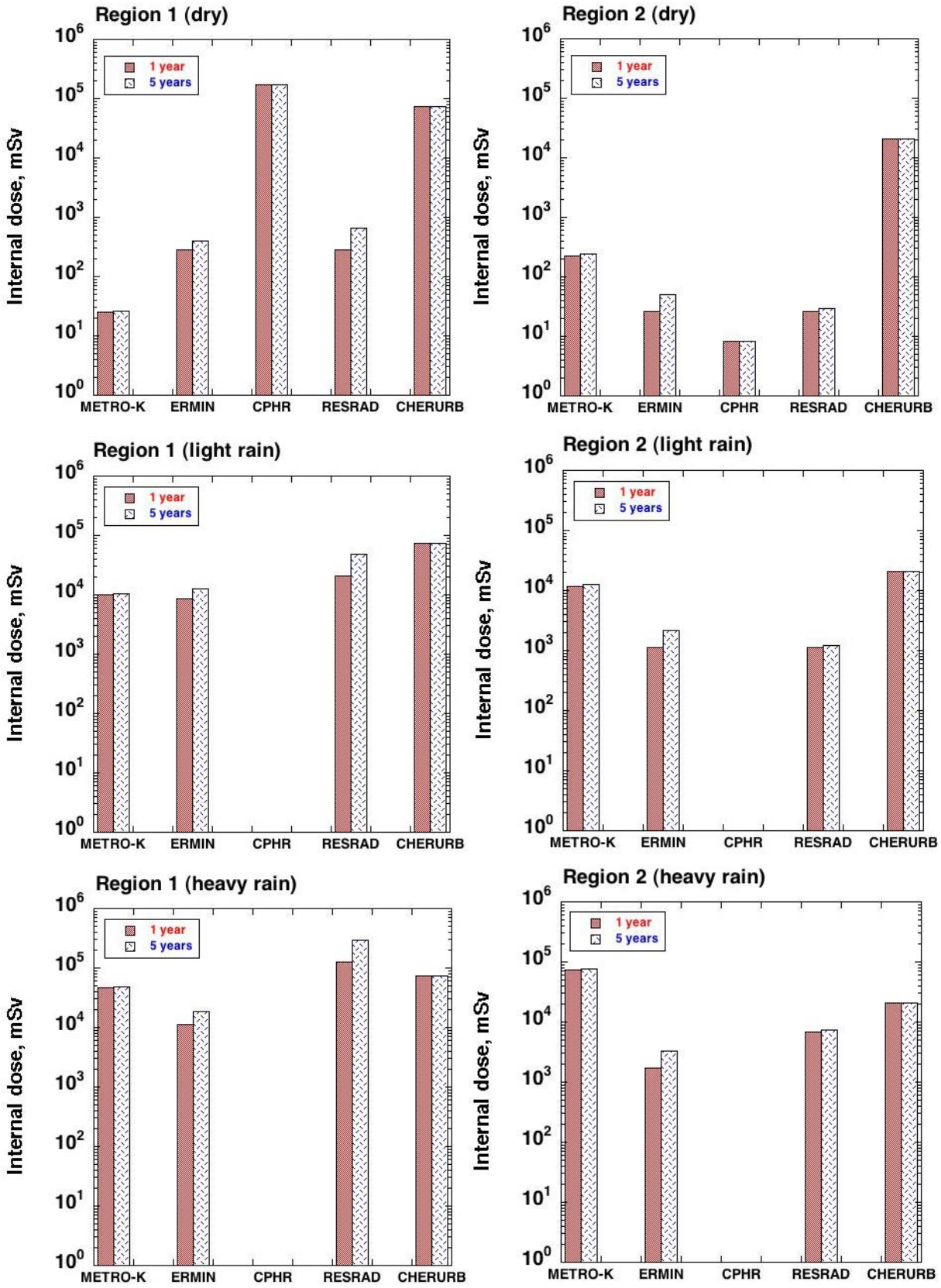

FIG. 4.29. Predicted cumulative inhalation doses (mSv) from ^{239}Pu during the first year and the first 5 years after the deposition event in Region 1 (left; business area) and Region 2 (right; park area). Predictions are shown for initial conditions in summer of dry weather (top), light rain (centre), and heavy rain (bottom).

4.3.6. Effectiveness of countermeasures

This section describes the predicted effectiveness of various countermeasures in terms of the reduction in cumulative external doses from ^{60}Co and inhalation doses from ^{239}Pu (discussed in Section 4.3.5) during the first year after the deposition event and during the first five years after the deposition event, for two specified exposure scenarios (described in Section 4.3.5 and Appendix V).

Tables 4.5 to 4.7 provide the predicted cumulative external doses from ^{60}Co during the first year and the first five years following a ^{60}Co release during the summer, under different weather conditions at the time of initial deposition (dry, light rain, assumed to be 3 mm/d; and heavy rain, assumed to be 20 mm/d; see Section 4.1 and Appendix V), assuming no countermeasures. Equivalent tables for cumulative inhalation doses following a release of ^{239}Pu during the summer are given in Tables 4.8 to 4.10. In addition, the tables present examples of the percent reduction in predicted cumulative external doses expected during the first year and the first five years following the deposition event, assuming application of specified countermeasures. These countermeasures include temporary relocation (six weeks), tree removal, soil and grass removal, road cleaning (vacuuming or sweeping), road cleaning (washing or hosing), washing of roofs and exterior walls, tree removal plus road cleaning, and relocation plus road cleaning (as described in Appendix V). Predictions for radioactive releases under dry initial conditions (Tables 4.5 and 4.8) were made using all five models (METRO-K, ERMIN, CPHR, RESRAD-RDD, CHERURB), and predictions under initial conditions of light rain (Tables 4.6 and 4.9) and heavy rain (Tables 4.7 and 4.10) were made using four models (METRO-K, ERMIN, RESRAD-RDD, CHERURB). The predicted doses are for defined exposure scenarios in either Region 1 (business area) or Region 2 (park area), as described in Section 4.3.5 and Appendix V.

4.3.6.1. Relocation

All models predicted a reduction in cumulative internal (inhalation) dose from ^{60}Co due to relocation of the population for the first six weeks following the deposition event. In Region 1, the predicted effectiveness of relocation, in terms of percent reduction of the cumulative external dose from indoor and outdoor surfaces, ranged from 11% to 47% during the first year after the deposition and from 6% to 28% during the first five years, under dry initial conditions (Table 4.5). In Region 2, the predicted effectiveness of relocation, assuming contributions to external dose from only outdoor surfaces, ranged from 8% to 33% during the first year and from 4% to 11% during the first five years, under dry initial conditions. For METRO-K in Region 2 and for ERMIN, RESRAD-RDD, and CHERURB in both regions, the predicted effectiveness of relocation for six weeks had little or no dependence on the initial weather conditions (dry, light rain, heavy rain) at the time of the deposition event. METRO-K predicted a 28–34% reduction in the cumulative external dose in Region 1 under dry initial conditions, but a lower effectiveness in external dose reduction under wet initial conditions (19–23% reduction under light rain conditions and 23–29% reduction under heavy rain conditions; see Tables 4.5 to 4.7).

4.3.6.2. Other Countermeasures: Effectiveness in reducing external dose (Cobalt-60)

For the other countermeasures included in Tables 4.5 to 4.7, their effectiveness in reducing cumulative external doses from ^{60}Co depended greatly on the predicted contribution of the surface to the cumulative external dose, prior to their implementation. For example, in Region 1, a business area with little or no expected contribution to external dose from soil or grass surfaces, removal of soil and grass had no effect on predicted cumulative external dose.

However, in Region 2, a park area with primarily unpaved surfaces contributing to external dose, removal of soil and grass was predicted to reduce the cumulative external dose by 46 to 87% during the first year after the deposition event and by 56 to 92% during the first five years after the deposition event, under dry initial conditions; similar reductions were predicted under conditions of wet deposition for most models considered (METRO-K, ERMIN, and RESRAD-RDD). By comparison, the CHERURB model predicted a higher effectiveness in reduction of cumulative external dose for initial deposition under wet conditions (88–89% reduction during the first five years after the deposition event) than for initial deposition under dry conditions (56% reduction during the first five years after the deposition event).

The opposite results are seen for countermeasures involving the cleaning of roads (vacuuming or washing); reductions in cumulative external dose of up to 44% (RESRAD-RDD for dry initial conditions) to 68% (METRO-K for wet initial conditions) were predicted in Region 1, whereas little or no reduction in cumulative external dose was predicted in Region 2. For all models, washing or hosing roads was more effectives than vacuuming or sweeping. Washing of roofs and walls was predicted to result in small reductions in cumulative external dose in Region 1, ranging from 2 to 16% (METRO-K, ERMIN, RESRAD-RDD, CHERURB, depending on initial weather conditions) on the lower end of the range and from 27 to 38% (CPHR, dry conditions) on the higher end of the range. Essentially no reduction (0–3%) in cumulative external dose in Region 2 was predicted to result from washing of roofs and walls.

The effectiveness of removing trees in terms of reduction in cumulative external dose varied amongst models, depending on the expected contribution of trees to the external dose. For example, METRO-K predicted a 28% reduction in cumulative external dose in Region 1 during the first year after the deposition event due to removal of trees (for dry deposition), whereas ERMIN and CHERURB predicted 10% and 3% reductions in cumulative external dose, respectively, in Region 1, for the same time period. Predicted reductions in cumulative external dose for Region 2 under dry initial conditions and for either Region 1 or 2 under wet initial conditions, ranged from 0 to 7% for the METRO-K, ERMIN, and CHERURB models. CPHR predicted no reduction in cumulative external dose in Region 1 due to removal of trees and predicted a 5 to 6% reduction in cumulative external dose in Region 2. RESRAD-RDD does not include trees as a specific contributor to external doses, and therefore did not predict the effect of tree removal on cumulative external dose.

Two combinations of countermeasures were assessed, tree removal plus road cleaning, and relocation plus road cleaning (Tables 4.5 to 4.7). In Region 1, where both trees and road surfaces contributed to predicted external doses, the combination of tree removal plus road cleaning resulted in approximately additive reductions in cumulative external doses (13–66% total reductions in cumulative external doses for dry initial conditions, and 27–71% total reductions in cumulative external doses for wet initial conditions), since the contributions to cumulative external dose from two separate surfaces were both reduced. In Region 2, predicted reductions in cumulative external doses for the combination of tree removal plus road cleaning ranged from 1–6% (METRO-K and ERMIN, wet or dry initial conditions) to 14–19% (CHERURB, dry initial conditions).

The combination of relocation plus road cleaning resulted in overall reductions in the predicted cumulative external doses that were less than the sum of the dose reductions predicted for the two individual countermeasures. Relocation reduces the amount of time a person can be exposed to contaminated surfaces in general, whereas road cleaning reduces the contribution to external dose rate from one surface, thereby reducing the cumulative external dose received, but only during the time a person was not relocated. In Region 1, the combination of relocation

plus road cleaning resulted in predicted reductions in cumulative external dose of 23 to 64% under dry initial conditions and 8 to 83% under wet initial conditions (Tables 4.5 to 4.7). The METRO-K, ERMIN, and RESRAD-RDD models predicted that the reductions in the cumulative external dose in Region 2 due to road cleaning were only 0 to 3%, and the reductions in the predicted cumulative external dose due to the combination of relocation and road cleaning (4–17%) were only slightly larger than the predicted dose reductions due only to relocation (4–16%); the road surfaces do not contribute greatly to cumulative external doses in Region 2, and therefore, cleaning the roads will not produce much reduction in the predicted cumulative external doses. CHERURB predicted 11 to 15% reductions in cumulative external doses from road cleaning for dry initial conditions in Region 2, and hence predicted 24 to 37% reductions in cumulative external doses in Region 2 due to the combination of relocation and road cleaning.

4.3.6.3. Other Countermeasures: Effectiveness in reducing internal inhalation dose (Plutonium-239)

For cumulative inhalation doses from ^{239}Pu (Tables 4.8 to 4.10), the effectiveness of countermeasures depended on the exposure pathways included in the dose calculation. Two models (CPHR and CHERURB) included inhalation exposures from the initial plume. Three models (METRO-K, ERMIN, RESRAD-RDD) included inhalation exposures from resuspension of material from contaminated surfaces. None of the models in this exercise included both routes of exposure. Thus, for two models (CPHR and CHERURB), the predicted cumulative inhalation doses were contributed only by the inhalation exposure from the initial plume. Therefore, temporary relocation (six weeks in this exercise) entirely eliminated the predicted cumulative inhalation dose. The other countermeasures reduced contamination densities on various surfaces but did not have an effect on the initial plume, and therefore this led to much lower reductions in cumulative inhalation does compared to those predicted by CPHR and CHERURB.

For the models that considered only resuspension (METRO-K, ERMIN, and RESRAD-RDD), relocation for six weeks was predicted to reduce cumulative inhalation doses by 8 to 33% (METRO-K, ERMIN, RESRAD-RDD; all initial weather conditions). However, in contrast to the case with models that include only the dose from the initial plume, countermeasures that reduce the contamination available for resuspension are potentially effective in reducing the predicted cumulative inhalation doses, depending on the importance of a given surface in contributing to the exposure to resuspended material for a given model. For example, in Region 1, METRO-K predicted a 52 to 70% reduction in the cumulative inhalation dose due to cleaning of roads, but no reduction in cumulative inhalation dose in Region 2 due to cleaning of roads. In contrast, METRO-K predicted that removal of soil and grass would reduce the cumulative inhalation doses from ^{239}Pu by 76% in Region 2, compared to 0% in Region 1. For the ERMIN model, predicted reductions in cumulative inhalation doses due to road cleaning were 1 to 13% in Region 1 (depending on initial weather conditions) and 1 to 10% in Region 2 (also depending on initial weather conditions), whereas dose reductions due to removal of soil and grass were 20 to 52% (depending on initial weather conditions) in Region 2 and 0% in Region 1. For RESRAD-RDD, predicted reductions in cumulative inhalation doses due to road cleaning were 6 to 16% in Region 1 and 0% in Region 2, whereas dose reductions due to removal of soil and grass were 44 to 49% in Region 2 and 0% in Region 1. ERMIN also predicted a 24 to 31% reduction in cumulative inhalation dose under dry initial conditions in Region 2 due to removal of trees, decreasing to 18 to 23% under initial light rain conditions and 15 to 19% under initial heavy rain conditions, but only a 1 to 2% reduction in cumulative inhalation doses were predicted in Region 1 due to fewer trees present in the scenario modelled.

The combination of tree removal and road cleaning made a difference in predicted cumulative inhalation dose only for ERMIN, which was the only model that predicted a reduction in cumulative inhalation dose due to removal of trees. As mentioned above, the percent reduction in cumulative inhalation dose in Region 2 due to removal of trees decreased from 24–31% under dry initial conditions, to 18–23% under initial light rain conditions, to 15–19% under initial heavy rain conditions; however, the dose reduction in Region 2 due to road cleaning increased from 1–2% under dry initial conditions, to 3–4% under initial light rain conditions, to 7–10% under initial heavy rain conditions. Thus, the effectiveness of the combined countermeasures was similar for all initial weather conditions (i.e. 26–33% under dry initial conditions, 21–27% under initial light rain conditions, and 23–29% under initial heavy rain conditions).

For all three models (METRO-K, ERMIN, RESRAD-RDD), reductions in cumulative inhalation doses in Region 2 that were only slightly larger than those for relocation alone were predicted for the combination of relocation and road cleaning because road cleaning had little or no effect on predicted cumulative inhalation doses in Region 2 (0–10%, as described above). However, in Region 1, where road cleaning was predicted to cause a larger reduction in cumulative inhalation doses (up to 70% for METRO-K), the combined effect of relocation and road cleaning was predicted to result in a larger reduction than either single countermeasure, but less than the sum of the individual dose reductions. The METRO-K model predicted that the combination of relocation and road cleaning resulted in a reduction in predicted cumulative inhalation dose in Region 1 of 86 to 87% (all initial weather conditions); the corresponding predicted dose reductions are 17 to 40% for ERMIN (depending on initial weather conditions) and 13 to 30% for RESRAD-RDD (depending on initial weather conditions).

As described previously for ^{60}Co (Section 4.3.6), relocation reduces the amount of time a person can be exposed to resuspended contaminated material, whereas road cleaning reduces the contribution to resuspension from paved surfaces, thereby reducing the cumulative inhalation dose from resuspension, but only during the time a person was not relocated. Thus, the two individual dose reductions cannot simply be added; in fact, for the METRO-K model, if added, the sum of the dose reductions for the two individual countermeasures would exceed 100%.

TABLE 4.5. EXAMPLES OF PREDICTED EFFECTIVENESS OF COUNTERMEASURES FOR CUMULATIVE EXTERNAL DOSES FROM Co-60, ASSUMING DRY INITIAL CONDITIONS IN SUMMER

Model	Time period	Cumulative external dose (mSv), No action	Countermeasure, % reduction in cumulative external dose							
			Relocation (6 weeks)	Tree removal	Soil and grass removal	Vacuuming or sweeping roads	Washing or hosing roads	Washing roofs and walls	Tree removal plus road cleaning	Relocation plus road cleaning
Region 1 (business area)										
METRO-K	1 year	8.2×10^{0}	34	28	0	28	38	4	66	64
	5 years	9.9×10^{0}	28	23	0	30	40	9	64	55
ERMIN	1 year	3.3×10^{1}	19	10	0.04	15	17	9	26	33
	5 years	7.8×10^{1}	8	6	0.02	10	11	13	17	18
CPHR	1 year	4.7×10^{0}	47	0	–[a]	0	8	38	–[a]	–[a]
	5 years	2.9×10^{1}	16	0	–[a]	1	39	27	–[a]	–[a]
RESRAD-RDD	1 year	1.7×10^{2}	11	–[a]	0	27	44	13	–[a]	51
	5 years	3.0×10^{2}	6	–[a]	0	23	37	16	–[a]	41
CHERURB	1 year	4.1×10^{1}	28	3	–[a]	4	10	3	13	36
	5 years	1.1×10^{2}	10	5	–[a]	5	14	5	18	23
Region 2 (park area)										
METRO-K	1 year	4.6×10^{1}	16	4	72	0	0	0	5	16
	5 years	1.1×10^{2}	7	2	77	0	0	0	3	7
ERMIN	1 year	4.5×10^{1}	16	5	50	2	2	1	6	17
	5 years	1.4×10^{2}	5	2	74	1	1	0	3	6
CPHR	1 year	7.3×10^{-1}	33	5	–[a]	0	0	0	–[a]	–[a]
	5 years	2.2×10^{0}	11	6	–[a]	0	0	0	–[a]	–[a]
RESRAD-RDD	1 year	9.1×10^{1}	8	–[a]	87	0	0	0	–[a]	8
	5 years	1.8×10^{2}	4	–[a]	92	0	0	0	–[a]	4
CHERURB	1 year	2.2×10^{1}	28	3	46	4	11	1	14	37
	5 years	6.0×10^{1}	10	5	56	6	15	3	19	24

[a] Endpoint not included by participant.

TABLE 4.6. EXAMPLES OF PREDICTED EFFECTIVENESS OF COUNTERMEASURES FOR CUMULATIVE EXTERNAL DOSES FROM Co-60, ASSUMING INITIAL CONDITIONS OF LIGHT RAIN IN SUMMER

Model	Time period	Cumulative external dose (mSv) No action	Countermeasure, % reduction in cumulative external dose							
			Relocation (6 weeks)	Tree removal	Soil and grass removal	Vacuuming or sweeping roads	Washing or hosing roads	Washing roofs and walls	Tree removal plus road cleaning	Relocation plus road cleaning
Region 1 (business area)										
METRO-K	1 year	1.8×10^3	23	4	0	50	67	2	71	83
	5 years	2.3×10^3	19	7	0	51	68	3	71	80
ERMIN	1 year	1.7×10^3	19	6	0.06	30	33	4	39	47
	5 years	3.7×10^3	9	4	0.03	21	23	7	27	30
RESRAD-RDD	1 year	1.1×10^4	11	–[a]	0	31	50	9	–[a]	57
	5 years	1.9×10^4	7	–[a]	0	28	44	12	–[a]	48
CHERURB	1 year	2.6×10^3	25	0	–[a]	–[a]	–[a]	–[a]	0	25
	5 years	8.4×10^3	8	0	–[a]	–[a]	–[a]	–[a]	0	8
Region 2 (park area)										
METRO-K	1 year	2.4×10^3	15	2	75	0	0	0	2	15
	5 years	5.6×10^3	6	1	78	0	0	0	1	6
ERMIN	1 year	2.3×10^3	16	3	41	3	3	1	6	17
	5 years	7.2×10^3	5	1	74	1	1	0.2	3	6
RESRAD-RDD	1 year	3.8×10^3	8	–[a]	87	0	0	0	–[a]	8
	5 years	7.5×10^3	4	–[a]	92	0	0	0	–[a]	4
CHERURB	1 year	1.5×10^3	26	0	85	–[a]	–[a]	–[a]	0	26
	5 years	4.6×10^3	8	0	89	–[a]	–[a]	–[a]	0	8

[a] Endpoint not included by participant.

TABLE 4.7. EXAMPLES OF PREDICTED EFFECTIVENESS OF COUNTERMEASURES FOR CUMULATIVE EXTERNAL DOSES FROM Co-60, ASSUMING INITIAL CONDITIONS OF HEAVY RAIN IN SUMMER

Model	Time period	Cumulative external dose (mSv), No action	Countermeasure, % reduction in cumulative external dose							
			Relocation (6 weeks)	Tree removal	Soil and grass removal	Vacuuming or sweeping roads	Washing or hosing roads	Washing roofs and walls	Tree removal plus road cleaning	Relocation plus road cleaning
Region 1 (business area)										
METRO-K	1 year	8.4×10^3	29	4	0	50	67	2	71[b]	82
	5 years	1.0×10^4	23	4	0	51	68	3	72[b]	80
ERMIN	1 year	7.0×10^3	18	3	0	35	38	3	41[b]	50
	5 years	1.6×10^4	8	2	0	24	26	5	28[b]	31
RESRAD-RDD	1 year	6.8×10^4	11	–[a]	0	31	50	9	–[a]	57
	5 years	1.1×10^5	7	–[a]	0	28	44	12	–[a]	48
CHERURB	1 year	9.9×10^3	25	0	–[a]	–[a]	–[a]	–[a]	0	25
	5 years	3.0×10^4	8	0	–[a]	–[a]	–[a]	–[a]	0	8
Region 2 (park area)										
METRO-K	1 year	1.4×10^4	15	2	76	0	0	0	2	15
	5 years	3.4×10^4	7	1	78	0	0	0	1	7
ERMIN	1 year	1.3×10^4	14	1	41	2	2	0.16	3	16
	5 years	4.0×10^4	5	0.5	76	1	1	0.05	1	5
RESRAD-RDD	1 year	2.3×10^4	8	–[a]	87	0	0	0	–[a]	8
	5 years	4.6×10^4	4	–[a]	92	0	0	0	–[a]	4
CHERURB	1 year	5.4×10^3	26	0	83	–[a]	–[a]	–[a]	0	26
	5 years	1.6×10^4	9	1	88	–[a]	–[a]	–[a]	1	19

a Endpoint not included by participant.

[b] Assumed reduction for road cleaning was washing/hosing.

TABLE 4.8. EXAMPLES OF PREDICTED EFFECTIVENESS OF COUNTERMEASURES FOR CUMULATIVE INHALATION DOSES FROM Pu-239, ASSUMING DRY INITIAL CONDITIONS IN SUMMER

Model	Time period	Cumulative internal dose (mSv), No action	Countermeasure, % reduction in cumulative internal dose							
			Relocation (6 weeks)	Tree removal	Soil and grass removal	Vacuuming or sweeping roads	Washing or hosing roads	Washing roofs and walls	Tree removal plus road cleaning	Relocation plus road cleaning
Region 1 (business area)										
METRO-K	1 year	2.6×10^{1}	33	0	0	52	70	0	70	87
	5 years	2.6×10^{1}	32	0	0	52	70	0	70	86
ERMIN	1 year	2.9×10^{2}	22	1	0	1	1	4	2	22
	5 years	4.0×10^{2}	16	1	0	1	1	6	3	17
CPHR	1 year	1.7×10^{5}	100	–[a]	–[a]	–[a]	–[a]	–[a]	–[a]	–[a]
	5 years	1.7×10^{5}	100	–[a]	–[a]	–[a]	–[a]	–[a]	–[a]	–[a]
RESRAD-RDD	1 year	2.9×10^{2}	19	–[a]	0	14	16	0	–[a]	30
	5 years	6.6×10^{2}	8	–[a]	0	6	7	0	–[a]	13
CHERURB	1 year	7.2×10^{4}	100	–[a]	–[a]	–[a]	–[a]	–[a]	–[a]	–[a]
	5 years	7.2×10^{4}	100	–[a]	–[a]	–[a]	–[a]	–[a]	–[a]	–[a]
Region 2 (park area)										
METRO-K	1 year	2.2×10^{2}	27	0	76	0	0	0	0	27
	5 years	2.4×10^{2}	26	0	76	0	0	0	0	26
ERMIN	1 year	2.6×10^{1}	43	24	43	1	1	0	26	39
	5 years	4.9×10^{1}	23	31	52	1	2	0	33	22
CPHR	1 year	8.4×10^{0}	100	–[a]	–[a]	–[a]	–[a]	–[a]	–[a]	–[a]
	5 years	8.4×10^{0}	100	–[a]	–[a]	–[a]	–[a]	–[a]	–[a]	–[a]
RESRAD-RDD	1 year	2.7×10^{1}	66	–[a]	44	0	0	0	–[a]	66
	5 years	2.9×10^{1}	60	–[a]	49	0	0	0	–[a]	60
CHERURB	1 year	2.1×10^{4}	100	–[a]	–[a]	–[a]	–[a]	–[a]	–[a]	–[a]
	5 years	2.1×10^{4}	100	–[a]	–[a]	–[a]	–[a]	–[a]	–[a]	–[a]

[a] Endpoint not included by participant.

TABLE 4.9. EXAMPLES OF PREDICTED EFFECTIVENESS OF COUNTERMEASURES FOR CUMULATIVE INHALATION DOSES FROM Pu-239, ASSUMING INITIAL CONDITIONS OF LIGHT RAIN IN SUMMER

Model	Time period	Cumulative internal dose (mSv), No action	Countermeasure, % reduction in cumulative internal dose							
			Relocation (6 weeks)	Tree removal	Soil and grass removal	Vacuuming or sweeping roads	Washing or hosing roads	Washing roofs and walls	Tree removal plus road cleaning	Relocation plus road cleaning
Region 1 (business area)										
METRO-K	1 year	1.0×10^4	33	0	0	52	70	0	70	87
	5 years	1.1×10^4	32	0	0	52	70	0	70	86
ERMIN	1 year	8.7×10^3	25	1	0	2	3	6	4	26
	5 years	1.3×10^4	17	1	0	4	4	9	6	20
RESRAD-RDD	1 year	2.1×10^4	19	–[a]	0	14	16	0	–[a]	30
	5 years	4.8×10^4	8	–[a]	0	6	7	0	–[a]	13
CHERURB	1 year	7.2×10^4	100	–[a]	–[a]	–[a]	–[a]	–[a]	–[a]	–[a]
	5 years	7.2×10^4	100	–[a]	–[a]	–[a]	–[a]	–[a]	–[a]	–[a]
Region 2 (park area)										
METRO-K	1 year	1.2×10^4	27	0	76	0	0	0	0	27
	5 years	1.3×10^4	26	0	76	0	0	0	0	26
ERMIN	1 year	1.1×10^3	43	18	42	3	3	0	21	41
	5 years	2.1×10^3	23	23	49	3	4	0	27	24
RESRAD-RDD	1 year	1.1×10^3	66	–[a]	44	0	0	0	–[a]	65
	5 years	1.2×10^3	60	–[a]	49	0	0	0	–[a]	60
CHERURB	1 year	2.1×10^4	100	–[a]	–[a]	–[a]	–[a]	–[a]	–[a]	–[a]
	5 years	2.1×10^4	100	–[a]	–[a]	–[a]	–[a]	–[a]	–[a]	–[a]

[a] Endpoint not included by participant.

TABLE 4.10. EXAMPLES OF PREDICTED EFFECTIVENESS OF COUNTERMEASURES FOR CUMULATIVE INHALATION DOSES FROM Pu-239, ASSUMING INITIAL CONDITIONS OF HEAVY RAIN IN SUMMER

Model	Time period	Cumulative internal dose (mSv), No action	Countermeasure, % reduction in cumulative internal dose							
			Relocation (6 weeks)	Tree removal	Soil and grass removal	Vacuuming or sweeping roads	Washing or hosing roads	Washing roofs and walls	Tree removal plus road cleaning	Relocation plus road cleaning
Region 1 (business area)										
METRO-K	1 year	4.6×10^4	33	0	0	52	70	0	70	87
	5 years	4.8×10^4	32	0	0	52	70	0	70	86
ERMIN	1 year	1.1×10^4	34	1	0	9	10	16	11	40
	5 years	1.9×10^4	20	2	0	12	13	22	15	31
RESRAD-RDD	1 year	1.3×10^5	19	–[a]	0	14	16	0	–[a]	30
	5 years	2.9×10^5	8	–[a]	0	6	7	0	–[a]	13
CHERURB	1 year	7.2×10^4	100	–[a]	–[a]	–[a]	–[a]	–[a]	–[a]	–[a]
	5 years	7.2×10^4	100	–[a]	–[a]	–[a]	–[a]	–[a]	–[a]	–[a]
Region 2 (park area)										
METRO-K	1 year	7.3×10^4	27	0	76	0	0	0	0	27
	5 years	7.8×10^4	26	0	76	0	0	0	0	26
ERMIN	1 year	1.7×10^3	43	15	20	7	8	0	23	45
	5 years	3.2×10^3	23	19	43	8	10	0	29	29
RESRAD-RDD	1 year	6.7×10^3	66	–[a]	44	0	0	0	–[a]	66
	5 years	7.3×10^3	60	–[a]	49	0	0	0	–[a]	60
CHERURB	1 year	2.1×10^4	100	–[a]	–[a]	–[a]	–[a]	–[a]	–[a]	–[a]
	5 years	2.1×10^4	100	–[a]	–[a]	–[a]	–[a]	–[a]	–[a]	–[a]

[a] Endpoint not included by participant.

4.4. CONCLUSIONS FROM THE CONTAMINANT TRANSPORT AND COUNTERMEASURES EXERCISE

The contaminant transport and countermeasures exercise provided an opportunity to compare model predictions of deposition densities, external dose rates, and external and internal (inhalation) doses, and to discuss explanations for similarities and differences amongst model predictions [4.2]. Predicted contamination densities and subsequent modelling endpoints in this exercise were highly dependent on weather conditions at the time of deposition (especially wet versus dry conditions) but were not greatly dependent on seasonality (summer versus winter). As anticipated, differences in the surfaces contributing to external dose rates were predicted between the business area (Region 1) and the park area (Region 2) by the five models participating in the exercise, which subsequently influenced the external and inhalation doses predicted.

In general, the predicted effectiveness of countermeasures (protective actions, including remedial actions) implemented on a given surface, in terms of reduction in cumulative external dose, depended on the predicted contribution of that surface to external dose rates and the cumulative external dose. Thus, cleaning of paved surfaces (roads) was predicted as being effective in Region 1 (the business area), with reductions in the external dose over the first year ranging from about 10% to 45% across the five models, while removal grass and soil surfaces was effective in Region 2, the park area, with reductions in external dose in the first year ranging from 45% to 90% between the five models. In selecting a model to be used to evaluate the effectiveness of countermeasures in an urban environment, it is important that the model is able to take into account the deposition onto, and transfer between, the different surfaces (e.g. trees or other individual outdoor surfaces; individual interior surfaces) as a function of time within the environment being considered, and that it is able to take into account the contribution of the activity on these surfaces to the doses received (external or internal (inhalation)). The surfaces that could be important could vary with the location of interest.

For internal dose, models considering only the initial plume (no resuspension) predicted elimination of the internal (inhalation) dose from relocation during the 6 week relocation period after the release event; other countermeasures were not assessed using these models but are not expected to reduce the inhalation dose from the initial plume. Models considering resuspension predicted reductions in internal (inhalation) dose from a variety of countermeasures, such as cleaning of roads (in Region 1) and removal of soil (in Region 2), as well as from relocation. None of the models in this exercise included contributions to inhalation dose from both the initial plume and resuspension; the inclusion of inhalation of the plume in the models depends on the purpose for which the model is to be used. The exercise shows that countermeasures can potentially be useful in reducing inhalation doses, particularly for radionuclides that can give rise to high inhalation doses, for example, ^{239}Pu.

Participants in this exercise started with the same information but produced different predictions for many modelling endpoints. This result is due to differences in model capabilities for a given release and exposure scenario, interpretation of input information, and experience and interests of assessors. Comparing and discussing predictions from several models provides an opportunity for better understanding of model results and can lead to reduced uncertainty in the modelling. The models used in this exercise and similar models, can be used to compare various remediation strategies following a release of radioactive material, and thus, to guide in the setting of priorities and the allocation of resources for specific strategies [4.2].

4.5. REFERENCES TO SECTION 4

[4.1] THIESSEN, K.M., ANDERSSON, K.G., BERKOVSKYY, V., CHARNOCK, T.W., CHOUHAN, S.L., De WITH, G., ĎÚRAN, J., FUKA, V., HELEBRANT, J., HŮLKA, J., HWANG, W.T., KUČA, P., MANCINI, F., NAVARRO, E., PERIÁÑEZ, R., PROUZA, Z., SDOUZ, G., TOMÁS, J., TRIFUNOVIĆ, D., URSO, L., WALTER H., Assessing emergency situations and their aftermath in urban areas: The EMRAS II Urban Areas Working Group, Radioprotection **46** (2011) S601.

[4.2] THIESSEN, K.M., CHARNOCK, T.W., CHOUHAN, S.L., HWANG, W.T., KAMBOJ, S., TOMÁS, J., YU, C., "Modeling the effectiveness of remediation efforts in contaminated urban areas: An EMRAS II Urban Areas Working Group exercise", Proc. of 41st Annual Conference on Waste Management, WM2015, Phoenix, AZ (2015) paper #15631.

[4.3] INTERNATIONAL ATOMIC ENERGY AGENCY, IAEA Safety Glossary: Terminology Used in Nuclear Safety and Radiation Protection: 2018 Edition, IAEA, Vienna (2019).

[4.4] INTERNATIONAL ATOMIC ENERGY AGENCY, Environmental Modelling for Radiation Safety (EMRAS). A Summary Report of the Results of the EMRAS Programme (2003–2007), IAEA-TECDOC-1678, IAEA, Vienna (2012).

[4.5] BROWN, J., MORTIMER, K., ANDERSSON, K., DURANOVA, T., MRSKOVA, A., HÄNNINEN, R., IKÄHEIMONEN, T., KIRCHNER, G., BERTSCH, V., GALLAY, F., REALES, N., HAMMOND, D., KWAKMAN, P., Generic Handbook for Assisting in the Management of Contaminated Inhabited Areas in Europe following a Radiological Emergency, Parts I-VI, EURANOS(CAT1)-TN(07)-02, Luxembourg (2007).

[4.6] GALLAY, F., Modelling the Rehabilitation of Contaminated Urban Environments. Bibliographic Survey, Report IRSN/DEI/SESUC/08-70, Institut de Radioprotection et de Sûreté Nucléaire, Fontenay-aux-Roses (2008).

[4.7] PETERSON, S.-R., CHOUHAN, S., HEINMILLER, B., KOCH, J., CHERURB-95: Urban Contamination and Dose Model, Research report prepared for the Atomic Energy Control Board, Canada (1995).

[4.8] GALLAY, F., Current status of the international experience in modeling the rehabilitation of accidentally contaminated urban environments, Report DEI/SARG/2006-007, Institut de Radioprotection et de Sûreté Nucléaire, Fontenay-aux-Roses (2006).

[4.9] INTERNATIONAL COMMISSION ON RADIOLOGICAL PROTECTION, Compendium of Dose Coefficients based on ICRP Publication 60, Publication 119, Pergamon Press, Oxford and New York (2012).

[4.10] EUROPEAN COMMISSION, FOOD AND AGRICULTURE ORGANIZATION OF THE UNITED NATIONS, INTERNATIONAL ATOMIC ENERGY AGENCY, INTERNATIONAL LABOUR ORGANIZATION, OECD NUCLEAR ENERGY AGENCY, PAN AMERICAN HEALTH ORGANIZATION, UNITED NATIONS ENVIRONMENT PROGRAMME, WORLD HEALTH ORGANIZATION, Radiation Protection and Safety of

Radiation Sources: International Basic Safety Standards, IAEA Safety Standards Series No. GSR Part 3, IAEA, Vienna (2014).

[4.11] CANADIAN STANDARDS ASSOCIATION, Guidelines for Calculating Derived Release Limits for Radioactive Material in Airborne and Liquid Effluents for Normal Operation of Nuclear Facilities, CSA N288.1, CSA Group, Toronto (2008).

[4.12] INTERNATIONAL COMMISSION ON RADIOLOGICAL PROTECTION, Age-Dependent Doses to Members of the Public from Intake of Radionuclides: Part 5 Compilation of Ingestion and Inhalation Dose Coefficients, Publication 72, Pergamon Press, Oxford and New York (1995).

[4.13] MECKBACH, R., JACOB, P., PARETZKE, H.G., Gamma exposures due to radionuclides deposited in urban environments. Part I: Kerma rates from contaminated urban surfaces, Radiation Protection Dosimetry **25** (1988) 167.

[4.14] JACOB, P., MECKBACH, R., Shielding factors and external dose evaluation, Radiation Protection Dosimetry **21** (1987) 79.

[4.15] KIS, Z, EGED, K., VOIGT, G, MECKBACH, R., MUELLER, H., Guidelines for Planning Interventions against External Exposure in Industrial Area after a Nuclear Accident. Part II: Calculation of doses using Monte-Carlo method, GSF-Report 02/03, GSF – National Research Centre for Environment and Health, Institute of Radiation Protection, Munich (2003).

[4.16] ECKERMAN, K.F., RYMAN, J.C., Federal Guidance Report No. 12, External Exposure to Radionuclides in Air, Water, and Soil, EPA-402-R-93-081, U.S. Environmental Protection Agency, Washington, DC (1993).

[4.17] INTERNATIONAL COMMISSION ON RADIOLOGICAL PROTECTION, Conversion Coefficients for use in Radiological Protection against External Radiation, Publication 74, Pergamon Press, Oxford and New York (1996).

5. CONCLUSIONS AND RECOMMENDATIONS

This publication covers the results of three modelling exercises conducted by EMRAS II WG 9: a short range atmospheric dispersion exercise (distances <2 km), a mid-range atmospheric dispersion exercise (distances up to about 70 km), and an exercise dealing with contaminant transport and effectiveness of countermeasures. Each modelling exercise and a detailed description of the exercise scenario is described. Details of the models used by participants in each exercise are given. The results of the exercises, including the model predictions and an intercomparison between the models, are presented and discussed.

In each of the modelling exercises, participants received the same starting information and had the opportunity to discuss how to best use the input information provided. In some cases, there were attempts to agree on specific input information, for example, the dimensions of the initial plume for the field experiments (short range atmospheric dispersion exercise). However, differences in model predictions remained for many of the endpoints predicted by the participants, and in some cases, these were large. The differences in model predictions reflect differences in the purpose and scope of the models, experience of the participants, the types of dispersion modelling used, processes included in the models, interpretation of input information and selection of parameter values. To understand the similarities and differences in results, it is necessary to understand individual modelling approaches and the effects of different assumptions and parameter values on the model results. Comparing and discussing predictions from several models provides an opportunity to better understand the model results and to reduce modelling errors. Although uncertainties in individual model predictions were not estimated for each exercise, the range of results produced by a number of models for each of the exercises is indicative of the overall level of uncertainty that can be expected.

A general recommendation from these model testing exercises is that it is very important that the models chosen are appropriate for the assessment conditions for which they are to be used. In the context of the 'countermeasures' exercise, for example, in selecting a model to be used to evaluate the effectiveness of the implementation of countermeasures in an urban environment, it is important that the model is able to take into account the deposition onto and transfer between the different surfaces as a function of time within the environment being considered and to also take into account the contribution of the activity on these surfaces to the doses received (external or internal (inhalation)). For the atmospheric dispersion models, to the extent possible, the scale (domain size or range) of the model needs to be appropriate for the conditions being modelled.

Atmospheric dispersion models, such as those used in the short range and mid-range exercises, can be valuable tools for planning appropriate emergency preparedness and response actions. The models used in the 'countermeasures' exercise can facilitate comparison of the relative effectiveness of various remediation strategies and countermeasures (protective actions, including remedial actions) in terms of the reduction in external and inhalation doses that can be achieved following the implementation of countermeasures in response to an accidental or intentional event involving the release of radioactive material.

APPENDIX I. SCENARIO DESCRIPTION AND DOCUMENTATION OF DATA FOR THE SHORT RANGE ATMOSPHERIC DISPERSION EXERCISE

I.1. INTRODUCTION

The overall objective of the EMRAS II Urban Areas Working Group ('WG9') was to test and improve the capabilities of models used in assessment of radioactive contamination in urban settings, including dispersion and deposition events, short and long term contaminant redistribution following deposition events, and potential countermeasures or remediation efforts for reducing human exposures and doses. The short range atmospheric dispersion exercise was based on experimental data obtained from the dispersal of a short lived radionuclide (^{99m}Tc) with a small amount of explosive. The exercise was intended to provide an opportunity to test model predictions for a short range dispersion event, including the deposition resulting from the event.

Input information for the exercise included information about each of four explosion events, the amount of radioactivity involved, the arrangement of the various detectors in the vicinity of the explosion, meteorological information, and particle size information. Modelling endpoints for which comparisons with measurements could be made include surface contamination and dose rates as a function of distance, and air concentrations as a function of height and distance. Additional modelling endpoints for intercomparison amongst participants in the exercise include the surface contamination, dose rates, and air concentrations beyond the domain of the measurements, and estimated 50%, 75%, and 95% contamination zones. Additional areas of effort could include validation of location factors[14], use of data assimilation[15] to improve initial modelling results, and estimation of the source term from measurements.

This appendix provides information about the scenario to be modelled (i.e. the input information) and a list of the endpoints to be modelled. Measurements for selected modelling endpoints are also provided. Additional information about the tests was provided to Working Group participants in electronic format.

I.2. DESCRIPTION OF THE EXPERIMENT

Several field tests were performed by the Czech National Radiation Protection Institute (SÚRO) on a test area belonging to the National Institute for Nuclear, Chemical and Biological Protection (SÚJCHBO) in Kamenná, near Prague (Fig. I.1). The radioactive material, a short lived radionuclide in liquid form, was spread by detonation of a small amount of explosive under different spatial conditions, including in an open field (flat terrain) and in an open field with some simulated structures. The measurements performed included monitoring of dose rate, surface contamination of ground and (when relevant) structures, air concentration, particle size distribution, time distribution of dust particles in air, and thermocamera snapshots. The test area was selected for a stable wind direction under usual meteorological conditions.

[14] A location factor is the ratio of the exposure rate determined or estimated for a location of interest and a reference exposure rate [I.1, I.2]; the location factor accounts for the geometry at the location, e.g. the presence and configuration of buildings and trees.

[15] Data assimilation techniques combine measurements with model results to improve the predictive power of assessment models [I.1].

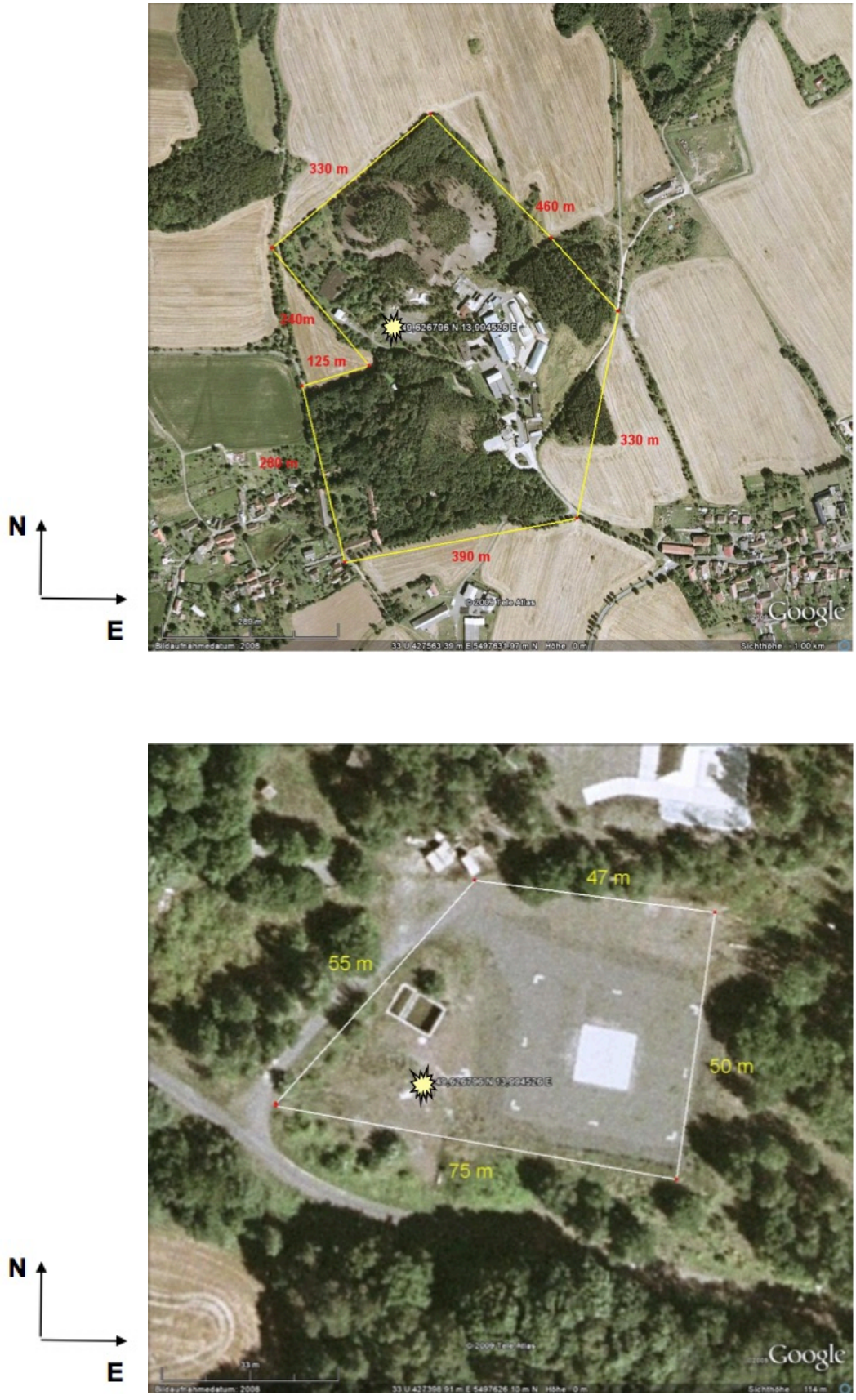

FIG. I.1. Aerial views of the test site with dimensions indicated. The origin of the explosion is indicated by the yellow symbol. (©2008 Google Earth Images)

For the open field tests, a combined booby-trap explosive system was selected, with the explosion in free space with a selected space angle. The radionuclide ^{99m}Tc was selected for its well detected gamma radiation energy, short radioactive half-life (6 h), and availability in suitable liquid form (^{99m}Tc as $NaTcO_4$ in 0.9% NaCl solution). Each test used approximately 1 GBq in a volume of 1.5 L (Test 1) or 6 mL (Tests 2 to 4), as summarized in Table I.1. The amount and type of explosive are also summarized in Table I.1.

The following measuring equipment was used:

- Infrared imaging technology (thermo camera ThermaCAM P25) to record the time development of the scene before and after the controlled explosion.
- Portable dose rate meters (Exploranium GR135 miniSpec, Tesla NB 3201) for dose rate area mapping.
- Spectrometric measurement (low background HPGe semiconductor spectrometry) for measuring of filters used for collecting samples of surface activities.
- Air sampling devices, including a 6 level cascade impactor for setting the aerosol size distribution, for measurement of the volume activity of the radionuclide in air.
- DustTrak laser nephelometers (DT model 8520, TSI) [I.3] to set the concentration of the atmospheric aerosol weight with a short integration time. The size fractions (μm) are selected with a pre-impactor at the equipment input.
- Weather monitoring station (Davis Vantage Pro2 meteo station, Windsonic sensor for wind measurement, height ~2 m) for detecting and recording meteorological parameters, especially the wind speed and direction, humidity, and temperature.

Collecting filters and other devices were distributed densely, both directly on the surface of an area of approximately 50 m × 40 m, and in specified places on vertically placed posts. Selected filters were changed several times after the explosion on a specified time schedule to estimate the time distribution of the dispersal of the radioactive material.

The following sections provide some additional details of the experiments and the equipment used. Information about Tests 1 to 3 has been reported by Prouza et al. [I.4][16].

I.3. INPUT INFORMATION

Information about Tests 1 to 4 is summarized in Table I.1. For Tests 1 and 2, all available data were provided to the participants, including measurements of surface contamination (Tests 1 and 2), dose rates (Test 2), and time integrated air concentrations (Test 2). These data could be used for calibration of models as desired. For Tests 3 and 4, only the input information was provided to participants during the exercise.

Meteorological information for the four tests is summarized in Table I.2. Detailed (time dependent) meteorological information is provided in Tables I.3 to I.7. The height of the wind measurements is ~2 m.

[16] The numbering of the field tests in this publication and in Ref. [I.4] is not the same. Readers need to use the dates, not the numbers, when comparing the two sources of information.

TABLE I.1. SUMMARY INFORMATION FOR THE FIELD TESTS

Test No.	Date	Explosion time	Activity of Tc-99m (MBq)	Time of measurement of Tc-99m activity	Amount of liquid containing the activity	Amount and type of explosive used[a]
Test 1	6 December 2007	12:45	780	10:20	1.5 L	Permon 10T, 350 g
Test 2	15 May 2008	11:30	1058	10:10	6 mL	Permon 10T, 350 g
Test 3	5 May 2009	12:22	1222	12:22	6 mL	Permon 10T, 350 g
Test 4	14 July 2009	12:42	1088	11:00	6 mL	Permon 10T, 350 g

[a] Descriptions of the explosives were provided separately.

TABLE I.2. SUMMARY OF WEATHER CONDITIONS DURING THE FIELD TESTS[a]

Experiment	Test 1	Test 2	Test 3	Test 4
Date	6 December 2007	15 May 2008	5 May 2009	14 July 2009
Temperature (°C)	6.9–7.1	22.2–22.4	10.1–10.7	25.4–25.6
Relative air humidity (%)	85–87	41–47	48–54	56–61
Condensation point (°C)	4.7–5.1	8.4–10.6	0.3–1.3	16.1–17.4
Wind speed[b] (km/h)	7.9–16.2	1.2–5.4	1.4–16.2	0–1.4
Gust wind speed (km/h)	–	–	4.7−16.2	0−3.2
Wind direction[b]	SW–SSW	S–SSW	SW–NNE	WSW–SSE
Air pressure (h Pa)	1011.1–1011.2	1009.1–1009.2	1021.3–1021.5	1012.6–1012.8

[a] More detailed meteorological data were provided in a separate Excel workbook.

[b] Wind measurements are at approximately 2 m height. The indicated direction is the direction wind is blowing from.

TABLE I.3. TIME DEPENDENT METEOROLOGICAL DATA FOR TEST 1 (6 DECEMBER 2007)

Time	Temperature (°C)	Relative air humidity (%)	Condensation point (°C)	Wind speed (m/s)	Wind direction	Maximum wind speed (m/s)	Air pressure (hPa)	Precipitation (mm)
09:33	7.2	85	4.8	2.7	SW	3.1	1011.8	0
09:34	7.2	84	4.6	2.7	WSW	4.0	1011.8	0
09:35	7.2	84	4.6	2.2	W	3.1	1011.8	0
09:36	7.2	85	4.8	2.7	SW	4.5	1011.8	0
09:37	7.2	84	4.6	1.8	SW	2.7	1011.8	0
09:38	7.2	85	4.8	3.6	WSW	4.9	1011.8	0
09:39	7.1	84	4.6	2.7	WSW	4.0	1011.8	0
09:40	7.1	84	4.6	2.7	SW	4.0	1011.8	0
09:41	7.1	84	4.6	2.7	WSW	3.1	1011.8	0
09:42	7.1	85	4.8	2.7	SW	3.1	1011.8	0
09:43	7.2	85	4.8	2.2	SW	3.1	1011.8	0
09:44	7.2	85	4.8	2.7	SW	4.5	1011.8	0
09:45	7.2	85	4.8	3.6	SW	5.4	1011.4	0
09:46	7.2	85	4.8	3.1	WSW	4.9	1011.4	0
09:47	7.2	85	4.8	2.2	SW	4.0	1011.4	0
09:48	7.3	85	4.9	2.2	SW	4.0	1011.4	0
09:49	7.3	85	4.9	2.7	WSW	4.5	1011.4	0
09:50	7.3	84	4.8	2.7	SW	4.0	1011.4	0
09:51	7.3	84	4.8	2.7	SW	4.0	1011.4	0
09:52	7.3	85	4.9	2.7	SW	4.9	1011.4	0
09:53	7.3	85	4.9	3.6	WSW	4.5	1011.4	0
09:54	7.3	85	5.0	2.2	WSW	3.1	1011.4	0
09:55	7.3	85	5.0	3.1	WSW	5.8	1011.4	0
09:56	7.3	85	5.0	4.0	WSW	6.3	1011.4	0
09:57	7.4	85	5.1	2.7	SW	4.5	1011.4	0
09:58	7.4	84	4.9	3.1	SW	6.3	1011.4	0
09:59	7.5	84	5.0	3.6	SW	5.4	1011.4	0
10:00	7.5	84	5.0	4.0	SW	6.3	1011.6	0
10:01	7.6	84	5.1	3.1	SW	4.5	1011.6	0
10:02	7.6	84	5.1	3.1	SW	4.9	1011.6	0

10:03	7.7	84	5.1	3.6	WSW	5.4	1011.6	0
10:04	7.7	84	5.1	4.5	WSW	5.4	1011.6	0
10:05	7.7	83	5.0	3.6	WSW	5.4	1011.6	0

TABLE I.3. TIME DEPENDENT METEOROLOGICAL DATA FOR TEST 1 (6 DECEMBER 2007) (cont.)

Time	Temperature (°C)	Relative air humidity (%)	Condensation point (°C)	Wind speed (m/s)	Wind direction	Maximum wind speed (m/s)	Air pressure (hPa)	Precipitation (mm)
10:06	7.7	83	5.0	3.1	SW	5.4	1011.6	0
10:07	7.8	83	5.1	3.6	SW	4.9	1011.6	0
10:08	7.8	82	4.9	5.4	WSW	7.2	1011.6	0
10:09	7.8	82	4.9	4.5	SW	5.4	1011.6	0
10:10	7.8	83	5.1	4.0	SW	5.8	1011.6	0
10:11	7.8	82	4.9	4.0	SW	6.3	1011.6	0
10:12	7.8	82	4.9	4.5	SW	6.7	1011.6	0
10:13	7.8	82	4.9	4.0	SW	5.8	1011.6	0
10:14	7.8	82	4.9	3.6	SW	4.5	1011.6	0
10:15	7.8	82	4.9	4.9	SW	6.7	1011.6	0
10:16	7.8	82	4.9	4.0	SW	5.4	1011.6	0
10:17	7.8	82	4.9	4.5	SW	6.7	1011.6	0
10:18	7.7	82	4.8	4.0	SW	6.3	1011.6	0
10:19	7.7	82	4.8	4.0	SW	6.3	1011.6	0
10:20	7.7	82	4.8	4.9	SW	8.5	1011.6	0
10:21	7.7	82	4.8	5.8	SW	7.2	1011.6	0
10:22	7.7	82	4.8	4.9	SW	6.7	1011.6	0
10:23	7.7	82	4.8	3.6	WSW	5.8	1011.6	0
10:24	7.7	82	4.8	4.5	SW	5.8	1011.6	0
10:25	7.7	82	4.8	4.0	SW	5.4	1011.6	0
10:26	7.7	82	4.8	4.0	SW	6.3	1011.6	0
10:27	7.7	83	5.0	3.6	WSW	5.4	1011.6	0
10:28	7.7	83	5.0	4.0	SW	4.9	1011.6	0
10:29	7.7	82	4.8	4.0	SW	6.3	1011.6	0
10:30	7.7	82	4.8	4.0	SW	5.4	1011.6	0
10:31	7.8	82	4.9	4.0	SW	5.4	1011.6	0

TABLE I.3. TIME DEPENDENT METEOROLOGICAL DATA FOR TEST 1 (6 DECEMBER 2007) (cont.)

Time	Temperature (°C)	Relative air humidity (%)	Condensation point (°C)	Wind speed (m/s)	Wind direction	Maximum wind speed (m/s)	Air pressure (hPa)	Precipitation (mm)
10:32	7.8	82	4.9	3.1	SW	4.5	1011.6	0
10:33	7.8	82	4.9	4.0	SW	5.8	1011.6	0
10:34	7.8	82	4.9	4.9	SW	6.3	1011.6	0
10:35	7.8	82	4.9	3.6	SW	4.5	1011.6	0
10:36	7.8	83	5.1	3.1	SW	4.9	1011.6	0
10:37	7.9	82	5.0	3.6	SW	4.5	1011.6	0
10:38	7.9	83	5.2	3.1	SW	4.9	1011.6	0
10:39	7.9	83	5.2	3.6	WSW	5.8	1011.6	0
10:40	7.9	83	5.2	3.1	SW	4.0	1011.6	0
10:41	7.9	86	5.7	4.0	SW	4.9	1011.6	0
10:42	7.9	83	5.2	4.0	SW	5.4	1011.6	0
10:43	8.0	83	5.3	3.1	SW	4.9	1011.6	0
10:44	7.9	83	5.2	3.6	SW	5.8	1011.6	0
10:45	7.9	83	5.2	3.6	SW	4.9	1011.9	0
10:46	7.9	83	5.2	3.1	WSW	4.5	1011.9	0
10:47	7.9	83	5.2	2.2	SW	3.1	1011.9	0
10:48	7.9	84	5.4	1.8	SW	2.7	1011.9	0
10:49	7.9	84	5.4	2.7	SW	4.5	1011.9	0
10:50	7.8	84	5.3	3.6	SW	4.5	1011.9	0
10:51	7.8	84	5.3	2.7	SW	5.4	1011.9	0
10:52	7.7	84	5.2	1.8	WSW	2.2	1011.9	0
10:53	7.7	84	5.2	2.7	SW	3.6	1011.9	0
10:54	7.7	85	5.4	2.2	SW	4.0	1011.9	0
10:55	7.7	85	5.4	1.8	SW	3.6	1011.9	0
10:56	7.7	84	5.2	2.7	SW	4.5	1011.9	0
10:57	7.7	85	5.4	2.2	SW	4.0	1011.9	0
10:58	7.7	85	5.4	2.7	SW	4.0	1011.9	0
10:59	7.7	85	5.4	2.2	SW	4.5	1011.9	0
11:00	7.7	85	5.4	3.6	SW	5.4	1011.6	0
11:01	7.7	85	5.4	1.8	SW	3.1	1011.6	0

TABLE I.3. TIME DEPENDENT METEOROLOGICAL DATA FOR TEST 1 (6 DECEMBER 2007) (cont.)

Time	Temperature (°C)	Relative air humidity (%)	Condensation point (°C)	Wind speed (m/s)	Wind direction	Maximum wind speed (m/s)	Air pressure (hPa)	Precipitation (mm)
11:02	7.7	85	5.4	2.2	SW	4.5	1011.6	0
11:03	7.7	85	5.4	2.2	SW	5.4	1011.6	0
11:04	7.7	84	5.2	3.6	SW	4.5	1011.6	0
11:05	7.7	84	5.2	1.8	SW	3.1	1011.6	0
11:06	7.7	84	5.2	3.6	SSW	6.7	1011.6	0
11:07	7.7	83	5.0	2.7	SW	4.0	1011.6	0
11:08	7.7	84	5.2	2.7	SW	4.5	1011.6	0
11:09	7.7	84	5.2	3.1	SW	5.4	1011.6	0
11:10	7.7	84	5.1	2.7	SW	4.0	1011.6	0
11:11	7.7	84	5.1	3.1	SSW	6.3	1011.6	0
11:12	7.7	85	5.3	2.2	SW	3.1	1011.6	0
11:13	7.7	84	5.1	2.2	SW	5.4	1011.6	0
11:14	7.6	84	5.1	3.6	SW	5.4	1011.6	0
11:15	7.6	84	5.1	2.7	SW	4.5	1011.6	0
11:16	7.5	84	5.0	2.7	SW	4.5	1011.6	0
11:17	7.5	85	5.1	3.6	SW	4.9	1011.6	0
11:18	7.4	85	5.1	2.7	SW	5.8	1011.6	0
11:19	7.4	85	5.1	1.8	SW	2.7	1011.6	0
11:20	7.4	86	5.3	3.1	SW	4.0	1011.6	0
11:21	7.4	85	5.1	3.1	SW	5.4	1011.6	0
11:22	7.4	86	5.3	3.1	SW	4.5	1011.6	0
11:23	7.4	85	5.1	3.6	SW	5.4	1011.6	0
11:24	7.4	85	5.1	3.1	SW	5.4	1011.6	0
11:25	7.4	85	5.1	3.1	SW	4.9	1011.6	0
11:26	7.4	85	5.1	3.1	SW	5.4	1011.6	0
11:27	7.4	85	5.1	3.1	SW	5.4	1011.6	0
11:28	7.4	85	5.1	4.0	SW	5.4	1011.6	0
11:29	7.4	85	5.1	2.7	SW	4.0	1011.6	0
11:30	7.4	85	5.1	3.1	SW	5.4	1011.4	0
11:31	7.4	85	5.1	2.2	SSW	4.9	1011.4	0

TABLE I.3. TIME DEPENDENT METEOROLOGICAL DATA FOR TEST 1 (6 DECEMBER 2007) (cont.)

Time	Temperature (°C)	Relative air humidity (%)	Condensation point (°C)	Wind speed (m/s)	Wind direction	Maximum wind speed (m/s)	Air pressure (hPa)	Precipitation (mm)
11:32	7.4	85	5.1	3.6	SW	4.5	1011.4	0
11:33	7.4	85	5.1	3.1	SW	4.9	1011.4	0
11:34	7.4	85	5.1	4.0	SW	6.3	1011.4	0
11:35	7.4	84	4.9	3.6	SW	4.9	1011.4	0
11:36	7.4	84	4.9	2.7	SW	4.5	1011.4	0
11:37	7.4	84	4.9	2.2	WSW	4.5	1011.4	0
11:38	7.4	85	5.1	2.7	SW	4.0	1011.4	0
11:39	7.4	84	4.9	2.7	SW	4.9	1011.4	0
11:40	7.4	84	4.9	3.1	WSW	6.3	1011.4	0
11:41	7.4	84	4.9	2.7	SW	4.9	1011.4	0
11:42	7.4	84	4.9	3.6	SW	5.8	1011.4	0
11:43	7.4	84	4.9	4.0	SW	5.8	1011.4	0
11:44	7.4	84	4.9	4.9	SW	6.3	1011.4	0
11:45	7.4	83	4.7	4.0	SW	5.8	1011.6	0
11:46	7.3	84	4.8	3.1	SW	4.0	1011.6	0
11:47	7.3	84	4.8	3.1	SW	4.9	1011.6	0
11:48	7.3	85	5.0	3.1	SW	5.4	1011.6	0
11:49	7.3	85	4.9	3.1	SW	4.5	1011.6	0.2
11:50	7.3	86	5.1	2.7	SW	6.3	1011.6	0
11:51	7.3	86	5.1	4.5	SW	6.3	1011.6	0
11:52	7.3	86	5.1	4.9	SW	8.5	1011.6	0
11:53	7.3	86	5.1	3.6	SW	4.9	1011.6	0
11:54	7.3	86	5.1	3.1	SW	5.4	1011.6	0
11:55	7.3	86	5.1	3.6	WSW	4.9	1011.6	0
11:56	7.3	86	5.1	3.1	SW	4.9	1011.6	0
11:57	7.3	86	5.1	4.0	SW	6.3	1011.6	0
11:58	7.3	85	4.9	3.1	SW	4.9	1011.6	0
11:59	7.3	86	5.1	3.6	SW	4.9	1011.6	0
12:00	7.3	86	5.1	2.2	SW	4.5	1011.5	0
12:01	7.2	87	5.1	2.7	SW	4.9	1011.5	0

TABLE I.3. TIME DEPENDENT METEOROLOGICAL DATA FOR TEST 1 (6 DECEMBER 2007) (cont.)

Time	Temperature (°C)	Relative air humidity (%)	Condensation point (°C)	Wind speed (m/s)	Wind direction	Maximum wind speed (m/s)	Air pressure (hPa)	Precipitation (mm)
12:02	7.2	87	5.1	3.1	SW	4.9	1011.5	0.2
12:03	7.2	87	5.1	2.7	SW	4.0	1011.5	0
12:04	7.1	87	5.1	2.7	WSW	4.5	1011.5	0
12:05	7.1	87	5.1	2.7	SW	4.0	1011.5	0
12:06	7.1	87	5.1	2.2	SW	3.1	1011.5	0.2
12:07	7.1	88	5.2	2.7	SW	3.6	1011.5	0
12:08	7.1	88	5.2	1.8	SW	3.1	1011.5	0
12:09	7.1	88	5.2	2.7	SW	3.6	1011.5	0
12:10	6.9	88	5.1	2.7	SW	3.6	1011.5	0
12:11	6.9	88	5.1	2.2	SW	3.1	1011.5	0
12:12	6.9	88	5.1	2.7	SW	4.0	1011.5	0
12:13	6.9	88	5.1	3.1	SW	4.0	1011.5	0
12:14	6.9	88	5.1	2.7	SW	3.1	1011.5	0
12:15	6.9	88	5.1	2.2	SW	2.7	1011.2	0.2
12:16	7.1	88	5.2	2.7	SW	3.6	1011.2	0
12:17	7.1	88	5.2	3.6	SW	5.8	1011.2	0
12:18	7.1	88	5.2	3.1	SW	4.0	1011.2	0
12:19	7.1	88	5.2	3.6	SW	5.8	1011.2	0
12:20	7.1	88	5.2	4.5	SW	6.3	1011.2	0
12:21	7.1	87	5.0	4.5	SW	5.4	1011.2	0
12:22	7.1	87	5.0	3.1	SW	4.9	1011.2	0
12:23	7.1	87	5.0	4.5	SW	6.3	1011.2	0
12:24	7.1	87	5.0	3.6	SW	5.8	1011.2	0
12:25	6.9	86	4.8	4.5	SW	6.3	1011.2	0
12:26	6.9	86	4.8	3.1	SW	4.0	1011.2	0
12:27	6.9	87	4.9	3.1	SW	4.5	1011.2	0
12:28	6.9	87	4.9	2.7	SW	5.4	1011.2	0
12:29	6.9	87	4.9	2.2	SW	3.1	1011.2	0
12:30	6.9	87	4.9	3.6	SW	6.7	1011.2	0
12:31	6.9	87	4.9	3.6	SW	4.9	1011.2	0

TABLE I.3. TIME DEPENDENT METEOROLOGICAL DATA FOR TEST 1 (6 DECEMBER 2007) (cont.)

Time	Temperature (°C)	Relative air humidity (%)	Condensation point (°C)	Wind speed (m/s)	Wind direction	Maximum wind speed (m/s)	Air pressure (hPa)	Precipitation (mm)
12:32	6.9	87	4.9	3.6	SW	4.9	1011.2	0
12:33	6.9	87	4.9	3.6	SW	4.9	1011.2	0
12:34	6.9	87	4.9	4.0	SW	5.4	1011.2	0
12:35	6.9	87	4.9	3.1	SW	4.5	1011.2	0
12:36	6.9	87	4.9	3.1	SW	4.5	1011.2	0
12:37	6.9	87	4.9	4.0	SW	5.4	1011.2	0
12:38	6.9	87	4.9	3.6	SW	5.4	1011.2	0
12:39	6.9	87	4.9	3.1	SW	4.9	1011.2	0
12:40	6.9	87	4.9	2.7	SW	4.5	1011.2	0
12:41	6.9	87	4.9	3.6	SW	5.8	1011.2	0
12:42	6.9	86	4.8	2.2	SSW	3.1	1011.2	0
12:43	6.9	86	4.8	3.1	SW	4.0	1011.2	0
12:44	7.1	86	4.9	3.6	SW	5.4	1011.2	0
12:45	7.1	86	4.9	4.0	SW	5.8	1011.1	0
12:46	7.1	85	4.7	4.5	SW	6.3	1011.1	0
12:47	7.1	86	4.9	3.1	SW	4.9	1011.1	0
12:48	7.1	86	4.9	2.7	SW	4.5	1011.1	0
12:49	7.2	86	5.0	3.1	SW	5.4	1011.1	0
12:50	7.2	86	5.0	2.2	SW	3.1	1011.1	0
12:51	7.2	87	5.1	2.2	SW	3.1	1011.1	0
12:52	7.2	86	5.0	3.6	SSW	5.8	1011.1	0
12:53	7.2	86	5.0	2.2	SW	4.0	1011.1	0
12:54	7.3	86	5.1	2.2	SW	3.1	1011.1	0
12:55	7.3	86	5.1	2.2	SW	4.0	1011.1	0
12:56	7.3	87	5.3	2.7	SSW	6.7	1011.1	0
12:57	7.3	86	5.1	3.6	SW	6.7	1011.1	0
12:58	7.3	84	4.8	3.6	SW	4.5	1011.1	0
12:59	7.3	85	4.9	3.1	SW	4.5	1011.1	0
13:00	7.3	85	5.0	2.7	SW	3.6	1011.2	0
13:01	7.3	85	5.0	3.1	SW	4.9	1011.2	0

TABLE I.3. TIME DEPENDENT METEOROLOGICAL DATA FOR TEST 1 (6 DECEMBER 2007) (cont.)

Time	Temperature (°C)	Relative air humidity (%)	Condensation point (°C)	Wind speed (m/s)	Wind direction	Maximum wind speed (m/s)	Air pressure (hPa)	Precipitation (mm)
13:02	7.3	85	5.0	4.0	SW	5.8	1011.2	0
13:03	7.3	85	5.0	3.6	SW	4.9	1011.2	0
13:04	7.3	85	5.0	2.2	SW	4.5	1011.2	0
13:05	7.3	86	5.1	3.1	SW	6.7	1011.2	0
13:06	7.3	84	4.8	6.3	SW	7.6	1011.2	0
13:07	7.3	84	4.8	4.5	WSW	6.7	1011.2	0
13:08	7.3	84	4.8	4.0	SW	5.8	1011.2	0
13:09	7.3	83	4.6	4.5	SW	7.2	1011.2	0
13:10	7.4	83	4.7	4.5	SW	7.6	1011.2	0
13:11	7.4	83	4.7	5.8	SW	6.7	1011.2	0
13:12	7.5	83	4.8	4.5	SW	6.7	1011.2	0
13:13	7.5	83	4.8	3.6	SW	5.8	1011.2	0
13:14	7.5	83	4.8	4.5	SW	6.3	1011.2	0
13:15	7.5	82	4.6	4.5	SW	6.7	1011.0	0
13:16	7.5	82	4.6	4.5	SW	6.3	1011.0	0
13:17	7.5	83	4.8	3.1	SW	4.9	1011.0	0
13:18	7.4	83	4.7	3.6	SW	5.4	1011.0	0
13:19	7.4	83	4.7	4.5	SW	5.4	1011.0	0
13:20	7.4	83	4.7	4.0	SW	5.4	1011.0	0
13:21	7.5	84	5.0	3.1	SW	5.4	1011.0	0
13:22	7.5	83	4.8	2.7	SW	4.5	1011.0	0
13:23	7.4	83	4.7	4.0	SW	6.3	1011.0	0
13:24	7.4	83	4.7	3.1	SW	4.5	1011.0	0
13:25	7.4	84	4.9	3.6	SW	5.4	1011.0	0
13:26	7.5	83	4.8	3.1	SW	4.9	1011.0	0
13:27	7.5	84	5.0	2.7	SW	4.0	1011.0	0
13:28	7.6	84	5.1	3.1	SSW	5.4	1011.0	0
13:29	7.6	83	4.9	3.6	SW	4.9	1011.0	0
13:30	7.6	84	5.1	3.1	SW	5.4	1010.9	0
13:31	7.6	84	5.1	2.7	SW	4.5	1010.9	0

TABLE I.3. TIME DEPENDENT METEOROLOGICAL DATA FOR TEST 1 (6 DECEMBER 2007) (cont.)

Time	Temperature (°C)	Relative air humidity (%)	Condensation point (°C)	Wind speed (m/s)	Wind direction	Maximum wind speed (m/s)	Air pressure (hPa)	Precipitation (mm)
13:32	7.5	83	4.8	3.6	SW	5.8	1010.9	0
13:33	7.5	83	4.8	2.2	SW	2.7	1010.9	0
13:34	7.5	83	4.8	3.1	SSW	4.9	1010.9	0
13:35	7.4	82	4.6	3.1	SW	4.5	1010.9	0
13:36	7.4	83	4.7	2.7	SSW	4.5	1010.9	0
13:37	7.3	82	4.5	4.9	SW	7.2	1010.9	0
13:38	7.3	82	4.5	4.0	SW	6.3	1010.9	0
13:39	7.3	83	4.6	3.6	SW	5.8	1010.9	0
13:40	7.3	83	4.6	3.6	SW	5.8	1010.9	0
13:41	7.3	83	4.6	3.1	SW	4.9	1010.9	0
13:42	7.3	83	4.6	3.6	SW	5.8	1010.9	0
13:43	7.3	83	4.6	4.0	SW	5.4	1010.9	0
13:44	7.3	83	4.6	2.7	SW	5.4	1010.9	0
13:45	7.2	83	4.5	2.7	SW	3.6	1010.8	0
13:46	7.2	83	4.5	2.2	SSW	3.1	1010.8	0
13:47	7.2	83	4.5	3.1	SW	4.5	1010.8	0
13:48	7.2	84	4.6	3.1	SW	4.9	1010.8	0
13:49	7.2	84	4.6	2.2	SW	2.7	1010.8	0
13:50	7.2	84	4.6	3.1	SW	4.9	1010.8	0
13:51	7.2	84	4.6	1.8	SW	2.2	1010.8	0
13:52	7.2	84	4.6	2.2	SW	3.1	1010.8	0
13:53	7.2	84	4.6	2.2	SW	3.6	1010.8	0
13:54	7.2	84	4.6	1.8	SW	3.1	1010.8	0
13:55	7.1	84	4.6	2.2	SW	3.1	1010.8	0
13:56	7.1	84	4.6	1.8	SSW	3.1	1010.8	0
13:57	7.1	84	4.6	3.1	SW	5.4	1010.8	0
13:58	7.1	83	4.4	2.2	SW	4.5	1010.8	0
13:59	7.1	84	4.6	2.2	SW	2.7	1010.8	0
14:00	7.1	84	4.6	1.8	SW	2.7	1010.7	0
14:01	7.2	84	4.6	1.8	SW	2.2	1010.7	0

TABLE I.3. TIME DEPENDENT METEOROLOGICAL DATA FOR TEST 1 (6 DECEMBER 2007) (cont.)

Time	Temperature (°C)	Relative air humidity (%)	Condensation point (°C)	Wind speed (m/s)	Wind direction	Maximum wind speed (m/s)	Air pressure (hPa)	Precipitation (mm)
14:02	7.2	84	4.6	3.1	SW	4.9	1010.7	0
14:03	7.2	84	4.6	2.7	SW	4.0	1010.7	0
14:04	7.2	84	4.6	1.3	SW	2.2	1010.7	0
14:05	7.2	83	4.5	2.7	SW	4.0	1010.7	0
14:06	7.2	83	4.5	1.3	SW	2.2	1010.7	0
14:07	7.2	84	4.6	1.3	SW	1.8	1010.7	0
14:08	7.2	84	4.6	0.9	SW	1.8	1010.7	0
14:09	7.2	85	4.8	0.4	SW	1.3	1010.7	0
14:10	7.2	85	4.8	0.4	SSW	0.9	1010.7	0
14:11	7.2	85	4.8	0.4	SSW	1.3	1010.7	0
14:12	7.2	85	4.8	1.3	SW	1.8	1010.7	0
14:13	7.1	85	4.8	1.3	WSW	1.8	1010.7	0
14:14	7.1	86	4.9	0.4	SW	0.9	1010.7	0
14:15	7.1	86	4.9	1.3	SW	2.2	1010.5	0.2
14:16	7.1	85	4.8	0	S	0.4	1010.5	0.2
14:17	7.2	85	4.8	0		0	1010.5	0
14:18	7.2	86	5.0	0		0	1010.5	0
14:19	7.2	86	5.0	0		0	1010.5	0
14:20	7.2	86	5.0	0		0	1010.5	0
14:21	7.2	86	5.0	0		0	1010.5	0
14:22	7.2	86	5.0	0		0	1010.5	0
14:23	7.2	86	5.0	0		0	1010.5	0
14:24	7.2	86	5.0	0		0	1010.5	0
14:25	7.2	86	5.0	0		0	1010.5	0
14:26	7.2	85	4.8	0		0	1010.5	0
14:27	7.1	85	4.8	0		0	1010.5	0
14:28	7.1	85	4.8	0		0	1010.5	0
14:29	7.1	85	4.8	0		0	1010.5	0
14:30	7.1	85	4.8	0		0	1010.1	0
14:31	7.1	85	4.8	0		0	1010.1	0

TABLE I.3. TIME DEPENDENT METEOROLOGICAL DATA FOR TEST 1 (6 DECEMBER 2007) (cont.)

Time	Temperature (°C)	Relative air humidity (%)	Condensation point (°C)	Wind speed (m/s)	Wind direction	Maximum wind speed (m/s)	Air pressure (hPa)	Precipitation (mm)
14:32	7.1	85	4.8	0		0	1010.1	0
14:33	7.1	85	4.8	0		0	1010.1	0
14:34	7.1	85	4.8	0		0	1010.1	0
14:35	7.1	85	4.8	0		0	1010.1	0
14:36	7.1	85	4.8	0	SW	0.9	1010.1	0
14:37	7.1	85	4.8	0		0	1010.1	0.2
14:38	7.1	85	4.8	0		0	1010.1	0
14:39	7.1	85	4.8	0		0	1010.1	0

TABLE I.4. TIME DEPENDENT METEOROLOGICAL DATA FOR TEST 2 (15 MAY 2008)

Time	Temperature (°C)	Relative air humidity (%)	Condensation point (°C)	Wind speed (m/s)	Wind direction	Air pressure (hPa)	Precipitation (mm)
11:15	22.2	45	9.7	1.07		1009.1	0
11:16	22.3	48	10.8	0.85		1009.1	0
11:17	22.4	45	9.9	0.96		1009.1	0
11:18	22.4	48	10.9	0.45	SSE	1009.1	0
11:19	22.4	45	9.9	0.28		1009.1	0
11:20	22.5	46	10.3	1.22		1009.1	0
11:21	22.5	45	10.0	0.79		1009.1	0
11:22	22.5	44	9.6	1.24	SSW	1009.1	0
11:23	22.5	45	10.0	1.84	SSW	1009.1	0
11:24	22.4	45	9.9	1.39		1009.1	0
11:25	22.3	44	9.5	1.47		1009.1	0
11:26	22.2	42	8.7	1.02		1009.1	0
11:27	22.2	45	9.7	0.38		1009.1	0
11:28	22.2	45	9.7	0.91	S	1009.1	0
11:29	22.2	45	9.7	0.98		1009.1	0
11:30	22.2	45	9.7	0.59		1009.2	0
11:31	22.2	45	9.7	0.93		1009.2	0
11:32	22.2	45	9.7	0.57		1009.2	0
11:33	22.3	45	9.8	0.34		1009.2	0
11:34	22.3	41	8.4	0.80		1009.2	0
11:35	22.3	43	9.1	0.81		1009.2	0
11:36	22.4	43	9.2	0.69		1009.2	0
11:37	22.4	44	9.6	0.82		1009.2	0
11:38	22.4	47	10.6	0.74		1009.2	0
11:39	22.4	47	10.6	1.49		1009.2	0
11:40	22.4	44	9.6	0.74		1009.2	0
11:41	22.5	46	10.3	0.79	SE	1009.2	0
11:42	22.5	50	11.6	1.13		1009.2	0
11:43	22.5	43	9.3	1.60	SSE	1009.2	0
11:44	22.5	44	9.6	0.72	S	1009.2	0

11:45	22.5	44	9.6	0.67		1008.9	0
11:46	22.5	42	8.9	1.54	S	1008.9	0
11:47	22.6	44	9.7	0.47		1008.9	0

TABLE I.4. TIME DEPENDENT METEOROLOGICAL DATA FOR TEST 2 (15 MAY 2008) (cont.)

Time	Temperature (°C)	Relative air humidity (%)	Condensation point (°C)	Wind speed (m/s)	Wind direction	Air pressure (hPa)	Precipitation (mm)
11:48	22.6	47	10.7	1.85		1008.9	0
11:49	22.6	42	9.0	1.02		1008.9	0
11:50	22.6	40	8.3	0.95		1008.9	0
11:51	22.6	42	9.0	1.38		1008.9	0
11:52	22.7	45	10.2	0.82	SSE	1008.9	0
11:53	22.7	42	9.1	1.35		1008.9	0
11:54	22.7	44	9.8	0.77		1008.9	0
11:55	22.8	43	9.6	0.95	ESE	1008.9	0
11:56	22.9	43	9.6	0.91		1008.9	0

TABLE I.5. TIME DEPENDENT METEOROLOGICAL DATA FOR TEST 3 (5 MAY 2009), STATION 1

Time	Temperature (°C)	Relative air humidity (%)	Condensation point (°C)	Wind speed (m/s)	Maximum wind speed (m/s)	Wind direction	Air pressure (hPa)	Precipitation (mm)
11:30	9.9	51	0.3	1.3	1.8	WNW	1021.4	0
11:31	9.9	51	0.3	1.8	2.7	NW	1021.4	0
11:32	9.9	51	0.3	1.3	2.7	NW	1021.4	0
11:33	9.9	51	0.3	1.3	2.2	NW	1021.4	0
11:34	9.9	51	0.2	0.9	1.8	NW	1021.4	0
11:35	9.9	52	0.5	1.3	1.8	NW	1021.4	0
11:36	9.9	55	1.3	1.3	2.7	WNW	1021.4	0
11:37	9.8	52	0.4	1.3	2.2	NW	1021.4	0
11:38	9.8	54	0.9	0.9	1.3	N	1021.4	0
11:39	9.7	54	0.8	1.8	3.1	SNW	1021.4	0

11:40	9.7	52	0.3	1.8	3.1	N	1021.4	0
11:41	9.7	53	0.6	1.3	2.7	NW	1021.4	0
11:42	9.7	53	0.5	0.9	1.8	NW	1021.4	0
11:43	9.7	52	0.3	1.3	2.7	SNW	1021.4	0
11:44	9.7	54	0.8	1.3	2.2	NW	1021.4	0
11:45	9.7	53	0.5	0.9	1.8	N	1021.2	0
11:46	9.7	55	1.1	0.9	2.2	NW	1021.2	0
11:47	9.7	56	1.4	1.8	3.1	SNW	1021.2	0

TABLE I.5. TIME DEPENDENT METEOROLOGICAL DATA FOR TEST 3 (5 MAY 2009), STATION 1 (cont.)

Time	Temperature (°C)	Relative air humidity (%)	Condensation point (°C)	Wind speed (m/s)	Maximum wind speed (m/s)	Wind direction	Air pressure (hPa)	Precipitation (mm)
11:48	9.7	52	0.3	1.3	2.7	N	1021.2	0
11:49	9.7	49	-0.5	2.7	3.1	NW	1021.2	0
11:50	9.7	50	-0.2	1.8	3.1	SNW	1021.2	0
11:51	9.7	49	-0.5	0.9	1.3	N	1021.2	0
11:52	9.8	49	-0.4	1.8	3.1	WNW	1021.2	0
11:53	9.8	50	-0.2	1.8	4.5	SNW	1021.2	0
11:54	9.9	47	-0.9	1.8	3.1	NW	1021.2	0
11:55	9.9	49	-0.3	2.2	4.5	NW	1021.2	0
11:56	9.9	47	-0.9	2.2	2.7	NW	1021.2	0
11:57	9.9	47	-0.9	1.3	2.7	NNW	1021.2	0
11:58	9.9	48	-0.6	1.8	3.1	NNW	1021.2	0
11:59	10.1	52	0.6	1.3	2.2	WSW	1021.2	0
12:00	10.1	51	0.4	1.3	2.2	W	1021.3	0
12:01	9.9	47	-0.9	1.8	3.1	WSW	1021.3	0
12:02	9.9	50	0.0	1.3	2.2	W	1021.3	0
12:03	9.9	48	-0.6	1.8	4.0	WSW	1021.3	0
12:04	9.9	52	0.5	1.8	3.6	W	1021.3	0
12:05	9.8	50	-0.2	1.8	3.6	WNW	1021.3	0
12:06	9.8	52	0.4	2.2	4.5	W	1021.3	0
12:07	9.8	51	0.1	1.8	4.0	WNW	1021.3	0
12:08	9.8	50	-0.2	0.9	2.2	WNW	1021.3	0

TABLE I.5. TIME DEPENDENT METEOROLOGICAL DATA FOR TEST 3 (5 MAY 2009), STATION 1 (cont.)

Time	Temperature (°C)	Relative air humidity (%)	Condensation point (°C)	Wind speed (m/s)	Maximum wind speed (m/s)	Wind direction	Air pressure (hPa)	Precipitation (mm)
12:09	9.8	48	-0.7	0.9	2.2	WNW	1021.3	0
12:10	9.8	52	0.4	1.3	2.2	WNW	1021.3	0
12:11	9.9	51	0.2	0.4	0.9	NW	1021.3	0
12:12	9.9	51	0.2	0.9	1.3	NW	1021.3	0
12:13	9.9	53	0.8	1.3	1.8	WSW	1021.3	0
12:14	9.9	50	0.0	0.9	2.2	WSW	1021.3	0
12:15	9.9	48	-0.6	1.3	5.4	JSW	1021.3	0
12:16	9.9	49	-0.3	1.3	2.7	WNW	1021.3	0
12:17	9.9	48	-0.6	0.9	2.7	NW	1021.3	0
12:18	10.1	52	0.6	1.8	2.7	W	1021.3	0
12:19	10.1	53	0.9	1.8	3.1	WNW	1021.3	0
12:20	10.1	53	0.9	2.7	4.0	WNW	1021.3	0
12:21	10.1	48	-0.5	2.2	4.0	WNW	1021.3	0
12:22	10.1	50	0.1	1.3	2.2	WNW	1021.3	0
12:23	10.2	54	1.3	1.8	2.7	WSW	1021.3	0
12:24	10.2	49	0.0	1.8	3.1	WSW	1021.3	0
12:25	10.2	48	-0.3	1.3	2.2	W	1021.3	0
12:26	10.4	48	-0.2	1.8	4.0	WNW	1021.3	0
12:27	10.4	48	-0.1	1.3	2.2	WNW	1021.3	0
12:28	10.6	51	0.8	1.3	3.6	W	1021.3	0
12:29	10.6	50	0.6	0.9	1.3	WSW	1021.3	0
12:30	10.6	50	0.6	1.3	2.2	WNW	1021.5	0
12:31	10.7	49	0.4	2.2	4.5	WNW	1021.5	0
12:32	10.7	48	0.1	1.3	3.1	W	1021.5	0
12:33	10.7	44	-1.1	2.2	3.1	W	1021.5	0
12:34	10.6	47	-0.2	2.7	4.9	W	1021.5	0
12:35	10.6	47	-0.2	0.9	1.3	WNW	1021.5	0
12:36	10.6	46	-0.5	1.8	2.7	WNW	1021.5	0
12:37	10.6	49	0.3	0.9	1.8	WNW	1021.5	0
12:38	10.6	48	0.0	1.3	3.1	WNW	1021.5	0

TABLE I.5. TIME DEPENDENT METEOROLOGICAL DATA FOR TEST 3 (5 MAY 2009), STATION 1 (cont.)

Time	Temperature (°C)	Relative air humidity (%)	Condensation point (°C)	Wind speed (m/s)	Maximum wind speed (m/s)	Wind direction	Air pressure (hPa)	Precipitation (mm)
12:39	10.6	51	0.9	1.3	2.2	W	1021.5	0
12:40	10.7	50	0.7	1.8	2.7	W	1021.5	0
12:41	10.7	48	0.1	2.2	3.6	WSW	1021.5	0
12:42	10.7	48	0.1	2.7	4.0	W	1021.5	0
12:43	10.7	51	1.0	1.8	2.7	WNW	1021.5	0
12:44	10.8	49	0.5	1.3	2.7	WNW	1021.5	0
12:45	10.9	47	0.0	1.3	2.7	WNW	1021.5	0
12:46	10.9	46	-0.3	2.2	3.1	WSW	1021.5	0
12:47	10.9	46	-0.2	1.3	2.2	W	1021.5	0
12:48	10.9	48	0.3	1.3	1.8	WNW	1021.5	0
12:49	11.1	49	0.7	1.8	3.1	W	1021.5	0
12:50	11.1	49	0.8	2.2	4.5	WSW	1021.5	0
12:51	11.2	44	-0.6	2.2	4.0	W	1021.5	0
12:52	11.3	44	-0.5	2.2	3.6	WNW	1021.5	0
12:53	11.4	45	-0.1	1.3	1.8	WNW	1021.5	0
12:54	11.4	42	-1.0	2.2	4.0	WNW	1021.5	0
12:55	11.6	46	0.3	1.8	5.4	NW	1021.5	0
12:56	11.6	44	-0.2	1.3	4.5	WNW	1021.5	0
12:57	11.7	48	1.1	2.2	4.0	W	1021.5	0
12:58	11.7	46	0.5	1.8	2.7	NW	1021.5	0
12:59	11.8	47	0.8	1.3	2.2	W	1021.5	0
13:00	11.8	46	0.5	1.8	4.5	WSW	1021.9	0
13:01	11.8	46	0.6	1.8	3.1	WNW	1021.9	0
13:02	11.8	46	0.6	2.2	4.9	W	1021.9	0
13:03	11.8	51	2.0	3.6	7.2	WNW	1021.9	0
13:04	11.8	47	0.8	2.2	4.5	WNW	1021.9	0
13:05	11.7	44	-0.1	2.2	3.1	W	1021.9	0
13:06	11.6	46	0.4	1.8	2.7	W	1021.9	0
13:07	11.6	47	0.6	2.2	3.1	W	1021.9	0
13:08	11.4	48	0.8	3.1	4.9	WSW	1021.9	0

TABLE I.5. TIME DEPENDENT METEOROLOGICAL DATA FOR TEST 3 (5 MAY 2009), STATION 1 (cont.)

Time	Temperature (°C)	Relative air humidity (%)	Condensation point (°C)	Wind speed (m/s)	Maximum wind speed (m/s)	Wind direction	Air pressure (hPa)	Precipitation (mm)
13:09	11.2	48	0.6	3.1	5.4	WNW	1021.9	0
13:10	11.1	44	-0.7	1.8	2.7	WNW	1021.9	0
13:11	11.1	47	0.2	1.3	2.2	W	1021.9	0
13:12	11.1	47	0.2	1.3	2.2	W	1021.9	0
13:13	11.1	45	-0.4	1.8	2.7	WSW	1021.9	0
13:14	11.1	45	-0.4	2.7	4.5	WNW	1021.9	0
13:15	11.2	42	-1.2	2.2	3.1	WSW	1021.8	0
13:16	11.3	47	0.4	2.2	3.1	SW	1021.8	0
13:17	11.3	43	-0.9	2.2	4.9	WNW	1021.8	0
13:18	11.3	47	0.4	1.8	2.7	WSW	1021.8	0
13:19	11.4	47	0.5	1.8	3.1	W	1021.8	0

TABLE I.6. TIME DEPENDENT METEOROLOGICAL DATA FOR TEST 3 (5 MAY 2009), STATION 2

Time	Temperature (°C)	Relative air humidity (%)	Condensation point (°C)	Wind speed (m/s)	Maximum wind speed (m/s)	Wind direction	Air pressure (hPa)	Precipitation (mm)
11:30	9.9	51	0.3	2.2	3.1	NNW	1022.2	0
11:31	9.9	51	0.2	2.7	4.0	NW	1022.1	0
11:32	9.9	51	0.2	2.7	3.6	NW	1022.1	0
11:33	9.8	51	0.2	2.2	3.1	NW	1022.2	0
11:34	9.8	53	0.7	1.8	2.7	NNW	1022.0	0
11:35	9.8	53	0.6	2.7	4.0	NW	1022.1	0
11:36	9.8	55	1.2	2.7	4.5	WNW	1022.1	0
11:37	9.7	52	0.3	2.2	3.1	NW	1022.0	0
11:38	9.7	52	0.3	2.2	3.1	NW	1021.9	0
11:39	9.7	54	0.8	2.2	3.6	NW	1022.0	0
11:40	9.7	53	0.5	2.2	3.6	NW	1022.2	0
11:41	9.7	53	0.6	2.2	4.0	NW	1022.0	0
11:42	9.7	51	0.0	2.2	3.1	NW	1021.9	0
11:43	9.7	53	0.5	1.8	2.7	NNW	1022.0	0
11:44	9.7	53	0.5	2.2	3.1	NNW	1021.9	0
11:45	9.7	54	0.8	1.8	3.1	NW	1022.0	0
11:46	9.7	55	1.1	1.8	3.6	NW	1022.0	0
11:47	9.7	55	1.1	2.7	4.0	WNW	1022.0	0
11:48	9.7	52	0.3	2.2	4.5	NW	1021.9	0
11:49	9.7	50	-0.2	3.1	4.9	NW	1022.0	0
11:50	9.7	49	-0.5	3.6	4.0	NW	1021.8	0
11:51	9.8	50	-0.2	2.7	3.6	NW	1022.0	0
11:52	9.8	51	0.1	2.7	4.0	WNW	1022.0	0
11:53	9.8	49	-0.4	4.0	5.8	NW	1022.0	0
11:54	9.8	47	-1.0	4.0	5.8	WNW	1022.1	0
11:55	9.8	48	-0.7	2.7	5.8	NW	1022.0	0
11:56	9.8	47	-1.0	3.1	4.9	NW	1022.1	0
11:57	9.8	48	-0.7	2.7	4.9	NNW	1022.0	0
11:58	9.8	50	-0.1	2.2	3.1	NNW	1022.0	0
11:59	9.8	51	0.2	2.2	3.6	NW	1022.1	0

12:00	9.8	50	-0.1	2.2	3.6	NW	1022.2	0
12:01	9.8	47	-1.0	1.8	3.1	NW	1022.2	0
12:02	9.8	49	-0.4	2.2	3.6	NW	1022.2	0

TABLE I.6. TIME DEPENDENT METEOROLOGICAL DATA FOR TEST 3 (5 MAY 2009), STATION 2 (cont.)

Time	Temperature (°C)	Relative air humidity (%)	Condensation point (°C)	Wind speed (m/s)	Maximum wind speed (m/s)	Wind direction	Air pressure (hPa)	Precipitation (mm)
12:03	9.8	50	-0.1	2.2	3.6	NW	1022.1	0
12:04	9.8	51	0.2	2.2	3.1	W	1022.2	0
12:05	9.8	50	-0.1	3.6	5.4	NW	1022.1	0
12:06	9.8	49	-0.4	3.1	4.9	NW	1022.0	0
12:07	9.9	49	-0.3	3.1	3.6	NNW	1022.0	0
12:08	9.8	46	-1.3	3.1	4.0	NW	1021.8	0
12:09	9.8	46	-1.3	2.2	2.7	NW	1021.9	0
12:10	9.8	50	-0.1	3.1	5.8	NW	1022.0	0
12:11	9.8	48	-0.7	1.8	2.7	WNW	1022.0	0
12:12	9.8	49	-0.4	1.3	2.2	NW	1022.0	0
12:13	9.8	52	0.4	1.3	2.2	WNW	1021.9	0
12:14	9.8	51	0.2	2.2	3.1	WNW	1022.0	0
12:15	9.9	48	-0.6	0.9	2.7	NW	1021.9	0
12:16	9.9	48	-0.6	2.2	4.0	W	1021.8	0
12:17	9.9	48	-0.6	1.8	2.7	W	1021.9	0
12:18	10.0	50	0.0	2.7	5.4	NW	1021.9	0
12:19	10.1	51	0.4	2.2	3.6	NNW	1021.9	0
12:20	10.1	50	0.1	2.7	3.6	NNW	1021.8	0
12:21	10.1	48	-0.4	2.7	4.0	NW	1021.9	0
12:22	10.2	48	-0.4	3.1	5.4	NW	1021.9	0
12:23	10.2	52	0.8	2.7	4.0	NW	1021.9	0
12:24	10.3	48	-0.3	2.7	4.0	NW	1021.8	0
12:25	10.3	48	-0.3	2.7	3.6	NW	1021.9	0
12:26	10.4	51	0.7	2.2	3.1	NW	1021.9	0
12:27	10.5	49	0.2	2.7	4.0	NW	1021.9	0
12:28	10.6	49	0.3	2.2	3.1	NW	1021.9	0

TABLE I.6. TIME DEPENDENT METEOROLOGICAL DATA FOR TEST 3 (5 MAY 2009), STATION 2 (cont.)

Time	Temperature (°C)	Relative air humidity (%)	Condensation point (°C)	Wind speed (m/s)	Maximum wind speed (m/s)	Wind direction	Air pressure (hPa)	Precipitation (mm)
12:29	10.6	47	-0.3	2.2	3.1	WNW	1021.9	0
12:30	10.6	48	0.0	2.2	3.1	NW	1021.9	0
12:31	10.7	51	0.9	3.1	5.8	NW	1021.9	0
12:32	10.7	49	0.4	3.1	4.5	NW	1022.0	0
12:33	10.7	44	-1.1	3.6	4.9	NW	1021.9	0
12:34	10.6	44	-1.2	3.1	5.4	NW	1021.9	0
12:35	10.6	45	-0.8	2.7	4.0	NW	1022.0	0
12:36	10.6	45	-0.9	2.7	4.0	NW	1022.0	0
12:37	10.6	47	-0.3	1.3	2.2	NW	1022.0	0
12:38	10.6	51	0.8	1.8	3.1	NNW	1021.9	0
12:39	10.6	49	0.3	2.7	5.8	NNW	1021.9	0
12:40	10.6	46	-0.5	3.6	6.3	WNW	1021.9	0
12:41	10.6	46	-0.5	3.6	6.3	WNW	1021.9	0
12:42	10.6	48	0.0	3.1	5.4	NW	1021.8	0
12:43	10.7	47	-0.2	2.7	3.6	NNW	1021.9	0
12:44	10.7	49	0.4	2.7	3.6	NW	1021.9	0
12:45	10.8	46	-0.4	2.2	4.0	NNW	1021.9	0
12:46	10.8	44	-1.0	3.6	5.4	NW	1021.9	0
12:47	10.8	46	-0.4	2.2	2.7	NW	1021.9	0
12:48	10.8	47	0.0	2.2	3.1	NNW	1022.0	0
12:49	10.8	49	0.5	3.1	4.0	NW	1022.0	0
12:50	10.9	46	-0.2	2.7	4.9	W	1021.9	0
12:51	11.0	45	-0.5	4.0	5.8	NNW	1022.1	0
12:52	11.1	47	0.2	3.1	5.4	NW	1022.2	0
12:53	11.2	49	0.8	2.2	4.0	NW	1022.4	0
12:54	11.3	42	-1.2	2.7	4.5	NNW	1022.4	0
12:55	11.3	45	-0.2	2.7	3.6	SSV	1022.3	0
12:56	11.4	44	-0.4	3.1	4.5	NW	1022.4	0
12:57	11.4	45	-0.1	3.1	4.9	NW	1022.4	0
12:58	11.4	45	-0.1	3.1	6.3	NNW	1022.6	0

TABLE I.6. TIME DEPENDENT METEOROLOGICAL DATA FOR TEST 3 (5 MAY 2009), STATION 2 (cont.)

Time	Temperature (°C)	Relative air humidity (%)	Condensation point (°C)	Wind speed (m/s)	Maximum wind speed (m/s)	Wind direction	Air pressure (hPa)	Precipitation (mm)
12:59	11.4	46	0.2	3.1	4.5	NW	1022.7	0
13:00	11.4	46	0.2	2.2	3.6	WNW	1022.8	0
13:01	11.5	48	0.9	2.2	3.1	NW	1022.6	0
13:02	11.6	49	1.2	3.1	4.9	NW	1022.8	0
13:03	11.6	50	1.5	4.5	6.7	NNW	1022.9	0
13:04	11.6	47	0.7	2.7	4.0	NNW	1022.8	0
13:05	11.6	50	1.5	2.7	3.6	WNW	1022.9	0
13:06	11.6	47	0.7	3.6	5.4	NW	1022.7	0
13:07	11.5	45	0.0	3.6	5.8	NW	1022.7	0
13:08	11.4	43	-0.7	4.0	6.3	NW	1022.7	0
13:09	11.3	44	-0.5	3.1	4.5	NW	1022.7	0
13:10	11.3	43	-0.9	3.1	5.4	NW	1022.5	0
13:11	11.2	44	-0.6	2.2	3.6	WNW	1022.4	0
13:12	11.2	45	-0.3	3.1	4.9	NW	1022.4	0
13:13	11.2	45	-0.3	3.1	4.0	NW	1022.4	0
13:14	11.1	43	-1.0	3.1	4.5	NW	1022.4	0
13:15	11.1	44	-0.7	3.1	4.0	NW	1022.3	0
13:16	11.1	47	0.2	1.8	2.7	WNW	1022.3	0
13:17	11.2	45	-0.3	3.1	5.4	NW	1022.3	0
13:18	11.2	46	0.0	2.2	3.6	NW	1022.2	0
13:19	11.1	43	-1.0	2.7	4.0	NW	1022.3	0
13:20	11.1	45	-0.4	2.2	3.6	NW	1022.3	0
13:21	11.1	45	-0.4	1.8	3.6	NW	1022.2	0
13:22	11.1	44	-0.8	1.8	3.6	NW	1022.3	0
13:23	11.0	44	-0.8	1.3	2.2	SSV	1022.3	0
13:24	10.9	47	0.1	2.7	4.9	NW	1022.1	0
13:25	10.9	48	0.3	3.1	4.9	NW	1022.2	0
13:26	10.8	47	0.0	3.1	4.9	NNW	1022.0	0
13:27	10.8	48	0.2	3.6	6.7	NW	1022.0	0
13:28	10.7	48	0.1	2.7	3.6	NNW	1022.0	0

TABLE I.6. TIME DEPENDENT METEOROLOGICAL DATA FOR TEST 3 (5 MAY 2009), STATION 2 (cont.)

Time	Temperature (°C)	Relative air humidity (%)	Condensation point (°C)	Wind speed (m/s)	Maximum wind speed (m/s)	Wind direction	Air pressure (hPa)	Precipitation (mm)
13:29	10.7	51	0.9	2.2	4.0	NNW	1021.8	0
13:30	10.6	51	0.9	2.7	4.9	NNW	1021.7	0

TABLE I.7. TIME DEPENDENT METEOROLOGICAL DATA FOR TEST 4 (14 JULY 2009)

Time	Temperature (°C)	Relative air humidity (%)	Condensation point (°C)	Wind speed (m/s)	Maximum wind speed (m/s)	Wind direction	Air pressure (hPa)	Precipitation (mm)
11:00	23.6	71	18.0	0	0		1013.4	0
11:01	23.7	66	17.0	0.4	0.9	SSW	1013.3	0
11:02	23.7	65	16.7	0	0.4	SSW	1013.3	0
11:03	23.8	64	16.6	0	0.4	SSW	1013.2	0
11:04	23.8	65	16.8	0	0		1013.2	0
11:05	23.8	66	17.1	0.4	0.9	SSW	1013.2	0
11:06	23.9	64	16.7	0.4	0.4	SSW	1013.2	0
11:07	23.9	64	16.7	0	0.4	SSW	1013.1	0

TABLE I.7. TIME DEPENDENT METEOROLOGICAL DATA FOR TEST 4 (14 JULY 2009) (cont.)

Time	Temperature (°C)	Relative air humidity (%)	Condensation point (°C)	Wind speed (m/s)	Maximum wind speed (m/s)	Wind direction	Air pressure (hPa)	Precipitation (mm)
11:08	23.9	63	16.5	0	0.4	SSW	1013.0	0
11:09	24.0	64	16.8	0.4	0.4	SSW	1013.0	0
11:10	24.0	63	16.5	0.4	0.9	SSW	1013.0	0
11:11	24.1	60	15.8	0.4	1.8	SSE	1013.0	0
11:12	24.1	65	17.1	0.4	0.9	SW	1013.0	0
11:13	24.1	62	16.4	0.4	0.9	W	1013.0	0
11:14	24.1	62	16.4	0	0.9	SW	1013.1	0
11:15	24.1	61	16.1	0.4	0.9	WSW	1013.1	0

TABLE I.7. TIME DEPENDENT METEOROLOGICAL DATA FOR TEST 4 (14 JULY 2009) (cont.)

Time	Temperature (°C)	Relative air humidity (%)	Condensation point (°C)	Wind speed (m/s)	Maximum wind speed (m/s)	Wind direction	Air pressure (hPa)	Precipitation (mm)
11:16	24.1	61	16.1	0.4	0.4	S	1013.0	0
11:17	24.1	63	16.6	0	0.9	SW	1013.0	0
11:18	24.1	62	16.4	0.4	0.4	SSW	1013.0	0
11:19	24.1	60	15.9	0	0.4	SSE	1013.0	0
11:20	24.1	60	15.9	0	0.9	SSE	1013.0	0
11:21	24.2	61	16.2	0.4	1.3	W	1013.0	0
11:22	24.2	62	16.4	0.4	1.3	SSW	1013.0	0
11:23	24.2	61	16.2	0	0.4	SSE	1013.1	0
11:24	24.3	61	16.3	0	0.4	SSE	1013.1	0
11:25	24.3	61	16.3	0	0.4	SSE	1013.2	0
11:26	24.3	61	16.3	0	0.9	WSW	1013.2	0
11:27	24.4	62	16.6	0.9	1.3	SW	1013.1	0
11:28	24.4	60	16.1	0.9	1.8	WSW	1013.2	0
11:29	24.4	61	16.4	0	0.4	W	1013.1	0
11:30	24.5	60	16.2	0.4	0.9	WSW	1013.0	0
11:31	24.5	60	16.2	0	0.4	WSW	1013.0	0
11:32	24.6	61	16.5	0	0.4	WSW	1013.0	0
11:33	24.6	61	16.6	0	0.4		1013.0	0
11:34	24.7	60	16.4	0.9	1.8	S	1012.9	0
11:35	24.7	60	16.4	0	0.4	SSE	1013.1	0
11:36	24.8	59	16.2	0.4	0.9	SSE	1013.1	0
11:37	24.8	60	16.5	0.4	1.8	WSW	1013.1	0
11:38	24.8	58	16.0	0.4	0.9	SW	1013.1	0
11:39	24.9	59	16.3	0	0.4	WSW	1013.1	0
11:40	24.9	60	16.6	0	0.4	WSW	1013.0	0
11:41	24.9	61	16.9	0	0.9	W	1013.0	0
11:42	24.9	60	16.6	0	0.4	W	1013.0	0
11:43	25.0	61	17.0	0	0.4	W	1013.0	0
11:44	25.0	61	17.0	0.4	0.9	W	1013.0	0
11:45	25.1	59	16.5	0.4	0.9	SSW	1013.1	0

TABLE I.7. TIME DEPENDENT METEOROLOGICAL DATA FOR TEST 4 (14 JULY 2009) (cont.)

Time	Temperature (°C)	Relative air humidity (%)	Condensation point (°C)	Wind speed (m/s)	Maximum wind speed (m/s)	Wind direction	Air pressure (hPa)	Precipitation (mm)
11:46	25.1	58	16.2	0.9	1.8	SW	1013.0	0
11:47	25.1	58	16.2	0.9	1.3	SW	1012.9	0
11:48	25.1	58	16.2	0.4	0.9	SSE	1013.0	0
11:49	25.1	57	15.9	0.4	1.8	SSW	1013.0	0
11:50	25.1	59	16.5	0.4	1.3	WSW	1013.0	0
11:51	25.1	59	16.5	0	0		1013.1	0
11:52	25.2	60	16.9	0	0.4	WSW	1013.1	0
11:53	25.2	57	16.1	0.9	2.7	SSE	1013.1	0
11:54	25.2	57	16.1	0.4	0.9	S	1013.0	0
11:55	25.3	58	16.4	0.4	0.4	SW	1013.0	0
11:56	25.3	58	16.4	0.4	1.8	SSW	1012.9	0
11:57	25.3	58	16.5	0	0.4	SSW	1013.0	0
11:58	25.3	58	16.5	0	0		1013.0	0
11:59	25.4	60	17.1	0	0.9	SW	1013.0	0
12:00	25.4	56	16.0	0.9	1.3	S	1013.0	0
12:01	25.4	56	16.0	0.4	0.9	W	1012.9	0
12:02	25.4	57	16.3	0	0.9	W	1012.9	0
12:03	25.4	57	16.3	0.9	2.2	SSE	1013.0	0
12:04	25.4	58	16.6	0.4	1.8	W	1013.0	0
12:05	25.4	58	16.6	0.4	0.4	W	1013.0	0
12:06	25.4	57	16.3	0.4	0.9	W	1013.0	0
12:07	25.4	57	16.3	0.4	0.9	W	1013.0	0
12:08	25.4	58	16.6	0.4	0.9	W	1013.0	0
12:09	25.4	58	16.6	0.4	0.9	SW	1013.1	0
12:10	25.4	58	16.5	0.4	0.9	SW	1013.1	0
12:11	25.4	60	17.1	0.9	1.8	WSW	1013.1	0
12:12	25.4	58	16.5	0	0.4	WSW	1013.1	0
12:13	25.4	59	16.8	0.4	0.9	WSW	1013.1	0
12:14	25.4	59	16.8	0.4	0.9	WSW	1013.1	0
12:15	25.4	58	16.5	0	0		1013.0	0

TABLE I.7. TIME DEPENDENT METEOROLOGICAL DATA FOR TEST 4 (14 JULY 2009) (cont.)

Time	Temperature (°C)	Relative air humidity (%)	Condensation point (°C)	Wind speed (m/s)	Maximum wind speed (m/s)	Wind direction	Air pressure (hPa)	Precipitation (mm)
12:16	25.4	58	16.5	0	0		1013.0	0
12:17	25.4	58	16.6	0	0.4	WSW	1013.0	0
12:18	25.4	60	17.1	0.4	0.9	SSE	1013.0	0
12:19	25.4	58	16.6	0	0.4	SE	1012.9	0
12:20	25.4	59	16.8	0	0.4	S	1012.9	0
12:21	25.5	60	17.2	0.4	0.9	W	1012.9	0
12:22	25.5	60	17.2	0.4	1.8	SSE	1012.8	0
12:23	25.5	58	16.6	0.9	1.8	SW	1012.8	0
12:24	25.5	59	16.9	0.4	0.9	SW	1012.7	0
12:25	25.5	58	16.6	0.4	0.9	SW	1012.7	0
12:26	25.5	59	16.9	0.4	0.9	S	1012.7	0
12:27	25.5	58	16.6	0	0.4	SSE	1012.8	0
12:28	25.4	59	16.8	0	0.4	SSE	1012.7	0
12:29	25.5	59	16.9	0	0.4	SSE	1012.7	0
12:30	25.4	60	17.1	0	0.4	SSE	1012.7	0
12:31	25.5	60	17.2	0.4	0.9	WSW	1012.8	0
12:32	25.5	59	16.9	0.4	0.9	SSE	1012.7	0
12:33	25.5	57	16.4	0.4	0.9	VSE	1012.7	0
12:34	25.5	58	16.6	0	0.9	WSW	1012.7	0
12:35	25.5	59	16.9	0	0.9	SSW	1012.8	0
12:36	25.4	59	16.8	0	0.4	SW	1012.8	0
12:37	25.5	58	16.6	0	0.9	WSW	1012.7	0
12:38	25.4	62	17.6	0	0.4	WSW	1012.7	0
12:39	25.4	59	16.8	0	0.9	S	1012.7	0
12:40	25.4	58	16.6	0.4	1.8	SSE	1012.7	0
12:41	25.4	57	16.3	0.9	0.9	S	1012.6	0
12:42	25.4	58	16.5	0	0.4	S	1012.7	0
12:43	25.4	58	16.5	0	0.4	S	1012.6	0
12:44	25.4	58	16.5	0.4	0.9	SW	1012.7	0
12:45	25.4	60	17.1	0	0.4	WSW	1012.8	0

TABLE I.7. TIME DEPENDENT METEOROLOGICAL DATA FOR TEST 4 (14 JULY 2009) (cont.)

Time	Temperature (°C)	Relative air humidity (%)	Condensation point (°C)	Wind speed (m/s)	Maximum wind speed (m/s)	Wind direction	Air pressure (hPa)	Precipitation (mm)
12:46	25.4	60	17.1	0	0		1012.8	0
12:47	25.4	61	17.4	0	0		1012.8	0
12:48	25.4	58	16.6	0	0		1012.8	0
12:49	25.4	58	16.6	0	0.4	SW	1012.7	0
12:50	25.5	59	16.9	0.4	0.9	SSW	1012.7	0
12:51	25.6	57	16.4	0	0.9	SW	1012.7	0
12:52	25.6	56	16.1	0.4	0.9	SE	1012.7	0
12:53	25.6	57	16.5	0.9	1.8	SW	1012.7	0
12:54	25.7	59	17.1	0.4	0.9	WSW	1012.6	0
12:55	25.7	58	16.8	0	0.4	WSW	1012.7	0
12:56	25.7	58	16.8	0.4	0.9	WSW	1012.7	0
12:57	25.8	58	16.9	0.9	1.8	SW	1012.7	0
12:58	25.8	59	17.2	0.4	0.9	W	1012.7	0
12:59	25.8	57	16.7	0.4	0.9	W	1012.7	0
13:00	25.9	57	16.7	0.4	0.9	WSW	1012.7	0
13:01	25.9	58	17.0	0.9	2.7	SSE	1012.7	0
13:02	26.0	58	17.1	0.4	0.9	SSW	1012.6	0
13:03	26.1	57	16.9	0.9	1.8	W	1012.7	0
13:04	26.2	58	17.3	0.4	0.9	SW	1012.7	0
13:05	26.3	57	17.1	0.9	1.8	SW	1012.7	0
13:06	26.3	59	17.7	0.4	0.9	SW	1012.6	0
13:07	26.4	57	17.2	1.3	2.7	SSW	1012.7	0
13:08	26.5	56	17.0	0.4	0.9	SW	1012.8	0
13:09	26.5	55	16.7	0.4	1.8	W	1012.7	0
13:10	26.6	56	17.1	0.4	1.8	S	1012.7	0
13:11	26.7	55	16.9	0.4	0.9	W	1012.7	0
13:12	26.7	53	16.3	0	0.4	SSW	1012.6	0
13:13	26.8	55	17.0	0	0.4	SSW	1012.6	0
13:14	26.9	55	17.1	0.4	0.9	SW	1012.6	0
13:15	26.9	57	17.7	0.4	0.9	WSW	1012.6	0

TABLE I.7. TIME DEPENDENT METEOROLOGICAL DATA FOR TEST 4 (14 JULY 2009) (cont.)

Time	Temperature (°C)	Relative air humidity (%)	Condensation point (°C)	Wind speed (m/s)	Maximum wind speed (m/s)	Wind direction	Air pressure (hPa)	Precipitation (mm)
13:16	27.0	55	17.2	0.9	1.3	W	1012.6	0
13:17	27.1	55	17.3	1.3	3.1	SSW	1012.6	0
13:18	27.2	53	16.8	0.4	1.8	SSW	1012.5	0
13:19	27.2	55	17.4	1.3	2.2	SW	1012.5	0
13:20	27.3	55	17.4	0.9	2.2	WSW	1012.6	0
13:21	27.3	53	16.9	0.4	0.9	SSW	1012.6	0
13:22	27.4	55	17.5	0.9	2.2	WSW	1012.6	0
13:23	27.4	51	16.4	0.9	1.3	S	1012.6	0
13:24	27.4	52	16.7	0.4	0.9	SW	1012.6	0
13:25	27.5	54	17.4	0.4	0.9	SW	1012.6	0
13:26	27.6	54	17.4	0.9	1.8	WSW	1012.6	0
13:27	27.6	54	17.5	0.4	1.3	SW	1012.6	0
13:28	27.7	56	18.1	1.3	2.2	SSW	1012.7	0
13:29	27.7	53	17.3	1.3	2.7	W	1012.7	0
13:30	27.8	54	17.6	0.9	2.7	SSW	1012.6	0
13:31	27.9	56	18.3	0.9	1.8	S	1012.6	0
13:32	27.9	53	17.4	1.3	1.8	WSW	1012.6	0
13:33	27.9	53	17.4	1.8	4.9	WSW	1012.7	0
13:34	27.9	54	17.8	0.4	0.9	SW	1012.7	0
13:35	27.9	53	17.4	1.3	3.1	WSW	1012.7	0
13:36	27.9	53	17.4	0.9	2.2	WSW	1012.7	0
13:37	27.9	55	18.1	1.3	2.2	W	1012.8	0
13:38	27.9	54	17.8	0.9	2.2	SW	1012.8	0
13:39	27.9	53	17.5	1.3	3.1	WSW	1012.8	0
13:40	27.9	55	18.0	0.4	0.9	SSW	1012.9	0
13:41	27.9	53	17.4	1.3	2.2	W	1012.9	0
13:42	27.9	57	18.6	1.3	2.2	WSW	1012.9	0
13:43	27.9	54	17.7	1.3	3.1	WSW	1012.8	0
13:44	27.9	55	18.0	1.8	2.7	W	1012.8	0
13:45	27.9	55	18.0	1.3	2.2	W	1012.9	0

TABLE I.7. TIME DEPENDENT METEOROLOGICAL DATA FOR TEST 4 (14 JULY 2009) (cont.)

Time	Temperature (°C)	Relative air humidity (%)	Condensation point (°C)	Wind speed (m/s)	Maximum wind speed (m/s)	Wind direction	Air pressure (hPa)	Precipitation (mm)
13:46	27.9	55	18.0	1.3	3.1	WSW	1012.9	0
13:47	27.9	55	18.1	1.8	2.7	WSW	1012.8	0
13:48	27.9	54	17.7	1.8	3.6	WSW	1012.9	0
13:49	27.9	54	17.7	1.8	2.7	SW	1012.8	0
13:50	27.8	53	17.4	0.9	2.7	WSW	1012.8	0
13:51	27.8	54	17.6	1.8	2.7	W	1012.8	0
13:52	27.7	54	17.6	0.9	2.2	W	1012.9	0
13:53	27.6	55	17.8	1.3	3.6	W	1012.9	0
13:54	27.6	55	17.7	1.3	1.8	SSW	1012.9	0
13:55	27.5	56	17.9	0.4	1.8	SW	1012.9	0
13:56	27.4	56	17.9	1.8	3.6	W	1012.9	0
13:57	27.4	55	17.5	1.8	4.0	SW	1013.0	0
13:58	27.4	56	17.8	1.8	2.7	WSW	1013.0	0
13:59	27.4	56	17.8	0.9	1.8	WSW	1013.0	0
14:00	27.4	57	18.1	0.9	1.8	SW	1013.0	0

The geometry of the test material is illustrated in Fig. I.2 for Tests 1 and 2. Tests 3 and 4 used a similar configuration to that used for Test 2 (see also Fig. I.3). The outer plastic case (blue in Fig. I.3) is made from a standard 1 L PET plastic bottle, approximately 20 cm long. The technetium solution is in a 6 mL spherical glass bottle inside the larger bottle. A set of schematic drawings of the configuration used for Tests 2 to 4 was provided to the participants.

The arrangements of detectors for Tests 1 and 2 are included with the available measurements (see Section I.4). The arrangements for Tests 3 and 4 are provided in Figs I.4 and I.5. Test 4 (14 July 2009) included two obstacles (shown in Fig. I.5). The small obstacle has dimensions of 3 m × 3 m × 1.5 m (width, height, length). The large obstacle has dimensions of 11 m × 2.5 m × 6 m (width, height, length).

For Test 1, most of the released inventory was in the form of drops (Fig. I.6). For Tests 2 to 4, most of the released inventory is thought to have been in an aerosol (Fig. I.6).

The explosion sequences for Tests 1 and 2 are provided in Figs I.7 and I.8. Video footage of all four tests (in most cases from more than one location) was made available to participants in the exercise.

DustTrak data for Test 2 are provided in Fig. I.9. Volume activities in various size intervals and distances from the place of radioactive material dispersal, as a percentage of total activities, are provided in Table I.8.

I.4. DATA FOR CALIBRATION

Measurement data for the first two field tests (6 December 2007 and 15 May 2008) include surface contamination (Bq/m^2) for Tests 1 and 2, dose rates (nSv/h) for Test 2, and time integrated air concentrations at selected locations (Test 2). Dose rates need to be used with caution, due to high background dose rates at the test site. The surface contamination and dose rates were made available to participants as GIS and Excel files. Plots of the data are provided in Figs I.10 to I.12. The time integrated air concentrations (Test 2) are provided in Table I.9. The measurements on which the time integrated air concentrations are based are provided in Tables I.10 and I.11. Suggested values for aerosol diameters and deposition velocities are provided in Table I.12; these values are based on the information for Test 2 in Tables I.8 and I.11. The measured surface contamination for Tests 1 and 2 and the measured dose rates for Test 2 are provided in Tables I.13 to I.15.

I.5. MODELLING ENDPOINTS

Tests 3 and 4 (5 May 2009 and 14 July 2009) were used in the exercise for blind testing of models. Model predictions were compared with each other (model intercomparisons) and eventually with the available measurements, to the extent possible (endpoints 1, 2, and 3 below, within the range of measurements).

Test 1:

Test 2:

Test 1:

Test 2:

FIG. I.2. Geometry of field tests.

FIG. I.3. Photographs of box holding the explosive setup.

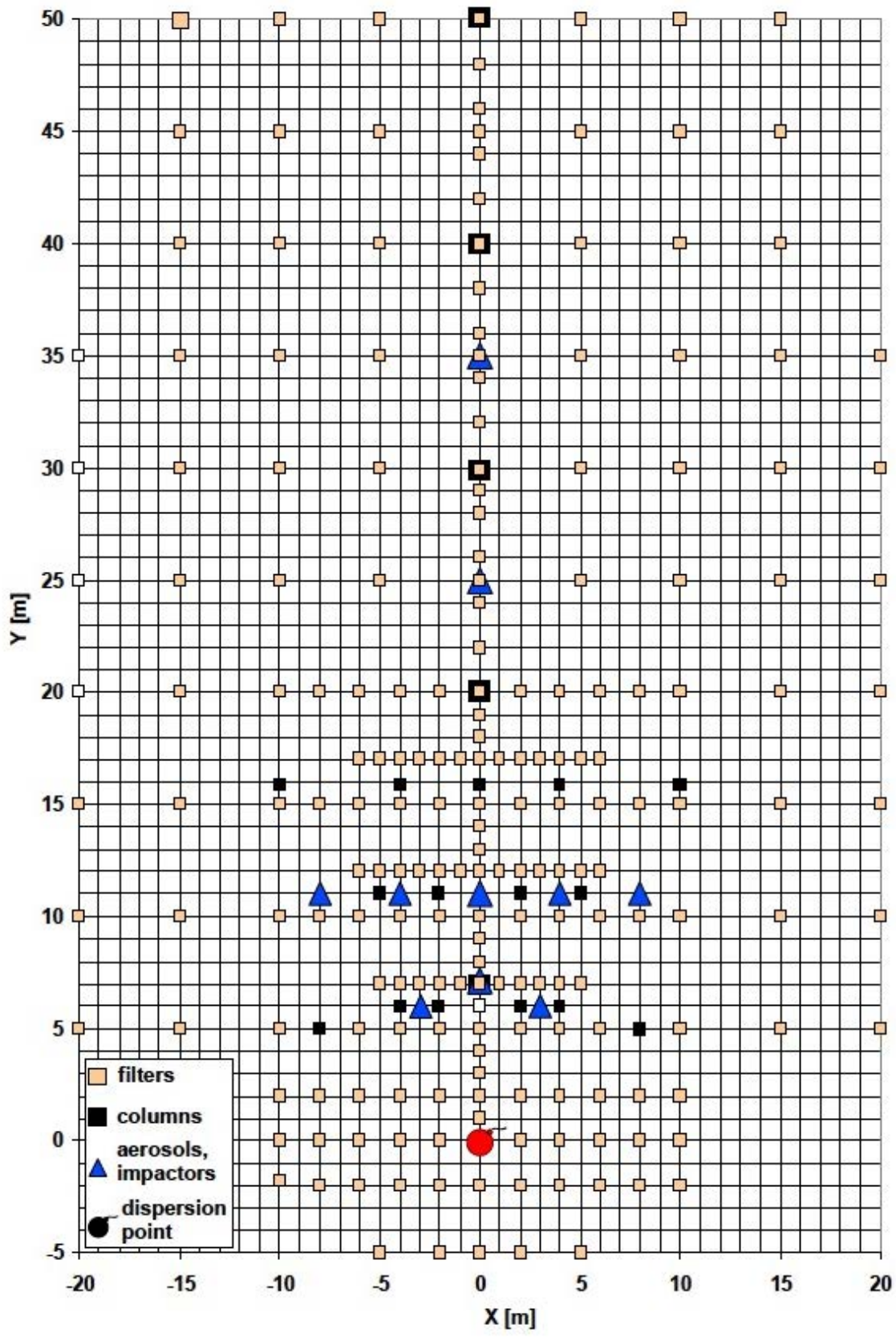

FIG. I.4. Arrangement of detectors for Test 3 (5 May 2009).

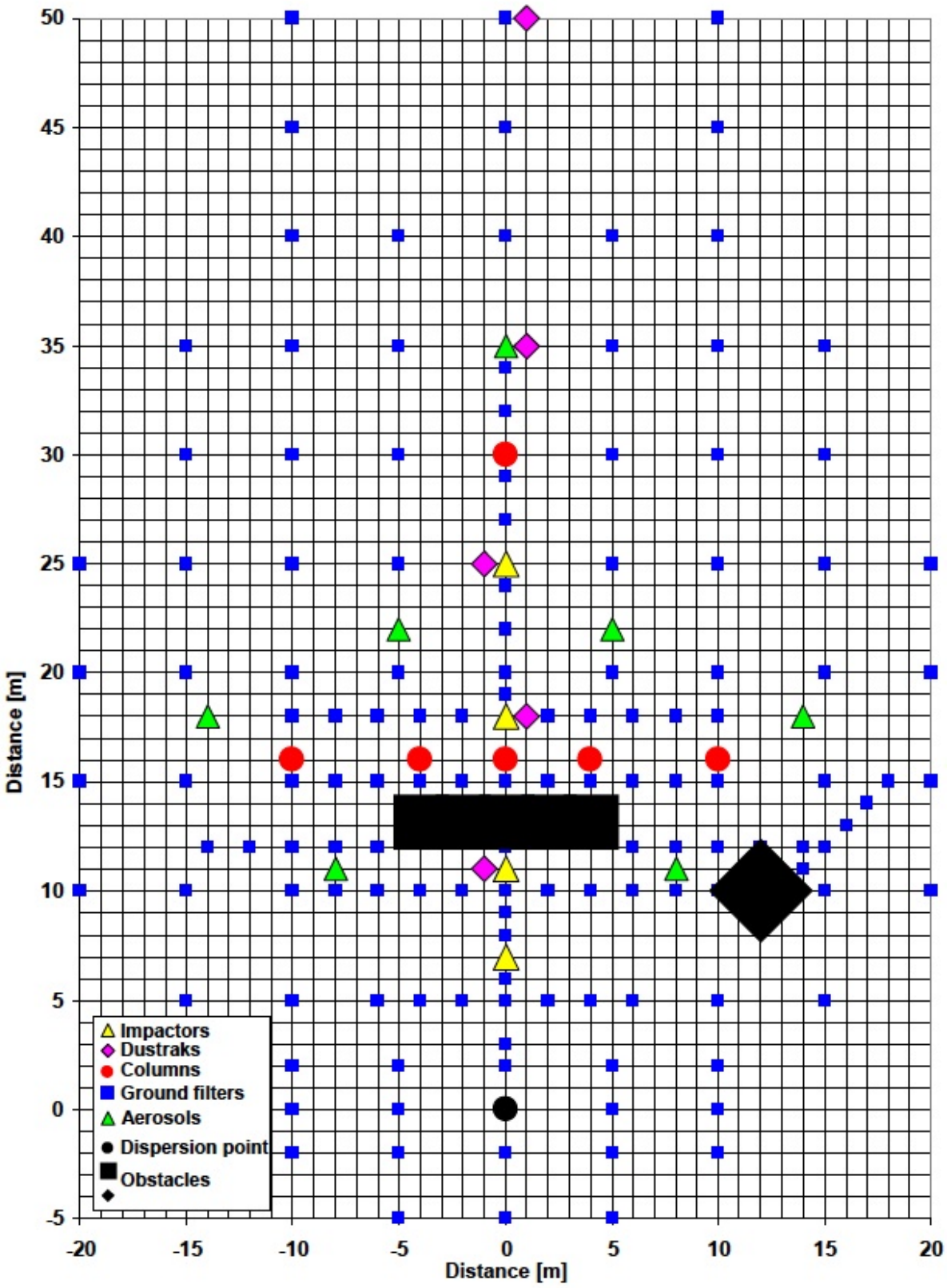

FIG. I.5. Arrangement of detectors for Test 4 (14 July 2009).

Test 1:

Test 2:

FIG. I.6. Photographs of the released material.

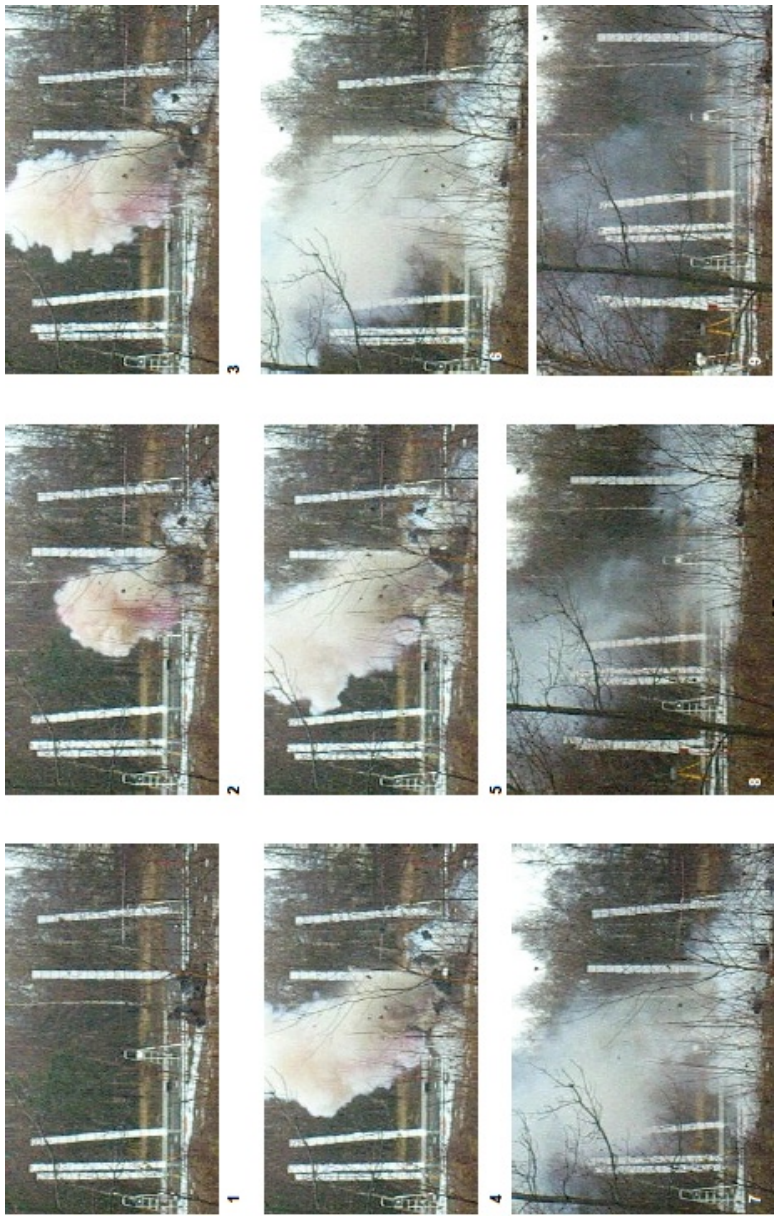

FIG. I.7. Explosion sequence for Test 1 (6 December 2007).

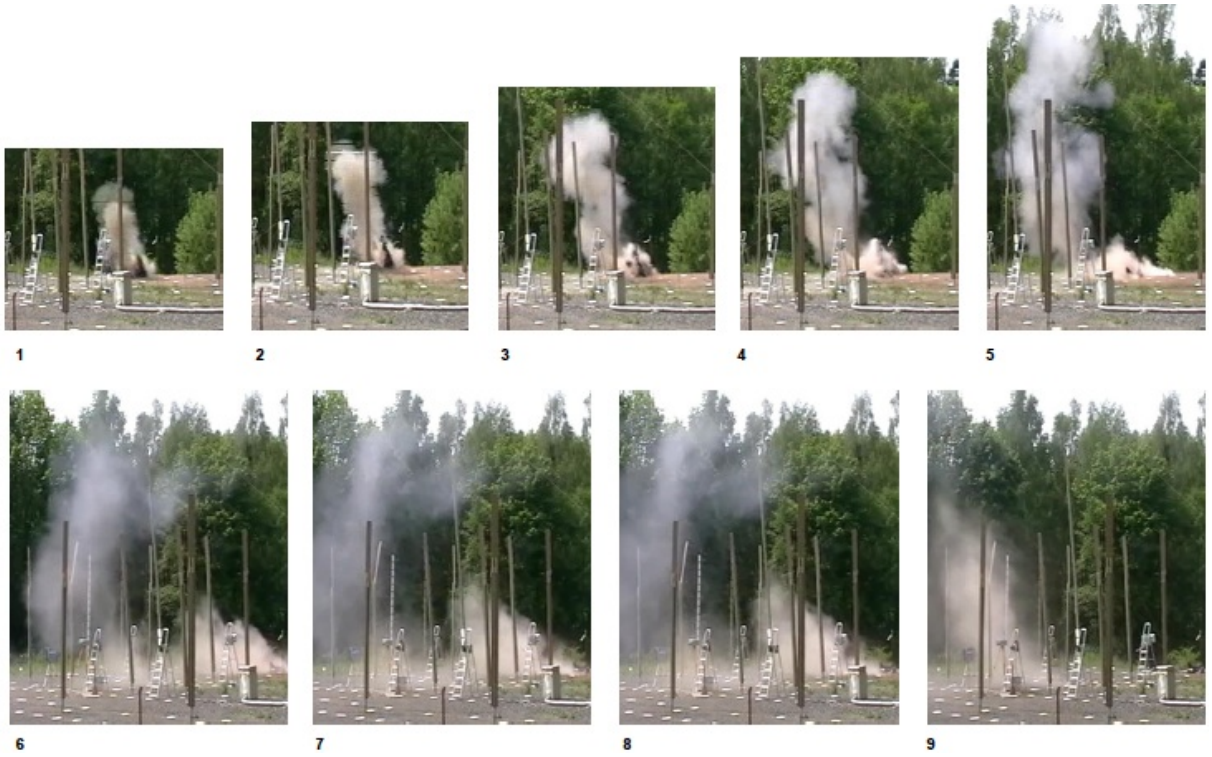

FIG. I.8. Explosion sequence for Test 2 (15 May 2008).

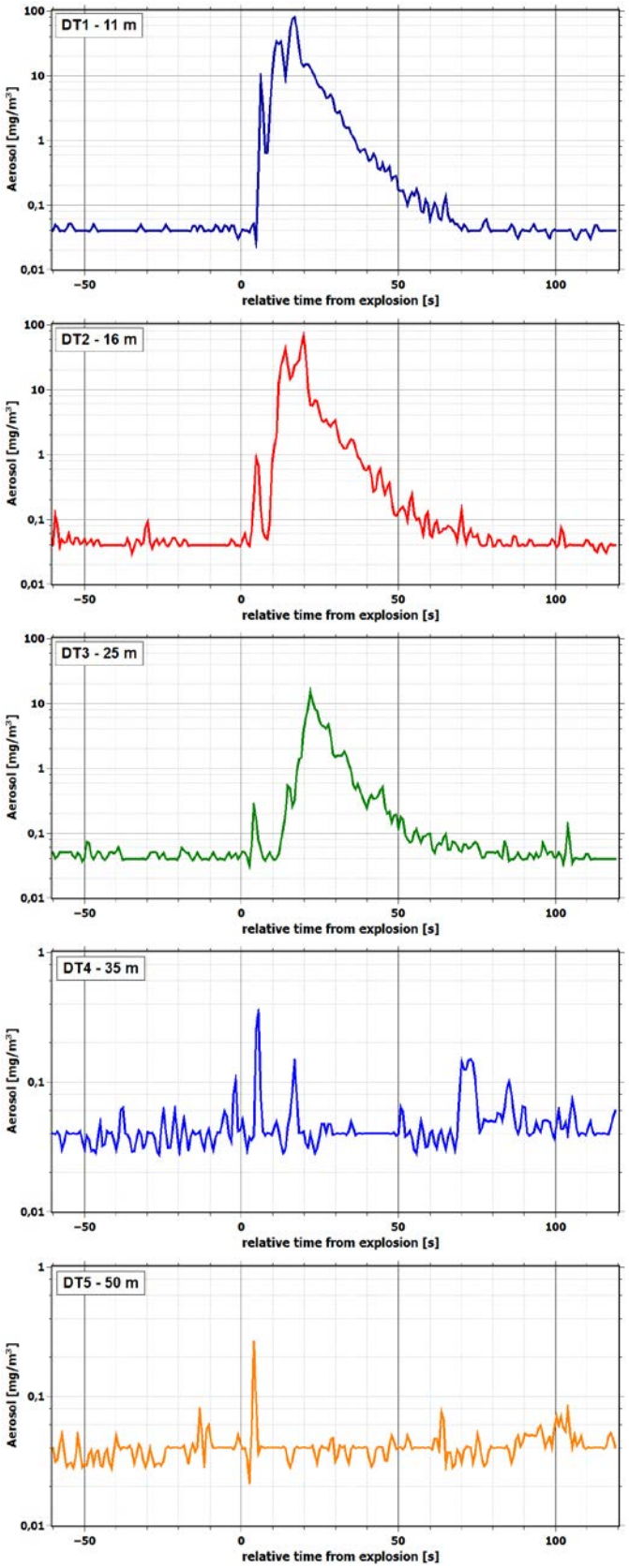

FIG. I.9. DustTrak data for Test 2 (15 May 2008). The devices were placed at distances of 11 m, 16 m, 25 m, 35 m and 50 m from the dispersion point, in parallel with the y-axis of the test grid, and at a distance of 1 m to the right or left of the y-axis of the test grid. The sampling heads were 1.8 m above

ground level. Integration time was 1 s. The x-axes represent time before and after the explosion; y-axes represent aerosol concentrations in mg/m^3.

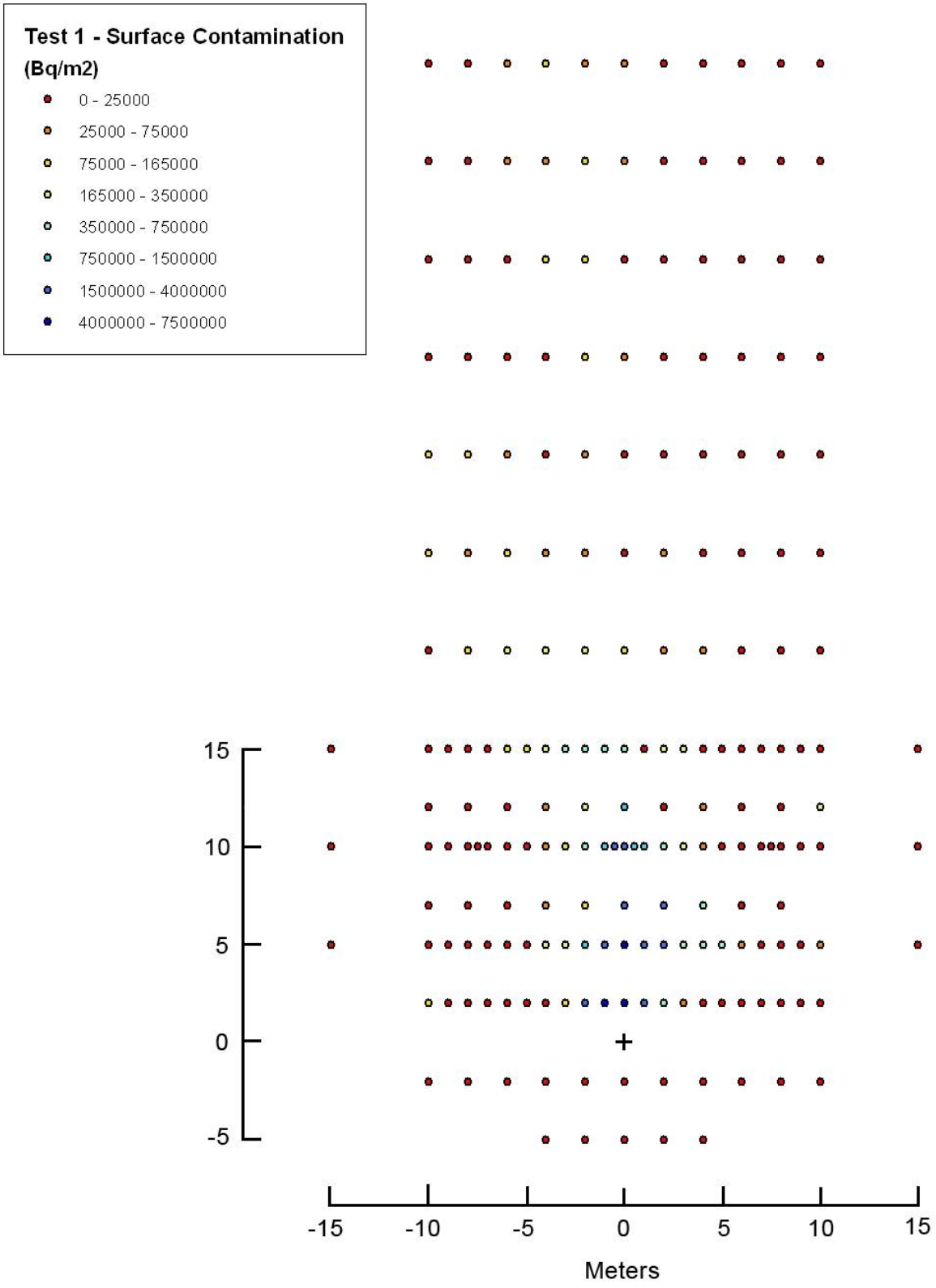

FIG. I.10. Surface contamination measurements for Test 1 (6 December 2007).

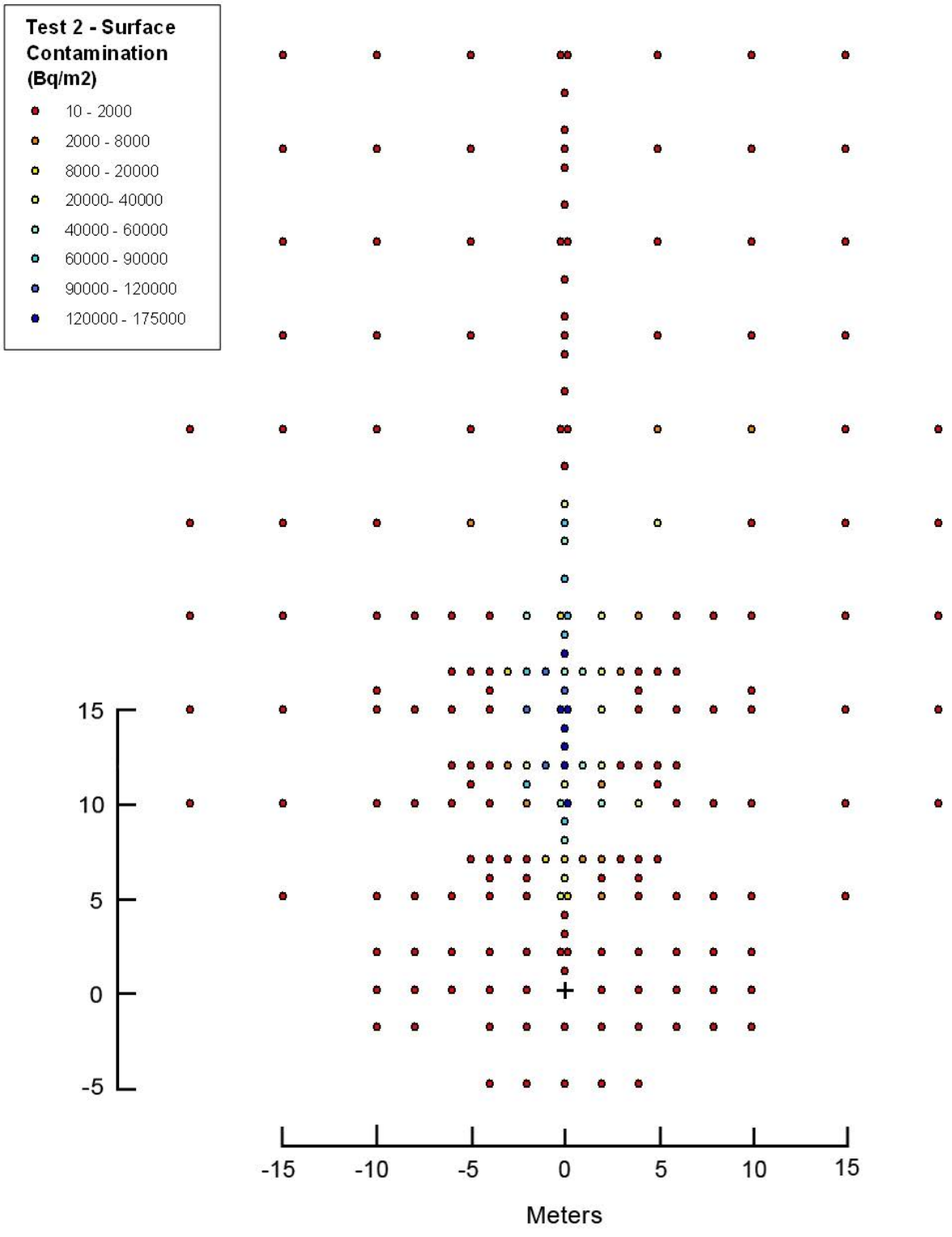

FIG. I.11. Surface contamination measurements for Test 2 (15 May 2008).

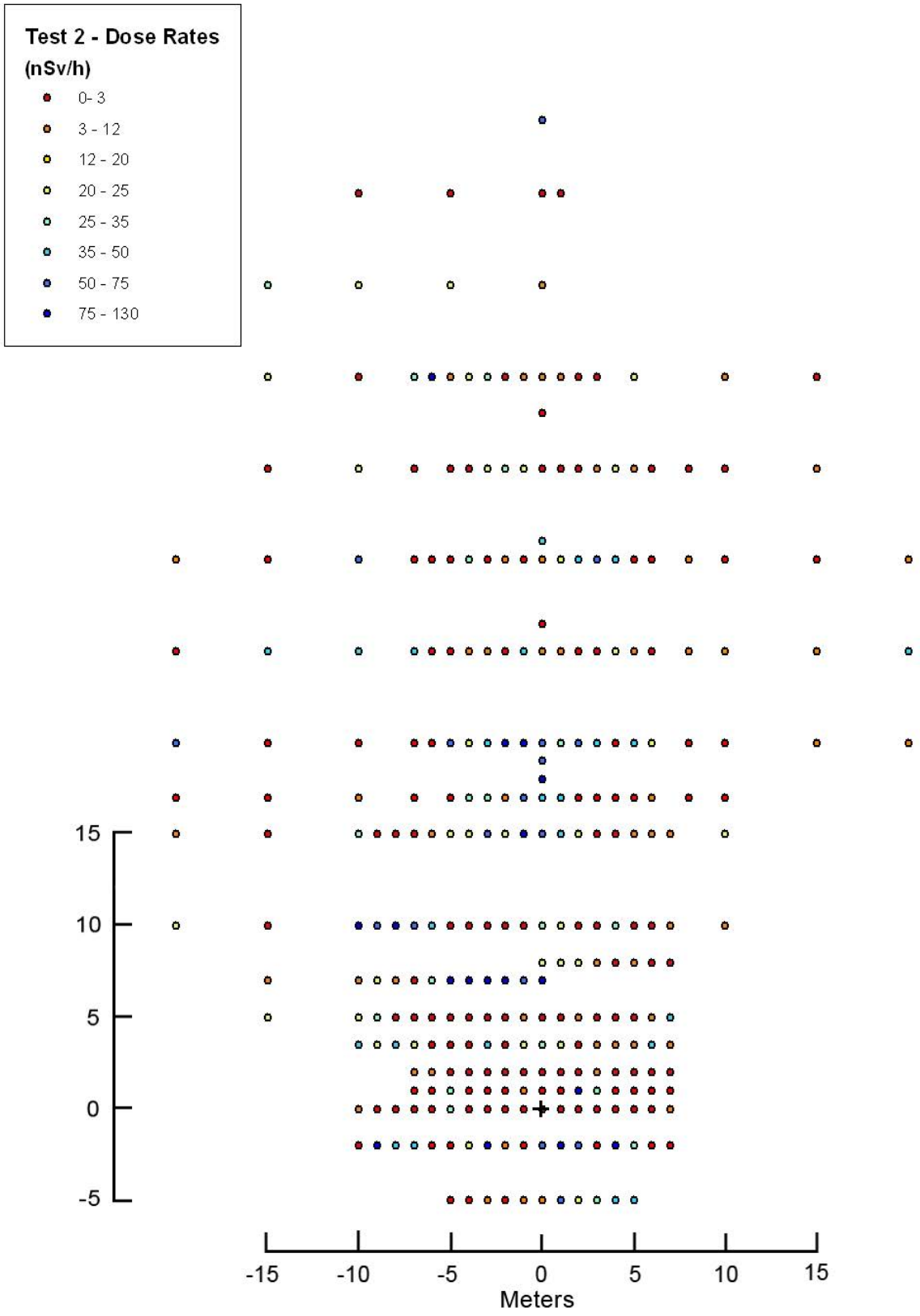

FIG. I.12. Dose rate measurements for Test 2 (15 May 2008).

TABLE I.8. VOLUME ACTIVITIES IN VARIOUS SIZE INTERVALS AND DISTANCES FROM THE PLACE OF RADIOACTIVE MATERIAL DISPERSAL, AS A PERCENTAGE OF TOTAL ACTIVITY (Test 2, 15 May 2008)

Sampling interval (min)	*0–117*	*0–129*	*0–117*
Distance (m)	*11*	*25*	*35*
Selection interval (μm)	Volume activity (% of total)		
>10.2	10.0	4.3	18.1
1.3–10.2	46.6	20.5	46.4
0.39–1.3	15.0	5.9	14.4
<0.39	28.4	69.3	21.1

TABLE I.9. TIME INTEGRATED AIR CONCENTRATIONS AT SELECTED LOCATIONS FOR TEST 2[a]

Location (Coordinates in m)	Time integrated air concentration[b] (Bq min m^{-3})
-8;11	11.0
8;11	28.5
4;11	119
-4;11	2690
-3;6	30.6
3;6	29.3
Centerline distance (m)	
11	73 400
25	13 100
35	194

[a] 'Less than' values were included at the nominal value.

[b] Based on measurements in Tables I.10 and I.11.

TABLE I.10. TOTAL VOLUME ACTIVITIES OF AEROSOLS IN THE INDICATED SAMPLING INTERVALS[a]

Sample		AERO 1/1	AERO 1/2	AERO 1/3	AERO 1/4
Sampling time [b]	mm:ss	15:48	29:25	43:50	53:13
Mean volume activity [c]	Bq/m^3	0.14	0.06	0.10	0.05
Sampler position [d]	m	(-8;11)			
Sample		AERO 2/1	AERO 2/2	AERO 2/3	AERO 2/4
Sampling time	mm:ss	18:08	28:22	43:48	53:00
Mean volume activity	Bq/m^3	0.77	0.29	<0.01	0.11
Sampler position	m	(8;11)			
Sample		AERO 3/1	AERO 3/2	AERO 3/3	AERO ¾
Sampling time	mm:ss	18:58	28:40	43:37	53:11
Mean volume activity	Bq/m^3	5.12	0.14	0.06	0.28
Sampler position	m	(4; 11)			
Sample		AERO 4/1	AERO 4/2	AERO 4/3	AERO 4/4
Sampling time	mm:ss	20:18	28:33	43:44	53:01
Mean volume activity	Bq/m^3	121	<0.36	0.18	<4.06
Sampler position	m	(-4;11)			
Sample		AERO 5/1	AERO 5/2	AERO 5/3	AERO 5/4
Sampling time	mm:ss	21:48	28:10	44:00	52:39
Mean volume activity	Bq/m^3	0.67	0.36	0.11	<0.02
Sampler position	m	(-3;6)			
Sample		AERO 6/1	AERO 6/2	AERO 6/3	AERO 6/4
Sampling time	mm:ss	23:03	28:15	44:15	52:32
Mean volume activity	Bq/m^3	0.50	0.20	0.12	0.13
Sampler position	m	(3;6)			

[a] The time necessary for changes of the aerosol filter was neglected.

[b] Time period of the sampling (15:48 means period from 0 to 15:48 minutes, 29:25 means the next 29:25 minutes after the first period, etc.).

[c] Total activity divided by total air volume in the sampler for appropriate sampling period.

[d] Explosion point is x = 0, y = 0. The sign '-' ('+') means left (right) from axis of radioactive material dispersion.

TABLE I.11. VOLUME ACTIVITIES IN VARIOUS SIZE INTERVALS AND DISTANCES FROM THE PLACE OF RADIOACTIVE MATERIAL DISPERSAL (height = 1 m)

Sampling interval (min)	0–117	0–129	0–117
Distance (m)	11	25	35
Selection interval (μm)	Volume activity (Bq/m^3)		
>10.2	63	4.4	0.3
1.3–10.2	292	20.8	0.77
0.39–1.3	94	6.0	0.24
<0.39	178	70.5	0.35
Total	627	101.7	1.66

TABLE I.12. SUGGESTED VALUES FOR AEROSOL DIAMETERS AND DEPOSITION VELOCITIES (TEST 2)[a]

Size range (μm)	Average diameter (μm)	Deposition velocity (10^{-4} m/s)
<0.39	0.2	0.5
0.39–1.3	1	1.5
1.3–10.2	8	10
>10.2	20	80

[a] Based on information in Tables I.8 and I.11.

TABLE I.13. MEASURED SURFACE CONTAMINATION (DEPOSITION) FOR TEST 1, 6 DECEMBER 2007 (Bq/m^2)

Coordinates (m)[a]		Deposition (Bq/m^2)
X	Y	
-15	5	292.49
-15	10	618.28
-15	15	1201.81
-10	-2	18 788.91
-10	2	97 906.06
-10	5	1494.06
-10	7	0
-10	10	534.19
-10	12	410.87
-10	15	1878.89
-10	20	7130.73
-10	25	12 1264.89
-10	30	119 977.36
-10	35	24 787.78
-10	40	8092.81
-10	45	0
-10	50	9054.9
-9	2	18 109.79
-9	5	43.15
-9	10	1216.75
-9	15	2337.29
-8	-2	701.75
-8	2	5942.28
-8	5	32.26
-8	7	1019.57
-8	10	727.51
-8	12	297.83
-8	15	1963.78
-8	20	127 900.4
-8	25	27 366.52
-8	30	90 548.95
-8	35	15 959.25
-8	40	11 262.03
-8	45	7583.47

-8	50	5942.28
-7.5	10	912.22
-7	2	4878.32

TABLE I.13. MEASURED SURFACE CONTAMINATION (DEPOSITION) FOR TEST 1, 6 DECEMBER 2007 (Bq/m^2) (cont.)

Coordinates (m)[a]		Deposition (Bq/m^2)
X	Y	
-7	5	905.49
-7	10	8156.23
-7	15	22 184.49
-6	-2	667.8
-6	2	2682.51
-6	5	735.71
-6	7	3326.09
-6	10	1383.79
-6	12	7543.48
-6	15	84 889.64
-6	20	324 844.37
-6	25	86 830.89
-6	30	63 384.27
-6	35	14 657.61
-6	40	9847.2
-6	45	47 311.83
-6	50	54 782.12
-5	2	1794
-5	5	899.83
-5	10	11 941.14
-5	15	131 295.98
-4	-5	44.43
-4	-2	301.64
-4	2	1499.72
-4	5	29 2586.3
-4	7	56 325.79
-4	10	58 290.89
-4	12	37608.7
-4	15	318619.13
-4	20	280 135.82
-4	25	53 285.07
-4	30	23 561.35
-4	35	21 844.93
-4	40	99037.92
-4	45	74 702.89
-4	50	120 543.29
-3	2	145 444.26
-3	5	219 581.21
-3	10	103 565.37
-3	15	473 684.21
-2	-5	20.51
-2	-2	365.03

TABLE I.13. MEASURED SURFACE CONTAMINATION (DEPOSITION) FOR TEST 1, 6 DECEMBER 2007 (Bq/m^2) (cont.)

Coordinates (m)[a]		Deposition (Bq/m^2)
X	Y	
-2	2	2 189 886.8
-2	5	882 852.29
-2	7	162 826.09
-2	10	496 537.77
-2	12	350 000
-2	15	730 050.93
-2	20	216 185.63
-2	25	60 524.89
-2	30	35 087.72
-2	35	99 603.85
-2	40	146 010.19
-2	45	129 032.26
-2	50	41 539.33
-1	2	4 933 623.19
-1	5	2 096 040.58
-1	10	1 359 793.59
-1	15	469 312.29
-0.5	10	1 790 339.48
0	-5	11.04
0	-2	17 204.3
0	2	7 406 632.86
0	5	4 091 014.89
0	7	3 294 341.48
0	10	1 835 100
0	12	1 015 188.68
0	15	409 734.01
0	20	84323.71
0	25	426.43
0	30	24561.4
0	35	40 860.22
0	40	18 788.91
0	45	29 145.44
0	50	31 239.39
0.5	10	1 034 225.23
1	2	1 748 956.37
1	5	3 703 683.35
1	10	1 084 407.5
1	15	6276.92
2	-5	137.52
2	-2	13 412.56
2	2	472 690.45
2	5	1 776 547.02
2	7	2 043 548.73
2	10	622 524.05
2	12	628.26
2	15	287 492.93
2	20	35 710.24

TABLE I.13. MEASURED SURFACE CONTAMINATION (DEPOSITION) FOR TEST 1, 6 DECEMBER 2007 (Bq/m^2) (cont.)

Coordinates (m)[a]		Deposition (Bq/m^2)
X	Y	
2	25	53 556.35
2	30	14 883.98
2	35	12 563.67
2	40	22 127.9
2	45	6451.61
2	50	2818.34
3	2	31 745.86
3	5	48 6134.69
3	10	218 449.35
3	15	228 070.18
4	-5	23.06
4	-2	956.42
4	2	17 543.86
4	5	616 864.74
4	7	533 840.75
4	10	69 043.58
4	12	31 086.96
4	15	11 714.77
4	20	56 310.13
4	25	5104.07
4	30	2048.67
4	35	2076.97
4	40	5772.5
4	45	3101.3
4	50	2229.77
5	2	10 604.68
5	5	469 722.69
5	10	24 052.07
5	15	22 976.8
6	-2	341.82
6	2	4974.53
6	5	62 252.41
6	7	6500
6	10	1573.29
6	12	765.22
6	15	17 770.23
6	20	18.11
6	25	14.41
6	30	102.57
6	35	14.41
6	40	102.57
6	45	537.07
6	50	18.25
7	2	2724.92
7	5	4125.64
7	10	46.69
7	15	735.71

TABLE I.13. MEASURED SURFACE CONTAMINATION (DEPOSITION) FOR TEST 1, 6 DECEMBER 2007 (Bq/m^2) (cont.)

Coordinates (m)[a]		Deposition (Bq/m^2)
X	Y	
7.5	10	4807.24
8	-2	315.79
8	2	899.83
8	5	5772.5
8	7	269.57
8	10	19.81
8	12	363.04
8	15	28.86
8	20	32.4
8	25	10.75
8	30	451.05
8	35	667.8
8	40	28.86
8	45	22.78
8	50	64.37
9	2	2376.91
9	5	9620.83
9	10	14.86
9	15	43.01
10	-2	24.34
10	2	844.52
10	5	30 786.64
10	10	328.24
10	12	211 388.9
10	15	464.06
10	20	22.92
10	25	299
10	30	17.69
10	35	91.54
10	40	22.78
10	45	28.3
10	50	58.01
15	5	1628.96
15	10	926.7
15	15	165.79

[a] Coordinates represent distances (m) from the dispersion point (0,0) in the grid area of the field test.

TABLE I.14. MEASURED SURFACE CONTAMINATION (DEPOSITION) FOR TEST 2, 15 MAY 2008 (Bq/m^2)

Coordinates (m)[a]		Deposition (Bq/m^2)
X	Y	
0	-5	76.89
-2	-5	135.78

-4	-5	39.56
2	-5	107.33
4	-5	113.11
0	-2	40.89
-2	-2	20.44
-4	-2	68.67
-8	-2	40.44
-10	-2	109.78
2	-2	41.11
4	-2	21.78
6	-2	40.22
8	-2	64
10	-2	25.11
-2	0	84.89
2	0	15.11
-4	0	12.44
4	0	65.11
-6	0	10
6	0	76.67
-8	0	14.67
8	0	291.11
-10	0	205.11
10	0	182.67
0	1	598.22
-0.2	2	737.78
-10	2	38.44

TABLE I.14. MEASURED SURFACE CONTAMINATION (DEPOSITION) FOR TEST 2, 15 MAY 2008 (Bq/m^2) (cont.)

Coordinates (m)[a]		Deposition (Bq/m^2)
X	Y	
-8	2	14.22
-6	2	59.56
-4	2	14
-2	2	16.89
0.2	2	182
2	2	79.11
4	2	108.67
6	2	9.56
8	2	10
10	2	78.67
0	3	322.22
0	4	465.11
-0.2	5	22 454.22
-15	5	70.22
-10	5	218.67
-8	5	79.33
-6	5	23.56
-4	5	65.33
-2	5	412.44

TABLE I.14. MEASURED SURFACE CONTAMINATION (DEPOSITION) FOR TEST 2, 15 MAY 2008 (Bq/m^2) (cont.)

Coordinates (m)[a]		Deposition (Bq/m^2)
X	Y	
0.2	5	8946.89
2	5	5614.22
4	5	154.89
6	5	109.11
8	5	67.78
10	5	46.67
15	5	14.22
0	6	35 669.33
-4	6	66.44
-2	6	1713.78
2	6	562.67
4	6	69.78
0	7	8937.78
-5	7	118.89
-4	7	23.33
-3	7	138.44
-2	7	126.67
-1	7	16 922.22
1	7	4231.11
2	7	4477.33
3	7	165.78
4	7	91.33
5	7	91.56
0	8	46 084.22
0	9	67 708.67
-0.2	10	53 718.89
-20	10	37.11
20	10	80.44
-15	10	478.44
-10	10	145.78
-8	10	332
-6	10	36.44
-4	10	221.78
-2	10	2059.78
0.2	10	146 699.22
2	10	58 872.44
4	10	21 684.61
6	10	25.56
8	10	25.78
10	10	54.22
15	10	94.22
0	11	37 295.56
-5	11	97.78
-2	11	81 542.22
2	11	4659.78
5	11	80.67
0	12	161 428.89

TABLE I.14. MEASURED SURFACE CONTAMINATION (DEPOSITION) FOR TEST 2, 15 MAY 2008 (Bq/m^2) (cont.)

Coordinates (m)[a]		Deposition (Bq/m^2)
X	Y	
-6	12	482.67
-5	12	67.56
-4	12	457.56
-3	12	7618.67
-2	12	24 742.67
-1	12	105 702.22
1	12	53 130.67
2	12	21 791.11
3	12	343.11
4	12	43.78
5	12	188.89
6	12	80
0	13	120 071.11
0	14	144 702.22
-0.2	15	161 282.22
-20	15	87.11
20	15	63.11
-15	15	59.78
-10	15	75.33
-8	15	157.78
-6	15	16.89
-4	15	207.11
-2	15	104 904.44
0.2	15	137 215.56
2	15	29 524.44
4	15	45.56
6	15	142.89
8	15	19.56
10	15	13.33
15	15	44.22
0	16	100 433.33
-10	16	13.78
-4	16	262.44
4	16	172.44
10	16	77.78
0	17	58 722.89
-6	17	287.56
-5	17	40.89
-4	17	222.89
-3	17	10 014.44
-2	17	69 686.44
-1	17	113 162.44
1	17	44 271.33
2	17	28 846.67
3	17	6151.56
4	17	459.78
5	17	127.78

TABLE I.14. MEASURED SURFACE CONTAMINATION (DEPOSITION) FOR TEST 2, 15 MAY 2008 (Bq/m^2) (cont.)

Coordinates (m)[a]		Deposition (Bq/m^2)
X	Y	
6	17	14.22
0	18	170 435.56
0	19	86 373.33
-0.2	20	14 503.78
-20	20	34
20	20	45.33
-15	20	148.89
-10	20	36.44
-8	20	26.89
-6	20	12.22
-4	20	1519.56
-2	20	57 211.11
0.2	20	80 424.44
2	20	28 209.56
4	20	5692.22
6	20	1075.56
8	20	952.22
10	20	32.44
15	20	22.89
0	22	77 843.11
0	24	58 779.22
-20	25	82
20	25	19.56
-15	25	477.78
-10	25	137.33
-5	25	3022.22
0	25	87 196.67
5	25	20 541.11
10	25	1585.56
15	25	459.11
0	26	22 883.33
0	28	1270.22
-0.2	30	22.89
-20	30	259.78
20	30	336.44
-15	30	262.67
-10	30	41.11
-5	30	122.89
0.2	30	77.78
5	30	3232.67
10	30	2789.11
15	30	903.33
0	32	260.22
0	34	993.67
-15	35	1605.78
-10	35	87.11
-5	35	175.78

TABLE I.14. MEASURED SURFACE CONTAMINATION (DEPOSITION) FOR TEST 2, 15 MAY 2008 (Bq/m^2) (cont.)

Coordinates (m)[a]		Deposition (Bq/m^2)
X	Y	
0	35	428
5	35	1038
10	35	1160.67
15	35	84.67
0	36	136.89
0	38	388.89
-0.2	40	417.78
-15	40	147.33
-10	40	782.89
-5	40	364.44
0.2	40	198.67
5	40	715.33
10	40	52.67
15	40	73.11
0	42	398.44
0	44	181.56
-15	45	513.33
-10	45	516.89
-5	45	132.89
0	45	657.33
5	45	453.11
10	45	188.89
15	45	757.33
0	46	120.22
0	48	21.33
-0.2	50	90
-15	50	80.22
-10	50	68.44
-5	50	79.33
0.2	50	382.22
5	50	1078
10	50	752
15	50	1012

[a] Coordinates represent distances (m) from the dispersion point (0,0) in the grid area of the field test.

TABLE I.15. MEASURED EXTERNAL DOSE RATES FOR TEST 2, 15 MAY 2008 (nSv/h)

Coordinates (m)[a]		Dose rate (nSv/h)
X	Y	
0	-5	0
-1	-5	10.027816
-2	-5	0
-3	-5	10.027816
-4	-5	0

-5	-5	0
0	-2	0
-1	-2	0
-2	-2	11.426308
-3	-2	125.689389
-4	-2	22.852616
-5	-2	0
-6	-2	0
-7	-2	45.57845
-8	-2	45.57845

TABLE I.15. MEASURED EXTERNAL DOSE RATES FOR TEST 2, 15 MAY 2008 (nSv/h) (cont.)

Coordinates (m)[a]		Dose rate (nSv/h)
X	Y	
-9	-2	102.551512
-10	-2	0
-10	0	11.394612
-9	0	0
-8	0	0
-7	0	0
-6	0	0
-5	0	30.083449
-4	0	0
-3	0	0
-2	0	0
-1	0	0
0	0	0
-7	1	0
-6	1	0
-5	1	33.525572
-4	1	0
-3	1	0
-2	1	0
-1	1	10.027816
0	1	0
0	2	0
-1	2	0
-2	2	0
-3	2	0
-4	2	0
-5	2	0
-6	2	10.990481
-7	2	10.959994
-10	3.5	43.718368
-9	3.5	21.859184
-8	3.5	43.597097
-7	3.5	21.798548
-6	3.5	0
-5	3.5	0

TABLE I.15. MEASURED EXTERNAL DOSE RATES FOR TEST 2, 15 MAY 2008 (nSv/h) (cont.)

Coordinates (m)[a]		Dose rate (nSv/h)
X	Y	
-4	3.5	0
-3	3.5	43.476162
-2	3.5	0
-1	3.5	21.677781
0	3.5	21.677781
0	5	21.617649
-1	5	10.808824
-2	5	0
-3	5	0
-4	5	0
-5	5	0
-6	5	0
-7	5	0
-8	5	0
-9	5	32.157375
-10	5	21.43825
-15	5	21.43825
-15	7	10.689391
-10	7	10.689391
-9	7	21.319479
-8	7	10.65974
-7	7	0
-6	7	31.625861
-5	7	94.877582
-4	7	84.101688
-3	7	105.12711
-2	7	115.639821
-1	7	52.417748
0	7	104.835495
0	10	10.48355
-1	10	0
-2	10	0
-3	10	0
-4	10	0
-5	10	0
-6	10	41.586198
-7	10	51.982748
-8	10	83.172397
-9	10	72.573973
-10	10	103.677104
-15	10	0
-20	10	20.677902
-20	15	10.338951
-15	15	0
-10	15	30.083449
-9	15	0
-8	15	0

TABLE I.15. MEASURED EXTERNAL DOSE RATES FOR TEST 2, 15 MAY 2008 (nSv/h) (cont.)

Coordinates (m)[a]		Dose rate (nSv/h)
X	Y	
-7	15	0
-6	15	10.281672
-5	15	20.506302
-4	15	20.506302
-3	15	71.772058
-2	15	20.506302
-1	15	92.022388
0	15	61.348258
0	17	81.797678
-1	17	71.37443
-2	17	10.196347
-3	17	30.589042
-4	17	30.50419
-5	17	0
-7	17	0
-10	17	10.027816
-15	17	0
-20	17	0
-20	20	70.585771
-15	20	0
-10	20	0
-7	20	0
-6	20	0
-5	20	50.139082
-4	20	20.055633
-3	20	40.111266
-2	20	90
-1	20	90
0	20	20
0	25	0
-1	25	35.342502
-2	25	0
-3	25	11.748155
-4	25	11.748155
-5	25	0
-6	25	0
-7	25	35.146699
-10	25	35.146699
-15	25	35.049205
-20	25	0
-20	30	11.683068
-15	30	0
-10	30	58.253302
-7	30	0
-6	30	0
-5	30	0
-4	30	34.758342

TABLE I.15. MEASURED EXTERNAL DOSE RATES FOR TEST 2, 15 MAY 2008 (nSv/h) (cont.)

Coordinates (m)[a]		Dose rate (nSv/h)
X	Y	
-3	30	0
-2	30	11.586114
-1	30	0
0	30	0
0	35	57.609626
-1	35	23.04385
-2	35	34.565776
-3	35	22.979929
-4	35	0
-5	35	0
-7	35	0
-10	35	22.916184
-15	35	0
-15	40	22.852616
-10	40	0
-7	40	34.278924
-6	40	91.156899
-5	40	11.394612
-4	40	22.789225
-3	40	34.089014
-2	40	0
-1	40	11.363005
0	40	0
0	45	11.331485
-5	45	22.662969
-10	45	22.600104
-15	45	33.900156
-10	50	0
-5	50	2.253741
0	50	0
1	50	0
0	54	56.187239
0	-5	11.586114
1	-5	57.93057
2	-5	23.236685
3	-5	34.855027
4	-5	46.602642
5	-5	46.602642
0	-2	57.769875
1	-2	92.4318
2	-2	57.769875
3	-2	0
4	-2	103.985775
5	-2	34.661925
0	0	0
1	0	0
2	0	0

TABLE I.15. MEASURED EXTERNAL DOSE RATES FOR TEST 2, 15 MAY 2008 (nSv/h) (cont.)

Coordinates (m)[a]		Dose rate (nSv/h)
X	Y	
3	0	0
4	0	0
5	0	0
0	1	0
1	1	0
2	1	101.983361
3	1	33.994454
4	1	0
5	1	0
6	1	0
7	1	0
6	0	0
7	0	11.144192
6	-2	0
7	-2	0
7	2	0
6	2	0
5	2	0
4	2	0
3	2	11.082451
2	2	0
1	2	0
0	2	0
0	3.5	33.063158
1	3.5	22.042105
2	3.5	0
3	3.5	10.990481
4	3.5	10.959994
5	3.5	10.959994
6	3.5	43.718368
7	3.5	10.929592
0	5	0
1	5	0
2	5	10.86904
3	5	0
4	5	0
5	5	0
6	5	10.838891
7	5	43.476162
0	8	21.43825
1	8	21.378782
2	8	21.378782
3	8	10.65974
4	8	0
5	8	10.63017
6	8	0
7	8	0

TABLE I.15. MEASURED EXTERNAL DOSE RATES FOR TEST 2, 15 MAY 2008 (nSv/h) (cont.)

Coordinates (m)[a]		Dose rate (nSv/h)
X	Y	
0	10	31.625861
1	10	21.083907
2	10	0
3	10	0
4	10	31.713832
5	10	0
6	10	0
7	10	10.600683
10	10	10.600683
0	15	52.272345
1	15	41.817876
2	15	20.908938
3	15	0
4	15	0
5	15	10.39655
6	15	10.39655
7	15	10.39655
10	15	20.793099
0	17	41.012605
1	17	41.012605
2	17	0
3	17	0
4	17	0
5	17	0
6	17	10.168063
8	17	0
10	17	0
0	20	50.840317
1	20	30.50419
2	20	50.699289
3	20	40.559432
4	20	0
5	20	40.559432
6	20	20.279716
8	20	0
10	20	0
15	20	10.083682
20	20	10.083682
0	25	11.748155
1	25	11.748155
2	25	0
3	25	0
4	25	23.49631
5	25	11.748155
0	19	50.981736
0	18	81.570778
6	25	0

TABLE I.15. MEASURED EXTERNAL DOSE RATES FOR TEST 2, 15 MAY 2008 (nSv/h) (cont.)

Coordinates (m)[a]		Dose rate (nSv/h)
X	Y	
8	25	10
10	25	10
15	25	10
20	25	40
0	26.5	0
0	30	11.683068
1	30	23.366137
2	30	46.732274
3	30	58.415342
4	30	46.732274
5	30	0
6	30	0
8	30	11.618342
10	30	0
15	30	0
20	30	11.618342
0	35	0
1	35	0
2	35	0
3	35	11.363005
4	35	22.726009
5	35	11.426308
6	35	0
8	35	0
10	35	0
15	35	11.426308
0	31	45.705232
0	38	0
0	40	11.331485
1	40	11.331485
2	40	0
3	40	0
5	40	22.662969
10	40	11.331485
15	40	0

[a] Coordinates represent distances (m) from the dispersion point (0,0) in the grid area of the field test.

For purposes of model intercomparison, participants were requested to use the following grid size, subject to model constraints:

— downwind distance 0–50 m: use a 5 × 5 m grid (Δx = 5 m);
— downwind distance 50–2000 m: use a 25 × 25 m grid (Δx = 25 m);
— upwind distance: to 100 m;

— width: Model dependent (measurements cover an area of 50 m × 40 m, or 20 m each side of the centerline).

For purposes of model intercomparison, participants were requested to use the following initial volume for the plume from the explosion: a cuboid with edge lengths of 7 m × 7 m × 12 m, with a homogeneous concentration of the material within the plume. As desired, participants could make additional calculations with one or more different specifications of the initial plume.

The activity of ^{99m}Tc at the time of the explosion needs to be used.

Endpoints to be modelled for Tests 3 and 4:

(1) Surface contamination (Bq/m^2) as a function of distance, assuming the grid described above. Assume that the deposition has been completed.
(2) Dose rates (mGy/h, at 1 m height) as a function of distance, assuming the grid described above. Assume that the deposition has been completed.
(3) Time integrated air concentrations (Bq · min · m^{-3}) as a function of height and distance along the center line, out to 1000 m, for heights from 0–5 m.
(4) Estimated percentile contamination zones (50%, 75% and 95%) for each explosion event. The contamination zone is the area (for example, defined in terms of a radius from the explosion, or an angle and distance from the explosion, or some selected contour) which is expected to contain a given percentage of the contamination released by the explosion event. Specify whether the zones are defined as a percentage of total activity or a percentage of total deposition.

Where possible, uncertainties on the model predictions were requested.

I.6. ADDITIONAL MODELLING ACTIVITIES

Additional modelling activities can be carried out for the four tests, using the measurements of dose rate or surface activity. The measured surface contamination for Tests 3 and 4 was not available to participants during the exercise but are provided in Tables I.16 and I.17. These activities include estimation of the source term from available measurements, validation of location factors, and use of data assimilation to improve initial model predictions. One example of using the data to estimate a source term from surface activity measurements is described in Annex I.

TABLE I.16. MEASURED SURFACE CONTAMINATION (DEPOSITION) FOR TEST 3, 5 MAY 2009 (Bq/m^2)

Coordinates (m)[a]		Deposition (Bq/m^2)
X	Y	
-20	5	104.24
-20	10	349.33
-20	15	241.56
-20	20	133.60
-20	25	23.93
-20	30	85.93
-20	35	97.98

-15	5	129.02
-15	10	303.56
-15	15	168.98
-15	20	305.56
-15	25	360.67
-15	30	42.89
-15	35	97.49
-15	40	76.84
-15	45	97.29
-15	50	84.22
-10	0	244.44
-10	2	281.11

TABLE I.16. MEASURED SURFACE CONTAMINATION (DEPOSITION) FOR TEST 3, 5 MAY 2009 (Bq/m^2) (cont.)

Coordinates (m)[a]		Deposition (Bq/m^2)
X	Y	
-10	5	1105.33
-10	10	881.56
-10	15	535.56
-10	20	901.11
-10	25	648.00
-10	30	110.87
-10	35	206.42
-10	40	140.07
-10	45	172.29
-10	50	211.84
-8	-2	3.01
-8	0	3.21
-8	2	588.44
-8	5	1178.22
-8	10	677.18
-8	15	1694.89
-8	20	1609.11
-6	-2	22.73
-6	0	23.31
-6	2	531.33
-6	5	1576.00
-6	10	4284.44
-6	12	2260.00
-6	15	1539.78
-6	17	2462.22
-6	20	2591.11
-5	-5	23.64
-5	7	7173.33
-5	12	3482.22
-5	17	1767.56
-5	25	2948.89
-5	30	1166.22
-5	35	1224.67

TABLE I.16. MEASURED SURFACE CONTAMINATION (DEPOSITION) FOR TEST 3, 5 MAY 2009 (Bq/m^2) (cont.)

Coordinates (m)[a]		Deposition (Bq/m^2)
X	Y	
-5	40	459.56
-5	45	592.67
-5	50	1090.89
-4	-2	25.69
-4	0	25.13
-4	2	350.00
-4	5	10 300.00
-4	7	12 664.44
-4	10	12 395.56
-4	12	33 933.33
-4	15	4526.67
-4	17	5924.44
-4	20	6955.56
-3	7	226 000.00
-3	12	45 577.78
-3	17	14 048.89
-2	-5	36.82
-2	-2	8.87
-2	0	6.56
-2	2	33 044.44
-2	5	182 466.67
-2	7	170 355.56
-2	10	122 111.11
-2	12	70 644.44
-2	15	120 288.89
-2	17	44 400.00
-2	20	55 400.00
-1	7	209 266.67
-1	12	69 422.22
-1	17	58 733.33
0	-5	13.96
0	2	121.56
0	3	255 555.56
0	4	1 432 000.00
0	5	363 777.78
0	6	224 888.89
0	7	592 000.00
0	8	97 222.22
0	9	247 777.78
0	10	75 248.89
0	12	78 111.11
0	13	184 200.00
0	14	208 066.67
0	15	66 600.00
0	17	78 000.00
0	18	69 488.89
0	19	49 088.89

TABLE I.16. MEASURED SURFACE CONTAMINATION (DEPOSITION) FOR TEST 3, 5 MAY 2009 (Bq/m^2) (cont.)

Coordinates (m)[a]		Deposition (Bq/m^2)
X	Y	
0	20	36 022.22
0	22	35 977.78
0	24	27 132.00
0	25	18 991.11
0	26	15 226.67
0	28	8524.44
0	29	10 428.89
0	30	5666.67
0	32	7068.89
0	34	14 036.38
0	35	10 444.44
0	36	7813.33
0	38	5046.67
0	40	5191.11
0	42	5077.78
0	44	6475.56
0	45	7997.78
0	46	10 075.56
0	48	12 793.33
0	50	10 057.78
1	7	18 6511.11
1	12	113 644.44
1	17	85 533.33
2	-5	10.98
2	-2	27.84
2	0	31.58
2	2	3106.67
2	5	199 066.67
2	7	922 888.89
2	10	103 311.11
2	12	86 844.44
2	15	72 688.89
2	17	79 666.67
2	20	51 533.33
3	7	155 777.78
3	12	84 266.67
3	17	66 688.89
4	-2	27.24
4	0	990.89
4	2	1036.89
4	5	3353.33
4	7	74 111.11
4	10	109 582.22
4	12	50 977.78
4	15	83 488.89
4	17	48 377.78
4	20	2457.78

TABLE I.16. MEASURED SURFACE CONTAMINATION (DEPOSITION) FOR TEST 3, 5 MAY 2009 (Bq/m^2) (cont.)

Coordinates (m)[a]		Deposition (Bq/m^2)
X	Y	
5	-5	7.94
5	7	5440.00
5	12	64 022.22
5	17	34 044.44
5	25	31 066.67
5	30	52 355.56
5	35	20 473.33
5	40	8915.56
5	45	9471.11
5	50	8388.89
6	-2	49.98
6	0	39.73
6	2	921.11
6	5	2968.89
6	10	28 800.00
6	12	155 200.00
6	15	41 644.44
6	17	1680.22
6	20	3411.11
8	-2	45.64
8	0	98.07
8	2	786.67
8	5	1461.78
8	10	2911.60
8	15	16 086.67
8	20	13 491.11
10	-2	36.47
10	0	48.93
10	2	444.67
10	5	5.00
10	10	134.96
10	15	1571.33
10	20	469.33
10	25	11 262.22
10	30	28 377.78
10	35	25 044.44
10	40	12 728.89
10	45	31 400.00
10	50	8500.00
15	5	109.67
15	10	99.84
15	15	555.11
15	20	982.22
15	25	3035.56
15	30	5944.44
15	35	27 377.78
15	40	25 466.67

TABLE I.16. MEASURED SURFACE CONTAMINATION (DEPOSITION) FOR TEST 3, 5 MAY 2009 (Bq/m^2) (cont.)

Coordinates (m)[a]		Deposition (Bq/m^2)
X	Y	
15	45	18 991.11
15	50	9800.00
20	5	128.53
20	10	8.67
20	15	563.78
20	20	532.89
20	25	652.67
20	30	1190.22
20	35	7695.56

[a] Coordinates represent distances (m) from the dispersion point (0,0) in the grid area of the field test.

TABLE I.17. MEASURED SURFACE CONTAMINATION (DEPOSITION) FOR TEST 4, 14 JULY 2009 (Bq/m^2)

Coordinates (m)[a]		Deposition (Bq/m^2)
X	Y	
-5	-5	1486.00
0	-5	347.30
5	-5	18.57
-10	-2	5548.00
-5	-2	2716.00
0	-2	187.00
5	-2	30.92
10	-2	3.27
-10	0	4412.00
-5	0	3032.00
5	0	17.94
10	0	1.83
-10	2	6235.00
-5	2	8045.00
0	2	2094.00
5	2	181.30
10	2	7.76
0	3	1010.00
-15	5	2582.00
-10	5	12 620.00
-6	5	18 860.00
-4	5	15 740.00
-2	5	2652.00
0	5	881.80
2	5	136.60
4	5	39.19

TABLE I.17. MEASURED SURFACE CONTAMINATION (DEPOSITION) FOR TEST 4, 14 JULY 2009 (Bq/m^2) (cont.)

Coordinates (m)[a]		Deposition (Bq/m^2)
X	Y	
6	5	24.82
10	5	12.18
15	5	11.08
0	6	3067.00
0	8	855.00
0	9	1450.00
-20	10	594.30
-15	10	3317.00
-10	10	9065.00
-8	10	8641.00
-6	10	4863.00
-4	10	3542.00
-2	10	2663.00
0	10	1587.00
2	10	1921.00
4	10	1153.00
6	10	39.51
8	10	26.66
10	10	18.89
12	10	17.07
15	10	12.09
20	10	16.77
14	11	16.29
0	12	1785.00
15	12	24.21
-14	13	915.60
-12	13	2053.00
-10	13	4542.00
-8	13	2724.00
-6	13	4419.00
6	13	111.30
8	13	60.86
10	13	35.49
12	13	42.21
14	13	27.60
15	13	16.67
17	14	19.94
-20	15	25.28
-15	15	67.59
-10	15	313.50
-8	15	583.10
-6	15	1080.00
-4	15	17.63
-2	15	29.82
0	15	22.42
2	15	11.31
4	15	24.06

TABLE I.17. MEASURED SURFACE CONTAMINATION (DEPOSITION) FOR TEST 4, 14 JULY 2009 (Bq/m^2) (cont.)

Coordinates (m)[a]		Deposition (Bq/m^2)
X	Y	
5	15	7.51
8	15	8.40
10	15	6.25
15	15	3.29
18	15	1.73
20	15	1.07
-10	18	13.76
-8	18	15.06
-6	18	36.18
-4	18	11.52
-2	18	18.19
2	18	20.38
4	18	9.24
6	18	7.21
8	18	5.10
10	18	8.27
0	19	9.82
-20	20	9.48
-15	20	11.22
-10	20	13.10
-5	20	14.58
0	20	10.06
5	20	5.89
10	20	5.71
15	20	2.25
20	20	0.84
0	22	9.33
0	24	5.07
-20	25	6.97
-15	25	18.21
-10	25	15.65
-5	25	7.29
5	25	4.82
10	25	2.71
15	25	0.54
20	25	9.02
0	27	5.78
0	29	5.00
-15	30	6.27
-10	30	9.97
-5	30	6.69
5	30	3.84
10	30	1.70
15	30	3.32
0	32	3.21
0	34	4.36
-15	35	3.28
-10	35	6.36

TABLE I.17. MEASURED SURFACE CONTAMINATION (DEPOSITION) FOR TEST 4, 14 JULY 2009 (Bq/m^2) (cont.)

Coordinates (m)[a]		Deposition (Bq/m^2)
X	Y	
-5	35	3.39
5	35	3.69
10	35	2.42
15	35	5.04
-10	40	8.27
-5	40	1.99
0	40	3.20
4	40	2.03
10	40	3.02
-10	45	0.98
-5	45	1.71
0	45	2.03
4	45	3.90
10	45	1.93

[a] Coordinates represent distances (m) from the dispersion point (0,0) in the grid area of the field test.

I.7. REFERENCES TO APPENDIX I

[I.1] INTERNATIONAL ATOMIC ENERGY AGENCY, Environmental Modelling for Radiation Safety (EMRAS). A Summary Report of the Results of the EMRAS Programme (2003–2007), IAEA-TECDOC-1678, IAEA, Vienna (2012).

[I.2] MECKBACH, R., JACOB, P., Gamma exposures due to radionuclides deposited in urban environments. Part II: Location factors for different deposition patterns, Radiation Protection Dosimetry **25** (1988) 181.

[I.3] HOVORKA, J., Dust-Tracks Measurements, Contract—SÚRO—Institute of the Environmental Studies, Charles University, Praha (in Czech) (2008).

[I.4] PROUZA, Z., BECKOVA, V., CESPIROVA, I., HELEBRANT, J., HULKA, J., KUCA, P., MICHALEK, V., RULIK, P., SKRKAL, J., HOVORKA, J., Field tests using radioactive matter, Radiation Protection Dosimetry **139** (2010) 519.

APPENDIX II. DESCRIPTION OF MODELS USED TO RUN THE SHORT RANGE ATMOSPHERIC DISPERSION EXERCISE

The short range atmospheric dispersion exercise was executed by eight participants using eight models. These included:

- Atmospheric Dispersion and Dose Analysis Method (ADDAM) (run by S.L. Chouhan, Canada);
- Canadian Standards Association (CSA-ERM) code (run by S.L. Chouhan);
- Computational Fluid Dynamics (CFD) code (run by G. de With, Netherlands);
- CLMM (run by V. Fuka, Czech Republic);
- HOTSPOT 2.07.1 (run by T.W. Charnock, UK and D. Trifunović, Croatia);
- LASAIR (run by H. Walter, Germany);
- RDD_MMC (run by J. Ďúran, Slovakia); and
- University of Seville Model (USev) (run by R. Periáñez, Spain).

Descriptions of each of these models and their assumptions are provided in the sections that follow.

II.1. DESCRIPTION OF ADDAM AND CSA-ERM

The Atmospheric Dispersion and Dose Analysis Method (ADDAM) and Canadian Standards Association CSA-ERM code were used for the short range modelling exercise by S.L. Chouhan of the Canadian Nuclear Laboratories (formerly Atomic Energy of Canada Limited).

II.1.1. Introduction

The following are the general aspects of ADDAM (Atmospheric Dispersion and Dose Analysis Method)[17] [II.1–II.4]:

- The code was developed for safety assessment of Canadian nuclear facilities;
- It can be used to calculate doses to members of the public following a hypothetical accidental release of radioactivity to the atmosphere;
- It is based on the models described in Canadian Standards Association (CSA) guidance document CSA N288.2 [II.5];
- It runs repeatedly, combining release data with historical meteorological data collected over the course of many years;
- It predicts a distribution of doses, which allows statements regarding the consequences of the accident to be made in terms of probabilities; and
- It is fully documented and quality assured.

A second code, CSA-ERM, which contains most of same equations as ADDAM, was developed to implement the same approach as ADDAM, but for application at locations not addressed by ADDAM. In particular, ADDAM makes predictions only along the plume centerline for each meteorological record, starting at a downwind distance of 100 m. In the current exercise, the

[17] The ADDAM and CSA-ERM codes are not designed for modelling very short term releases (fractions of seconds) of explosive materials. Testing of these codes in this exercise is simply to learn how they will compare with other kinds of models and with the experimental data.

calculations were necessary over a 50 m grid starting at 5 m; as a result, these calculations were made using CSA-ERM rather than ADDAM. CSA-ERM is not yet documented, but it was quality assured while verifying ADDAM, and it is considered indirectly validated because ADDAM is validated.

II.1.2. Key assumptions

The ADDAM code is based upon the following assumptions:

- Meteorological conditions are constant over the averaging time of the meteorological data;
- The terrain is flat;
- Terrain roughness and cover are uniform by sector;
- Precipitation type and rate are uniform over the region of analysis;
- Inversion height has a set value for a given atmospheric stability class and is constant with downwind distance; and
- The activity of radionuclides deposited on the ground decreases through decay only.

II.1.3. Modelling approaches

ADDAM is a Gaussian plume model that considers the following atmospheric dispersion phenomena, all of which have been validated (see Figs II.1 and II.2 for more details):

- Plume rise, downwash, and entrainment (effective release height);
- Fumigation;
- Reflection from an elevated inversion;
- Transport and dispersion (plume broadening and plume diffusion);
- Wet and dry deposition and plume depletion;
- Air concentration;
- Radioactive decay and buildup;
- External exposure due to cloudshine (including a finite cloud model) and groundshine to humans; and
- Internal exposure due to inhalation to humans.

The following improvements were made to ADDAM to update the code that had been included in CSA N288.2 [II.5]:

- The model can be run probabilistically with respect to the meteorological data;
- It can now quantify some areas of plume rise models where CSA N288.2 [II.5] is vague (e.g. buoyant plume rise);
- The plume rise model can treat buoyant horizontal releases, and can accept stack gas temperature and exit velocity as inputs;
- The model has a lower threshold speed for entrainment;

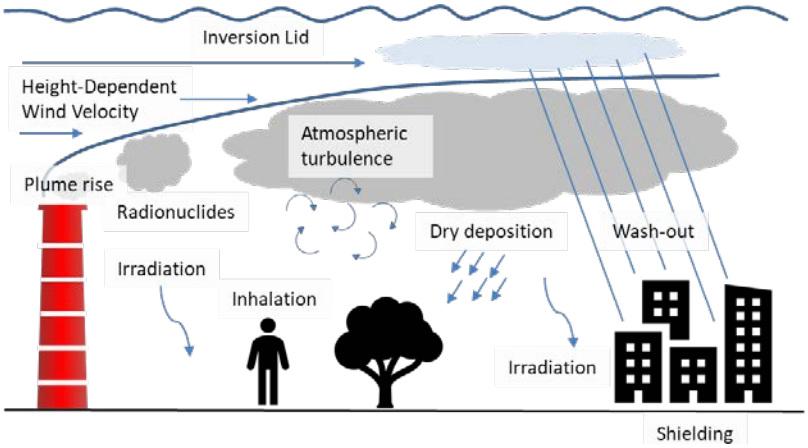

FIG. II.1. Processes modelled in ADDAM (figure modified from Ref. [II.6]).

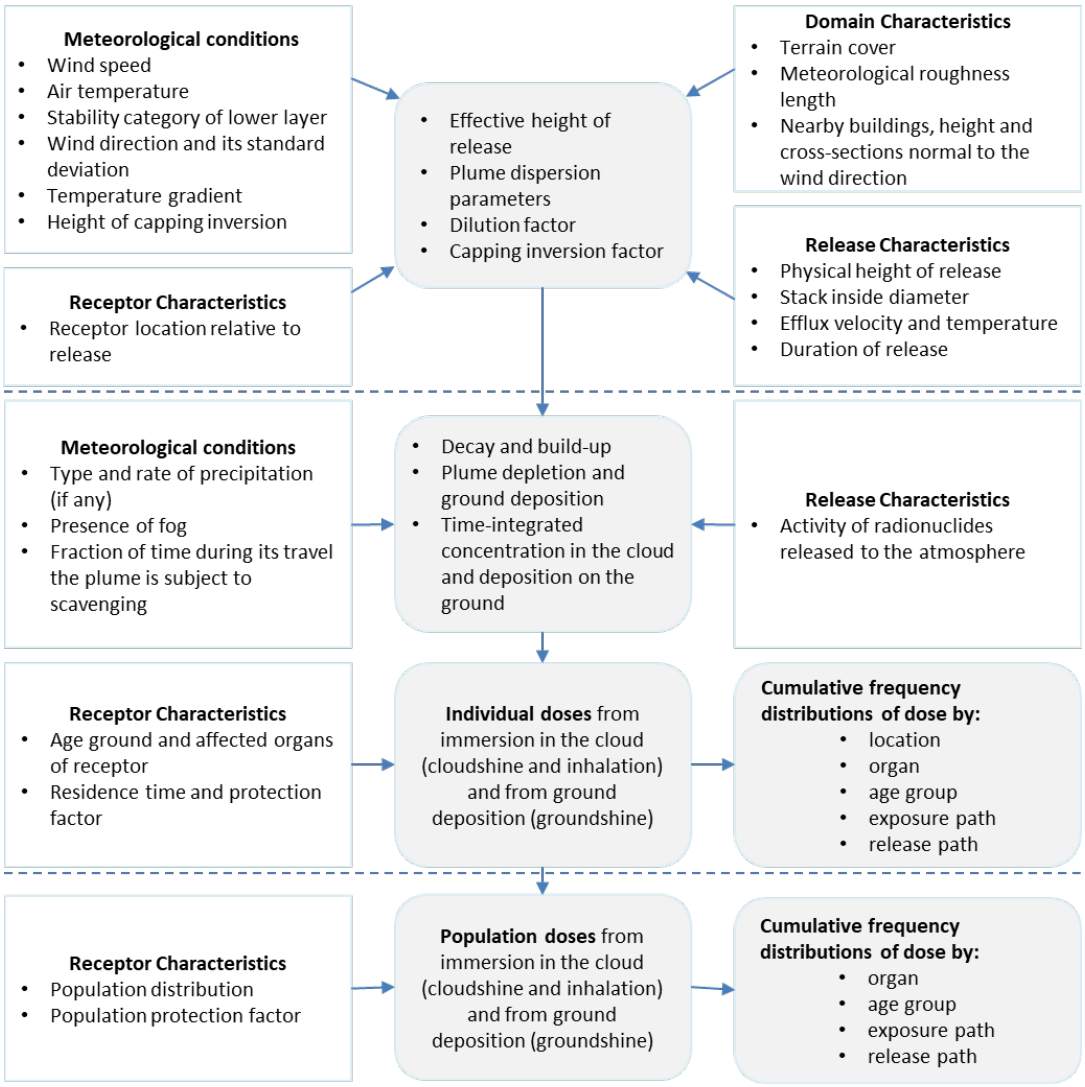

FIG. II.2. Data requirements and calculations in ADDAM (figure modified from Ref. [II.4]).

— The lateral dispersion parameter can be calculated directly from the standard deviation in wind direction;
— The model handles deposition due to fog using a special algorithm;
— The latest dose conversion factors (DCFs) have been incorporated into the model as input parameters;
— The model uses a more refined finite cloud model;
— Sheltering by individuals can be credited to more realistically reflect dose; and
— Assessments can be made for tritiated hydrogen gas (HT).

The above improvements have also been incorporated in CSA-ERM.

II.1.3.1. Model outputs

For a given release, dilution factors (i.e. concentration divided by release rate) and doses are calculated at each distance in the affected wind direction sector(s). In addition, dilution factors can be broken down by release pathway, and individual doses can be broken down by release pathway, exposure pathway, age group (adult, infant or other), and organ (effective, thyroid or other).

II.1.3.2. Results generated by ADDAM

The predictions are made for realistic critical groups located on the grid, as defined by the geographic area being modelled for a given modelling exercise. The individual receiving the highest dose, corresponding to a given cut-off percentile, is used in the assessment.

II.1.3.3. Limitations of ADDAM

The limitations of ADDAM are as follows:

— The model is not suitable for puff releases (release duration needs to be greater than the travel time);
— The release period needs to be divided into intervals within which the release rate is assumed to be constant;
— Uncertainties increase for downwind distances of less than three building heights and of greater than 30 km from the source;
— Activity concentrations and individual doses are calculated on the plume centerline; off-axis estimates are not available in ADDAM, but can be determined using a second code, CSA-ERM;
— ADDAM cannot treat calm winds;
— ADDAM can handle point sources only. It cannot treat line, area or volume sources;
— ADDAM cannot treat dense gases (heavier than air);
— The endpoint of ADDAM is dose. The model cannot be used to calculate risks; and
— Due to the lack of test data, ADDAM has not been adequately validated for wet deposition, plume depletion by snow, or dry deposition to vegetation and snow.

II.1.4. Input parameter values

The following are the input parameters to ADDAM (their values are discussed in Section II.1.6):

— Site characteristics, including:
  - Ground cover;
  - Roughness length;
  - Release location and configuration; and
  - Locations and dimensions of nearby buildings.

— Release characteristics, including:
  - Time dependent mass and energy released;
  - Time dependent activity of each radionuclide released; and
  - Four release pathways (Stack, Inlet, Leakage and Hole).

— Receptor characteristics, including:
  - Locations (downwind distance, direction) of realistic critical groups; and
  - Ages; and
  - Individual organs receiving a dose.

— Meteorological conditions, including:
  - Wind speed;
  - Wind direction;
  - Standard deviation in wind direction;
  - Air temperature;
  - Vertical temperature gradient;
  - Stability class;
  - Precipitation rate; and
  - Presence or absence of fog.

II.1.5. Handling of uncertainties within ADDAM

The uncertainty features are implemented in ADDAM as follows:

— Multiple calculations of doses are performed using ADDAM, with successive calculations beginning at the next record in the meteorological file.
— Each calculation produces a prediction of a dose at each radial distance in the affected sector(s).
— Doses are set equal to zero in unaffected sectors for a given calculation.
— The final output is a set of doses at each radial distance in each sector. These sets include zeros.
— A number of statistics can be derived from these sets, including:
  - Minimum and maximum doses;
  - Cumulative frequency distributions; and
  - Doses corresponding to a given percentile in the cumulative frequency distributions.

The following are generic estimates of uncertainties in ADDAM predictions for a given hour:

— The 90% confidence intervals for the maximum activity concentrations in air and for the cloudshine and inhalation doses cover a range within a factor of approximately 2 to 5.
— The 90% confidence intervals for the maximum ground activity concentrations and for groundshine doses cover a range within at least a factor of 10.

— The uncertainties at the extreme ends of a distribution of doses are similar, but the uncertainties at a given interior percentile within the distribution tend to be lower than those at the extreme ends of the distribution.

II.1.6. Application of the model to the short range exercise

ADDAM has options for making either conservative or realistic predictions; most of the realistic options were used in the calculations that were made for the short range exercise.

II.1.6.1. Inputs to the model calculations

The nuclide released was ^{99m}Tc, which has a radioactive half-life of approximately 6 hours. For Test 3, the total activity of ^{99m}Tc that was released was 1.222 GBq. For Test 4, the initial activity was 1088 MBq. There was a 1 hour and 42 minute delay between when the activity was measured and when the explosion took place. After accounting for radioactive decay, the final activity released was 895 MBq.

II.1.6.2. Assumptions used in the model calculations

The assumptions that were made in ADDAM for the short range modelling exercise were as follows:

— The actual release occurred as an instantaneous explosion; however, the release duration was as assumed to be 10 minutes in ADDAM.[18]
— The explosion time was noon.
— Air temperatures of 10.8°C and 26.9°C were assumed for Tests 3 and 4, respectively.
— No wet deposition was assumed to occur.
— It was assumed that it was not raining at the time of the explosion.
— It was assumed that there was no fog at the time of the explosion.
— The wind speed was estimated to be 2.7 m/s for Test 3 and 0.7255 m/s for Test 4.

For Test 3, the stability class was estimated to be Class C (slightly unstable conditions) using the information provided in the exercise (see Appendix I), in addition to the meteorological data measured during the 8 minutes from just before to immediately after the explosion occurred and during which the wind conditions were constant (5 May 2009, 12:21–12:28). Although the stability class is normally estimated using at least 10 minutes of meteorological data, there was a wind change prior to and after these 8 minutes. Additionally, it would have only taken 8 minutes for the plume to reach 2 km downwind.

For Test 4, the stability class was estimated to be Class A (extremely unstable conditions) using the information provided in the exercise (see Appendix I), in addition to the meteorological data from the 12th minute (when the wind speed became 0.9 m/s) to the 59th minute following the

[18] For prevailing circumstances similar to those that occurred during Test 4, because of the low wind speed, ADDAM switched to a long term model, with a prolonged time-frame (minutes rather than seconds). The activity concentration at any downwind distance in the receiving wind sector then became uniform and independent of y (the actual distance). The activity concentrations in neighbouring sectors, therefore, became zero, which will not produce a smooth contour. As a result, this switching wind speed was lowered from 2 m/s to 0 m/s. This is a deviation from ADDAM, and consequently, predictions with ADDAM will not be comparable to those generated using CSA-ERM for Test 4.

explosion (14 July 2009, 12:52–13:39). The meteorological data for the first 11 minutes was ignored because of a very low wind (0.4 m/s) for three minutes and no wind for another eight minutes. The wind in the first three minutes was also blowing roughly in the same direction as the wind afterward. The plume might have travelled 50 m in the first three minutes of very low wind, but this was ignored, and the plume was assumed to start from the origin of the explosion when starting the simulation using all available data.

Within ADDAM, the parameter value database has three different deposition velocity values (high, low and average) for five different surfaces (water, soil, snow, grass and forest). Ideally, the calculations are to have been performed using the average value (1.0×10^{-2} m/s) of the dry deposition for ^{99m}Tc. On the contrary, in the current exercise, the participants were encouraged to calibrate their models using data and results from Tests 1 and 2 before applying their model for Tests 3 and 4. The results from Tests 1 and 2 show that most of the contamination remained within 2 km of the origin of the explosion. This amount of deposition in the near range can only occur by assuming that because ^{99m}Tc was in a liquid solution, it might have not fully converted to the gaseous form during the explosion. Therefore, as the ^{99m}Tc was in the form of a liquid solution, most of it would have been deposited within a few meters of the origin of explosion. In applying the ADDAM code to this exercise, the highest value (1.0×10^{-1} m/s) of the dry deposition to the forest surface was assumed for both Tests 3 and 4.

II.1.6.3. Specific parameter values used for the exercise

Both the ADDAM and CSA-ERM codes are based on the standard CSA N288.2 [II.5], but with some differences. ADDAM is fully documented, fully quality assured, fully validated, and used for safety assessments. CSA-ERM is not yet documented and is used for research and development (R&D) or experimental purposes. CSA-ERM can be considered quality assured to the extent that it produces the same results as ADDAM, which is validated for scenarios where both codes are applicable. The current modelling exercise is similar to an R&D application; therefore, for the purposes of this exercise, CSA-ERM was quality assured with ADDAM over an applicable range, and CSA-ERM was then used in the exercise for the final calculations. ADDAM makes predictions only for the plume centerline, for each meteorological record, starting at a downwind distance of 100 m. In this exercise, the calculations were to be done on a specified the grid starting at a downwind distance of 5 m; as a result, the calculations were made using CSA-ERM, which contains most of the equations from ADDAM.

ADDAM applies the same residence time to all the receptors. For example, for Test 3, it took 12.35 minutes for the predicted plume to reach a distance of 2 km downwind. The groundshine dose predicted by ADDAM is dependent upon a single value of residence time, which applies to the entire population. To correctly predict 1 hour of groundshine dose for a receptor located 2 km downwind, the residence time at 2 km downwind has to be set at 1 hour plus 12.35 minutes of travel time; this will ensure that a receptor at a distance of 2 km from the source (origin) will be exposed for 1 hour; however, all of the receptors at distances that are nearer than 2 km from the source will be exposed for a slightly longer time period. CSA-ERM was modified to ensure that each receptor was exposed for only 1 hour. For this reason, for Test 3, the ADDAM and CSA-ERM dose predictions were comparable only at a receptor distance of 2 km from the source, but not at other locations. This comparison was sufficient for quality assurance purposes, and for all subsequent calculations, all the predictions on the set grid were made using CSA-ERM, assuming a residence time of 1 hour for each receptor.

The effective release height was assumed to be 6.45 m. The initial plume cloud was 12.9 m high, and it was expected to have the same activity concentration throughout this height. The downwash, plume rise, and entrainment were not applied.

Both σ_y and σ_z were calculated using the relevant stability class, and a short term dilution factor model was used.

Just following the explosion, the plume cloud was 7 m wide, 7 m long and 12.9 m high. This spread was accounted for, to some degree, by applying a building wake of 12.9 m high and 7 m wide to the Σ_y and Σ_z.

ADDAM runs four simulations using four different values of the building constant (C_b = 0.5, 1, 1.5 and 2) and uses the results of whichever one gives the most conservative (highest) results. A value of C_b = 0.5 was selected within the ADDAM code for both Tests 3 and 4, and accordingly, this value was used in the CSA-ERM code also.

The inversion layer height was assumed to be 5000 m and the terrain cover was assumed to be grass, with a roughness length of 0.4 m. A receptor height of 0 m was assumed. Although the dose rates were requested at a 1 m height, they are expected to be the same as at a 0 m height because gamma rays from ^{99m}Tc can travel a distance of approximately 170 m.

The finite cloud correction factor for the cloudshine dose was not applied. This submodel has been accurately implemented in the ADDAM code but not in CSA-ERM as of yet. The semi-infinite model predicts higher than realistic doses for ground level releases and lower than realistic doses for elevated releases. Therefore, by not applying the finite cloud correction factor, the prediction of cloudshine dose that was generated using CSA-ERM is expected to be slightly higher than realistic.

The effective DCF from immersion in air[19] for an adult is 5.3×10^{-15} Sv/s per Bq/m^3, and the effective DCF from groundshine[20] for an adult is 1.1×10^{-16} Sv/s per Bq/m^2. It is noted that the DCF values for both exposure pathways are 50% higher for infants than those for adults.

Integrated immersion dose was calculated for the plume duration (10 minutes) and was summed with the groundshine dose for 1 hour to determine the total dose in Sv during the specified 1 hour of exposure.

II.1.7. Results

Results generated using the ADDAM code are summarized in Section 2 and in Figs II.3 and II.4. The results are as expected, based upon the selected input parameter values that were used. The predictions of air concentrations at the plume centerline that were generated using the ADDAM code did not vary greatly with the height of the receptor (0 to 5 m).

II.1.8. Acknowledgements

The contributions from previous and current members of the ADDAM development and meteorological data collection team (N. Scheier, V. Korolevych, P. Davis, R. Moffett, P. Hernu, P. Leeson and B. Reavie) are gratefully acknowledged. The prompt assistance from D. Killey in creating the plume contours is also much appreciated.

[19] The effective dose conversion factor (DCF) is taken from Ref. [II.7].

[20] The effective DCF for groundshine is taken from Ref. [II.8].

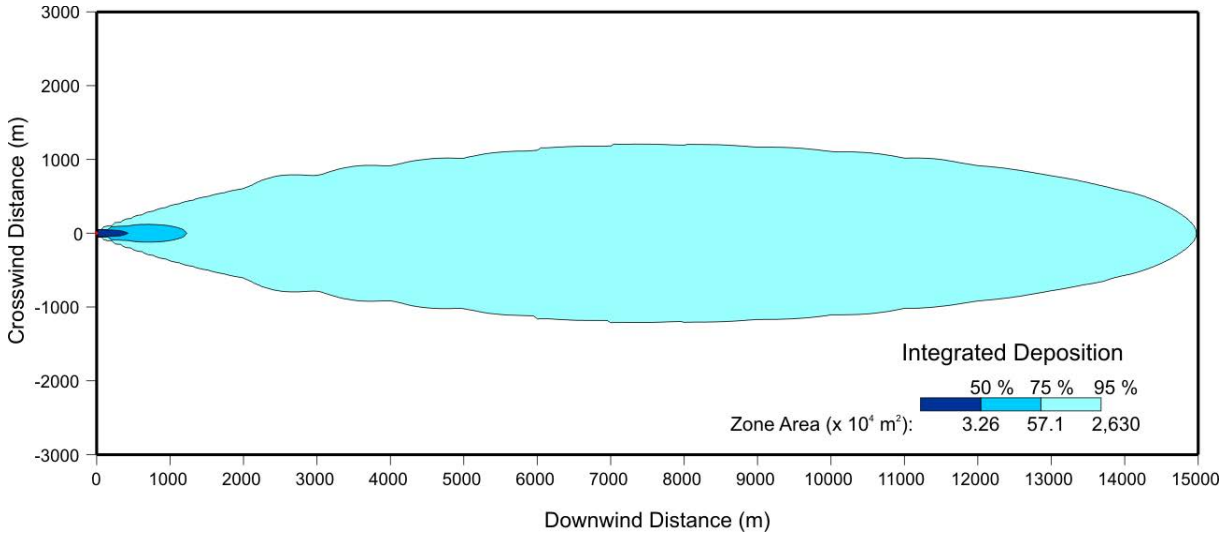

FIG. II.3. Contamination zones (integrated deposition percentiles of the total activity released) for Test 3.

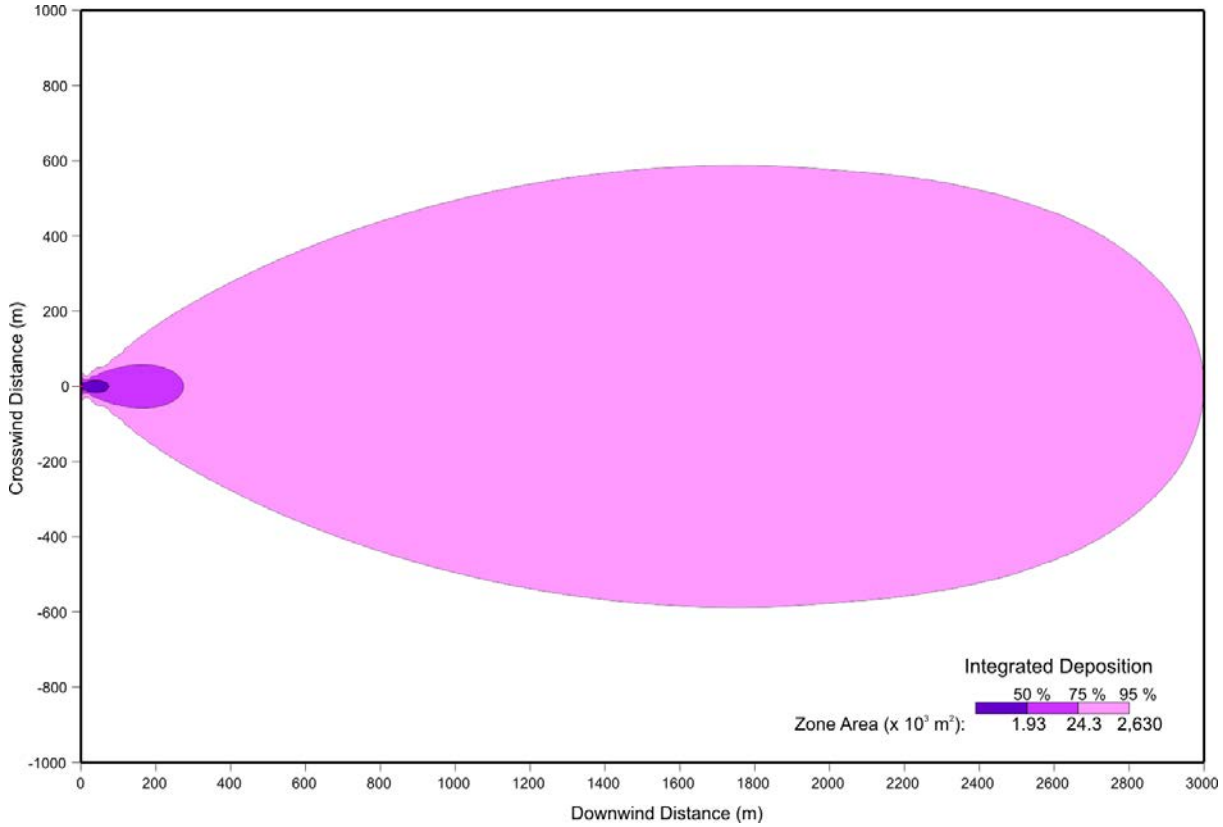

FIG. II.4. Contamination zones (integrated deposition percentiles of the total activity released) for Test 4.

II.2. DESCRIPTION OF HOTSPOT 2.07.1 (HPA)

The HotSpot 2.07.1 code was used for the short range modelling exercise by T.W. Charnock of Public Health England (PHE)[21] in the United Kingdom. In this publication, the code as used by the above participant is referred to as HotSpot 2.07.1 (HPA) to distinguish it from the same code used by a different participant (see Section II.3).

II.2.1. Introduction

The HotSpot 2.07.1 model was developed by the Lawrence Livermore National Laboratory and is freely available. HotSpot contains a number of models for different scenarios and for this modeling exercise the general explosion model was used.

The developers of HotSpot are quite clear about the purpose and scope of the software. The following text is extracted from the HotSpot 2.07.1 help tool:

"The HotSpot Health Physics codes were created to provide emergency response personnel and emergency planners with a fast, field-portable set of software tools for evaluating incidents involving radioactive material. The software is also used for safety-analysis of facilities handling nuclear material. HotSpot codes are a first-order approximation of the radiation effects associated with the atmospheric release of radioactive materials."

Full details of the model can be found in the HotSpot User's Guide [II.9], but in summary, the general explosion model uses the well-established straight line Gaussian plume formulation and applies it to a set of virtual source terms that are generated using a simple formulation to represent the vertical distribution of the activity in the column immediately following the explosion. Deposition onto the ground surface is modelled using dry deposition velocities and a rain out coefficient.

HotSpot considers partitioning of the activity within the column and subsequent atmospheric dispersion within a three dimensional frame of reference, and deposition onto a two dimensional frame of reference.

The user has to provide the total activity of each radionuclide and the fraction of activity that is airborne. HotSpot necessitates the activity to be partitioned into two particle size groups – respirable and non-respirable – and the user has to specify the fraction of activity in the groups and their dry deposition velocities.

Additionally, the user has to provide a meteorological description, including wind speed at a 2 m height, wind direction and stability category. The user has to choose a terrain type (either 'standard' or 'urban'; the latter assumes taller buildings).

The user has to provide an amount of explosive in pounds of TNT equivalent[22] and can adjust the way the activity is distributed in the initial column or can accept the default parameters. There are also various options concerned with estimating dose (e.g. with different sets of dose coefficients), but these were not used in this modeling exercise.

---

[21] Public Health England (PHE) since 1 April 2013, was formerly the Health Protection Agency (HPA), formerly the National Radiological Protection Board (NRPB).

[22] TNT (trinitrotoluene) equivalent in pounds (lb. TNT equivalent; 1 pound = 0.454 kg) is a commonly used measure of the energy released from an explosion [II.9].

The HotSpot general explosion model endpoints include:

- Time integrated activity concentration in air;
- Total deposition to the ground surface;
- Total effective dose equivalent from internal exposure to inhaled radionuclides;
- Dose rate from radionuclides deposited on the ground; and
- Plume arrival time.

Key assumptions, modelling approaches and parameter values can be found in the HotSpot User's Guide [II.9]. HotSpot does not handle uncertainties.

II.2.2. Application of the model to the short range atmospheric dispersion exercise

HotSpot is intended to provide a first order approximation on the extent of consequences of a release of radioactivity to the atmosphere. It uses a straight line Gaussian plume formulation and does not claim to simulate the complex pattern of air activity concentration and ground deposition in response to changing meteorological conditions and complex terrain. Because of this and because of the need to keep the modelling exercise simple with minimal effort, for this exercise, HotSpot is only calibrated against and only used to generate results for comparison of the deposition on the supposed plume centreline.

The scenario description describes four experiments. For Tests 1 and 2, a complete set of measurement information was provided for participants to use for calibration purposes. For Test 3 and Test 4 only starting conditions and meteorological information were provided, as these were to be the subject of blind runs.

II.2.3. Calibration runs

Test 1 was rejected for calibration as the mass of material to be dispersed by the explosion was very much larger than for the subsequent three experiments. Therefore, HotSpot was only calibrated against results from Test 2.

Calibration proceeded by a process of trial and error, starting with default factors, where possible, and varying inputs within reasonable ranges.

The exercise description includes the measurements from meteorological stations within the region. These indicate stability Class B (moderately unstable conditions) at around the time of Test 2 and this parameter was taken to be fixed. The meteorological measurements also include wind speed and this ranged from about 0.3 to 1.8 m/s. It is noted that the Gaussian plume model does not perform well in low wind speeds.

Wind direction is less important, as the modeling exercise focused on the plume centreline; however, the direction is needed in order pick out the ground deposition measurements that fall on this line. The experimenters laid out a rectangular grid of measurement devices that was approximately 50 m long by 40 m wide, with the explosive device located half way along the shorter side (see Appendix I). They designed the detonation so that material would be directed both upwards and forwards towards the grid. Ideally, the detonation would occur when the wind was blowing parallel with the centreline of the grid; however, the configuration of the experimental site, surrounded by trees and adjacent to a large mine waste heap, means that the wind can be gusty and erratic.

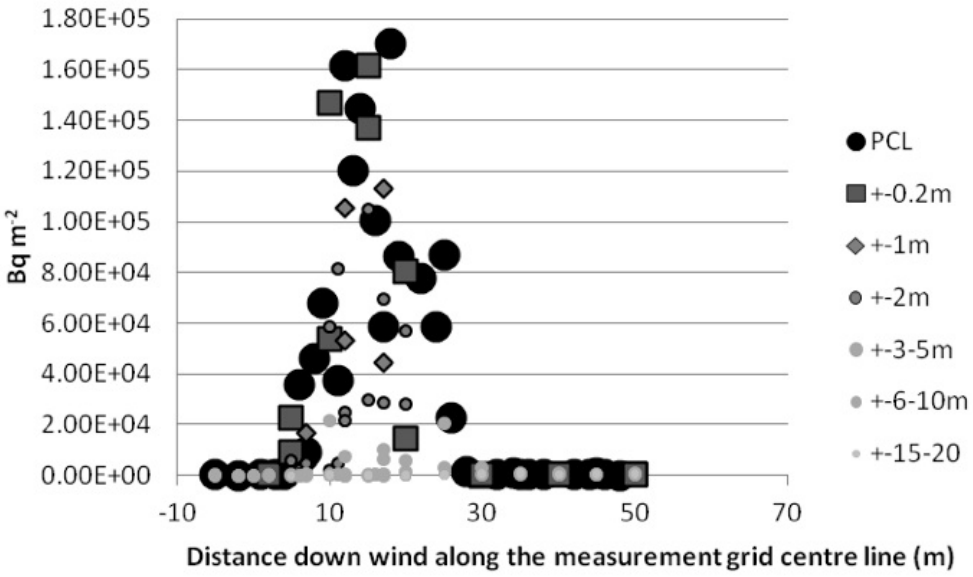

FIG. II.5. Plot of observed deposition against distance along the measurement grid of Test 2.

Figure II.5 shows the deposition measurements for Test 2 plotted against distance downwind. Different symbols are used for measurements on the grid centreline and in bands parallel to the grid centreline. The figure indicates that the highest results were observed on or near the grid centreline. The experimental designers have been successful in timing the explosion of Test 2, such that the grid centreline can be considered as the plume centreline.

As stated above, the terrain of the experimental site is complex and not very well suited to HotSpot. Therefore, the standard terrain option was chosen and considered fixed.

HotSpot allows for two particle size groups: a respirable fraction[23] of small particles (AMAD ≤10 μm); and a non-respirable fraction of large particles (AMAD >10 μm). These groups can be given different deposition velocities. For the purposes of calibration, the proportion of respirable particles by activity was varied between 90% and 99.9% and the deposition velocity of the respirable fraction was varied between 0.3 (the default value in HotSpot) and 0.01 cm/s. The value for non-respirable deposition was held constant at 40 cm/s, which is the default for the general explosion model in HotSpot. This is a very large value compared with even the largest value 0.8 cm/s suggested for the largest particles in the exercise; however, the HotSpot model does not include gravitational settlement, which may be an important mechanism and the use of a high deposition velocity will compensate for this to some extent.

HotSpot allows the user to specify the height of the explosion column indirectly by specifying an amount of explosive in pounds of TNT (lb. TNT) equivalent. The height reached can be further adjusted using a correction factor (e.g. to customize the height or to use a different methodology for estimation of the height) and more factors can be set to alter the distribution of activity vertically in the explosion column. HotSpot allows more complex geometries for the

[23] The respirable fraction is the fraction of aerosolized material that is respirable, generally considered as having an Activity Median Aerodynamic Diameter (AMAD) ≤10 μm; the non-respirable fraction is the fraction of aerosolized material that has an AMAD >10 μm. In HotSpot, the respirable fraction is assumed to have an AMAD of 1 μm [II.9].

source to be set, but this functionality was not used for this modelling exercise. During the calibration, HotSpot was used with an unconstrained height, by a height constrained to 12 m and to 5 m, as agreed by participants and based on estimates of the height of the visible column in videos and photos. Originally, the agreed height was 12 m, but upon further review, this was revised to 5 m. It was assumed that the 0.02 kg of the explosive Vesuvit used was equivalent to about 0.04 lb. (0.018 kg) TNT. HotSpot predicted that even this small amount of explosive would produce a column that is 34 m high and well above the visible column of 5 m observed.

Table II.1 lists the input parameters used in the calibration process for the HotSpot model. Figure II.6 depicts plots of the predicted deposition and the observed values, and it can be seen that calibration can very quickly turn into a curve fitting exercise with little reference to the physics of the experiment.

HotSpot does not easily generate results for distances upwind or that are less than 10 m downwind of source. Therefore, initially, the calibration exercise was aimed at representing the peak in observed values that occurs at approximately 10 to 20 m downwind and the sharp decline that follows. In the event, it proved very difficult to represent the decline, which is very steep, and even runs that look a reasonable fit on the standard plot (Fig. II.6) do not capture the decline very well when the scale is reduced (as in Fig. II.7).

This difficulty may be because the peak is dominated by gravitational settling, a process that HotSpot does not include. In the HotSpot results, the peak is dominated by activity in the non-respirable fraction, which has been assigned a very high deposition velocity. The amount of non-respirable material is very sensitive to the respirable fraction parameter, as varying the respirable fraction from 90% to 99.9% varies the non-respirable fraction by a factor of 100 between different runs. Figure II.8 shows one calibration run split into the respirable and non-respirable components.

For radiation protection purposes, achieving a good representation of the peak and decline might be considered less important than a good representation of the low deposition area beyond. For a real incident or for planning purposes, low deposition areas present the bigger challenge to decision makers, particularly when considering appropriate protective actions (including remedial actions) to be taken. They will be much more extensive than the high deposition area, and as a result, more monitoring resources will be needed. Countermeasures, such as restricting access or cleanup, will be much more disruptive, particularly if the area encompasses residences or commercial or industrial facilities, and cleanup will generate much larger quantities of waste albeit at a lower activity concentration. In contrast, the high deposition area is much smaller and can be quickly and intensively monitored, so that highly accurate modelling is far less crucial. Furthermore, it is much less disruptive and expensive to restrict access to a small area or clean it up, and much more justifiable to do so when the predicted doses are high.

For this reason, the decision was taken not to experiment with different deposition velocities for the non-respirable fraction to improve the representation of the peak and decline, but instead to focus on the respirable fraction, which becomes more important in the far range. Unfortunately, in this exercise, there are few measurements available for the area beyond the peak to calibrate against. Therefore, out of the set of runs generated, the run W1.0_VD0.01_40_RF0.999_UC (Table II.1; Figs II.6 and II.7) was selected as being in best agreement with the measured data. This run was replaced with run W1.0_VD0.01_40_RF0.999_C5m (Table II.1; Figs II.6 and II.7) when EMRAS II WG9 participants agreed on a changed specification of the observed column height; in the end, this made no difference to the HotSpot predictions.

TABLE II.1. SUMMARY OF INPUT PARAMETERS USED FOR CALIBRATING HOTSPOT TO TEST 2

Parameter[a]	Value used
Wind speed	Varied between 0.33 to 1.8 m/s
Stability category	Fixed B
Respirable fraction	Varied between 90% and 99.9%
Respirable fraction deposition velocity	Varied between 0.3 and 0.01 cm/s
Non-respirable deposition velocity	Fixed at 40 cm/s
Explosive and Column height	Varied between 0.004 lb. (0.0018 kg) and 0.04 lb. (0.018 kg) TNT equivalent or ignored and the column height constrained to 12 m or 5 m.

[a] Input parameters for each model run are indicated by a code, as follows: W is Wind speed; RF is Respirable fraction; VD is Deposition velocity; EX is the quantity of explosive (lb. TNT equivalent); UC is Column height constrained to 12 m; C5 is Column height constrained to 5 m and that activity was distributed according to HotSpot defaults. Same conventions are used in figures.

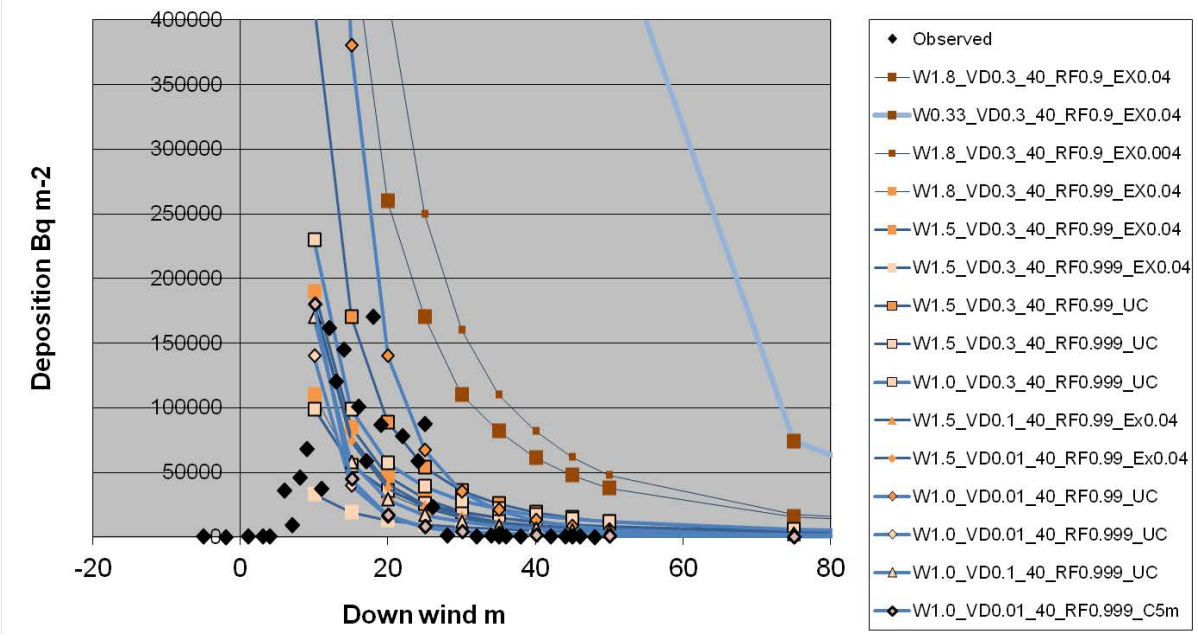

FIG. II.6. Predicted deposition on the plume centreline from the various calibration runs plotted against observations along the measurement grid centreline.

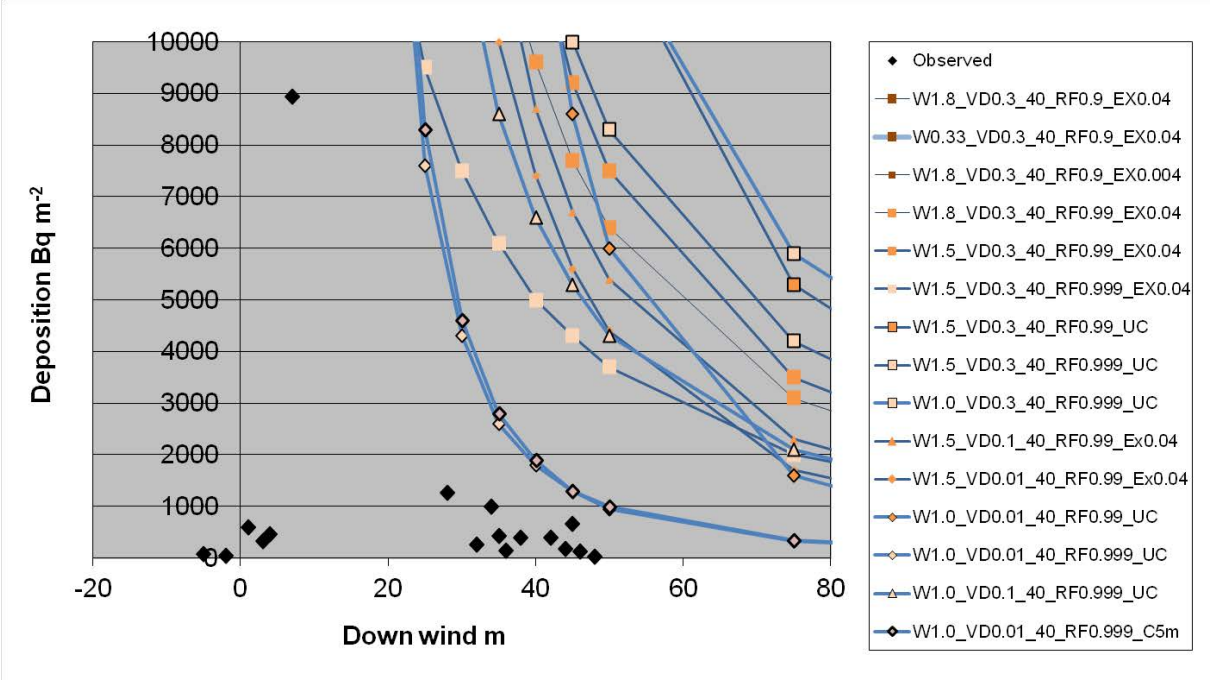

FIG. II.7. Predicted depositions on the plume centreline from the various calibration runs plotted against observations along the measurement grid centreline with the scale adjusted to show the low values at 40 m distance downwind.

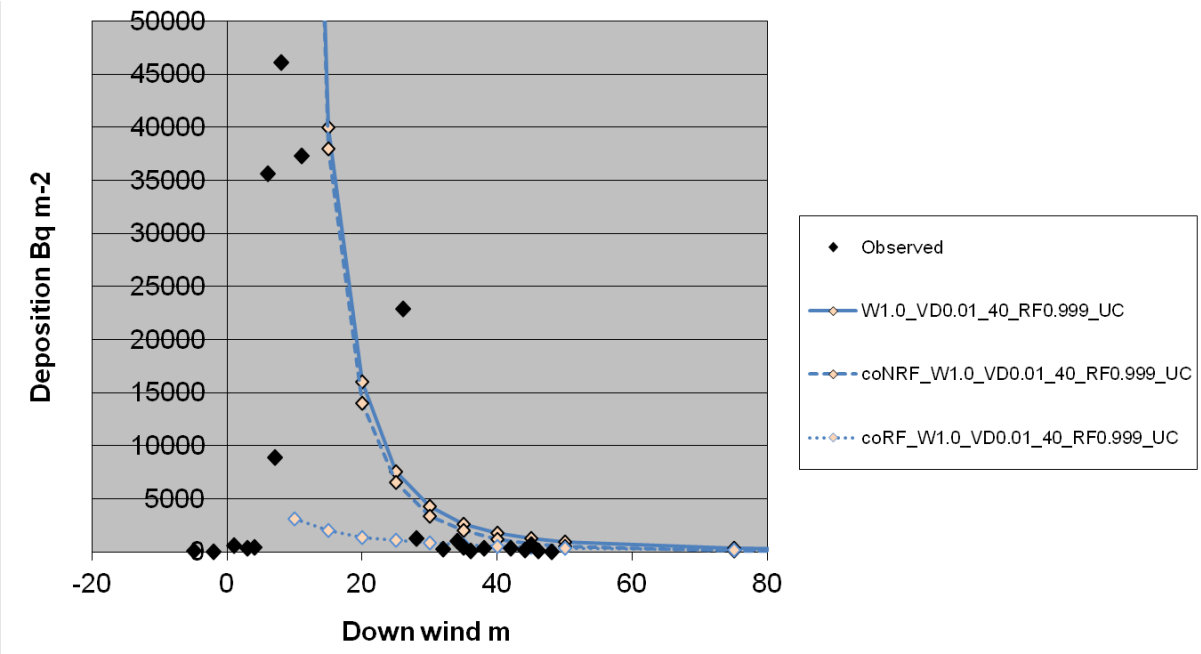

FIG. II.8. Predicted deposition from one calibration run split into non-respirable fraction component (coNRF) and respirable fraction component (coRF).

TABLE II.2. HOTSPOT INPUTS FOR THE BLIND RUNS ON TESTS 3 AND 4

Parameter	Test 3	Test 4
Wind speed m/s	1.5	0.4
Stability class	D	C
Respirable fraction	0.999	0.999
Respirable deposition velocity (cm/s)	0.01	0.01
Non-respirable deposition velocity (cm/s)	40	40
Column height	Constrained to 13 m	Constrained to 13 m

II.2.4. Blind runs

The inputs for the blind runs were taken from the selected calibration run and adapted for the prevailing weather conditions and for constraints on the column height, as agreed by the group (Table II.2).

Figure II.9 shows the predicted results over two downwind distance scales. The high deposition predicted for Test 4 in the near range is mainly due to the very low wind speed.

II.2.5. Remarks

Taking note of the limitations of the HotSpot model, there is the potential for it to not perform well for the tests that were carried out in support of the short range modelling exercise. The model is not well suited to the experimental conditions, which include very complex terrain, low and variable wind speeds and directions, and possibly gravitational settling.

The overall predictiveness of HotSpot in this exercise is probably best evaluated by assessing how well it performs in the far range away from the point of release and considering how well it predicts the maximum deposition with distance rather than the exact location of the maximum value. Unfortunately, there are no observations beyond 50 m downwind, and as a result, it is necessary to evaluate the overall predictiveness of HotSpot by comparing its model outputs with those generated by the more complex models in the intercomparison exercise. HotSpot needs to be evaluated in the light of its stated aim as a model for a ‘first order approximation’.

In the near range, it will be important to distinguish between the centreline of the grid and the centreline of the plume. If the two are misaligned by even a few degrees, then HotSpot can be expected to overestimate the deposition on the grid centreline, possibly by several orders of magnitude. It is by no means certain that the experimenters were as successful in aligning the plume direction with the grid centreline in Tests 3 and 4, as they were for Test 2.

II.3. DESCRIPTION OF HOTSPOT 2.07.1 (HR)

The HotSpot 2.07.1 code was used for the short range modelling exercise by D. Trifunovic of the State Office for Radiological and Nuclear Safety in Croatia. In this publication, the code as used by the above participant is referred to as HotSpot 2.07.1 (HR) to distinguish it from the same code used by a different participant (see Section II.2).

II.3.1. Introduction

HotSpot 2.07.1 is a code that was developed by and accessed from Lawrence Livermore National Laboratory of the USA, and full details are available in the User’s Guide [II.9].

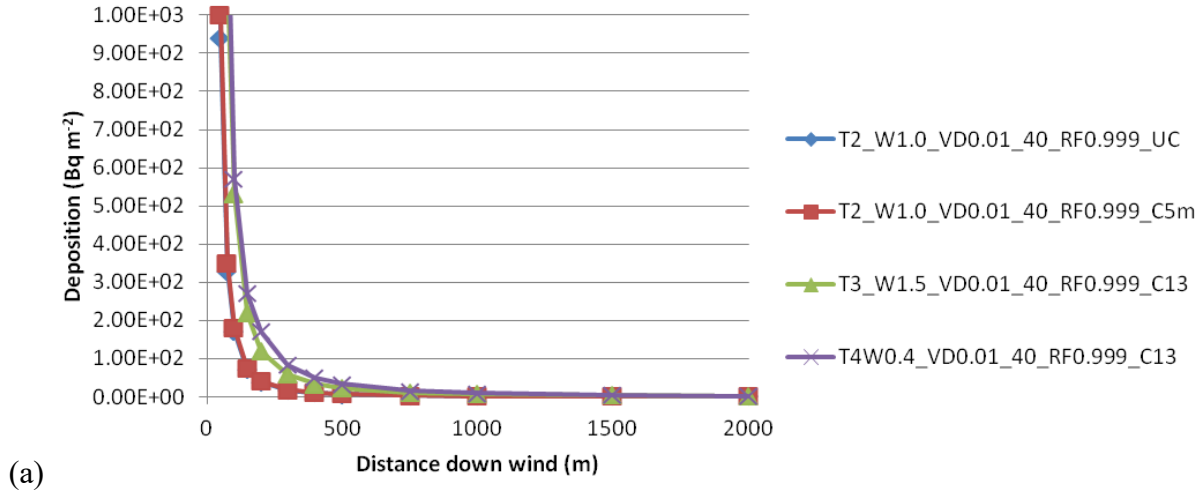

(a)

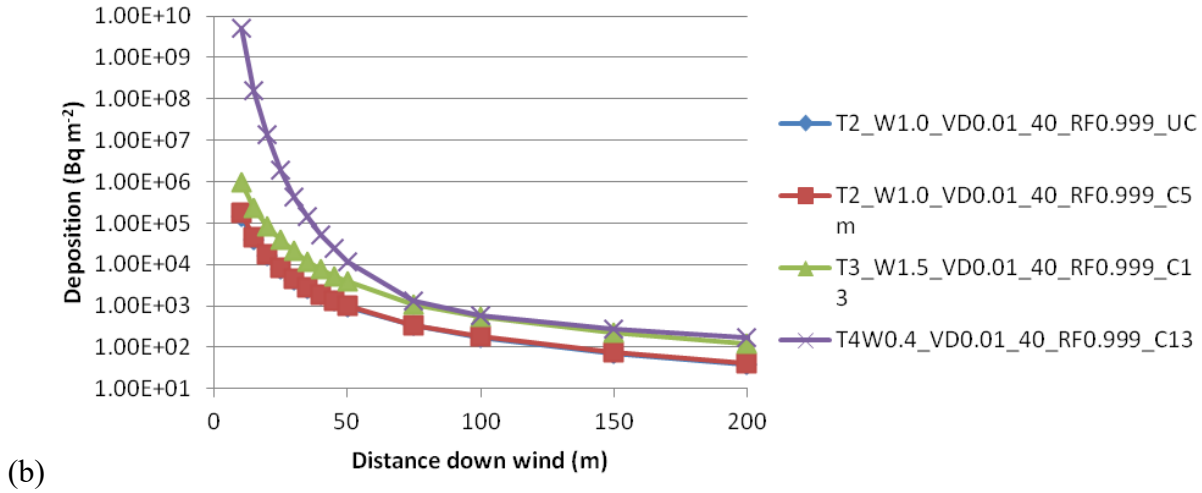

(b)

FIG. II.9. The predicted deposition on the plume centreline in the two chosen calibration runs and the two blind runs.

TABLE II.3. HOTSPOT INPUT PARAMETER VALUES FOR THE SHORT RANGE MODELLING EXERCISE

Parameter	Test 2 (calibration)	Test 3	Test 4
Wind speed (m/s)	0.6	1.3	0.1
Stability class	B	D	C
Source term (MBq)	1058	1222	1088
Cloud top (m)	5	13	13
Respirable fraction (%)	99	99	99
Deposition velocity (m/s) for the respirable fraction	0.0008	0.0008	0.0008

II.3.2. Application to the short range exercise

The HotSpot 2.07.1 code is intended to model an unbounded upward explosion, with an unrestricted 360° geometry. In contrast, the field tests that were considered in the short range exercise were arranged such that the blast was approximately parallel to the ground, with a back blast wave due to the impact of the blast on the metal plates that directed the force of the explosion. This produced a shift in the location of maximum deposition from the area around the explosion point to a location that was approximately 10–15 m in front of the explosion point.

The release was partitioned by describing a virtual source term upwind of the explosion point, such that the predicted cloud at the location of the explosion approximately corresponded to the actual cloud from the explosion. This was done for each layer of the cloud, and the source term was distributed amongst the layers of the cloud. The cloud radius (m) was defined as 0.2 times the cloud top (m), and the cloud top (m) was defined as 76 $w^{0.25}$, where w is the number of pounds of high explosive. For each virtual source term, σ_y was assumed to be 0.5 times the cloud radius (at $x = 0$) and σ_z was set at 0.2 times the cloud top (also at $x = 0$). The source term was partitioned as follows: 4% at h(1), which was at the ground level; 16% at h(2), which was at 0.2 cloud top; 25% at h(3), which was at 0.4 cloud top; 35% at h(4), which was at 0.6 cloud top; and 20% at h(5), which was at 0.8 cloud top. The HotSpot 2.07.1 code describes the dispersion based on a standard Gaussian model.

The input information that was used in the exercise is provided in Table II.3.

II.4. DESCRIPTION OF RDD_MMC CODE

The RDD_MMC code was used for the short range modelling exercise by J. Ďúran of VÚJE Inc. in Slovakia.

II.4.1. Introduction

The RDD_MMC code is intended for calculating the results of an event involving a radiological dispersal device (RDD) using a Monte Carlo approach (‘Method Monte Carlo’, MMC). The RDD_MMC code is a Lagrangian particle model, which simulates fluctuation using the Monte Carlo method. The code was developed using FORTRAN 77.

II.4.2. Application to the short range exercise

The meteorological wind field is time independent and is assumed to be homogeneous. The CALMET and MATHEW computer codes are used.

The initial volume of the source term can be composed of up to eight independent volumes. Up to eight particle diameters can be considered as aerosols, and each particle class (grouped by diameter) can have its own density. The initial distribution of particles in the source volumes can be random or Gaussian.

The model takes account of several removal processes, including gravitational settlement, dry and wet deposition, and radioactive decay.

The model calculates a dose rate for one monoenergetic photon emission, in terms of a dose rate (Gy/h) in air from ground exposure. Contributions from all areas are numerically integrated in a 1 m × 1 m step. A Berger form of the buildup factor is used for approximation. The energy of gamma rays is set at $E = 0.140510$ MeV.

TABLE II.4. INPUT INFORMATION USED WITH RDD_MMC IN THE SHORT RANGE MODELLING EXERCISE

Parameter	Test 1 6 December 2007	Test 2 15 May 2008	Test 3 5 May 2009	Test 4 14 July 2009
Explosion time	12:45	11:30	12:22	12:42
Wind speed (m/s)	4.00	0.59	1.30c	0.20
Wind direction[a]	SW	S	WNW	S
Stability category	C (ETE)[b]	A (ETE)	B (ETE)[c]	A (estimated)

a Measured value of wind direction; for the calculation, a direction of South +10 degrees (190 degrees) direction was used.
b ETE is the meteorological station near NPP Temelin (Elektrárna Temelín, abbreviated as ETE) in Czech Republic.
c For Test 3 on 5 May 2009, the data from the first meteorological station was used (of the two sets provided).

TABLE II.5. PARAMETER VALUES USED FOR THE SIMULATED PARTICLES IN THE SHORT RANGE EXERCISE

Particle diameter (μm)	Density (g/cm^3)	Dry deposition velocity (m/s)	Fraction of emission (unitless)
0.2	1.0	5.0×10^{-3}	0.20
1.0	1.0	1.5×10^{-4}	0.15
8.0	1.5	1.0×10^{-3}	0.50
20.0	2.0	8.0×10^{-3}	0.15

A number of uncertainties are considered, including meteorological uncertainties (wind speed, wind direction, category of stability), geometric shape and dimension of the initial clouds, distribution of volume activity in initial clouds, distribution of the activity as a function of the aerosol (particle) diameters, distribution of particles with different diameters as a function of the height, and the density for each diameter of aerosols (particles).

Input information used in the exercise is provided in Table II.4. Descriptions of the parameters of the simulated particles are provided in Table II.5.

II.5. DESCRIPTION OF UNIVERSITY OF SEVILLE MODEL

The University of Seville model (USev) was used for the short range modelling exercise by R. Periáñez of the University of Seville in Spain.

II.5.1. Introduction

The model applied by the University of Seville is a FORTRAN code that has been specifically designed and developed for this scenario and for research purposes. It is a dynamic, process oriented numerical model which simulates the dispersion of liquid and gas particles released after an explosion, based upon a Lagrangian approach.

The activity released by the explosion is considered to be in two forms: liquid and gas particles. A total amount of 10 000 particles are assumed to be released (5000 liquid and 5000 gas particles). Each particle contains a certain amount of activity, depending on the ^{99m}Tc activity used in the experiment and on its fractionation between liquid and gas. Different dispersion processes are considered for liquid and gas, but in both cases, the trajectories followed by

individual particles are calculated until deposition, radioactive decay, or until they leave the model domain.

The model does not try to reproduce the explosion itself, but the dispersion just after it. Thus, the initial conditions for liquid particles assume an initial velocity for these particles, which is set as a calibration parameter. Liquid particles are released from the explosion container with this velocity. In the case of gas particles, a cloud above the explosion site is assumed to be formed about a given effective height, which is also set as a calibration parameter. The HotSpot formulation, based on a cloud top, has also been tested using the model, and sensitivity tests have been carried out; however, the results show a better agreement with observations if a formulation based on an effective release height is applied.

Dispersion of both liquid and gas particles is computed starting from this initial time and going forward. The geometry of the model domain is shown in Fig. II.10. The origin of coordinates is at the explosion site (exactly in the center of the explosive shielding), and the z-axis is directed upwards. The rectangular box is one of the areas over which results are provided. Its length and width are 100 m and 40 m, respectively.

Results are provided for this area with a spatial resolution of 1 m; however, according to the model endpoints defined in the scenario, results are also provided with a spatial resolution of 5 m to a distance of 50 m from the explosion site and with a spatial resolution of 25 m from 100 m upstream to 2000 m downstream of the explosion point.

It is interesting to point out that, due to the model design, there is not any limitation with respect to the model output resolution. It is, therefore, possible to simultaneously generate results at a short scale (1 m resolution in the near field, i.e. up to 50 m from the explosion site) and at a larger scale (25 m resolution, up to 2000 m from the explosion site). Also, computation times are very short, on the order of 30 seconds for a 15 minute simulation on a PC. Finally, the role of liquid droplets in the transport of radionuclides in the short scale seems essential, since it seems that most of the deposition in a short distance from the explosion site is due to liquid droplets. Other models, such as HotSpot, do not include the different dispersion processes for liquid and gas particles.

II.5.2. Modelling approach

The processes considered for simulation of the movement of liquid and gas particles released after an explosion are described in this section. Liquid and gas particles are considered separately. Differences between these two types of particles are due to: (a) different initial conditions for liquid and gas particles; and (b) different dispersion mechanisms.

Given the Lagrangian nature of the model, space is treated as continuous, i.e. no spatial discretization is necessary. Model results can be provided over any resolution grid after a simple averaging process, and there is not any limitation in this sense. A temporal discretization is necessary, and a time step is provided as input data, which is typically on the order of 10^{-2} seconds.

II.5.2.1. Liquid particles

Liquid particles are considered to follow a parabolic motion, including friction with air. This friction is formulated in terms of a quadratic law with particle velocity. The friction coefficient is provided as input data. Additionally, particles are advected with wind velocity. Wind velocity and direction is provided in the scenario description and is assumed to be uniform over the

model domain, although varying in time. A standard vertical logarithmic profile for wind velocity is constructed from the 2 m height of the wind data provided with the scenario. Particles which touch the ground (i.e. with a z-coordinate of less than or equal to zero) are deposited and are assumed not to move any farther; calculation stops for such particles. Radioactive decay is simulated using a Monte Carlo method. Calculation also stops for decayed particles.

The explosive is initially confined by a box, which is open in the top and on one side. This shielding is considered to limit the direction of the initial velocity of liquid particles, both horizontally and vertically. Thus, in the horizontal direction, particles are initially confined by the angle –α and +α. In the vertical direction, particles are released between angles of β1 and β2. These angles may be seen in Fig. II.11. The actual direction of the initial velocity of each liquid particle is determined by applying a Monte Carlo method, assuming that all permitted directions have the same probability. All angles are provided as input data. The magnitude of the initial velocity and a given error or tolerance (in %) for this parameter are also specified as input data through model calibration. The actual initial magnitude of the velocity for each particle is again determined by applying a Monte Carlo method; however, the magnitude of the velocity is assumed to have a normal probability distribution, with the specified mean value and standard deviation.

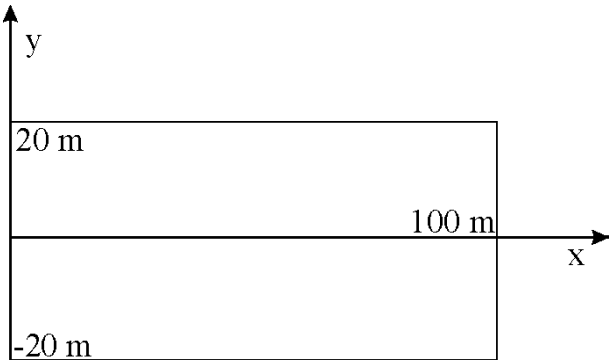

FIG. II.10. Geometry of the model domain.

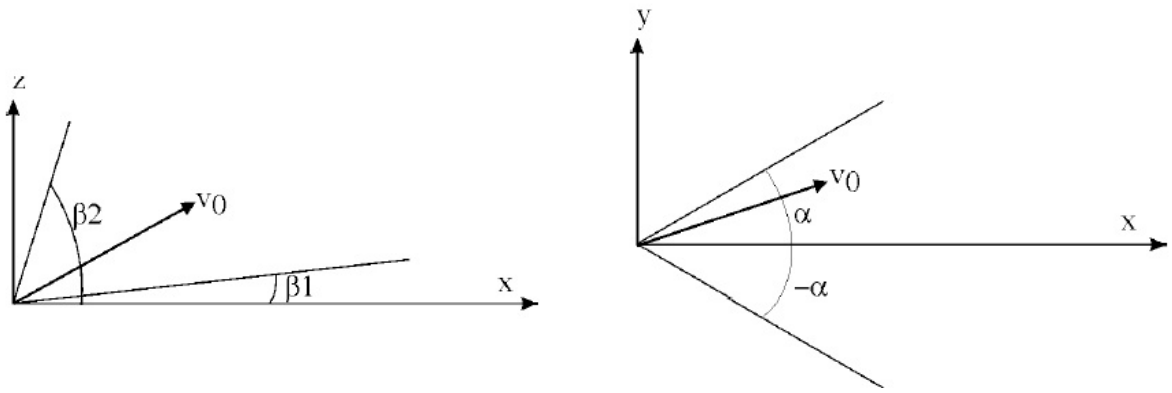

FIG. II.11. Vertical (left-hand side) and horizontal (right-hand side) projections of the initial velocity of a given liquid particle. The possible direction is limited by the specified angles.

II.5.2.2. Gas particles

Gas particles are considered to form a cloud (also, called a plume) over the explosion site. The dimensions of this plume are given by: CR × CR × CH m^3, where CR is a cloud radius (m) and CH is a cloud height (m). Horizontally, the plume is centred over the explosion site. Vertically, it is centred about an effective release height provided as input data to the model. This effective height has been generated through a calibration process. The particles are, initially, homogeneously distributed within this cloud. Again, the actual position of each gas particle within the cloud is obtained by applying a Monte Carlo method.

Once the initial positions of gas particles are determined, these particles are advected by wind velocity. Of course, the same wind vertical profile as for liquid particles is used. Three dimensional turbulent diffusion is calculated using a Monte Carlo method. The diffusion coefficient is specified as input data. Particles which touch the ground are deposited and do not move any farther. Radioactive decay is again calculated using a stochastic method.

In order to calculate deposition, dose and time integrated activity concentrations in air over the grids defined in the scenario description, the spatial density of particles (liquid and gas) is calculated for each specified grid.

II.5.3. Model parameters

A number of different types of parameters are used by the University of Seville model, including calibrated parameters, those that have been deduced or directly taken from the scenario description (see Appendix I), standard values and simulation inputs. Table II.6 provides a list of each type of parameter, along with relevant information describing each.

II.5.4. Uncertainties

No uncertainty assessments were carried out.

II.5.5. Model output

The model predicts deposited activity on the ground with a spatial resolution of 1 m (on a 1 m × 1 m grid), time integrated activity in air with the same resolution (1 m × 1 m grid) in the horizontal, and as a function of height (1 m vertical resolution), up to 30 m, and also dose rates with the same grid resolution as the deposited activity.

The model output has been arranged to provide results requested in the scenario description in the form of a series of files, as described in Table II.7.

It is important to note that time integrated activity concentrations in air on 5 m × 5 m and 25 m × 25 m grids, 5 minutes and 10 minutes after the explosion, were also requested for the exercise; however, differences in contour maps cannot be discerned if compared with the 15 minutes maps. This is because particles leave the model domain or are deposited before 5 minutes. Thus, only the output for the 15 minutes time point is provided. Results at shorter time intervals after the explosion (e.g. 1 minute) are necessary to identify significant differences in contour maps for the time integrated activity concentrations in air.

TABLE II.6. SUMMARY OF PARAMETER TYPES AND PARAMETERS USED BY THE UNIVERSITY OF SEVILLE MODEL IN THE SHORT RANGE MODELING EXERCISE

Type of Parameter	Parameter	Units
Calibrated Parameters	Initial velocity for liquid particles just after the explosion	m/s
	Tolerance of the initial velocity for liquid particles just after the explosion	%
	Friction coefficient of liquid particles with air	dimensionless
	Effective mean release height of gas particles	m
	Fraction of activity released as aerosol particles[a]	dimensionless
Parameters deduced or directly taken from the scenario description	Horizontal dispersion angle (α)	degrees
	Vertical dispersion angles ($\beta 1$ and $\beta 2$)	degrees
	Wind velocity vector components	m/s
	Explosive shielding dimensions	m × m
	Total activity released	Bq
	Time from activity determination in explosive to explosion itself	min
	Cloud radius (CR)	m
	Cloud height (CH)	m
Standard values	Diffusion coefficient in air[b]	m^2/s
	Radioactive decay constant for Tc-99m	s^{-1}
	Dose conversion factor	mGy/h per Bq/m^2
Simulation Input	Simulation time	s
	Time step	s

[a] Some information on this parameter is provided in the scenario (Appendix I), but the actual values had to be calibrated.

[b] A standard value does not exist, but a reasonable value of 30 m^2/s has been used.

TABLE II.7. LIST OF MODEL OUTPUT FILES AND DESCRIPTIONS

File Name	Description of Output File
percentiles.out	95^{th}, 75^{th} and 50^{th} percentiles are provided in terms of the radius of a circle containing the corresponding percentage of activity released by the explosion.
surface_dose5.out	Surface contamination (Bq/m^2) and dose rate (nGy/h) on a 5 m × 5 m grid. The first two columns of the file are the coordinates of the centre of the grid cell (y and x); the third column is surface contamination, and the last column is dose rate.
surface_dose25.out	Surface contamination (Bq/m^2) and dose rate (nGy/h) on a 25 m × 25 m grid. The first two columns of the file are the coordinates of the centre of the grid cell (y and x); the third column is surface contamination, and the last column is dose rate.
conc5_15min.out	Time integrated activity concentrations in air ($Bq \times min/m^3$) on a 5 m × 5 m grid, 15 minutes after the explosion, at heights of 5, 10, and 15 m above the ground (columns 3, 4, and 5, respectively). The first two columns of the file are the coordinates of the centre of the grid cell (y and x).
conc25_15min.out	Time integrated activity concentrations in air ($Bq \times min/m^3$) on a 25 m × 25 m grid, 15 minutes after the explosion, at heights of 5, 10, and 15 m above the ground (columns 3, 4, and 5, respectively). The first two columns of the file are the coordinates of the centre of the grid cell (y and x).

II.5.6. Model application to the scenario

The dose rate was calculated using a conversion factor given by the USEPA [II.10], which gives the effective dose from the ground surface concentration of the radionuclide of interest.

Tests 1 and 2 were used to calibrate the model. Once model parameters were defined for these tests, the same values were used for Tests 3 and 4 (with the exception of activity and time from the activity measurement to the explosion). Different values for the effective release height and size of the gas cloud were also used for Tests 3 and 4. The input data file for Test 1 is reproduced in Fig. II.12 as an example.

For Test 2, the effective release height was set to 35 m and the cloud radius again to 3.5 m. According to supplied information, it seems that the cloud top and radius were larger for Tests 3 and 4. For these two tests, the effective height and cloud radius were set at 50 and 5 m, respectively.

Some examples of results are provided in Figs II.13 and II.14[24]. Figure II.13 shows vertical sections of the predicted time integrated activity concentrations in air along the y-axis at several distances from the explosion site for Test 2. Figure II.14 shows horizontal maps of time integrated activity concentrations in air at several heights above the ground for Test 2. For this test experiment, most of the activity (95%) is released as aerosol at an effective height of 35 m; thus, it is not surprising that time integrated activity concentrations in air increase with increasing distance from the ground, as shown in both figures.

The model has a running time of approximately 30 seconds for a 15 minute simulation on a PC compatible computer.

Contour maps over the 5 m and 25 m spatial resolution grids were generated with Matlab, using the model output files. Since the dose rate is directly proportional to the deposited activity, maps of the dose rate over the 25 m grid are not provided.

```
input data for explosion code: test1
-----------------------------
6.,40.              initial particle velocity (m/s), tolerance (%)
40.                 initial horizontal dispersion angle
30.,90.             vertical angles
0.001               friction coefficient of liquid particles with air
30.                 diffusion coefficient in air (m^2/s)
16                  simulated time (minutes)
.01                 time step (s)
.80,.50             box explosive dimensions x,y (m)
780.e6              total activity (Bq)
3.20e-5             radioactive decay constant (s-1)
145.                time in minutes from activity determination to explosion
.35                 fraction of activity in aerosol
30.                 effective mean release height for aerosol particles/ct (m)
3.5                 cloud radius (m)
```

FIG. II.12. Input data file reproduction for Test 1.

[24] Note that in Figs II.13 and II.14, the explosion site is located at the origin of the coordinates.

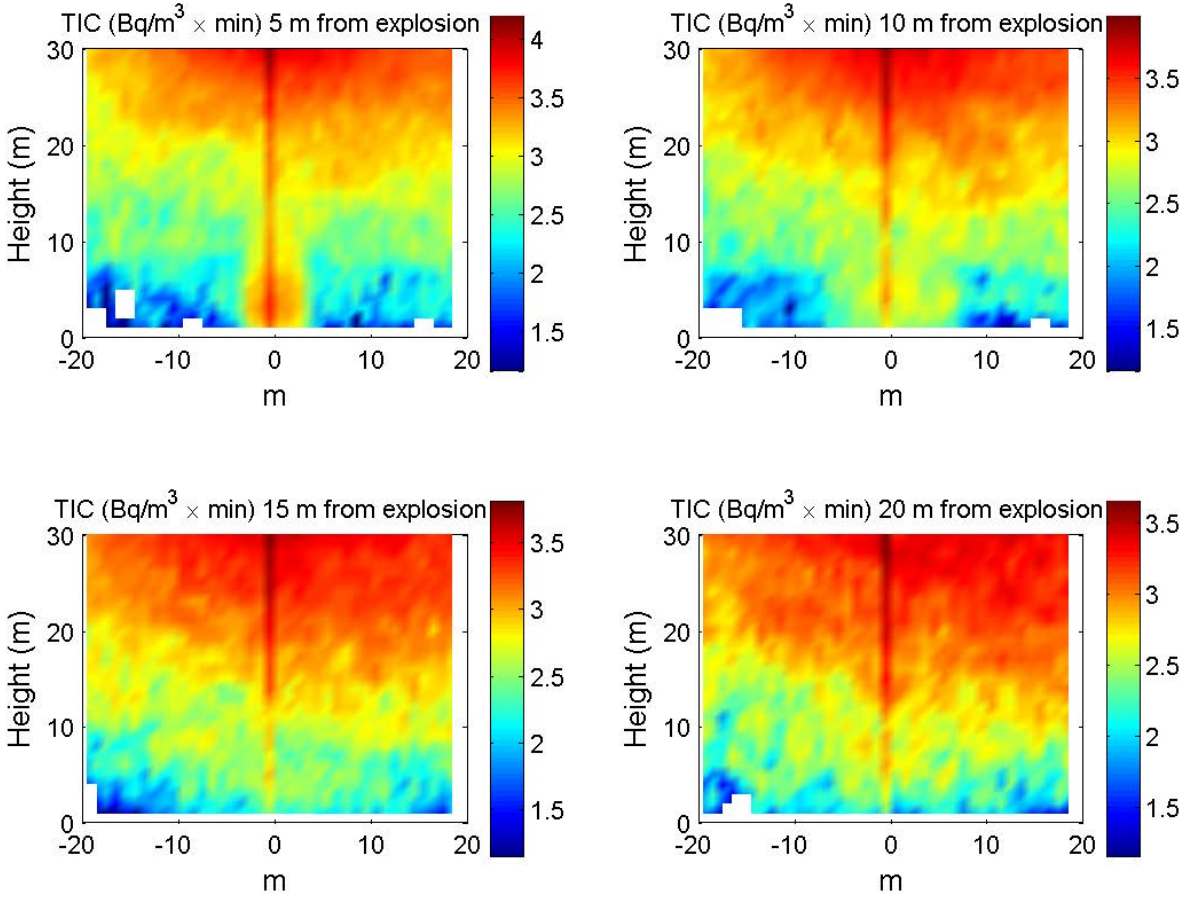

FIG. II.13. Time integrated activity concentrations in air, shown in logarithmic scale for vertical sections at different distances from the explosion site.

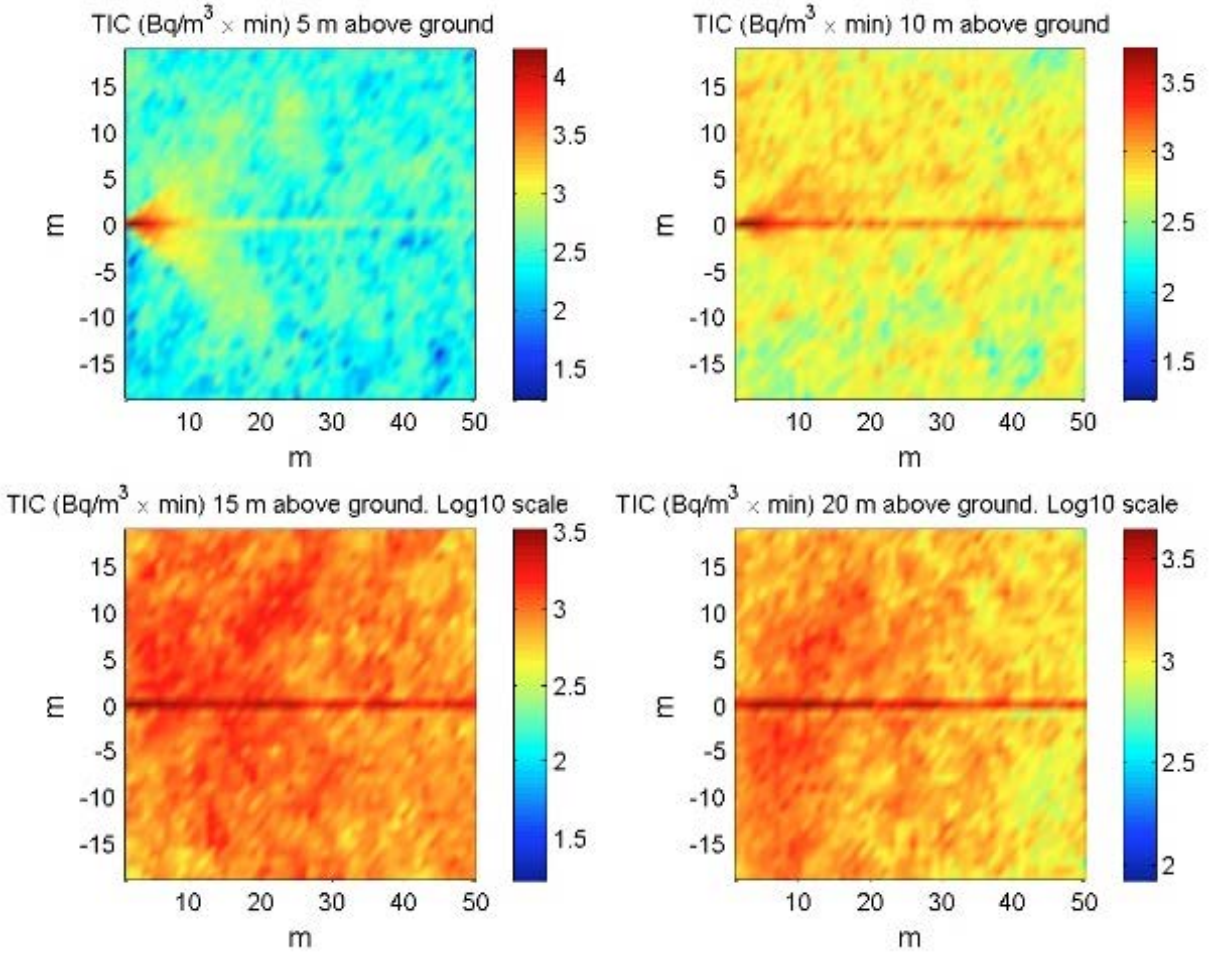

FIG. II.14. Time integrated activity concentrations in air, shown in logarithmic scale, at several heights above the ground.

II.5.7. Results

Results from Test 2 were made available to participants for use in model calibration and for evaluation of options for model parameterization (see Section II.7.1), as more data were available for Test 2 than for other tests.

Results from Test 1 (Section II.7.2) were also made available to participants for use in testing of the parameterization of their model, based on the model calibration that was carried out using data from Test 2.

Results from Tests 3 and 4 were then used for blind model testing.

II.5.7.1. Test 2

Measured deposition and predicted dose at the end of the experiment are presented in Figs II.15 and II.16. These contour plots were created using WinSURF Reconstruction Software (Windows SURFdriver, http://www.surfdriver.com/) using information provided with the scenario (see Tables I.8 and I.9 in Appendix I). Test 2 was used to test the two different formulations for the release of aerosol particles, based either on an effective release height or on a cloud top formulation (as is done in the HotSpot model).

Contour plots were then generated from the model output (Figs II.17 to II.19). These plots correspond to the surface deposition on a 5 m × 5 m grid. The first map was generated using the effective release height formulation (Fig II.17). The second and third maps were generated using the cloud top formulation in the model (Figs II.18 and II.19). In the second map, 'real situation' values were used for the cloud height and radius (with values of 5 m and 1 m, respectively). 'Theoretical' values were used to generate the third map (with values of 34.8 m and 7 m, respectively, for the cloud height and radius).

It may be concluded that for the cloud top formulation (as used in the HotSpot model), deposition values tended to be overestimated. Also, qualitative shapes of isolines seemed more realistic for the effective release height formulation. Considering that the present model is a different type of model than HotSpot, it was preferred to retain the formulation based on the effective height formulation.

The order of magnitude of dose rates computed using the effective height formulation was also comparable with measured values, as may be seen in Fig. II.20. Thus, in what follows, only results obtained using the effective release height formulation are presented.

Predicted surface deposition on a 25 m × 25 m grid for Test 2 is presented in Fig. II.21.

II.5.7.2. Test 1

Surface deposition measured for Test 1 is presented in Fig. II.22, and the corresponding computed deposition is presented in Fig. II.23 on a 5 m × 5 m grid. In general, measured data indicated that the deposition was restricted to the area near the explosion site, to a distance of approximately 20 meters; this was quite well reproduced by the model.

Deposition map on a 25 m resolution grid is presented in Fig. II.24, and the corresponding dose rates on a 5 m resolution grid are presented in Fig. II.25.

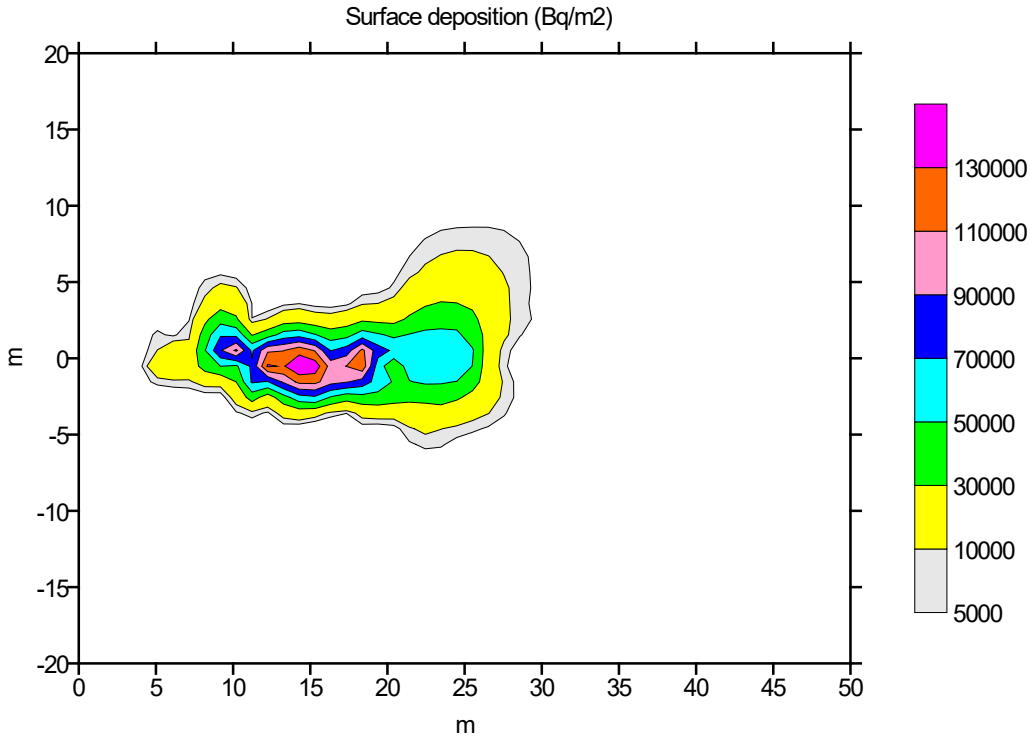

FIG. II.15. Measured surface deposition in Test 2.

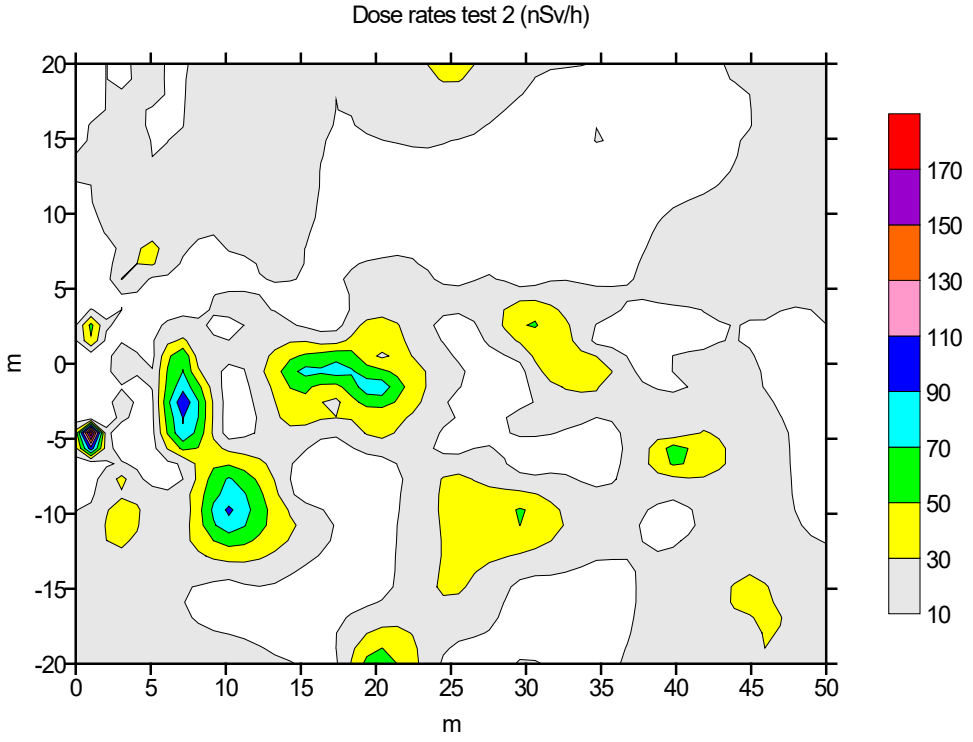

FIG. II.16. Measured dose rates in Test 2.

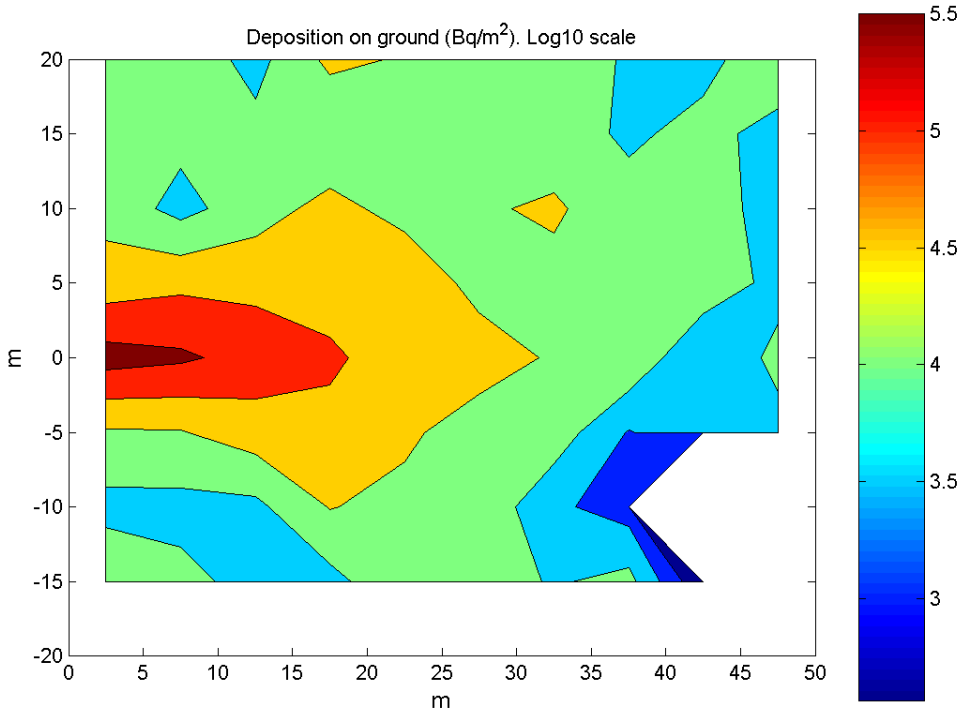

FIG. II.17. Surface deposition for Test 2 generated using the effective release height formulation.

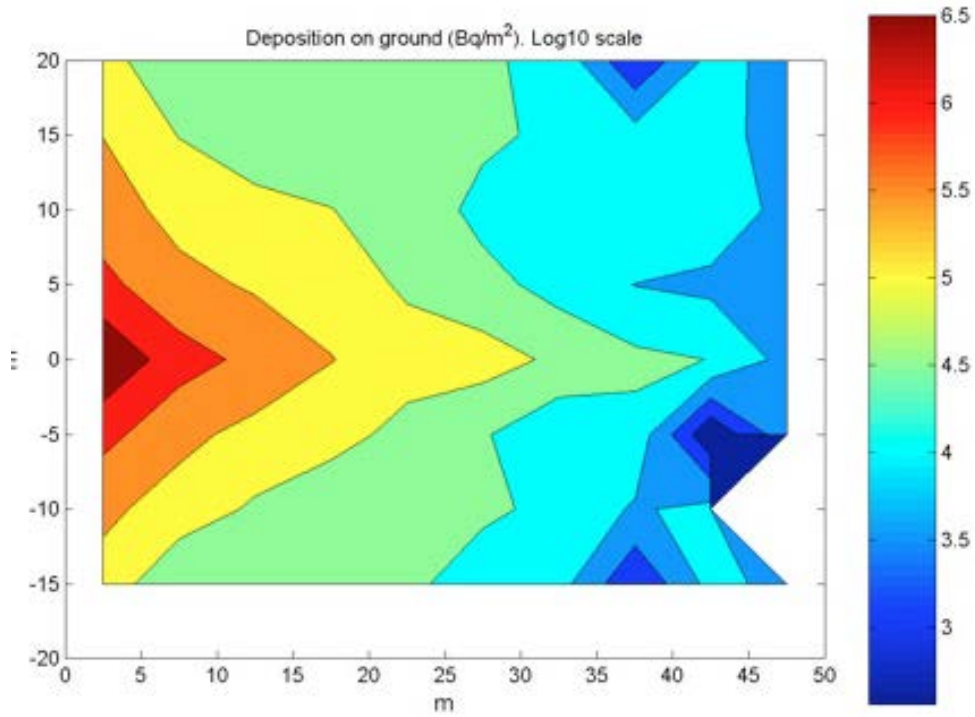

FIG. II.18. Surface deposition for Test 2 generated using the cloud top formulation and 'real situation' parameters.

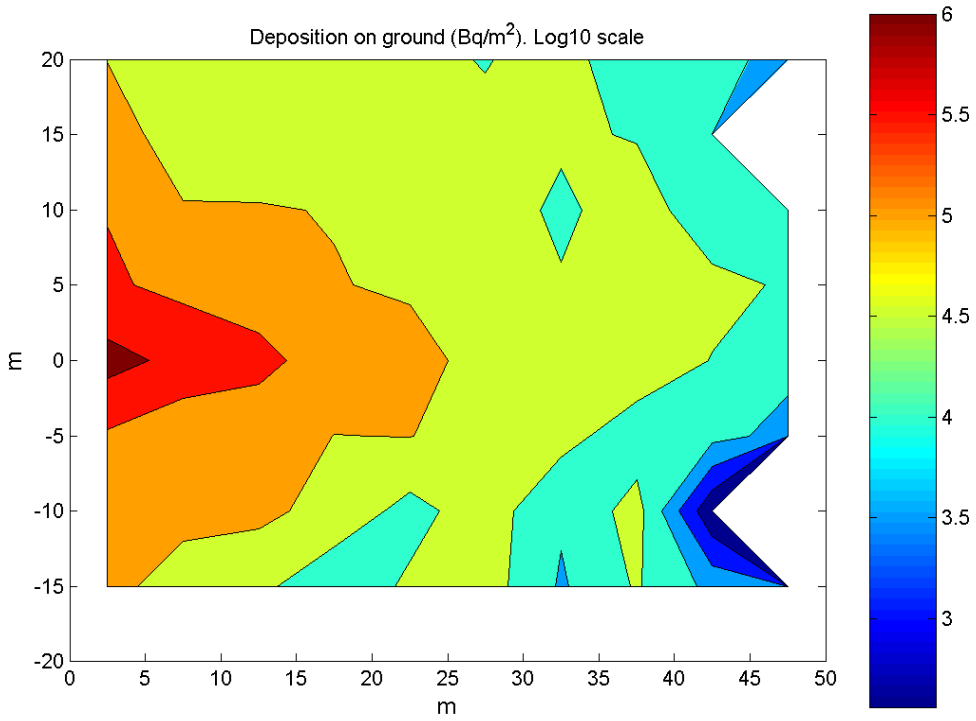

FIG. II.19. Surface deposition for Test 2 generated using the cloud top formulation and 'theoretical' parameters.

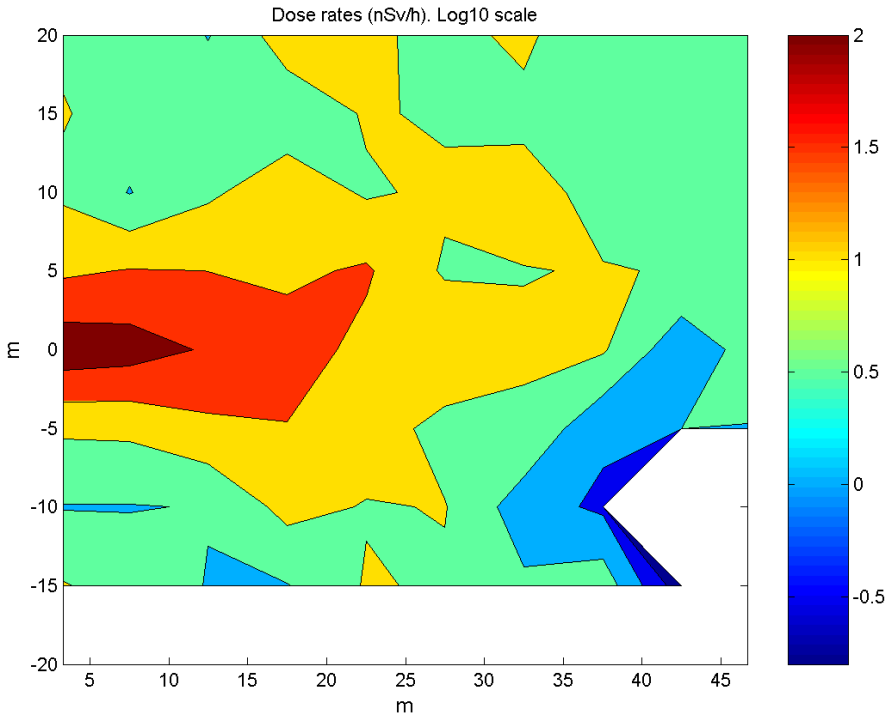

FIG. II.20. Dose rates for Test 2 generated using the effective release height formulation.

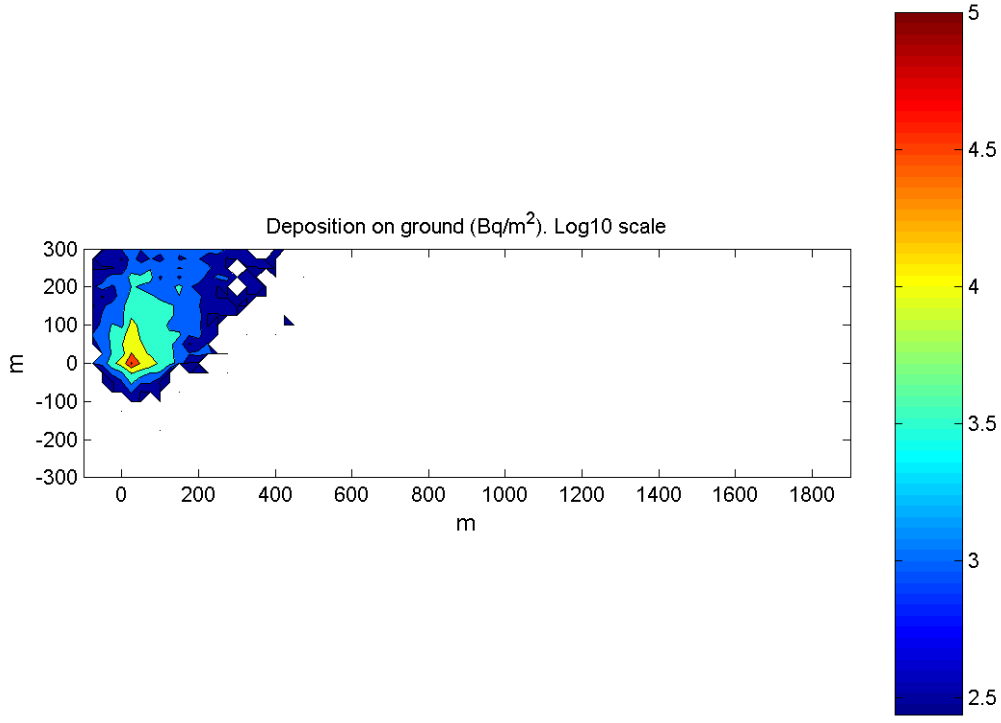

FIG. II.21. Predicted surface deposition on a 25 m × 25 m grid for Test 2.

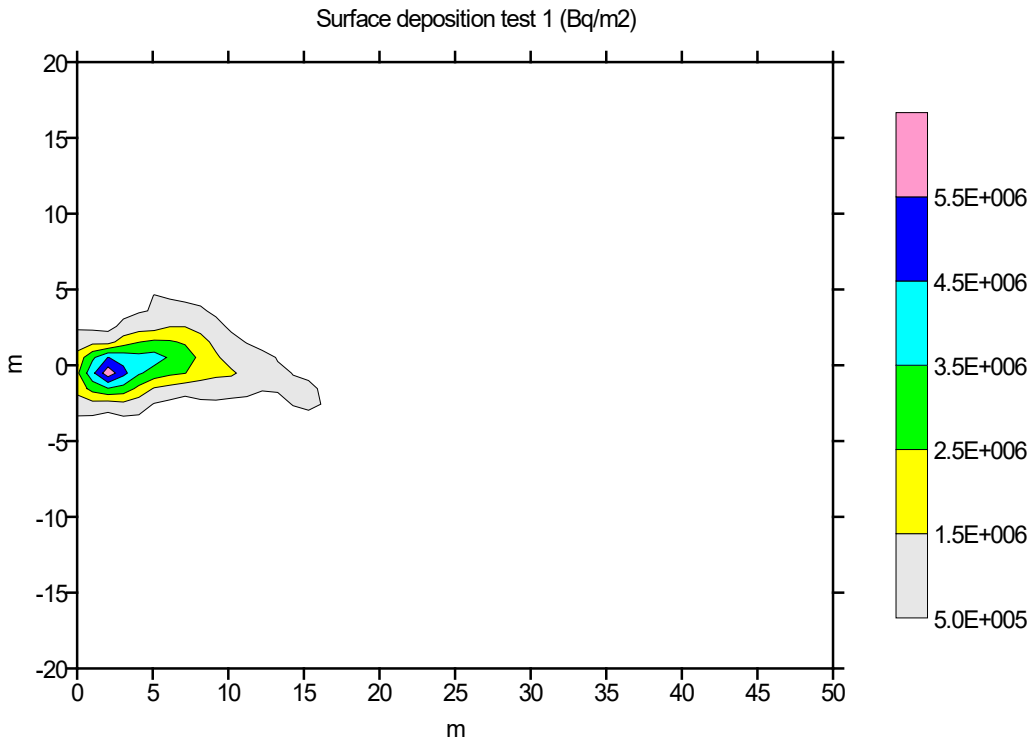

FIG. II.22. Measured surface deposition for Test 1.

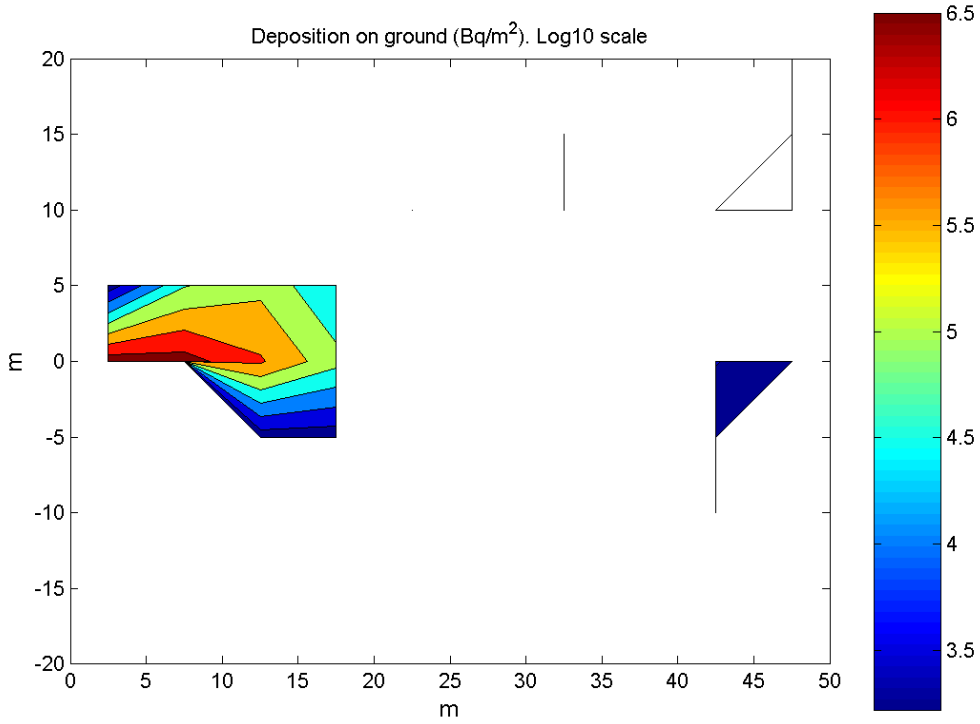

FIG. II.23. Computed surface deposition for Test 1.

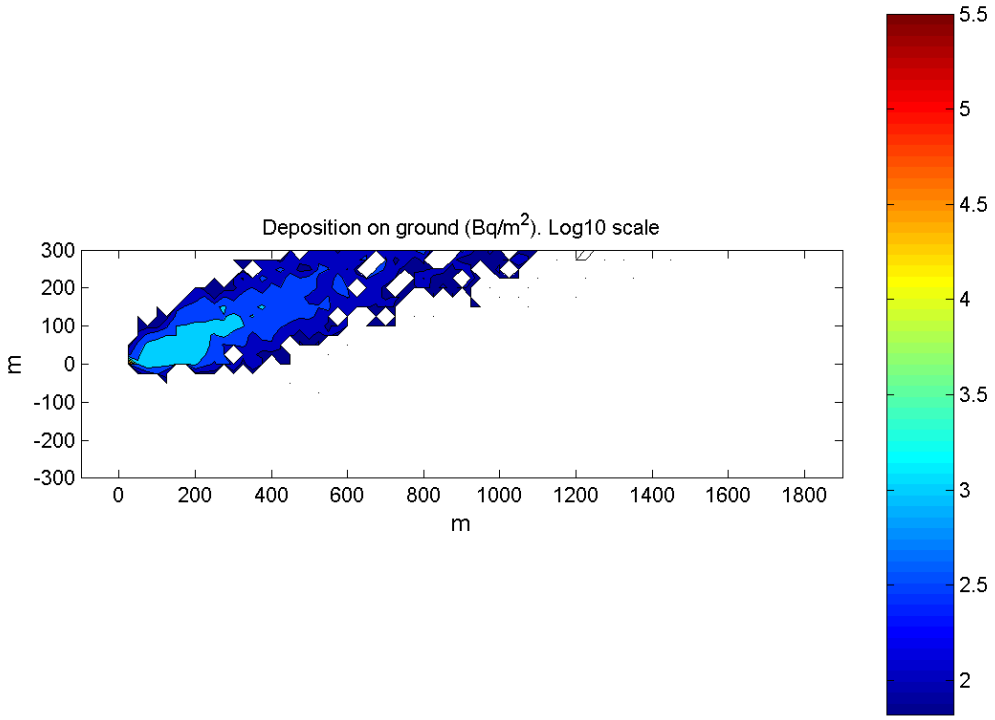

FIG. II.24. Deposition map computed on a 25 m resolution grid for Test 1.

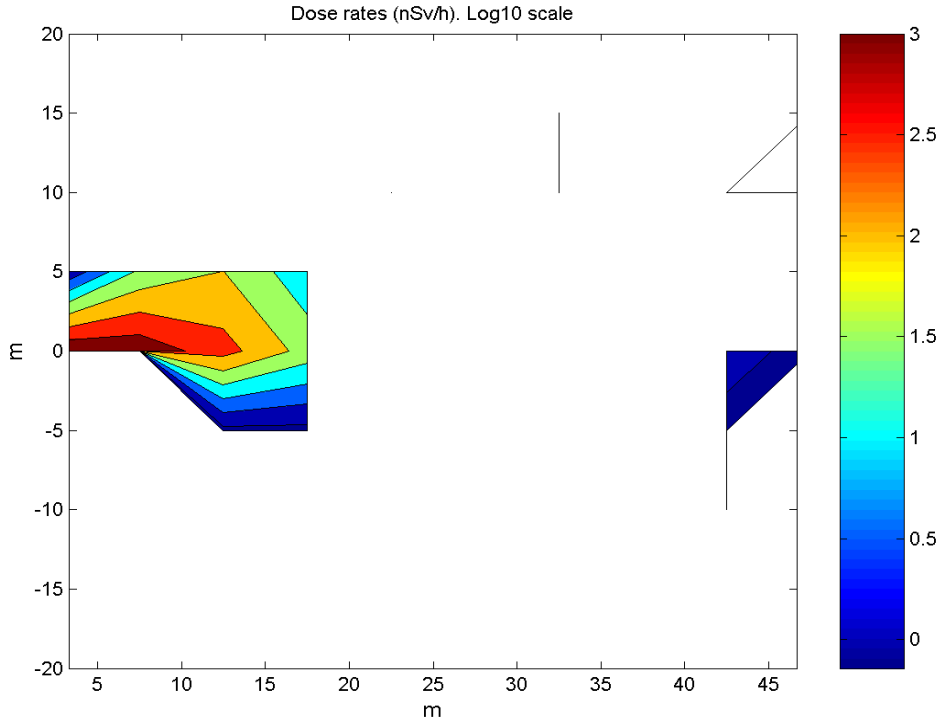

FIG. II.25. Computed dose rates for Test 1 on a 5 m resolution grid.

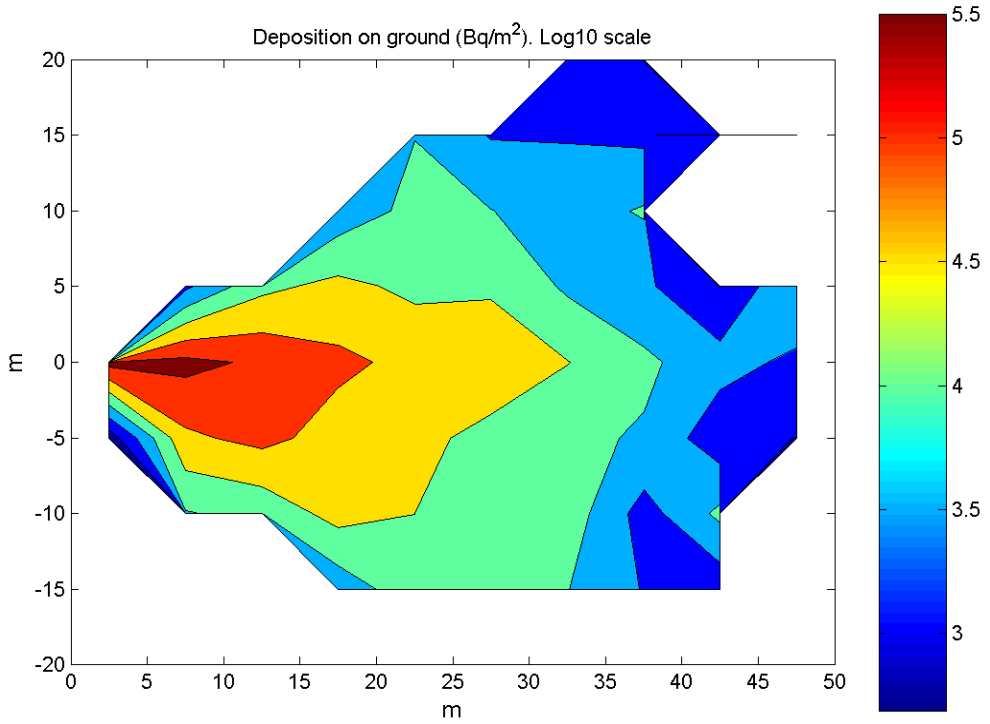

FIG. II.26. Surface deposition on a 5 m resolution grid for Test 3.

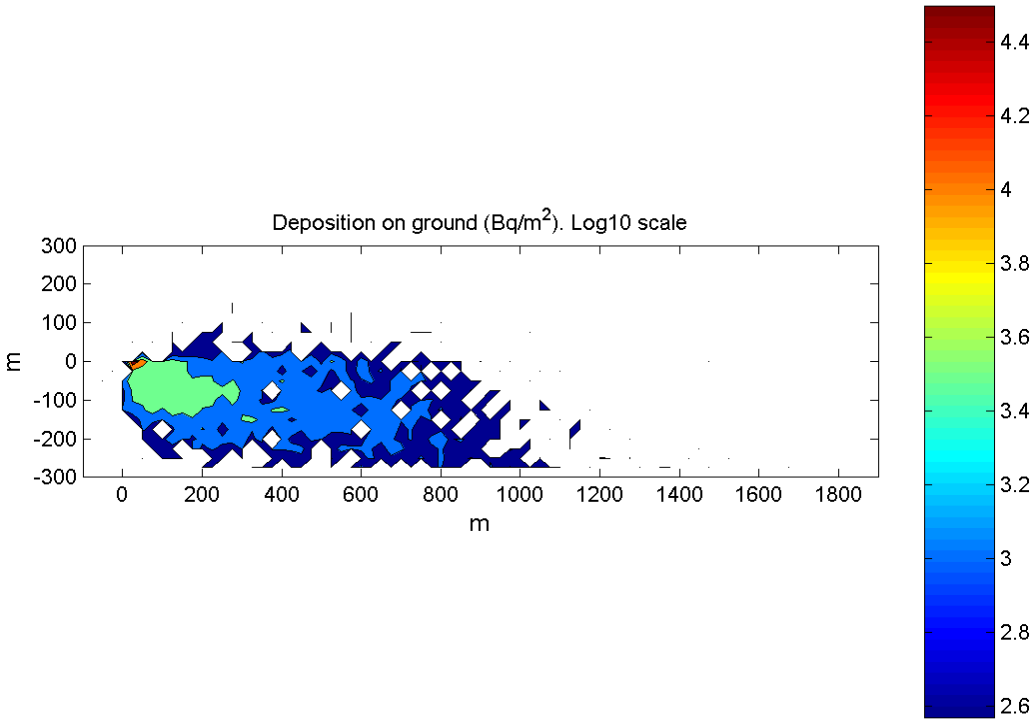

FIG. II.27. Computed surface deposition on a 25 m resolution grid for Test 3.

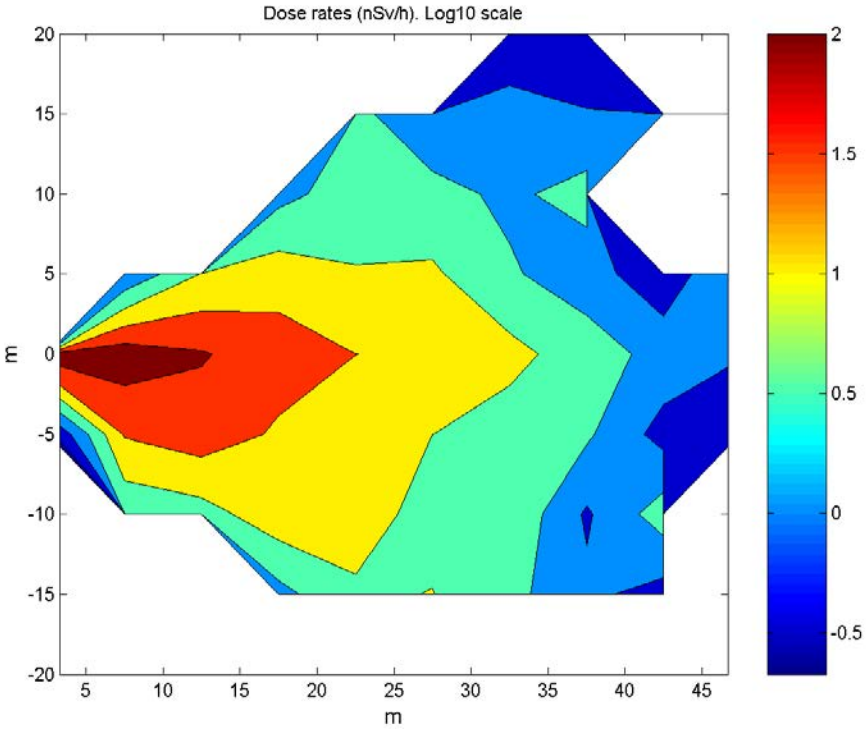

FIG. II.28. Computed dose rate on a 5 m resolution grid for Test 3.

II.5.7.3. Test 3

Tests 3 and 4 were used for blind model testing. As discussed earlier, the cloud top and cloud radius were larger for these tests than for Tests 1 and 2, by approximately a factor of 2. Thus, the effective release height and cloud radius have been increased for both Tests 3 and 4 to 50 m and 5 m, for the effective height and cloud radius respectively. Remaining parameters were set as in Test 2; in particular, it was assumed that 95% of the activity was released as aerosol particles. Figures II.26 and II.27 depict the predicted surface deposition on the 5 m and 25 m resolution grids, respectively, for Test 3. Figure II.28 depicts the corresponding predicted dose rates on the 5 m resolution grid.

II.5.7.4. Test 4

For this last test, collision with obstacles used in the experiment was included in the model. Obstacles are shown as black objects in the figures that follow. It is noted that these obstacles have been treated in a very simple way; specifically, how the presence of the obstacle modifies the wind field and turbulence around it was not considered. Thus, an obstacle was taken into account only when a liquid or aerosol particle collided with it, in which case, the particle was removed from the computation. Figures II.29 and II.30 depict the predicted surface deposition on the 25 m and 5 m resolution grids, respectively, for Test 4. Figure II.31 depicts the corresponding predicted dose rates on the 5 m resolution grid.

The effect of obstacles may be appreciated in the deposition map that was generated on a 1 m × 1 m grid, thus after a minimum averaging process (see Fig. II.32). In this case, there was no deposition in the area behind the main obstacle. Also, maximum values in this map were larger than in the 5 m resolution map, which is due to the averaging process that was used to

generate this map. In addition, as expected, the maximum values were even lower on the 25 m resolution map, as may be seen in Fig. II.29. This effect was evident for the other tests, as well.

II.5.7.5. Additional output

Maps of time integrated activity concentrations in air at three heights above the ground, as requested in the scenario description, are presented in Figs II.33 to II.36. Maps are only provided for the 25 m resolution grids, but were calculated on the 5 m resolution grid, as well. All the maps correspond to 15 minutes after the explosion. As noted above, there were no significant differences 5 and 10 minutes after the explosion.

Percentile contamination zones (95%, 75% and 50%) for each test are presented in Table II.8. These zones are defined in terms of the radius of a circle centered at the explosion site, as a percentage of total deposition. The short distances of the radii for the 75% and 50% zones, in the case of Test 1, are due to the assumption that most of the activity was released as liquid particles for this test. Thus, most of the deposition occurred near the explosion site. For the other three tests, it was assumed that most of the activity was released as aerosol particles.

Based on a comparison of the results of Tests 2, 3 and 4 (Table II.8), it is evident that relatively larger percentile areas were generated for Test 3. This result is consistent with those presented in Figs II.21, II.27 and II.29, which show surface deposition on the 25 m resolution grid, when results in these figures are compared. Radionuclides were transported a longer distance in the case of Test 3 because of the prevailing wind conditions during this test experiment.

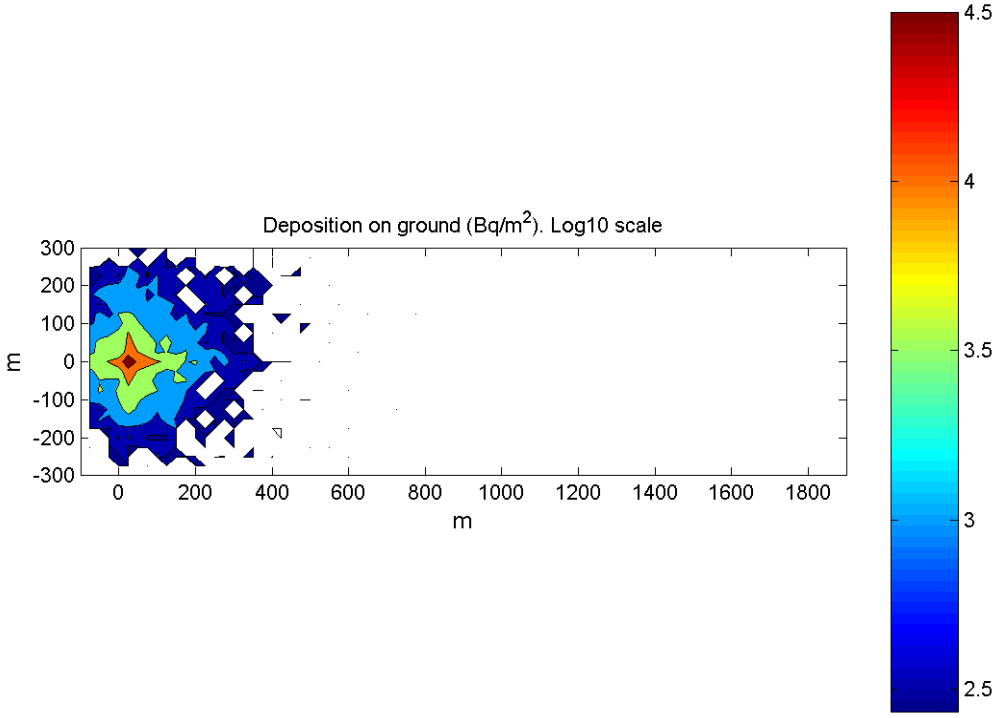

FIG. II.29. Computed surface deposition on a 25 m resolution grid for Test 4.

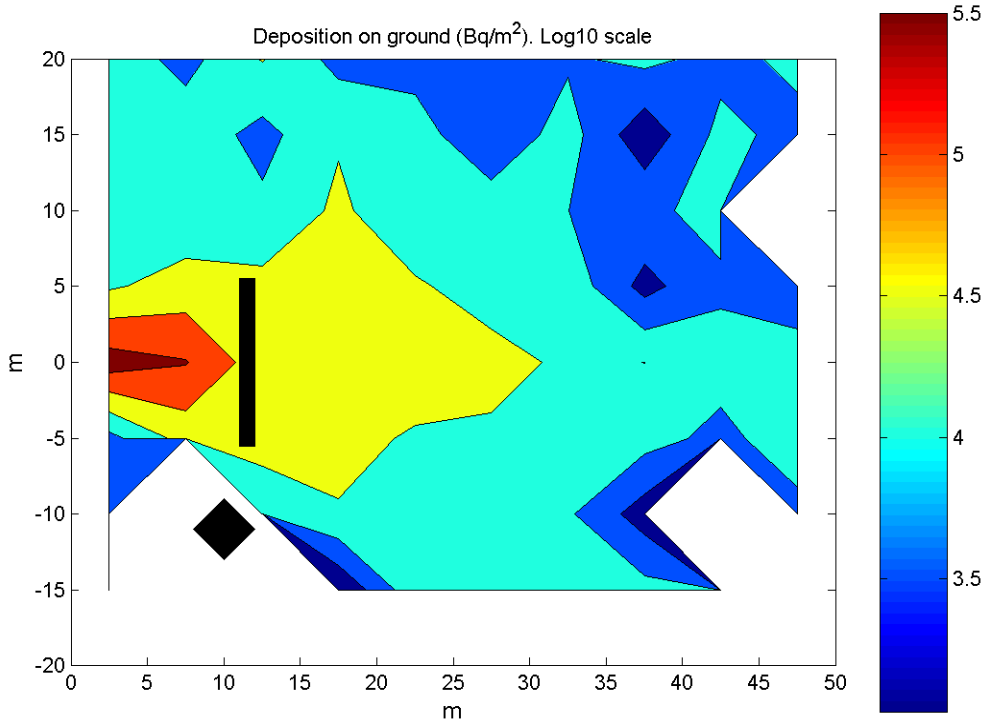

FIG. II.30. Computed deposition for Test 4 on a 5 m resolution grid.

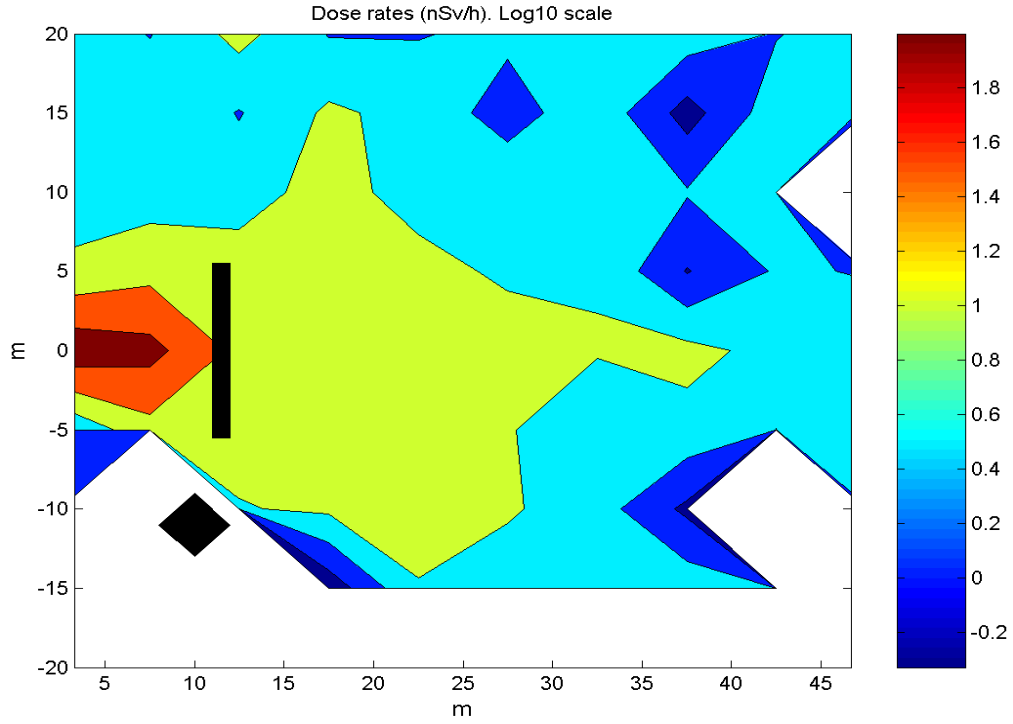

FIG. II.31. Computed dose rate on a 5 m resolution grid for Test 4.

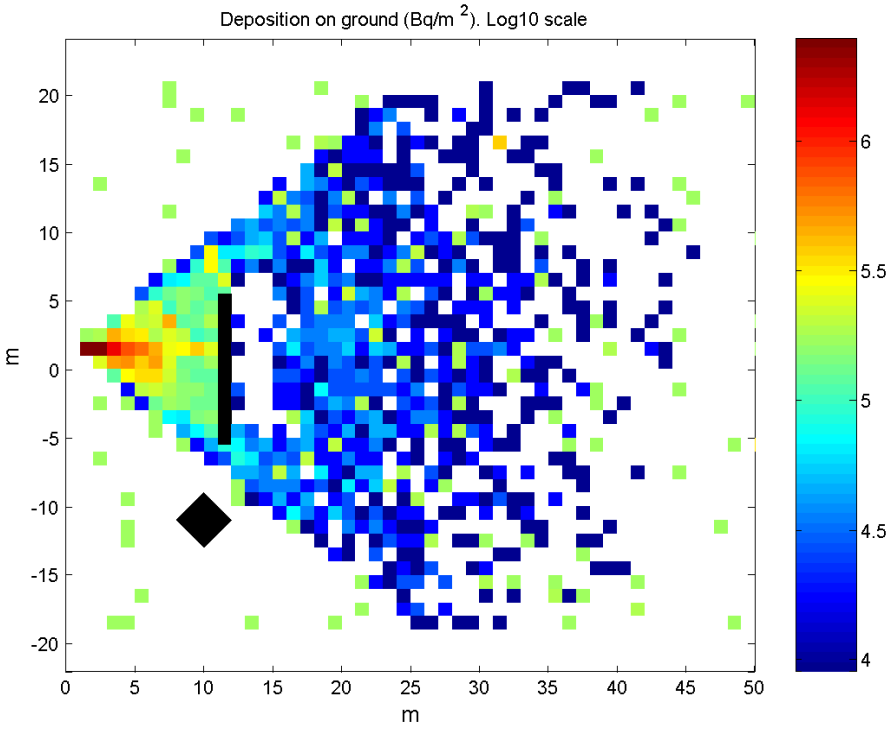

FIG. II.32. Computed surface deposition on a 1 m resolution grid for Test 4.

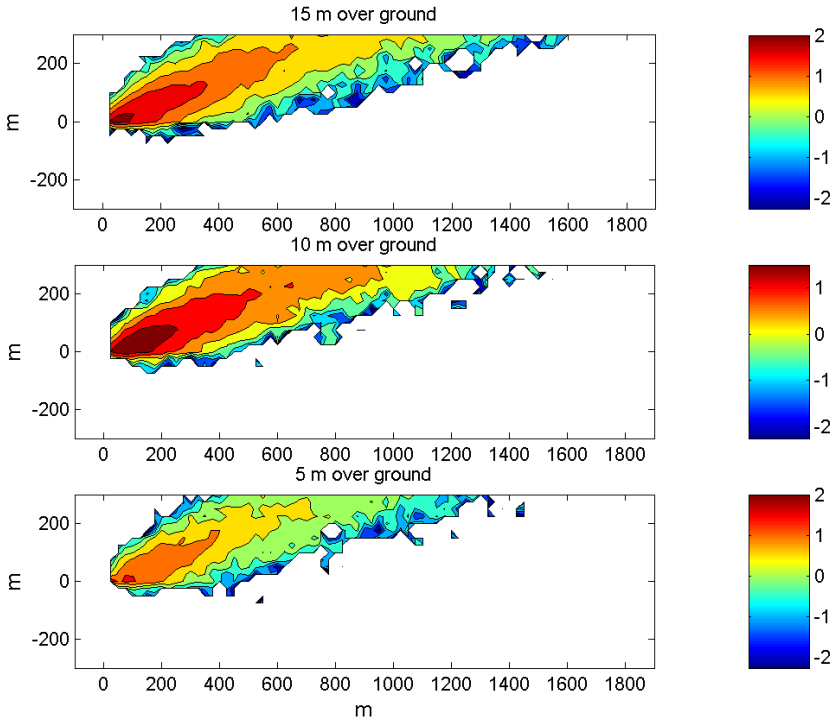

FIG. II.33. Computed time integrated activity concentration in air (Bq/m^3 × min) for Test 1 on a 25 m resolution grid.

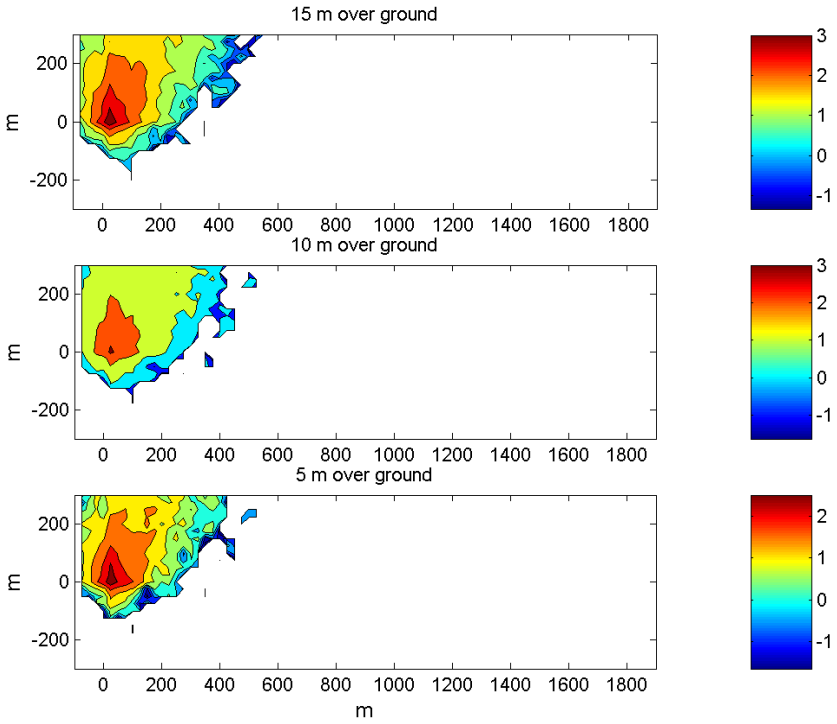

FIG. II.34. Computed time integrated activity concentration in air (Bq/m^3 × min) for Test 2 on a 25 m resolution grid.

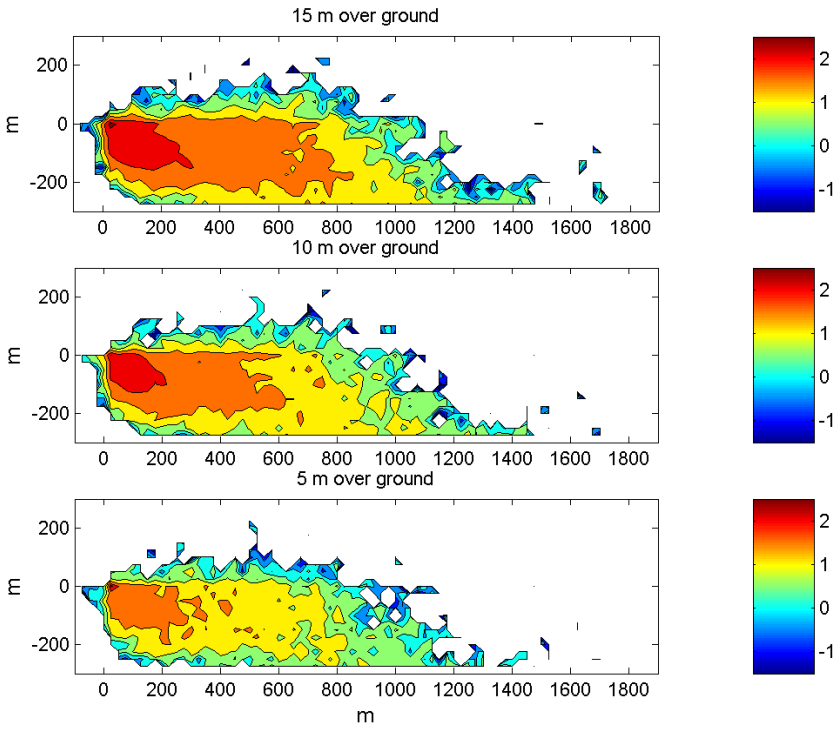

FIG. II.35. Computed time integrated activity concentration in air (Bq/m^3 × min) for Test 3 on a 25 m resolution grid.

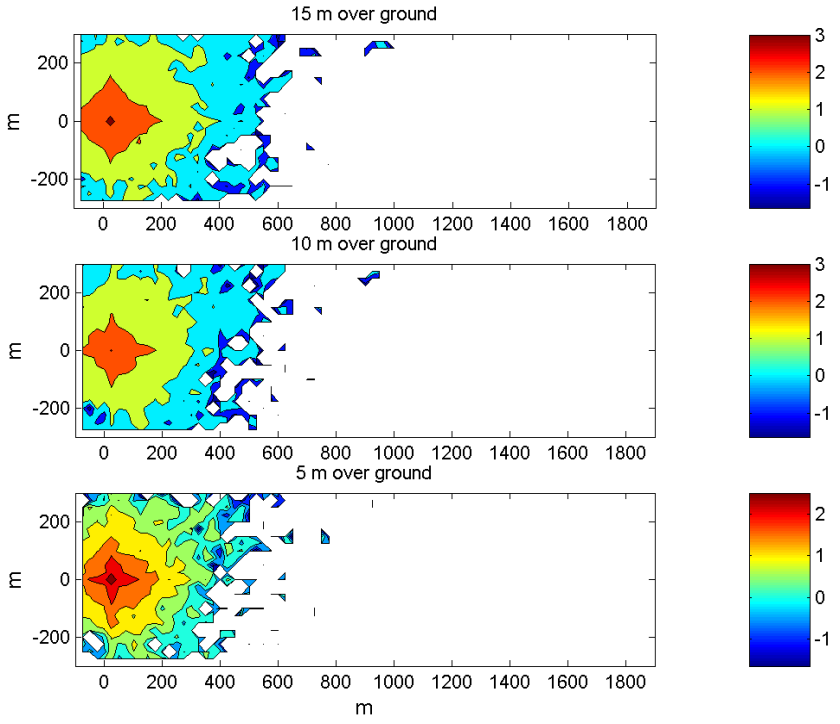

FIG. II.36. Computed time integrated activity concentration in air (Bq/m^3 × min) for Test 4 on a 25 m resolution grid.

TABLE II.8. PERCENTILE CONTAMINATION ZONES (95%, 75% AND 50%)

Test	95%	75%	50%
1	427	12	7
2	304	189	102
3	812	511	277
4	348	189	111

II.5.8. Summary

A model specifically designed for the short range scenario has been developed. It is a simple model based on a Lagrangian method to simulate particle dispersion, decay and deposition. The main characteristics of the model are:

- Separate simulation of the dispersion and deposition of liquid and aerosol particles; different initial conditions are set for both types of particles, and different dispersion mechanisms are assumed.
- Running times are extremely short (approximately 30 seconds for a 15 minutes simulation on a personal computer).
- There are no limitations on output resolutions due to the Lagrangian nature of the model. The model can be used to generate deposition maps, dose rate maps and time integrated air concentration maps at any desired resolution and spatial scale.
- Collisions with obstacles are included in a very simple way.
- The order of magnitude of surface deposition and dose rates computed for Tests 1 and 2 are in relatively good agreement with measured values.
- Once calibrated, the model has been applied to Tests 3 and 4. Only the effective release height and cloud radius, for aerosol particles, have been modified for these simulations.

II.6. DESCRIPTION OF LASAIR

The LASAIR code was used for the short range modelling exercise by H. Walter of the Bundesamt für Strahlenschutz in Germany.

II.6.1. Introduction

LASAIR is a decision support model developed for the Lagrange-Simulation of the dispersion (German translation: ‘Ausbreitung’) and Inhalation of Radionuclides. The model is designed to simulate the effects after a ‘dirty bomb’ explosion.

The LASAIR model is a two dimensional flow model (no orographic structure). It is a Lagrangian particle model, using 60 000 particles. The roughness length can be characterized for the individual scenario being modelled. Up to five radionuclides can be computed simultaneously, and approximately 860 radionuclides are available. LASAIR offers a very quick response time (1–10 minutes).

LASAIR input parameters include meteorology data (wind speed, wind direction, stability class), information on the type of atmospheric release (short term or continuous release), and topography (individual roughness length, two dimensional simulation). LASAIR outputs, for up to five radionuclides, include the activity concentrations in the base layer, deposition on the surface, and cloud arrival time. Human exposure is calculated for inhalation, groundshine, and cloudshine.

The basic computation in LASAIR is:

$$B_r = V_g \times C^*_r \quad \text{(II.1)}$$

where:

B_r is the deposition of radionuclide r (Bq/m^2);
V_g is the deposition velocity (m/s); and
C^*_r is the time integrated activity concentration in air of radionuclide r (Bq · min · m^{-3}).

II.6.2. Application to the short range exercise

Table II.9 summarizes the aerosol characteristics used in the short range exercise.

The input data used by LASAIR in the short range exercise are summarized in Table II.10. The source term was characterized in terms of the initial cloud, represented as a volume, as described by its height (m) and the width and depth of the cloud base (m; width and depth have the same value).

II.6.3. Summary of predicted deposition

Table II.11 summarizes the predicted deposition after 60 minutes for each test.

TABLE II.9. SUMMARY OF AEROSOL CHARACTERISTICS USED IN THE SHORT RANGE EXERCISE

Size range (μm)	Deposition velocity (10^{-4} m/s)	Fraction of aerosols (%)
0–2.5	1	40
2.5–10	10	40
10–50	80	10
>50	80	10

TABLE II.10. SUMMARY OF INPUT DATA USED WITH LASAIR IN THE SHORT RANGE EXERCISE

Parameter	Test 1 2007-12-06	Test 2 2008-05-15	Test 3 2009-05-05	Test 4 2009-07-14
Explosion time	12:45	11:30	12:22	12:42
Explosive	Permon 10T	Vesuvit TN	Permon 10T	Permon 10T
Explosive mass	30 g	20 g	350 g	350 g
Defined cloud height (m)	7	5	13	13
Defined cloud base (m)	3	2	5	5
Particle sizes (μm)				
0–2.5	40%	40%	40%	40%
2.5–10	40%	40%	40%	40%
10–50	10%	10%	10%	10%
>50	10%	10%	10%	10%
Wind speed at 2 m height	0–6.3 m/s	0.28–1.85 m/s	0.9–7.2 m/s	0–4.9 m/s
Stability class	D	B–C	D	C
Land use class and roughness length	explosion test ground: 0.1 m vicinity 1.0 m	explosion test ground: 0.1 m vicinity 1.0 m	explosion test ground: 0.1 m vicinity 1.0 m	explosion test ground: 0.1 m vicinity 1.0 m obstacle 1.5 m
Radionuclide and radioactive half-life	Tc-99 6.01 h	Tc-99 6.01 h	Tc-99 6.01 h	Tc-99 6.01 h
Activity (time of measurement)	780 MBq at 10:20	1058 MBq at 10:10	1222 MBq at 12:22	1088 MBq at 11:00
Activity (time of explosion)	590 MBq at 12:45	907 MBq at 11:30	1222 MBq at 12:22	894 MBq at 12:42

TABLE II.11. SUMMARY OF PREDICTED DEPOSITION AFTER 60 MINUTES

Parameter	Test 1 2007-12-06	Test 2 2008-05-15	Test 3 2009-05-05	Test 4 2009-07-14
Activity released (Bq)	5.90×10^8	9.07×10^8	1.22×10^9	8.94×10^8
Activity deposited (Bq)	7.28×10^7	1.91×10^8	2.33×10^8	2.0×10^8
Deposition/release (%)	12.4	21.1	19.1	22.3
Area affected (m^2)	6.5×10^9	1.0×10^8	1.6×10^9	1.0×10^8

II.7. DESCRIPTION OF COMPUTATIONAL FLUID DYNAMICS (CFD) CODE

The Computational Fluid Dynamics (CFD) code was used for the short range modelling exercise by G. de With of the Nuclear Research and Consultancy Group (NRG) in the Netherlands.

II.7.1. Introduction

In recent years, there has been increasing interest in predicting the possible consequences of the release of nuclear material or other radioactive material into the atmosphere. Such releases can occur due to an accidental release from a nuclear facility or as a result of a malicious act, such as a dirty bomb. In all such cases, the consequences to the general public in the vicinity of the release are of key interest, as they are potentially most at risk from radiation exposure. However, making an accurate prediction of the consequences to those in the vicinity of the release is a

difficult task. Climatic conditions and building arrangement or vegetation surrounding the release, as well as the radioactive material and the type of detonation used in the release, can greatly influence the dispersion of the nuclear substance. As a result, any radiation exposure varies strongly both spatially and temporally, making accurate prediction very difficult. It is for these reasons that most mainstream assessment tools for radiation exposure are not designed to study the exposure close to a release. To address such shortcomings, a benchmark study was initiated within the EMRAS II programme. The benchmark study was aimed at evaluating and improving the capabilities of simulation tools used in the assessment of radioactive contamination in urban settings. The work presented here was part of this benchmark study and was aimed at modelling the dispersion of radioactive material in the atmosphere.

During the benchmark study, simulations were performed to model the dispersion of ^{99m}Tc in the vicinity of a release. The simulations were based on numerical computations using the CFD tool FLUENT. The results were benchmarked against field experiments from the National Radiation Protection Institute (SÚRO) in Prague (Czech Republic) (Appendix I). These field experiments had been carried out on the premises of the National Institute for Nuclear, Chemical and Biological Protection (SÚJCHBO) in Kamenná, near Prague (Czech Republic). The experiments were performed using a limited amount of ^{99m}Tc that was stored in liquid form and released into the atmosphere using a small industrial explosive. As part of the experiment, activity concentrations of ^{99m}Tc in the air were measured, as well as the deposition of ^{99m}Tc on the ground surface and the subsequent radiation dose rates at 1 m above the ground surface (Appendix I).

In the CFD simulation model, all climatic conditions at the time of the experiment were incorporated. The local topography and the surrounding vegetation formed the basis of the model geometry, and the essential aspects of the explosion were also considered in the simulation. In the CFD computation, the time dependent wind and temperature driven airflows were modelled using standard available CFD algorithms. To take account of turbulent vortex motions, a k-ε turbulence model was applied, and effects of vegetation and forest were accounted for using a porosity model. The dispersion of ^{99m}Tc was modelled using NRG's algorithms. These algorithms were developed to compute the nuclear decay, deposition and terminal velocity, as well as the radiation exposure from the deposited ^{99m}Tc. Using this selection of CFD algorithms, all aspects of the release, dispersion, decay, and deposition of the radioactive material can be modelled in detail. During the simulation, the computation was initiated following the initial release of radioactive material and continued until the ^{99m}Tc was predicted to have been deposited on the ground surface or dispersed beyond the area considered in the model (beyond the model domain).

Section II.7.2 describes the computational models used in the short range exercise. Section II.7.3 describes the model setup, along with the details of the boundary conditions, followed by a summary of all relevant input parameters. Section II.7.4 describes the findings of the work, including a detailed comparison of model results against experimental data and a sensitivity analysis.

II.7.2. Mathematical models

The CFD software FLUENT was used for the short range exercise. The computational models used for airflow modelling and deposition have been described by de With and de Jong [II.11]. The calculation of radiation exposure (dose rate) from deposited activity is described in this section.

Following the release of ^{99m}Tc, the radiation exposure in the surrounding area is primarily from the gamma rays emitted by the ^{99m}Tc that has been deposited on the ground surface. Calculation routines were implemented in the CFD model to calculate the absorbed dose rate at a 1 m height above the ground using the following equation:

$$\dot{K}_{a,j} = \Gamma_a \sum_{p=0}^{p=P_b} \frac{A_p}{r_{p,j}^2} \tag{II.2}$$

where:

$\dot{K}_a$ is the absorbed dose rate at a 1 m height above the ground surface (μGy/h);
j is an index for the grid element;
p is an index for the boundary facet;
P_b is the total number of boundary facets;
Γ_a is the air kerma rate constant (μGy·m^2 MBq^{-1} h^{-1});
A is the activity from deposition on the ground surface (Bq); and
$r_{p,j}$ is the distance between the radiation source (p) and the grid element (j).

In addition, the equivalent dose rate is calculated using the following equation:

$$\dot{H}_j = \eta \sum_{p=0}^{p=P_b} \frac{A_p}{r_{p,j}^2} \tag{II.3}$$

where:

$\dot{H}$ is the equivalent dose rate (μSv/h); and
η is the equivalent dose rate constant (μSv·m^2 MBq^{-1} h^{-1}).

The kerma rate constant (Γ_a) for ^{99m}Tc in air is 0.018 μGy·m^2 MBq^{-1} h^{-1}, and the equivalent dose rate constant (η) is 0.023 μSv·m^2 MBq^{-1} h^{-1}.

The activity A is based on the accumulated surface contamination and the surface area of the boundary facet, and is calculated by means of Eq. (II.4), as follows:

$$A_p = \sum_{t=0}^{t=t_p} J_{d,t,p} \cdot a_{b,p} \tag{II.4}$$

where:

A_p is the activity of the boundary facet p (Bq);
$J_{d,t,p}$ is the deposition (accumulated surface contamination) in the j^{th} grid element during time step t (Bq/m^2); and
$a_{b,p}$ is the surface area of the boundary facet p (m^2).

The dose rate is computed during the calculation at the end of each time step t, for each grid element j that lies approximately 1 m above the ground surface. For each grid element, the dose rates from all individual boundary facets are computed and accumulated. A sketch of the calculation procedure is presented in Fig. II.37.

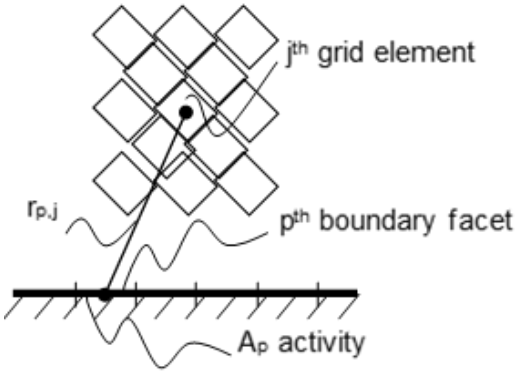

FIG. II.37. Sketch of the dose rate calculation in the CFD model.

II.7.3. Model setup and boundary conditions

II.7.3.1. Model setup

II.7.3.1.1. Model geometry

For the CFD computation, a three dimensional model of the area surrounding the explosion was constructed (the computational domain is shown in Fig. II.38; also, see Appendix I, Fig. I.1). The outer dimensions of the model are length (x) × width (z) × height (y) = 1000 m × 950 m × 100 m, and the model contains more than 2 million grid elements. The sand hills located adjacent to the institute have been incorporated into the model. The locations and geometry of the sand hills were estimated, based on publicly available topographic information and information received verbally from the SÚRO. The remaining ground surface was assumed to be horizontal, and therefore, irregularities and disturbances in the ground surface are not included in the model geometry. These types of irregularities are accounted for in the model constant for roughness height.

II.7.3.1.2. Simulation type

The CFD simulations are transient, with a total physical time of 500 s and a time step of 1 s. At the start of the simulation, at time $t = 0$ s, a fully developed initial cloud with spatially uniform flow properties was assumed, and a fully developed and converged atmospheric boundary flow was applied. These boundary flow conditions were continuously updated during the CFD calculation.

II.7.3.1.3. Vegetation

Using publicly available topographic information, the patches with intense forest were identified, and a mean height for each patch of forest was chosen by means of best guess. The areas were incorporated into the model geometry, and the airflow in the forest patch was modelled as a porous medium. Based on work presented by Endalew et al. [II.12], the porosity was assumed to be isotropic, and a resistance coefficient of 0.1 m^{-1} was applied. The resistance coefficient is a measure of the airflow obstruction from tree branches and leaves. The resistance coefficient is dependent on the season of the year and the type of vegetation; nevertheless, the selected value of 0.1 m^{-1} was considered a reasonable average and was applied to all forest patches in the CFD model.

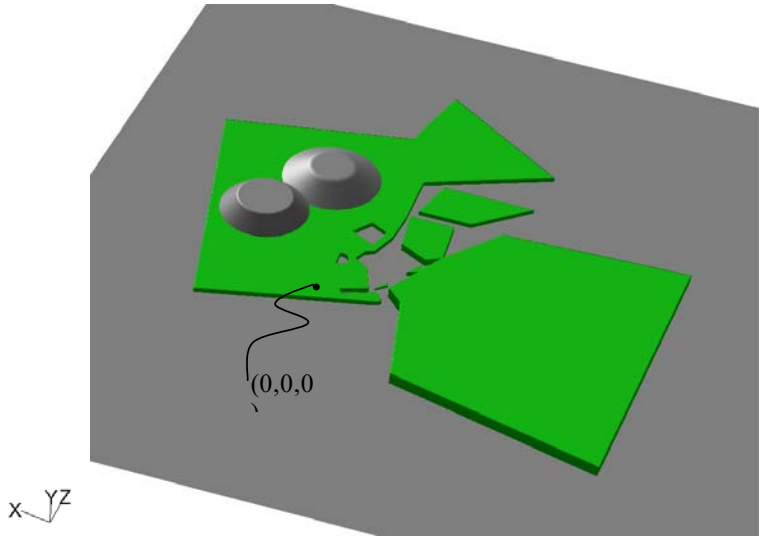

FIG. II.38. Sketch of the computational domain. The green patches represent the forest and building plots. The outer dimensions of the computational domain are Length (x) × Width (z) × Height (y) = 1000 m × 950 m × 100 m. The coordinates (0,0,0) indicate the location of the explosion.

Disturbances in the ground surface due to the presence of hedges, bushes and other irregularities, which were not included in the patches of forest, were accounted for. These features were included in the physical roughness height K_s and the aerodynamic roughness length y_0. Based on the surrounding vegetation and irregularities, the physical roughness height was estimated to be approximately 0.9 m. The aerodynamic roughness length y_0 of 0.03 m was derived using Eq. (II.5), as proposed by Durbin and Petterson Reif [II.13]:

$$K_s = 30 y_0 \tag{II.5}$$

where:

K_s is the physical roughness height (m); and
y_0 is the aerodynamic roughness length (m).

II.7.3.1.4. Droplet release

During the initial stage of the explosion, droplet dispersion and surrounding airflow were driven by the energy released from the explosive material. This initial stage was not considered in the computation. The computation started when the explosive energy was fully dispersed and the air movement and droplet transport were driven by the atmospheric flow only. Photographs of the exercise scenario presented during the EMRAS II Technical Meetings (Appendix I) were used to construct the geometry of the initial cloud. The cloud was assumed to have a height of 4 m and a radius of 1 m. Within the initial cloud, thermal energy, activity concentrations of the radionuclide, and droplet sizes were assumed to be spatially uniformly distributed.

II.7.3.1.5. Droplet spectrum

Based on the available information on the exercise scenario provided during the EMRAS II Technical Meetings (Appendix I), a droplet spectrum was selected that consisted of a total of

four droplet diameters. The droplet diameters and the available volume activity as a percentage of the total volume activity are provided in Table II.12.

TABLE II.12. DROPLET DIAMETER AND THE PERCENTAGE OF TOTAL VOLUME ACTIVITY

Droplet diameter (m)	Volume activity (%)
2×10^{-5}	10.0
6×10^{-6}	46.6
1×10^{-6}	15.0
2×10^{-7}	28.4

The droplet spectrum, together with the associated droplet size, were assumed to remain constant throughout the entire computational domain and throughout the duration of the computation. Shrinkage of the droplets due to evaporation and droplet collision were not considered in this simulation model. Droplet deposition and radioactive decay resulted in a decline in the activity concentration of the radionuclide in air. Both mechanisms were considered in the computation by means of an extra source term.

II.7.3.1.6. Release volume

The total volume of the initial cloud at the start of the computation was 11.8 m^3, with a total activity of 1.058 GBq during detonation and a corresponding normalized activity concentration in the cloud of 89.5 MBq/m^3.

II.7.3.1.7. Droplet temperature

The total thermal energy captured within the explosive material was 6.12 GJ, which led to a mean temperature rise in the initial cloud of 5 K. This temperature rise was based on the assumption that both the droplets and the surrounding air were uniformly heated. Based on an external temperature of 22°C, the initial temperature in the cloud was 27°C.

II.7.3.2. Boundary conditions

II.7.3.2.1. Wind conditions

The conditions for wind, which were imposed at the inlet, were described by three parameters, which included the wind speed, the turbulent energy and the turbulent dissipation, as functions of the height above the ground surface, as described by the following equations:

$$U(y) = u^*_{ABL} \ln\left(\frac{y + y_0}{y_0}\right) \tag{II.6}$$

where:

$U(y)$ is the wind speed (U) as a function of height above the ground surface (y);
u^*_{ABL} is the friction velocity from the atmospheric flow (m/s);
y is the height above the ground surface (m); and
y_0 is the aerodynamic roughness length (m).

$$k(y) = \frac{u^{*2}_{ABL}}{\sqrt{C_\mu}} \tag{II.7}$$

where:

k is the turbulent kinetic energy (m^2/s^2), which is independent of the height above the ground surface; and
C_μ is a model constant of the k-ε turbulence model.

$$\varepsilon(y) = \frac{u_{ABL}^{*3}}{\kappa(y + y_0)} \tag{II.8}$$

where:

ε is the turbulent dissipation (m^2/s^3); and
κ is the Von Karmann constant (dimensionless).

Equations (II.6) and (II.7) for U and k, respectively, are commonly used as inlet profiles for CFD simulations when measured profiles of U and k are not available. These profiles are not only used for simulations with the standard k–ε model, but also with other types of turbulence models (e.g. Re-Normalisation Group, k–ε; realizable k–ε, standard k–ω, Shear Stress Transport, k–ω; and the Spalart–Allmaras model [II.14]).

In the CFD computation, the default wind direction imposed at the inlet boundary was –30° relative to the positive axis. For this assumption, the resulting wind direction in the vicinity of the release point was broadly similar to the positive z-axis.

II.7.3.2.2. Temperature conditions

The approaching wind was assumed to be thermally uniform, with a temperature of 22°C. On the side boundaries and at the ground surface, an adiabatic temperature condition was applied.

II.7.3.2.3. Concentration and exhalation of ^{99m}Tc

The activity concentration of ^{99m}Tc imposed at the inlet boundary was 0 Bq/m^3 and the exhalation of ^{99m}Tc from the ground was 0 Bq m^{-2} s^{-1}.

II.7.3.3. Input parameters of the CFD model

Details of the input parameters used in the CFD model are shown in Table II.13.

II.7.4. Simulation results

Results are presented for a set of CFD simulations that predicted the release of ^{99m}Tc into the atmosphere to reproduce the findings from the second field experiment dated 15 May 2008 (Appendix I). Results from a single CFD simulation using the best available input parameters are described in Section II.7.4.1. Prior to this CFD simulation, a sensitivity analysis on the most relevant input parameters was performed (see Section II.7.4.2). All simulation results were compared with available experimental data, including surface activity concentrations and the corresponding dose rates at 1 m above ground surface. Where appropriate, predicted activity concentrations of ^{99m}Tc in the air were also compared with experimental data.

II.7.4.1. Release of ^{99m}Tc into the atmosphere

The predicted contamination resulting from the release of ^{99m}Tc into the atmosphere on 15 May 2008 was based on a single simulation using the best available input parameters. The best available input parameters were obtained from the documentation describing the field

experiments from the SÚRO in Prague (Appendix I), as described in Section II.7.3. A sensitivity analysis (Section II.7.4.2) was then conducted to fine tune the simulation model.

TABLE II.13. RELEASE AND DEPOSITION OF ^{99m}Tc FOR THE FOUR DIFFERENT DROPLET DIAMETERS

Input parameter	Model input	Section
Geometry / airflow and thermal calculation		
Geometry	Length (x) = 1000 m Height (y) = 100 m Width (z) = 950 m	II.7.3.1.1
CFD simulation	Transient t = 0 s to t = 500 s	II.7.3.1.2
Imposed wind profile	Logarithmic velocity profile	II.7.3.2.1
Imposed wind speed (U)	4 m/s at 10 m above ground	II.7.3.2.1
Imposed wind direction (°)	-30° relative to the positive z-axis	II.7.3.2.1
Aerodynamic roughness length (y_0)	0.03 m	II.7.3.1.3
Physical roughness height (K_s)	0.9 m	II.7.3.1.3
Turbulence model	k-ε	[II.11]
Imposed turbulent kinetic energy (k)	0.27 m^2/s^2	II.7.3.2.1
Imposed turbulent dissipation (ε)	Linear profile	II.7.3.2.1
Ambient temperature (T_e)	22°C	II.7.3.2.2
Resistance coefficient, forest (C_n)	0.1 m^{-1}	II.7.3.1.3
Geometry and properties of the initial cloud		
Volume (V_c)	11.8 m^3	II.7.3.1.6
Initial temperature ($T_{c,i}$)	27°C	II.7.3.1.7
Initial activity ($A_{c,i}$)	1.06×10^9 Bq	II.7.3.1.6
Initial concentration ($C_{c,i}$)	8.95×10^7 Bq/m^3	II.7.3.1.6
Droplet diameters and their percentage of the total volume activity	2×10^{-5} m; 10.0% 6×10^{-6} m; 46.6% 1×10^{-6} m; 15.0% 2×10^{-7} m; 28.4%	II.7.3.1.5
Droplet density (ρ_d)	1000 kg m^{-3}	II.7.3.1.4
Dispersion of ^{99m}Tc		
^{99m}Tc background concentration	0 Bq/m^3	II.7.3.2.3
^{99m}Tc exhalation from the ground	0 Bq m^{-2} s^{-1}	II.7.3.2.3
^{99m}Tc deposition	Deposition on the horizontal ground surface only	[II.11]

II.7.4.1.1. Airflow field

The atmospheric airflow prior to the release of ^{99m}Tc was predicted using the boundary conditions for wind speed, wind direction, turbulent kinetic energy (k) and turbulent dissipation (ε), as described in Section II.7.3. Figure II.39 shows details of the predicted velocity field and the imposed velocity conditions at the inlet. In the figure, the open areas on the ground surface (flat white areas) represent patches of forest and the blue mounds represent sand hills (see Fig. II.38). In addition, it is important to note that the wind direction is not lined up with the velocity contour plot, as indicated by the velocity vectors at the inlet boundary (shown at the upper and lower right hand edges of the figure). The contour plot shows a reduced wind speed

(blue colour) in the forest areas due to the additional resistance from trees and bushes. Above the sand hills, there is an increase in wind speed due to limited model height.

II.7.4.1.2. Surface contamination

Contamination of the ground surface was primarily a result of gravitational settling from the droplets that were formed during the explosion. The droplets varied in size, leading to greater deposition with larger diameter droplets. A detailed plot of the accumulated surface contamination 500 s after the ^{99m}Tc release is shown in Fig. II.40. The surface contamination is a product of the deposition from the four different droplet sizes that were modelled (see Tables II.12 and II.13). Although the contamination spread over a large downwind area (≥ 1 km from the explosion site), most of the contamination was found around the release point and within 20 m downwind from the release point.

The deposition of ^{99m}Tc and the activity of ^{99m}Tc in the atmosphere during the 500 s of simulation time are shown in Fig. II.41. The deposition and the activity in the atmosphere are products of the four different droplet sizes that were included in the simulation model. The activity at the start of the simulation was 1058 MBq; this remained constant during the first 100 s. After approximately 150 s, some of the activity began to leave the computational domain, and only a marginal activity of ^{99m}Tc was present in the atmosphere inside the computational domain after a 500 s simulation time. The deposition occurred during the first 200 s, and by the end of the simulation, the total ^{99m}Tc on the ground surface was approximately 1.6% of the activity released at the start. It is important to stress that the deposition had little effect on the activity concentrations of ^{99m}Tc in the atmosphere for the droplet diameters chosen in this simulation.

A detailed overview of the ^{99m}Tc release and deposition for the four different droplet diameters is shown in Table II.14. While the average deposition was 1.6% of the activity released, the deposition was dominated by the largest droplets, which had a diameter of 20 μm and a deposition of 10.6%. The smaller droplets contributed little to no deposition, with an insignificant deposition of 0.01% for the smallest droplets. More detailed plots of the activity and deposition of ^{99m}Tc, as a function of time, are shown in Fig. II.42.

The accumulated surface contamination after the release was measured as part of the field experiments performed by the SÚRO. A comparison of the predicted and measured surface contamination is shown in Fig. II.43. Specifically, the figure shows that the predicted surface contamination was broadly similar to the measured contamination. Nevertheless, there were some distinct differences. For example, along the center line, the measured surface activity was highest approximately 10 to 30 m downwind from the release point; however, the simulation predicted the highest surface activity at the release point itself. This discrepancy was most likely a result of the assumptions that were made in the CFD model to construct the location and geometry of the initial cloud. In the CFD model, the initial cloud was located at the release point itself, and its geometry was based on photographs taken during the experiment. It is possible that the geometry and the location of the initial cloud needed to be determined in a more robust manner. Unfortunately, the experimental data were insufficient to allow for further improvement of the characterization of the initial cloud.

Detailed plots of the surface contamination from the four different droplet diameters are shown in Fig. II.44. The predicted surface contamination was compared against the total accumulated contamination (all particle diameters) as measured by the SÚRO.

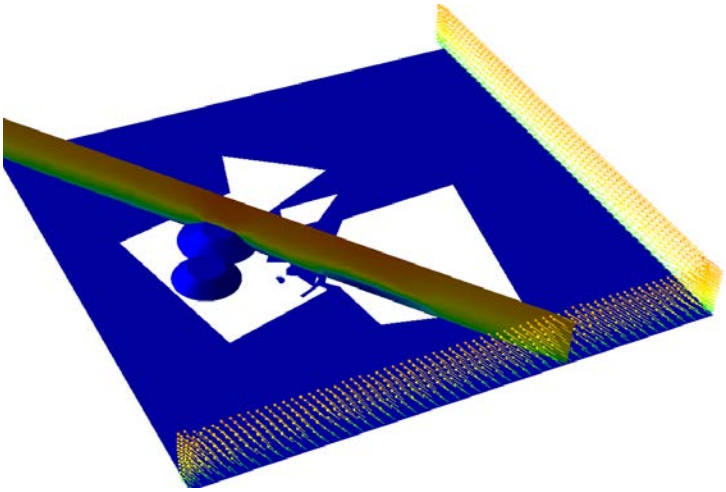

FIG. II.39. Velocity contour and vector plot of the wind driven airflow. The logarithmic velocity profile at the inlet is the imposed velocity boundary condition. The diagonal velocity contour plot is part of the predicted flow field.

(a)

(b)

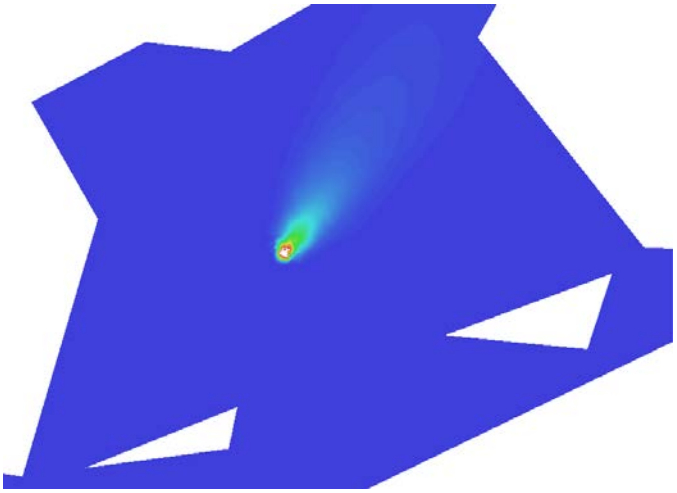

FIG. II.40. The predicted surface contamination of ^{99m}Tc at the end of the simulation at t = 500 s. The uncoloured surface patches represent forest and building plots (see Fig. II.38). The blue areas are the general terrain without forest or buildings (e.g. grass). (a) A plot of the complete computational domain; and (b) a detailed plot of the computational domain in the immediate vicinity of the detonation.

TABLE II.14. RELEASE AND DEPOSITION OF ^{99m}Tc FOR THE FOUR DIFFERENT DROPLET DIAMETERS

Droplet diameter (m)	Released activity (Bq)	Deposition (Bq)	Percentage deposition (%)
$2 \times 10^{-5} – 2 \times 10^{-7}$	*1.06×10^{9}*	*1.65×10^{7}*	*1.6*
2×10^{-5}	1.05×10^{8}	1.11×10^{7}	10.6
6×10^{-6}	4.97×10^{8}	5.24×10^{6}	1.1
1×10^{-6}	1.58×10^{8}	5.30×10^{4}	0.03
2×10^{-7}	2.97×10^{8}	3.54×10^{4}	0.01

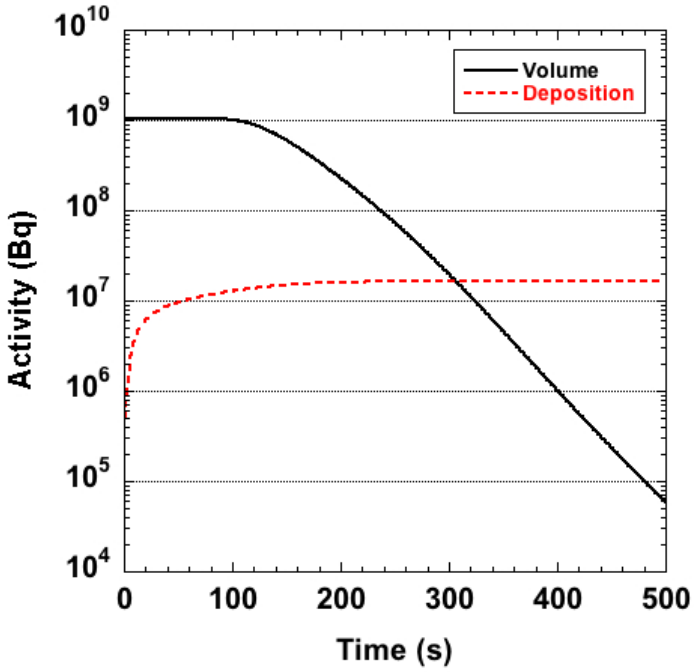

FIG. II.41. Predicted ^{99m}Tc activity (Bq) in the computational domain as a function of time, where t = 0 is the start of the simulation. The solid black line represents the predicted ^{99m}Tc activity dispersed in the air (volume) inside the computational domain. The red dashed line represents the predicted ^{99m}Tc activity deposited on the ground surface of the domain.

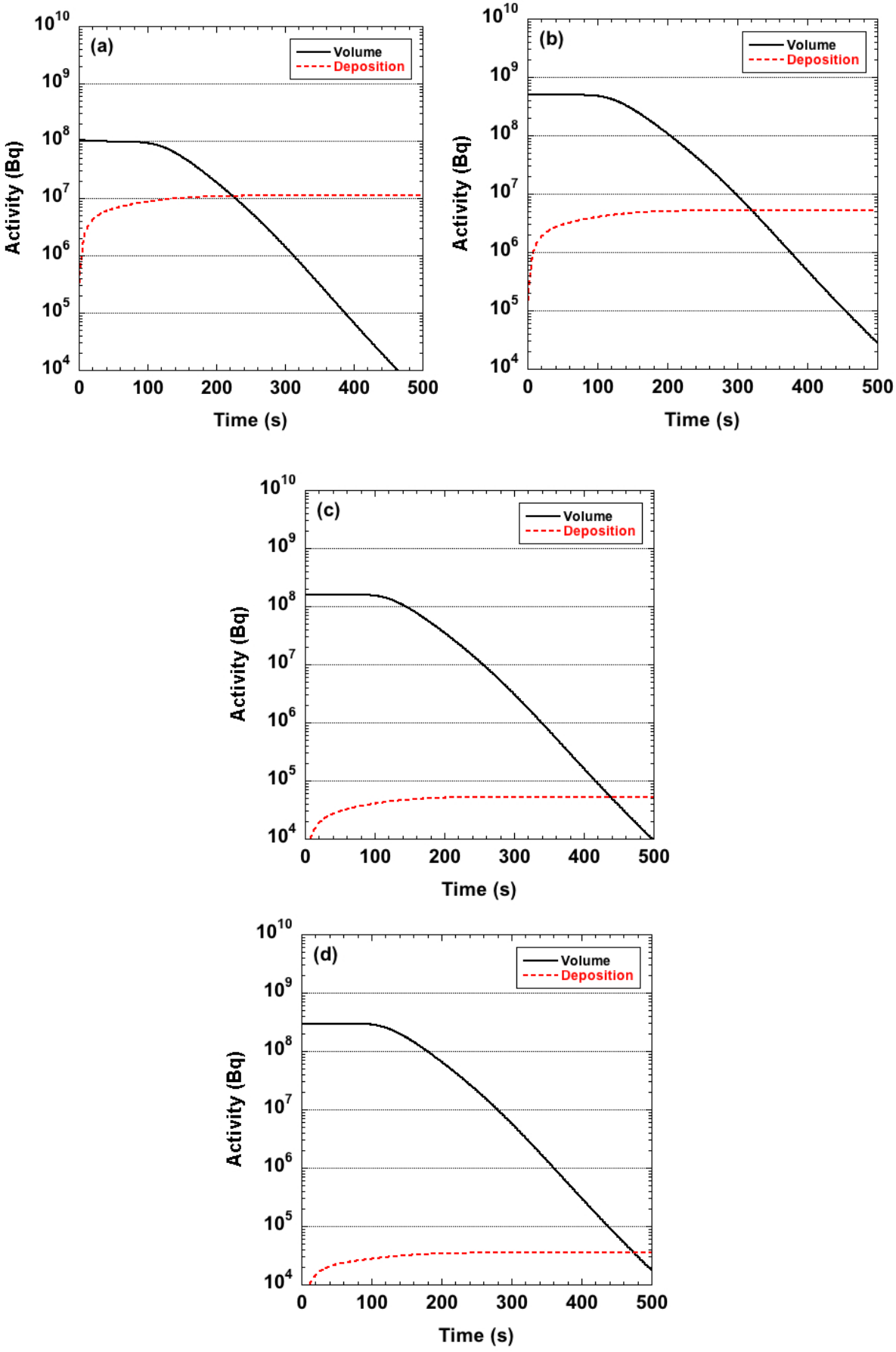
(a)
Volume
Deposition
Activity (Bq)
Time (s)
(b)
Volume
Deposition
Activity (Bq)
Time (s)
(c)
Volume
Deposition
Activity (Bq)
Time (s)
(d)
Volume
Deposition
Activity (Bq)
Time (s)

FIG. II.42. Predicted ^{99m}Tc activity (Bq) in the computational domain as a function of time for the four different droplet diameters, where t = 0 is the start of the simulation. The solid black lines represent the ^{99m}Tc activity dispersed in the air (volume) inside the computational domain, and the red dashed lines represent the ^{99m}Tc activity deposited on the ground surface of the domain. (a) Droplet diameter is 2.0 × 10^{-5} m, (b) droplet diameter is 6.0 × 10-6 m, (c) droplet diameter is 1.0 × 10^{-6} m, and (d) droplet diameter is 2.0 × 10^{-7} m.

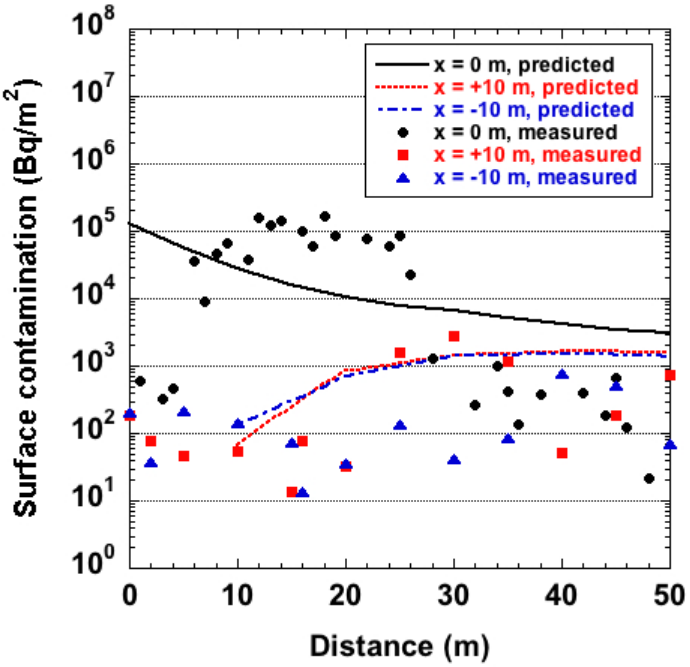

FIG. II.43. The surface contamination from ^{99m}Tc (Bq/m^2), estimated using default input parameters. The solid black line represents the predicted activity along the centreline at x = 0 m, the red dashed line represents the predicted activity parallel to the centreline at x = +10 m, and the blue dashed line represents the predicted activity parallel to the centreline at x = −10 m. Black circles, red squares, and blue triangles indicate measured surface contamination at the centreline (x = 0 m), parallel to the centreline at x = +10 m, and parallel to the centreline at x = −10 m, respectively.

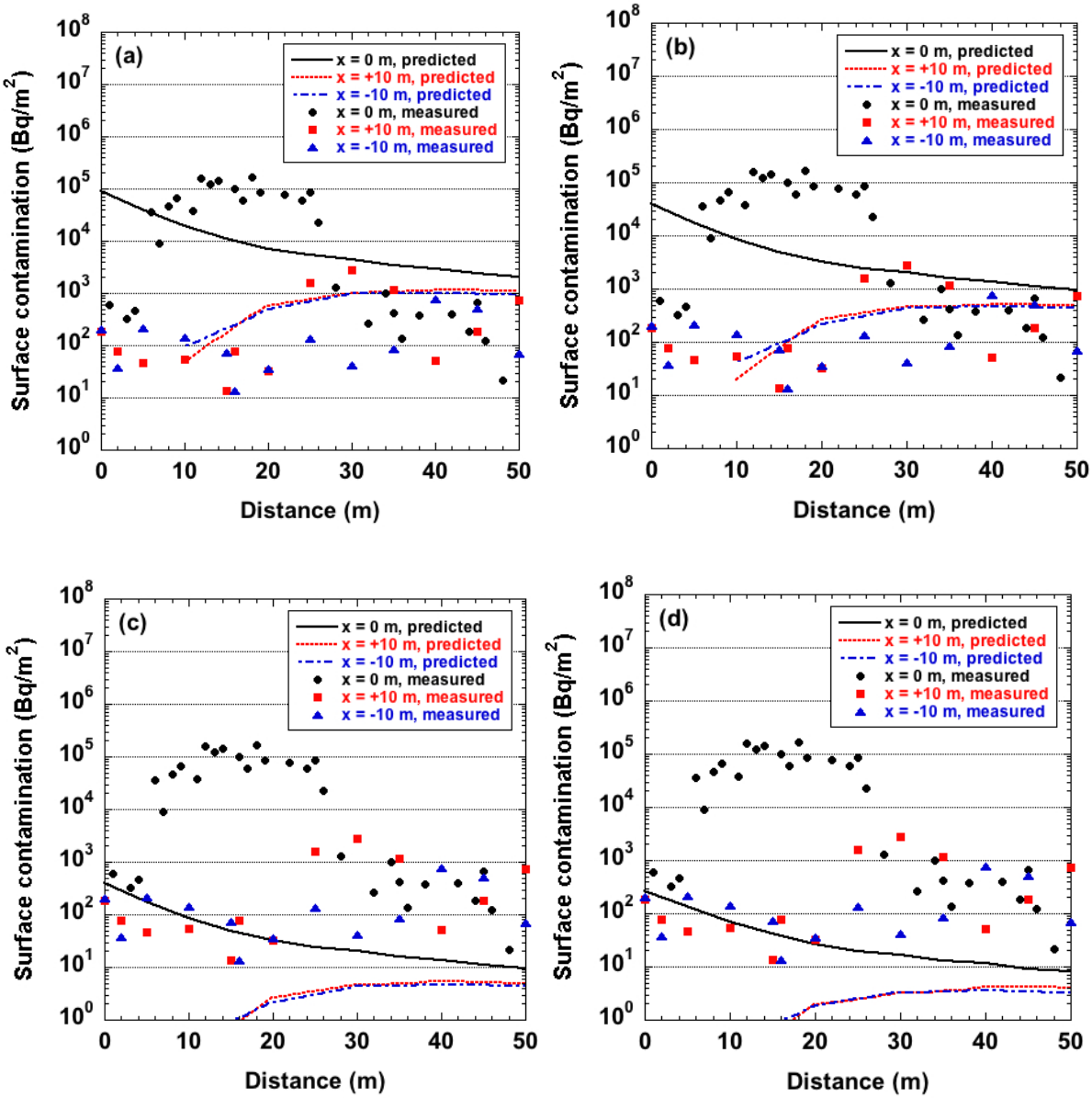

FIG. II.44. The surface contamination from ^{99m}Tc (Bq/m^2), estimated using default input parameters, shown by droplet diameter: (a) Droplet diameter is 2.0 × 10^{-5} m, (b) droplet diameter is 6.0 × 10^{-6} m, (c) droplet diameter is 1.0 × 10^{-6} m, and (d) droplet diameter is 2.0 × 10^{-7} m. The solid black lines represent the predicted activity along the centreline at x = 0 m, the red dashed lines represent the predicted activity parallel to the centreline at x = +10 m, and the blue dashed lines represent the predicted activity parallel to the centreline at x = −10 m. Black circles, red squares, and blue triangles indicate measured surface contamination (total for all particle diameters) at the centreline (x = 0 m), parallel to the centreline at x = +10 m, and parallel to the centreline at x = −10 m, respectively.

TABLE II.15. RADIUS OF THE 50th PERCENTILE, 75th PERCENTILE AND 95th PERCENTILE CONTAMINATION ZONES FOR THE TOTAL CONTAMINATION AND THE CONTAMINATION FROM THE FOUR INDIVIDUAL DROPLET DIAMETERS

Droplet diameter (m)	R_{50} zone (m)	R_{75} zone (m)	R_{95} zone (m)
$2 \times 10^{-5} - 2 \times 10^{-7}$	7.4	16.6	42.1
2×10^{-5}	7.2	16.3	41.9
6×10^{-6}	7.8	17.2	42.5
1×10^{-6}	7.8	17.3	43.9
2×10^{-7}	6.1	15.8	46.1

II.7.4.1.3. Percentile contamination zones

Table II.15 presents the radius of three contamination zones that have been defined for the four different droplet diameters and the total droplet deposition. These contamination zones were set at the 50th percentile, 75th percentile and 95th percentiles and have been expressed in terms of a circle with its center located at the release point.

The 95th percentile radius R_{95} is approximately 42 m for all droplet diameters. The 50th percentile radius R_{50} is approximately 7 m, which suggests that amongst the four droplet diameters, deposition was fastest for the smallest and largest diameters. While the relatively fast deposition of the largest droplet diameters is fairly intuitive, the relatively fast deposition of the smallest droplet diameters was unexpected. In the case of the smallest droplets that were deposited in the vicinity of the explosion, this pattern was likely caused by the large deposition velocity for these droplets. In the close vicinity of the explosion, the droplet concentration in the air near the ground surface was relatively high, leading to high deposition when combined with the high deposition velocity. As the smallest droplets dispersed into the atmosphere, the droplet concentration in the air near the ground surface decreased. Consequently, the deposition of the smallest droplets further downwind was lower. An interesting side effect of this phenomenon was the relatively large 95th percentile contamination zone, which had a diameter of 46.1 m (Table II.15). A graphical depiction of the percentage deposition as a function of the contamination zone is shown in Fig. II.45. Very little difference in predicted deposition can be seen with respect to particle size, except that the smallest particle size had the highest percentage deposition close to the explosion site (<10 m) but the lowest percentage deposition at the farther distances (>30 m).

II.7.4.1.4. Dose rates

As part of the CFD simulation, dose rates at a 1 m height above ground resulting from surface contamination were computed. The dose rates were computed both in terms of mSv/h and Gy/h. The results are shown in Fig. II.46, and where possible, compared with experimental data. Comparison with experimental data suggested that the dose rates were underpredicted by the CFD model. Nevertheless, the CFD predictions indicated a continuous decrease in doses with distance away from the release point, whereas the experimentally obtained doses rates were highly variable. It is, therefore, important to treat the experimental dose rates with a considerable degree of caution, as the experimental dose rates include effects of background radioactivity and possible effects of geometry not included in the model.

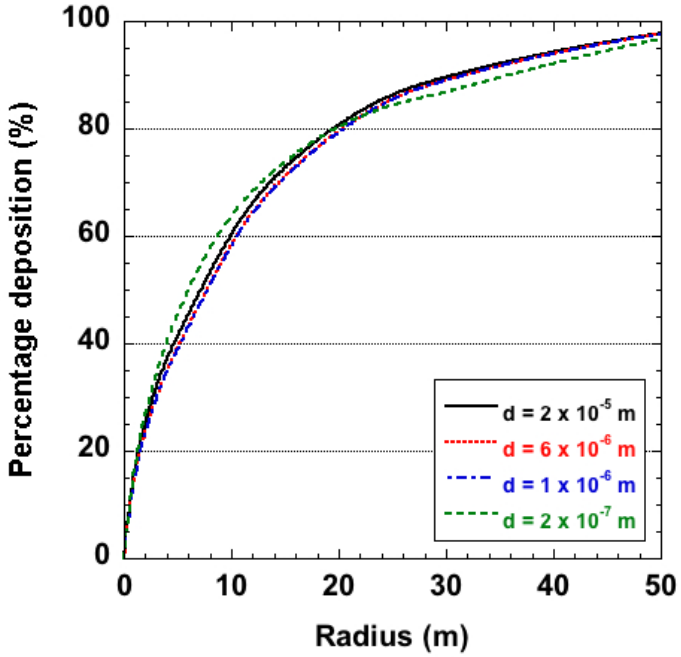

FIG. II.45. Predicted percentage deposition as a function of the contamination zone radius for the four different droplet diameters. The solid black line represents a droplet diameter of 2 × 10^{-5} m, the red dashed line represents a droplet diameter of 6 × 10^{-6} m, the blue dashed line represents a droplet diameter of 1 × 10^{-6} m, and the green dashed line represents a droplet diameter of 2 × 10^{-7} m.

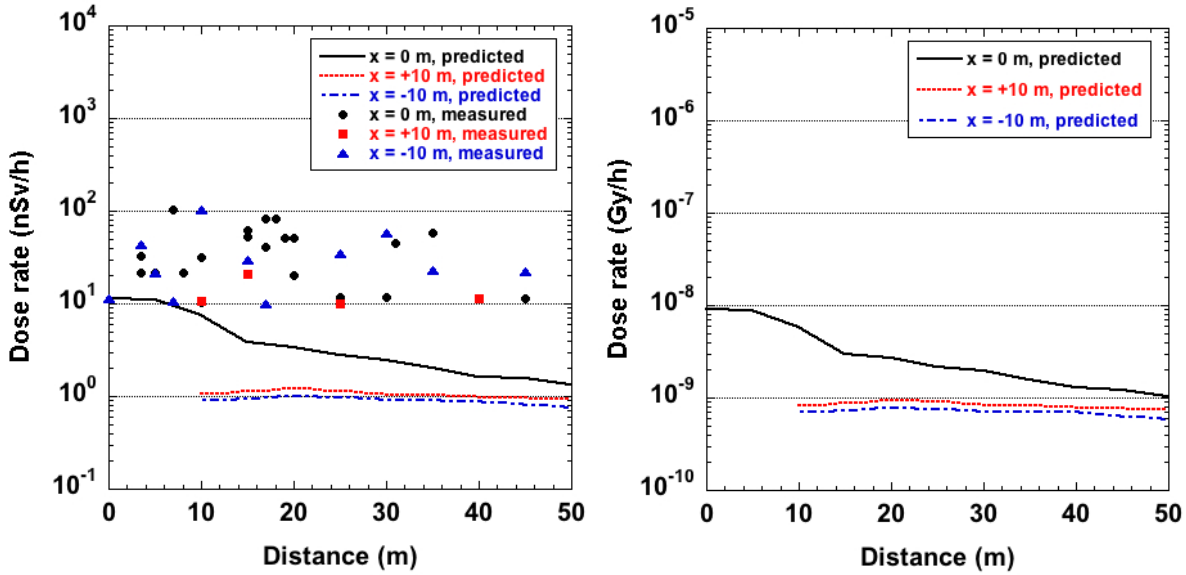

FIG. II.46. Predicted dose rates from ^{99m}Tc at 1 m above ground after deposition was completed, shown in nSv/h (left) and in Gy/h (right). The solid black line represents the predicted dose rate along the z-axis at x = 0 m, the red dashed line represents the predicted dose rate parallel to the z-axis at x = +10 m, and the blue dashed line represents the predicted dose rate parallel to the z-axis at x = −10 m. Black circles, red squares, and blue triangles indicate measured surface contamination (total for all particle diameters) at the centreline (x = 0 m), parallel to the centreline at x = +10 m, and parallel to the centreline at x = −10 m, respectively.

II.7.4.1.5. Activity concentrations in air

The predicted activity concentrations of ^{99m}Tc in air are presented in Fig. II.47 for four locations in the near vicinity of the release. The activity concentrations were averaged over a 1 minute time interval, and for each of the four locations, activity concentrations are presented at 1 m, 2 m and 5 m above the ground surface. The four locations were located along the center line at the release point itself and 10 m, 30 m and 50 m downwind of the release point. All concentration plots in Fig. II.47 show the highest predicted average concentration during the first minute.

For all locations, the average activity concentration in air during the second minute was at least five orders of magnitude lower than during the first minute and can be considered negligible. Based on these findings, it can be concluded that for this event, the activity concentrations of ^{99m}Tc in air would not contribute significantly to doses to humans in comparison with the dose from the surface contamination alone.

II.7.4.2. Sensitivity analysis

A total of ten CFD simulations were performed to study the sensitivity of the various input parameters. As part of the sensitivity analysis, a total of five input parameters were studied. These included: wind direction, wind speed, forest vegetation, droplet diameter and explosion energy.

The model setup is described in detail in Section II.7.3. However, it is important to note that for two input parameters, the default values that were applied in this sensitivity study differed

slightly from those reported in Section II.7.3 (Table II.13). The input parameters that differed are listed in Table II.16.

In Table II.17, an overview of the predicted deposition is provided for all ten simulations. The deposition was based on the total accumulated deposition on the ground surface, as defined in the model, by the end of the simulation. The results clearly demonstrated that the diameter of the droplets greatly affected the surface contamination and the size of the 95th percentile contamination zone. Other parameters, such as wind speed and wind direction, also had a measurable effect, but their effects were considerably less significant.

II.7.4.2.1. Default model setup

The predicted surface contamination (Bq/m^2) and dose rates (Gy/h) are presented in Fig. II.48 below. In line with previous findings, the predicted surface contamination and dose rates were highest at the release point, with values of 1.0×10^5 Bq/m^2 and 10 nGy/h, respectively, at this point. For an imposed wind direction at the inlet boundaries on the outside of the model, the wind direction near the release did not line up with the centreline of the model. This was partly caused by the surrounding forest, which deflected the wind. As a result, the predicted surface contamination 40 m to 50 m downwind from the release point was highest at 10 m from the centreline (x = +10 m), as indicated by the red dashed line in Fig. II.48.

TABLE II.16. DEFAULT MODEL SETTINGS FOR THE CFD MODEL

Default settings	Units	Input parameter
Wind direction	Degrees (o)	0° relative to the positive z-axis
Droplet diameter	μm	5.6

TABLE II.17. RELEASE, PREDICTED DEPOSITION AND PREDICTED RADIUS OF THE 95th PERCENTILE CONTAMINATION ZONE (R_{95})

Simulation	Input parameter	Released activity (Bq)	Deposition (Bq)	Percentage deposition (%)	R_{95} zone (m)
Default model input	*Default*	*1.06×10^9*	*9.16×10^6*	*0.9*	*38.4*
Wind direction *option 1*	+30 (°)	1.06×10^9	7.86×10^6	0.7	42.6
Wind direction *option 2*	-30 (°)	1.06×10^9	1.01×10^7	0.9	25.3
Wind speed *option 1*	2.0 (m/s)	1.06×10^9	1.66×10^7	1.6	36.5
Wind speed *option 2*	8.0 (m/s)	1.06×10^9	7.84×10^6	0.7	30.1
Forest vegetation *option 1*	1.0 (m^{-1})	1.06×10^9	1.14×10^7	1.1	33.3
Droplet diameter *option 1*	1×10^3 (μm)	1.06×10^9	8.20×10^8	77.5	0.2
Droplet diameter *option 2*	1×10^2 (μm)	1.06×10^9	7.75×10^8	73.3	6.4
Droplet diameter *option 3*	1×10^1 (μm)	1.06×10^9	3.52×10^7	3.3	38.2
Explosion energy *option 1*	100 (dimensionless)	1.06×10^9	9.16×10^6	0.9	38.4

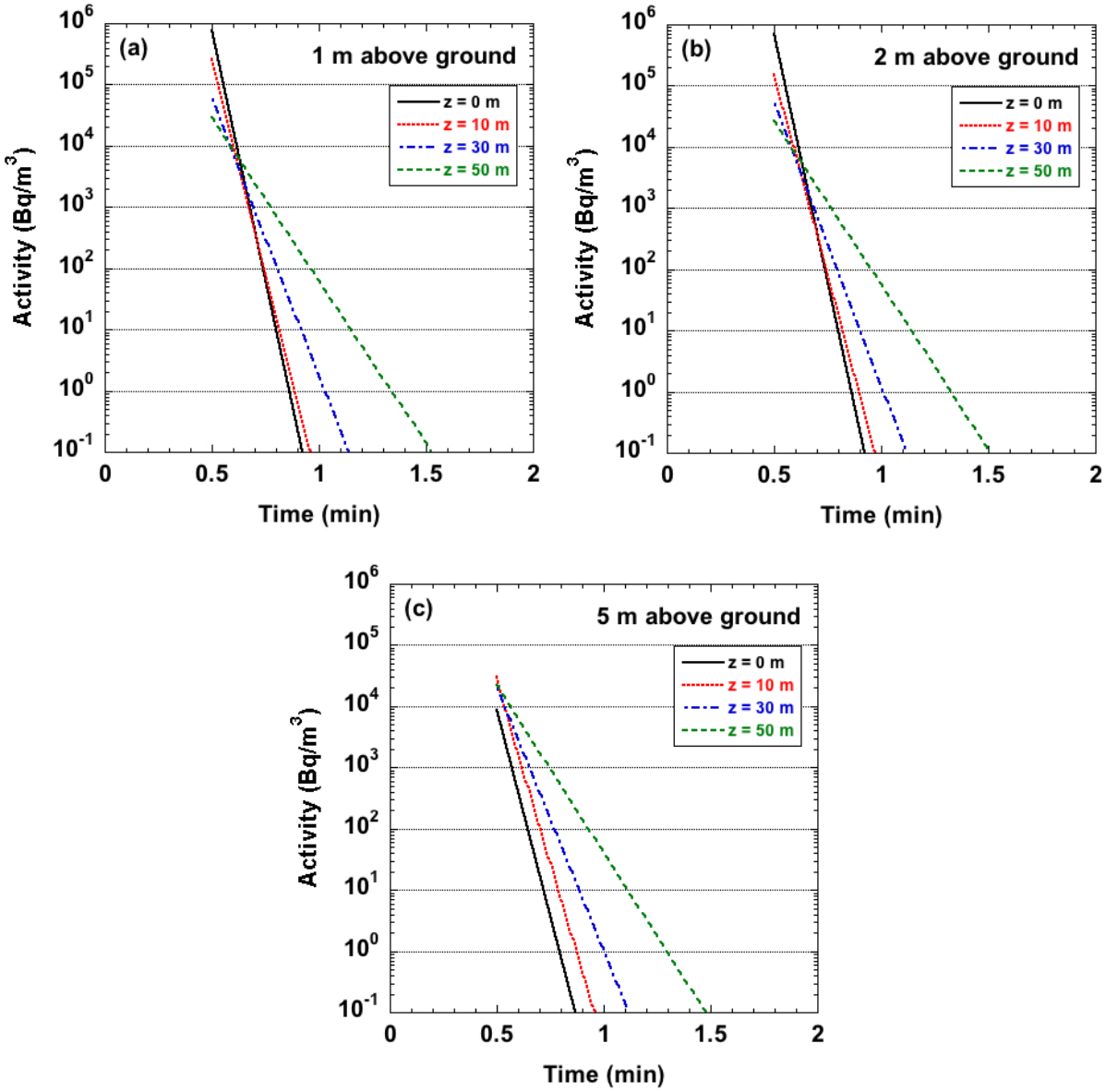

FIG. II.47. Predicted 1 minute averaged ^{99m}Tc activity concentration (Bq/m^3) in air along the z-axis. (a) Predicted ^{99m}Tc activity concentration at 1 m above ground, (b) predicted ^{99m}Tc activity concentration at 2 m above ground, and (c) predicted ^{99m}Tc activity concentration at 5 m above ground. The solid black lines represent the predicted ^{99m}Tc activity concentration at 0 m from the release, the red dashed lines represent the predicted ^{99m}Tc activity concentration at 10 m from the release, the blue dashed lines represent the predicted ^{99m}Tc activity concentration at 30 m from the release, and the green dashed lines represent the predicted ^{99m}Tc activity concentration at 50 m from the release.

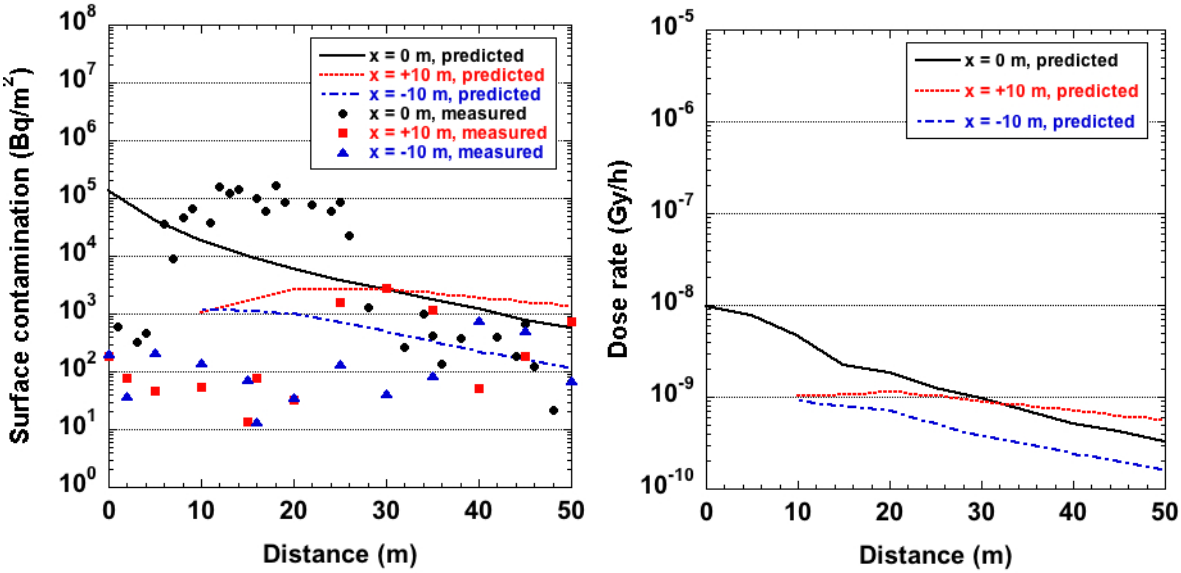

FIG. II.48. The predicted and measured surface contamination from ^{99m}Tc (Bq/m^2; left) and predicted dose rates from ^{99m}Tc (Gy/h) at 1 m above ground (right), using default input parameter values. The solid black lines represent the predicted activity or dose rate along the z-axis at x = 0 m, the red dashed lines represent the predicted activity or dose rate parallel to the z-axis at x = +10 m, and the blue dashed lines represent the predicted activity or dose rate parallel to the z-axis at x = −10 m. The black circles, red squares, and blue triangles represent the measured surface contamination along or parallel to the x-axis at x = 0 m, +10 m, and −10 m, respectively.

II.7.4.2.2. Wind direction

Two simulations were performed for wind directions that were 30° clockwise and 30° anticlockwise, respectively, relative to the z-axis at x = 0 m. The predicted surface contamination (Bq/m^2) and dose rates (Gy/h) are presented in Fig. II.49. Graphs (a) and (b) in Fig. II.49 show the highest predicted contamination along the z-axis at x = 0 m and symmetrically decreased contamination with distance away from the z-axis at either x = +10 m or x = −10 m. The results suggest that for the model setup that was used, the wind near the release was aligned with the z-axis, as seen in the experimental data.

Graphs (c) and (d) in Fig. II.49 show the predicted contamination when the wind direction at the inlet boundary was 30° clockwise relative to the z-axis at x = 0 m. For this simulation, the predicted contamination in the downwind region was highest parallel to the z-axis at x = +10 m. In this case, the wind was assumed to be driving the ^{99m}Tc activity away from the z-axis, with little transport of activity along the z-axis. As a result, the predicted activity downwind was highest at x = +10 m and predicted ^{99m}Tc activities were considerably lower than those measured in the field experiment.

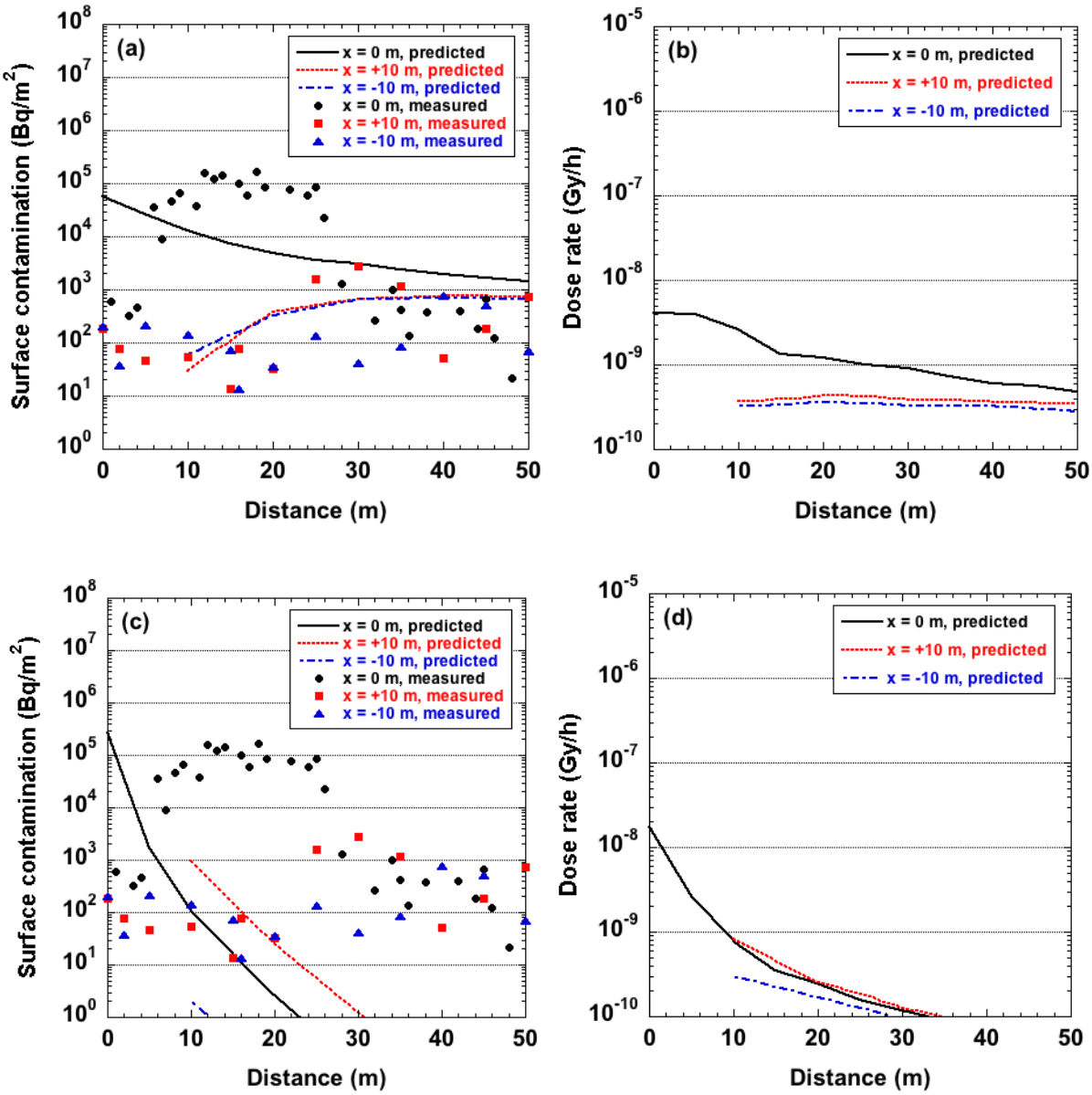

FIG. II.49. The predicted and measured surface contamination from ^{99m}Tc (Bq/m^2; left) and predicted dose rates from ^{99m}Tc (Gy/h) at 1 m above ground (right). (a) and (b) Simulation with a wind direction along the z-axis (x = 0 m), (c) and (d) simulation with a wind direction of 30^o clockwise from the z-axis. The solid black lines represent the predicted activity or dose rate along the z-axis at x = 0 m, the red dashed lines represent the predicted activity or dose rate parallel to the z-axis at x = +10 m, and the blue dashed lines represent the predicted activity or dose rate parallel to the z-axis at x = −10 m. The black circles, red squares, and blue triangles represent the measured surface contamination along or parallel to the x-axis at x = 0 m, +10 m, and −10 m, respectively.

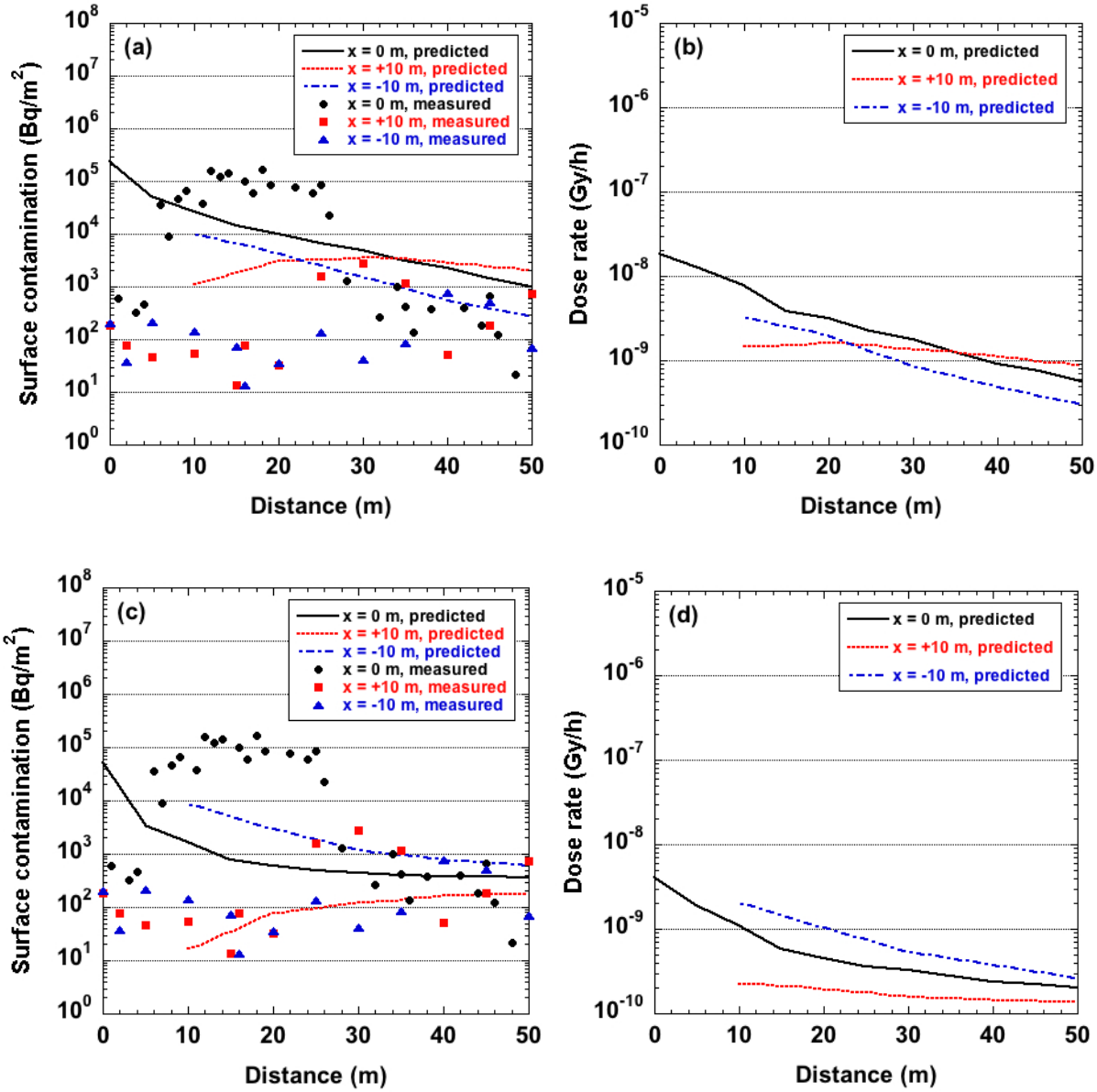

FIG. II.50. The predicted and measured surface contamination from ^{99m}Tc (Bq/m^2; left) and predicted dose rates from ^{99m}Tc (Gy/h) at 1 m above ground (right). (a, b) Simulation with a wind speed of 2 m/s; (c, d) simulation with a wind speed of 8 m/s. The solid black lines represent the predicted activity or dose rate along the z-axis at x = 0 m, the red dashed lines represent the predicted activity or dose rate parallel to the z-axis at x = +10 m, and the blue dashed lines represent the predicted activity or dose rate parallel to the z-axis at x = −10 m. The black circles, red squares, and blue triangles represent the measured surface contamination along or parallel to the x-axis at x = 0 m, +10 m, and −10 m, respectively.

II.7.4.2.3. Wind speed

Two simulations were performed with wind speeds of 2.0 m/s and 8.0 m/s. The findings from those simulations are presented in Fig. II.50.

An interesting observation can be made regarding the simulations shown in graphs (c) and (d) of Fig. II.50 above, when a speed of 8.0 m/s was applied. While previous simulations using a 0° wind direction showed the highest predicted contamination along the *z*-axis at $x = 10$ m, this simulation showed an opposite effect. In this case, the predicted contamination in the downwind region was highest parallel to the *z*-axis at $x = -10$ m. This difference was due to the effects of the Reynolds number, which led to reversed air flow behind the patches of forest surrounding the release zone.

II.7.4.2.4. Explosive energy

The predicted surface contamination and dose rate using a higher explosive energy are shown in Fig. II.51. Contrary to common expectations, a higher explosive energy, as represented in the form of an increased temperature in the initial cloud, had very little effect on the predicted surface contamination. It is, therefore, anticipated that a more robust calculation method is necessary to represent the early stages of the explosion. The assumptions that were made in the current exercise to construct the initial cloud conditions were insufficient, and the increase in temperature was not a correct reflection of the effects from an increased explosion energy.

II.7.4.2.5. Forest vegetation

Similar to previous results obtained with a wind speed of 8.0 m/s (see Section II.7.4.2.3), an increase in the resistance coefficient of the forest also led to a reverse flow field in the area around the release point. The increase in the resistance coefficient changed the aerodynamic behaviour of the forest, leading to a more solid forest patch. This resulted in a stronger flow separation at the rear edge of the forest patch encouraging the formation of a wake region with a reverse flow. Consequently, the predicted contamination levels at >10 m downwind from the release point were highest parallel to the z-axis at $x = -10$ m (Fig. II.52).

II.7.4.2.6. Droplet size distribution

As described at the start of Section II.7.4.2, the most dominant feature influencing the predicted deposition was the droplet diameter. This was also seen in the predicted surface contamination and dose rates, as presented in Fig. II.53 using different values for the droplet diameter. Graphs (a) and (b) of Fig. II.53 show the contamination for a droplet diameter of 1×10^3 μm and suggest that there was little deposition at distances >10 m away from the release point. Graphs (c) and (d) show that for a droplet diameter of 1×10^2 μm, the predicted deposition close to the release point was lower than in graphs (a) and (b), but the predicted surface contamination within the first 50 m from the release point was as much as two orders of magnitude higher than the measured values. Graphs (e) and (f) show that for a droplet diameter of 1×10^1 μm, the predicted deposition in most areas was higher than the measurements, although not consistently so.

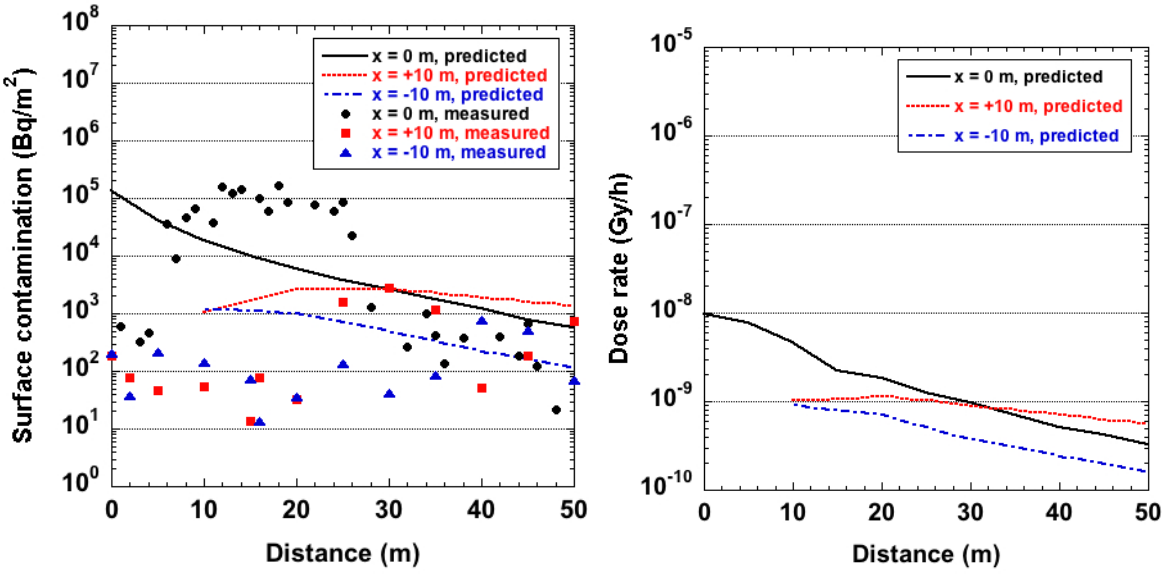

FIG. II.51. The predicted and measured surface contamination from ^{99m}Tc (Bq/m^2; left) and predicted dose rates from ^{99m}Tc (Gy/h) at 1 m above ground (right). Simulation with an explosive energy that is 100 times the default energy. The solid black lines represent the predicted activity or dose rate along the z-axis at x = 0 m, the red dashed lines represent the predicted activity or dose rate parallel to the z-axis at x = +10 m, and the blue dashed lines represent the predicted activity or dose rate parallel to the z-axis at x = −10 m. The black circles, red squares, and blue triangles represent the measured surface contamination along or parallel to the x-axis at x = 0 m, +10 m, and −10 m, respectively.

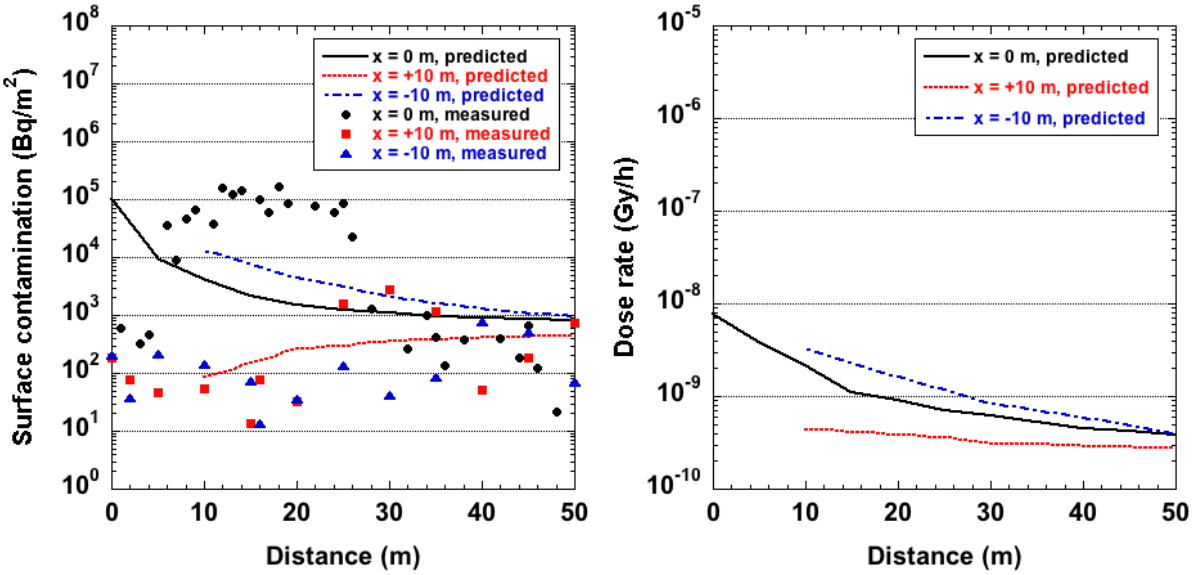

FIG. II.52. The predicted and measured surface contamination from ^{99m}Tc (Bq/m^2; left) and predicted dose rates from ^{99m}Tc (Gy/h) at 1 m above ground (right). Simulation with a resistance coefficient of 1 m^{-1} for the forest vegetation. The solid black lines represent the predicted activity or dose rate along the z-axis at x = 0 m, the red dashed lines represent the predicted activity or dose rate parallel to the z-axis at x = +10 m, and the blue dashed lines represent the predicted activity or dose rate parallel to the z-axis at x = −10 m. The black circles, red squares, and blue triangles represent the measured surface contamination along or parallel to the x-axis at x = 0 m, +10 m, and −10 m, respectively.

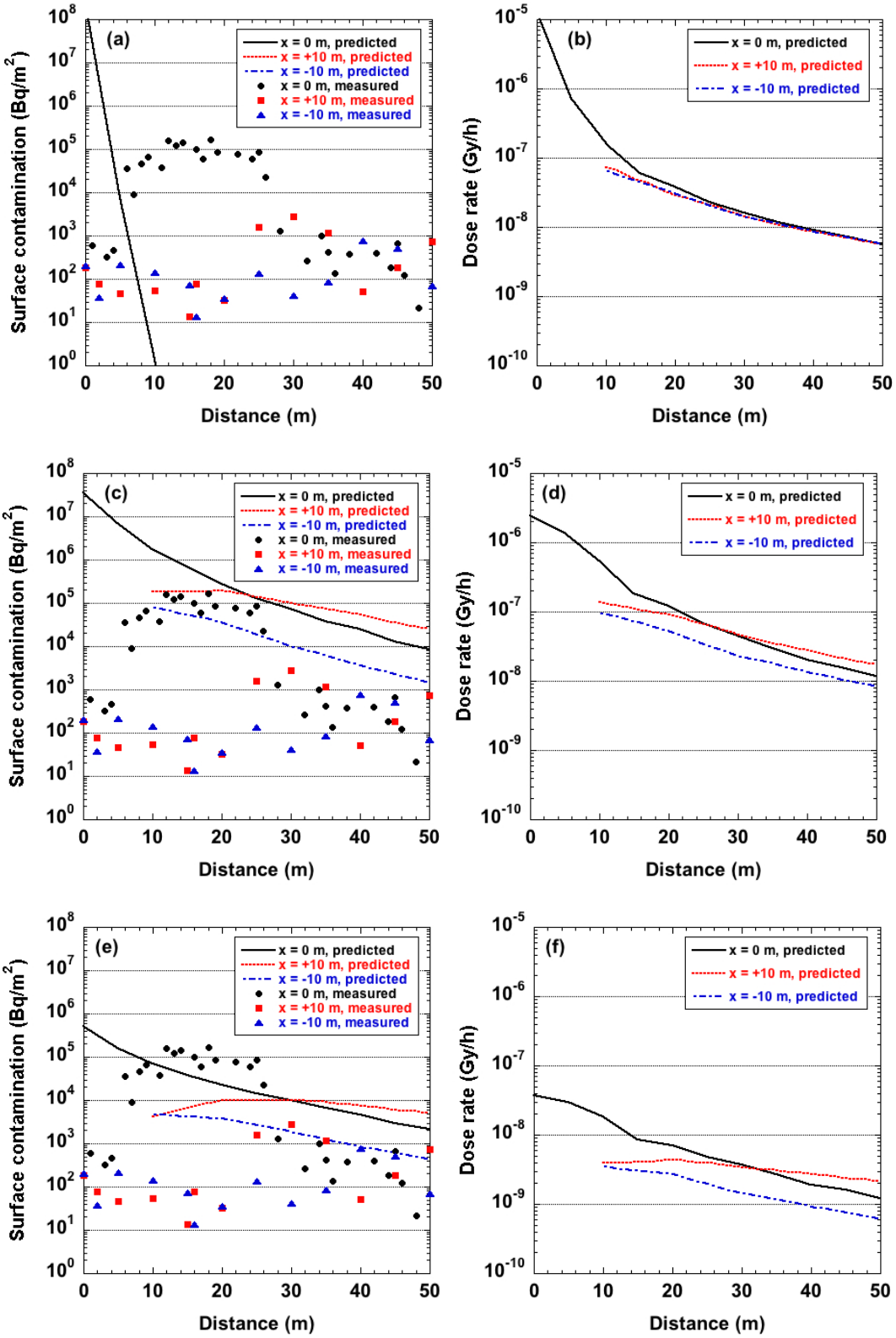

FIG. II.53. The predicted and measured surface contamination from ^{99m}Tc (Bq/m^2; left) and predicted dose rates from ^{99m}Tc (Gy/h) at 1 m above ground (right). (a, b) A droplet size of 1 × 10^3 μm, (c, d) a droplet size of 1 × 10^2 μm, and (e, f) a droplet size of 1 × 10^1 μm. The solid black lines represent the predicted activity or dose rate along the z-axis at x = 0 m, the red dashed lines represent the predicted activity or dose rate parallel to the z-axis at x = +10 m, and the blue dashed lines represent the predicted activity or dose rate parallel to the z-axis at x = −10 m. The black circles, red squares, and blue triangles

represent the measured surface contamination along or parallel to the x-axis at x = 0 m, +10 m, and −10 m, respectively.

II.8. DESCRIPTION OF CLMM

The CLMM code was used for the short range modelling exercise by V. Fuka of Charles University in the Czech Republic.

II.8.1. Introduction

The CLMM code is an in-house code developed for research, primarily for simulating flows in complex geometry [II.15, II.16]. This code is still under development and not yet been validated. CLMM is an atmospheric computational fluid dynamics (CFD) code designed for large eddy simulation [II.17]. The transport processes considered are turbulent and molecular diffusion, advection by wind, and dry deposition. No biological or environmental compartments are considered. Model endpoints are time dependent fields of flow and pollutant concentrations.

II.8.2. Key assumptions

The key assumptions for this model are: (a) Flat terrain; (b) Prescribed (logarithmic for this exercise) inflow wind profile; (c) A constant roughness parameter on the ground of 3 mm; and (d) A constant turbulent Schmidt number.[25]

II.8.3. Modelling approaches (conceptual and mathematical)

Transfers between compartments are modelled as turbulent, diffusive and advective fluxes between control volumes, with semiempirical parametrization of particle deposition.

Concentrations in compartments were calculated as fluxes (as described above). Temporal and spatial discretization of the model can be described as Runge Kutta (3^{rd} order) and Crank Nicolson (2^{nd} order) schemes in time, and as a central (2^{nd} order) scheme in space, limited to preserve monotonicity in space.

The input data that were needed for this exercise were: (a) wind direction and profile; (b) roughness parameter distribution; (c) location and size of obstacles; (d) initial concentration of contaminant; and (e) particle diameter distribution.

II.8.4. Parameter values

Values of the environmental parameters used in the CLMM model are described below. The coefficient in the deposition scheme was used exactly as described by Piskunov [II.18].

Constant environmental parameters were used for spatial and temporal averaging. The model itself is time dependent, with time integrated concentrations calculated from time averaged concentrations.

[25] The turbulent Schmidt number is defined as the ratio of the eddy viscosity (m^2/s) and the eddy diffusivity (m^2/s); in this exercise, this ratio was kept constant.

II.8.5. Uncertainties

Estimating uncertainties in the model predictions is only possible by assessing their sensitivity to different parameters and sets of parameter values (ensemble calculations). This was not done during the timeframe of the modelling exercise.

II.8.6. Application of the model to the specific exercise

The data that were provided in the exercise description were used as input to the model, as follows:

- A 5 minute average wind speed and direction at the time of the explosion;
- Initial particle distribution of 39.6% of size 0.2 μm, 11.8% of size 1 μm, 37.8% of size 8 μm, and 10.8% of size 20 μm; and
- Initial cloud, as described by HotSpot 2.07.1 (HR) (see Table 2.3 in Section 2.3).

Specific parameter values used for the exercise were as follows:

- Roughness parameters of the ground of 1 cm;
- Roughness parameter for the incoming flow of 0.1 m;
- Initial particle distribution, as stated above.

An assumption of flat terrain was made to match the model to the conditions of the exercise. Separate calculations were made for a small (50 m) domain and a large (2000 m) domain.

II.9. REFERENCES TO APPENDIX II

[II.1] SCHEIER, N.W., CHOUHAN, S.L., ADDAM Version 1.4 User's Manual, Rep. COG SQAD-07-5009, CANDU Owners Group, Toronto (2009).

[II.2] SCHEIER, N.W., CHOUHAN, S.L. ADDAM Version 1.4.2 Model Development and Verification, Rep. SQAD-10-5087, AECL, Chalk River (2010).

[II.3] SCHEIER, N.W., CHOUHAN, S.L., ADDAM Version 1.4.1 Model Development and Verification, Rep. COG SQAD-09-5079, AECL, Chalk River (2010).

[II.4] SCHEIER, N.W., ADDAM Version 1.4 Theory Manual, Rep. COG SQAD-07-5008, AECL, Chalk River (2009).

[II.5] CANADIAN STANDARDS ASSOCIATION, Guidelines for Calculating Radiation Doses to the Public from a Release of Airborne Radioactive Material under Hypothetical Accident Conditions in Nuclear Reactors, CAN/CSA-N288.2-M91, CSA Group, Toronto (1991).

[II.6] U.S. DEPARTMENT OF ENERGY, GENII Computer Code, Application Guidance for Documented Safety Analysis, Rep. 20585-2040, U.S. Department of Energy, Office of Environment, Safety, and Health, Washington, DC, (2004).

[II.7] KOCHER, D.C., Dose rate conversion factors for external exposure to photons and electrons, Health Physics **45** (1983) 665.

[II.8} ECKERMAN, K.F., LEGGETT, R.W., DCFPAK: Dose coefficient data file package for Sandia National Laboratory, Oak Ridge National Laboratory Report ORNL/TM-13347, Oak Ridge, TN (1996).

[II.9] HOMANN, S.G., HotSpot Health Physics Codes Version 2.07.1 User's Guide, LLNL-TM-411345, Rev. 1, Lawrence Livermore National Laboratory, CA (2009).

[II.10] UNITED STATES ENVIRONMENTAL PROTECTION AGENCY, External Exposure to Radionuclides in Air, Water and Soil, Federal Guidance Report 12, EPA-402-R-93-081, USEPA, Washington, DC (1993).

[II.11] DE WITH, G., DE JONG, P., Impact from indoor air mixing on the thoron progeny concentration and attachment fraction, Journal of Environmental Radioactivity **158–159** (2016) 56.

[II.12] ENDALEW, M.A., HERTOG, M., DELELE, M.A., BAETENS, K., PERSOONS, T., BAELMANS, M., RAMON, H., NICOLAÏ, B.M., VERBOVEN, P., CFD modeling and wind tunnel validation of airflow through plant canopies using 3D canopy architecture, International Journal of Heat and Fluid Flow **30** (2009) 356.

[II.13] DURBIN, P.A., PETTERSON REIF, B.A., Statistical theory and modeling for turbulent flows, John Wiley & Sons Ltd, Chichester (2001) 285 pp.

[II.14] LAUNDER, B.E., SPALDING, D.B., The numerical computation of turbulent flows, Computer Methods in Applied Mechanics and Engineering **3** (1974) 269.

[II.15] FUKA, V., BRECHLER, J., "LES of contaminant dispersion in an idealized geometry", Proceedings of the Conference on Modelling Fluid Flow, Budapest, Hungary (2009) 138−142.

[II.16] FUKA, V., BRECHLER, J., "Dispersion of aerosol around solid obstacles – experiment and simulation", Proceedings of the Conference on Topical Problems of Fluid Mechanics, Prague Institute of Thermomechanics, Prague, Czech Republic (2010) 47–50.

[II.17] VREMAN, A.W., An eddy-viscosity subgrid-scale model for turbulent shear flow: Algebraic theory and applications, Physics of Fluids **16** (2004) 3070.

[II.18] PISKUNOV, V.N., Parameterization of aerosol dry deposition velocities onto smooth and rough surfaces, Journal of Aerosol Science **40** (2009) 664.

APPENDIX III. SCENARIO DESCRIPTION FOR THE MID-RANGE ATMOSPHERIC DISPERSION EXERCISE

III.1. INTRODUCTION

The overall objective of the EMRAS II Urban Areas Working Group ('WG 9') is to test and improve the capabilities of models used in assessment of radioactive contamination in urban settings, including dispersion and deposition events, short and long term contaminant redistribution following deposition events, and potential countermeasures or remediation efforts for reducing human exposures and doses. The present scenario is based on a hypothetical release of radioactivity from a nuclear power plant (NPP). The scenario is intended to provide an opportunity to test model predictions for a mid-range dispersion event, including the dispersion of radioactivity from the NPP and the deposition resulting from the event in an urban area. The exercise is based upon real geographic information. The effects of different meteorological conditions on dispersion and deposition may be studied.

Input information for the scenario includes a description of the hypothetical accident event, the amount and types of radioactivity involved, meteorological information, location of the cities of interest, locations for modelling endpoints, and information on the terrain and topography. Modelling endpoints for intercomparison among participants in the exercise include the deposition on ground (reference lawn surface), time integrated air concentrations, a contour map of deposition, and a time series for contamination at selected locations.

This publication and accompanying files provide information about the scenario to be modelled (input information) and a list of the endpoints to be modelled.

III.2. INPUT DATA

III.2.1. Geographic data

The nuclear power plant chosen for the exercise is Trillo, in the central part of Spain, about 70 km from the Madrid metropolitan area (Fig. III.1) and 46 km from Guadalajara, which is a smaller town in central Spain located between Trillo NPP and Madrid.

The topography of the area of interest has been downloaded from the NOAA (U.S. National Oceanic and Atmospheric Administration) Geodas database, with a 1 minute resolution both in longitude and latitude. The limits of the area of interest are the following:

Longitude: from 3º49' W to 2º28' W
Latitude: from 40º09' N to 40º50' N

The resulting grid consists of 82 columns × 42 rows (3444 grid cells). Topography is provided in the file 'trillo.xyz'. The file consists of three columns: longitude, latitude, and elevation above mean sea level (m). A map showing the topography of the region, the position of the Trillo NPP and the two main cities in the area (Madrid and Guadalajara) is presented in Fig. III.2.

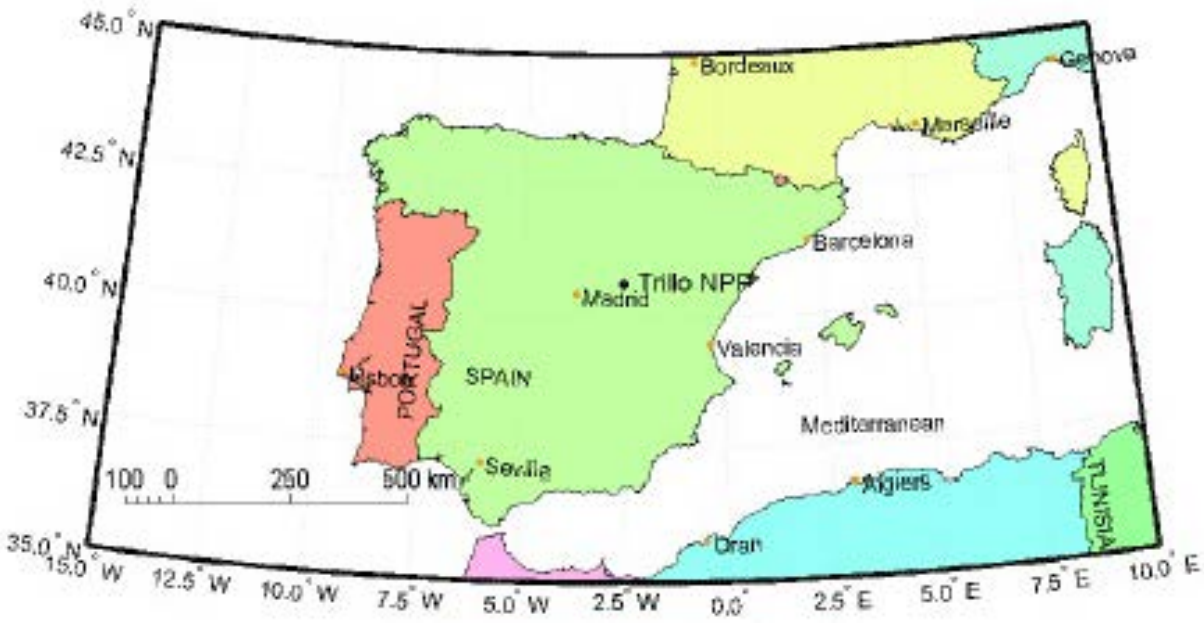

FIG. III.1. Map of Spain showing the location of Trillo NPP.

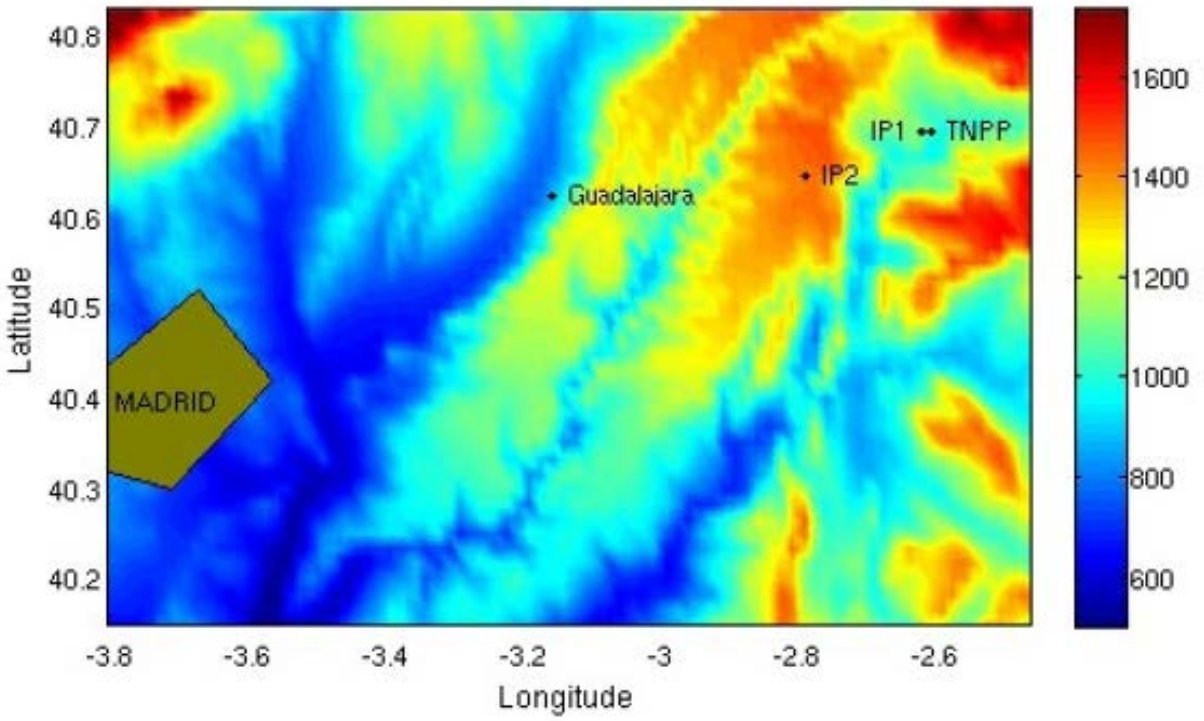

FIG. III.2. Topography (m) of the area of interest from the NOAA Geodas database.

Geographic coordinates of the locations of interest are the following:

Trillo NPP: 2.62º W, 40.70º N
Guadalajara: 3.17º W, 40.63º N

Madrid is represented schematically as a polygon with the following vertices:

Latitudes = (40.33, 40.30, 40.42, 40.52, 40.43)
Longitudes = (–3.87, –3.72, –3.57, –3.68, –3.82)

The Trillo NPP started its operation in 1987 and is a pressurized water reactor (PWR) with 1043 MW power. Refrigeration is carried out through two cooling towers.

Guadalajara is a small town (81 221 habitants in 2008, population density 345 inhabitants per km^2) located 55 km from Madrid and 46 km from Trillo NPP. The Madrid metropolitan area is about 70 km from Trillo NPP; the Madrid population in 2008 was 3 213 271 inhabitants (density 5294 inhabitants per km^2).

III.2.2. Meteorological data

Specific meteorological conditions, which would be representative of a worst case scenario, will be used for the simulations. Wind fields 10 m above the ground are provided. These were obtained from the WINMOD model, developed at the University of Wales [III.1]. WINMOD calculates such wind fields from the geostrophic wind and atmosphere stability. Essentially, the model diagnoses the local modification of the wind field in regions of complex topography. A geostrophic wind speed and direction, as well as the atmospheric lapse rate, are specified, and the model iterates the horizontal momentum and temperature equations at the surface towards a steady state.

Two scenarios are considered: one with a stable atmosphere, and one with neutral stability. This will allow assessment of the effects of stability conditions in radionuclide dispersion. Files containing wind fields 10 m above the ground are provided for the two scenarios (‘trillostuv.dat’ for stable conditions, ‘trillonsuv.dat’ for neutral stability). Each file consists of 6 columns: *x* (grid coordinates), *y* (grid coordinates), longitude, latitude, *u* (m/s), *v* (m/s).

The *x* coordinate runs from 1 to 82 (west to east), and the *y* coordinate runs from 1 to 42 (south to north). Thus, each grid cell is specified both from its grid coordinates and its geographic coordinates. Geographic coordinates correspond to the center of each grid cell. *u* and *v* are velocity vector components in the *x* and *y* directions, respectively. Table III.1 provides additional information concerning each scenario.

In both cases, the same geostrophic wind direction is considered. However, stable stratification and neutral conditions are found at low wind speeds, thus it is 3.0 m/s and 6.0 m/s for the stable and neutral conditions, respectively.

As an example, the representation of the wind field 10 m above the ground provided by WINMOD for the stable atmosphere is given in Fig. III.3. Generally speaking, the presence of the ground, because of friction, slows down the wind speed and deviates it to the left from the geostrophic wind direction. Topographic variations produce a local modification of the wind field; thus, it may be observed that it tends to blow along valleys from higher to lower altitude.

TABLE III.1. METEOROLOGICAL CONDITIONS FOR THE STABLE AND NEUTRAL STABILITY SCENARIOS

Parameter	Stable conditions	Neutral stability
Boundary layer height (m)	1000	1500
Geostrophic wind (m/s)	3.0	6.0
Direction[a] (deg)	140	140
Atmospheric lapse rate (K/m)	0.006	0.009
Pasquill stability class	E	D
File name	trillostuv.dat	trillonsuv.dat

[a] Direction from which the wind blows, degrees clockwise from north.

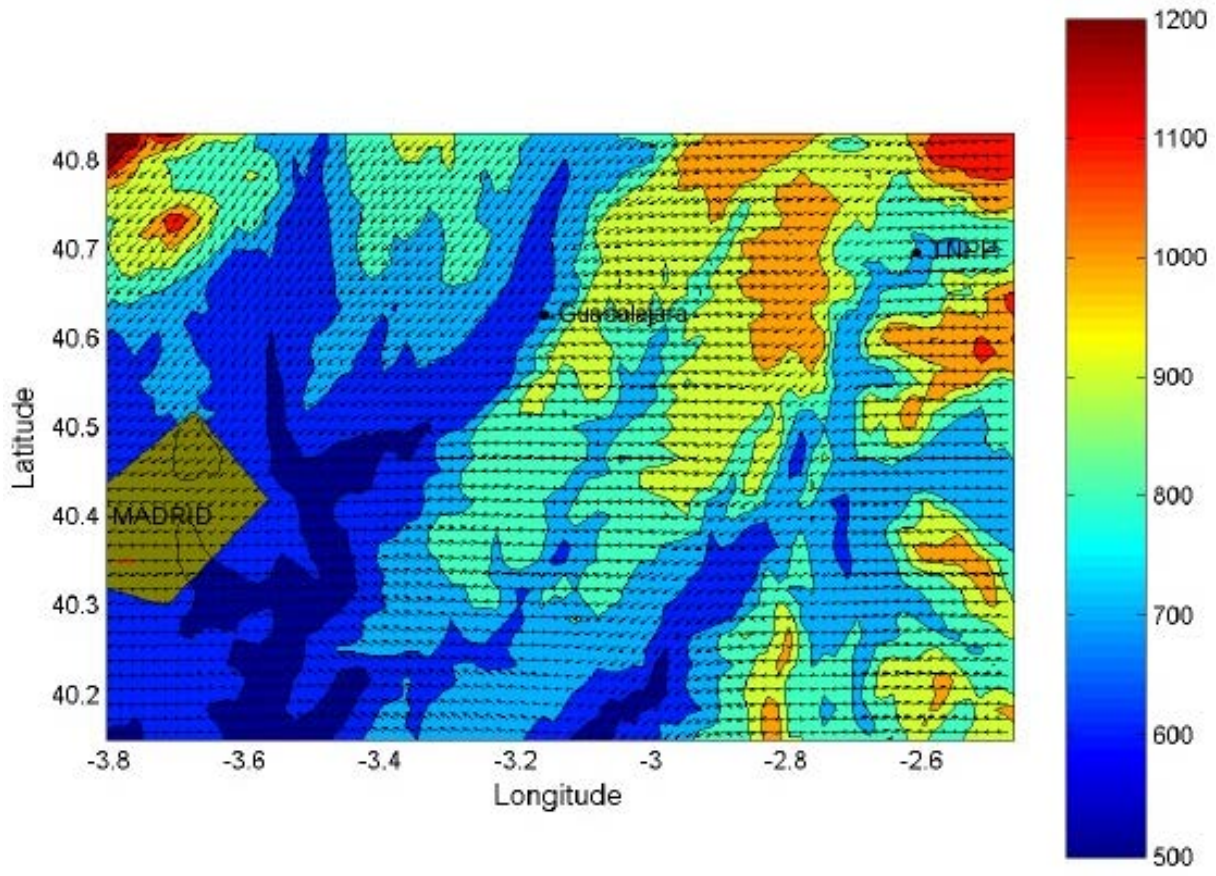

FIG. III.3. Wind field 10 m above the ground calculated by WINMOD for a stable atmosphere. The colour scale (m) is the topography of the area. The red vector (left side of figure, inside Madrid) gives a scale for the wind speed, corresponding to 2 m/s.

III.2.3. Release data

The same hypothetical accident is considered for both meteorological scenarios. The radionuclides are assumed to be released as gas, and only dry deposition is considered. Two radionuclides with different half-lives are considered, ^{137}Cs and ^{131}I, with all of the latter in molecular form. Of course, many more than two radionuclides, and different chemical forms of them, would be released during a real accident, but considering these two radionuclides with different half-lives is enough for modelling intercomparison purposes.

The hypothetical accident considered here consists of a steam generator tube rupture, a scenario which was developed IRSN. The duration of the release is 1 hour, and the release rate is variable for both radionuclides. Release data are provided in Table III.2 and in an Excel file ('release.xlsx'). An effective release height of 50 m is considered.

This exercise uses steady wind conditions for the dispersion calculations, so it is not reasonable to assume longer release episodes (of the order of a few days, for instance). Steady winds over such longer periods are not realistic.

III.3. SIMULATION ENDPOINTS

A simulation over 10 hours needs to be carried out. The following results are to be provided by the modellers participating in the exercise for each simulation:

(1) Contour map of deposited activity (Bq/m^2) on the ground at the end of the simulation, at the same resolution as the topographic data.
(2) Contour map of time integrated air activity concentration ($Bq \cdot min \cdot m^{-3}$) at ground level (averaged value up to 50 m over the ground), at the same resolution as the topographic data.
(3) Time series, with a temporal resolution of 10 minutes, of activity concentrations in air (averaged value from ground level to 50 m) at four points: Guadalajara, downtown Madrid, and two intermediate points between Trillo NPP and Guadalajara (coordinates given in Table III.3). Locations of these points may also be seen in the map in Fig. III.2. These time series are also be averaged values over the 1 minute spatial resolution grid cell where the point of interest is located. Geographic coordinates of all relevant points are summarized in Table III.3. The units for activity concentrations are in Bq/m^3.

TABLE III.2. RATE OF RADIONUCLIDE RELEASE (Bq/s) OVER TIME FOR A HYPOTHETICAL STEAM GENERATOR TUBE RUPTURE

Time (hh:mm:ss)	Iodine-131	Caesium-137
12:01:00 AM	0.00×10^{0}	0.00×10^{0}
12:02:00 AM	0.00×10^{0}	0.00×10^{0}
12:03:00 AM	0.00×10^{0}	0.00×10^{0}
12:04:00 AM	1.31×10^{6}	3.35×10^{5}
12:05:00 AM	7.45×10^{5}	1.87×10^{5}
12:06:00 AM	1.37×10^{6}	3.34×10^{5}
12:07:00 AM	1.10×10^{6}	2.61×10^{5}
12:08:00 AM	1.28×10^{6}	2.96×10^{5}
12:09:00 AM	2.29×10^{6}	5.16×10^{5}
12:10:00 AM	1.81×10^{6}	3.98×10^{5}
12:11:00 AM	1.00×10^{6}	2.18×10^{5}
12:12:00 AM	3.06×10^{8}	6.54×10^{7}
12:13:00 AM	3.86×10^{8}	8.15×10^{7}
12:14:00 AM	4.17×10^{8}	8.69×10^{7}
12:15:00 AM	4.50×10^{8}	9.25×10^{7}
12:16:00 AM	4.84×10^{8}	9.84×10^{7}
12:17:00 AM	5.18×10^{8}	1.04×10^{8}
12:18:00 AM	5.55×10^{8}	1.10×10^{8}
12:19:00 AM	5.91×10^{8}	1.17×10^{8}
12:20:00 AM	6.29×10^{8}	1.23×10^{8}
12:21:00 AM	6.67×10^{8}	1.30×10^{8}
12:22:00 AM	7.07×10^{8}	1.36×10^{8}
12:23:00 AM	7.47×10^{8}	1.43×10^{8}
12:24:00 AM	7.88×10^{8}	1.50×10^{8}
12:25:00 AM	8.29×10^{8}	1.57×10^{8}
12:26:00 AM	8.72×10^{8}	1.64×10^{8}
12:27:00 AM	9.14×10^{8}	1.71×10^{8}
12:28:00 AM	9.57×10^{8}	1.79×10^{8}
12:29:00 AM	1.00×10^{9}	1.86×10^{8}
12:30:00 AM	1.05×10^{9}	1.94×10^{8}
12:31:00 AM	1.09×10^{9}	2.02×10^{8}
12:32:00 AM	1.13×10^{9}	2.10×10^{8}
12:33:00 AM	1.18×10^{9}	2.18×10^{8}
12:34:00 AM	1.23×10^{9}	2.26×10^{8}
12:35:00 AM	1.27×10^{9}	2.34×10^{8}
12:36:00 AM	1.32×10^{9}	2.42×10^{8}
12:37:00 AM	1.36×10^{9}	2.50×10^{8}
12:38:00 AM	1.41×10^{9}	2.59×10^{8}
12:39:00 AM	1.46×10^{9}	2.67×10^{8}
12:40:00 AM	1.50×10^{9}	2.74×10^{8}
12:41:00 AM	1.55×10^{9}	2.78×10^{8}
12:42:00 AM	1.59×10^{9}	2.82×10^{8}
12:43:00 AM	1.63×10^{9}	2.85×10^{8}
12:44:00 AM	1.66×10^{9}	2.88×10^{8}
12:45:00 AM	1.70×10^{9}	2.90×10^{8}
12:46:00 AM	1.73×10^{9}	2.92×10^{8}
12:47:00 AM	1.76×10^{9}	2.94×10^{8}
12:48:00 AM	1.78×10^{9}	2.95×10^{8}
12:49:00 AM	1.81×10^{9}	2.96×10^{8}
12:50:00 AM	1.83×10^{9}	2.96×10^{8}
12:51:00 AM	1.85×10^{9}	2.96×10^{8}
12:52:00 AM	1.86×10^{9}	2.97×10^{8}
12:53:00 AM	1.87×10^{9}	2.96×10^{8}
12:54:00 AM	1.87×10^{9}	2.96×10^{8}

TABLE III.2. RATE OF RADIONUCLIDE RELEASE (Bq/s) OVER TIME FOR A HYPOTHETICAL STEAM GENERATOR TUBE RUPTURE (cont.)

Time (hh:mm:ss)	Iodine-131	Caesium-137
12:55:00 AM	1.87×10^9	2.95×10^8
12:56:00 AM	1.88×10^9	2.94×10^8
12:57:00 AM	1.87×10^9	2.93×10^8
12:58:00 AM	1.87×10^9	2.92×10^8
12:59:00 AM	1.87×10^9	2.91×10^8
1:00:00 AM	1.87×10^9	2.89×10^8

TABLE III.3. GEOGRAPHIC COORDINATES OF MODELLING LOCATIONS FOR THE SCENARIO

Location	Longitude	Latitude
Trillo NPP	2.62º W	40.70º N
IP-1[a]	2.70º W	40.70º N
IP-2[a]	2.80º W	40.65º N
Guadalajara	3.17º W	40.63º N
Downtown Madrid	3.68º W	40.43º N

[a] IP-1 and IP-2 are intermediate points between Trillo NPP and Guadalajara.

III.4. REFERENCE TO APPENDIX III

[III.1] JONES, B., A user guide and model description for WINMOD. Unit for Coastal and Estuarine Studies, Marine Science Laboratories. University of Wales, Menai Bridge, Anglesey, United Kingdom (1998).

APPENDIX IV. DESCRIPTION OF MODELS USED TO RUN THE MID-RANGE ATMOSPHERIC DISPERSION EXERCISE

The mid-range atmospheric dispersion exercise was executed by five participants using six models. These included:

- Atmospheric Dispersion and Dose Analysis Method (ADDAM) (run by S.L. Chouhan, Canada);
- Canadian Standards Association (CSA-ERM) code (run by S.L. Chouhan);
- HOTSPOT 2.07.1 (run by D. Trifunović, Croatia);
- JRODOS (run by G. Sdouz, Austria);
- RASCAL 3.0.3 (**R**adiological **AS**sessment for **C**onsequence **A**na**L**ysis for Windows) (run by F. Mancini, Italy); and
- University of Seville Model (USev) (run by R. Periáñez, Spain).

Descriptions of each of these models and their assumptions are provided in the sections that follow.

IV.1. DESCRIPTION OF ADDAM AND CSA-ERM (MID-RANGE)

The ADDAM and CSA-ERM codes were used for the mid-range modelling exercise by S.L. Chouhan of the Canadian Nuclear Laboratories (formerly Atomic Energy of Canada Limited) in Canada [IV.1].

IV.1.1. Introduction

The ADDAM and CSA-ERM codes were also used for the short range modelling exercise (see Appendices I and II). Therefore, the model descriptions already provided for that exercise apply here also and are not repeated.

IV.1.2. Application of the model to the mid-range exercise

Both the ADDAM and CSA-ERM codes are based on CSA N288.2 [IV.2], but they were written for slightly different purposes, as described in Appendix II. ADDAM is a fully documented, quality assured, and validated code that can be used for safety assessments. By comparison, CSA-ERM is not yet documented and is used for R&D or experimental purposes. CSA-ERM can be considered quality assured to the extent that it produces the same results as the ADDAM code, which is validated for scenarios where both codes are applicable.

The mid-range exercise has similar objectives to a R&D initiative. Therefore, for the purposes of the exercise, CSA-ERM was quality assured with ADDAM over an applicable range, and CSA-ERM was then used for the final calculations.

ADDAM can make predictions only for the plume centerline for each meteorological record at 10 specified downwind distances. In this exercise, the calculations were needed at a very fine resolution (500 m × 500 m grid interval) for a 90 km downwind distance and a 30–40 km cross wind distance.

ADDAM can only predict dilution factors and doses; however, in the current exercise, ground depositions and activity concentrations in air were to be predicted. Therefore, most of the predictions were made using CSA-ERM, although predictions at the plume centreline were also

made using ADDAM at four locations (IP-1, IP-2, Guadalajara and downtown Madrid) for the Neutral scenario, and the predictions compared well.[26]

Both ADDAM and CSA-ERM have some options (e.g. choice of parameter values) for making either conservative (protective or potentially overestimated) predictions or realistic predictions. In most cases, the realistic options were used in these calculations.

IV.1.2.1. Inputs to the model calculations

The radionuclides released were ^{137}Cs (half-life of 30.17 years) and ^{131}I (half-life of 8.04 days). Caesium-137 decays to form ^{137m}Ba and ^{137}Ba through β^- decay, and ^{137m}Ba decays to produce ^{137}Ba through γ decay. Barium-137m reaches a level of the ^{137}Cs level within 1 hour and remains at approximately this level from there onward; thus, the activity concentrations of ^{137m}Ba in air and soil will be comparable to those of ^{137}Cs.

Iodine-131 decays to form ^{131m}Xe through β decay, and ^{131m}Xe then undergoes γ decay to produce ^{131}Xe. The amount of ^{131m}Xe is four orders of magnitude lower than that of ^{131}I at 1 hour. As a result, the activity concentrations of ^{131m}Xe in air and soil will be four orders of magnitude lower than that of ^{131}I.

For the sake of simplicity, the daughter products were not considered in these simulations and the following values of the total activity released were used as input to the model calculations:

— For ^{137}Cs, 643 GBq were assumed to be released within 1 hour; and
— For ^{131}I, 3.69 TBq were assumed to be released within 1 hour.

IV.1.2.2. Assumptions used in the model calculations

The release duration was 3 hours; however, for these calculations, it was assumed to be one hour. For prediction of the integrated activity concentration in air and the ground deposition, and an assumption that the wind speed and direction do not change, a 1 hour release duration is expected to produce comparable results to those of a 3 hour release duration. There would be differences in predictions of the time series, but these differences are corrected manually.

An air temperature of 20°C was assumed for the exercise, although, it is not important for these calculations. No wet deposition was assumed to occur, and it was assumed that there was neither rain nor fog at the time of the release.

The wind speeds were estimated by adding the wind vectors provided in the scenario description for the exercise. A value of 1.78 m/s was predicted under stable conditions, and a value of 3.16 m/s was predicted under neutral conditions.

The stability class was Class E under stable conditions and Class D under neutral conditions.

[26] Under stable conditions, because of the low wind speed, ADDAM switches to a long term model. The activity concentration at any downwind distance in the receiving sector then becomes uniform and independent of *y* (the downwind distance), the activity concentrations in neighbouring sectors become zero, and this will not produce a smooth contour. Therefore, the wind speed at which the switch occurs was lowered from 2 m/s to 0 m/s. This is a deviation from the ADDAM code, and therefore, predictions made using ADDAM will not be comparable to those of CSA-ERM under stable conditions.

Best estimate dry deposition velocity values of 0.01 m/s for ^{137}Cs and 0.008 m/s for ^{131}I, corresponding to the grass surface, were used.

IV.1.2.3. Specific parameter values used for the exercise

The effective release height was assumed to be 50 m, corresponding to a stack. The downwash, plume rise, entrainment and building wake effect were not applied.

Both σ_y and σ_z were calculated using the stability class, and the short term dilution factor model was used.

The building constant ($C_b = 1$) was used, but it had no impact on the calculations.

Inversion layer height values of 1000 m under stable conditions and 1500 m under neutral conditions were used.

The terrain cover was assumed to be grass, with a roughness length of 0.4 m.

The receptor height was assumed to be 0 m.

IV.1.3. Results

The results that were generated using the ADDAM code are provided in Figs IV.1 to IV.10 and described in Section 2. The results are completely as expected, based upon the selections of the input parameter values that were used as input information in ADDAM.

IV.1.4. Acknowledgements

The contributions from the previous and the current members of the ADDAM development and meteorological data collection team (N. Scheier, V. Korolevych, P. Davis, R. Moffett, P. Hernu, P. Leeson and B. Reavie) are gratefully acknowledged. The prompt help from D. Killey in creating the plume contours is also much appreciated.

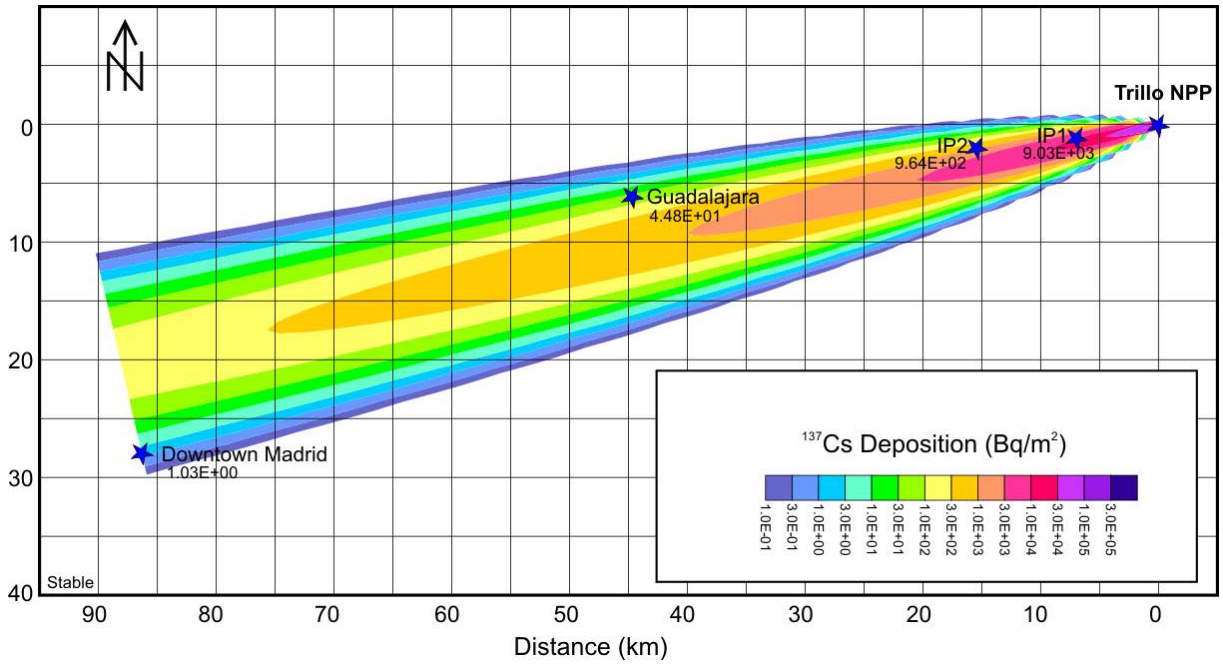

FIG. IV.1. Deposited activity (Bq/m^2) on the ground at the end of the simulation for ^{137}Cs released under stable meteorological conditions.

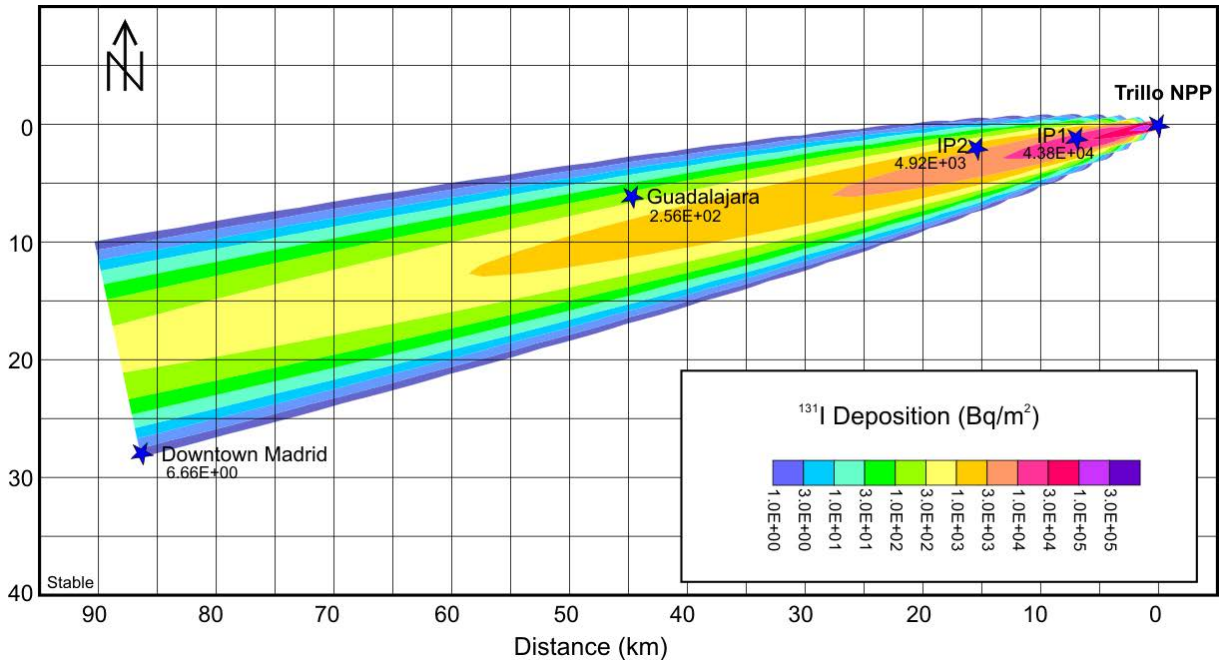

FIG. IV.2. Deposited activity (Bq/m^2) on the ground at the end of the simulation for ^{131}I released under stable meteorological conditions.

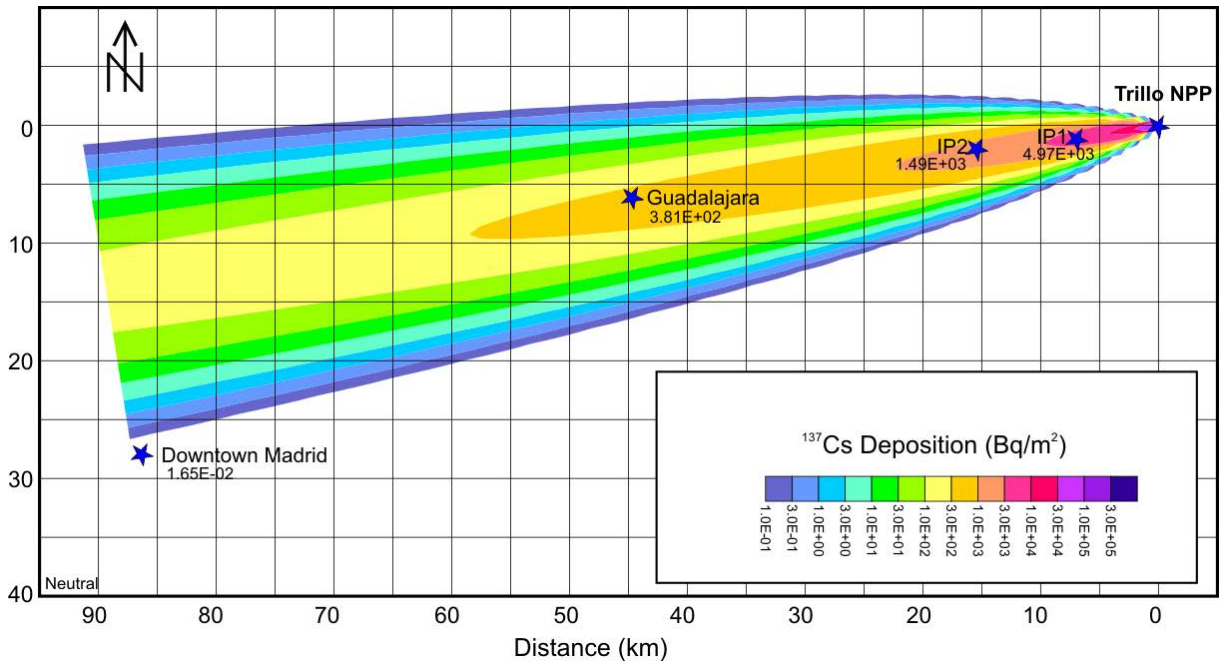

FIG. IV.3. Deposited activity (Bq/m^2) on the ground at the end of the simulation for ^{137}Cs released under neutral meteorological conditions.

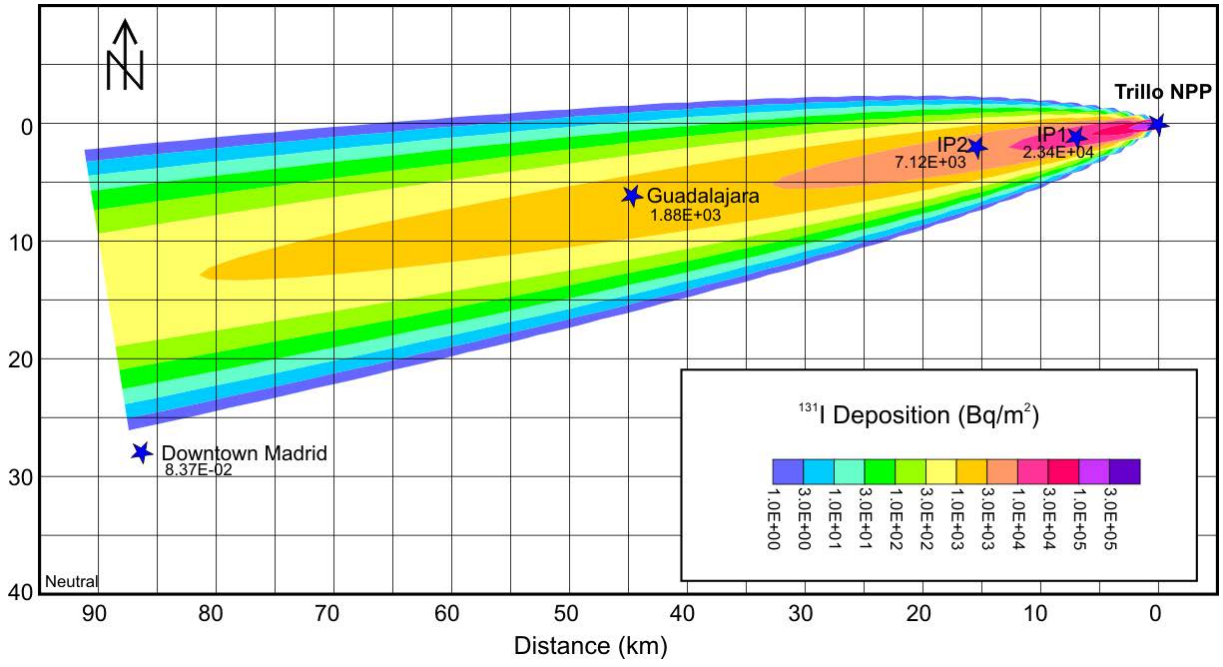

FIG. IV.4. Deposited activity (Bq/m^2) on the ground at the end of the simulation for ^{131}I released under neutral meteorological conditions.

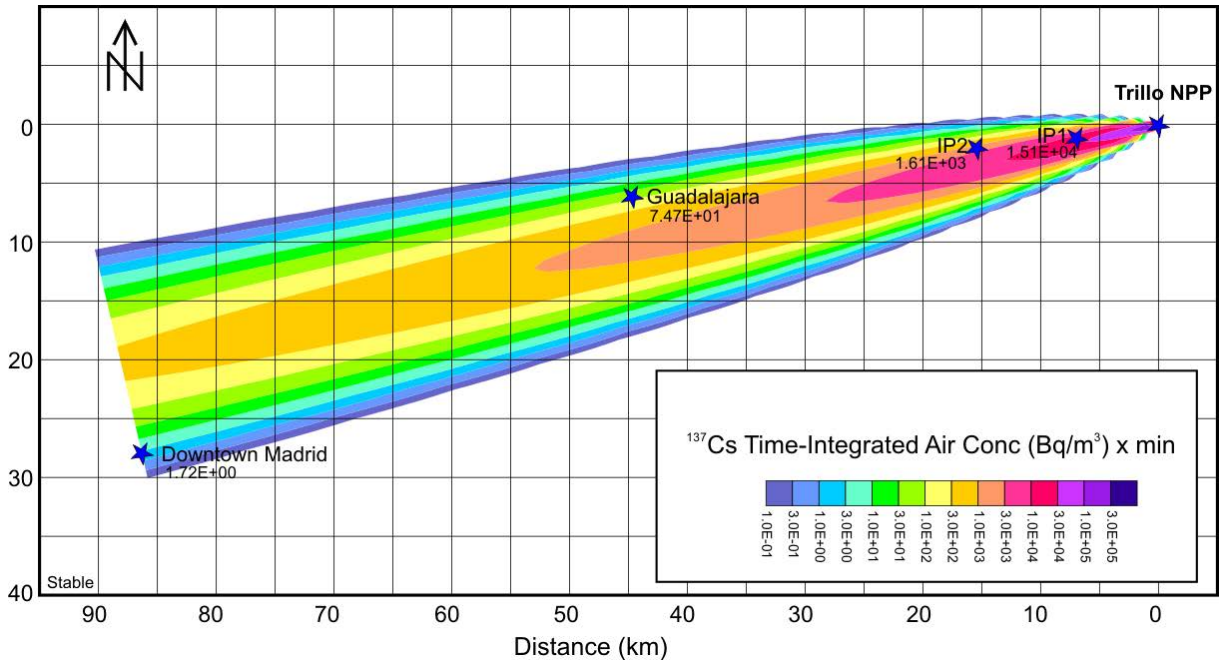

FIG. IV.5. Time integrated air activity concentration at ground level (Bq/m^3 × min) for ^{137}Cs released under stable meteorological conditions.

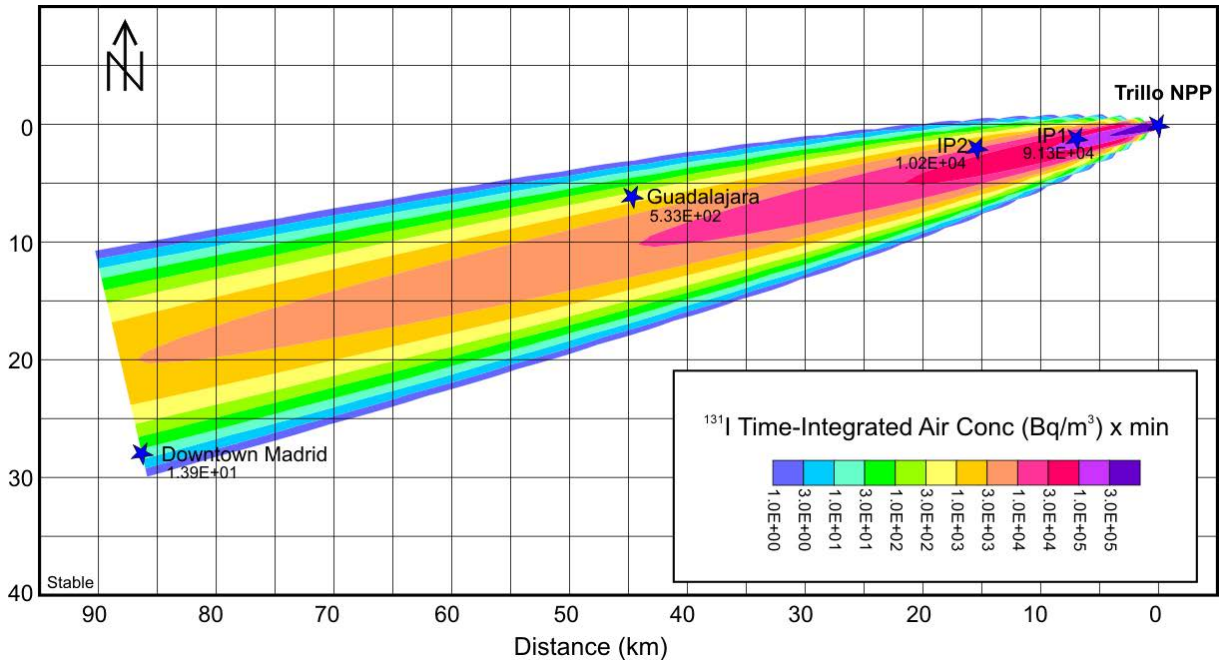

FIG. IV.6. Time integrated air activity concentration at ground level (Bq/m^3 × min) for ^{131}I released under stable meteorological conditions.

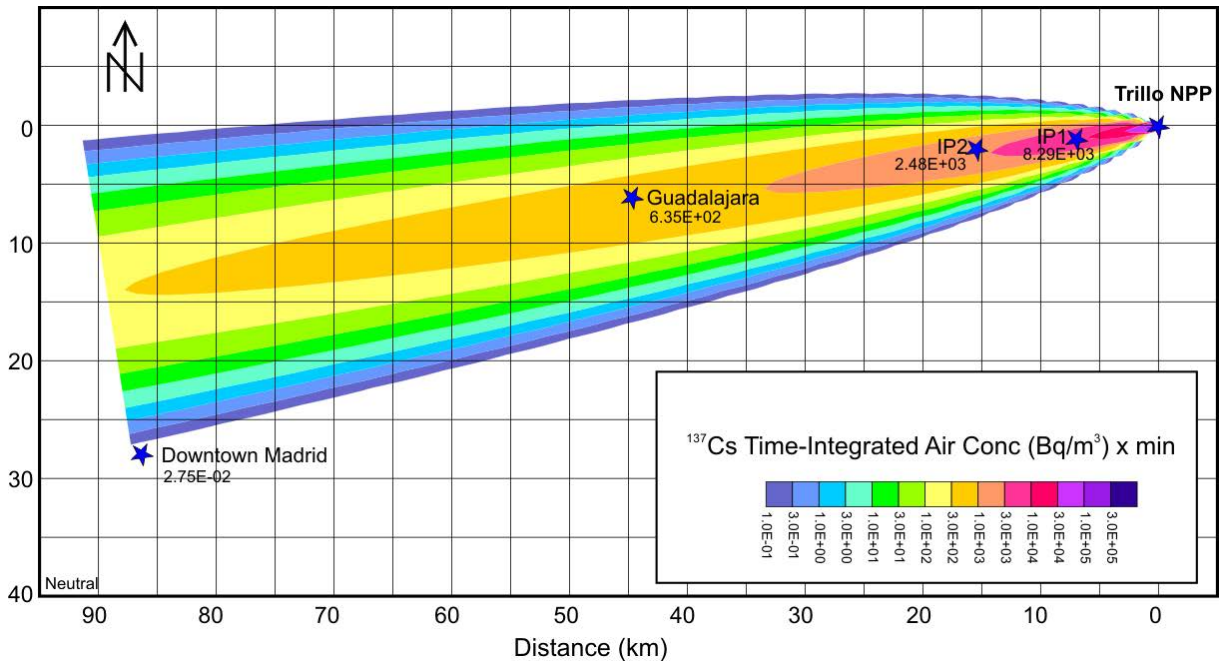

FIG. IV.7. Time integrated air activity concentration at ground level (Bq/m^3 × min) for ^{137}Cs released under neutral meteorological conditions.

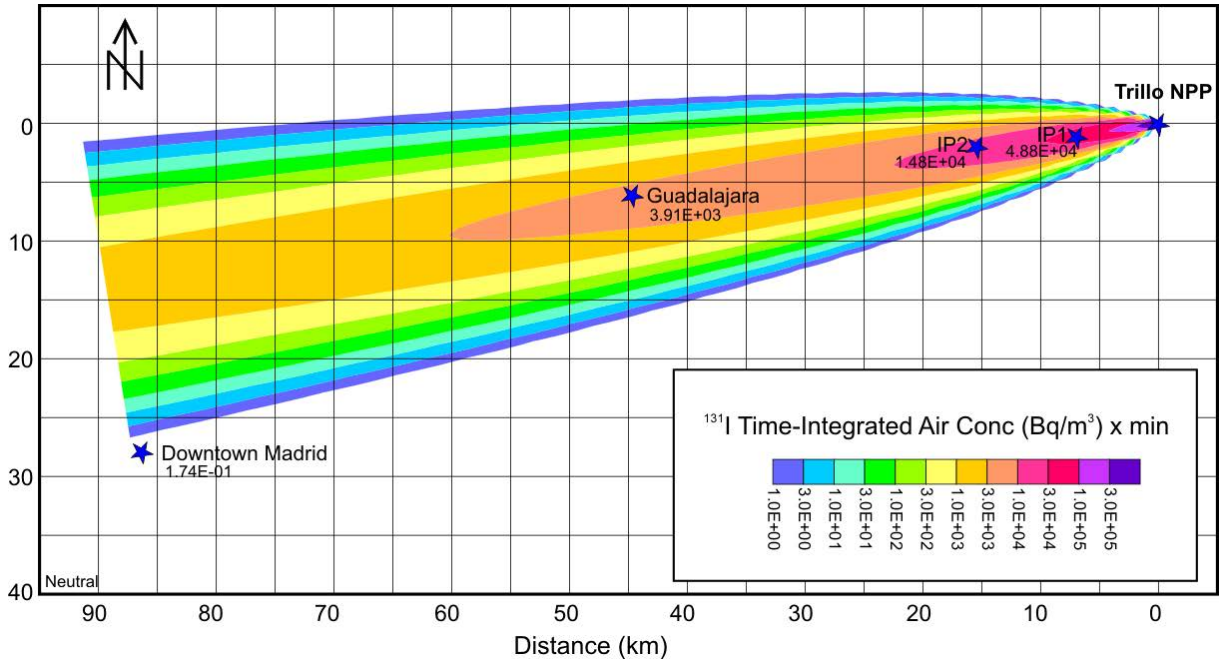

FIG. IV.8. Time integrated air activity concentration at ground level (Bq/m^3 × min) for ^{131}I released under neutral meteorological conditions.

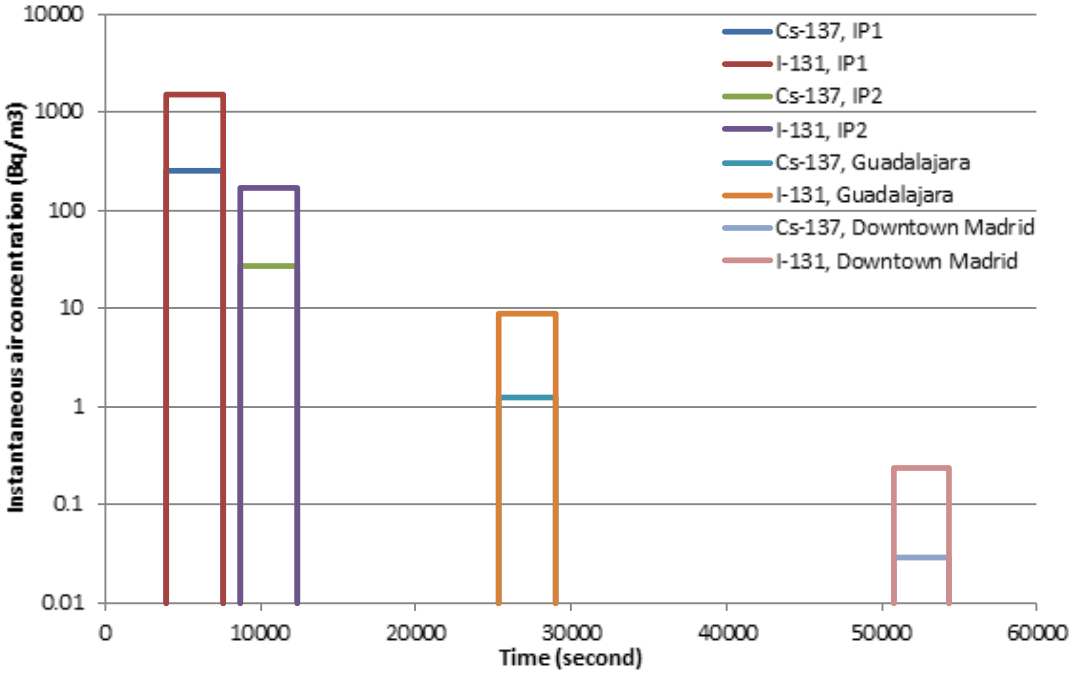

FIG. IV.9. Predicted time series of activity concentrations in air (Bq/m^3) at four points for releases under stable meteorological conditions.

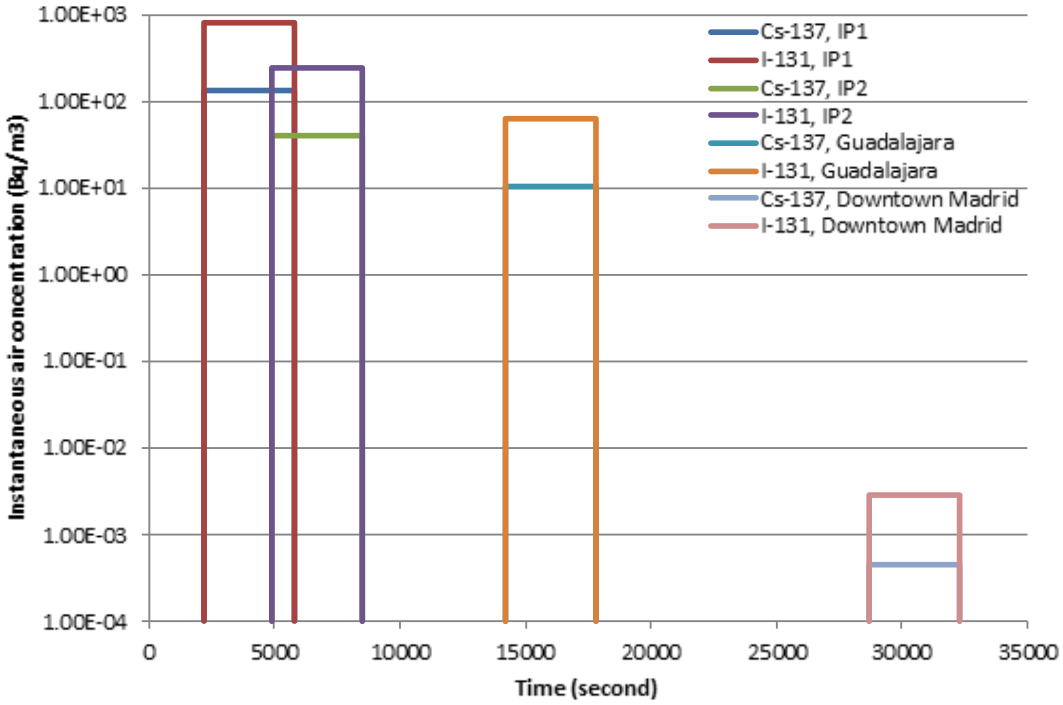

FIG. IV.10. Predicted time series of activity concentrations in air (Bq/m^3) at four points for releases under neutral meteorological conditions.

IV.2. DESCRIPTION OF RASCAL 3.0.3

The RASCAL 3.0.3 code was used for the mid-range modelling exercise by F. Mancini of SOGIN S.p.A. in Italy [IV.1].

IV.2.1. Introduction

The calculations were performed using RASCAL 3.0.3 (**R**adiological **AS**sessment for **C**onsequence **A**na**L**ysis for Windows) [IV.3]. RASCAL was developed for use by the U.S. Nuclear Regulatory Commission (NRC). It includes three sets of tools for use in consequence analysis: (1) STDose; (2) FMDose; and (3) DecayCalc. STDose can be used to estimate:

— Source terms for radiological accidents;
— Atmospheric transport, diffusion, and deposition of releases from accidents; and
— Doses from exposure to the releases.

IV.2.2. Transport, diffusion

The RASCAL 3.0.3 code applies Gaussian models to describe the atmospheric dispersion of radioactive and chemical releases from nuclear facilities. These types of models have frequently been used in calculations in support of licensing and emergency response (e.g. PAVAN [IV.4], XOQDOQ [IV.5], MESORAD [IV.6, IV.7], and RASCAL Version 2.0 [IV.8]), as they can quickly provide reasonable estimates of atmospheric activity concentrations, deposition, and doses, using relatively limited information on topography and meteorology. TADPLUME is a straight line Gaussian plume model that can be used near a release point, in cases where travel times are short and the plume depletion associated with dry deposition is small [IV.9].

TADPUFF is a Lagrangian-trajectory Gaussian puff model that can be used at longer distances, in cases where temporal or spatial variations in meteorological conditions or the depletion of the plume due to dry deposition may be significant [IV.9].

IV.2.2.1. Model Domains

TADPLUME and TADPUFF apply different model domains. Specifically, the TADPLUME domain consists of a 4 to 5 polar grid with receptor nodes set at 10° intervals on circles at eight radial distances, which may be adjusted to address the problem at hand. By comparison, the TADPUFF domain consists of a square Cartesian grid with receptor nodes that are uniformly spaced throughout the domain. The polar grid has a relatively higher node density near the release point than the Cartesian grid; by comparison, the Cartesian grid has a higher node density in the far field than the polar grid.

IV.2.2.2. Transport

IV.2.2.2.1. TADPLUME Transport

The TADPLUME model is a straight line Gaussian model, which assumes straight line transport based on the wind direction at the time and location of a release. In calculating the transport direction to ensure that the plume axis passes directly over receptors, the wind direction is rounded up to the closest 10°. Similar to other straight line Gaussian models, the transit time is not considered in determining when material arrives at the receptors; instead, it is assumed that the radioactive material arrives at the receptors at the time of release.

Transit time is calculated using the wind speed at the height of the release and is used to calculate the decay of radionuclides between the source and the receptors. Transit time is also used to calculate depletion of the radioactive material in the plume due to wet deposition. Decay calculations are made at 5 minute intervals and depletion is calculated for the full transit time.

IV.2.2.2.2. TADPUFF Transport

Unlike TADPLUME, the TADPUFF model explicitly accounts for the transit time in all calculations, as the model tracks the movement of individual puffs and calculates activity concentrations and doses based on puff positions. The decay and ingrowth of radionuclides and the depletion of the puffs due to wet and dry deposition, are calculated at 5 minute intervals.

In cases where the topography modifies the wind patterns, TADPUFF may generate more realistic patterns of activity concentration and dose, compared to TADPLUME, as the wind fields used in TADPUFF can be modified to account for topography; by comparison, it is not possible to modify assumptions within TADPLUME to account for topography.

The movement of puffs is controlled by the wind at the centre of the puff as the puffs move through the model domain. In the TADPUFF model, the spatial variation of winds is represented by two dimensional fields of vectors, which estimate the speed and direction of puff movement at 15 minute intervals, using available wind data.

Calculation of puff movement is a sequential six step process, as follows:

(1) Initial estimation of the speed and direction of puff movement, given the current puff position and height above the ground, using bilinear interpolation of the vectors at the nearest nodes of the field [IV.10];

(2) Initial estimation of the puff position at the end of the interval, based on the initial estimates of puff speed and direction (from Step 1);
(3) Second estimation of the speed and direction of puff movement, based on the puff position that was estimated at the end of the interval (from Step 2);
(4) Second estimation of the puff position at the end of the interval, based on the estimate of speed and direction (from Step 3);
(5) Averaging of the endpoints that have been calculated in Steps 2 and 4; and
(6) Calculation of the final estimate of speed and direction of puff movement, based on the initial position of the puff and the average endpoint (calculated in Step 5).

The vector fields that were established using a meteorological program are for a height of 10 m above the ground. These vectors are relevant for puffs that represent ground level releases. For release heights exceeding 12 m above the ground, a wind speed profile is used to adjust the speed of transport for a puff at a height of 10 m (i.e. ground level releases) to the actual height of puff transport. The profile that is used to adjust the wind speed considers both the atmospheric stability and the surface friction.

IV.2.2.3. Dispersion parameters

The horizontal dispersion parameters that are used in TADPLUME and TADPUFF are based on the results of many dispersion experiments that have been conducted in the 1950s and 1960s. The experiments were conducted in areas with relatively flat terrain and typically involved releases of tracer over durations of approximately 10 minutes to 1 hour; ground level measurements of activity concentration were made at distances that ranged from 100 m to several kilometers from the release point.

Dispersion parameters, based on the experiments, were then documented, for example, including the set of dispersion parameter curves, known as the Pasquill-Gifford curves [IV.11]. NRC regulatory guidance includes a graphic depiction of these curves, and many computer codes that are used by the NRC include numerical approximations of the curves. In the RASCAL 3.0.3 model, the same basic algorithms are used to estimate dispersion parameters as in other NRC codes (including PAVAN [IV.4]; XOQDOQ [IV.5]). These parameterizations can be attributed to Eimutis and Konicek [IV.12] (in general), Tadmor and Gur [IV.13] (σ_Y parameterization), and Martin and Tikvart [IV.14] (σ_Z parameterization).

IV.2.3. Release data

Table IV.1 summarizes the source term and release rate used in the modelling. Table IV.2 summarizes the release height and the duration of the simulated dispersion.

IV.2.4. Meteorological data

Only a limited number of wind vectors provided in the files *trillostuv.dat* and *trillonsuv.dat* are used. The wind vectors that have been used are compiled below in Table IV.3 and Table IV.4. The topographic data of the file *trillo.xvz* did not use wind vectors.

IV.2.4.1. Scenario 1 (Stable conditions)

For Scenario 1, assuming stable conditions, the stability class was assumed to be E. Assumed wind vectors are summarized in Table IV.3.

IV.2.4.2. Scenario 2 (Neutral conditions)

For Scenario 2, assuming neutral conditions, the stability class was assumed to be D. Assumed wind vectors are summarized in Table IV.4.

IV.2.4.3. Output files

A list of the output files that were generated using the RASCAL 3.0.3 code is provided in Table IV.5, along with a description of each file.

IV.2.5. Results

The results that were generated using RASCAL 3.0.3 are described in Section 3. The results were provided for points of topographic data, with the exception of distances exceeding 50 miles (80.5 km), as the code does not allow for calculations exceeding this distance. The activity concentrations in air are provided with a temporal resolution of 15 minutes only for ^{131}I. The activity concentration was not calculated at the endpoint, 'downtown Madrid', because it is located at a distance that exceeds 50 miles (80.5 km) from the radionuclide release point, and therefore, cannot be calculated using the RASCAL 3.0.3 code.

TABLE IV.1. DESCRIPTION OF SOURCE

Isotopes	Release rate (Bq/h)
Cs-137	6.43×10^{11}
I-131	3.69×10^{12}

TABLE IV.2. DESCRIPTION OF RELEASE HEIGHT AND TIME

Parameter	Assumption
Effective release height	50 m
Duration of simulated dispersion	10 hours

TABLE IV.3. WIND VECTORS FOR STABLE CONDITIONS

W	N	*u*	*v*
-3,598	40,401	0.25	0.41
-3,598	40,498	1.15	0.81
-3,598	40,595	1.12	1.23
-3,598	40,692	1.2	1.57
-3,4	40,401	1.64	0.1
-3,4	40,498	1.7	0.54
-3,4	40,595	1.9	0.92
-3,4	40,692	2.16	1.16
-3,203	40,401	1.96	0.13
-3,203	40,498	2.15	0.05
-3,203	40,595	1.62	0.77
-3,203	40,692	1.43	1.35
-3,005	40,401	2.14	0.18
-3,005	40,498	2.05	0.07
-3,005	40,595	1.93	0.35
-3,005	40,692	2.18	0.52
-2,807	40,401	1.59	0.59

-2,807	40,498	1.4	0.56
-2,807	40,595	1.8	0.51
-2,807	40,692	1.96	0.32
-2,593	40,401	2.18	0.23
-2,593	40,498	1.84	0.01
-2,593	40,595	2	0.08
-2,593	40,692	1.95	0.12
-2,495	40,401	1.6	0.04
-2,495	40,498	1.72	0.04
-2,495	40,595	2	0.1
-2,495	40,692	2.31	0.05
-2,593	40,692	1.95	0.12

TABLE IV.4. WIND VECTORS FOR NEUTRAL CONDITIONS

W	N	*u*	*V*
-3,598	40,401	-3.05	-0.61
-3,598	40,498	-2.97	-0.68
-3,598	40,595	-2.92	-0.89
-3,598	40,692	-2.93	-1.04
-3,4	40,401	-3.32	-0.36
-3,4	40,498	-3.21	-0.58
-3,4	40,595	-3.21	-0.75
-3,4	40,692	-3.3	-0.86
-3,203	40,401	-3.27	-0.44
-3,203	40,498	-3.39	-0.3
-3,203	40,595	-3.21	-0.5
-3,203	40,692	-3.03	-0.83

TABLE IV.4. WIND VECTORS FOR NEUTRAL CONDITIONS (cont.)

W	N	*u*	*V*
-3,005	40,401	-3.28	-0.56
-3,005	40,498	-3.3	-0.43
-3,005	40,595	-3.22	-0.52
-3,005	40,692	-3.3	-0.5
-2,807	40,401	-3.04	-0.57
-2,807	40,498	-2.86	-0.62
-2,807	40,595	-3.02	-0.62
-2,807	40,692	-3.13	-0.45
-2,593	40,401	-3.24	-0.47
-2,593	40,498	-3.13	-0.35
-2,593	40,595	-3.3	-0.31
-2,593	40,692	-3.3	-0.36
-2,495	40,401	-2.99	-0.42
-2,495	40,498	-3.13	-0.4
-2,495	40,595	-3.23	-0.33
-2,495	40,692	-3.37	-0.33
-2,61	40,692	-3.24	-0.38

TABLE IV.5. WIND VECTORS FOR A NEUTRAL WIND CLASS

Name of Output File	Description of File
stable_class.xls	Deposited activity; integrated air activity concentration, activity concentrations – stable atmosphere
neutral_class.xls	Deposited activity; integrated air activity concentration, activity concentrations – neutral atmosphere

IV.3. DESCRIPTION OF UNIVERSITY OF SEVILLE MODEL (MID-RANGE)

The Atmospheric Dispersion Model code was used for the mid-range modelling exercise by R. Periáñez of the University of Seville in Spain [IV.1].

IV.3.1. Introduction

A Lagrangian three dimensional particle tracking dispersion model, developed at the University of Seville, was used for the mid-range scenario within EMRAS II WG9. Essentially, the radionuclide release was simulated in terms of a number of particles, each one equivalent to a number of units (Bq, in this case), whose trajectories were computed over time.

IV.3.2. Description of model

The physical processes affecting particle behaviour are advection, turbulent diffusion, radioactive decay and deposition on the ground. Advection is estimated for each particle by solving a simple equation of the form:

$$\frac{d\vec{r}}{dt} = \vec{u} \quad \text{(IV.1)}$$

where:

$\vec{r}$ is the position vector of the particle; and
$\vec{u}$ is the wind speed vector at the particle position.

Wind fields provided in the scenario consist of the wind speed at a height of 10 m above the ground. A standard logarithmic profile is applied to obtain wind speed at any height above the ground:

$$u_z = \frac{u\sqrt{C_d}}{k} ln\left(\frac{z}{z_0}\right) \quad \text{(IV.2)}$$

where:

k is the von Karman constant[27] and is equal to 0.4;
u is wind speed 10 m over the ground;
u_z is wind speed at height z;
C_d is a friction coefficient; and

[27] The von Karman constant is a dimensionless constant in the logarithmic law that describes the distribution of the longitudinal velocity in the wall-normal direction of a turbulent fluid flow near a boundary with a no-slip condition.

z_0 is surface rugosity.

The last two parameters (C_d and z_0) have different values for land and water.

Radioactive decay and turbulent diffusion are simulated using stochastic methods. A horizontal and a vertical diffusion coefficient needs to be specified. Particles are assumed to be deposited when their height is less than 10 cm above ground level, and deposited particles are assumed not to move any more following deposition. On the other hand, a particle that reaches the top of the atmospheric boundary layer is assumed to be at the top the of this boundary layer.

Standard values were used for friction coefficients and ground surface rugosity. In the case of land, friction coefficient and rugosity were assumed to be 0.015 and 40 cm, respectively. In the case of water (not relevant in this application), they are 0.0015 and 0.05 cm, respectively.

Particles were assumed to have been released at the accident position and effective height at a constant rate of 200 particles per time step. The activity (in Bq) corresponding to each particle depended on the release data at the considered instant of time.

The only free parameters in the model are the horizontal and vertical diffusivities. Values of 60 m^2/s and 30 m^2/s were used in the simulation for the horizontal and vertical diffusion coefficients, respectively. A higher value was used for the horizontal diffusion coefficient given the larger spatial scale in the horizontal than in the vertical direction (the latter of which was limited by the boundary layer height). An example of an input data file for a model run is included in Fig. IV.11 below.

IV.3.3. Results

Three output files were produced for each simulation (Table IV.6), which contain the ground deposition (in Bq/m^2), the time integrated air activity concentration averaged to 50 m ($Bq/m^3 \times min$), and the time series of air concentrations at the four locations (in Bq/m^3), respectively.

```
INPUT DATA FOR ATMOSPHERIC DISPERSION MODEL

1409. 1853.              dx,dy (m)
-3.82  -2.47             geographyic limits (long)
40.15  40.83             geographyic limits (lat)
82,42                    nx,ny
10.                      time step (s)
1000.                    boundary layer height
3.0                      geostrophic wind magnitude
trillost.OUT             output file from WINMOD
trillo.xyz               topography (lon,lat,height)
60. 30.                  horizontal and vertical diffusivities
10.                      simulation time (hours)
-2.62 40.7 50.           release position (long,lat) and height (m)
iodine.dat           source data file
1.                       release duration (hours)
1.                       release data resolution (minutes)
9.98e-7              decay constant (s-1)
-2.80,40.65              intermediate point
-3.17,40.63              guadalajara
-3.68,40.43          downtown madrid
```

FIG. IV.11. Example of an input data file for a model run of the University of Seville model.

TABLE IV.6. NAMES, DESCRIPTIONS AND FORMATS OF OUTPUT FILES GENERATED DURING EACH SIMULATION USING THE UNIVERSITY OF SEVILLE MODEL

File Name[a]	File Content	File Format
depositbq_XY.out	Ground deposition	The format is x,y,deposition, where x,y are grid coordinates.
integrated_XY.out	Time integrated activity concentration in air	The format is x,y,concentration, where x,y are grid coordinates.
timeseries_XY.out	time series	The format is t,IP-1,IP-2,G,M, where t is time (hours) and IPs, IPS-2, G and M are activity concentrations in air at the intermediate points 1 and 2, Guadalajara and downtown Madrid, respectively.

[a] In the file names, X may be 'cs' or 'i' for Cs and I, respectively; Y may be 'st' or 'ns' for stable conditions and neutral stability, respectively.

IV.4. DESCRIPTION OF JRODOS

The JRODOS code was used for the mid-range modelling exercise by G. Sdouz of the Austrian Institute of Technology GmbH in Austria [IV.1].

IV.4.1. Introduction

JRODOS is a Java based version of the European Commission's Real Online Decision Support system (https://resy5.iket.kit.edu/JRODOS/; https://resy5.iket.kit.edu/JRODOS/). In this exercise, JRODOS was used to model releases due to a hypothetical steam generator tube rupture accident. The objective was to model the ground deposition of ^{137}Cs and ^{131}I, the corresponding time integrated radionuclide activity concentrations in air, and time series of contamination at selected locations.

JRODOS incorporates several dispersion models, including Gaussian puff models (ATSTEP and RIMPUFF), and a particle model for complex terrains (DIPCOT) (https://www.eu-alara.net/images/stories/pdf/program17/Session3/14%20jrodos-2017-alara.pdf) (Fig. IV.12). JRODOS also includes a Lagrangian particle model (LASAT) for use with powerful servers, which is available with a licence (although, the RIMPUFF, DIPCOT and LASAT models were not addressed by WG2 as part of this exercise).

For this exercise, the ATSTEP model was used. ATSTEP is a Gaussian model with properties of a simplified puff model. The dispersion parameters used in this exercise for high roughness are from Karlsruhe-Jülich (Germany), and the dispersion parameters used in this exercise for moderate roughness are from Mol (Belgium), as provided within the model. The Standard/Briggs plumes rise formulas are used.

IV.4.2. Application to the mid-range exercise

The exercise involved a steam generator tube rupture scenario, which was developed by IRSN (Appendix III).

IV.4.2.1. Input information for the release

A file was provided containing the release rates (Bq/s) for 17 radionuclides at 1 minute intervals during a 1 hour release. JRODOS uses a release time step of 0.5 h. The data that were provided for ^{137}Cs and ^{131}I (Appendix III) were averaged for the first half hour and the second half hour (Table IV.7). The release height was assumed to be 10 m, corresponding to the calculated wind field provided with the scenario description (Appendix III).

The calculation range for the exercise was assumed to be less than 100 km. The grid size was 1.2 km.

IV.4.2.2. Meteorological input per time-step

The wind direction (°) was derived from WINMOD model data (http://winmod.de/en/), as described in Appendix III. The wind velocity (m/s) was also derived from the WINMOD model data (the velocity vector components u and v in the input file were supplied for the exercise) (Appendix III). There was assumed to be no rain (rain intensity = 0.0 mm/h) and no clouds. The atmospheric stability class (diffusion category) was assumed to be E.

IV.4.2.3. Modelling approach

Step 1 was to estimate the cloud path. Mean values for the velocity vector components *u* and *v* were calculated in terms of one single wind speed and one single wind direction, which were then used as JRODOS input data for the whole calculation. Specifically, the input velocity was 1.78 m/s and the direction was 76.4°. The result of these assumptions was a cloud arrival time at Madrid, Spain, of 7 h.

Step 2 was to introduce the changes in wind speed and direction. This involved preparation of 7 sets of meteorological input data, each covering a 1 h interval. The starting point for the exercise (Trillo NPP in Spain) is located at cell 73/35. The ending point (in Madrid, Spain) is located at cell 8/16. The area between these two cells was divided into 7 approximately equal areas covering the approximate path of the cloud. For each of these 7 areas, the mean values of the velocity vector components were determined, resulting in 1 wind speed and 1 wind direction for each area. Then, new JRODOS calculations were performed, using the 7 different sets of wind speed and direction (Table IV.8).

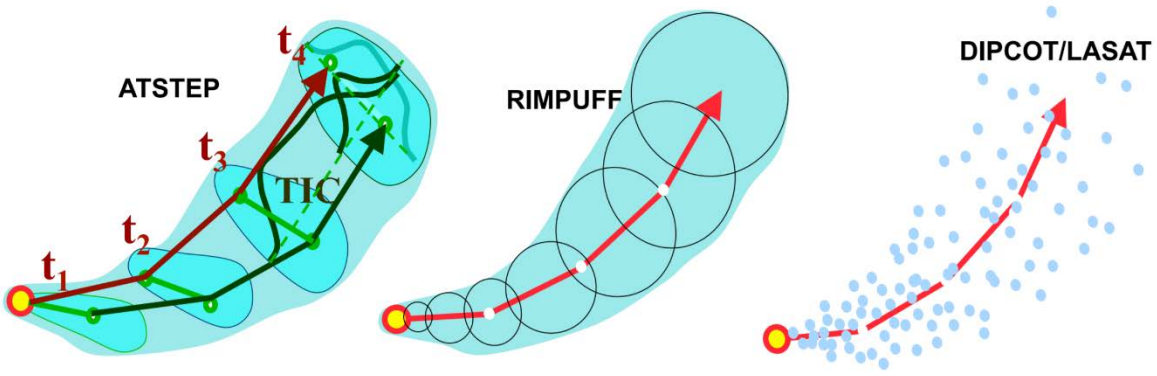

FIG. IV.12. Depiction of models available within JRODOS.

TABLE IV.7. RELEASE DATA USED WITH JRODOS

Time step (h)	I-131 (Bq)	Cs-137 (Bq)
0–0.5	7.7×10^{11}	1.5×10^{11}
0.5–1	2.9×10^{12}	4.9×10^{11}

TABLE IV.8. SUMMARY OF METEOROLOGICAL INPUT USED WITH JRODOS

Area	Wind velocity (m/s)	Wind direction (°)
1	1.43	74.8
2	2.07	80.2
3	2.03	82.6
4	1.98	87.5
5	1.94	81.8
6	1.47	76.1
7	1.36	70.5

IV.5. DESCRIPTION OF HOTSPOT 2.07.1 (HR) (MID-RANGE)

The HotSpot 2.07.1 code was used for the mid-range modelling exercise by D. Trifunovic of the State Office for Radiological and Nuclear Safety in Croatia [IV.1]. In this publication, the code as used by the above participant is referred to as 'HotSpot 2.07.1 (HR)' to distinguish it from the same code used by a different participant (see Section II.2).

IV.5.1. Introduction

HotSpot 2.07.1 is a code that was obtained from Lawrence Livermore National Laboratory, and full details are available in the User's Guide [IV.15].

IV.5.2. Application to the mid-range exercise

IV.5.2.1. Input information

The exercise involved two sets of model predictions, one assuming stable atmospheric conditions, and one assuming neutral stability. Under stable conditions, the atmospheric stability class was assumed to be Class E, and the wind speed at 10 m height was assumed to be 3.0 m/s. Under neutral conditions, the atmospheric stability class was assumed to be Class D, with a wind speed at 10 m height of 6.0 m/s.

For both sets of predictions, the effective release height was assumed to be 50 m, and the release duration was 1 h. For ^{137}Cs, the source term was 640 GBq, and the deposition velocity was 0.04 cm/s. For ^{131}I, the source term was 3.67 TBq, and the deposition velocity was 0.22 cm/s.

IV.5.2.2. Results

The results of the modelling are summarized in Table IV.9.

TABLE IV.9. SUMMARY OF HOTSPOT 2.07.1 RESULTS

Location and stability class	Ground deposition (Bq/m^2)		Air concentrations[a] (Bq/m^3 × min)	
	Cs-137	I-131	Cs-137	I-131
Stability Class D				
Guadalajara	2.3	71	95	533
Madrid	1.4	45	60	333
Stability Class E				
Guadalajara	20	610	817	4500
Madrid	13	390	517	3000

[a] The activity concentrations in air are assumed to be homogeneous up to 50 m height.

IV.6. REFERENCES TO APPENDIX IV

[IV.1] PERIÁÑEZ, R., THIESSEN, K.M., CHOUHAN, S.L., MANCINI, F., NAVARRO, E., SDOUZ, G., TRIFUNOVIĆ, D., Mid-range atmospheric dispersion modelling. Intercomparison of simple models in EMRAS-2 project, Journal of Environmental Radioactivity **162–163** (2016) 225.

[IV.2] CANADIAN STANDARDS ASSOCIATION, Guidelines for Calculating Radiation Doses to the Public from a Release of Airborne Radioactive Material under Hypothetical Accident Conditions in Nuclear Reactors, Rep. CAN/CSA-N288.2-M91, CSA Group, Toronto (1991).

[IV.3] SJOREEN, A.L., RAMSDELL, J.V. JR., MCKENNA, T.J., MCGUIRE, S.A., FOSMIRE, C., ATHEY, G.F., RASCAL 3.0: Description of models and methods, Rep. NUREG-1741, U.S. Nuclear Regulatory Commission, Office of Standards Development, Washington, DC (2001).

[IV.4] BANDER, T.J., PAVAN: An Atmospheric Dispersion Program for Evaluating Design Basis Accidental Releases for Radioactive Materials from Nuclear Power Stations, Rep. NUREG/CR-2858, U.S. Nuclear Regulatory Commission, Office of Standards Development, Washington, DC (1982).

[IV.5] SAGENDORF, J.F., GOLL, J.T., SANDUSKY, W.F., XOQDOQ: Computer Program for the Meteorological Evaluation of Routine Effluent Releases at Nuclear Power Stations, Rep. NUREG/CR-4380, U.S. Nuclear Regulatory Commission, Office of Standards Development, Washington, DC (1982).

[IV.6] SCHERPELZ, R.I., BANDER, T.J., ATHEY, G.F., RAMSDELL, J.F. JR., The Mesorad Dose Assessment Model, Vol. 1. U.S. Nuclear Regulatory Commission, NUREG/CR-4000, Vol. 1, Office of Standards Development, Washington, DC (1986).

[IV.7] RAMSDELL, J.V. JR., ATHEY, G.F., BANDER, T.J., SCHERPELZ, R.I., The MESORAD Dose Assessment Model, Vol. 2: Computer Code, Rep. NUREG/CR-4000, U.S. Nuclear Regulatory Commission, Vol. 2, Office of Standards Development, Washington, DC (1988).

[IV.8] ATHEY, G.F., SJOREEN, A.L., RAMSDELL, J.V. JR., MCKENNA, T.J. RASCAL Version 2.0 User's Guide. Vol. 1, Rev. 1, Rep. NUREG/CR-5247, U.S. Nuclear Regulatory Commission, Office of Standards Development, Washington, DC (1993).

[IV.9] RAMSDELL, J.V. JR, ATHEY, G.F., MCGUIRE, S.A., BRANDON, L.K., RASCAL 4: Description of Models and Methods, Rep. NUREG-1940, Office of Standards Development, Washington, DC (2012).

[IV.10] PRESS, W.H., FLANNERY, B.P., TEUKOLSKY, S.A., Numerical recipes, The art of scientific computing, Cambridge University Press, New York (1986) 818 pp.

[IV.11] GIFFORD, F.A., Turbulent diffusion-typing schemes: A review, Nuclear Safety **17** (1976) 68.

[IV.12] EIMUTIS, E.C., KONICEK, M.G., Derivations of continuous functions for the lateral and vertical atmospheric dispersion coefficients, Atmospheric Environment **6** (1972) 859.

[IV.13] TADMORE, J., GUR, Y., Analytical expressions for vertical and lateral dispersion coefficients in atmospheric diffusion, Atmospheric Environment **3** (1969) 688.

[IV.14] MARTIN, D.O., TIKVART, J.A., "A general atmospheric diffusion model for estimating the effects on air quality of one or more source", Proceedings of the 61st Annual Meeting of the Air Pollution Control Association for NAPCA (National Air Pollution Control Administration), St. Paul, MN (1968) 68–148.

[IV.15] HOMANN, S.G., HotSpot Health Physics Codes Version 2.07 User's Guide, Rep. LLNL-TM-411345, Lawrence Livermore National Laboratory, CA (2009).

APPENDIX V. SCENARIO DESCRIPTION FOR THE CONTAMINANT TRANSPORT AND COUNTERMEASURES EXERCISE

V.1. INTRODUCTION

The overall objective of the EMRAS II Urban Areas Working Group ('WG 9') is to test and improve the capabilities of models used in assessment of radioactive contamination in urban settings, including dispersion and deposition events, short and long term contaminant redistribution following deposition events, and potential countermeasures (protective actions including remedial actions) for reducing human exposures and doses. The present scenario is intended to provide an opportunity to test model predictions for contaminant transport and countermeasures following a release of radioactivity. The scenario is based on a hypothetical deposition of radioactivity in a city from a defined activity concentration in air and makes use of detailed geographical information for an actual urban area.

Input information for the scenario includes information about the radionuclides, the conditions of the initial deposition, meteorological information, locations for modelling endpoints, and descriptions of the countermeasures to be modelled. Modelling endpoints for intercomparison amongst participants include the deposition at specified outdoor locations, external dose rates at specified locations and times, contributions to external dose rate from relevant surfaces, external and internal doses to specified reference persons, and the effectiveness of the countermeasures considered. This publication provides information about the scenario to be modelled (input information) and a list of the endpoints to be predicted.

V.2. DESCRIPTION OF THE EXERCISE

This exercise makes use of the availability of detailed geographic information for part of an actual city. The exercise starts with a defined activity concentration in air at ground level in specified areas. The radionuclides of interest are ^{60}Co and ^{239}Pu (considered separately). Given a defined activity concentration in air, participants were asked to estimate the partitioning of each radionuclide on various urban surfaces (deposition). The impact of different weather conditions at the time of the initial deposition is considered; average weather conditions for the region are considered for the longer term estimation of contaminant transport.

Two 'regions' or areas of the city have been selected for the modelling exercise: Region 1 is a business area, and Region 2 is a park area near an apartment town. Several locations within each region have been selected as test locations for which model calculations will be made. More detailed descriptions of these regions are provided in the following sections.

V.2.1. Climatological characteristics

The city was selected for use in a simulation of radioactive contamination and subsequent exposure dose to humans due to a release of radioactivity. This city has a temperate zone climate with four distinctive seasons (spring, summer, fall and winter). In winter it is cold and dry under the influence of continental high pressure with cold air. In summer it is hot and humid under the influence of a high pressure from the ocean, with high temperature and humidity. In both spring and fall, it is clear and dry under the influence of a migratory high pressure on many days. The annual average temperature is 10°C to 16°C. The hottest month is August, with an average temperature of 23°C to 27°C, while the coldest month is January, with an average temperature of –6°C to +7°C. The annual average precipitation is 1100 mm to 1400 mm. Precipitation from June to September accounts for around 70% of the annual total amount; precipitation in July accounts for 20% of the annual total amount.

Predominant wind directions are between north and west in winter, and between south and west in summer. Figure V.1 shows a surface wind rose in 2007. The prevailing wind direction is west-northwest. The probability of occurrence of calm (defined as wind speed <0.5 m/s) is 3.6%. Relative humidity in summer is more than 80%, and in fall, around 70%. The annual average wind speed is 2.4 m/s, with monthly averages from 2 m/s to 2.8 m/s. The rainy season begins in late June and lasts for a month. Typhoons are generated from the ocean in summer, and 2 to 3 typhoons each year typically affect this region directly or indirectly.

Detailed information on the annual and monthly climate elements over 30 years is provided in Tables V.1 and V.2, respectively. Detailed information on the annual and monthly climate elements in 2007 is provided in Tables V.3 and V.4, respectively. As with many other cities of the world, the temperature in this city is rising steeply due to construction of new high-rise buildings and sustained centralization of the population. This may cause a heat island effect, which is a common phenomenon in urbanized areas.

V.2.2. Human geographical characteristics

The test site is a well-developed urbanized region. The population density can be as high as 14 000 persons/km^2. The age distribution includes 16% below 16 years old, 73% between 16 and 64 years old, and 11% more than 65 years old. Living quarters of residents include 30% in detached houses, 60% in apartment houses, 5% in terrace houses, 3% in semidetached houses, and 2% in other types of houses. The average number of residents in a household is 3.7 persons.

In terms of area, the windows take up 30–40% of the outer walls in detached houses, semidetached houses and terrace houses, and 60–80% in apartment houses. The outer walls of business buildings are almost covered with glasses and aluminum plates for the beauty of the external appearance. The height between floors is 3–3.5 m for business buildings and schools, and 2.5 m–3 m for residential buildings. Land use distribution includes 20% fields, 16% forests, 40% residential areas, 4% schools, 16% roads, 3% park areas, and 1% other purposes. The soil type is acid loamy sand or acid loamy with pH 5.5 to 6.0.

Traffic speed in the city is 20.8 km/h (daily average); it is 22.1 km/h in the morning and 17.9 km/h in the afternoon. Traffic conditions during rush hours (07:00–09:00 and 17:00–19:00) are more severe.

Street cleaning is done at daybreak every day by vacuum cleaning vehicles or water spray vehicles. Vacuum cleaning may be effective in removing wastes, earth and sand, and fallen leaves accumulated in the middle or at the edges of roadways. On the other hand, water spray cleaning may be effective in removing particles less than 60 μm throughout the entire surfaces of roadways. The necessary water amount is approximately 100 t/km^2.

V.2.3. Description of the test site

Figure V.2 shows an aerial photograph of the test site (from Google Earth). In addition to the aerial photograph, three dimensional GIS (Geographical Information System) was provided to EMRAS II WG9 participants for better understanding of the structure forms and for such information as land use and building attributes. A large river runs south-north with a width of 400 m. Traversing the river, there is a large bridge 1.3 km in length and 31 m wide. The circular structure in the upper part of the figure near the center is a sports stadium. A large apartment town is visible in the lower right hand side. Detailed information on the buildings of the test site was provided to the participants.

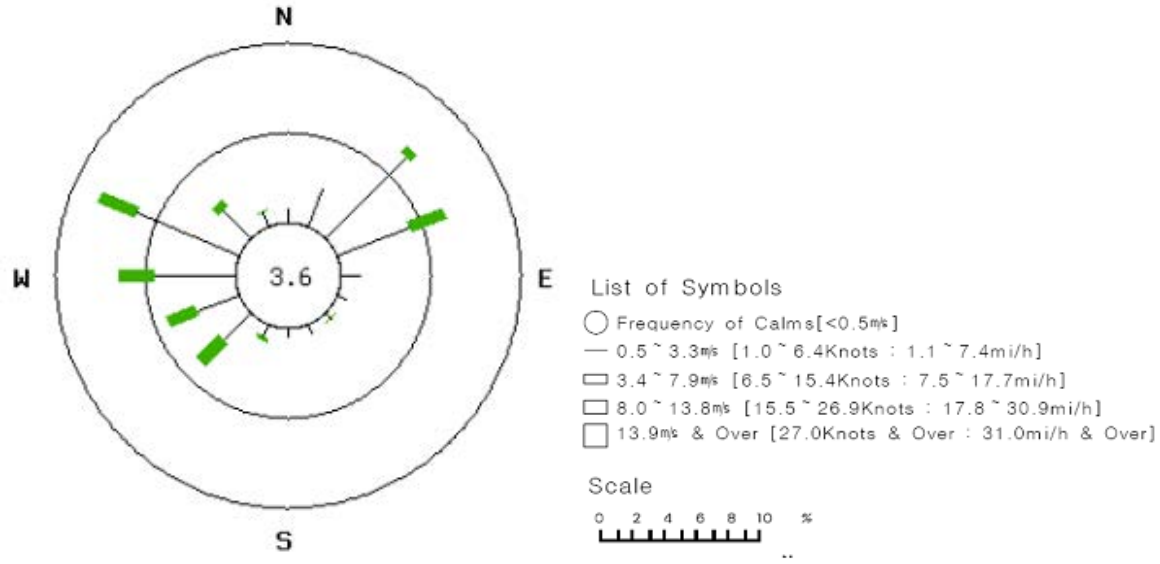

FIG. V.1. Surface wind rose in the city in 2007.

FIG. V.2. Aerial photograph of the test site. 'Region 1' is a business area, and 'Region 2' is a park area (©2007 Google, Image ©2009 DigitalGlobe).

TABLE V.1. ANNUAL CLIMATE ELEMENTS IN THE CITY OVER 30 YEARS (1971–2000)

Climate elements	Values
Temperature (°C)	12.5
Highest temperature (°C)	16.9
Lowest temperature (°C)	8.2
Precipitation (mm)	1344.3
Wind speed (m/s)	2.4
Humidity (%)	66.9
Time of sunshine (hours)	2114.1
Heat energy (MJ/m^2)	11.35

TABLE V.2. MONTHLY CLIMATE ELEMENTS IN THE CITY OVER 30 YEARS (1971–2000)

Climate elements	Jan.	Feb.	Mar.	Apr.	May	Jun.	Jul.	Aug.	Sep.	Oct.	Nov.	Dec.
Temperature (°C)	-2.5	-0.3	5.2	12.1	17.4	21.9	24.9	25.4	20.8	14.4	6.9	0.2
Highest temperature (°C)	1.6	4.1	10.2	17.6	22.8	26.9	28.8	29.5	25.6	19.7	11.5	4.2
Lowest temperature (°C)	-6.1	-4.1	1.1	7.3	12.6	17.8	21.8	22.1	16.7	9.8	2.9	-3.4
Temp. on the ground (°C)	-2.4	-0.3	5.6	13.4	19.7	24.8	26.8	27.4	22.5	14.8	6.2	-0.1
Precipitation (mm)	21.6	23.6	45.8	77.0	102.2	133.3	327.9	348.0	137.6	49.3	53.0	24.9
No. of days in precipitation (>1.0 mm)	3.9	3.7	4.5	5.9	6.9	7.8	12.8	11.2	6.7	4.8	6.9	4.3
No. of days in precipitation (>0.1 mm)	7.1	6.0	6.8	8.0	8.8	10.0	15.5	13.8	8.7	6.6	9.0	7.3
Wind speed (m/s)	2.5	2.7	2.9	2.9	2.6	2.3	2.3	2.1	1.9	2.0	2.3	2.3
Humidity (%)	62.6	61.0	61.2	59.3	64.1	71.0	79.8	77.4	71.0	66.2	64.6	63.8
Time of sunshine (hours)	158.4	163.3	197.5	210.7	224.3	187.8	130.7	155.3	184.5	200.5	151.3	149.9
Heat energy (MJ/m^2)	7.04	9.58	12.37	15.19	16.49	15.53	12.11	12.43	12.16	10.33	7.08	5.88

TABLE V.3. ANNUAL CLIMATE ELEMENTS IN THE CITY IN 2007

Climate elements	Values
Temperature (°C)	13.3
Highest temperature (°C)	33.2
Lowest temperature (°C)	-8.6
Precipitation (mm)	1212.3
Daily greatest precipitation (mm)	76
No. of days of precipitation (>1.0 mm)	90
No. of days of precipitation (>0.1 mm)	132
Relative humidity (%)	62
Wind speed (m/s)	2.4
Most frequent wind direction	WNW
No. of days with phenomena:	
clear (days)	94
cloudy (days)	105
thunderstorm (days)	25
fog (days)	4
frost (days)	60
freezing (days)	99
snow cover (days)	20

TABLE V.4. MONTHLY CLIMATE ELEMENTS IN THE CITY IN 2007

Climate elements	Jan.	Feb.	Mar.	Apr.	May	Jun.	Jul.	Aug.	Sep.	Oct.	Nov.	Dec.
Temperature (°C)	0.4	4	6.1	11.4	18.1	23.2	24.2	26.5	21.5	15.1	6.7	1.8
Highest temperature (°C)	11.8	14.8	16.2	22.5	30.1	33.2	31.2	33.2	31.1	26.2	19.3	13.8
Lowest temperature (°C)	-7.6	-8.6	-7.6	1.6	9	14.1	17.7	19.8	14.1	3.2	-5.5	-7.4
Precipitation (mm)	10.8	12.6	123.5	41.1	137.6	54.5	274.1	237.6	241.9	39.5	26.4	12.7
No. of days of precipitation (>1.0 mm)	2	2	10	7	8	5	11	16	13	7	4	5
No. of days of precipitation (>0.1 mm)	5	3	14	9	9	12	15	19	20	7	8	11
Relative humidity (%)	56	53	60	53	62	61	75	75	8	63	55	60
Wind speed (m/s)	2	2.3	2.7	2.8	2.6	2.3	2.4	2.6	2.5	2.1	2.2	2.4
Maximum wind speed (m/s)	8	8.6	10	9.4	8.7	6.9	7.3	9.9	8	8	7.7	8.5
No. of days with phenomena:												
clear (days)	14	13	6	9	6	5	0	3	3	8	16	11
cloudy (days)	2	3	8	8	9	12	16	13	19	8	2	5
thunderstorm (days)	1	0	3	1	4	1	4	5	2	1	3	0
fog (days)	1	0	2	0	0	0	1	0	0	0	0	0
frost (days)	20	8	3	0	0	0	0	0	0	0	0	18
snow cover (days)	3	2	5	0	0	0	0	0	0	0	0	11

Figure V.3 shows a close up photograph of Region 1, a center of business. The roadway running north-south is 16 lanes in two directions; the roadway running east-west is 12 lanes. Each lane is 3.5 m wide. The surface is covered with asphalt. A subway station is located below the street crossing, and there are four entrances at the edges of the street crossing. The floating population utilizing this station is 160 000 persons per day.

Building 1 is a 24 storey building for business, with a height of 66 m and an area of 903 m^2, with a rounded shape. Building 2 is a 30 storey building for business, with a height of 82 m and an area of 1193 m^2, with a shape of angled edges. Building 3 is a 16 storey building for business with a height of 44 m and an area of 607 m^2, and with a mixed shape of angled and round edges. Building 4 is a pavilion of 15 m in height and an area of 2566 m^2. The roof of building 4 is made of steel plates with a rounded shape. All of the business buildings are made of strengthened concrete with reinforcing rods, and the surfaces of the outer walls are covered with aluminum plates or strengthened glass. The roofs are flat and unpainted. Generally, the outer walls of non-high rise buildings are made of concrete or red bricks with flat roofs.

In the case of high rise buildings, air ventilation, heating and cooling are done by their own central systems. Therefore, most of the time, the windows are closed. On the other hand, in the case of residential houses, air ventilation is done by natural circulation via windows. Heating is done by central systems, while cooling (air conditioning) is done independently in every house.

Sidewalks are 10 m wide and are covered with ceramic tiles or cement bricks. There are storm sewers to prevent flooding between roadways and walkways. Avenues are lined with plane trees, which are deciduous trees with broad leaves. Plane trees 7 m in height are planted at 8 m intervals. The leaves of the plane tree emerge in early April and fall in late November.

Figure V.4 shows a close up photograph of Region 2, which is about 1.5 km to the northeast of Region 1. Region 2 is a park area of 66 027 m^2 for the rest and relaxation of residents. The pine tree (a coniferous tree) is a typical species in the park area. In addition to pine trees, deciduous trees and shrubs are sparsely planted in the park. Pine trees are 3 to 10 m tall, depending on age. Walking paths are 1.5 m wide and covered with cement bricks. There is a small plaza at the entrance of the park, and its surface is covered with cement bricks or ceramic tiles. Other areas are covered with soil or lawn. Sports facilities are provided for the health of residents in some places, and benches are provided for rest.

Around the park, there are apartment towns for residential purposes. Most of the apartments are 12 storey buildings with flat roofs; the height between floors is 2.5 m. In the park area, there is an office building of 3 stories with a flat roof, and a parking lot covered with concrete. The outer walls of the office building are covered with red bricks. The roadway running east-west, adjacent to the park, is 56 m wide; the roadways running south-north are 25 m wide.

V.3. INPUT INFORMATION

For each scenario described below, participants were asked to assume an initial time integrated radionuclide concentration in air at ground level of 1 $MBq \cdot d \cdot m^{-3}$. Modelling is done separately for: (1) each of two radionuclides (^{60}Co or ^{239}Pu); (2) three types of weather (dry, light rain, or heavy rain) at the time of deposition; and (3) two locations (Region 1 or Region 2). Participants were asked to assume that the initial deposition event occurred on 1 June of Year 0. Additional calculations assuming an event occurring on 1 January of Year 0 were encouraged, but not mandatory. Radionuclides were assumed to be in an unspecified chemical form with a particle size of 1 μm. For this exercise, ‘light rain’ was defined as 3 mm per day, and ‘heavy rain’ was defined as 20 mm per day.

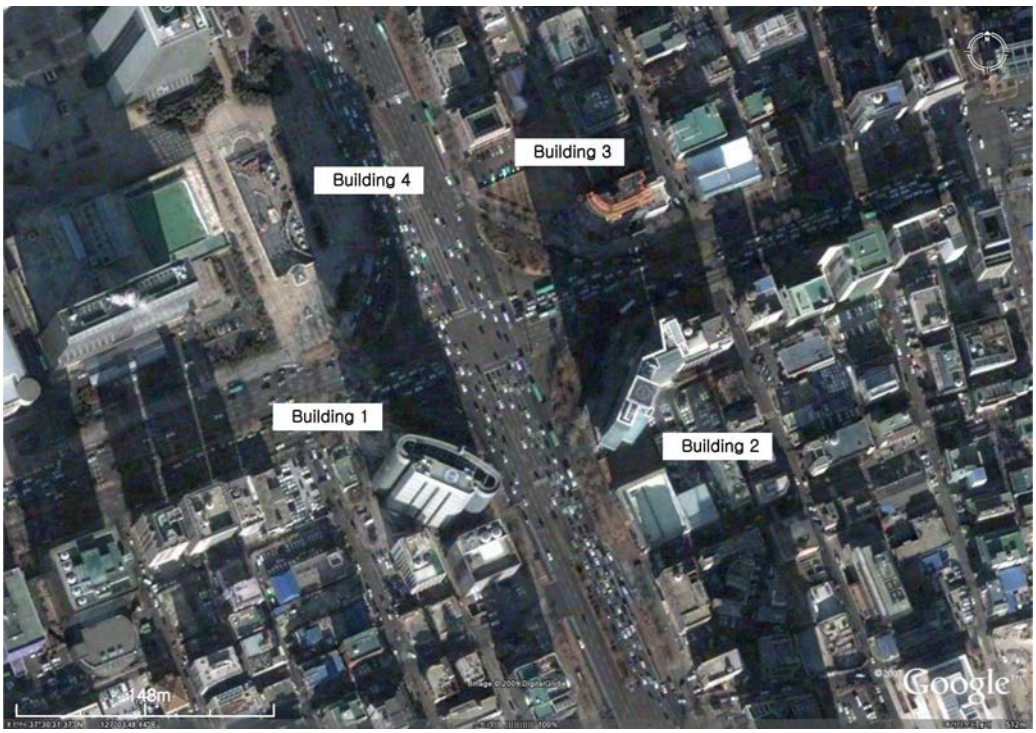

FIG. V.3. Close up photograph of Region 1 (business area). Three test locations are inside Building 1 (Location #1, ground floor; Location #2, 10th floor; Location #3, 24th floor, which is the top floor). Location #4 is outside, at street level on a concrete sidewalk in front of Building 1 (©2007 Google, Image ©2009 DigitalGlobe).

FIG. V.4. Close up photograph of Region 2 (park area). Both test locations are outside. Location #5 (labelled E1) is at the center of the park, outdoors on a dirt (soil) pathway. Location #6 (labelled E2) is at the east side of the park, outdoors on a paved (concrete) parking lot (©2007 Google, Image ©2009 DigitalGlobe).

TABLE V.5. LIST OF COUNTERMEASURES (PROTECTIVE ACTIONS, INCLUDING REMEDIAL ACTIONS) AND THE CORRESPONDING TIME OF APPLICATION FOR USE IN THE MODELING EXERCISE

	Countermeasure	Time of application (after the accident)
1	No countermeasures	–
2	Relocation of population (temporary)	For the first 6 weeks
3	Removal of trees (or leaves)	Day 30
4	Vacuuming or sweeping of roads	Day 14 (no rain)
5	Washing or hosing of roads	Day 14 (no rain)
6	Washing of roofs and exterior walls	Day 14 (no rain)
7	Cutting and removal of soil (5 cm) and grass (park location)	Day 7 for grass, day 180 for soil
8	Combination (1)—tree removal plus road cleaning	
9	Combination (2)—relocation plus road cleaning	

Test locations for Region 1 include three indoor locations in Building 1 (ground floor, 10th floor, and 24th floor; the 24th floor is the top floor) and one outdoor location, outside Building 1. These locations are shown in Fig. V.3. Test locations for Region 2 include the center of the park and a location in the parking lot at the edge of the park. These locations are shown in Fig. V.4.

V.4. MODELLING ENDPOINTS FOR MODEL INTERCOMPARISON

The modelling endpoints described below were to be calculated for this exercise. These endpoints were used for intercomparison among participants in the exercise. Example formats for submitting model predictions were provided to the participants. Where possible, uncertainties on the model predictions need to be provided.

For each test location and each applicable countermeasure (Table V.5), participants were asked to calculate the dose rates and radionuclide concentrations first without any countermeasure, i.e. 'no countermeasures' and then with the indicated countermeasure. For dose calculations, participants were asked to predict the annual doses for each reference exposure scenario (listed below) with no countermeasures and then with the indicated countermeasure. Internal doses need to be identified as the initial dose (cloud), the dose from resuspension, or both.

V.4.1. Cobalt-60

For ^{60}Co, the default modelling endpoints for this scenario are as follows:

(1) Contamination density (Bq/m^2) on a paved (concrete) surface at outdoor locations;
(2) External exposure rates (external dose rates, mGy/h) at each location, from all relevant surfaces (by surface and total);
(3) Contributions to the external dose rates (%) from each surface, for the most important surfaces;
(4) Annual and cumulative external doses (mSv) for specified reference (hypothetical) exposure scenarios; and
(5) Effectiveness of countermeasures in terms of the reduction in external dose rates and external doses.

Optional modelling endpoints for ^{60}Co are as follows:

(1) Annual and cumulative internal doses (mSv) for specified reference (hypothetical) exposure scenarios; and
(2) Effectiveness of countermeasures in terms of the reduction in internal doses.

V.4.2. Plutonium-239

For ^{239}Pu, the default modelling endpoints for this scenario are as follows:

(1) Contamination density (Bq/m^2) on a paved (concrete) surface at outdoor locations;
(2) Annual and cumulative internal doses (mSv) for specified reference (hypothetical) exposure scenarios; and
(3) Countermeasure effectiveness in terms of the reduction in internal doses.

Optional modelling endpoints for ^{239}Pu are as follows:

(1) External exposure rates (external dose rates, mGy/h) at each location, from all relevant surfaces (by surface and total);
(2) Contributions to the external dose rates (%) from each surface, for the most important surfaces;
(3) Annual and cumulative external doses (mSv) for specified reference (hypothetical) exposure scenarios; and
(4) Effectiveness of countermeasures in terms of the reduction in external dose rates and external doses.

Model calculations need to start following the initial deposition and carried forward for 5 years (1 day, 1 week, 1 month, 3 months, 1 year, 2 years, and 5 years). Results can then be presented as a time series, with the date specified for each predicted dose rate, dose, or radionuclide concentration. Example formats were provided to the participants. Participants were asked to include uncertainties on the predictions, where possible.

V.4.3. Exposure scenarios for dose calculations

Exposure scenarios for dose calculations are as follows:

(1) Business area (Region 1). Assume 40 hours per week indoors (at work) and 5 hours per week outside building (lunch break). Assume an inhalation rate of 0.5 m^3/h indoors (sitting) and 1 m^3/h outdoors (standing or walking). Assume that the person is an adult.
(2) Park area (Region 2). Assume 3 hours per week (0.5 hours per day, 6 days per week) for an older man exercising in the park. Assume an inhalation rate of 1.5 m^3/h (moderate exercise).

The countermeasures (protective actions, including remedial actions) to be considered are listed in Table V.5, together with the time of application to be assumed.

APPENDIX VI. DESCRIPTION OF MODELS USED TO RUN THE CONTAMINANT TRANSPORT AND COUNTERMEASURES EXERCISE

The contaminant transport and countermeasures exercise was executed by six participants using five models. These included:

- CPHR model (run by J. Tomás Zerquera, Cuba);
- CHERURB model (run by S.L. Chouhan, Canada);
- ERMIN model (run by T.W. Charnock, UK);
- METRO-K (run by W.T. Hwang, Korea); and
- RESRAD-RDD (run by S. Kamboj and C. Yu, USA).

Descriptions of each of these models and their assumptions are provided in the following sections.

VI.1. DESCRIPTION OF CPHR

The CPHR code was developed and used for the Countermeasures exercise (which covered contaminant transfer and effectiveness of countermeasures (protective actions, including remedial actions) by J. Tomás Zerquera of the Centro de Protección e Higiene de las Radiaciones in Cuba [VI.1].

VI.1.1. Introduction

The CPHR code was developed by the Centro de Protección e Higiene de las Radiaciones (CPHR) in support of an emergency preparedness programme in Cuba and in the framework of the EMRAS I Programme [VI.2–VI.4]. The code uses information (parameter values and approaches) available from best practices. Some parameter values were chosen using professional judgment. The code is based on the ECOLEGO code developed by Facilia AB in Sweden[28].

VI.1.2. General features

CPHR is a compartment model and uses a conservative approach (tending towards overestimation) for an average set of conditions. The model considers the contribution of each compartment to a location 'cluster' configured at the point of interest, on a percentage basis. As developed during the EMRAS I programme, the model considered the following compartments:

- Paved surfaces (for artificially covered surfaces);
- Surface soil (for all open areas, not artificially covered);
- Roofs (for covers of all buildings);
- Trees (for areas covered by trees);
- Walls (for all vertical surfaces in buildings); and
- Deep soil (for considering the migration from the top layers of soil to the deeper layers).

For the present exercise, which was carried out during the EMRAS II programme, the model considered the same set of compartments plus two additional compartments, as follows:

- Air (the initially contaminated compartment); and
- Drains (for considering the sewerage systems).

[28] https://home.facilia.se

TABLE VI.1. SUMMARY OF PARAMETER VALUES USED IN THE COUNTERMEASURES EXERCISE

Parameter		Values
Dry deposition velocity		400 m/d for Co; 800 m/d for Pu
Washout coefficient		0.001 mm m d^{-2}
Environmental half-lives	Roofs	170 d for Co; 480 d for Pu
	Walls	180 d
	Trees	180 d
	Paved surfaces	30 d
	Soil	30 d
Filtration factor		0.7

VI.1.3. Key assumptions

Key assumptions for the Countermeasures exercise included the following:

- The resuspension transport process was assumed to be negligible.
- Transport of contaminants out of the modelled system occurred only through the 'drains' compartment.
- Both external and internal dose rates were considered.
- No rain and light rain at the time of deposition were considered, as specified.

Table VI.1 summarizes key parameter values used in the exercise.

VI.2. DESCRIPTION OF CHERURB

The CHERURB (Chalk River Environmental Research Branch Urban Contamination and Dose Model) code was used for the Countermeasures exercise by S.L. Chouhan of the Canadian Nuclear Laboratories (formerly Atomic Energy of Canada Limited) in Canada [VI.1].

VI.2.1. Introduction

CHERURB is a time dependent code that can be used to assess the impact of an accidental atmospheric release of ^{137}Cs, ^{131}I, ^{103}Ru, ^{106}Ru, and/or ^{238}U in the vicinity of a city [VI.5]. In order to complete the EMRAS II WG9 Countermeasures exercise, ^{60}Co and ^{239}Pu were added and DCFs were updated in CHERURB; most other parameter values for these radionuclides were kept the same as for ^{103}Ru because the size of contamination particles was consistent (1 μm).

The code can be used to calculate inhalation, immersion, and groundshine doses to an adult, child (age 10) and infant (age 1) at indoor and outdoor locations during the passage of a plume, and doses from deposited activity years after (see Fig. VI.1). The code predicts a best estimate and a 95% confidence interval and can be used to calculate reductions in dose due to weathering and decontamination processes (see Fig. VI.2). The code can help in the estimating of the cost effectiveness of dose reduction measures.

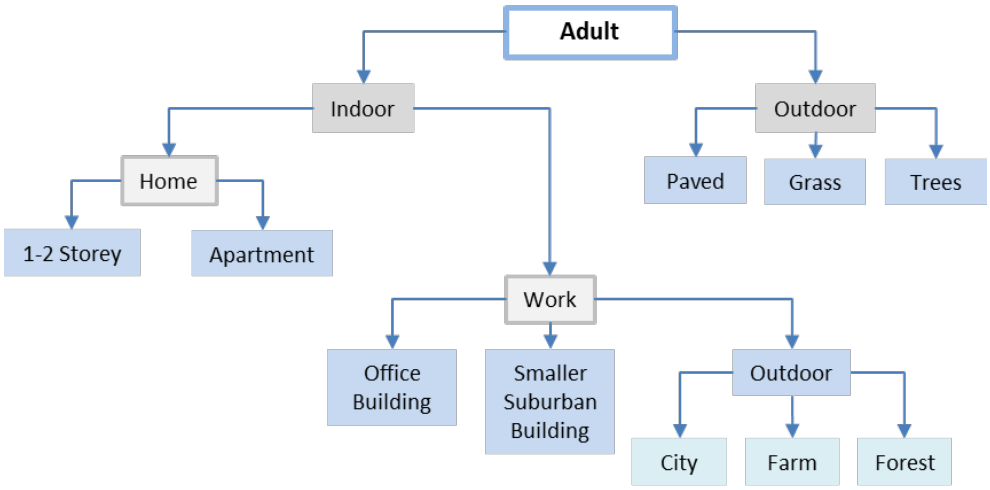

FIG.VI.1. Example of lifestyle and building characteristics modelled by CHERURB (modified from Ref. [VI.5]).

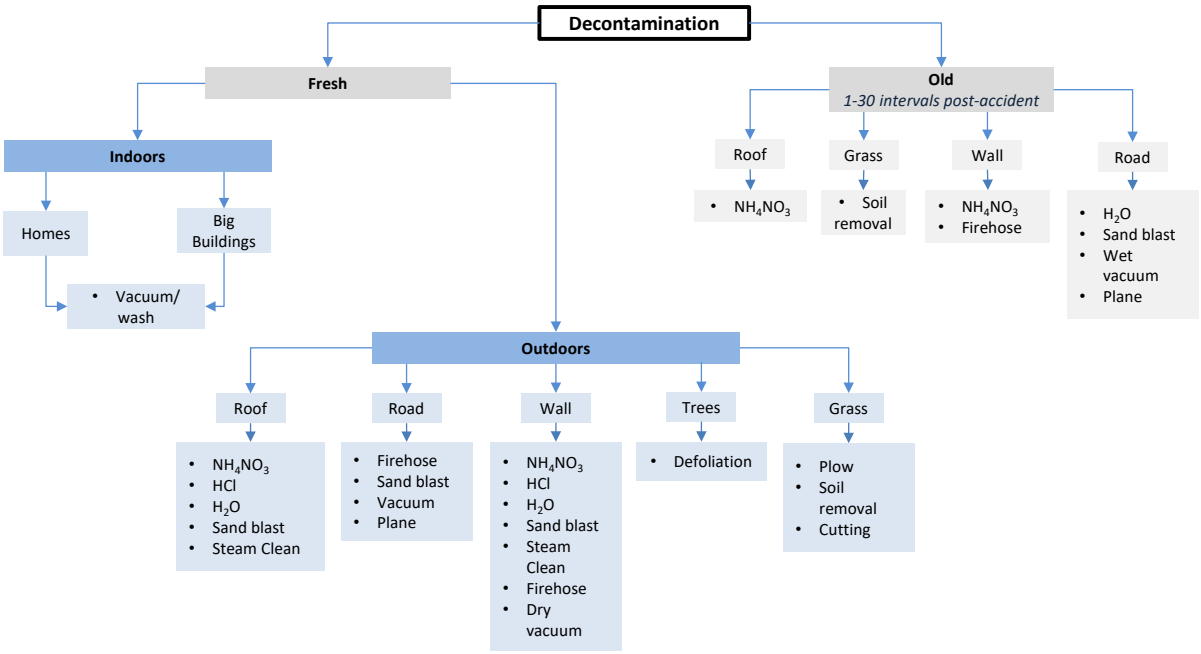

FIG.VI.2. Decontamination processes.

VI.2.2. Model details for CHERURB

CHERURB can be used to model elemental, organic and particulate forms for Iodine. The code can handle various building sizes (single family house, prefabricated house, semidetached house, townhouse, apartment house, workplace and school) and outdoor environments. Indoor locations that can be modelled using the CHERURB code include the basement to the fifth floor, and the attic. Outdoor locations that can be modelled include front, side, back, street and courtyard locations.

Dry and wet deposition on five surfaces (roof top, walls, roads, lawn, trees) can be modelled using the code, in addition to fresh and old deposition, and fixation of contaminants.

The code can handle rain events using surface type specific parameter values (e.g. runoff occurs after a certain critical amount of precipitation).

VI.2.3. Inputs

Model input parameters include [VI.5]:

- Radionuclide activity concentration in air and precipitation data (the preferred starting point);
- Measured deposition on any surface (an optional starting point);
- Fraction of time an adult, child and infant spent in different locations (data specific to conditions in Toronto, Canada, are already in the code);
- Many general and nuclide specific parameters [VI.5];
- Dimensions of rooms (representing relevant rooms in the indoor living area);
- Decontamination information; and
- Distributions of input parameters (normal, lognormal, uniform, triangular, and user specific) and correlation coefficients between the parameters.

VI.3. DESCRIPTION OF ERMIN

The ERMIN code was used for the Countermeasures exercise by T.W. Charnock of the Health Protection Agency in the United Kingdom [VI.1].

VI.3.1. Introduction

The ERMIN (European Model for Inhabited Areas) tool was applied to the Countermeasures exercise.

The purpose of the ERMIN model is to provide a tool for a user to explore different recovery options following the contamination of an urban environment with radioactive material and, ultimately, to develop an appropriate remediation strategy. It is intended to be used both for planning and for evaluation of different remediation strategies after an incident.

The model has been implemented as an interactive tool within the Real-time On-line DecisiOn Support (RODOS) and ARGOS Nuclear Emergency Decision Support Systems. In both systems, a map-based interface is used; users delineate zones of different urban environments and different levels of radionuclide deposition on a map. Users also indicate areas where different combinations of recovery countermeasures are to be applied. Figure VI.3 shows a screen shot from the RODOS implementation of ERMIN.

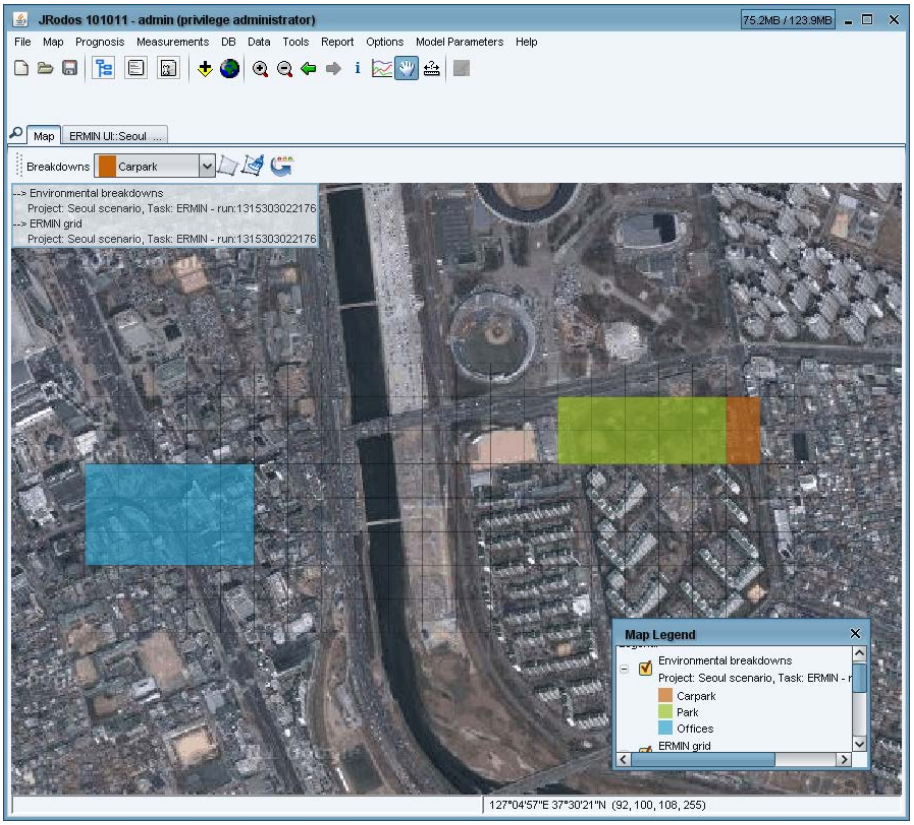

FIG. VI.3. A typical screen shot of the RODOS ERMIN user interface. Here the user delineates three zones in the environment, representing office blocks in Region 1 of the scenario and representing park and car parks in Region 2.

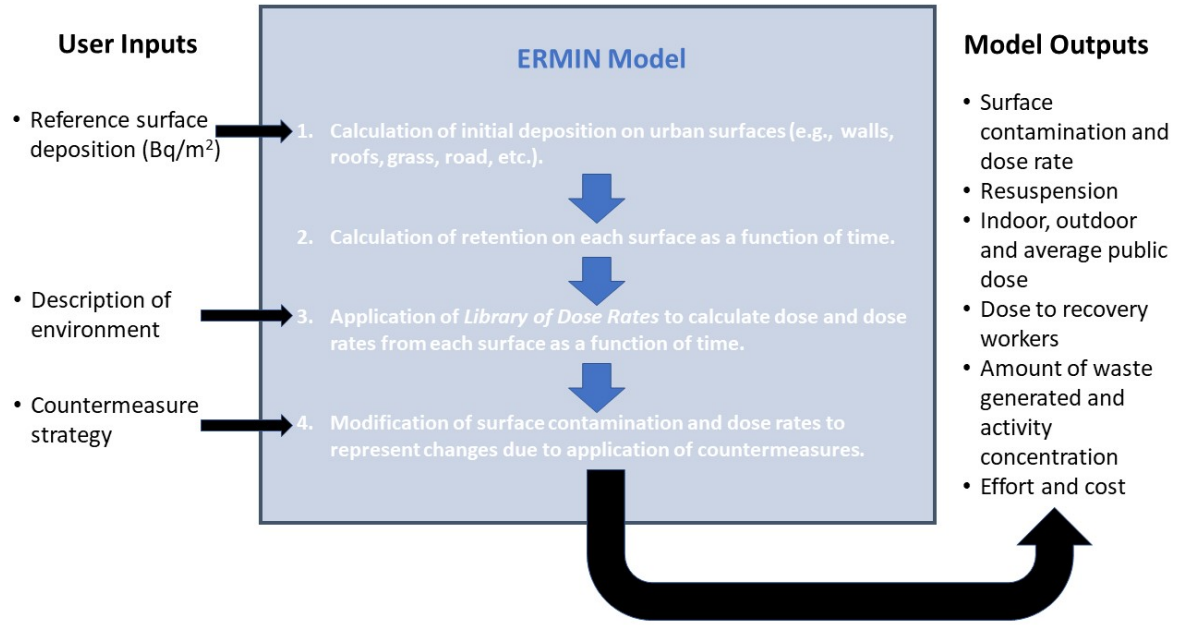

FIG. VI.4. Stages of the ERMIN calculation (modified from Ref. [VI.6]).

ERMIN applies ratios to estimate the deposition on representative urban surfaces, based on the input deposition to the grass reference surface. Long term surface retention of radionuclides on each surface and transfers between surfaces are represented as empirical functions; radionuclide migration in soil is simulated using a convective dispersive model. A library of dose rates for surfaces in idealized urban environments is applied to calculate dose rates indoors and outdoors. Different countermeasures are represented through modifying the surface contamination and dose rates. Outdoors, resuspension is modelled using an approach involving a simple resuspension factor; indoors, resuspension is modelled using an indoor resuspension factor together with a filter factor applied to the outdoor activity concentration in air. Full details of the models are provided in the ERMIN model description [VI.6, VI.7], and Fig. VI.4 illustrates the stages of the ERMIN calculation.

The ERMIN model considers the following urban surfaces:

— Paved surfaces, subdivided into roads, sidewalks and other paved surfaces;
— External walls of buildings;
— Roofs of buildings;
— Internal surfaces of buildings;
— Grass and 9 soil layers under the grass;
— Plants and 9 soil layers under the plants;
— Bare soil with 9 layers; and
— Trees, subdivided into deciduous and coniferous trees.

In addition, ERMIN can be used to estimate activity concentrations in outdoor and indoor air, as a result of the resuspension of deposited activity.

Output information generated by the ERMIN includes estimates of:

— Average doses to members of the public from external exposure to gamma and beta radiation from deposited radionuclides and from inhalation of resuspended radioactivity;
— Contamination on urban surfaces;
— Activity concentrations in air due to resuspension;
— Doses to workers undertaking the recovery work;
— The quantity and activity of waste generated; and
— The cost and work necessary to implement various countermeasures.

The outputs generated using ERMIN can then be used with RODOS and ARGOS; results can be presented as a grid overlain onto a background map for visualization or summarized over a region, or in table format.

VI.3.2. Key assumptions

ERMIN makes a number of key assumptions appropriate to its function for planning and for scoping the consequences of possible recovery strategies after a real event.

ERMIN considers a number of urban surfaces but treats the activity as averaged over a given surface. Within an urban environment, the model does not account for the patchiness of deposition that could be caused, for example, by the different orientations with respect to wind direction of different parts of a surface, or the effects of small scale differences in surface roughness.
In using ERMIN, the real urban environment of concern is represented by the user, based on proportions of idealized urban environments for which complex Monte Carlo dose modelling has been performed. Generally, the Monte Carlo modelling exercises have used a few receptor locations indoors and a few outdoors to be representative of all locations indoors or outdoors. The ERMIN dose library includes dose rates for all of these receptor locations; however, the doses calculated and presented to the user are weighted averages, and for each environment, ERMIN generates only one overall indoor and one overall outdoor dose. For this reason and because ERMIN cannot be used to represent patchiness, the doses and dose rates are not for specific indoor and outdoor locations but are representative of the doses received by a person moving around in that environment. A person remaining at a specific location within an environment, for an example, an invalid in a bedroom close to the roof, may receive a very different dose, and the relative contribution of various urban surfaces to that dose may be different from that calculated using ERMIN.

ERMIN cannot be used to model short term changes caused by varying weather conditions. Instead, it uses retention factors to represent the long term effects of weathering on the retention of activity on urban surfaces. It also cannot be used to model the effects of individual rainfall events that might wash material away more quickly over a short period of time, that might temporarily suppress resuspension or that might lead to a wet surface that effectively shields beta radiation over a period of time. The overall effect is a temporal smoothing of the dose profile.

VI.3.3. Modelling approaches (conceptual and mathematical)

Full details of the modelling approaches used in ERMIN are provided in the ERMIN model description [VI.7] and in two published papers [VI.6, VI.8].

VI.3.4. Parameter values

Full details of parameters are given in the ERMIN model description [VI.7].

VI.3.5. Uncertainties

ERMIN cannot be used to calculate uncertainties.

VI.3.6. Application of the model to the countermeasures exercise

VI.3.6.1. Initial deposition

The principal input to ERMIN is the initial deposition of radionuclides onto a lawn. The Countermeasures exercise, as presented, does not provide this input, but provides only the integrated activity concentration in air. Therefore, the initial deposition that was calculated using the METRO-K model was used as the input into the ERMIN model.

For a 1 $MBq \cdot d \cdot m^{-3}$ integrated activity concentration in air and for each deposition condition specified in the exercise, the following initial depositions where used:

- Dry deposition: 52.9 MBq/m^2
- Deposition in light rain: 2.83 GBq/m^2
- Deposition in heavy rain: 17.2 GBq/m^2

TABLE VI.2. IDEALISED URBAN ENVIRONMENTS IN THE ERMIN LIBRARY

ERMIN Ideal Environments	Available Parameter Sets for Adjustment of Proportions of Outdoor Surfaces
Street of detached prefabricated houses	No trees – low – medium (default) – high trees Low paved – medium (default) – high paved
Street of semidetached houses with basements	No trees – low – medium (default) – high trees Low paved – medium (default) – high paved
Street of semidetached houses without basements	No trees – low – medium (default) – high trees Low paved – medium (default) – high paved
Street of terraced houses	No trees – low – medium (default) – high trees Low paved – medium (default) – high paved
Multistorey block of flats amongst other house blocks	No trees – low – medium (default) – high trees Low paved – medium (default) – high paved
Multistorey block of flats opposite parkland	No trees – low – medium (default) – high trees Low paved – medium (default) – high paved
Industrial site (incomplete library)	Medium trees and medium paved
Large open area	Park (default); mostly grass, some trees, some paved Playing fields; mostly grass, few trees, little paved Car park; mostly paved, few trees, little grass Ideal; all grass, no trees, no paved

In accordance with the aim of making ERMIN easy to use, ERMIN users can choose between three deposition options, rather than specifying actual rainfall rates. The deposition options are:

— Completely dry deposition;
— The scenario where depositions from dry and wet components are roughly equal; and
— Mostly wet deposition.

For the current modelling exercise, these were assumed to correspond to the conditions as specified in the exercise.

VI.3.6.2. Urban environment

ERMIN has a number of idealized urban environments, which the user can assemble in different proportions to represent the real environment that is of interest. Each idealized environment has a number of named parameter sets representing different proportions of outside surfaces that can be used to refine a given environment description. Table VI.2 provides a list of the environments available in the ERMIN library.

Unfortunately, none of the environments is a satisfactory match for the high rise glass office blocks in Region 1 of the modelling exercise. The closest match is the 'Multistorey block of flats amongst other house blocks' environment; however, this environment has largely concrete walls and is not a high rise. This environment has two outdoor locations: 1. outside in the street; and 2. outside in a central courtyard. It also has four indoor locations: 1. basement; 2. first floor (ground floor in the UK); 3. third floor (second floor in the UK); and 4. fifth floor (fourth floor in the UK), which is the top floor. For a normal ERMIN run, these receptor locations would be given equal weight and an average dose rate for the building would be calculated; however, in order to represent the locations in the business region, the weights were changed for this modelling exercise (described below), as were the assumptions about the contributing surfaces (also described below).

Figure VI.5 shows the sources and indoor receptors in the 'multistorey' environment. In the ERMIN library, all source surfaces contribute to dose rate at all receptor locations. Figure VI.6 shows how contributions can increase or decrease rapidly with height over just a few floors. The office block in Region 1 of the exercise has 24 floors, and as a result, some modifications and simplifications in assumptions were justified.

Figure VI.7 shows how the contributions to dose rate at the indoor receptor locations were modified. To represent Location 1 (i.e. the ground floor of the office block), the receptor location on the 1st floor of the multistorey building was used, and it was assumed that there was no contribution to dose from the roof. To represent Location 2 (i.e. the 10th floor of the office block), the 3rd floor receptor location in the multistorey building was used, and it was assumed that there was no contribution to dose from the roof, paved, soil or tree surfaces. To represent Location 3 (i.e. the top floor of the office block), the top floor receptor location was used, and it was assumed that there was no contribution from paved, grass or tree surfaces. To represent Location 4 (i.e. outdoors next to the office block), the outdoor in the street receptor location was used, and it was assumed that there was no contribution from the roof.

Locations 5 and 6 in a park and a car park, respectively, were easier to represent, having obvious matches in the ERMIN environment library. Table VI.3 summarizes how each location was represented in ERMIN.

The model comparison exercise also specifies two dose scenarios (Table VI.4): 1. an office worker who spends 40 hours per week inside Building 1 and 5 hours per week outside Building 1; and 2. a person who spends 3 hours per week using the park in Region 2.

It is not clear from the exercise where in the building the office worker is located; however, wherever he or she works, the office worker will have to pass through the ground floor to enter and leave the building. Therefore, in order to represent the office worker, the ERMIN library was weighted to use the 3rd floor location, but unlike for the dose rate scenario at Location 2 (Table VI.4), contributions from all surfaces were included. This is a conservative assumption, as it is unlikely that the office worker would be receiving significant contributions from the roof and paved/tree/grass surfaces at the same time. The results from this part of the modelling exercise are similar to those that would be generating using RODOS and ARGOS users.

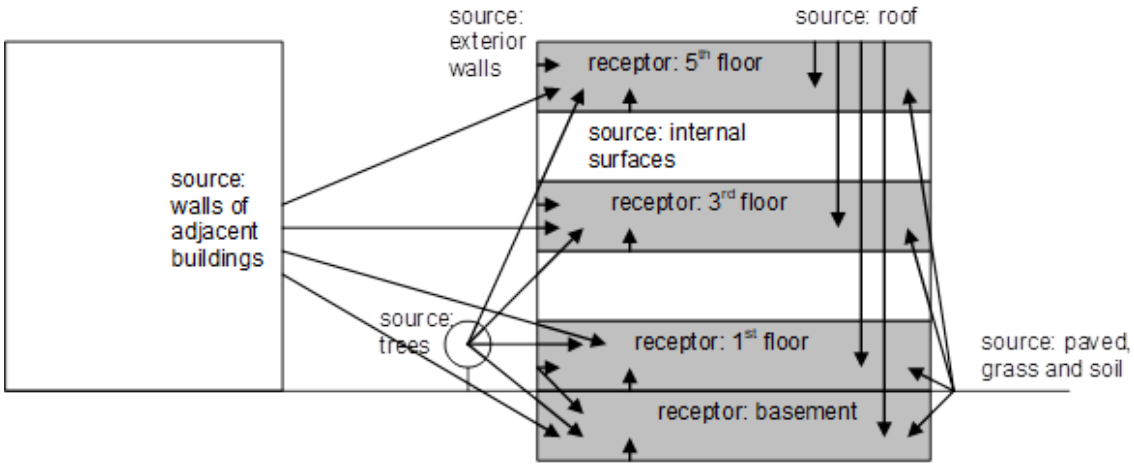

FIG. VI.5. The sources and receptors in the multistorey environment.

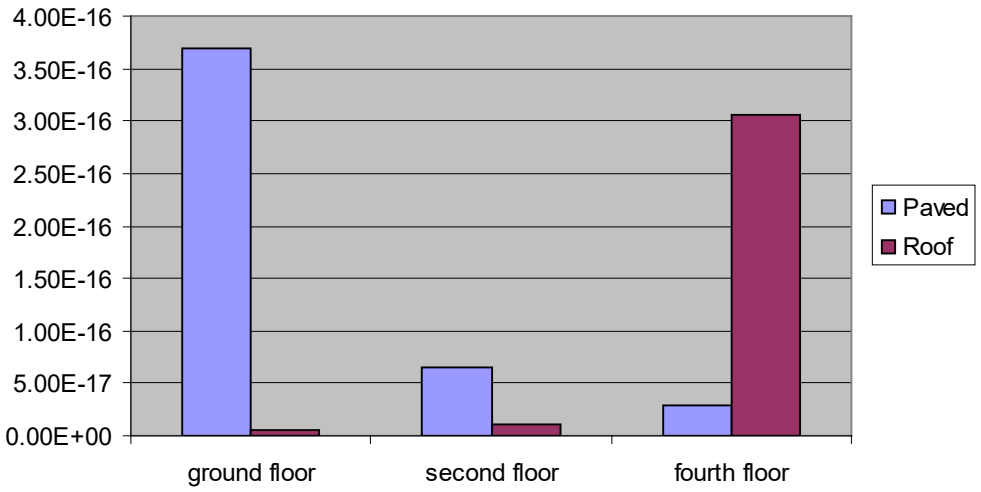

FIG. VI.6. Dose rates from ^{60}Co at various indoor locations in a multistorey environment from activity deposited on paved and roofed surfaces per unit area of surface (Gy day^{-1} m^{-2} per Bq).

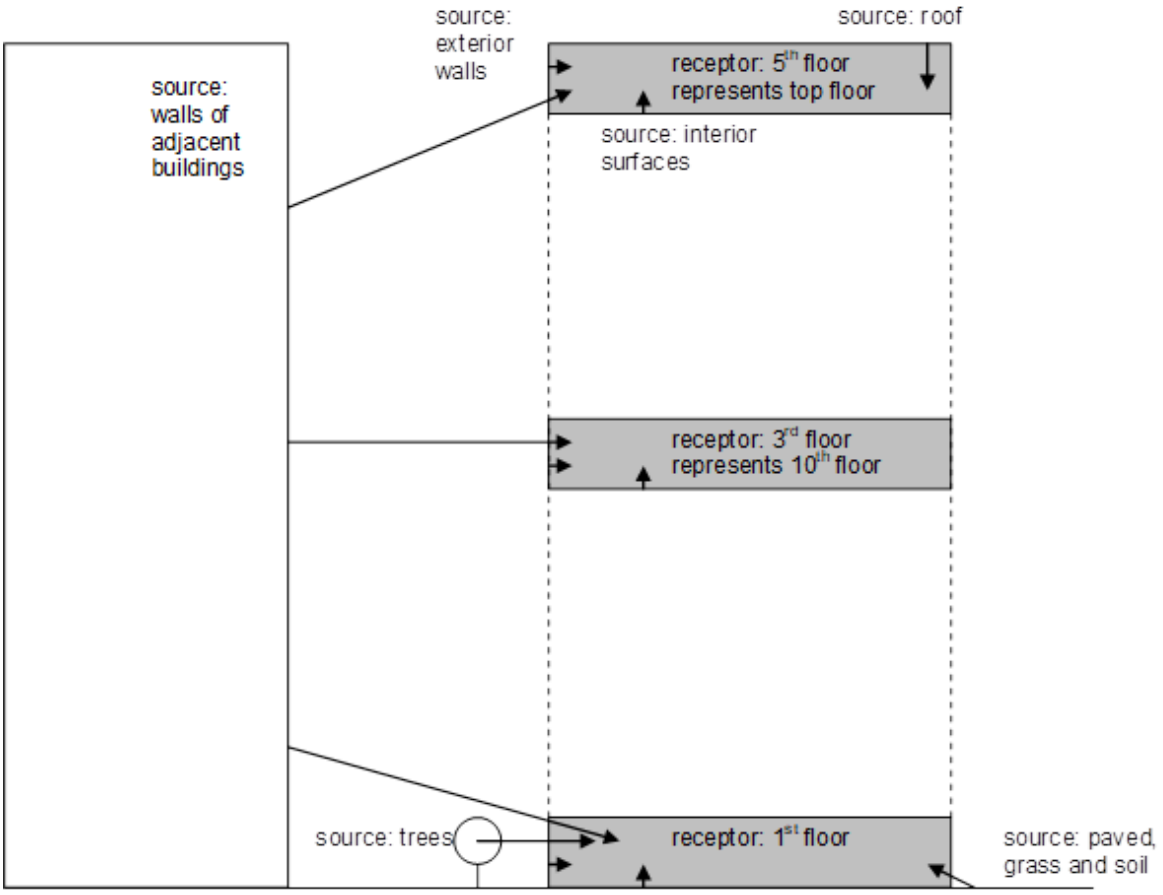

FIG. VI.7 Modification of the receptor locations in the ERMIN 'multistorey' environment to represent the glass office block in the modelling scenario.

TABLE VI.3. SCENARIO LOCATIONS AND THEIR REPRESENTATION IN ERMIN

Scenario location	Representation in ERMIN
Location 1 (1st floor (ground floor) inside Building 1)	Indoor location in the multistorey environment with 'default trees and high paved' parameter set. The unit dose rates were weighted to use the 1st floor (ground floor in the UK) location and to ignore the basement, 3rd and 5th floors. No contribution from roofs was included.
Location 2 (10th floor inside Building 1)	Indoor location in the multistorey environment. The library was weighted to use the 3rd floor location (2nd floor in the UK). No contribution from roofs, paved, grass or tree surfaces was included.
Location 3 (top floor of Building 1)	Indoor location in the multistorey environment. The library was weighted to use the 5th floor location (4th floor in the UK). No contribution from paved, grass or tree surfaces was included.
Location 4 (outdoors near Building 1)	Same as for Location 1, but outside. The library was weighted to use the outdoor in the street location.
Location 5 (centre of park)	'Open area' using 'Park' parameter set
Location 6 (east side of park on paved surface)	'Open area' using 'Car park' parameter set

TABLE VI.4. EXPOSURE SCENARIOS AND THEIR REPRESENTATION IN ERMIN

Scenario No.	Scenario Location	Representation in ERMIN
1	An office worker who spends 40 hours per week inside Building 1 and 5 hours per week outside of Building 1	The office worker is assumed to spend their time in the multistorey environment with the 'default trees and high paved' parameter set at 3rd floor receptor location (2nd floor in the UK) and outdoors at the street location.
2	An older person exercising in the park for 3 hours per week	The person is assumed to spend their time in the open area environment with the 'Park' parameter set

TABLE VI.5. RATIOS OF DEPOSITION ON URBAN SURFACES RELATIVE TO DEPOSITION ON LAWN FOR TWO PARTICLE SIZE GROUPS IN ERMIN. THESE RATIOS ACCOUNT FOR INTERCEPTION AND FOR IMMEDIATE RUNOFF WITH RAIN WATER

Weather	Aerosol AMAD[a]	Paved	Roof	Walls	Interior	Tree	Grass	Plants	Soil
Dry	<2 μm	0.3	0.7	0.05	0.0417	2.5	1	1.5	0.3
	2–5 μm	0.7	4	0.1	0.0411	5	1	1.5	0.3
Dry/wet	<2 μm	0.57	0.7125	0.02	0.0208	1.53	0.8	1.105	0.65
	2–5 μm	0.8075	2.28	0.05	0.00205	2.55	0.8	1.105	0.65
Wet	<2 μm	0.45	0.425	0.01	0.00208	0.5	0.1	0.2	1
	2–5 μm	0.45	0.3825	0.01	0.00205	0.25	0.1	0.3	1

[a] AMAD: activity median aerodynamic diameter.

VI.3.6.3. Particle size

The modelling exercise specifies a particle size of 1 μm activity median aerodynamic diameter (AMAD); however, in ERMIN, by default, both of the radionuclides included in this exercise (^{60}Co and ^{239}Pu) are in the 2–5 μm AMAD particle size group. For the current exercise, both radionuclides were reassigned to the <2 μm AMAD particle size group. Generally, ERMIN assumes that the smaller sized particles (<2 μm AMAD) deposit to a relatively lesser extent on most urban surfaces under dry conditions compared to the larger particle size group (2–5 μm AMAD), as shown in Table VI.5.

VI.3.6.4. Countermeasure effectiveness

The parameters describing decontamination effectiveness for the scenario were the default parameters taken from the ERMIN database which account for both particle size group and time after deposition. For techniques that remove activity from a surface, a decontamination factor (DF) is calculated and applied to the remaining activity on the surface. For techniques that remove the surface, ERMIN assumes that virtually all the radioactivity is removed with the

surface, and so the effectiveness of the technique depends on how much radioactivity has been retained on the surface up to the time of decontamination. Table VI.6 summarizes the assumptions used for each of the countermeasure options in the modelling exercise.

VI.3.6.5. Example results

The results generated using the ERMIN model are described in detail in Section 4 of this publication. For the two radionuclides (^{60}Co and ^{239}Pu), two times of year, three sets of weather conditions and nine countermeasure combinations (including no countermeasures) that are included in the current exercise, the number of combinations of results sets is very large. The results presented here are a subset chosen to illustrate key aspects of the ERMIN model.

VI.3.6.6. Time of year

Within the ERMIN model, the time of the year can be used to indicate whether there are leaves on the trees, and if so, how long those leaves will remain. If there are leaves on the trees, the deposition on the trees is increased, and as a result, the overall deposition in the area is increased, which leads to higher dose rates. This can be seen in Fig. VI.8, which depicts the predicted dose rates from ^{60}Co at different times of the year at two locations (Locations 1 and 6) and under different initial weather conditions, as defined in the exercise (see Appendix V). The dose rates for January are consistently less than the corresponding dose rates for June. The effect is more pronounced at Location 1, where trees on the street can contribute to doses indoors, compared with Location 6, which is a car park away from trees.

VI.3.6.7. Effect of deposition conditions

The effect of the weather at the time of deposition is very marked in Fig. VI.8, where the wet conditions lead to an enhanced overall deposition in an area, and consequently, higher dose rates regardless of the time of year. However, deposition can have a more subtle effect in changing the relative importance of surfaces, which will then change the relative effectiveness of countermeasures. Figure VI.9 depicts the effect of different countermeasures on Exposure Scenario 2; grass cutting is effective under dry conditions, but not under wet conditions, as the activity is deposited on the soil and not on the grass where it can be removed.

TABLE VI.6. DECONTAMINATION OPTION EFFECTIVENESS ASSUMPTIONS USED BY ERMIN FOR THE MODELLING EXERCISE

Countermeasure	ERMIN assumption
No countermeasures	–
Relocation of population (temporary)	Population receives no dose during period of relocation
Tree removal at 30 days	All radioactivity remaining on leaves of tree removed[b]
Vacuuming or sweeping roads at 14 days	DF2.5 to 7 days, reducing to DF1 by 28 days[a]
High pressure hosing roads at 14 days	DF4 to 7 days, reducing to DF1 by 28 days[a]
High pressure hosing roof and high pressure hosing exterior walls at 14 days	DF1.75 to 7 days reducing to DF1 by 28 days[a] DF1.75 to 7 days reducing to DF1 by 28 days[a]
Cutting and removal of grass at 7 days	All radioactivity remaining on grass leaves removed[b]
Soil removal at 180 days	All radioactivity to 5 cm depth removed[b]
Tree removal at 30 days high pressure hosing roads 14 days	All radioactivity remaining on leaves of tree removed[b] DF4 to 7 days, reducing to DF1 by 28 days[a]

Relocation for 6 weeks and high pressure hosing roads at 14 days	DF4 to 7 days, reducing to DF1 by 28 days[a]

[a] Applied to particles of size <2 µm.
[b] Applied to all particle sizes.

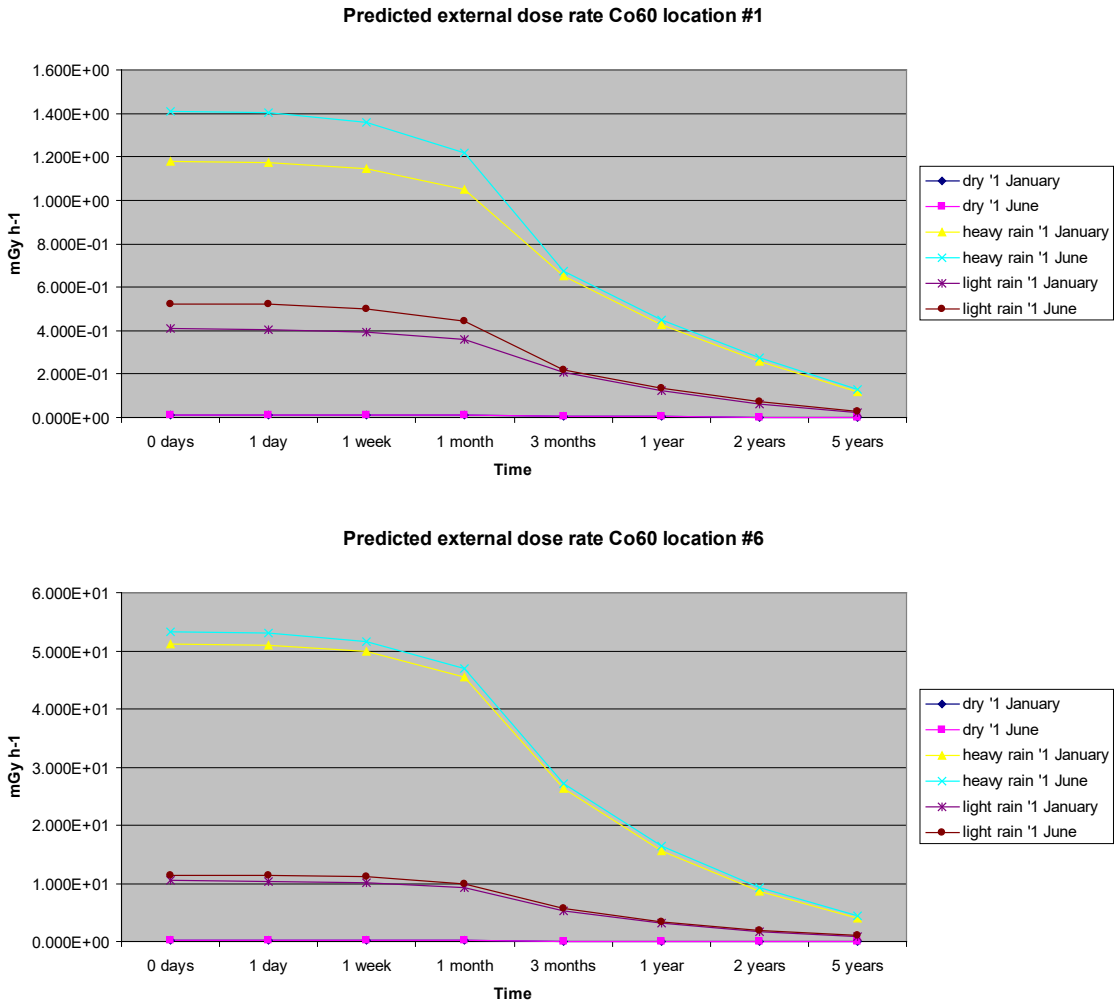

FIG. VI.8. Predicted external dose rates at different times of the year and under different deposition conditions at Locations 1 and 6, as defined in the exercise (see Appendix V).

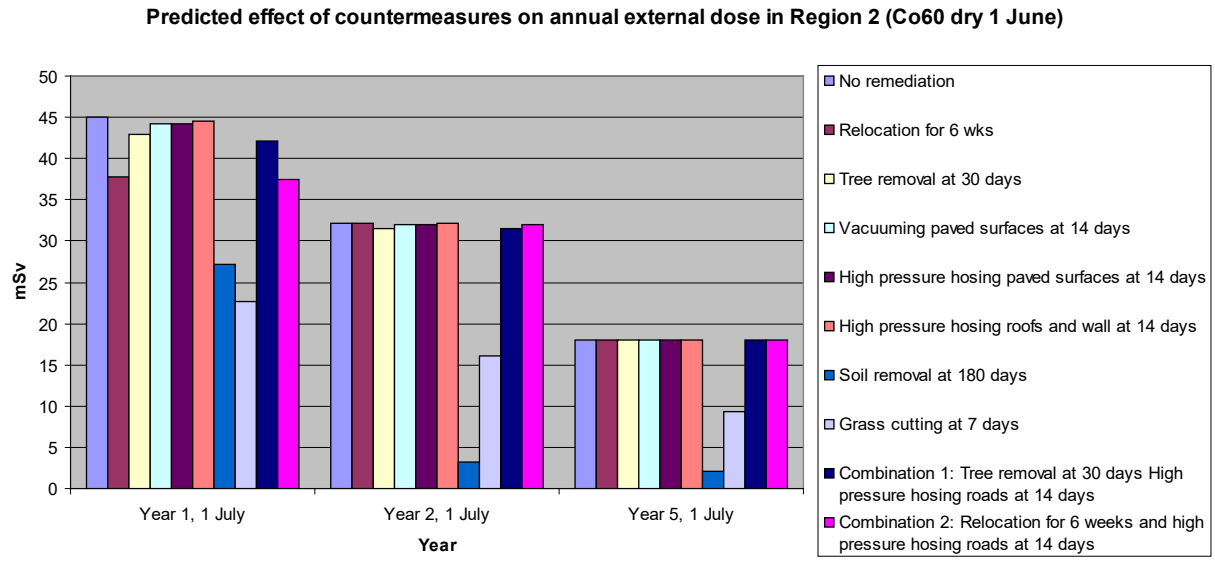

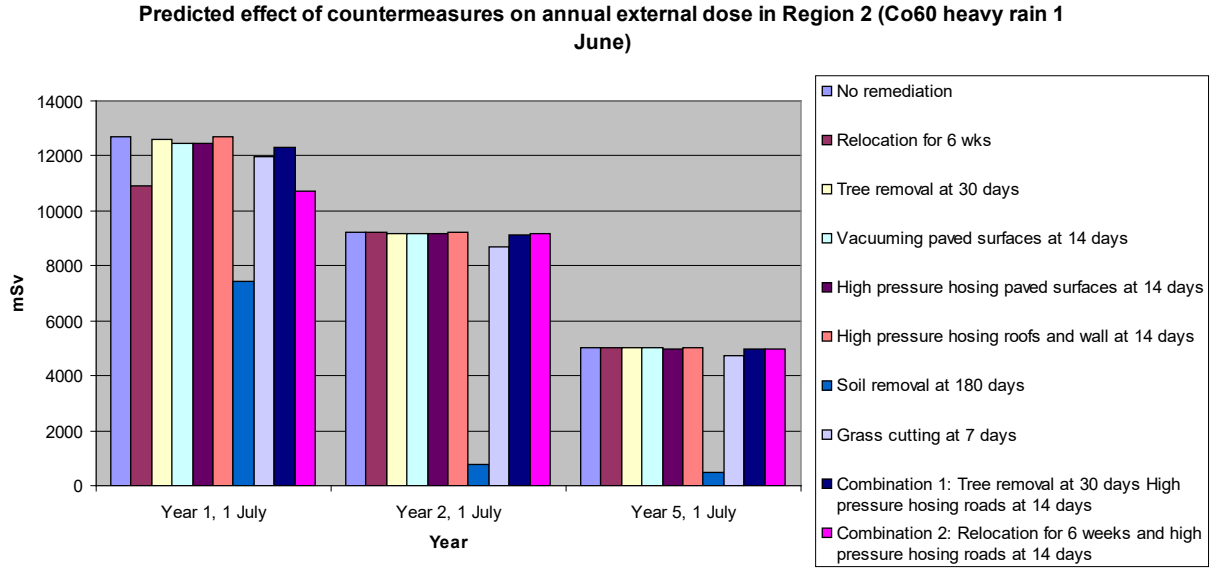

FIG. VI.9. The effect of different countermeasures on annual external dose for Exposure Scenario 2 in June for dry and heavy rain conditions.

VI.3.6.8. Glass office building

In order to better represent glass buildings, a second set of ERMIN runs was performed. For these runs, ERMIN was adapted in two ways: Firstly, it was assumed that material deposited on the walls produced a dose rate that was equivalent to activity deposited on interior surfaces, i.e. it was assumed that the glass offered no shielding to the activity; Secondly, it was assumed that material weathered more quickly from the glass than from concrete. ERMIN by default assumes that the half-life of material on walls is seven years. This was arbitrarily changed to seven months. The expected overall consequence of these changes was to alter the profile of dose from the walls from a long, slow decline to a larger peak with a sharper decline. These changes introduced some inconsistencies into the input, for example, although it is assumed that the glass walls offer no shielding of people indoors to material deposited externally on the glass, the glass walls still offer shielding to material deposited on other outdoor surfaces. Furthermore, it is emphasized that these two assumptions are arbitrary; in particular, it is by no means certain that activity deposited on glass will, in all cases, weather more quickly than activity deposited on concrete. Another factor that has not been addressed is that initial deposition to smooth glass walls may be very different to that on rougher concrete walls. Therefore, results need to be treated with caution and are included for illustrative purposes only. The runs were repeated only for ^{60}Co and not for ^{239}Pu, for which the main hazard is internal exposure.

The modifications had little effect on overall dose rates or doses, likely reflecting the relative unimportance of the external walls under most sets of conditions. As expected, indoor dose rates were generally a little higher for glass buildings than for concrete buildings, particularly for earlier time periods, because of the reduced shielding of the glass; however, the effect of shortening the retention half-life of material on walls was barely discernable. Figure VI.10 shows predicted dose rates at Location 2 for June deposition under dry conditions for both runs of ERMIN. This location was on the 10th floor of the office building and was expected to be the location where differences between glass and concrete walls would be the most significant. As expected, the dose was higher at earlier times for the modified runs (glass buildings). Also, as expected, high pressure hosing of roofs and walls was more effective in the modified run (glass walls rather than concrete walls), although doses remained higher for the glass buildings, reflecting the increased importance of the wall surface in contributing to doses. Finally, the expected effect that doses in the long term were higher in the unmodified run than in the modified run was just discernable.

In conclusion, the attempt to modify the dose libraries for glass buildings made little difference overall. The main difference was to raise the dose slightly during the first few years, due to the low shielding with respect to material deposited on exterior walls. This being the case, it is likely that a more important effect that was not captured in these model runs was the lower shielding that glass walls present to doses from other outdoor surfaces, especially paved areas and trees, compared to concrete walls.

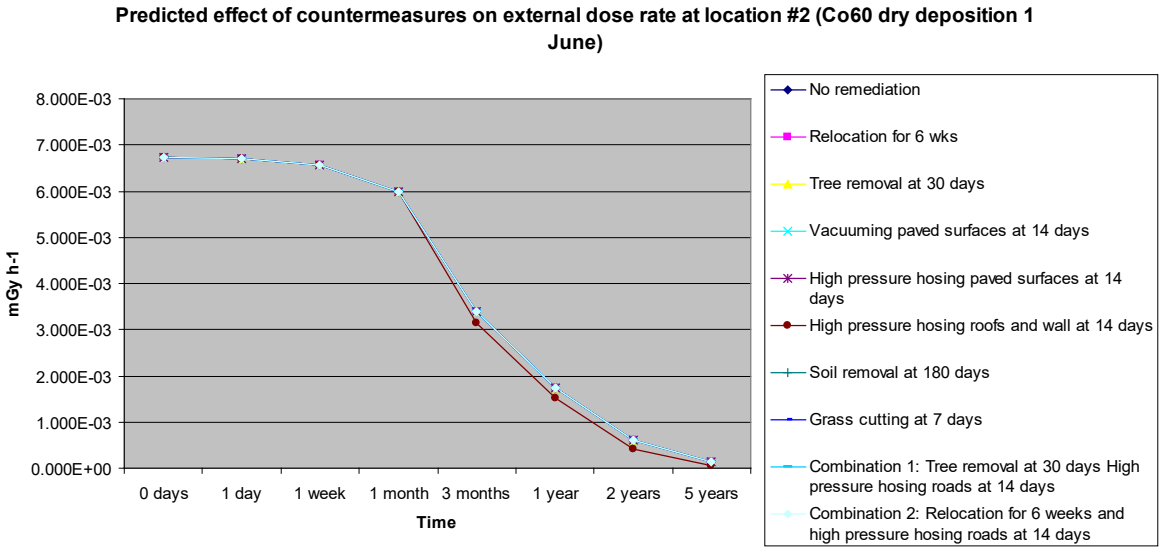

(a)

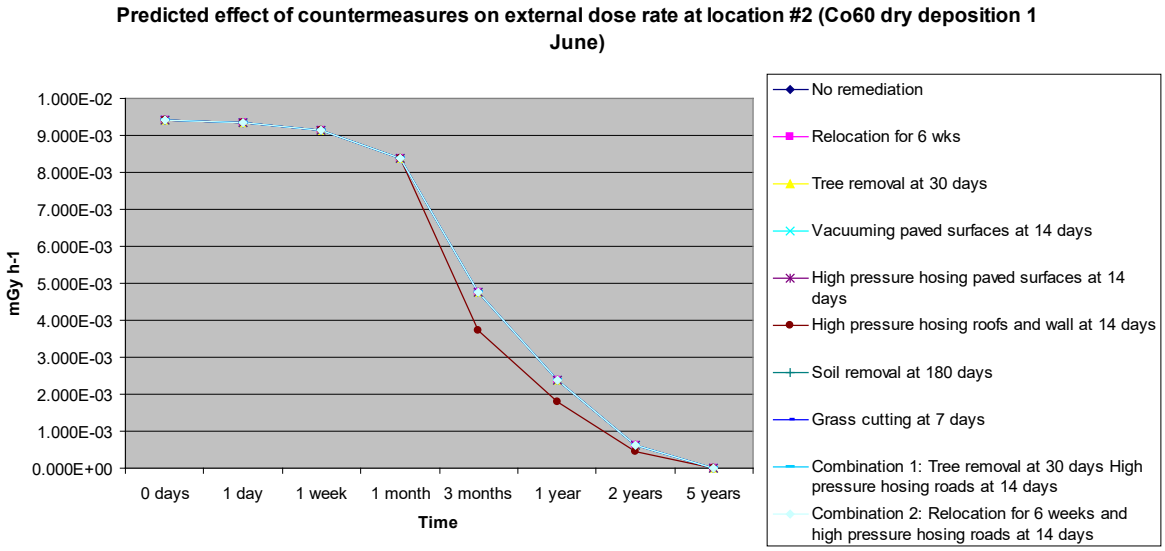

(b)

327

FIG. VI.10. Predicted external doses rate in June under dry conditions for location 2. (a) Using default ERMIN parameters and (b) using parameters modified to more closely resemble glass office buildings.

VI.4. DESCRIPTION OF METRO-K

The METRO-K code was used for the Countermeasures exercise by W.T. Hwang of the Korea Atomic Energy Research Institute (KAERI) in the Republic of Korea [VI.1].

VI.4.1. General description of METRO-K

The METRO-K (Model for Evaluating the Transient Behavior of RadiOactive Materials in the Korean Urban Environment) model was developed by KAERI for use in dose assessment following radioactive contamination in the Korean urban environment, with funding from the Ministry of Science and Technology (MOST) in Korea. Modelling approaches are similar to those of the Canadian model, CHERURB-95 [VI.9], with modifications to describe the Korean urban environment as accurately as possible. Major features of METRO-K are as follows:

(1) Simple mathematical structures, which reduces the input parameters and facilitates understanding of the model; the foundational analytical approaches in the METRO-K model apply empirical and experimental data obtained following the Chernobyl accident;
(2) Easy construction of geometrically complex urban environments using only five types of surfaces (roofs, paved roads, outer walls, lawn or soil, and trees); and
(3) Application of various remediation measures to different surfaces by calculation of the exposure doses from each contaminated surface.

In the case of accidental releases from nuclear facilities, radioactive materials released into the atmosphere will be deposited onto surfaces through both dry deposition processes (e.g. atmospheric turbulence and gravitation) and wet deposition processes (e.g. precipitation). Surface contamination from dry and wet deposition processes can be predicted, based on radionuclide activity concentrations in air, in terms of well known processes, including the deposition velocity and the washout ratio, respectively. If there is no precipitation during a release of radioactive materials, deposition of the radioactive materials by dry deposition processes is predicted from the activity concentrations in air (Bq/m^3) and the amount of precipitation (mm). Predicted radionuclide activity concentrations on surfaces are corrected to account for radioactive decay during the period of deposition; however, losses due to other environmental processes are not considered. External dose rates are calculated as a function of the location of a receptor using air kerma (pGy per photon/mm^2) and the geometry of the location.

At this time, the METRO-K model can be used to calculate the external exposure from contaminated outdoor surfaces. Internal exposure through inhalation of contaminated air and external exposure from contaminated indoor surfaces in buildings, which may be important contributors to dose in some cases, are not considered.

Outputs of the METRO-K model are radionuclide activity concentrations on different surfaces and subsequent external doses as a function of time following a deposition for a receptor in a residential location. Three types of radionuclides (Cs, Ru, I) and three forms of iodine (elemental, organic, particulate) are considered in the model. Figure VI.11 shows a schematic of the processes included in the METRO-K model. Dry deposited radionuclides are classified in terms of a mobile fraction and a fixed fraction. Mobile radionuclides can be easily removed from surfaces by external factors in the environment, such as wind and precipitation, while fixed radionuclides cannot be easily removed. A certain fraction of the mobile radionuclides accumulated during a given day will be fixed overnight due to moisture occurring in the nighttime air. As a result, the amount of fixed radionuclides will increase by a certain fraction each day.

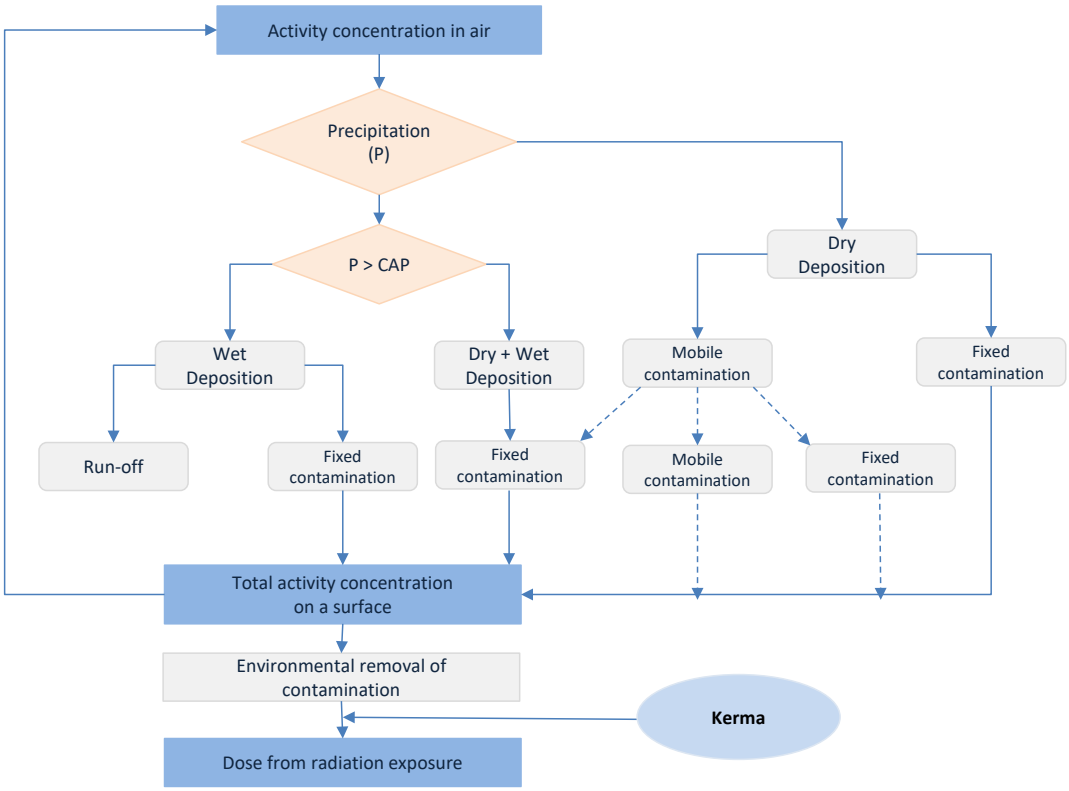

FIG. VI.11. Schematic diagram of METRO-K. CAP represents a critical amount of precipitation. Dotted lines represent the behaviour of the radionuclides deposited during previous days.

In the case of wet deposition processes, the term 'critical amount of precipitation' (CAP) is introduced to quantify runoff. CAP is the minimum precipitation at which runoff can occur. If there is a slight precipitation below the CAP during a release of radioactive materials, both dry and wet deposition processes will occur. Deposited radionuclides will be fixed, and mobile radionuclides that have been deposited through dry deposition processes in the previous days will be fixed.

If there is heavy precipitation exceeding the CAP during a release of radioactive materials, radionuclides will be deposited through wet deposition processes. Some radionuclides will be fixed; however, others will be removed via runoff water. A certain fraction of the radionuclides in the runoff water will be retained on surfaces. Following deposition, radionuclide activity concentrations on surfaces will be affected by environmental removal processes, including wind, pedestrians and traffic, and migration into soil. Information from the Chernobyl experience indicates that radioactive materials may be released for several days in the case of a severe accident. In such cases, total depositions on different surfaces are calculated step-by-step using the METRO-K model.

VI.4.2. Surface contamination through deposition processes

Dry deposition onto surfaces is quantified in terms of a deposition velocity (v_g, m/s), which is a proportionality constant describing the relationship between radionuclide activity concentrations in air and on the ground. A certain fraction of dry deposited radionuclides, known as the fixed fraction, binds strongly to surfaces due to moisture; as a result, this fraction is not easily removed by external environmental factors. The remaining fraction, known as the

mobile fraction, will show less binding with surfaces and can easily be removed. It is assumed that 90% of initial deposition is fixed and 10% is mobile, regardless of the radionuclide. The amount of daily deposition can be calculated using Eqs (VI.1) and (VI.2), as follows:

$$D_m(\Delta t, s) = 86400\ f_m(s)\ C_{air}(\Delta t)\ v_g(s) \quad \text{(VI.1)}$$

$$D_f(\Delta t, s) = 86400\ (1 - f_m)\ C_{air}(\Delta t)\ v_g(s) \quad \text{(VI.2)}$$

where:

$D_m(\Delta t, s)$ is the daily initial deposition of mobile radionuclides for surface s (Bq/m^2);
$D_f(\Delta t, s)$ is the daily initial deposition of fixed radionuclides for surface s (Bq/m^2);
$C_{air}(\Delta t)$ is the daily radionuclide activity concentration in air (Bq/m^3);
v_g is the deposition velocity (m/s);
f_m is the mobile fraction of deposited radionuclides; and
86400 is a unit conversion factor (s/d).

It is assumed that, following deposition, mobile radionuclides will become fixed at a rate of 70% per day [VI.9]. Table VI.7 presents the deposition velocities used in METRO-K for different types of surfaces and radionuclides.

Wet deposition can be quantified in terms of a washout ratio, which is a proportionality constant describing the relationship between radionuclide activity concentrations in air and in precipitation. In METRO-K, this constant is assumed to be 9.26×10^5 for particulates, and 8.44×10^3 and 2.03×10^5 for organic iodine and elemental iodine, respectively. It is assumed that run off occurs in cases where the daily precipitation exceeds the CAP during a release of radioactive materials. The values of the CAP were assumed to be 3, 4.28, 0.06, 6 and 2 mm for roofs, paved roads, outer walls, lawn or soil, and trees, respectively. In the case of slight precipitation less than the CAP during a release, both dry and wet deposition processes will occur. In such cases, it is assumed that the deposited radionuclides are fixed onto surfaces.

In the case of heavy precipitation that exceeds the CAP, wet deposition processes will occur. In such cases, run off will occur for amounts of precipitation exceeding the CAP, and a certain fraction of radionuclides in the run off water will be retained on surfaces. Table VI.8 presents the assumptions made in the METRO-K model regarding the fraction of radionuclides retained on the surfaces from run off water for different types of surfaces and radionuclides. The mathematical expressions describing these assumptions are as follows:

$$D_{SP} = 1 \times 10^{-3}\ C_{air}(\Delta t)\ P(\Delta t)\ \omega_p + 86400\ C_{air}(\Delta t)\ v_g(s) \quad \text{(VI.3)}$$

$$D_{HP} = 1 \times 10^{-3}\ C_{air}(\Delta t)\ [CAP(s) + (P(\Delta t) - CAP(s))\ f_{ret}(s)]\ \omega_p \quad \text{(VI.4)}$$

where:

$D_{SP}(\Delta t, s)$ is the daily initial deposition on surfaces during slight precipitation (P < CAP) (Bq/m^2);
$D_{HP}(\Delta t, s)$ is the daily initial deposition on surfaces during heavy precipitation (P > CAP) (Bq/m^2);
$P(\Delta t)$ is the daily precipitation (mm);
f_{ret} is the fraction of radionuclides retained on surfaces from run off water; and
1×10^{-3} is a unit conversion factor (mm/m).

TABLE VI.7. DEPOSITION VELOCITY OF RADIONUCLIDES (m/s)

Surface	Radionuclide				
	Cs	Ru	I (particulate)	I (organic)	I (elemental)
Roofs	4.32×10^{-4}	4.32×10^{-4}	1.07×10^{-3}	4.00×10^{-6}	4.26×10^{-3}
Paved roads	8.14×10^{-5}	8.14×10^{-5}	2.45×10^{-4}	4.00×10^{-6}	9.79×10^{-4}
Outer walls	1.80×10^{-5}	1.80×10^{-5}	1.28×10^{-4}	8.55×10^{-7}	5.13×10^{-4}
Lawn or Soil	6.12×10^{-4}	6.12×10^{-4}	1.62×10^{-3}	1.28×10^{-5}	7.43×10^{-3}
Trees	1.21×10^{-3}	1.21×10^{-3}	1.99×10^{-3}	2.00×10^{-5}	7.94×10^{-3}

TABLE VI.8. FRACTION OF RADIONUCLIDES RETAINED ON SURFACES FROM RUN OFF WATER

Surface	Radionuclide		
	Cs	Ru	I
Roofs	0.86	0.86	0.02
Paved roads	0.60	0.60	0.02
Outer walls	0.02	0.02	0.02
Lawn or soil	0.90	0.90	0.75
Trees	0.75	0.75	0.02

VI.4.3. Exposure dose assessment

Prediction of external doses in an urban environment may be a difficult task because of the geometrical complexity of surrounding structures, including buildings. For simplicity of assessment, METRO-K uses predetermined kerma values, which represent dose rate per unit deposition. The external dose rate for a specified location i can be calculated using Eq. (VI.5), as follows:

$$\dot{H}_i(t) = 8.64 \times 10^{-14} DCF_i \sum_k y_k \sum_j \omega_j D_j(t)\ k_{ijk} \tag{VI.5}$$

where:

i is the location of a receptor (indoors or outdoors);
j is the contaminated surface;
k is the specified gamma energy;
$\dot{H}_i(t)$ is the effective dose rate (Sv/d);
DCF_i is the dose conversion factor at receptor location i (Sv/Gy);
ω_j is the dose reduction by surface roughness on surface j (dimensionless);
y_k is the yield of gamma energy k (γ sec^{-1} Bq^{-1});
D_j(t) is the radionuclide activity concentration on surface j (Bq/m^2); and
k_{ijk} is the kerma at receptor location i on surface j for gamma energy k (pGy per γ/mm^2).

Meckbach et al. [VI.10] calculated kerma values as a function of the location of the receptor, the contaminated surface, and the gamma energy for four types of representative European buildings, using the Monte Carlo method. Although the types of buildings and surrounding environments differ not only between countries, but also between regions, kerma values derived

by Meckbach et al. [VI.10] are widely used to predict external doses in existing urban models (see e.g. [VI.9], [VI.11]).

METRO-K considers seven representative Korean building types:

(1) Prefabricated one storey houses;
(2) One storey semidetached houses with flat concrete roofs;
(3) Two storey semidetached houses with flat concrete roofs;
(4) Two storey semidetached houses with tile roofs;
(5) Three storey terrace houses with tile roofs;
(6) Large, five storey public or commercial buildings; and
(7) Ten-storey apartment buildings.

To generate kerma values for these building types, the kerma values of Meckbach et al. [VI.10] have been rearranged or modified. Figure VI.12 shows an example of how this rearrangement was done for two different building types.

For the contamination of the roofs, it is assumed that kerma values on the top floor of a 10 storey apartment are the same as those on the top floor of a five storey building, symbolized as K_1. K_2 and K_3 symbolize kerma values on the third and fifth floors from the top, respectively, due to contamination on the roof. For the 5 storey building, K_3 corresponds to the kerma on the ground floor from contamination of the roof, while for the 10 storey building, K_3 corresponds to the kerma on the sixth floor from the ground, from contamination of the roof.

For the contamination of the trees, it is assumed that kerma values on the 5^{th} floor of a five storey building are the same as those on the 5^{th} floor of a 10 storey building, symbolized as K_A. K_B and K_C symbolize kerma values on the third and ground floors, respectively, due to contamination of the tree. For the 5 storey building, K_A, K_B, and K_C contribute to the external dose rate on the same floors affected by K_1, K_2, and K_3 (from the roof), while for the 10 storey building, K_A, K_B, and K_C (from the tree) affect different floors than K_1, K_2, and K_3 (from the roof).

A data library for the kerma values of the seven types of buildings considered in the METRO-K model has been established using a similar approach for three different gamma energies (0.3 MeV, 0.662 MeV, 3 MeV). Table VI.9 shows kerma values for a 10 storey apartment building as a representative example. Those for other building types are presented elsewhere [VI.12]. METRO-K considers not only the external doses resulting from a contaminated building where a receptor resides, but also those resulting from the contaminated surfaces of neighboring buildings and a large park. Kerma values for other energies and locations are estimated using logarithmic interpolation. These kerma values are averaged for a residential location of a receptor, not a specified location.

Additional exposures resulting from daughter products are implicitly included in calculated dose rates by considering the yields of gamma energies from their radioactive decay scheme. The range of gamma energies considered in this calculation is between 0.3 MeV and 3 MeV. Table VI.10 shows the yields of gamma energies for five types of radionuclides.

DCFs are assumed to be 0.8 Sv/Gy and 0.7 Sv/Gy for adults located outdoors and indoors, respectively [VI.13]. Dose reductions due to surface roughness are set at 1.0, 0.9, 0.95, 0.8, and 0.9, for roofs, paved roads, outer walls, soil or lawn, and trees, respectively.

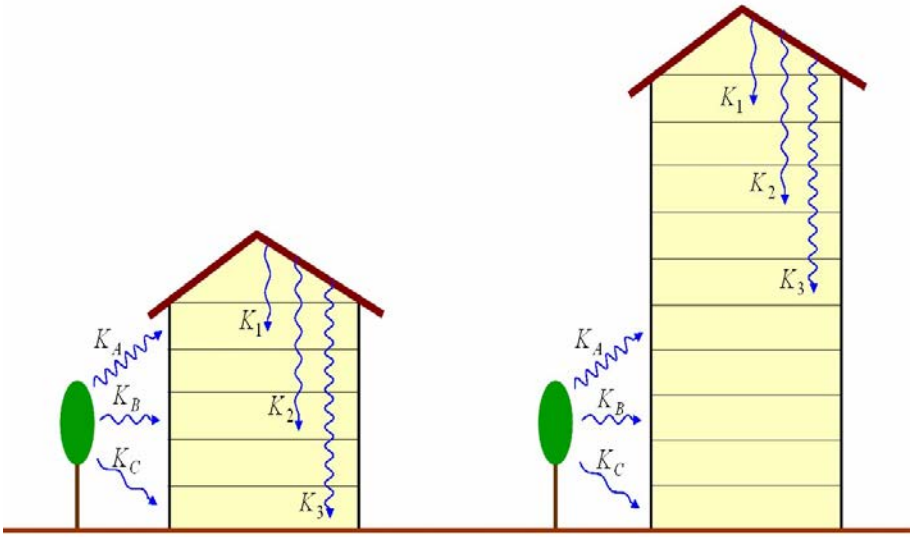

FIG. VI.12. An example of the rearrangement of kerma values derived in Ref. [VI.10] applied to the building types and environment described in METRO-K. The houses in the figure correspond to a simplified European building (left) and a Korean building (right).

TABLE VI.9. KERMA VALUES GENERATED FOR SPECIFIED PARTS OF A 10 STOREY APARTMENT BUILDING (pGy per γ mm^{-2})

Location	Surface	A near building					Neighboring buildings across roads			A park across roads				
		Walls	Outer walls	Roofs	Garden	Garden trees	Paved roads	Outer wall	Roofs	Paved Roads	Park	Outer walls	Roofs	Trees
0.3 MeV 333	Basement	0.001	0.002	0	0.004	0	0.004	0.01	0	0.004	0.001	0.003	0	0.004
	1st floor	2.9	0.5	0	1.8	0.33	1	2	0	1.4	1.6	0.7	0	0.65
	5th floor	2.9	0.6	0	0.25	0.03	0.09	1.8	0.01	0.15	0.9	0.7	0.03	0.05
	10th floor	2.8	0.4	0.6	0	0	0	1.1	0.3	0	0.51	0.4	0.1	0
	Roads	8.1	57	0	0.25	0.01	200	130	2	230	66	32	1	25
	Garden	6.6	45	0	252	10	0.2	57	3	0.2	3	56	3	0.05
0.662 MeV	Basement	0.009	0.008	0	0.01	0.0005	0.018	0.042	0	0.013	0.004	0.024	0	0.013
	1st floor	6.5	2.1	0	5.1	0.9	2.6	5.4	0	3.9	4.8	2	0	1.8
	5th floor	6.5	2.1	0	0.5	0.06	0.15	5.3	0.08	0.3	2.2	2	0.05	0.09
	10th floor	6.5	2	3.8	0	0	0	3	0.6	0	1	0.9	0.25	0
	Roads	16	115	0	0.3	0.02	430	270	3	495	140	68	1.5	52
	Garden	14	89	0	530	21	0.4	110	4	0.5	4	110	4	0.1
3 MeV	Basement	0.05	0.4	0	0.2	0.02	0.3	1.7	0.2	0.2	0.07	1.2	0	0.2
	1st floor	24	26	0	39	4.7	2.4	32	0	34	43	14	0	10
	5th floor	25	28	0.01	3.3	0.4	1.1	33	1	2	20	14	0.7	0.8
	10th floor	24	26	56	0	0	0	21	3.3	0	9.3	10	2.1	0
	Roads	48	315	0	1	0.08	1260	810	8.5	1490	585	220	2.5	154
	Garden	38	250	0	1580	61	4	320	9.5	2	10	320	9	0.5

TABLE VI.10. GAMMA ENERGIES OF RADIONUCLIDES AND THEIR YIELDS

Radionuclide	Energy (MeV)	Yield (%)
Ru-103	0.444/0.497/0.557 0.610/0.612	0.3/86.4/0.8 5.3/0.1
Ru-106	0.428/0.435/0.512 0.616/0.622/0.873 1.050/1.128/1.194 1.562	0.1/0.1/20.6 0.7/9.8/0.4 1.5/0.4/0.1 0.1
Cs-134	0.475/0.563/0.569 0.605/0.796/0.802 1.039/1.168/1.365	1.5/8.4/15.4 97.6/85.4/8.7 1.0/1.8/3.0
Cs-137	0.662	85.0
I-131	0.326/0.364/0.503 0.637/0.643/0.723	0.3/81.2/0.4 7.3/0.2/1.8

TABLE VI.11. PARAMETER VALUES FOR TIME DEPENDENT DOSE RATES TO DESCRIBE ENVIRONMENTAL REMOVAL PROCESSES FOR SPECIFIED SURFACES

Parameter		Surface				
		Roofs	Paved roads	Outer walls	Lawn or Soil	Trees
A	Cs	0.5	0.6	0.2	0.63	0.8
	Ru	0.29	0.3	0.17	0.95	0.95
	I	0.75	0.75	0.3	0.95	0.8
$T_{w,a}$ (day)	Cs	340	80	365	317.6	36.5
	Ru	29.2	69.4	314	91	36.5
	I	17	40	182.5	160	18
$T_{w,b}$ (day)	Cs	2420	10100	6930	15600	36500
	Ru	2420	10100	6930	4450	36500
	I	2420	10100	6930	15600	36500

TABLE VI.12. PARAMETER VALUES FOR THE ENVIRONMENTAL REMOVAL PROCESSES, AS USED FOR THE COUNTERMEASURES EXERCISE

Parameter	Surface				
	Roofs	Paved roads	Outer walls	Lawn or soil	Trees
A	0.5	0.70	1	0.575	1
$T_{w,a}$ (day)	365	120	2740	1200	100
$T_{w,b}$ (day)	13700	1100	0	7670	0

TABLE VI.13. PHOTON ENERGIES OF RADIONUCLIDES TO BE TESTED AND THEIR YIELDS

Radionuclide	Energy (MeV)	Yield (%)
^{60}Co	0.6938/1.173/1.333	0.016/100/100
^{239}Pu	0.044/0.0005	0.014/0.113

VI.4.4. Time dependent external dose (exposure dose)

In the METRO-K model, an urban environment is assumed to be composed of only five types of surfaces (roofs, paved roads, outer walls, soil or lawn, and trees). Radionuclides deposited onto surfaces will be removed or diluted, not only due to natural processes, such as wind, precipitation and migration into soil, but also due to artificial processes, such as traffic and pedestrians. Time dependent dose rates due to environmental removal processes following deposition are described using two different exponential terms, as follows:

$$\dot{H}(t) = \dot{H}_0 \exp\left(-\frac{0.693\,t}{T_{1/2,d}}\right)\cdot\left[A\exp\left(-\frac{-0.693\,t}{T_{w,a}}\right)+(1-A)\exp\left(-\frac{0.693\,t}{T_{w,b}}\right)\right] \quad \text{(VI.6)}$$

where:

$\dot{H}(t)$ is the time dependent exposure dose rate (Sv/d);

$\dot{H}_0$ is the external dose rate just after a deposition (Sv/d);

A is the fraction of contamination subject to short term environmental removal processes, and $(1-A)$ is the fraction of contamination subject to long term environmental processes;

$T_{w,a}$ is the short term environmental half-life (d);

$T_{w,b}$ is the long term environmental half-life (d); and

$T_{1/2,d}$ is the half-life for radioactive decay (d).

Table VI.11 provides the parameter values that were used to describe the time dependent dose rates, depending on the types of surfaces and radionuclides.

VI.4.5. Application of METRO-K to the Countermeasures exercise

A variety of calculations for the Countermeasures exercise (Seoul scenarios; Appendix III), which was designed by the EMRAS II WG9, were performed using the Korean model, METRO-K. Although this exercise involved the radionuclides ^{60}Co and ^{239}Pu, a variety of parameter values describing their environmental behaviour are based on data for ^{137}Cs (with the exception of the inherent physical characteristics of the radionuclides), because the parameter values for ^{137}Cs have been relatively well established in the scientific literature and specific data for other radionuclides are often not available.

For this exercise, the parameter values in Table VI.11 (used in Eq. (VI.6)) describing environmental removal processes following deposition, were replaced with values reported in a recent study by Andersson et al. [VI.14], as shown in Table VI.12. The more recent values (Table VI.12) are expected to better describe long term radionuclide behaviour in an urban environment.

Kerma values were rearranged or modified to account for different sizes of contaminated areas, assuming that kerma values are inversely proportional to the square of the distance from a

calculation location. The contaminated area is divided into several partitions of equivalent size for use in METRO-K, as shown in Fig. VI.13.

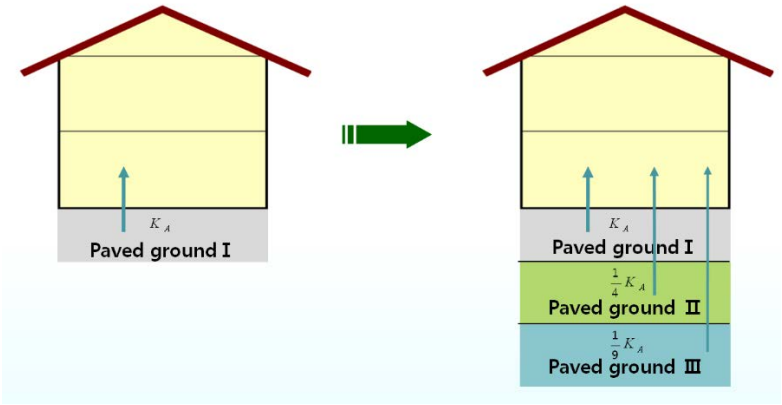

FIG. VI.13. An example of the modification of kerma values for application to environments of different sizes of contaminated areas. K_A is the kerma value for a paved area (paved ground I); paved ground II and III are the same size as paved ground I. For paved ground II, the kerma value is one quarter of K_A, and for paved ground III, the kerma value is one ninth of K_A.

Cobalt-60 is a beta emitter with a radioactive half-life of approximately 5.27 years. It decays to form a nuclear excited state of ^{60}Ni, which emits one or two gamma ray photons to ultimately form a stable ^{60}Ni isotope. Plutonium-239 is an alpha emitter with a radioactive half-life of approximately 2.42×10^4 years. It decays to form ^{234}U, which has a much longer radioactive half-life of approximately 7.04×10^8 years. Therefore, the contribution to external dose from daughter products was not considered for these radionuclides. Table VI.13 presents the photon energies of the radionuclides to be tested and their yields. External dose resulting from surface depositions of ^{239}Pu was not calculated due to its weak photon energies and low yields; in addition, METRO-K does not generate results for photon energies below 0.3 MeV.

METRO-K cannot be used to estimate inhalation dose resulting from air contamination. For the Countermeasures exercise, inhalation dose was independently calculated using time dependent deposition amounts generated using METRO-K and a resuspension factor. The resuspension factor is an empirical constant deduced from the ratio of air to surface activity concentrations. The time dependent resuspension factor following a deposition was selected assuming regular disturbance by pedestrian or vehicular traffic [VI.15], as follows:

$$K(t) = 10^{-6} \exp(-0.01t) + 10^{-9} \quad \text{(VI.7)}$$

where:

$K(t)$ is the time dependent resuspension factor (m^{-1}); and
t is the time (days).

The inhalation dose resulting from resuspension following deposition was calculated in terms of effective dose using dose coefficients provided in ICRP 119 [VI.16]. A chemical form

(M type) was selected for lung absorption of both radionuclides, which may be applied in the case of insufficient information, as described in IAEA Safety Reports Series No. 19 [VI.17].

TABLE VI.14. COUNTERMEASURES AND THEIR DOSE RATE REDUCTION FACTORS (DRRFs)

Countermeasure	Time of application after the event	DRRF
No countermeasure	–	–
Relocation of population	For the first 6 weeks	–
Removal of trees (or leaves)	Day 30	20
Vacuuming or sweeping of roads	Day 14 (no rain)	2.5
Washing or hosing of roads	Day 14 (no rain)	5
Cutting of grass plus removal of soil[a]	Cutting grass: Day 7 Removal soil: Day 180	5 20
Removal of trees plus washing of roads	–	–
Relocation plus washing of road	–	–
Washing building[b]	Day 14 –	Roof: 5 Wall: 7

[a] Applied to park area only.

[b] Applied to business area only.

Dose reductions through application of countermeasures were calculated using dose rate reduction factors (DRRFs). Table VI.14 presents the countermeasures to be considered, their application times, and their DRRFs, which have been summarized in the EMRAS I report [VI.16]. DRRF is defined as the reduction in photon dose rate above a surface just following decontamination. Therefore, absorbed dose rates following application of a countermeasure are calculated by dividing the absorbed dose rate before the countermeasure by the DRRF corresponding to the given countermeasure.

In the application of the METRO-K model to the Countermeasures exercise, customized interpretations were made for each countermeasure, as appropriate. Relocation of the population was assumed to be a temporary stoppage of use for both the business area (for work) and the park area (for recreation). Removal of trees (or leaves) was assumed to involve the removal of trees (or leaves) along the streets in the business area, and removal of trees (or leaves), including shrubs, in the park area. In addition, the washing of roads was interpreted as washing of roads in the business area and washing of a parking lot in the park area.

Amongst the several environmental components that are considered in METRO-K, trees may show a unique seasonal dependence with respect to both deposition and retention of environmental contamination. The presence or absence of leaves affects the amount of contaminated material deposited on deciduous trees, and the retention of contamination on trees depends greatly on the timing of leaf fall. For the Countermeasures exercise, it was assumed that trees along the streets of business areas are completely deciduous, whereas trees in park areas are 50% deciduous and 50% coniferous (pine tree), respectively. Most deciduous leaves may have already fallen in winter. Thus, it was assumed that for deposition onto trees in winter,

the deposited amounts are 5% and 50% in comparison with the amounts in summer, for the business area and the park area, respectively.

In defining the climatological characteristics of Seoul, snow may be more likely than rain in the winter. Due to the lack of information on deposition and environmental removal processes related to snow, the environmental behaviour of radionuclides for snow was regarded in the same way as for rain.

In cases where deposition occurs in the winter, removal of trees along the streets in the business area and removal of grass in the park area may be unavailable as cost-effective countermeasures. Thus, these countermeasures were regarded as unavailable for reduction of dose. It was assumed that resuspension occurred only from paved surfaces (road) and soil (or grass). Thus, internal dose due to inhalation of resuspended radionuclides was calculated for a receptor standing on these surfaces.

VI.4.6. Predicted results

Doses from radiation exposure were calculated as a function of time following a deposition event, with combined scenarios for the season in which the deposition occurs, for different rainfall conditions on the day that the deposition occurs, and for a variety of countermeasures that could be implemented following a deposition event. The predicted results are discussed in Section 4 and summarized in Appendix V.

VI.4.7. Lessons learned

The lessons learned from the countermeasures exercise are as follows:

(1) External doses are distinctly different depending on the location of a receptor because of the differences in contamination of surfaces and their contributions to external dose.

(2) The reduction in external dose rates over time following a deposition event differs with receptor location due to the differing contributions of surfaces and their environmental removal processes.

(3) The rainfall conditions on the day when a deposition event occurs may play an important role in surface contamination.

(4) External dose resulting from contaminated surfaces may depend on the season during which an event occurs due to seasonal changes in the attributes of urban environments.

(5) METRO-K can only estimate the external exposure from radionuclides deposited onto outdoor surfaces. Additional efforts would be necessary to improve the model capability for a variety of exposure pathways in an urban environment, for example, to account for:
- Resuspension of radioactive materials; and
- Indoor contamination of buildings by ventilation.

(6) Additional efforts would be necessary to improve the reliability of model predictions with respect to:
- Radionuclide behaviour on outer walls made of glass, since outer walls of modern high rise buildings frequently have glass surfaces;
- Radionuclide behaviour on and in snow; and
- Dose reduction for different application times of countermeasures following a deposition event.

(7) Additional efforts would be necessary to provide the following information to decision makers:
- Uncertainty analysis of predicted results and sensitivity analysis of parameters (due to the complexity and variability of urban environments); and
- Economic and social impacts of countermeasures.

VI.5. DESCRIPTION OF RESRAD-RDD

The RESRAD-RDD code was used for the Countermeasures exercise of the EMRAS II WG9 (the 'Seoul Scenario') by S. Kamboj and C. Yu of the Argonne National Laboratory in the United States [VI.1].

VI.5.1. Introduction

The modelling of the changes in the activity concentrations of radionuclides dispersed in an urban environment caused by a hypothetical radiological event in Seoul, Korea was performed using a methodology consistent with that of RESRAD-RDD, a computer code developed by the Argonne National Laboratory for the Interagency Operational Guidelines Task Group (OGT) in the USA [VI.18]. The RESRAD-RDD code can be used to evaluate exposures of humans to radiation during the early, intermediate, or late phase of response following an incident involving a radiological dispersal device (RDD).

VI.5.2. RESRAD-RDD conceptual model

The RESRAD-RDD code considers the dispersion of radionuclides and their subsequent partitioning in the environment following an event involving an RDD, as illustrated in Fig. VI.14. It was assumed that the RDD event occurred outdoors and resulted in surface contaminations on the paved areas, lawn, and exterior walls and roofs of residential and commercial buildings. In addition, the contaminants were assumed to penetrate the residential and commercial buildings and deposit on indoor floors and walls, either directly during the event through open windows or indirectly after the event through indoor/outdoor air exchange or through contaminants trapped on shoes of people who entered the buildings.

The RESRAD-RDD code uses the partitioning factors to consider differences in the initial radionuclide activity concentrations on different surfaces and applies the weathering parameters to consider the changes in radionuclide activity concentrations on various surfaces as time progresses. The code uses a time dependent resuspension factor to allow calculation of air activity concentrations. The partitioning factors and weathering parameters were incorporated on the basis of the Chernobyl accident data, which showed that in an urban environment, different surfaces have different initial retentions of radioactivity when compared with the reference surface and that they behave differently over time [VI.19]. The reference surface was defined as an infinite smooth air-ground interface (i.e. a surface with no roughness associated with it), with radionuclides deposited on the ground and with no initial penetration. According to a study by Andersson et al. [VI.19], the weathering process and the effect of migration generally follow a two component exponential behaviour with time, as represented by Eq. (VI.8):

$$w(t) = ae^{-(bt)} + (1-a)e^{-(ct)} \quad \text{(VI.8)}$$

where:

$w(t)$ is the activity fraction retained after weathering at time t; and

a, *b*, and *c* are weathering parameters for each surface.

In Eq. (VI.8), there is a mobile fraction *a* with a shorter half-life *b* due to loose binding to the surface or due to the higher migration rate in the case of permeable surfaces. There is also a fixed fraction (1 – *a*) with a longer half-life *c* due to strong binding to the surface or the lower migration rate.

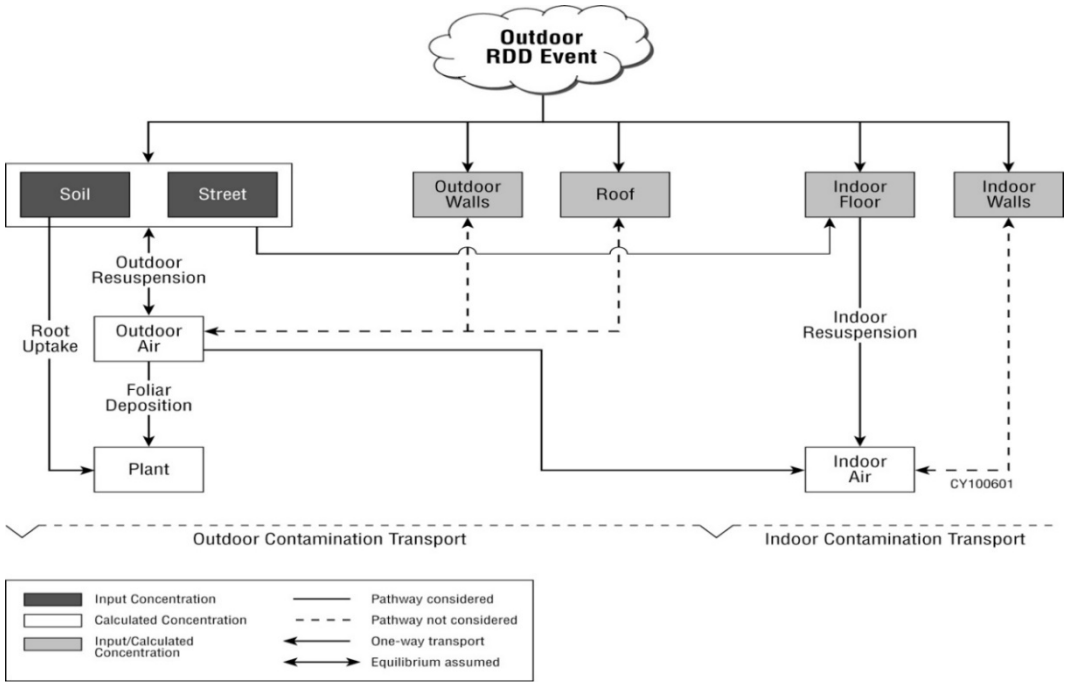

FIG.VI.14. Conceptual model of environmental transport after an RDD event.

TABLE VI.15. INITIAL ESTIMATED CONCENTRATIONS (Bq/m^2) ON THE REFERENCE SURFACE USED IN THE MODELLING UNDER THREE WEATHER CONDITIONS

Weather Conditions	Initial Estimated Concentrations (Bq/m^2) on Reference Surface
Dry	5.29×10^7
Light rain	2.83×10^9
Heavy rain	1.72×10^{10}

[a] Initial estimated concentrations used with RESRAD-RDD were generated using METRO-K (Section 4, Table 4.2).

TABLE VI.16. INITIAL PARTITIONING FACTORS RELATIVE TO IDEALIZED REFERENCE LAWN

Type of Deposition	Surface					
	Lawn	Exterior walls	Roofs	Interior floor	Interior walls	Paved areas
Dry	0.9	0.1	0.7	0.04	0.02	0.4
Wet	0.7	0.015	0.7	0.055	0.0275	0.55

TABLE VI.17. WEATHERING COEFFICIENTS USED FOR THE COUNTERMEASURES SCENARIO

Surface	Mobile fraction (a)	Shorter half-life (ln 2/b), years	Longer half-life (ln 2/c), years
Street (paved areas)	0.5	0.2	2
Soil (lawn)	0.46	1.5	50
Roof/Sloped roofs	0.5	4	50
Exterior Wall	0.2	0.2	20
Interior Floor	0.5	0.2	2
Interior Wall	0.2	0.2	20

VI.5.3. Source

The exercise started with a defined air activity concentration of two radionuclides, ^{60}Co and ^{239}Pu (considered separately). The impact of different weather conditions at the time of initial deposition was to be evaluated. The initial estimated activity concentrations on reference surfaces under three sets of weather conditions are listed in Table VI.15. Two regions, a business area and a park area, were considered. Test locations for Region 1 (business area) included three indoor locations in Building 1 (ground floor, 10th floor, and 24th floor to top floor) and one outdoor location just outside Building 1. Test locations for Region 2 included the centre of the park and a location in the parking lot. For each test location, the annual doses for each reference scenario were to be calculated first without countermeasures and then with the indicated countermeasure (see Appendix V for details).

Table VI.16 lists the partitioning factors assumed for this modelling exercise for the initial retention of radionuclides on different surfaces. The partitioning for lawn, paved areas, roof and exterior walls are from Andersson et al. [VI.19]. The initial floor concentration inside the building was assumed to be 10% of the initial outdoor concentration. The initial interior wall concentration was assumed to be half (a factor of 0.5) of the initial concentration on the floor, which is consistent with indoor deposition patterns [VI.20]. For this modelling exercise, the initial concentrations of radionuclides on interior floor, and interior walls were calculated by multiplying the initial concentration on paved area with the corresponding partitioning factor.

Table VI.17 provides a summary of the values for the weathering parameters used in this exercise [VI.19]. The parameters for the interior floor were assumed to be the same as those for the outdoor paved areas to take account of the transport of contaminants by human activities (e.g. walking from outdoors to indoors) and air exchange. Therefore, the concentration ratio between these two surfaces would stay the same at any given point in time. The weathering parameters for the interior walls were assumed to be the same as for the exterior walls.

In addition to weathering, the activity concentrations on different surfaces were also corrected for radioactive decay. Therefore, the average weathering correction factor (WCF) from time t_1 to t_2, which includes correction for both weathering and radioactive decay, can be given by Eq. (VI.9):

$$\overline{WCF} = \frac{1}{t_2 - t_1} \int_{t_1}^{t_2} [\, a\, e^{-(bt)} + (1-a) e^{-(ct)} \,] e^{-\lambda t} dt \tag{VI.9}$$

The correction factor at a given time t can be given by Eq. (VI.10), as follows:

$$WCF(t) = [\, a e^{-(bt)} + (1-a)\, e^{-(ct)} \,] e^{-\lambda t} \tag{VI.10}$$

Figure VI.15 shows the effect of weathering on different surfaces as a function of time. The following weathering effects are observed:

— The fraction of the initial activity concentration remaining on paved surfaces changes very rapidly compared with the fraction of the initial activity concentration remaining on other surfaces. This is due to smaller values for both the shorter and longer half-life (Table VI.17).

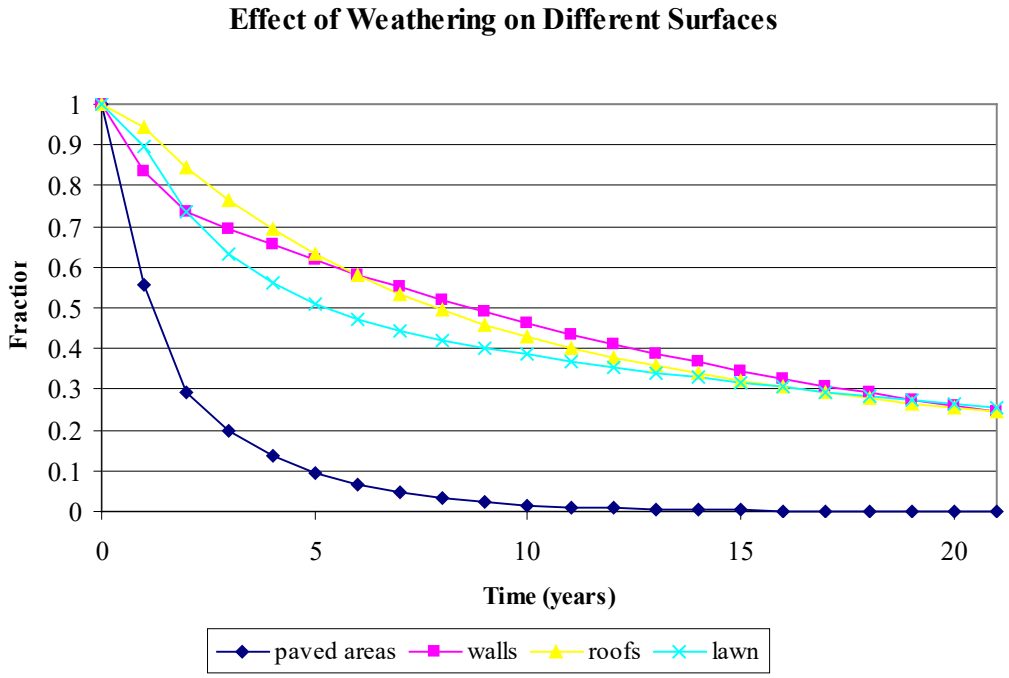

FIG. VI.15. Fraction of the initial activity concentration remaining on the indicated surfaces over time, demonstrating the effect of weathering on the different surfaces.

— The fraction of the initial activity concentration remaining on walls initially changes more rapidly than the fraction of the initial activity concentration remaining on roofs and lawns. This is due to a smaller value for the shorter half-life (Table VI.17). Later, the fraction of the initial activity concentration remaining on lawns and roofs changes faster than for walls because lawns and roofs have much higher mobile fractions compared with walls (Table VI.17).
— The fraction of the initial activity concentration remaining on lawns changes more rapidly than the fraction of the initial activity concentration remaining on roofs. This is due to a smaller value of the shorter half-life for lawns than for roofs (Table VI.17).

VI.5.4. Exposure pathways

The RESRAD-RDD model considers the following 13 exposure pathways for a receptor:

(1) External exposure (groundshine) to contaminants on streets or soils while staying outdoors;

(2) External exposure to contaminants on exterior walls while staying indoors;
(3) External exposure to contaminants on roofs while staying indoors;
(4) External exposure to contaminants on interior walls while staying indoors;
(5) External exposure to contaminants on interior floors while staying indoors;
(6) External exposure to contaminants on streets or soils while staying indoors,
(7) Inhalation exposure while staying outdoors (resuspension of contaminants from streets or soils only);
(8) Inhalation exposure while staying indoors (indoor air contamination results from both outdoor air contamination and resuspension from contaminants on interior floors);
(9) Submersion in contaminated air while staying outdoors;
(10) Submersion in contaminated air while staying indoors;
(11) Ingestion of dust particles on streets/soils while staying outdoors;
(12) Ingestion of dust particles while staying indoors (assumed to be from the floors or walls, whichever is more conservative); and
(13) Radon inhalation while staying indoors.

The first six exposure pathways contribute to the external radiation dose, and Pathways 7 and 8 are inhalation exposure pathways. Only external and inhalation exposure pathways are considered in this exercise.

VI.5.5. Resuspension factor correction

The RESRAD-RDD software has the flexibility of accepting two user defined coefficients, A and B, for use in resuspension factor calculations, as shown in Eq. (VI.11):

$$RF_o(t) = \frac{A}{t} + B \tag{VI.11}$$

where:

t is time in days after deposition; and
A and B were the coefficients for the initial and long term resuspension factors, respectively.

The default assumption in the code is that the resuspension factor is fixed at 1×10^{-6} m^{-1} for the first day; for days 1 to 1000, it varies with time as $1 \times 10^{-6}/t$ (m^{-1}); it then remains fixed at 1×10^{-9} m^{-1} after 1000 days [VI.21].

Combined with the average weathering correction factor, an average outdoor air concentration correction factor from time t_1 to t_2 that accounts for radioactive decay, resuspension, and source depletion due to weathering and leaching can be defined by means of Eq. (VI.12), as follows:

$$\overline{WCF \times RF_o} = \frac{\int_{t_1}^{t_2} RF_o(t)[a\,e^{-(bt)} + (1-a)e^{-(ct)}]e^{-\lambda t}dt}{t_2 - t_1} \tag{VI.12}$$

This factor is used in the analyses to estimate an average activity concentration of contaminants in outdoor air from a contaminated surface source.

In addition to the resuspension factors discussed above, the RESRAD-RDD code has a list of 'rule of thumb' multiplication factors, as given by Walsh [VI.22], to adjust for resuspended activity concentrations in air resulting from variations in atmospheric conditions. The

multiplication factors (Table VI.18) can be used to adjust the average resuspension factors in accordance with specific scenarios.

Table VI.19 lists the assumptions that have been made for the two exposure scenarios for the dose calculations carried out during this exercise. The exposures were calculated for an adult member of the public. One exposure scenario was considered in Region 1 (in the business area), and the other exposure scenario was considered in Region 2 (in the park area).

Table VI.20 lists the dimensions and characteristics assumed for Building 1, as well as the dimensions for the outdoor ground source (i.e. lawn and paved area).

TABLE VI.18. MULTIPLICATION FACTORS TO BE APPLIED TO THE RESUSPENSION FACTOR RESULTS

Conditions	Multiplication Factor[a]
Rural conditions, light-medium winds	1
Arid climate	10
Urban conditions, light traffic, light pedestrian activity[a]	10
Urban conditions, heavy traffic	100
Plowing in dry conditions	100

[a] Given that some countermeasures might restrict the movement of vehicles, this factor need not always be applied.

TABLE VI.19. ASSUMPTIONS FOR THE EXPOSURE SCENARIOS

Region	Indoor		Outdoor	
	Duration (h/week)	Inhalation rate (m^3/h)	Duration (h/week)	Inhalation rate (m^3/h)
Region 1 (Business area)	40	0.5	5	1.0
Region 2 (Park area)	0	N/A	3	1.5

N/A = not applicable.

TABLE VI.20. DIMENSIONS AND CHARACTERISTICS ASSUMED FOR THE OUTDOOR GROUND SOURCE AND DIFFERENT TARGET BUILDINGS

Building/Source	Floor length (m)	Floor width (m)	Building/ floor height (m)	Thickness of walls (cm)	Thickness of roof (cm)	Material of walls/roof	Density of material (g/cm^3)
Office building	30	30	2.75	1	10	Aluminum/ Concrete	2.7/2.4
Lawn/paved area	Infinite	Infinite	N/A	N/A	N/A	N/A	N/A

N/A = not applicable.

TABLE VI.21. AVERAGE EXTERNAL SHIELDING FACTORS USED FOR THE CALCULATION OF INDOOR EXPOSURE TO AN OUTSIDE GROUND SOURCE

Building/floor location	Shielding factor (Co-60)	Shielding factor (Pu-239)
Office building (1st floor)	0.353	0.0541
Office building (10th floor)	0.253	0.0481
Office building 1 (24th floor)	0.167	0.0318

VI.5.6. Dose calculations

VI.5.6.1. External pathway dose

To calculate the doses from external pathways, first the dose to source ratios (DSR) for each of the six external dose components resulting from different contaminated surfaces (Section VI.5.4) were calculated using the RESRAD-BUILD computer code [VI.23].

For the first component pathway (outdoor exposure to paved area), an infinite, homogeneously contaminated concrete area and lawn were considered, and the DSR for a receptor located at the centre of each area was calculated. For component pathways 2 to 5 (indoor exposures to exterior walls, roofs, interior walls, and floor), the receptor was assumed to be located at the centre of the floor of a contaminated building.

For a multiple storey building, the floor area and height were assumed to be the same for different floor levels. Except for the ground floor, the floor for any other floor level was also considered as the roof for the floor beneath it. For this exercise, the activity concentrations of radionuclides on the floor, exterior walls, and interior walls were assumed to be independent of the floor level. It is possible that in a real situation, each floor may have different activity concentrations. Shielding between the surface source and the receptor was considered in the calculation of the DSR for each component pathway. For the last component pathway (indoor exposure to outside ground source), the DSR was determined by adjusting the DSR for the first component pathway using a shielding factor. Table VI.21 provides the shielding factors that were used for this component for different building floors. The RESRAD-BUILD computer code was used to calculate the shielding factors.

The indoor hourly external dose at a specific time for a receptor living or working on a specific floor level inside the office building was calculated as the sum of the doses from component pathways 2 to 5 using Eq. (VI.13), as follows:

$$hourly\ dose_{in,f}(t) = \sum_{n=2-5} C_{s,} \times P_n \times WCF_n(t) \times DSR_{n,f} \quad \text{(VI.13)}$$

where:

$hourly\ dose_{in,f}(t)$ is the indoor hourly external dose on the floor level *f* inside the building (Sv/a);

Cs is the initial outdoor ground surface concentration at the location of the building (Bq/m^2);
Pn is the partitioning factor for the surface source corresponding to component pathway n;
WCF_n (t) is the weathering and radiological decay correction factor for the initial concentration on the surface source corresponding to component pathway n at a given time t;
n is the index for the component pathway; and
$DSR_{n,f}$ is the dose to source ratio for component pathway n at the floor level f (mSv/h per Bq/m^2).

The outdoor hourly external dose was calculated using an approach that was similar to the approach used for the indoor hourly dose, with the exception that only the first component pathway was relevant; therefore, summation was not needed.

The indoor annual average external dose was calculated by multiplying the indoor average hourly dose by the average indoor exposure duration using Eq. (VI.14), as follows:

$$annual\ dose_{in,f}(t) = \left(\sum_{n=2-5} C_s \times P_n \times \overline{WCF_n(t)} \times DSR_{n,f} \right) \times ED_{in,f} \quad \text{(VI.14)}$$

where:

$\overline{WCF_n}$ *(t)* is the average weathering and radiological decay correction factor for the initial concentration on the surface source corresponding to component pathway n in a specific year t (see Eq. (VI.9) for its calculation); and
EDin,,f (t) is the indoor exposure duration on the floor level f in the building (h/a).

The outdoor annual average external dose was calculated by multiplying the outdoor average hourly dose by the average outdoor exposure duration. The total annual average external dose was calculated by summing the indoor annual average external dose and the outdoor annual average external dose.

VI.5.6.2. Inhalation pathway dose

To calculate the dose from inhalation pathways, first, the activity concentrations in air outdoors and indoors were calculated using Eqs (VI.15) and (VI.16) and a time dependent resuspension factor and weathering correction were applied, as follows:

$$C_o = C_s \times \overline{WCF_s \times RF_o} \times MF\ , \quad \text{(VI.15)}$$

$$C_i = C_o \times SHF1 + C_{floor} \times RF_i \times \overline{WCF_{floor}}\ , \quad \text{(VI.16)}$$

where:

C_o is the activity concentration in outdoor air (pCi/m^3);
C_i is the activity concentration in indoor air (pCi/m^3);
C_S is the activity concentration on streets or soil at t = 0 (pCi/m^2);
C_{floor} is the activity concentration on interior floors at t = 0 (pCi/m^2);
$\overline{WCF_s \times RF_o}$ is the average outdoor air concentration correction factor (weathering and radioactive decay included; see Eq. (VI.12)) (m^{-1});

MF is a multiplication factor to account for the influence of meteorological conditions or traffic (see Table VI.18);
SHF 1 is the indoor dust filtration factor = 0.55;
$\overline{WCF_{floor}}$ is the weathering correction factor for interior floors, including radioactive decay; and
RF_i is the indoor resuspension factor = 1×10^{-6} m^{-1}.

As shown in Eq. (VI.16), the activity concentration in indoor air is calculated from contamination in outdoor air corrected by the indoor dust filtration factor and from contamination on the interior floor corrected by a resuspension factor. The outdoor and indoor doses from inhalation exposure can be calculated with Eqs (VI.17) and (VI.18), respectively, as follows:

$$pathway\ dose_{inh-outdoor} = C_o \times OF_o \times IR_o \times DCF_{inh} \quad \text{(VI.17)}$$

$$pathway\ dose_{inh-indoor} = C_i \times OF_i \times IR_i \times DCF_{inh} \quad \text{(VI.18)}$$

where:

IR_o, IR_i is the inhalation rate while staying outdoors or indoors, respectively (m^3/a);
OF_o, OF_i is the occupancy factor (time fraction spent outdoors or indoors, respectively); and
DCF_{inh} is the dose conversion factor for inhalation taken from ICRP 72 [VI.24], which was the ICRP 60 [VI.25] based committed effective dose conversion factor (mrem/pCi).

The external and internal doses were predicted for the case without any countermeasure and for several cases with various countermeasures. The various countermeasures were specified for this modelling exercise (Appendix V). Table VI.22 lists the decontamination factors assumed for each of the various countermeasures. Radionuclide activity concentrations on an affected surface source following application of a countermeasure were assumed to be reduced by the decontamination factor. For example, cutting and removing grass at day 7 would result in the reduction of the lawn concentration by a factor of 3 at day 7. When a countermeasure was considered, the first year was divided into two time periods, from t = 0 to the time the countermeasure was applied, and from the time the countermeasure was applied to the end of the first year. The external and inhalation doses incurred during these two time periods were calculated separately and were subsequently added together to generate the total external and inhalation doses for the first year.

VI.5.7. Modelling endpoints

The following eight modelling endpoints were considered in this exercise:

(1) Contamination density (Bq/m^2) at outdoor test locations;
(2) External exposure rates (dose rates, mGy/h) at each location, from all relevant surfaces (by surface and by total);
(3) Contribution to the dose rates (%) from each surface, for the most important surfaces;
(4) Annual and committed external doses (mGy) for specified reference (hypothetical) exposure scenarios;
(5) Annual and cumulative internal doses (mSv) for specified reference (hypothetical) exposure scenarios;

(6) Effectiveness of countermeasures in terms of external dose rate reduction compared to 'no action';
(7) Effectiveness of countermeasures in terms of external dose reduction compared to 'no action'; and
(8) Effectiveness of countermeasures in terms of internal dose reduction compared to 'no action'.

For this exercise, the model calculations covered the period that started just following the initial deposition from the RDD event and were carried forward for five years. Results were presented as a time series, with the date specified for each predicted dose rate, dose, or radionuclide activity concentration. Example formats were provided for each phase of modelling.

Since this exercise was designed to model cases to test the changes in the radiological conditions over time with and without the implementation of various countermeasures, all the predictions were made first assuming no countermeasures were implemented and were then repeated for the different countermeasures, and were carried forward for five years.

TABLE VI.22. COUNTERMEASURES CONSIDERED AND DECONTAMINATION FACTORS ASSUMED FOR DOSE MODELLING

Countermeasure		Decontamination factor (DF)[a]	Time of application
1	No countermeasures	–	–
2	Relocation of population (temporary)	–	For the first six weeks
3	Tree removal[b]	Not modelled	
4	Vacuuming or sweeping of roads	2	At day 14 (no rain)
5	Washing or hosing of roads	5	At day 14 (no rain)
6	Washing of roof and exterior walls	10	At day 14 (no rain)
7	Cutting and removal of grass; soil removal	10	At day 7 for grass and day 180 for soil
8	Tree removal[b] + road cleaning	Not modelled	
9	Relocation + road cleaning	5	At day 14

[a] The decontamination factors were obtained from Ref. [VI.26].

[b] Trees are not included in the code.

VI.5.7.1. First modelling endpoint – Contamination density at three outdoor test locations

The contamination density was predicted for three outdoor test locations at different times starting at time zero and carried forward for five years into the future using the methodology described above. One test location was just outside Building 1 in Region 1 and the other two test locations were outdoors in Region 2.

VI.5.7.2. Second modelling endpoint – External exposure rates at six test locations (total from all surfaces)

The external dose rate at the six test locations (three inside Building 1 and three outdoor locations, as in first modelling endpoint described in Section VI.5.7.1 above) was predicted at different times starting at time zero and carried forward for five years into the future. The external dose rates included the dose rates from all contaminated surfaces.

VI.5.7.3. Third modelling endpoint – External exposure rates at six test locations from different surfaces and their percent contribution

The external dose rate at the six test locations (as in second modelling endpoint, as described in Section VI.5.7.2 above) from different contributing surfaces was predicted at different times starting at time zero and carried forward for five years into the future. The percent contribution to external dose rates from different contaminated surfaces was also estimated.

VI.5.7.4. Fourth modelling endpoint – External doses for two reference exposure scenarios

The annual and committed external dose was predicted for two reference exposure scenarios at different times starting at time zero and carried forward for twenty years into the future. Table VI.19 lists the assumptions used in the exposure scenario.

VI.5.7.5. Fifth modelling endpoint – Internal doses for two reference exposure scenarios

The annual and committed internal dose was predicted for two reference exposure scenarios at different times starting at time zero and carried forward for five years into the future. Table VI.19 lists the assumptions used in the exposure scenario.

TABLE VI.23. LISTING OF COUNTERMEASURES, THEIR EFFECTIVENESS AND APPLICABILITY IN BOTH PAVED AREAS AND SOIL AREAS

Case	Countermeasure	Decontamination Factor (DF)	Time	Applicability in paved area	Applicability in soil area
# 1	No countermeasures	None	Day 0	Yes	Yes
# 2	Relocation	Infinite	First six weeks	Yes	Yes
# 3	Tree removal[b]	Not modelled			
# 4	Vacuuming or sweeping of roads	2	Day 14	Yes	No
# 5	Washing or hosing of roads	5	Day 14	Yes	No
# 6	Washing of roof and exterior walls	1.4 (roof) and 10 (exterior walls)	Day 14	No	No
# 7	Cutting of grass and removal of soil	3 (grass cutting) and 10 (soil removal)	Day 7 (grass cutting) and Day 180 (soil removal)	No	Yes
# 8	Tree removal[b] + road cleaning	Not modelled			
# 9	Relocation and road cleaning by washing	Infinite (no dose during relocation) and 5 (washing of road)	First six weeks (relocation) and Day 14 (road cleaning)	Yes	Yes

[b] Trees are not included in the code.

VI.5.7.6. Sixth modelling endpoint – Effectiveness of countermeasures in terms of external dose rate reduction compared to 'no action'

349

The external dose rate was predicted for two reference exposure scenarios at different times starting at time zero and carried forward for five years into the future. Table VI.19 lists the assumptions used in the exposure scenario. The calculations were performed for cases with and without a given countermeasure. From these two sets of calculations, the external dose rate reduction compared to the 'no action' scenario was calculated for different countermeasures for both ^{60}Co and ^{239}Pu contamination. Table VI.23 lists the applicability of different countermeasures in both regions.

VI.5.7.7. Seventh modelling endpoint – Effectiveness of countermeasures in terms of external dose reduction compared to 'no action'

The external annual and cumulative doses were predicted for two reference exposure scenarios at different times starting at time zero and carried forward for five years into the future. Table VI.19 lists the assumptions used in the exposure scenario. The calculations were performed assuming cases with and without the countermeasures. From these two calculations, the external annual and cumulative dose reduction compared to the 'no action' scenario was calculated for different countermeasures for both ^{60}Co and ^{239}Pu contamination.

VI.5.7.8. Eighth modelling endpoint – Effectiveness of countermeasures in terms of internal dose reduction compared to 'no action'

The internal (inhalation) annual and cumulative dose was predicted for two reference exposure scenarios at different times starting from time zero and were carried forward for five years in the future. Table VI.19 lists the exposure scenario assumptions used. The calculations were performed with and without a given countermeasure. From these two calculations the internal (inhalation) annual and cumulative dose reduction compared to 'no countermeasures' scenario was calculated for different countermeasures for both ^{60}Co and ^{239}Pu contamination.

VI.5.8. Results and discussions

EXCEL spreadsheets were submitted that included all the results for the eight modelling endpoints assuming no countermeasures were implemented and for different countermeasures. The results were also provided for the sets of three weather conditions that were defined in the Countermeasures scenario (Appendix V). For wet deposition (light rain or heavy rain), only two countermeasures (relocation of population; cutting and removal of grass and soil removal) were considered.

VI.6. REFERENCES TO APPENDIX VI

[VI.1] THIESSEN, K.M., CHARNOCK, T.W., CHOUHAN, S.L., HWANG, W.T., KAMBOJ, S., TOMÁS, J., YU, C., "Modeling the effectiveness of remediation efforts in contaminated urban areas: An EMRAS II Urban Areas Working Group exercise", Proc. of 41st Annual Conference on Waste Management, WM2015, Phoenix, AZ (2015) paper #15631.

[VI.2] INTERNATIONAL ATOMIC ENERGY AGENCY, Environmental Modelling for Radiation Safety (EMRAS). A Summary Report of the Results of the EMRAS programme (2003–2007), IAEA-TECDOC-1678, IAEA, Vienna (2012).

[VI.3] THIESSEN, K.M., BATANDJIEVA, B., ANDERSSON, K.G., ARKHIPOV, A., CHARNOCK, T.W., GALLAY, F., GASCHAK, S., GOLIKOV, V.,

HWANG, W.T., KAISER, J.C., KAMBOJ, S., STEINER, M., TOMÁS, J., TRIFUNOVIC, D., YU, C., ZELMER, R., ZLOBENKO, B., Improvement of modelling capabilities for assessing urban contamination: The EMRAS Urban Remediation Working Group, Applied Radiation and Isotopes **66** (2008) 1741.

[VI.4] THIESSEN, K.M., ARKHIPOV, A., BATANDJIEVA, B., CHARNOCK, T.W., GASCHAK, S., GOLIKOV, V., HWANG, W.T., TOMÁS, J., ZLOBENKO, B., Modelling of a large-scale urban contamination situation and remediation alternatives, Journal of Environmental Radioactivity **100** (2009) 413.

[VI.5] ROBERTSON, E., BARRY, P.J., Urban Contamination and Dose Model. Atomic Energy Control Board, AECB Project No. 3.145.1 (1995).

[VI.6] CHARNOCK, T.W., JONES, J.A., SINGER, L.N., ANDERSSON, K.G., ROED, J., THYKIER-NIELSEN, S. MIKKELSEN, T., ASTRUP, P., KAISER, J.C., MÜLLER, H., PRÖHL, G., RASKOB, W., HOE, S.C., JACOBSEN, L.H., SCHOU-JENSEN, L., GERING, F., Calculating the consequences of recovery, a European model for inhabited areas, Radioprotection **44** (2009) 407.

[VI.7] JONES, J.A., CHARNOCK, T.W., SINGER, L.N., ROED, J., ANDERSSON, K.G., THYKIER-NIELSEN, S., MIKKELSEN, T., ASTRUP, P., KAISER, J.C., MÜLLER, H., PRÖHL, G., RASKOB, W., HOE, S.C., JACOBSEN, L.H., SCHOU-JENSEN, L., GERING, F., Description of inhabited area model, Rep. EURANOS(CAT2)-TN(05)-04, Health Protection Agency, Centre for Radiation, Chemical and Environmental Hazards, Chilton, UK (2007).

[VI.8] CHARNOCK, T.W., The European model for inhabited areas (ERMIN) – developing a description of the urban environment, Radioprotection **45** (2010) S55.

[VI.9] PETERSON, S.-R., CHOUHAN, S., HEINMILLER, B., KOCH, J., CHERURB-95: Urban Contamination and Dose Model, Research report prepared for the Atomic Energy Control Board, Canada (1995).

[VI.10] MECKBACH, R., JACOB, P., PARETZKE, H.G., Gamma exposures due to radionuclides deposited in urban environments. Part I: Kerma rates from contaminated urban surfaces, Radiation Protection Dosimetry **25** (1988) 167.

[VI.11] ROCHEDO, E.R.R., CONTI, F.F.C., PARETZKE, H.G. PARATI, A dynamic model for radiological assessments in urban areas, Part I. Modelling of urban areas, their contamination and radiation fields, Radiation and Environmental Biophysics **35** (1996) 243.

[VI.12] KOREA ATOMIC ENERGY RESEARCH INSTITUTE, Development of Environmental Radiation Protection Technology: Radiological Dose Assessments through the Atmospheric Environment, Rep. KAERI/RR-2769/2006, Korea Atomic Energy Research Institute (KAERI), Daejeon (2006).

[VI.13] JACOB, P., MECKBACH, R., Shielding factors and external dose evaluation, Radiation Protection Dosimetry **21** (1987) 79.

[VI.14] ANDERSSON, K.G., ROED, J., Estimation of doses received in a dry-contaminated residential area in the Bryansk region, Russia, since the Chernobyl accident, Journal of Environmental Radioactivity **85** (2006) 228.

[VI.15] U.S. NUCLEAR REGULATORY COMMISSION, Radiological Assessment: A Textbook on Environmental Dose Analysis, Rep. NUREG/CR-3332, ORNL-5969, USNRC, Office of Standards Development, Washington, DC (1983).

[VI.16] INTERNATIONAL COMMISSION ON RADIOLOGICAL PROTECTION, Compendium of Dose Coefficients based on ICRP Publication 60, Publication 119, Ann. ICRP 41 (Suppl.), Pergamon Press, Oxford and New York (2012).

[VI.17] INTERNATIONAL ATOMIC ENERGY AGENCY (IAEA), Generic Models for Use in Assessing the Impact of Discharges of Radioactive Substances to the Environment, Safety Reports Series No. 19, IAEA, Vienna (2001).

[VI.18] YU, C., CHENG, J.-J., KAMBOJ, S., DOMOTOR, S., WALLO, A., Preliminary Report on Operational Guidelines Developed for Use in Emergency Preparedness and Response to Radiological Dispersal Device Incident, Rep. DOE/HS-001, ANL/EVS/TM-09-1, Argonne National Laboratory, IL (2009).

[VI.19] ANDERSSON, K.G., ROED, J., EGED, K., KIS, Z., VOIGT, G., MECKBACH, R., OUGHTON, D.H., HUNT, J., LEE, R., BERESFORD, N.A., SANDALLS, F.J., Physical Countermeasures to Sustain Acceptable Living and Working Conditions in Radioactively Contaminated Residential Areas, Rep. Risø-R-1396(EN), National Laboratory, Roskilde, Denmark (2003).

[VI.20] RAUNEMAA, T., KULMALA, M., SAARI, H., OLIN, M., KULMALA, M.H., Indoor air aerosol model: Transport indoors and deposition of fine and coarse particles, Aerosol Science and Technology **11** (1989) 11.

[VI.21] NATIONAL COUNCIL ON RADIATION PROTECTION AND MEASUREMENTS), Recommended Screening Limits for Contaminated Surface Soil and Review of Factors Relevant to Site-Specific Studies, Rep. NCRP No. 129, NCRP, Bethesda, MD (1999).

[VI.22] WALSH, C., Calculation of Resuspension Doses for Emergency Response, Rep. NRPB-W1, National Radiological Protection Board, Chilton, Didcot, Oxon, U.K. (2002).

[VI.23] YU, C., LEPOIRE, D.J., CHENG, J.-J., GNANAPRAGASAM, E., KAMBOJ, S., ARNISH, J., BIWER, B.M., ZIELEN, A.J., WILLIAMS, W.A., WALLO, A. III, PETERSON, H.T. JR., User's Manual for RESRAD-BUILD Version 3, Rep. ANL/EAD/03-1, Argonne National Laboratory, Argonne, IL (2003).

[VI.24] INTERNATIONAL COMMISSION ON RADIOLOGICAL PROTECTION, Age-Dependent Doses to Members of the Public from Intake of Radionuclides: Part 5 Compilation of Ingestion and Inhalation Dose Coefficients, Publication 72, Pergamon Press, Oxford and New York (1995).

[VI.25] INTERNATIONAL COMMISSION ON RADIOLOGICAL PROTECTION, 1990 Recommendations of the International Commission on Radiological Protection, Publication 60, Pergamon Press, Oxford, England (1991).

[VI.26] GALLAY, F., Current status of the international experience in modeling the rehabilitation of accidentally contaminated urban environments, Report DEI/SARG/2006-007, Institut de Radioprotection et de Sûreté Nucléaire, Fontenay-aux-Roses (2006).

APPENDIX VII. SELECTED MODEL PREDICTIONS FOR THE CONTAMINANT TRANSPORT AND COUNTERMEASURES EXERCISE

The Contaminant Transport and Countermeasures Exercise is described in Section 4 and Appendix V of this publication. The tables that follow provide the model predictions for the no countermeasure scenario (i.e. without countermeasures implemented) corresponding to the figures in Section 4.

Tables VII.1 to VII.5 provide the predicted contamination densities over time at outdoor locations for each participating model.

Tables VII.6 to VII.10 provide the predicted external dose rates over time at both indoor and outdoor locations for each participating model.

Tables VII.11 to VII.14 provide the percent contributions to predicted external dose rate from the most important surfaces for each of the models for which these predictions were made. Participants were asked to provide the three most important surfaces contributing to external dose rate at each location. In some cases, more than three surfaces contributed; thus, the percentages do not always sum to 100%. In other cases, only one or two surfaces contributed to external dose rate.

Tables VII.15 to VII.19 provide the predicted external doses (annual doses and cumulative doses) for Regions 1 and 2, corresponding to specified exposure scenarios, as described in Appendix V. An annual dose is defined as the dose received during the year preceding the indicated ‘time since event’. A cumulative dose is defined as the dose received from the time of the event to the indicated ‘time since event’.

Tables VII.20 to VII.24 provide the predicted external doses (annual doses and cumulative doses) for Regions 1 and 2, corresponding to specified exposure scenarios, as described in Appendix V. An annual dose is defined as the dose received during the year preceding the indicated ‘time since event’. A cumulative dose is defined as the dose received from the time of the event to the indicated ‘time since event’.

As described in Section 4.1 and as shown in Figs V.3 to V.4 (Appendix V), Region 1 is a business area and Region 2 is a park area. Locations 1 to 3 are indoors in Region 1, Location 4 is outdoors in Region 1 (near buildings), and Locations 5 to 6 are outdoors in Region 2. Locations 4 and 6 are both on pavement.

TABLE VII.1. PREDICTED CONTAMINATION DENSITIES (Bq/m^2) FROM METRO-K (OUTDOOR LOCATIONS ONLY), WITHOUT COUNTERMEASURES

Time since event	Location 4	Location 5	Location 6
Co-60, summer release			
Dry conditions			
0 days	7.03×10^6	5.29×10^7	7.03×10^6
1 day	7.00×10^6	5.29×10^7	7.00×10^6
1 week	6.81×10^6	5.26×10^7	6.81×10^6
1 month	6.14×10^6	5.18×10^7	6.14×10^6
3 months	4.76×10^6	4.95×10^7	4.76×10^6
1 year	1.99×10^6	4.07×10^7	1.99×10^6
2 years	1.08×10^6	3.15×10^7	1.08×10^6
5 years	3.44×10^5	1.54×10^7	3.44×10^5
Light rain			
0 days	2.79×10^9	2.83×10^9	2.79×10^9
1 day	2.78×10^9	2.83×10^9	2.78×10^9
1 week	2.70×10^9	2.82×10^9	2.70×10^9
1 month	2.44×10^9	2.77×10^9	2.44×10^9
3 months	1.89×10^9	2.65×10^9	1.89×10^9
1 year	7.90×10^8	2.18×10^9	7.90×10^8
2 years	4.27×10^8	1.69×10^9	4.27×10^8
5 years	1.36×10^8	8.21×10^8	1.36×10^8
Heavy rain			
0 days	1.27×10^{10}	1.72×10^{10}	1.27×10^{10}
1 day	1.26×10^{10}	1.72×10^{10}	1.26×10^{10}
1 week	1.23×10^{10}	1.71×10^{10}	1.23×10^{10}
1 month	1.11×10^{10}	1.68×10^{10}	1.11×10^{10}
3 months	8.60×10^9	1.61×10^{10}	8.60×10^9
1 year	3.60×10^9	1.32×10^{10}	3.60×10^9
2 years	1.95×10^9	1.02×10^{10}	1.95×10^9
5 years	6.21×10^8	4.99×10^9	6.21×10^8
Co-60, winter release			
Dry conditions			
0 days	7.03×10^6	5.29×10^7	7.03×10^6
1 day	7.00×10^6	5.29×10^7	7.00×10^6
1 week	6.81×10^6	5.26×10^7	6.81×10^6
1 month	6.14×10^6	5.18×10^7	6.14×10^6
3 months	4.76×10^6	4.95×10^7	4.76×10^6
1 year	1.99×10^6	4.07×10^7	1.99×10^6
2 years	1.08×10^6	3.15×10^7	1.08×10^6
5 years	3.44×10^5	1.54×10^7	3.44×10^5
Light rain			
0 days	2.79×10^9	2.83×10^9	2.79×10^9
1 day	2.78×10^9	2.83×10^9	2.78×10^9
1 week	2.70×10^9	2.82×10^9	2.70×10^9
1 month	2.44×10^9	2.77×10^9	2.44×10^9
3 months	1.89×10^9	2.65×10^9	1.89×10^9
1 year	7.90×10^8	2.18×10^9	7.90×10^8
2 years	4.27×10^8	1.69×10^9	4.27×10^8
5 years	1.36×10^8	8.21×10^8	1.36×10^8
Heavy rain			
0 days	1.27×10^{10}	1.72×10^{10}	1.27×10^{10}
1 day	1.26×10^{10}	1.72×10^{10}	1.26×10^{10}
1 week	1.23×10^{10}	1.71×10^{10}	1.23×10^{10}

TABLE VII.1. PREDICTED CONTAMINATION DENSITIES (Bq/m^2) FROM METRO-K (OUTDOOR LOCATIONS ONLY), WITHOUT COUNTERMEASURES (cont.)

Time since event	Location 4	Location 5	Location 6
1 month	1.11×10^{10}	1.68×10^{10}	1.11×10^{10}
3 months	8.60×10^{9}	1.61×10^{10}	8.60×10^{9}
1 year	3.60×10^{9}	1.32×10^{10}	3.60×10^{9}
2 years	1.95×10^{9}	1.02×10^{10}	1.95×10^{9}
5 years	6.21×10^{8}	4.99×10^{9}	6.21×10^{8}
	Pu-239, summer release		
	Dry conditions		
0 days	7.03×10^{6}	5.29×10^{7}	7.03×10^{6}
1 day	7.00×10^{6}	5.29×10^{7}	7.00×10^{6}
1 week	6.83×10^{6}	5.28×10^{7}	6.83×10^{6}
1 month	6.21×10^{6}	5.23×10^{7}	6.21×10^{6}
3 months	4.92×10^{6}	5.12×10^{7}	4.92×10^{6}
1 year	2.27×10^{6}	4.64×10^{7}	2.27×10^{6}
2 years	1.40×10^{6}	4.10×10^{7}	1.40×10^{6}
5 years	6.64×10^{5}	2.97×10^{7}	6.64×10^{5}
	Light rain		
0 days	2.79×10^{9}	2.83×10^{9}	2.79×10^{9}
1 day	2.78×10^{9}	2.83×10^{9}	2.78×10^{9}
1 week	2.71×10^{9}	2.82×10^{9}	2.71×10^{9}
1 month	2.46×10^{9}	2.80×10^{9}	2.46×10^{9}
3 months	1.95×10^{9}	2.74×10^{9}	1.95×10^{9}
1 year	9.02×10^{8}	2.48×10^{9}	9.02×10^{8}
2 years	5.56×10^{8}	2.19×10^{9}	5.56×10^{8}
5 years	2.64×10^{8}	1.59×10^{9}	2.64×10^{8}
	Heavy rain		
0 days	1.27×10^{10}	1.72×10^{10}	1.27×10^{10}
1 day	1.26×10^{10}	1.72×10^{10}	1.26×10^{10}
1 week	1.23×10^{10}	1.72×10^{10}	1.23×10^{10}
1 month	1.12×10^{10}	1.70×10^{10}	1.12×10^{10}
3 months	8.89×10^{9}	1.66×10^{10}	8.89×10^{9}
1 year	4.10×10^{9}	1.51×10^{10}	4.10×10^{9}
2 years	2.53×10^{9}	1.33×10^{10}	2.53×10^{9}
5 years	1.20×10^{9}	9.64×10^{9}	1.20×10^{9}
	Pu-239, winter release		
	Dry conditions		
0 days	7.03×10^{6}	5.29×10^{7}	7.03×10^{6}
1 day	7.00×10^{6}	5.29×10^{7}	7.00×10^{6}
1 week	6.83×10^{6}	5.28×10^{7}	6.83×10^{6}
1 month	6.21×10^{6}	5.23×10^{7}	6.21×10^{6}
3 months	4.92×10^{6}	5.12×10^{7}	4.92×10^{6}
1 year	2.27×10^{6}	4.64×10^{7}	2.27×10^{6}
2 years	1.40×10^{6}	4.10×10^{7}	1.40×10^{6}
5 years	6.64×10^{5}	2.97×10^{7}	6.64×10^{5}
	Light rain		
0 days	2.79×10^{9}	2.83×10^{9}	2.79×10^{9}
1 day	2.78×10^{9}	2.83×10^{9}	2.78×10^{9}
1 week	2.71×10^{9}	2.82×10^{9}	2.71×10^{9}
1 month	2.46×10^{9}	2.80×10^{9}	2.46×10^{9}
3 months	1.95×10^{9}	2.74×10^{9}	1.95×10^{9}
1 year	9.02×10^{8}	2.48×10^{9}	9.02×10^{8}
2 years	5.56×10^{8}	2.19×10^{9}	5.56×10^{8}
5 years	2.64×10^{8}	1.59×10^{9}	2.64×10^{8}

TABLE VII.1. PREDICTED CONTAMINATION DENSITIES (Bq/m^2) FROM METRO-K (OUTDOOR LOCATIONS ONLY), WITHOUT COUNTERMEASURES (cont.)

Time since event	Location 4	Location 5	Location 6
	Heavy rain		
0 days	1.27×10^{10}	1.27×10^{10}	1.27×10^{10}
1 day	1.26×10^{10}	1.26×10^{10}	1.26×10^{10}
1 week	1.23×10^{10}	1.23×10^{10}	1.23×10^{10}
1 month	1.12×10^{10}	1.12×10^{10}	1.12×10^{10}
3 months	8.89×10^{9}	8.89×10^{9}	8.89×10^{9}
1 year	4.10×10^{9}	4.10×10^{9}	4.10×10^{9}
2 years	2.53×10^{9}	2.53×10^{9}	2.53×10^{9}
5 years	1.20×10^{9}	1.20×10^{9}	1.20×10^{9}

TABLE VII.2. PREDICTED CONTAMINATION DENSITIES (Bq/m^2) FROM ERMIN (OUTDOOR LOCATIONS ONLY), WITHOUT COUNTERMEASURES

Time since event	Location 4	Location 5	Location 6
	Co-60, summer release		
	Dry conditions		
0 days	1.587×10^{7}	5.290×10^{7}	1.587×10^{7}
1 day	1.581×10^{7}	5.288×10^{7}	1.580×10^{7}
1 week	1.545×10^{7}	5.277×10^{7}	1.536×10^{7}
1 month	1.415×10^{7}	5.236×10^{7}	1.381×10^{7}
3 months	8.412×10^{6}	5.480×10^{7}	7.085×10^{6}
1 year	5.035×10^{6}	5.142×10^{7}	3.425×10^{6}
2 years	2.573×10^{6}	4.535×10^{7}	1.268×10^{6}
5 years	7.783×10^{5}	3.092×10^{7}	4.126×10^{5}
	Light rain		
0 days	1.613×10^{9}	2.830×10^{9}	1.613×10^{9}
1 day	1.607×10^{9}	2.829×10^{9}	1.606×10^{9}
1 week	1.570×10^{9}	2.823×10^{9}	1.561×10^{9}
1 month	1.438×10^{9}	2.800×10^{9}	1.403×10^{9}
3 months	8.550×10^{8}	2.823×10^{9}	7.201×10^{8}
1 year	5.118×10^{8}	2.646×10^{9}	3.482×10^{8}
2 years	2.615×10^{8}	2.329×10^{9}	1.289×10^{8}
5 years	7.911×10^{7}	1.582×10^{9}	4.194×10^{7}
	Heavy rain		
0 days	7.740×10^{9}	1.720×10^{10}	7.740×10^{9}
1 day	7.710×10^{9}	1.719×10^{10}	7.704×10^{9}
1 week	7.534×10^{9}	1.716×10^{10}	7.491×10^{9}
1 month	6.902×10^{9}	1.702×10^{10}	6.733×10^{9}
3 months	4.102×10^{9}	1.646×10^{10}	3.455×10^{9}
1 year	2.456×10^{9}	1.541×10^{10}	1.671×10^{9}
2 years	1.255×10^{9}	1.353×10^{10}	6.184×10^{8}
5 years	3.796×10^{8}	9.143×10^{9}	2.012×10^{8}
	Co-60, winter release		
	Dry conditions		
0 days	1.587×10^{7}	5.290×10^{7}	1.587×10^{7}
1 day	1.581×10^{7}	5.288×10^{7}	1.580×10^{7}
1 week	1.545×10^{7}	5.277×10^{7}	1.536×10^{7}
1 month	1.415×10^{7}	5.236×10^{7}	1.381×10^{7}

TABLE VII.2. PREDICTED CONTAMINATION DENSITIES (Bq/m^2) FROM ERMIN (OUTDOOR LOCATIONS ONLY), WITHOUT COUNTERMEASURES (cont.)

Time since event	Location 4	Location 5	Location 6
3 months	8.412×10^6	4.974×10^7	7.085×10^6
1 year	5.035×10^6	4.668×10^7	3.425×10^6
2 years	2.573×10^6	4.119×10^7	1.268×10^6
5 years	7.783×10^5	2.812×10^7	4.126×10^5
	Light rain		
0 days	1.613×10^9	2.830×10^9	1.613×10^9
1 day	1.607×10^9	2.829×10^9	1.606×10^9
1 week	1.570×10^9	2.823×10^9	1.561×10^9
1 month	1.438×10^9	2.800×10^9	1.403×10^9
3 months	8.550×10^8	2.658×10^9	7.201×10^8
1 year	5.118×10^8	2.491×10^9	3.482×10^8
2 years	2.615×10^8	2.193×10^9	1.289×10^8
5 years	7.911×10^7	1.490×10^9	4.194×10^7
	Heavy rain		
0 days	7.740×10^9	1.720×10^{10}	7.740×10^9
1 day	7.710×10^9	1.719×10^{10}	7.704×10^9
1 week	7.534×10^9	1.716×10^{10}	7.491×10^9
1 month	6.902×10^9	1.702×10^{10}	6.733×10^9
3 months	4.102×10^9	1.613×10^{10}	3.455×10^9
1 year	2.456×10^9	1.510×10^{10}	1.671×10^9
2 years	1.255×10^9	1.326×10^{10}	6.184×10^8
5 years	3.796×10^8	8.961×10^9	2.012×10^8
	Pu-239, summer release		
	Dry conditions		
0 days	1.587×10^7	5.290×10^7	1.587×10^7
1 day	1.581×10^7	5.290×10^7	1.580×10^7
1 week	1.549×10^7	5.291×10^7	1.540×10^7
1 month	1.431×10^7	5.293×10^7	1.396×10^7
3 months	8.975×10^6	5.847×10^7	7.559×10^6
1 year	5.742×10^6	5.864×10^7	3.906×10^6
2 years	3.346×10^6	5.898×10^7	1.649×10^6
5 years	1.501×10^6	5.965×10^7	7.959×10^5
	Light rain		
0 days	1.613×10^9	2.830×10^9	1.613×10^9
1 day	1.607×10^9	2.830×10^9	1.606×10^9
1 week	1.574×10^9	2.830×10^9	1.565×10^9
1 month	1.454×10^9	2.831×10^9	1.419×10^9
3 months	9.122×10^8	3.012×10^9	7.683×10^8
1 year	5.837×10^8	3.018×10^9	3.971×10^8
2 years	3.401×10^8	3.029×10^9	1.676×10^8
5 years	1.526×10^8	3.051×10^9	8.089×10^7
	Heavy rain		
0 days	7.740×10^9	1.720×10^{10}	7.740×10^9
1 day	7.713×10^9	1.720×10^{10}	7.707×10^9
1 week	7.553×10^9	1.720×10^{10}	7.510×10^9
1 month	6.977×10^9	1.720×10^{10}	6.806×10^9
3 months	4.377×10^9	1.756×10^{10}	3.687×10^9
1 year	2.801×10^9	1.757×10^{10}	1.905×10^9
2 years	1.632×10^9	1.759×10^{10}	8.042×10^8
5 years	7.322×10^8	1.764×10^{10}	3.881×10^8

TABLE VII.2. PREDICTED CONTAMINATION DENSITIES (Bq/m^2) FROM ERMIN (OUTDOOR LOCATIONS ONLY), WITHOUT COUNTERMEASURES (cont.)

Time since event	Location 4	Location 5	Location 6
	Pu-239, winter release		
	Dry conditions		
0 days	1.587×10^7	5.290×10^7	1.587×10^7
1 day	1.581×10^7	5.290×10^7	1.580×10^7
1 week	1.549×10^7	5.291×10^7	1.540×10^7
1 month	1.431×10^7	5.293×10^7	1.396×10^7
3 months	8.975×10^6	5.307×10^7	7.559×10^6
1 year	5.742×10^6	5.324×10^7	3.906×10^6
2 years	3.346×10^6	5.357×10^7	1.649×10^6
5 years	1.501×10^6	5.424×10^7	7.959×10^5
	Light rain		
0 days	1.613×10^9	2.830×10^9	1.613×10^9
1 day	1.607×10^9	2.830×10^9	1.606×10^9
1 week	1.574×10^9	2.830×10^9	1.565×10^9
1 month	1.454×10^9	2.831×10^9	1.419×10^9
3 months	9.122×10^8	2.835×10^9	7.683×10^8
1 year	5.837×10^8	2.841×10^9	3.971×10^8
2 years	3.401×10^8	2.852×10^9	1.676×10^8
5 years	1.526×10^8	2.874×10^9	8.089×10^7
	Heavy rain		
0 days	7.740×10^9	1.720×10^{10}	7.740×10^9
1 day	7.713×10^9	1.720×10^{10}	7.707×10^9
1 week	7.553×10^9	1.720×10^{10}	7.510×10^9
1 month	6.977×10^9	1.720×10^{10}	6.806×10^9
3 months	4.377×10^9	1.721×10^{10}	3.687×10^9
1 year	2.801×10^9	1.722×10^{10}	1.905×10^9
2 years	1.632×10^9	1.724×10^{10}	8.042×10^8
5 years	7.322×10^8	1.729×10^{10}	3.881×10^8

TABLE VII.3. PREDICTED CONTAMINATION DENSITIES (Bq/m^2) FROM CPHR (OUTDOOR LOCATIONS ONLY), WITHOUT COUNTERMEASURES

Time since event	Location 4	Location 5	Location 6
	Co-60, summer release		
	Dry conditions		
1 day	3.96×10^5	3.96×10^5	5.28×10^5
1 week	5.98×10^5	5.98×10^5	7.98×10^5
1 month	5.94×10^5	5.92×10^5	7.91×10^5
3 months	5.81×10^5	5.76×10^5	7.74×10^5
1 year	5.27×10^5	5.10×10^5	7.02×10^5
2 years	4.63×10^5	4.33×10^5	6.16×10^5
5 years	3.13×10^5	2.66×10^5	4.16×10^5
	Light rain		
1 day	3.61×10^5	3.03×10^5	4.62×10^5
1 week	3.16×10^5	1.09×10^5	3.58×10^5
1 month	1.97×10^5	9.73×10^2	2.61×10^5
3 months	1.95×10^5	1.24×10^3	2.57×10^5
1 year	1.86×10^5	1.27×10^3	2.37×10^5
2 years	1.70×10^5	1.24×10^3	2.10×10^5
5 years	1.22×10^5	9.54×10^2	1.41×10^5

TABLE VII.3. PREDICTED CONTAMINATION DENSITIES (Bq/m^2) FROM CPHR (OUTDOOR LOCATIONS ONLY), WITHOUT COUNTERMEASURES (cont.)

Time since event	Location 4	Location 5	Location 6
Pu-239, summer release			
Dry conditions			
1 day	5.31×10^5	5.31×10^5	7.08×10^5
1 week	6.00×10^5	6.00×10^5	8.00×10^5
1 month	6.00×10^5	5.98×10^5	8.00×10^5
3 months	6.00×10^5	5.95×10^5	8.00×10^5
1 year	6.01×10^5	5.81×10^5	8.01×10^5
2 years	6.01×10^5	5.63×10^5	8.01×10^5
5 years	6.02×10^5	5.13×10^5	8.02×10^5
Light rain			
1 day	4.77×10^5	3.92×10^5	6.08×10^5
1 week	3.05×10^5	9.82×10^4	3.47×10^5
1 month	1.99×10^5	8.68×10^2	2.64×10^5
3 months	2.02×10^5	1.16×10^3	2.65×10^5
1 year	2.11×10^5	1.32×10^3	2.70×10^5
2 years	2.20×10^5	1.46×10^3	2.73×10^5
5 years	2.31×10^5	1.67×10^3	2.71×10^5

TABLE VII.4. PREDICTED CONTAMINATION DENSITIES (Bq/m^2) FROM RESRAD-RDD (OUTDOOR LOCATIONS ONLY), WITHOUT COUNTERMEASURES

Time since event	Location 4	Location 5	Location 6
Co-60, summer release			
Dry conditions			
0 days	2.12×10^7	4.76×10^7	2.12×10^7
1 day	2.10×10^7	4.75×10^7	2.10×10^7
1 week	2.03×10^7	4.73×10^7	2.03×10^7
1 month	1.80×10^7	4.62×10^7	1.80×10^7
3 months	1.37×10^7	4.37×10^7	1.37×10^7
1 year	6.84×10^6	3.43×10^7	6.84×10^6
2 years	4.13×10^6	2.61×10^7	4.13×10^6
5 years	9.67×10^5	1.35×10^7	9.67×10^5
Light rain			
0 days	1.56×10^9	1.98×10^9	1.56×10^9
1 day	1.54×10^9	1.98×10^9	1.54×10^9
1 week	1.49×10^9	1.97×10^9	1.49×10^9
1 month	1.32×10^9	1.92×10^9	1.32×10^9
3 months	1.01×10^9	1.82×10^9	1.01×10^9
1 year	5.03×10^8	1.43×10^9	5.03×10^8
2 years	3.04×10^8	1.09×10^9	3.04×10^8
5 years	7.11×10^7	5.64×10^8	7.11×10^7
Heavy rain			
0 days	9.46×10^9	1.20×10^{10}	9.46×10^9
1 day	9.38×10^9	1.20×10^{10}	9.38×10^9
1 week	9.08×10^9	1.20×10^{10}	9.08×10^9
1 month	8.05×10^9	1.17×10^{10}	8.05×10^9
3 months	6.14×10^9	1.11×10^{10}	6.14×10^9
1 year	3.06×10^9	8.68×10^9	3.06×10^9
2 years	1.85×10^9	6.60×10^9	1.85×10^9
5 years	4.32×10^8	3.43×10^9	4.32×10^8

TABLE VII.4. PREDICTED CONTAMINATION DENSITIES (Bq/m^2) FROM RESRAD-RDD (OUTDOOR LOCATIONS ONLY), WITHOUT COUNTERMEASURES (cont.)

Time since event	Location 4	Location 5	Location 6
	Pu-239, summer release		
	Dry conditions		
0 days	2.12×10^{7}	4.76×10^{7}	2.12×10^{7}
1 day	2.10×10^{7}	4.76×10^{7}	2.10×10^{7}
1 week	2.04×10^{7}	4.74×10^{7}	2.04×10^{7}
1 month	1.82×10^{7}	4.68×10^{7}	1.82×10^{7}
3 months	1.42×10^{7}	4.52×10^{7}	1.42×10^{7}
1 year	7.81×10^{6}	3.91×10^{7}	7.81×10^{6}
2 years	5.35×10^{6}	3.38×10^{7}	5.35×10^{6}
5 years	1.87×10^{6}	2.62×10^{7}	1.87×10^{6}
	Light rain		
0 days	1.56×10^{9}	1.98×10^{9}	1.56×10^{9}
1 day	1.54×10^{9}	1.98×10^{9}	1.54×10^{9}
1 week	1.50×10^{9}	1.97×10^{9}	1.50×10^{9}
1 month	1.34×10^{9}	1.95×10^{9}	1.34×10^{9}
3 months	1.04×10^{9}	1.88×10^{9}	1.04×10^{9}
1 year	5.74×10^{8}	1.63×10^{9}	5.74×10^{8}
2 years	3.94×10^{8}	1.41×10^{9}	3.94×10^{8}
5 years	1.37×10^{8}	1.09×10^{9}	1.37×10^{8}
	Heavy rain		
0 days	9.46×10^{9}	1.20×10^{10}	9.46×10^{9}
1 day	9.39×10^{9}	1.20×10^{10}	9.39×10^{9}
1 week	9.10×10^{9}	1.20×10^{10}	9.10×10^{9}
1 month	8.14×10^{9}	1.18×10^{10}	8.14×10^{9}
3 months	6.34×10^{9}	1.14×10^{10}	6.34×10^{9}
1 year	3.49×10^{9}	9.90×10^{9}	3.49×10^{9}
2 years	2.39×10^{9}	8.55×10^{9}	2.39×10^{9}
5 years	8.35×10^{8}	6.61×10^{9}	8.35×10^{8}

TABLE VII.5. PREDICTED CONTAMINATION DENSITIES (Bq/m^2) FROM CHERURB (OUTDOOR LOCATIONS ONLY), WITHOUT COUNTERMEASURES

Time since event	**Location 4**	**Location 5**	**Location 6**
	Co-60, summer release		
	Dry conditions		
0 days	2.44×10^{7}	not provided	2.44×10^{7}
1 day	2.40×10^{7}	not provided	2.40×10^{7}
1 week	2.23×10^{7}	not provided	2.23×10^{7}
1 month	1.67×10^{7}	not provided	1.67×10^{7}
3 months	9.73×10^{6}	not provided	9.73×10^{6}
1 year	5.90×10^{6}	not provided	5.90×10^{6}
2 years	5.64×10^{6}	not provided	5.64×10^{6}
5 years	5.03×10^{6}	not provided	5.03×10^{6}
	Light rain		
0 days	2.80×10^{9}	not provided	2.80×10^{9}
1 day	2.77×10^{9}	not provided	2.77×10^{9}
1 week	2.56×10^{9}	not provided	2.56×10^{9}
1 month	1.93×10^{9}	not provided	1.93×10^{9}
3 months	1.12×10^{9}	not provided	1.12×10^{9}
1 year	6.78×10^{8}	not provided	6.78×10^{8}
2 years	6.49×10^{8}	not provided	6.49×10^{8}
5 years	5.79×10^{8}	not provided	5.79×10^{8}

TABLE VII.5. PREDICTED CONTAMINATION DENSITIES (Bq/m^2) FROM CHERURB (OUTDOOR LOCATIONS ONLY), WITHOUT COUNTERMEASURES (cont.)

Time since event	Location 4	Location 5	Location 6
	Heavy rain		
0 days	9.49×10^{9}	not provided	9.49×10^{9}
1 day	9.37×10^{9}	not provided	9.37×10^{9}
1 week	8.68×10^{9}	not provided	8.68×10^{9}
1 month	6.52×10^{9}	not provided	6.52×10^{9}
3 months	3.79×10^{9}	not provided	3.79×10^{9}
1 year	2.30×10^{9}	not provided	2.30×10^{9}
2 years	2.20×10^{9}	not provided	2.20×10^{9}
5 years	1.96×10^{9}	not provided	1.96×10^{9}
	Pu-239, summer release		
	Dry conditions		
0 days	2.44×10^{7}	not provided	2.44×10^{7}
1 day	2.41×10^{7}	not provided	2.41×10^{7}
1 week	2.23×10^{7}	not provided	2.23×10^{7}
1 month	1.68×10^{7}	not provided	1.68×10^{7}
3 months	9.76×10^{6}	not provided	9.76×10^{6}
1 year	5.97×10^{6}	not provided	5.97×10^{6}
2 years	5.79×10^{6}	not provided	5.79×10^{6}
5 years	5.37×10^{6}	not provided	5.37×10^{6}
	Light rain		
0 days	2.80×10^{9}	not provided	2.80×10^{9}
1 day	2.77×10^{9}	not provided	2.77×10^{9}
1 week	2.56×10^{9}	not provided	2.56×10^{9}
1 month	1.93×10^{9}	not provided	1.93×10^{9}
3 months	1.12×10^{9}	not provided	1.12×10^{9}
1 year	6.87×10^{8}	not provided	6.87×10^{8}
2 years	6.66×10^{8}	not provided	6.66×10^{8}
5 years	6.18×10^{8}	not provided	6.18×10^{8}
	Heavy rain		
0 days	9.49×10^{9}	not provided	9.49×10^{9}
1 day	9.37×10^{9}	not provided	9.37×10^{9}
1 week	8.68×10^{9}	not provided	8.68×10^{9}
1 month	6.53×10^{9}	not provided	6.53×10^{9}
3 months	3.81×10^{9}	not provided	3.81×10^{9}
1 year	2.33×10^{9}	not provided	2.33×10^{9}
2 years	2.26×10^{9}	not provided	2.26×10^{9}
5 years	2.09×10^{9}	not provided	2.09×10^{9}

TABLE VII.6. PREDICTED EXTERNAL DOSE RATES (mGy/h) FROM METRO-K, WITHOUT COUNTERMEASURES

Time since event	Location 1	Location 2	Location 3	Location 4	Location 5	Location 6
			Co-60, summer release			
			Dry conditions			
0 days	3.22×10^{-3}	6.68×10^{-5}	3.25×10^{-3}	1.09×10^{-1}	5.38×10^{-1}	5.24×10^{-2}
1 day	3.20×10^{-3}	6.68×10^{-5}	3.25×10^{-3}	1.08×10^{-1}	5.37×10^{-1}	5.21×10^{-2}
1 week	3.07×10^{-3}	6.65×10^{-5}	3.24×10^{-3}	1.04×10^{-1}	5.30×10^{-1}	5.05×10^{-2}
1 month	2.64×10^{-3}	6.55×10^{-5}	3.19×10^{-3}	9.12×10^{-2}	5.05×10^{-1}	4.48×10^{-2}
3 months	1.80×10^{-3}	6.31×10^{-5}	3.07×10^{-3}	6.53×10^{-2}	4.53×10^{-1}	3.33×10^{-2}
1 year	4.07×10^{-4}	5.30×10^{-5}	2.59×10^{-3}	1.99×10^{-2}	3.29×10^{-1}	1.19×10^{-2}
2 years	1.50×10^{-4}	4.21×10^{-5}	2.08×10^{-3}	9.28×10^{-3}	2.49×10^{-1}	5.96×10^{-3}
5 years	5.14×10^{-5}	2.11×10^{-5}	1.10×10^{-3}	3.09×10^{-3}	1.21×10^{-1}	1.88×10^{-3}

TABLE VII.6. PREDICTED EXTERNAL DOSE RATES (mGy/h) FROM METRO-K, WITHOUT COUNTERMEASURES (cont.)

Time since event	Location 1	Location 2	Location 3	Location 4	Location 5	Location 6
			Light rain			
0 days	3.16×10^{-1}	4.73×10^{-3}	2.41×10^{-1}	2.17×10^{1}	2.52×10^{1}	1.56×10^{1}
1 day	3.14×10^{-1}	4.73×10^{-3}	2.41×10^{-1}	2.16×10^{1}	2.52×10^{1}	1.55×10^{1}
1 week	3.05×10^{-1}	4.71×10^{-3}	2.40×10^{-1}	2.10×10^{1}	2.50×10^{1}	1.51×10^{1}
1 month	2.72×10^{-1}	4.64×10^{-3}	2.37×10^{-1}	1.89×10^{1}	2.42×10^{1}	1.36×10^{1}
3 months	2.05×10^{-1}	4.47×10^{-3}	2.28×10^{-1}	1.45×10^{1}	2.24×10^{1}	1.05×10^{1}
1 year	7.87×10^{-2}	3.76×10^{-3}	1.92×10^{-1}	5.92×10^{0}	1.73×10^{1}	4.34×10^{0}
2 years	4.15×10^{-2}	2.98×10^{-3}	1.54×10^{-1}	3.18×10^{0}	1.33×10^{1}	2.33×10^{0}
5 years	1.37×10^{-2}	1.49×10^{-3}	8.18×10^{-2}	1.03×10^{0}	6.47×10^{0}	7.45×10^{-1}
			Heavy rain			
0 days	1.50×10^{0}	1.83×10^{-2}	3.39×10^{-2}	1.00×10^{2}	1.53×10^{2}	7.14×10^{1}
1 day	1.49×10^{0}	1.83×10^{-2}	3.39×10^{-2}	1.00×10^{2}	1.52×10^{2}	7.11×10^{1}
1 week	1.45×10^{0}	1.82×10^{-2}	3.38×10^{-2}	9.72×10^{1}	1.51×10^{2}	6.91×10^{1}
1 month	1.29×10^{0}	1.80×10^{-2}	3.33×10^{-2}	8.73×10^{1}	1.46×10^{2}	6.22×10^{1}
3 months	9.68×10^{-1}	1.73×10^{-2}	3.20×10^{-2}	6.70×10^{1}	1.36×10^{2}	4.80×10^{1}
1 year	3.61×10^{-1}	1.45×10^{-2}	2.70×10^{-2}	2.71×10^{1}	1.06×10^{2}	1.98×10^{1}
2 years	1.87×10^{-1}	1.15×10^{-2}	2.17×10^{-2}	1.45×10^{1}	8.11×10^{1}	1.07×10^{1}
5 years	6.14×10^{-2}	5.77×10^{-3}	1.15×10^{-2}	4.68×10^{0}	3.95×10^{1}	3.40×10^{0}
			Co-60, winter release			
			Dry conditions			
0 days	8.23×10^{-4}	6.68×10^{-5}	3.25×10^{-3}	5.58×10^{-2}	4.78×10^{-1}	4.54×10^{-2}
1 day	8.19×10^{-4}	6.68×10^{-5}	3.25×10^{-3}	5.55×10^{-2}	4.77×10^{-1}	4.52×10^{-2}
1 week	7.96×10^{-4}	6.65×10^{-5}	3.24×10^{-3}	5.40×10^{-2}	4.72×10^{-1}	4.39×10^{-2}
1 month	7.17×10^{-4}	6.55×10^{-5}	3.19×10^{-3}	4.87×10^{-2}	4.57×10^{-1}	3.92×10^{-2}
3 months	5.55×10^{-4}	6.31×10^{-5}	3.07×10^{-3}	3.78×10^{-2}	4.22×10^{-1}	2.97×10^{-2}
1 year	2.39×10^{-4}	5.30×10^{-5}	2.59×10^{-3}	1.62×10^{-2}	3.25×10^{-1}	1.14×10^{-2}
2 years	1.38×10^{-4}	4.21×10^{-5}	2.08×10^{-3}	9.02×10^{-3}	2.49×10^{-1}	5.93×10^{-3}
5 years	5.14×10^{-5}	2.11×10^{-5}	1.10×10^{-3}	3.09×10^{-3}	1.21×10^{-1}	1.88×10^{-3}
			Light rain			
0 days	2.58×10^{-1}	4.73×10^{-3}	2.41×10^{-1}	2.04×10^{1}	2.38×10^{1}	1.54×10^{1}
1 day	2.56×10^{-1}	4.73×10^{-3}	2.41×10^{-1}	2.03×10^{1}	2.37×10^{1}	1.53×10^{1}
1 week	2.50×10^{-1}	4.71×10^{-3}	2.40×10^{-1}	1.98×10^{1}	2.36×10^{1}	1.49×10^{1}
1 month	2.25×10^{-1}	4.64×10^{-3}	2.37×10^{-1}	1.78×10^{1}	2.30×10^{1}	1.34×10^{1}
3 months	1.75×10^{-1}	4.47×10^{-3}	2.28×10^{-1}	1.38×10^{1}	2.16×10^{1}	1.04×10^{1}
1 year	7.47×10^{-2}	3.76×10^{-3}	1.92×10^{-1}	5.83×10^{0}	1.72×10^{1}	4.33×10^{0}
2 years	4.12×10^{-2}	2.98×10^{-3}	1.54×10^{-1}	3.18×10^{0}	1.33×10^{1}	2.33×10^{0}
5 years	1.37×10^{-2}	1.49×10^{-3}	8.18×10^{-2}	1.03×10^{0}	6.47×10^{0}	7.45×10^{-1}
			Heavy rain			
0 days	1.17×10^{0}	1.83×10^{-2}	3.39×10^{-2}	9.32×10^{1}	1.44×10^{2}	7.04×10^{1}
1 day	1.17×10^{0}	1.83×10^{-2}	3.39×10^{-2}	9.28×10^{1}	1.44×10^{2}	7.01×10^{1}
1 week	1.14×10^{0}	1.82×10^{-2}	3.38×10^{-2}	9.03×10^{1}	1.43×10^{2}	6.82×10^{1}
1 month	1.03×10^{0}	1.80×10^{-2}	3.33×10^{-2}	8.14×10^{1}	1.40×10^{2}	6.15×10^{1}
3 months	7.98×10^{-1}	1.73×10^{-2}	3.20×10^{-2}	6.32×10^{1}	1.32×10^{2}	4.76×10^{1}
1 year	3.38×10^{-1}	1.45×10^{-2}	2.70×10^{-2}	2.66×10^{1}	1.05×10^{2}	1.97×10^{1}
2 years	1.86×10^{-1}	1.15×10^{-2}	2.17×10^{-2}	1.45×10^{1}	8.10×10^{1}	1.06×10^{1}
5 years	6.14×10^{-2}	5.77×10^{-3}	1.15×10^{-2}	4.68×10^{0}	3.95×10^{1}	3.40×10^{0}

TABLE VII.7. PREDICTED EXTERNAL DOSE RATES (mGy/h) FROM ERMIN, WITHOUT COUNTERMEASURES

Time since event	Location 1	Location 2	Location 3	Location 4	Location 5	Location 6
Co-60, summer release						
Dry conditions						
0 days	1.354×10^{-2}	6.734×10^{-3}	9.589×10^{-3}	1.632×10^{-1}	3.731×10^{-1}	1.528×10^{-1}
1 day	1.345×10^{-2}	6.708×10^{-3}	9.561×10^{-3}	1.622×10^{-1}	3.720×10^{-1}	1.520×10^{-1}
1 week	1.294×10^{-2}	6.553×10^{-3}	9.390×10^{-3}	1.568×10^{-1}	3.660×10^{-1}	1.470×10^{-1}
1 month	1.136×10^{-2}	5.991×10^{-3}	8.772×10^{-3}	1.398×10^{-1}	3.462×10^{-1}	1.311×10^{-1}
3 months	5.468×10^{-3}	3.383×10^{-3}	5.832×10^{-3}	8.269×10^{-2}	2.706×10^{-1}	7.853×10^{-2}
1 year	3.314×10^{-3}	1.746×10^{-3}	3.853×10^{-3}	6.383×10^{-2}	2.320×10^{-1}	5.436×10^{-2}
2 years	1.694×10^{-3}	5.967×10^{-4}	2.194×10^{-3}	4.665×10^{-2}	1.840×10^{-1}	3.649×10^{-2}
5 years	6.927×10^{-4}	1.512×10^{-4}	9.491×10^{-4}	2.531×10^{-2}	1.054×10^{-1}	2.028×10^{-2}
Light rain						
0 days	5.230×10^{-1}	1.772×10^{-1}	3.355×10^{-1}	9.765×10^{0}	1.883×10^{1}	1.146×10^{1}
1 day	5.197×10^{-1}	1.765×10^{-1}	3.346×10^{-1}	9.718×10^{0}	1.879×10^{1}	1.140×10^{1}
1 week	5.008×10^{-1}	1.724×10^{-1}	3.297×10^{-1}	9.441×10^{0}	1.856×10^{1}	1.108×10^{1}
1 month	4.419×10^{-1}	1.574×10^{-1}	3.116×10^{-1}	8.527×10^{0}	1.775×10^{1}	9.974×10^{0}
3 months	2.199×10^{-1}	8.805×10^{-2}	2.239×10^{-1}	5.030×10^{0}	1.401×10^{1}	5.680×10^{0}
1 year	1.344×10^{-1}	4.462×10^{-2}	1.616×10^{-1}	3.499×10^{0}	1.188×10^{1}	3.471×10^{0}
2 years	7.158×10^{-2}	1.436×10^{-2}	1.031×10^{-1}	2.313×10^{0}	9.329×10^{0}	1.999×10^{0}
5 years	3.006×10^{-2}	3.253×10^{-3}	4.758×10^{-2}	1.171×10^{0}	5.275×10^{0}	1.001×10^{0}
Heavy rain						
0 days	1.408×10^{0}	1.321×10^{-1}	7.068×10^{-1}	4.258×10^{1}	1.019×10^{2}	5.323×10^{1}
1 day	1.401×10^{0}	1.317×10^{-1}	7.058×10^{-1}	4.241×10^{1}	1.017×10^{2}	5.300×10^{1}
1 week	1.358×10^{0}	1.290×10^{-1}	7.003×10^{-1}	4.140×10^{1}	1.011×10^{2}	5.168×10^{1}
1 month	1.220×10^{0}	1.196×10^{-1}	6.796×10^{-1}	3.793×10^{1}	9.803×10^{1}	4.700×10^{1}
3 months	6.757×10^{-1}	7.528×10^{-2}	5.688×10^{-1}	2.361×10^{1}	7.930×10^{1}	2.719×10^{1}
1 year	4.488×10^{-1}	4.648×10^{-2}	4.714×10^{-1}	1.625×10^{1}	6.708×10^{1}	1.648×10^{1}
2 years	2.776×10^{-1}	2.410×10^{-2}	3.465×10^{-1}	1.061×10^{1}	5.239×10^{1}	9.321×10^{0}
5 years	1.304×10^{-1}	9.679×10^{-3}	1.707×10^{-1}	5.304×10^{0}	2.927×10^{1}	4.505×10^{0}
Co-60, winter release						
Dry conditions						
0 days	1.002×10^{-2}	6.734×10^{-3}	9.589×10^{-3}	1.109×10^{-1}	3.101×10^{-1}	1.214×10^{-1}
1 day	9.974×10^{-3}	6.708×10^{-3}	9.561×10^{-3}	1.106×10^{-1}	3.098×10^{-1}	1.209×10^{-1}
1 week	9.691×10^{-3}	6.553×10^{-3}	9.390×10^{-3}	1.086×10^{-1}	3.079×10^{-1}	1.180×10^{-1}
1 month	8.752×10^{-3}	5.991×10^{-3}	8.772×10^{-3}	1.011 × 10-1	2.996×10^{-1}	1.078×10^{-1}
3 months	5.115×10^{-3}	3.383×10^{-3}	5.832×10^{-3}	6.966×10^{-2}	2.435×10^{-1}	6.496×10^{-2}
1 year	2.983×10^{-3}	1.746×10^{-3}	3.853×10^{-3}	5.164×10^{-2}	2.066×10^{-1}	4.166×10^{-2}
2 years	1.404×10^{-3}	5.967×10^{-4}	2.194×10^{-3}	3.596×10^{-2}	1.617×10^{-1}	2.536×10^{-2}
5 years	4.973×10^{-4}	1.512×10^{-4}	9.491×10^{-4}	1.810×10^{-2}	9.034×10^{-2}	1.277×10^{-2}
Light rain						
0 days	4.079×10^{-1}	1.772×10^{-1}	3.355×10^{-1}	8.055×10^{0}	1.676×10^{1}	1.043×10^{1}
1 day	4.059×10^{-1}	1.765×10^{-1}	3.346×10^{-1}	8.027×10^{0}	1.675×10^{1}	1.038×10^{1}
1 week	3.945×10^{-1}	1.724×10^{-1}	3.297×10^{-1}	7.863×10^{0}	1.666×10^{1}	1.013×10^{1}
1 month	3.566×10^{-1}	1.574×10^{-1}	3.116×10^{-1}	7.260×10^{0}	1.622×10^{1}	9.210×10^{0}
3 months	2.084×10^{-1}	8.805×10^{-2}	2.239×10^{-1}	4.604×10^{0}	1.312×10^{1}	5.236×10^{0}
1 year	1.236×10^{-1}	4.462×10^{-2}	1.616×10^{-1}	3.100×10^{0}	1.105×10^{1}	3.055×10^{0}
2 years	6.209×10^{-2}	1.436×10^{-2}	1.031×10^{-1}	1.963×10^{0}	8.600×10^{0}	1.634×10^{0}
5 years	2.366×10^{-2}	3.253×10^{-3}	4.758×10^{-2}	9.347×10^{-1}	4.784×10^{0}	7.548×10^{-1}
Heavy rain						
0 days	1.180×10^{0}	1.321×10^{-1}	7.068×10^{-1}	3.919×10^{1}	9.776×10^{1}	5.118×10^{1}
1 day	1.175×10^{0}	1.317×10^{-1}	7.058×10^{-1}	3.905×10^{1}	9.769×10^{1}	5.098×10^{1}

TABLE VII.7. PREDICTED EXTERNAL DOSE RATES (mGy/h) FROM ERMIN, WITHOUT COUNTERMEASURES (cont.)

Time since event	Location 1	Location 2	Location 3	Location 4	Location 5	Location 6
1 week	1.147×10^{0}	1.290×10^{-1}	7.003×10^{-1}	3.827×10^{1}	9.730×10^{1}	4.979×10^{1}
1 month	1.051×10^{0}	1.196×10^{-1}	6.796×10^{-1}	3.542×10^{1}	9.499×10^{1}	4.548×10^{1}
3 months	6.528×10^{-1}	7.528×10^{-2}	5.688×10^{-1}	2.276×10^{1}	7.753×10^{1}	2.631×10^{1}
1 year	4.273×10^{-1}	4.648×10^{-2}	4.714×10^{-1}	1.546×10^{1}	6.543×10^{1}	1.565×10^{1}
2 years	2.588×10^{-1}	2.410×10^{-2}	3.465×10^{-1}	9.916×10^{0}	5.094×10^{1}	8.597×10^{0}
5 years	1.177×10^{-1}	9.679×10^{-3}	1.707×10^{-1}	4.835×10^{0}	2.829×10^{1}	4.017×10^{0}
Pu-239, summer release						
Dry conditions						
0 days	1.403×10^{-9}	1.245×10^{-9}	1.271×10^{-9}	8.030×10^{-9}	1.322×10^{-5}	5.415×10^{-6}
1 day	1.397×10^{-9}	1.241×10^{-9}	1.266×10^{-9}	7.975×10^{-9}	1.318×10^{-5}	5.386×10^{-6}
1 week	1.360×10^{-9}	1.213×10^{-9}	1.239×10^{-9}	7.663×10^{-9}	1.300×10^{-5}	5.221×10^{-6}
1 month	1.235×10^{-9}	1.112×10^{-9}	1.138×10^{-9}	6.758×10^{-9}	1.232×10^{-5}	4.687×10^{-6}
3 months	6.788×10^{-10}	6.341×10^{-10}	6.577×10^{-10}	4.008×10^{-9}	9.066×10^{-6}	2.852×10^{-6}
1 year	3.549×10^{-10}	3.194×10^{-10}	3.411×10^{-10}	3.265×10^{-9}	7.784×10^{-6}	2.037×10^{-6}
2 years	1.147×10^{-10}	8.719×10^{-11}	1.059×10^{-10}	2.671×10^{-9}	6.613×10^{-6}	1.495×10^{-6}
5 years	2.726×10^{-11}	8.734×10^{-12}	2.256×10^{-11}	2.064×10^{-9}	5.220×10^{-6}	1.188×10^{-6}
Light rain						
0 days	4.084×10^{-8}	3.316×10^{-8}	3.465×10^{-8}	4.718×10^{-7}	6.669×10^{-4}	4.059×10^{-4}
1 day	4.065×10^{-8}	3.304×10^{-8}	3.452×10^{-8}	4.692×10^{-7}	6.657×10^{-4}	4.041×10^{-4}
1 week	3.956×10^{-8}	3.230×10^{-8}	3.378×10^{-8}	4.542×10^{-7}	6.591×10^{-4}	3.934×10^{-4}
1 month	3.586×10^{-8}	2.962×10^{-8}	3.108×10^{-8}	4.077×10^{-7}	6.309×10^{-4}	3.567×10^{-4}
3 months	1.966×10^{-8}	1.686×10^{-8}	1.822×10^{-8}	2.442×10^{-7}	4.671×10^{-4}	2.085×10^{-4}
1 year	1.046×10^{-8}	8.464×10^{-9}	9.712×10^{-9}	1.782×10^{-7}	3.949×10^{-4}	1.317×10^{-4}
2 years	3.678×10^{-9}	2.273×10^{-9}	3.352×10^{-9}	1.307×10^{-7}	3.299×10^{-4}	8.211×10^{-5}
5 years	1.094×10^{-9}	1.933×10^{-10}	9.923×10^{-10}	9.306×10^{-8}	2.542×10^{-4}	5.775×10^{-5}
Heavy rain						
0 days	4.750×10^{-8}	2.080×10^{-8}	2.620×10^{-8}	1.982×10^{-6}	3.608×10^{-3}	1.886×10^{-3}
1 day	4.727×10^{-8}	2.072×10^{-8}	2.612×10^{-8}	1.974×10^{-6}	3.605×10^{-3}	1.878×10^{-3}
1 week	4.595×10^{-8}	2.027×10^{-8}	2.566×10^{-8}	1.927×10^{-6}	3.590×10^{-3}	1.835×10^{-3}
1 month	4.159×10^{-8}	1.864×10^{-8}	2.396×10^{-8}	1.769×10^{-6}	3.476×10^{-3}	1.680×10^{-3}
3 months	2.324×10^{-8}	1.086×10^{-8}	1.581×10^{-8}	1.122×10^{-6}	2.621×10^{-3}	9.902×10^{-4}
1 year	1.433×10^{-8}	5.727×10^{-9}	1.028×10^{-8}	8.030×10^{-7}	2.197×10^{-3}	6.144×10^{-4}
2 years	7.813×10^{-9}	1.909×10^{-9}	5.843×10^{-9}	5.744×10^{-7}	1.812×10^{-3}	3.692×10^{-4}
5 years	4.321×10^{-9}	5.092×10^{-10}	3.424×10^{-9}	3.967×10^{-7}	1.360×10^{-3}	2.438×10^{-4}
Pu-239, winter release						
Dry conditions						
0 days	1.317×10^{-9}	1.245×10^{-9}	1.271×10^{-9}	5.400×10^{-9}	1.099×10^{-5}	4.299×10^{-6}
1 day	1.312×10^{-9}	1.241×10^{-9}	1.266×10^{-9}	5.375×10^{-9}	1.098×10^{-5}	4.283×10^{-6}
1 week	1.281×10^{-9}	1.213×10^{-9}	1.239×10^{-9}	5.230×10^{-9}	1.093×10^{-5}	4.190×10^{-6}
1 month	1.171×10^{-9}	1.112×10^{-9}	1.138×10^{-9}	4.789×10^{-9}	1.065×10^{-5}	3.852×10^{-6}
3 months	6.712×10^{-10}	6.341×10^{-10}	6.577×10^{-10}	3.357×10^{-9}	8.040×10^{-6}	2.339×10^{-6}
1 year	3.472×10^{-10}	3.194×10^{-10}	3.411×10^{-10}	2.614×10^{-9}	6.758×10^{-6}	1.524×10^{-6}
2 years	1.070×10^{-10}	8.719×10^{-11}	1.059×10^{-10}	2.020×10^{-9}	5.587×10^{-6}	9.820×10^{-7}
5 years	1.960×10^{-11}	8.734×10^{-12}	2.256×10^{-11}	1.413×10^{-9}	4.194×10^{-6}	6.747×10^{-7}
Light rain						
0 days	3.802×10^{-8}	3.316×10^{-8}	3.465×10^{-8}	3.857×10^{-7}	5.939×10^{-4}	3.694×10^{-4}
1 day	3.787×10^{-8}	3.304×10^{-8}	3.452×10^{-8}	3.840×10^{-7}	5.935×10^{-4}	3.680×10^{-4}
1 week	3.695×10^{-8}	3.230×10^{-8}	3.378×10^{-8}	3.745×10^{-7}	5.915×10^{-4}	3.596×10^{-4}
1 month	3.375×10^{-8}	2.962×10^{-8}	3.108×10^{-8}	3.433×10^{-7}	5.762×10^{-4}	3.294×10^{-4}
3 months	1.941×10^{-8}	1.686×10^{-8}	1.822×10^{-8}	2.229×10^{-7}	4.335×10^{-4}	1.917×10^{-4}

TABLE VII.7. PREDICTED EXTERNAL DOSE RATES (mGy/h) FROM ERMIN, WITHOUT COUNTERMEASURES (cont.)

Time since event	Location 1	Location 2	Location 3	Location 4	Location 5	Location 6
1 year	1.021×10^{-8}	8.464×10^{-9}	9.712×10^{-9}	1.569×10^{-7}	3.613×10^{-4}	1.149×10^{-4}
2 years	3.428×10^{-9}	2.273×10^{-9}	3.352×10^{-9}	1.093×10^{-7}	2.963×10^{-4}	6.531×10^{-5}
5 years	8.430×10^{-10}	1.933×10^{-10}	9.923×10^{-10}	7.174×10^{-8}	2.207×10^{-4}	4.095×10^{-5}
			Heavy rain			
0 days	4.190×10^{-8}	2.080×10^{-8}	2.620×10^{-8}	1.811×10^{-6}	3.463×10^{-3}	1.813×10^{-3}
1 day	4.173×10^{-8}	2.072×10^{-8}	2.612×10^{-8}	1.805×10^{-6}	3.462×10^{-3}	1.807×10^{-3}
1 week	4.077×10^{-8}	2.027×10^{-8}	2.566×10^{-8}	1.769×10^{-6}	3.456×10^{-3}	1.768×10^{-3}
1 month	3.739×10^{-8}	1.864×10^{-8}	2.396×10^{-8}	1.641×10^{-6}	3.368×10^{-3}	1.625×10^{-3}
3 months	2.274×10^{-8}	1.086×10^{-8}	1.581×10^{-8}	1.080×10^{-6}	2.554×10^{-3}	9.568×10^{-4}
1 year	1.383×10^{-8}	5.727×10^{-9}	1.028×10^{-8}	7.607×10^{-7}	2.130×10^{-3}	5.810×10^{-4}
2 years	7.314×10^{-9}	1.909×10^{-9}	5.843×10^{-9}	5.320×10^{-7}	1.745×10^{-3}	3.359×10^{-4}
5 years	3.823×10^{-9}	5.092×10^{-10}	3.424×10^{-9}	3.543×10^{-7}	1.293×10^{-3}	2.105×10^{-4}

TABLE VII.8. PREDICTED EXTERNAL DOSE RATES (mGy/h) FROM CPHR, WITHOUT COUNTERMEASURES

Time since event	Location 1	Location 2	Location 3	Location 4	Location 5	Location 6
			Co-60, summer release			
			Dry conditions			
0 days	3.18×10^{-1}	3.18×10^{-1}	3.18×10^{-1}	4.54×10^{-1}	4.54×10^{-1}	4.54×10^{-1}
1 day	1.09×10^{-1}	1.09×10^{-1}	1.09×10^{-1}	1.55×10^{-1}	1.57×10^{-1}	1.58×10^{-1}
1 week	1.34×10^{-3}	1.34×10^{-3}	1.29×10^{-3}	2.39×10^{-3}	4.12×10^{-3}	6.37×10^{-3}
1 month	1.17×10^{-3}	1.17×10^{-3}	1.12×10^{-3}	2.14×10^{-3}	3.86×10^{-3}	6.09×10^{-3}
3 months	1.15×10^{-3}	1.15×10^{-3}	1.10×10^{-3}	2.10×10^{-3}	3.75×10^{-3}	5.96×10^{-3}
1 year	1.04×10^{-3}	1.04×10^{-3}	9.97×10^{-4}	1.90×10^{-3}	3.33×10^{-3}	5.40×10^{-3}
2 years	9.07×10^{-4}	9.07×10^{-4}	8.74×10^{-4}	1.67×10^{-3}	2.83×10^{-3}	4.74×10^{-3}
5 years	6.08×10^{-4}	6.08×10^{-4}	5.89×10^{-4}	1.12×10^{-3}	1.75×10^{-3}	3.20×10^{-3}
			Light rain			
0 days	3.18×10^{-1}	3.18×10^{-1}	3.18×10^{-1}	4.54×10^{-1}	4.54×10^{-1}	4.54×10^{-1}
1 day	1.08×10^{-1}	1.08×10^{-1}	1.08×10^{-1}	1.55×10^{-1}	1.56×10^{-1}	1.57×10^{-1}
1 week	5.25×10^{-4}	5.25×10^{-4}	4.78×10^{-4}	1.34×10^{-3}	9.71×10^{-4}	2.97×10^{-3}
1 month	5.00×10^{-6}	5.00×10^{-6}	4.00×10^{-6}	6.68×10^{-4}	6.99×10^{-6}	1.99×10^{-3}
3 months	3.35×10^{-6}	3.35×10^{-6}	2.68×10^{-6}	6.62×10^{-4}	8.25×10^{-6}	1.95×10^{-3}
1 year	2.51×10^{-6}	2.51×10^{-6}	2.01×10^{-6}	6.30×10^{-4}	8.30×10^{-6}	1.81×10^{-3}
2 years	1.74×10^{-6}	1.74×10^{-6}	1.40×10^{-6}	5.77×10^{-4}	7.92×10^{-6}	1.60×10^{-3}
5 years	5.86×10^{-7}	5.86×10^{-7}	4.69×10^{-7}	4.11×10^{-4}	5.93×10^{-6}	1.07×10^{-3}
			Pu-239, summer release			
			Dry conditions			
0 days	5.47×10^{-3}	5.47×10^{-3}	5.47×10^{-3}	7.81×10^{-3}	7.81×10^{-3}	7.81×10^{-3}
1 day	6.30×10^{-4}	6.30×10^{-4}	6.30×10^{-4}	9.00×10^{-4}	9.00×10^{-4}	9.01×10^{-4}
1 week	1.86×10^{-7}	1.86×10^{-7}	1.79×10^{-7}	3.40×10^{-7}	6.12×10^{-7}	9.64×10^{-7}
1 month	1.85×10^{-7}	1.85×10^{-7}	1.78×10^{-7}	3.38×10^{-7}	6.09×10^{-7}	9.62×10^{-7}
3 months	1.85×10^{-7}	1.85×10^{-7}	1.77×10^{-7}	3.38×10^{-7}	6.06×10^{-7}	9.62×10^{-7}
1 year	1.85×10^{-7}	1.85×10^{-7}	1.77×10^{-7}	3.39×10^{-7}	5.93×10^{-7}	9.63×10^{-7}
2 years	1.84×10^{-7}	1.84×10^{-7}	1.77×10^{-7}	3.39×10^{-7}	5.75×10^{-7}	9.63×10^{-7}
5 years	1.83×10^{-7}	1.83×10^{-7}	1.76×10^{-7}	3.39×10^{-7}	5.28×10^{-7}	9.64×10^{-7}

TABLE VII.8. PREDICTED EXTERNAL DOSE RATES (mGy/h) FROM CPHR, WITHOUT COUNTERMEASURES (cont.)

Time since event	Location 1	Location 2	Location 3	Location 4	Location 5	Location 6
			Light rain			
0 days	5.47×10^{-3}	5.47×10^{-3}	5.47×10^{-3}	7.81×10^{-3}	7.81×10^{-3}	7.81×10^{-3}
1 day	6.31×10^{-4}	6.31×10^{-4}	6.31×10^{-4}	9.01×10^{-4}	9.00 × 10-4	9.01×10^{-4}
1 week	5.33×10^{-8}	5.33×10^{-8}	4.59×10^{-8}	1.69×10^{-7}	1.06×10^{-7}	4.16×10^{-7}
1 month	7.25×10^{-10}	7.25×10^{-10}	5.80×10^{-10}	1.05×10^{-7}	9.81×10^{-10}	3.14×10^{-7}
3 months	4.88×10^{-10}	4.88×10^{-10}	3.90×10^{-10}	1.07×10^{-7}	1.21×10^{-9}	3.15×10^{-7}
1 year	4.03×10^{-10}	4.03×10^{-10}	3.22×10^{-10}	1.12×10^{-7}	1.34×10^{-9}	3.21×10^{-7}
2 years	3.19×10^{-10}	3.19×10^{-10}	2.55×10^{-10}	1.16×10^{-7}	1.46×10^{-9}	3.24×10^{-7}
5 years	1.59×10^{-10}	1.59×10^{-10}	1.27×10^{-10}	1.22×10^{-7}	1.62×10^{-9}	3.22×10^{-7}

TABLE VII.9. PREDICTED EXTERNAL DOSE RATES (mGy/h) FROM RESRAD-RDD, WITHOUT COUNTERMEASURES

Time since event	Location 1	Location 2	Location 3	Location 4	Location 5	Location 6
			Co-60, summer release			
			Dry conditions			
0 days	7.43×10^{-2}	5.68×10^{-2}	6.11×10^{-2}	1.76×10^{-1}	3.95×10^{-1}	1.76×10^{-1}
1 day	7.39×10^{-2}	5.65×10^{-2}	6.09×10^{-2}	1.74×10^{-1}	3.95×10^{-1}	1.74×10^{-1}
1 week	7.15×10^{-2}	5.47×10^{-2}	5.95×10^{-2}	1.69×10^{-1}	3.92×10^{-1}	1.69×10^{-1}
1 month	6.35×10^{-2}	4.86×10^{-2}	5.49×10^{-2}	1.49×10^{-1}	3.84×10^{-1}	1.49×10^{-1}
3 months	4.87×10^{-2}	3.73×10^{-2}	4.62×10^{-2}	1.14×10^{-1}	3.63×10^{-1}	1.14×10^{-1}
1 year	2.47×10^{-2}	1.90×10^{-2}	3.02×10^{-2}	5.68×10^{-2}	2.85×10^{-1}	5.68×10^{-2}
2 years	1.49×10^{-2}	1.16×10^{-2}	2.17×10^{-2}	3.43×10^{-2}	2.17×10^{-1}	3.43×10^{-2}
5 years	3.88×10^{-3}	3.08×10^{-3}	9.54×10^{-3}	8.03×10^{-3}	1.12×10^{-1}	8.03×10^{-3}
			Light rain			
0 days	5.38×10^{0}	4.09×10^{0}	4.00×10^{0}	1.29×10^{1}	1.64×10^{1}	1.29×10^{1}
1 day	5.35×10^{0}	4.07×10^{0}	3.98×10^{0}	1.28×10^{1}	1.64×10^{1}	1.28×10^{1}
1 week	5.18×10^{0}	3.94×10^{0}	3.88×10^{0}	1.24×10^{1}	1.63×10^{1}	1.24×10^{1}
1 month	4.59×10^{0}	3.49×10^{0}	3.55×10^{0}	1.10×10^{1}	1.60×10^{1}	1.10×10^{1}
3 months	3.51×10^{0}	2.67×10^{0}	2.93×10^{0}	8.38×10^{0}	1.51×10^{1}	8.38×10^{0}
1 year	1.76×10^{0}	1.34×10^{0}	1.83×10^{0}	4.18×10^{0}	1.18×10^{1}	4.18×10^{0}
2 years	1.05×10^{0}	8.01×10^{-1}	1.28×10^{0}	2.52×10^{0}	9.01×10^{0}	2.52×10^{0}
5 years	2.56×10^{-1}	1.96×10^{-1}	5.28×10^{-1}	5.90×10^{-1}	4.68×10^{0}	5.90×10^{-1}
			Heavy rain			
0 days	3.27×10^{1}	2.49×10^{1}	2.43×10^{1}	7.85×10^{1}	9.99×10^{1}	7.85×10^{1}
1 day	3.25×10^{1}	2.47×10^{1}	2.42×10^{1}	7.79×10^{1}	9.98×10^{1}	7.79×10^{1}
1 week	3.15×10^{1}	2.39×10^{1}	2.36×10^{1}	7.53×10^{1}	9.92×10^{1}	7.53×10^{1}
1 month	2.79×10^{1}	2.12×10^{1}	2.16×10^{1}	6.68×10^{1}	9.70×10^{1}	6.68×10^{1}
3 months	2.13×10^{1}	1.62×10^{1}	1.78×10^{1}	5.10×10^{1}	9.17×10^{1}	5.10×10^{1}
1 year	1.07×10^{1}	8.13×10^{0}	1.11×10^{1}	2.54×10^{1}	7.20×10^{1}	2.54×10^{1}
2 years	6.38×10^{0}	4.87×10^{0}	7.79×10^{0}	1.53×10^{1}	5.48×10^{1}	1.53×10^{1}
5 years	1.55×10^{0}	1.19×10^{0}	3.21×10^{0}	3.59×10^{0}	2.84×10^{1}	3.59×10^{0}
			Pu-239, summer release			
			Dry conditions			
0 days	3.72×10^{-6}	3.60×10^{-6}	3.36×10^{-6}	2.17×10^{-5}	4.88×10^{-5}	2.17×10^{-5}
1 day	3.71×10^{-6}	3.58×10^{-6}	3.35×10^{-6}	2.15×10^{-5}	4.87×10^{-5}	2.15×10^{-5}
1 week	3.59×10^{-6}	3.47×10^{-6}	3.25×10^{-6}	2.09×10^{-5}	4.85×10^{-5}	2.09×10^{-5}
1 month	3.22×10^{-6}	3.10×10^{-6}	2.92×10^{-6}	1.86×10^{-5}	4.79×10^{-5}	1.86×10^{-5}

TABLE VII.9. PREDICTED EXTERNAL DOSE RATES (mGy/h) FROM RESRAD-RDD, WITHOUT COUNTERMEASURES (cont.)

Time since event	Location 1	Location 2	Location 3	Location 4	Location 5	Location 6
3 months	2.51×10^{-6}	2.43×10^{-6}	2.31×10^{-6}	1.45×10^{-5}	4.62×10^{-5}	1.45×10^{-5}
1 year	1.38×10^{-6}	1.33×10^{-6}	1.31×10^{-6}	8.00×10^{-6}	4.01×10^{-5}	8.00×10^{-6}
2 years	8.71×10^{-7}	8.41×10^{-7}	8.64×10^{-7}	5.48×10^{-6}	3.46×10^{-5}	5.48×10^{-6}
5 years	3.54×10^{-7}	3.43×10^{-7}	3.97×10^{-7}	1.91×10^{-6}	2.68×10^{-5}	1.91×10^{-6}
			Light rain			
0 days	2.72×10^{-4}	2.62×10^{-4}	2.42×10^{-4}	1.59×10^{-3}	2.03×10^{-3}	1.59×10^{-3}
1 day	2.70×10^{-4}	2.61×10^{-4}	2.41×10^{-4}	1.58×10^{-3}	2.03×10^{-3}	1.58×10^{-3}
1 week	2.62×10^{-4}	2.53×10^{-4}	2.34×10^{-4}	1.53×10^{-3}	2.02×10^{-3}	1.53×10^{-3}
1 month	2.34×10^{-4}	2.26×10^{-4}	2.10×10^{-4}	1.37×10^{-3}	1.99×10^{-3}	1.37×10^{-3}
3 months	1.83×10^{-4}	1.76×10^{-4}	1.65×10^{-4}	1.07×10^{-3}	1.92×10^{-3}	1.07×10^{-3}
1 year	9.93×10^{-5}	9.58×10^{-5}	9.24×10^{-5}	5.88×10^{-4}	1.67×10^{-3}	5.88×10^{-4}
2 years	6.23×10^{-5}	6.01×10^{-5}	5.97×10^{-5}	4.03×10^{-4}	1.44×10^{-3}	4.03×10^{-4}
5 years	2.44×10^{-5}	2.36×10^{-5}	2.59×10^{-5}	1.41×10^{-4}	1.11×10^{-3}	1.41×10^{-4}
			Heavy rain			
0 days	1.65×10^{-3}	1.59×10^{-3}	1.47×10^{-3}	9.69×10^{-3}	1.23×10^{-2}	9.69×10^{-3}
1 day	1.64×10^{-3}	1.58×10^{-3}	1.47×10^{-3}	9.61×10^{-3}	1.23×10^{-2}	9.61×10^{-3}
1 week	1.59×10^{-3}	1.54×10^{-3}	1.42×10^{-3}	9.32×10^{-3}	1.23×10^{-2}	9.32×10^{-3}
1 month	1.42×10^{-3}	1.37×10^{-3}	1.28×10^{-3}	8.33×10^{-3}	1.21×10^{-2}	8.33×10^{-3}
3 months	1.11×10^{-3}	1.07×10^{-3}	1.00×10^{-3}	6.50×10^{-3}	1.17×10^{-2}	6.50×10^{-3}
1 year	6.04×10^{-4}	5.82×10^{-4}	5.62×10^{-4}	3.57×10^{-3}	1.01×10^{-2}	3.57×10^{-3}
2 years	3.78×10^{-4}	3.65×10^{-4}	3.63×10^{-4}	2.45×10^{-3}	8.76×10^{-3}	2.45×10^{-3}
5 years	1.48×10^{-4}	1.43×10^{-4}	1.57×10^{-4}	8.55×10^{-4}	6.77×10^{-3}	8.55×10^{-4}

TABLE VII.10. PREDICTED EXTERNAL DOSE RATES (mGy/h) FROM CHERURB, WITHOUT COUNTERMEASURES

Time since event	Location 1	Location 2	Location 3	Location 4	Location 5	Location 6
			Co-60, summer release			
			Dry conditions			
0 days	–[a]	5.43×10^{-2}	–	1.11×10^{0}	1.11×10^{0}	–
1 day	–	6.95×10^{-3}	–	5.41×10^{-1}	5.41×10^{-1}	–
1 week	–	6.35×10^{-3}	–	4.92×10^{-1}	4.92×10^{-1}	–
1 month	–	4.77×10^{-3}	–	3.55×10^{-1}	3.55×10^{-1}	–
3 months	–	3.10×10^{-3}	–	2.06×10^{-1}	2.06×10^{-1}	–
1 year	–	1.39×10^{-3}	–	9.51×10^{-2}	9.51×10^{-2}	–
2 years	–	1.08×10^{-3}	–	8.14×10^{-2}	8.14×10^{-2}	–
5 years	–	8.42×10^{-4}	–	7.11×10^{-2}	7.11×10^{-2}	–
			Light rain			
0 days	–	4.36×10^{-1}	–	3.34×10^{1}	3.34×10^{1}	–
1 day	–	3.81×10^{-1}	–	3.24×10^{1}	3.24×10^{1}	–
1 week	–	3.35×10^{-1}	–	3.01×10^{1}	3.01×10^{1}	–
1 month	–	2.25×10^{-1}	–	2.28×10^{1}	2.28×10^{1}	–
3 months	–	1.39×10^{-1}	–	1.35×10^{1}	1.35×10^{1}	–
1 year	–	8.27×10^{-2}	–	7.38×10^{0}	7.38×10^{0}	–
2 years	–	6.98×10^{-2}	–	6.81×10^{0}	6.81×10^{0}	–
5 years	–	5.21×10^{-2}	–	6.03×10^{0}	6.03×10^{0}	–
			Heavy rain			
0 days	–	1.75×10^{0}	–	1.22×10^{2}	1.22×10^{2}	–
1 day	–	1.66×10^{0}	–	1.20×10^{2}	1.20×10^{2}	–
1 week	–	1.48×10^{0}	–	1.11×10^{2}	1.11×10^{2}	–

TABLE VII.10. PREDICTED EXTERNAL DOSE RATES (mGy/h) FROM CHERURB, WITHOUT COUNTERMEASURES (cont.)

Time since event	Location 1	Location 2	Location 3	Location 4	Location 5	Location 6
1 month	–	1.01×10^{0}	–	8.51×10^{1}	8.51×10^{1}	–
3 months	–	6.24×10^{-1}	–	5.09×10^{1}	5.09×10^{1}	–
1 year	–	3.39×10^{-1}	–	2.60×10^{1}	2.60×10^{1}	–
2 years	–	2.78×10^{-1}	–	2.35×10^{1}	2.35×10^{1}	–
5 years	–	2.06×10^{-1}	–	2.08×10^{1}	2.08×10^{1}	–

[a] Results not provided for Locations 1, 3, and 6.

TABLE VII.11. PREDICTED MOST IMPORTANT CONTRIBUTORS TO EXTERNAL DOSE RATES (%) FROM METRO-K, WITHOUT COUNTERMEASURES

Time since event	Location 1	Location 2	Location 3	Location 4	Location 5	Location 6
Co-60, summer release						
Dry conditions						
0 days	paved 19.65 trees 78.34 walls 2.01	walls 100	walls 1.94 roofs 98.06	paved 47.02 trees 51.26 walls 1.72	trees 22.49 soil 77.51	paved 73.46 trees 26.53
1 year	paved 44.04 trees 43.31 walls 12.66	walls 100	walls 1.93 roofs 98.07	paved 72.92 trees 19.6 walls 7.48	trees 2.57 soil 97.43	paved 91.82 trees 8.18
5 years	paved 60.2 trees 0.01 walls 39.8	walls 100	walls 1.8 roofs 98.2	paved 80.91 walls 19.09	soil 100	paved 100
Light rain						
0 days	paved 79.14 trees 19.41 walls 1.45	walls 100	walls 1.84 roofs 98.2	paved 93.12 trees 6.27 walls 0.61	trees 11.7 soil 88.3	paved 97.79 trees 2.18
1 year	paved 89.94 trees 5.44 walls 4.62	walls 100	walls 1.84 roofs 98.16	paved 96.63 trees 1.6 walls 1.77	trees 1.18 soil 98.82	paved 99.46 trees 0.55
5 years	paved 89.43 walls 10.56	walls 100	walls 1.72 roofs 98.28	paved 95.96 walls 4.04	soil 100	paved 100
Heavy rain						
0 days	paved 75.86 trees 22.96 walls 1.18	walls 100	walls 1.22 roofs 98.8	paved 91.88 trees 7.61 walls 0.51	trees 10.88 soil 89.12	paved 97.33 trees 2.68
1 year	paved 89.43 trees 6.68 walls 3.89	walls 100	walls 1.21 roofs 98.79	paved 96.53 trees 1.97 walls 1.5	trees 1.1 soil 98.9	paved 99.33 trees 0.67
5 years	paved 90.9 walls 9.1	walls 100	walls 1.13 roofs 98.87	paved 96.55 walls 3.45	soil 100	paved 100
Co-60, winter release						
Dry conditions						
0 days	paved 76.81 trees 15.31 walls 7.88	walls 100	walls 1.94 roofs 98.06	paved 91.65 trees 5.0 walls 3.35	trees 12.67 soil 87.33	paved 84.71 trees 15.29

TABLE VII.11. PREDICTED MOST IMPORTANT CONTRIBUTORS TO EXTERNAL DOSE RATES (%) FROM METRO-K, WITHOUT COUNTERMEASURES (cont.)

Time since event	Location 1	Location 2	Location 3	Location 4	Location 5	Location 6
1 year	paved 74.82 trees 3.68 walls 21.5	walls 100	walls 1.93 roofs 98.07	paved 89.61 trees 1.2 walls 9.19	trees 1.3 soil 98.7	paved 95.73 trees 4.26
5 years	paved 60.2 walls 39.8	walls 100	walls 1.8 roofs 98.2	paved 80.91 walls 19.09	soil 100	paved 100
			Light rain			
0 days	paved 97.03 trees 1.78 walls 1.19	walls 100	walls 1.84 roofs 98.2	paved 99.02 trees 0.33 walls 0.65	trees 6.18 soil 93.82	paved 98.9 trees 1.1
1 year	paved 94.57 trees 0.57 walls 4.86	walls 100	walls 1.84 roofs 98.16	paved 98.12 trees 0.08 walls 1.8	trees 0.6 soil 99.4	paved 99.72 trees 0.27
5 years	paved 89.44 walls 10.56	walls 100	walls 1.72 roofs 98.28	paved 95.96 walls 4.04	soil 100	paved 100
			Heavy rain			
0 days	paved 97.03 trees 1.47 walls 1.51	walls 100	walls 1.22 roofs 98.8	paved 99.04 trees 0.41 walls 0.55	trees 5.75 soil 94.25	paved 98.64 trees 1.36
1 year	paved 95.49 trees 0.36 walls 4.16	walls 100	walls 1.21 roofs 98.79	paved 98.37 trees 0.1 walls 1.53	trees 0.55 soil 99.45	paved 99.66 trees 0.34
5 years	paved 90.9 walls 9.1	walls 100	walls 1.13 roofs 98.87	paved 96.55 walls 3.45	soil 100	paved 100

TABLE VII.12. PREDICTED MOST IMPORTANT CONTRIBUTORS TO EXTERNAL DOSE RATES (%) FROM ERMIN, WITHOUT COUNTERMEASURES

Time since event	Location 1	Location 2	Location 3	Location 4	Location 5	Location 6
			Co-60, summer release			
			Dry conditions			
0 days	paved 11.53 trees 32.89 interior 46.28	walls 6.96 interior 93.04	walls 4.01 interior 65.34 roofs 30.65	paved 34.55 trees 40.56 grass 17.65	paved 2.53 trees 21.10 grass 76.37	paved 55.61 trees 25.74 grass 18.64
1 year	paved 12.19 grass 25.86 interior 41.45	walls 21.32 interior 78.68	walls 7.92 interior 35.65 roofs 56.43	paved 22.86 grass 55.90 walls 12.62	paved 0.96 trees 2.21 grass 96.83	paved 34.11 trees 4.72 grass 61.17
5 years	paved 8.77 grass 69.32 walls 21.45	walls 2.10 interior 97.90	walls 12.79 interior 0.33 roofs 86.87	paved 8.67 grass 77.41 walls 12.66	paved 0.29 grass 99.71	paved 11.17 grass 88.83
			Light rain			
0 days	paved 30.35 trees 27.88 interior 31.97	walls 5.66 interior 94.34	walls 2.45 interior 49.84 roofs 47.71	paved 58.69 trees 22.19 grass 16.12	paved 5.1 trees 13.69 grass 81.21	paved 75.41 trees 11.24 grass 13.34
1 year	paved 30.56 grass 28.77 interior 27.27	walls 17.85 interior 82.15	walls 4.04 interior 22.68 roofs 73.27	paved 42.39 grass 47.03 walls 4.93	paved 1.91 trees 1.41 grass 96.68	paved 54.30 trees 2.42 grass 43.28

TABLE VII.12. PREDICTED MOST IMPORTANT CONTRIBUTORS TO EXTERNAL DOSE RATES (%) FROM ERMIN, WITHOUT COUNTERMEASURES (cont.)

Time since event	Location 1	Location 2	Location 3	Location 4	Location 5	Location 6
5 years	paved 20.55 grass 68.59 walls 10.58	walls 97.40 interior 2.60	walls 5.46 interior 0.18 roofs 94.36	paved 19.05 grass 73.60 walls 5.86	paved 0.58 grass 99.42	paved 23.02 grass 76.98
			Heavy rain			
0 days	paved 54.08 trees 20.56 grass 15.97	walls 23.07 interior 76.93	walls 3.54 interior 14.38 roofs 82.09	paved 64.58 trees 10.11 grass 23.22	paved 4.52 trees 5.02 grass 90.45	paved 77.88 trees 4.81 grass 17.31
1 year	paved 43.91 grass 41.29 walls 5.41	walls 52.07 interior 47.93	walls 4.21 interior 4.73 roofs 91.06	paved 43.79 grass 50.13 walls 3.22	paved 1.62 trees 0.50 grass 97.88	paved 54.88 trees 1.01 grass 44.11
5 years	paved 22.73 grass 69.81 walls 7.41	walls 99.47 interior 0.53	walls 4.63 interior 0.03 roofs 95.34	paved 20.18 grass 74.71 walls 3.93	paved 0.50 grass 99.50	paved 24.53 grass 75.47
			Co-60, winter release			
			Dry conditions			
0 days	paved 15.58 trees 9.35 interior 62.51	walls 6.96 interior 93.04	walls 4.01 interior 65.34 roofs 30.65	paved 50.83 trees 12.56 grass 25.97	paved 3.05 trees 5.08 grass 91.88	paved 70.04 trees 6.48 grass 23.48
1 year	paved 13.55 grass 17.64 interior 46.04	walls 21.32 interior 78.68	walls 7.92 interior 35.65 roofs 56.43	paved 28.26 grass 45.49 walls 15.59	paved 1.08 trees 2.48 grass 96.44	paved 44.50 trees 6.16 grass 49.34
5 years	paved 12.22 grass 57.26 walls 29.88	walls 2.10 interior 97.90	walls 12.79 interior 0.33 roofs 86.87	paved 12.12 grass 68.41 walls 17.70	paved 0.33 grass 99.67	paved 17.74 grass 82.26
			Light rain			
0 days	paved 38.91 grass 10.11 interior 40.99	walls 5.66 interior 94.34	walls 2.45 interior 49.84 roofs 47.71	paved 71.16 trees 5.66 grass 19.54	paved 5.73 trees 3.07 grass 91.20	paved 82.87 trees 2.47 grass 14.66
1 year	paved 33.24 grass 22.53 interior 29.66	walls 17.85 interior 82.15	walls 4.04 interior 22.68 roofs 73.27	paved 47.85 grass 40.21 walls 5.56	paved 2.05 trees 1.52 grass 96.43	paved 61.69 trees 2.75 grass 35.56
5 years	paved 26.10 grass 60.10 walls 13.44	walls 97.40 interior 2.60	walls 5.46 interior 0.18 roofs 94.36	paved 23.86 grass 66.94 walls 7.33	paved 0.64 grass 99.36	paved 30.51 grass 69.49
			Heavy rain			
0 days	paved 64.56 grass 19.06 interior 8.61	walls 23.07 interior 76.92	walls 3.54 interior 14.38 roofs 82.09	paved 70.18 trees 2.31 grass 25.23	paved 4.71 trees 1.05 grass 94.24	paved 81.00 trees 1.00 grass 18.00
1 year	paved 46.12 grass 38.33 walls 5.68	walls 52.04 interior 47.93	walls 4.21 interior 4.73 roofs 91.06	paved 46.04 grass 47.58 walls 3.39	paved 1.66 trees 0.51 grass 97.83	paved 57.78 trees 1.07 grass 41.16
5 years	paved 25.19 grass 66.55 walls 8.21	walls 99.47 interior 0.53	walls 4.63 interior 0.03 roofs 95.34	paved 22.13 grass 72.25 walls 4.31	paved 0.52 grass 99.48	paved 27.51 grass 72.49
			Pu-239, summer release			
			Dry conditions			
0 days	paved 2.3 trees 7.77 interior 87.87	walls 0.99 interior 99.01	walls 0.79 interior 97.00 roofs 2.21	paved 33.52 trees 41.48 grass 16.93	paved 2.53 trees 21.10 grass 76.37	paved 55.61 trees 25.74 grass 18.64

TABLE VII.12. PREDICTED MOST IMPORTANT CONTRIBUTORS TO EXTERNAL DOSE RATES (%) FROM ERMIN, WITHOUT COUNTERMEASURES (cont.)

Time since event	Location 1	Location 2	Location 3	Location 4	Location 5	Location 6
1 year	grass 4.79 walls 3.25 interior 86.86	walls 3.50 interior 96.50	walls 2.67 interior 90.37 roofs 6.96	paved 24.33 grass 50.16 walls 14.51	paved 1.16 trees 2.66 grass 96.18	paved 36.77 trees 5.09 grass 58.15
5 years	paved 8.9 grass 58.19 walls 28.5	walls 86.22 interior 13.78	walls 27.20 interior 5.34 roofs 67.47	paved 9.79 grass 71.80 walls 15.44	paved 0.39 grass 99.61	paved 13.04 grass 86.96
			Light rain			
0 days	paved 8.04 trees 8.74 interior 80.56	walls 0.80 interior 99.20	walls 0.62 interior 94.96 roofs 4.42	paved 58.00 trees 23.12 grass 15.14	paved 5.10 trees 13.69 grass 81.21	paved 75.41 trees 11.24 grass 13.34
1 year	paved 9.26 grass 7.10 interior 78.60	walls 2.83 interior 97.17	walls 2.01 interior 84.69 roofs 13.31	paved 45.32 grass 41.24 walls 5.69	paved 2.32 trees 1.72 grass 95.96	paved 57.81 trees 2.58 grass 39.61
5 years	paved 22.53 grass 59.33 walls 15.20	walls 83.38 interior 16.62	walls 13.23 interior 3.24 roofs 83.53	paved 22.07 grass 67.01 walls 7.33	paved 0.82 grass 99.18	paved 27.25 grass 72.75
			Heavy rain			
0 days	paved 33.18 trees 14.93 interior 42.10	walls 3.86 interior 96.14	walls 2.50 interior 76.31 roofs 21.19	paved 66.25 trees 10.93 grass 19.96	paved 4.52 trees 5.02 grass 90.45	paved 77.88 trees 4.81 grass 17.31
1 year	paved 32.45 grass 23.56 interior 34.88	walls 12.71 interior 87.29	walls 5.77 interior 48.64 roofs 45.59	paved 48.25 grass 43.45 walls 3.84	paved 2.00 trees 0.61 grass 97.38	paved 59.47 trees 1.10 grass 39.44
5 years	paved 27.37 grass 60.48 walls 11.69	walls 96.17 interior 3.83	walls 11.66 interior 0.57 roofs 87.77	paved 24.84 grass 66.87 walls 5.23	paved 0.74 grass 99.26	paved 30.97 grass 69.03
			Pu-239, winter release			
			Dry conditions			
0 days	paved 2.45 trees 1.74 interior 93.61	walls 0.99 interior 99.01	walls 0.79 interior 97.00 roofs 2.21	paved 49.85 trees 12.99 grass 25.18	paved 3.05 trees 5.08 grass 91.88	paved 70.04 trees 6.48 grass 23.48
1 year	paved 2.75 walls 3.33 interior 88.78	walls 3.50 interior 96.50	walls 2.67 interior 90.37 roofs 6.96	paved 30.39 grass 37.75 walls 18.12	paved 1.34 trees 3.07 grass 95.60	paved 49.14 trees 6.80 grass 44.06
5 years	paved 12.37 grass 41.84 walls 39.64	walls 86.22 interior 13.78	walls 27.20 interior 5.34 roofs 67.47	paved 14.30 grass 58.80 walls 22.56	paved 0.49 grass 99.51	paved 22.95 grass 77.05
			Light rain			
0 days	paved 8.64 grass 2.14 interior 86.53	walls 0.80 interior 99.20	walls 0.62 interior 94.96 roofs 4.42	paved 70.94 trees 5.95 grass 18.52	paved 5.73 trees 3.07 grass 91.20	paved 82.87 trees 2.47 grass 14.66
1 year	paved 9.49 grass 4.82 interior 80.54	walls 2.83 interior 97.17	walls 2.01 interior 84.69 roofs 13.31	paved 51.48 grass 33.25 walls 6.46	paved 2.54 trees 1.88 grass 95.58	paved 66.26 trees 2.95 grass 30.78
5 years	paved 29.24 grass 47.22 walls 19.72	walls 83.38 interior 16.62	walls 13.23 interior 3.24 roofs 83.53	paved 28.63 grass 57.20 walls 9.51	paved 0.95 grass 99.05	paved 38.43 grass 61.57

373

TABLE VII.12. PREDICTED MOST IMPORTANT CONTRIBUTORS TO EXTERNAL DOSE RATES (%) FROM ERMIN, WITHOUT COUNTERMEASURES (cont.)

Time since event	Location 1	Location 2	Location 3	Location 4	Location 5	Location 6
			Heavy rain			
0 days	paved 37.61 grass 9.12 interior 47.73	walls 3.86 interior 96.14	walls 2.50 interior 76.31 roofs 21.19	paved 72.51 trees 2.52 grass 21.85	paved 4.71 trees 1.05 grass 94.24	paved 81.00 trees 1.00 grass 18.00
1 year	paved 33.62 grass 20.81 interior 36.14	walls 12.71 interior 87.29	walls 5.77 interior 48.64 roofs 45.59	paved 50.93 grass 40.30 walls 4.05	paved 2.07 trees 0.63 grass 97.30	paved 62.88 trees 1.16 grass 35.96
5 years	paved 30.94 grass 55.33 walls 13.22	walls 96.17 interior 3.83	walls 11.66 interior 0.57 roofs 87.77	paved 27.81 grass 62.92 walls 5.85	paved 0.78 grass 99.22	paved 35.87 grass 64.13

TABLE VII.13. PREDICTED MOST IMPORTANT CONTRIBUTORS TO EXTERNAL DOSE RATES (%) FROM CPHR, WITHOUT COUNTERMEASURES

Time since event	Location 1	Location 2	Location 3	Location 4	Location 5	Location 6
			Co-60, summer release			
			Dry conditions			
0 days	air 100	air 100	air 100	air 100	air 100	air 100
1 year	walls 100	walls 100	roofs 17 walls 83	paved 94 walls 6	trees 7 soil 93	paved 99 trees 1
5 years	walls 100	walls 100	roofs 17 walls 83	paved 94 walls 6	trees 7 soil 93	paved 99 trees 1
			Light rain			
0 days	air 100	air 100	air 100	air 100	air 100	air 100
1 year	walls 100	walls 100	walls 100	paved 99.95 walls 0.05	trees 7 soil 92	paved 100
5 years	walls 100	walls 100	walls 100	paved 99.98 walls 0.02	trees 2 soil 98	paved 100
			Pu-239, summer release			
			Dry conditions			
0 days	air 100	air 100	air 100	air 100	air 100	air 100
1 year	walls 100	walls 100	roofs 17 walls 83	paved 94 walls 6	trees 7 soil 93	paved 99 trees 1
5 years	walls 100	walls 100	roofs 17 walls 83	paved 94 walls 6	trees 7 soil 93	paved 99 trees 1
			Light rain			
0 days	air 100	air 100	air 100	air 100	air 100	air 100
1 year	walls 100	walls 100	walls 100	paved 99.96 walls 0.04	trees 6 soil 94	paved 100
5 years	walls 100	walls 100	walls 100	paved 99.99 walls 0.01	trees 2 soil 98	paved 100

TABLE VII.14. PREDICTED MOST IMPORTANT CONTRIBUTORS TO EXTERNAL DOSE RATES (%) FROM RESRAD-RDD, WITHOUT COUNTERMEASURES

Time since event	Location 1	Location 2	Location 3	Location 4	Location 5	Location 6
			Co-60, summer release			
			Dry conditions			
0 days	from outside 83.22 roof 1.58 exterior wall 1.69 interior wall 0.42 floor 13.10	from outside 78.04 roof 2.07 exterior wall 2.21 interior wall 0.55 floor 17.14	from outside 47.85 roof 33.67 exterior wall 2.05 interior wall 0.51 floor 15.92	infinite area 100	infinite area 100	infinite area 100
1 year	from outside 81.32 roof 1.54 exterior wall 3.48 interior wall 0.86 floor 12.80	from outside 75.73 roof 2.00 exterior wall 4.52 interior wall 1.12 floor 16.63	from outside 31.41 roof 54.59 exterior wall 2.84 interior wall 0.70 floor 10.45	infinite area 100	infinite area 100	infinite area 100
5 years	from outside 73.05 roof 1.39 exterior wall 11.28 interior wall 2.79 floor 11.50	from outside 66.02 roof 1.75 exterior wall 14.22 interior wall 3.51 floor 14.50	from outside 14.04 roof 75.57 exterior wall 4.58 interior wall 1.13 floor 4.67	infinite area 100	infinite area 100	infinite area 100
			Light rain			
0 days	from outside 84.54 roof 1.60 exterior wall 0.13 interior wall 0.42 floor 13.31	from outside 79.67 roof 2.11 exterior wall 0.17 interior wall 0.56 floor 17.50	from outside 53.81 roof 27.54 exterior wall 0.17 interior wall 0.57 floor 17.91	infinite area 100	infinite area 100	infinite area 100
1 year	from outside 84.03 roof 1.59 exterior wall 0.26 interior wall 0.89 floor 13.23	from outside 79.04 roof 2.09 exterior wall 0.35 interior wall 1.17 floor 17.36	from outside 38.09 roof 48.14 exterior wall 0.25 interior wall 0.85 floor 12.67	infinite area 100	infinite area 100	infinite area 100

TABLE VII.14. PREDICTED MOST IMPORTANT CONTRIBUTORS TO EXTERNAL DOSE RATES (%) FROM RESRAD-RDD, WITHOUT COUNTERMEASURES (cont.)

Time since event	Location 1	Location 2	Location 3	Location 4	Location 5	Location 6
	from outside 81.57 roof 1.55	from outside 76.04 roof 2.01	from outside 18.69 roof 73.14			
5 years	exterior wall 0.93 interior wall 3.11 floor 12.84	exterior wall 1.20 interior wall 4.05 floor 16.70	exterior wall 0.45 interior wall 1.51 floor 6.22	infinite area 100	infinite area 100	infinite area 100
			Heavy rain			
	from outside 84.54 roof 1.60	from outside 79.67 roof 2.11	from outside 53.81 roof 27.54			
0 days	exterior wall 0.13 interior wall 0.42 floor 13.31	exterior wall 0.17 interior wall 0.56 floor 17.50	exterior wall 0.17 interior wall 0.57 floor 17.91	infinite area 100	infinite area 100	infinite area 100
	from outside 84.03 roof 1.59	from outside 79.04 roof 2.09	from outside 38.09 roof 48.14			
1 year	exterior wall 0.26 interior wall 0.89 floor 13.23	exterior wall 0.35 interior wall 1.17 floor 17.36	exterior wall 0.25 interior wall 0.85 floor 12.67	infinite area 100	infinite area 100	infinite area 100
	from outside 81.57 roof 1.55	from outside 76.04 roof 2.01	from outside 18.69 roof 73.14			
5 years	exterior wall 0.93 interior wall 3.11 floor 12.84	exterior wall 1.20 interior wall 4.05 floor 16.70	exterior wall 0.45 interior wall 1.51 floor 6.22	infinite area 100	infinite area 100	infinite area 100
			Pu-239, summer release			
			Dry conditions			
	from outside 31.40 roof 0.20	from outside 28.92 roof 0.20	from outside 20.44 roof 3.80			
0 days	exterior wall 0.96 interior wall 0.18 floor 67.27	exterior wall 0.99 interior wall 0.19 floor 69.69	exterior wall 1.06 interior wall 0.199 floor 74.50	infinite area 100	infinite area 100	infinite area 100

TABLE VII.14. PREDICTED MOST IMPORTANT CONTRIBUTORS TO EXTERNAL DOSE RATES (%) FROM RESRAD-RDD, WITHOUT COUNTERMEASURES (cont.)

Time since event	Location 1	Location 2	Location 3	Location 4	Location 5	Location 6
1 year	from outside 31.00 roof 0.19 exterior wall 2.02 interior wall 0.38 floor 66.41	from outside 28.54 roof 0.20 exterior wall 2.09 interior wall 0.39 floor 68.77	from outside 19.08 roof 8.85 exterior wall 2.12 interior wall 0.397 floor 69.55	infinite area 100	infinite area 100	infinite area 100
5 years	from outside 29.20 roof 0.18 exterior wall 6.78 interior wall 1.27 floor 62.56	from outside 26.83 roof 0.19 exterior wall 7.01 interior wall 1.32 floor 64.65	from outside 15.30 roof 21.73 exterior wall 6.05 interior wall 1.14 floor 55.78	infinite area 100	infinite area 100	infinite area 100
			Light rain			
0 days	from outside 31.68 roof 0.20 exterior wall 0.07 interior wall 0.18 floor 67.87	from outside 29.19 roof 0.20 exterior wall 0.07 interior wall 0.188 floor 70.34	from outside 20.86 roof 2.82 exterior wall 0.08 interior wall 0.204 floor 76.04	infinite area 100	infinite area 100	infinite area 100
1 year	from outside 31.59 roof 0.197 exterior wall 0.15 interior wall 0.39 floor 67.68	from outside 29.11 roof 0.20 exterior wall 0.16 interior wall 0.40 floor 70.13	from outside 19.96 roof 6.73 exterior wall 0.16 interior wall 0.416 floor 72.73	infinite area 100	infinite area 100	infinite area 100
5 years	from outside 31.16 roof 0.194 exterior wall 0.53 interior wall 1.36 floor 66.76	from outside 28.70 roof 0.20 exterior wall 0.55 interior wall 1.41 floor 69.14	from outside 17.30 roof 17.86 exterior wall 0.50 interior wall 1.28 floor 63.05	infinite area 100	infinite area 100	infinite area 100

TABLE VII.14. PREDICTED MOST IMPORTANT CONTRIBUTORS TO EXTERNAL DOSE RATES (%) FROM RESRAD-RDD, WITHOUT COUNTERMEASURES (cont.)

Time since event	Location 1	Location 2	Location 3	Location 4	Location 5	Location 6
			Heavy rain			
0 days	from outside 31.68 roof 0.20 exterior wall 0.07 interior wall 0.18 floor 67.87	from outside 29.19 roof 0.20 exterior wall 0.07 interior wall 0.188 floor 70.34	from outside 20.86 roof 2.82 exterior wall 0.08 interior wall 0.204 floor 76.04	infinite area 100	infinite area 100	infinite area 100
1 year	from outside 31.59 roof 0.197 exterior wall 0.15 interior wall 0.39 floor 67.68	from outside 29.11 roof 0.20 exterior wall 0.16 interior wall 0.40 floor 70.13	from outside 19.96 roof 6.73 exterior wall 0.16 interior wall 0.416 floor 72.73	infinite area 100	infinite area 100	infinite area 100
5 years	from outside 31.16 roof 0.194 exterior wall 0.53 interior wall 1.36 floor 66.76	from outside 28.70 roof 0.20 exterior wall 0.55 interior wall 1.41 floor 69.14	from outside 17.30 roof 17.86 exterior wall 0.50 interior wall 1.28 floor 63.05	infinite area 100	infinite area 100	infinite area 100

TABLE VII.15. PREDICTED EXTERNAL DOSES (mSv) FROM METRO-K, WITHOUT COUNTERMEASURES, FOR SPECIFIED EXPOSURE SCENARIOS

Time since event	Region 1 (Business area)		Region 2 (Park area)	
	Annual dose[a]	Cumulative dose[b]	Annual dose	Cumulative dose
		Co-60, summer release		
		Dry conditions		
1 year	8.19×10^{0}	8.19×10^{0}	4.58×10^{1}	4.58×10^{1}
2 years	9.71×10^{-1}	9.16×10^{0}	2.72×10^{1}	7.30×10^{1}
5 years	1.16×10^{-1}	9.88×10^{0}	6.23×10^{0}	1.06×10^{2}
		Light rain		
1 year	1.82×10^{3}	1.82×10^{3}	2.35×10^{3}	2.35×10^{3}
2 years	2.85×10^{2}	2.11×10^{3}	1.45×10^{3}	3.81×10^{3}
5 years	2.39×10^{1}	2.27×10^{3}	3.33×10^{2}	5.55×10^{3}
		Heavy rain		
1 year	8.38×10^{3}	8.38×10^{3}	1.43×10^{4}	1.43×10^{4}
2 years	1.29×10^{3}	9.67×10^{3}	8.87×10^{3}	2.32×10^{4}
5 years	1.06×10^{2}	1.04×10^{4}	2.03×10^{3}	3.38×10^{4}
		Co-60, winter release		
		Dry conditions		
1 year	4.86×10^{0}	4.86×10^{0}	4.41×10^{1}	4.41×10^{1}
2 years	9.46×10^{-1}	5.81×10^{0}	2.72×10^{1}	7.13×10^{1}
5 years	1.16×10^{-1}	6.53×10^{0}	6.23×10^{0}	1.04×10^{2}
		Light rain		
1 year	1.73×10^{3}	1.73×10^{3}	2.31×10^{3}	2.31×10^{3}
2 years	2.85×10^{2}	2.01×10^{3}	1.45×10^{3}	3.76×10^{3}
5 years	2.38×10^{1}	2.18×10^{3}	3.33×10^{2}	5.51×10^{3}
		Heavy rain		
1 year	7.87×10^{3}	7.87×10^{3}	1.41×10^{4}	1.41×10^{4}
2 years	1.29×10^{3}	9.16×10^{3}	8.87×10^{3}	2.29×10^{4}
5 years	1.06×10^{2}	9.93×10^{3}	2.03×10^{3}	3.36×10^{4}

[a] The annual dose is the dose received during the year preceding the indicated 'time since event'.

[b] The cumulative dose is the dose received from the time of the event to the indicated 'time since event'.

TABLE VII.16. PREDICTED EXTERNAL DOSES (mSv) FROM ERMIN, WITHOUT COUNTERMEASURES, FOR SPECIFIED EXPOSURE SCENARIOS

Time since event	Region 1 (Business area)		Region 2 (Park area)	
	Annual dose[a]	Cumulative dose[b]	Annual dose	Cumulative dose
		Co-60, summer release		
		Dry conditions		
1 year	3.286×10^{1}	3.286×10^{1}	4.499×10^{1}	4.499×10^{1}
2 years	1.635×10^{1}	4.921×10^{1}	3.220×10^{1}	7.719×10^{1}
5 years	7.605×10^{0}	7.752×10^{1}	1.798×10^{1}	1.427×10^{2}
		Light rain		
1 year	1.698×10^{3}	1.698×10^{3}	2.307×10^{3}	2.307×10^{3}
2 years	7.631×10^{2}	2.461×10^{3}	1.638×10^{3}	3.945×10^{3}
5 years	3.324×10^{2}	3.697×10^{3}	9.007×10^{2}	7.239×10^{3}

TABLE VII.16. PREDICTED EXTERNAL DOSES (mSv) FROM ERMIN, WITHOUT COUNTERMEASURES, FOR SPECIFIED EXPOSURE SCENARIOS (cont.)

Time since event	Region 1 (Business area)		Region 2 (Park area)	
	Annual dose[a]	Cumulative dose[b]	Annual dose	Cumulative dose
		Heavy rain		
1 year	6.988×10^{3}	6.988×10^{3}	1.271×10^{4}	1.271×10^{4}
2 years	3.316×10^{3}	1.030×10^{4}	9.227×10^{3}	2.194×10^{4}
5 years	1.488×10^{3}	1.581×10^{4}	5.009×10^{3}	4.034×10^{4}
		Co-60, winter release		
		Dry conditions		
1 year	2.761×10^{1}	2.761×10^{1}	4.014×10^{1}	4.014×10^{1}
2 years	1.326×10^{1}	4.086×10^{1}	2.847×10^{1}	6.862×10^{1}
5 years	5.519×10^{0}	6.199×10^{1}	1.547×10^{1}	1.255×10^{2}
		Light rain		
1 year	1.526×10^{3}	1.526×10^{3}	2.148×10^{3}	2.148×10^{3}
2 years	6.618×10^{2}	2.187×10^{3}	1.516×10^{3}	3.665×10^{3}
5 years	2.641×10^{2}	3.189×10^{3}	8.186×10^{2}	6.676×10^{3}
		Heavy rain		
1 year	6.647×10^{3}	6.647×10^{3}	1.239×10^{4}	1.239×10^{4}
2 years	3.115×10^{3}	9.762×10^{3}	8.985×10^{3}	2.138×10^{4}
5 years	1.352×10^{3}	1.480×10^{4}	4.845×10^{3}	3.922×10^{4}
		Pu-239, summer release		
		Dry conditions		
1 year	2.622×10^{-6}	2.622×10^{-6}	1.534×10^{-3}	1.534×10^{-3}
2 years	1.120×10^{-6}	3.742×10^{-6}	1.112×10^{-3}	2.646×10^{-3}
5 years	5.662×10^{-7}	5.661×10^{-6}	8.395×10^{-4}	5.362×10^{-3}
		Light rain		
1 year	1.092×10^{-4}	1.092×10^{-4}	7.828×10^{-2}	7.828×10^{-2}
2 years	4.667×10^{-5}	1.558×10^{-4}	5.581×10^{-2}	1.341×10^{-1}
5 years	2.406×10^{-5}	2.363×10^{-4}	4.095×10^{-2}	2.675×10^{-1}
		Heavy rain		
1 year	3.431×10^{-4}	3.431×10^{-4}	4.274×10^{-1}	4.274×10^{-1}
2 years	1.699×10^{-4}	5.129×10^{-4}	3.086×10^{-1}	7.360×10^{-1}
5 years	1.010×10^{-4}	8.434×10^{-4}	2.199×10^{-1}	1.459×10^{0}
		Pu-239, winter release		
		Dry conditions		
1 year	2.362×10^{-6}	2.362×10^{-6}	1.351×10^{-3}	1.351×10^{-3}
2 years	9.449×10^{-7}	3.307×10^{-6}	9.518×10^{-4}	2.303×10^{-3}
5 years	3.914×10^{-7}	4.702×10^{-6}	6.790×10^{-4}	4.537×10^{-3}
		Light rain		
1 year	1.006×10^{-4}	1.006×10^{-4}	7.232×10^{-2}	7.232×10^{-2}
2 years	4.095×10^{-5}	1.416×10^{-4}	5.056×10^{-2}	1.229×10^{-1}
5 years	1.834×10^{-5}	2.049×10^{-4}	3.569×10^{-2}	2.405×10^{-1}
		Heavy rain		
1 year	3.261×10^{-4}	3.261×10^{-4}	4.155×10^{-1}	4.155×10^{-1}
2 years	1.585×10^{-4}	4.846×10^{-4}	2.981×10^{-1}	7.137×10^{-1}
5 years	8.963×10^{-5}	7.810×10^{-4}	2.095×10^{-1}	1.406×10^{0}

[a] The annual dose is the dose received during the year preceding the indicated 'time since event'.

[b] The cumulative dose is the dose received from the time of the event to the indicated 'time since event'.

TABLE VII.17. PREDICTED EXTERNAL DOSES (mSv) FROM CPHR, WITHOUT COUNTERMEASURES, FOR SPECIFIED EXPOSURE SCENARIOS

Time since event	Region 1 (Business area)		Region 2 (Park area)	
	Annual dose[a]	Cumulative dose[b]	Annual dose	Cumulative dose
		Co-60, summer release		
		Dry conditions		
1 year	4.66 × 100	4.66 × 100	7.27 × 10-1	7.27 × 10-1
2 years	5.66 × 100	1.60 × 101	4.72 × 10-1	1.20 × 100
5 years	6.10 × 100	2.89 × 101	4.77 × 10-1	2.22 × 100
		Pu-239, summer release		
		Dry conditions		
1 year	1.59 × 10-2	1.59 × 10-2	1.50 × 10-3	1.50 × 10-3
2 years	1.09 × 10-3	3.40 × 10-2	1.21 × 10-3	1.60 × 10-3
5 years	1.53 × 10-3	3.73 × 10-2	1.33 × 10-4	1.85 × 10-3

[a] The annual dose is the dose received during the year preceding the indicated 'time since event'.

[b] The cumulative dose is the dose received from the time of the event to the indicated 'time since event'.

TABLE VII.18. PREDICTED EXTERNAL DOSES (mSv) FROM RESRAD-RDD, WITHOUT COUNTERMEASURES, FOR SPECIFIED EXPOSURE SCENARIOS

Time since event	Region 1 (Business area)		Region 2 (Park area)	
	Annual dose[a]	Cumulative dose[b]	Annual dose	Cumulative dose
		Co-60, summer release		
		Dry conditions		
1 year	6.49×10^{1}	1.74×10^{2}	3.87×10^{1}	9.12×10^{1}
2 years	4.62×10^{1}	2.20×10^{2}	2.98×10^{1}	1.21×10^{2}
3 years	3.39×10^{1}	2.54×10^{2}	2.37×10^{1}	1.45×10^{2}
4 years	2.54×10^{1}	2.79×10^{2}	1.94×10^{1}	1.64×10^{2}
5 years	1.94×10^{1}	2.99×10^{2}	1.61×10^{1}	1.80×10^{2}
		Light rain		
1 year	4.04×10^{3}	1.11×10^{4}	1.61×10^{3}	3.80×10^{3}
2 years	2.80×10^{3}	1.39×10^{4}	1.24×10^{3}	5.04×10^{3}
3 years	2.00×10^{3}	1.59×10^{4}	9.86×10^{2}	6.02×10^{3}
4 years	1.46×10^{3}	1.74×10^{4}	8.06×10^{2}	6.83×10^{3}
5 years	1.09×10^{3}	1.85×10^{4}	6.71×10^{2}	7.50×10^{3}
		Heavy rain		
1 year	2.46×10^{4}	6.77×10^{4}	9.80×10^{3}	2.31×10^{4}
2 years	1.70×10^{4}	8.47×10^{4}	7.53×10^{3}	3.06×10^{4}
3 years	1.22×10^{4}	9.69×10^{4}	5.99×10^{3}	3.66×10^{4}
4 years	8.89×10^{3}	1.06×10^{5}	4.90×10^{3}	4.15×10^{4}
5 years	6.64×10^{3}	1.12×10^{5}	4.08×10^{3}	4.56×10^{4}
		Pu-239, summer release		
		Dry conditions		
1 year	4.04×10^{-3}	1.13×10^{-2}	5.81×10^{-3}	1.27×10^{-2}
2 years	2.89×10^{-3}	1.42×10^{-2}	5.09×10^{-3}	1.78×10^{-2}
3 years	2.10×10^{-3}	1.63×10^{-2}	4.63×10^{-3}	2.24×10^{-2}
4 years	1.55×10^{-3}	1.78×10^{-2}	4.31×10^{-3}	2.67×10^{-2}
5 years	1.15×10^{-3}	1.90×10^{-2}	4.10×10^{-3}	3.08×10^{-2}

TABLE VII.18. PREDICTED EXTERNAL DOSES (mSv) FROM RESRAD-RDD, WITHOUT COUNTERMEASURES, FOR SPECIFIED EXPOSURE SCENARIOS (cont.)

Time since event	Region 1 (Business area)		Region 2 (Park area)	
	Annual dose[a]	Cumulative dose[b]	Annual dose	Cumulative dose
		Light rain		
1 year	2.89×10^{-1}	8.14×10^{-1}	2.42×10^{-1}	5.29×10^{-1}
2 years	2.04×10^{-1}	1.02×10^{0}	2.12×10^{-1}	7.41×10^{-1}
3 years	1.47×10^{-1}	1.16×10^{0}	1.93×10^{-1}	9.33×10^{-1}
4 years	1.07×10^{-1}	1.27×10^{0}	1.79×10^{-1}	1.11×10^{0}
5 years	7.80×10^{-2}	1.35×10^{0}	1.70×10^{-1}	1.28×10^{0}
		Heavy rain		
1 year	1.76×10^{0}	4.94×10^{0}	1.47×10^{0}	3.21×10^{0}
2 years	1.24×10^{0}	6.19×10^{0}	1.29×10^{0}	4.50×10^{0}
3 years	8.94×10^{-1}	7.08×10^{0}	1.17×10^{0}	5.67×10^{0}
4 years	6.49×10^{-1}	7.73×10^{0}	1.09×10^{0}	6.76×10^{0}
5 years	4.74×10^{-1}	8.20×10^{0}	1.04×10^{0}	7.80×10^{0}

[a] The annual dose is the dose received during the year preceding the indicated 'time since event'.

[b] The cumulative dose is the dose received from the time of the event to the indicated 'time since event'.

TABLE VII.19. PREDICTED EXTERNAL DOSES (mSv) FROM CHERURB, WITHOUT COUNTERMEASURES, FOR SPECIFIED EXPOSURE SCENARIOS

Time since event	Region 1 (Business area)		Region 2 (Park area)	
	Annual dose[a]	Cumulative dose[b]	Annual dose	Cumulative dose
		Co-60, summer release		
		Dry conditions		
1 year	4.08×10^{1}	4.08×10^{1}	2.18×10^{1}	2.18×10^{1}
2 years	1.93×10^{1}	6.01×10^{1}	1.05×10^{1}	3.23×10^{1}
5 years	1.64×10^{1}	1.11×10^{2}	8.80×10^{0}	5.99×10^{1}
		Light rain		
1 year	2.63×10^{3}	2.63×10^{3}	1.45×10^{3}	1.45×10^{3}
2 years	1.54×10^{3}	4.17×10^{3}	8.60×10^{2}	2.31×10^{3}
5 years	1.33×10^{3}	8.35×10^{3}	7.50×10^{2}	4.64×10^{3}
		Heavy rain		
1 year	9.85×10^{3}	9.85×10^{3}	5.37×10^{3}	5.37×10^{3}
2 years	5.45×10^{3}	1.53×10^{4}	2.96×10^{3}	8.33×10^{3}
5 years	4.60×10^{3}	2.98×10^{4}	2.60×10^{3}	1.64×10^{4}

[a] The annual dose is the dose received during the year preceding the indicated 'time since event'.

[b] The cumulative dose is the dose received from the time of the event to the indicated 'time since event'.

TABLE VII.20. PREDICTED INTERNAL DOSES (mSv) FROM METRO-K, WITHOUT COUNTERMEASURES, FOR SPECIFIED EXPOSURE SCENARIOS

Time since event	Region 1 (Business area)		Region 2 (Park area)	
	Annual dose[a]	Cumulative dose[b]	Annual dose	Cumulative dose
Co-60, summer release				
Dry conditions				
1 year	5.01×10^{-3}	5.01×10^{-3}	4.34×10^{-2}	4.34×10^{-2}
2 years	1.40×10^{-4}	5.15×10^{-3}	2.57×10^{-3}	4.59×10^{-2}
5 years	1.29×10^{-6}	5.15×10^{-3}	4.53×10^{-5}	4.62×10^{-2}
Light rain				
1 year	1.99×10^{0}	1.99×10^{0}	2.32×10^{0}	2.32×10^{0}
2 years	5.55×10^{-2}	2.04×10^{0}	1.37×10^{-1}	2.46×10^{0}
5 years	5.11×10^{-4}	2.05×10^{0}	2.42×10^{-3}	2.47×10^{0}
Heavy rain				
1 year	9.04×10^{0}	9.04×10^{0}	1.41×10^{1}	1.41×10^{1}
2 years	2.52×10^{-1}	9.30×10^{0}	8.35×10^{-1}	1.49×10^{1}
5 years	2.33×10^{-3}	9.31×10^{0}	1.47×10^{-2}	1.50×10^{1}
Co-60, winter release				
Dry conditions				
1 year	5.01×10^{-3}	5.01×10^{-3}	4.34×10^{-2}	4.34×10^{-2}
2 years	1.40×10^{-4}	5.15×10^{-3}	2.57×10^{-3}	4.59×10^{-2}
5 years	1.29×10^{-6}	5.15×10^{-3}	4.53×10^{-5}	4.62×10^{-2}
Light rain				
1 year	1.99×10^{0}	1.99×10^{0}	2.32×10^{0}	2.32×10^{0}
2 years	5.55×10^{-2}	2.04×10^{0}	1.37×10^{-1}	2.46×10^{0}
5 years	5.11×10^{-4}	2.05×10^{0}	2.42×10^{-3}	2.47×10^{0}
Heavy rain				
1 year	9.04×10^{0}	9.04×10^{0}	1.41×10^{1}	1.41×10^{1}
2 years	2.52×10^{-1}	9.30×10^{0}	8.35×10^{-1}	1.49×10^{1}
5 years	2.33×10^{-3}	9.31×10^{0}	1.47×10^{-2}	1.50×10^{1}
Pu-239, summer release				
Dry conditions				
1 year	2.56×10^{1}	2.56×10^{1}	2.23×10^{2}	2.23×10^{2}
2 years	7.97×10^{-1}	2.64×10^{1}	1.46×10^{1}	2.38×10^{2}
5 years	1.09×10^{-2}	2.65×10^{1}	3.84×10^{-1}	2.39×10^{2}
Light rain				
1 year	1.02×10^{4}	1.02×10^{4}	1.19×10^{4}	1.19×10^{4}
2 years	3.16×10^{2}	1.05×10^{4}	7.84×10^{2}	1.27×10^{4}
5 years	4.33×10^{0}	1.05×10^{4}	2.05×10^{1}	1.28×10^{4}
Heavy rain				
1 year	4.63×10^{4}	4.63×10^{4}	7.25×10^{4}	7.25×10^{4}
2 years	1.44×10^{3}	4.77×10^{4}	4.76×10^{3}	7.73×10^{4}
5 years	1.97×10^{1}	4.78×10^{4}	1.25×10^{2}	7.78×10^{4}
Pu-239, winter release				
Dry conditions				
1 year	2.56×10^{1}	2.56×10^{1}	2.23×10^{2}	2.23×10^{2}
2 years	7.97×10^{-1}	2.64×10^{1}	1.46×10^{1}	2.38×10^{2}
5 years	1.09×10^{-2}	2.65×10^{1}	3.84×10^{-1}	2.39×10^{2}

TABLE VII.20. PREDICTED INTERNAL DOSES (mSv) FROM METRO-K, WITHOUT COUNTERMEASURES, FOR SPECIFIED EXPOSURE SCENARIOS (cont.)

Time since event	Region 1 (Business area)		Region 2 (Park area)	
	Annual dose[a]	Cumulative dose[b]	Annual dose	Cumulative dose
		Light rain		
1 year	1.02×10^{4}	1.02×10^{4}	1.19×10^{4}	1.19×10^{4}
2 years	3.16×10^{2}	1.05×10^{4}	7.84×10^{2}	1.27×10^{4}
5 years	4.33×10^{0}	1.05×10^{4}	2.05×10^{1}	1.28×10^{4}
		Heavy rain		
1 year	4.63×10^{4}	4.63×10^{4}	7.25×10^{4}	7.25×10^{4}
2 years	1.44×10^{3}	4.77×10^{4}	4.76×10^{3}	7.73×10^{4}
5 years	1.97×10^{1}	4.78×10^{4}	1.25×10^{2}	7.78×10^{4}

[a] The annual dose is the dose received during the year preceding the indicated 'time since event'.

[b] The cumulative dose is the dose received from the time of the event to the indicated 'time since event'.

TABLE VII.21. PREDICTED INTERNAL DOSES (mSv) FROM ERMIN, WITHOUT COUNTERMEASURES, FOR SPECIFIED EXPOSURE SCENARIOS

Time since event	Region 1 (Business area)		Region 2 (Park area)	
	Annual dose[a]	Cumulative dose[b]	Annual dose	Cumulative dose
		Co-60, summer release		
		Dry conditions		
1 year	5.466×10^{-2}	5.466×10^{-2}	5.079×10^{-3}	5.079×10^{-3}
2 years	1.277×10^{-2}	6.743×10^{-2}	1.750×10^{-3}	6.829×10^{-3}
5 years	4.298×10^{-4}	7.245×10^{-2}	2.555×10^{-4}	8.491×10^{-3}
		Light rain		
1 year	1.653×10^{0}	1.653×10^{0}	2.178×10^{-1}	2.178×10^{-1}
2 years	4.078×10^{-1}	2.060×10^{0}	7.504×10^{-2}	2.928×10^{-1}
5 years	2.124×10^{-2}	2.258×10^{0}	1.096×10^{-2}	3.641×10^{-1}
		Heavy rain		
1 year	2.140×10^{0}	2.140×10^{0}	3.317×10^{-1}	3.317×10^{-1}
2 years	6.390×10^{-1}	2.779×10^{0}	1.143×10^{-1}	4.460×10^{-1}
5 years	7.002×10^{-2}	3.270×10^{0}	1.669×10^{-2}	5.545×10^{-1}
		Co-60, winter release		
		Dry conditions		
1 year	5.466×10^{-2}	5.466×10^{-2}	5.079×10^{-3}	5.079×10^{-3}
2 years	1.277×10^{-2}	6.743×10^{-2}	1.750×10^{-3}	6.829×10^{-3}
5 years	4.298×10^{-4}	7.245×10^{-2}	2.555×10^{-4}	8.491×10^{-3}
		Light rain		
1 year	1.653×10^{0}	1.653×10^{0}	2.178×10^{-1}	2.178×10^{-1}
2 years	4.078×10^{-1}	2.060×10^{0}	7.504×10^{-2}	2.928×10^{-1}
5 years	2.124×10^{-2}	2.258×10^{0}	1.096×10^{-2}	3.641×10^{-1}
		Heavy rain		
1 year	2.140×10^{0}	2.140×10^{0}	3.317×10^{-1}	3.317×10^{-1}
2 years	6.390×10^{-1}	2.779×10^{0}	1.143×10^{-1}	4.460×10^{-1}
5 years	7.002×10^{-2}	3.270×10^{0}	1.669×10^{-2}	5.545×10^{-1}

TABLE VII.21. PREDICTED INTERNAL DOSES (mSv) FROM ERMIN, WITHOUT COUNTERMEASURES, FOR SPECIFIED EXPOSURE SCENARIOS (cont.)

Time since event	Region 1 (Business area)		Region 2 (Park area)	
	Annual dose[a]	Cumulative dose[b]	Annual dose	Cumulative dose
		Pu-239, summer release		
		Dry conditions		
1 year	2.871×10^{2}	2.871×10^{2}	2.643×10^{1}	2.643×10^{1}
2 years	7.672×10^{1}	3.638×10^{2}	1.059×10^{1}	3.702×10^{1}
5 years	3.848×10^{0}	4.001×10^{2}	2.294×10^{0}	4.949×10^{1}
		Light rain		
1 year	8.670×10^{3}	8.670×10^{3}	1.133×10^{3}	1.133×10^{3}
2 years	2.452×10^{3}	1.112×10^{4}	4.541×10^{2}	1.587×10^{3}
5 years	1.903×10^{2}	1.257×10^{4}	9.834×10^{1}	2.122×10^{3}
		Heavy rain		
1 year	1.118×10^{4}	1.118×10^{4}	1.726×10^{3}	1.726×10^{3}
2 years	3.857×10^{3}	1.503×10^{4}	6.916×10^{2}	2.418×10^{3}
5 years	6.283×10^{2}	1.870×10^{4}	1.498×10^{2}	3.232×10^{3}
		Pu-239, winter release		
		Dry conditions		
1 year	2.871×10^{2}	2.871×10^{2}	2.643×10^{1}	2.643×10^{1}
2 years	7.672×10^{1}	3.638×10^{2}	1.059×10^{1}	3.702×10^{1}
5 years	3.848×10^{0}	4.001×10^{2}	2.294×10^{0}	4.949×10^{1}
		Light rain		
1 year	8.670×10^{3}	8.670×10^{3}	1.133×10^{3}	1.133×10^{3}
2 years	2.452×10^{3}	1.112×10^{4}	4.541×10^{2}	1.587×10^{3}
5 years	1.903×10^{2}	1.257×10^{4}	9.834×10^{1}	2.122×10^{3}
		Heavy rain		
1 year	1.118×10^{4}	1.118×10^{4}	1.726×10^{3}	1.726×10^{3}
2 years	3.857×10^{3}	1.503×10^{4}	6.916×10^{2}	2.418×10^{3}
5 years	6.283×10^{2}	1.870×10^{4}	1.498×10^{2}	3.232×10^{3}

[a] The annual dose is the dose received during the year preceding the indicated 'time since event'.

[b] The cumulative dose is the dose received from the time of the event to the indicated 'time since event'.

TABLE VII.22. PREDICTED INTERNAL DOSES (mSv) FROM CPHR, WITHOUT COUNTERMEASURES, FOR SPECIFIED EXPOSURE SCENARIOS

Time since event	Region 1 (Business area)		Region 2 (Park area)	
	Annual dose[a]	Cumulative dose[b]	Annual dose	Cumulative dose
		Co-60, summer release		
		Dry conditions		
1 year	7.26×10^{1}	7.26×10^{1}	1.73×10^{1}	1.73×10^{1}
2 years	0.00×10^{0}	7.26×10^{1}	0.00×10^{0}	1.73×10^{1}
5 years	0.00×10^{0}	7.26×10^{1}	0.00×10^{0}	1.73×10^{1}
		Pu-239, summer release		
		Dry conditions		
1 year	1.70×10^{5}	1.70×10^{5}	8.40×10^{0}	8.40×10^{0}
2 years	0.00×10^{0}	1.70×10^{5}	0.00×10^{0}	8.40×10^{0}
5 years	0.00×10^{0}	1.70×10^{5}	0.00×10^{0}	8.40×10^{0}

[a] The annual dose is the dose received during the year preceding the indicated 'time since event'.

[b] The cumulative dose is the dose received from the time of the event to the indicated 'time since event'.

TABLE VII.23. PREDICTED INTERNAL DOSES (mSv) FROM RESRAD-RDD, WITHOUT COUNTERMEASURES, FOR SPECIFIED EXPOSURE SCENARIOS

Time since event	Region 1 (Business area)		Region 2 (Park area)	
	Annual dose[a]	Cumulative dose[b]	Annual dose	Cumulative dose
Co-60, summer release				
Dry conditions				
1 year	2.17×10^{-2}	6.68×10^{-2}	4.20×10^{-4}	6.67×10^{-3}
2 years	1.82×10^{-2}	8.50×10^{-2}	1.87×10^{-4}	6.86×10^{-3}
3 years	1.54×10^{-2}	1.00×10^{-1}	1.05×10^{-4}	6.96×10^{-3}
4 years	1.30×10^{-2}	1.13×10^{-1}	6.66×10^{-5}	7.03×10^{-3}
5 years	1.10×10^{-2}	1.24×10^{-1}	4.52×10^{-5}	7.07×10^{-3}
Light rain				
1 year	1.59×10^{0}	4.92×10^{0}	1.75×10^{-2}	2.78×10^{-1}
2 years	1.34×10^{0}	6.25×10^{0}	7.77×10^{-3}	2.85×10^{-1}
3 years	1.13×10^{0}	7.38×10^{0}	4.38×10^{-3}	2.90×10^{-1}
4 years	9.55×10^{-1}	8.34×10^{0}	2.77×10^{-3}	2.92×10^{-1}
5 years	8.09×10^{-1}	9.15×10^{0}	1.88×10^{-3}	2.94×10^{-1}
Heavy rain				
1 year	9.69×10^{0}	2.99×10^{1}	1.06×10^{-1}	1.69×10^{0}
2 years	8.13×10^{0}	3.80×10^{1}	4.72×10^{-2}	1.73×10^{0}
3 years	6.87×10^{0}	4.49×10^{1}	2.66×10^{-2}	1.76×10^{0}
4 years	5.81×10^{0}	5.07×10^{1}	1.68×10^{-2}	1.78×10^{0}
5 years	4.92×10^{0}	5.56×10^{1}	1.14×10^{-2}	1.79×10^{0}
Pu-239, summer release				
Dry conditions				
1 year	1.02×10^{2}	2.85×10^{2}	1.96×10^{0}	2.66×10^{1}
2 years	9.76×10^{1}	3.83×10^{2}	9.98×10^{-1}	2.76×10^{1}
3 years	9.41×10^{1}	4.77×10^{2}	6.42×10^{-1}	2.82×10^{1}
4 years	9.08×10^{1}	5.68×10^{2}	4.64×10^{-1}	2.87×10^{1}
5 years	8.76×10^{1}	6.55×10^{2}	3.60×10^{-1}	2.90×10^{1}
Light rain				
1 year	7.51×10^{3}	2.10×10^{4}	8.15×10^{1}	1.11×10^{3}
2 years	7.18×10^{3}	2.82×10^{4}	4.15×10^{1}	1.15×10^{3}
3 years	6.92×10^{3}	3.51×10^{4}	2.67×10^{1}	1.17×10^{3}
4 years	6.68×10^{3}	4.18×10^{4}	1.93×10^{1}	1.19×10^{3}
5 years	6.44×10^{3}	4.82×10^{4}	1.50×10^{1}	1.21×10^{3}
Heavy rain				
1 year	4.56×10^{4}	1.27×10^{5}	4.95×10^{2}	6.72×10^{3}
2 years	4.37×10^{4}	1.71×10^{5}	2.52×10^{2}	6.97×10^{3}
3 years	4.21×10^{4}	2.13×10^{5}	1.62×10^{2}	7.14×10^{3}
4 years	4.06×10^{4}	2.54×10^{5}	1.17×10^{2}	7.25×10^{3}
5 years	3.92×10^{4}	2.93×10^{5}	9.10×10^{1}	7.34×10^{3}

[a] The annual dose is the dose received during the year preceding the indicated ‘time since event’.

[b] The cumulative dose is the dose received from the time of the event to the indicated ‘time since event’.

TABLE VII.24. PREDICTED INTERNAL DOSES (mSv) FROM CHERURB, WITHOUT COUNTERMEASURES, FOR SPECIFIED EXPOSURE SCENARIOS

Time since event	Region 1 (Business area)		Region 2 (Park area)	
	Annual dose[a]	Cumulative dose[b]	Annual dose	Cumulative dose
Co-60, summer release				
Dry conditions				
1 year	1.45×10^{1}	1.45×10^{1}	4.14×10^{0}	4.14×10^{0}
2 years	0	1.45×10^{1}	0	4.14×10^{0}
5 years	0	1.45×10^{1}	0	4.14×10^{0}
Light rain				
1 year	1.45×10^{1}	1.45×10^{1}	4.14×10^{0}	4.14×10^{0}
2 years	0	1.45×10^{1}	0	4.14×10^{0}
5 years	0	1.45×10^{1}	0	4.14×10^{0}
Heavy rain				
1 year	1.45×10^{1}	1.45×10^{1}	4.14×10^{0}	4.14×10^{0}
2 years	0	1.45×10^{1}	0	4.14×10^{0}
5 years	0	1.45×10^{1}	0	4.14×10^{0}
Pu-239, summer release				
Dry conditions				
1 year	7.24×10^{4}	7.24×10^{4}	2.07×10^{4}	2.07×10^{4}
2 years	0	7.24×10^{4}	0	2.07×10^{4}
5 years	0	7.24×10^{4}	0	2.07×10^{4}
Light rain				
1 year	7.24×10^{4}	7.24×10^{4}	2.07×10^{4}	2.07×10^{4}
2 years	0	7.24×10^{4}	0	2.07×10^{4}
5 years	0	7.24×10^{4}	0	2.07×10^{4}
Heavy rain				
1 year	7.24×10^{4}	7.24×10^{4}	2.07×10^{4}	2.07×10^{4}
2 years	0	7.24×10^{4}	0	2.07×10^{4}
5 years	0	7.24×10^{4}	0	2.07×10^{4}

[a] The annual dose is the dose received during the year preceding the indicated ‘time since event’.

[b] The cumulative dose is the dose received from the time of the event to the indicated ‘time since event’.

ANNEX I. USE OF MODELLING SCENARIO FOR ESTIMATION OF SOURCE TERM FROM SURFACE ACTIVITY MEASUREMENTS

One EMRAS II WG9 participant (L. Urso) used the information from the modelling exercise (given in Appendix I) to estimate the source term from surface activity measurements [I-1]. This was done through application of inverse fitting of a Gaussian dispersion model (HotSpot 2.07.01 [I-2]; using measurements for surface activity (Bq/m^2), in particular, data from Test 2, for which all measurements were available at the time of this work (see Section 2.2 and Appendix I). An optimization routine was written based on MINPACK [I-3] to inversely determine the source term by means of the Levenberg-Marquardt algorithm and the Gaussian dispersion model [I-4], as implemented in HotSpot 2.07.1 [I-2]. The same empirical formulas used in HotSpot 2.07.01 were applied to estimate dispersion coefficients, wind velocity at a reference height, and other parameters; however, unlike HotSpot 2.07.01, integration of the depletion factor was carried out using a Gaussian integration, instead of the less precise trapezoidal rule. The source term was then inversely determined by minimizing the function, as follows:

$$F(x,y) = log_{10}(B_{rmeas}(x,y)+1) - log_{10}(B_{rcalc}(x,y)+1) \quad \text{(I-1)}$$

where B_{rmeas} and B_{rcalc} are the experimental and calculated surface activity, respectively, at a given point in the grid area (x,y). The values of the surface activities were log-transformed in order to guarantee stability during the minimisation process.

The known activity at the time of the explosion was 910 MBq, and the wind velocity at a height of 2 m was 1.1 m/s. Based on the reported weather conditions (shown in Tables 2.1 and 2.2 and also in Appendix I), the stability class was assumed to be Class B (moderately unstable conditions). Based on experimental observations, the release height (H) during the explosion was estimated to be 5 m. The greatest uncertainty in the experiment was, by far, contributed by the deposition velocity, since no measurements were available to characterize the partitioning of the source term amongst the four different aerosol sizes defined in the exercise (see Appendix I).

To measure the surface activity, 221 detectors were placed over a 50 m × 40 m area (see Appendix I). The behaviour of the data in the x-direction (downwind) did not follow an exponential decay, but instead could be predicted using a typical Gaussian plume model. In addition, the very slow wind velocity suggested that in the x-direction, a diffusive process may have taken place. Indeed, Fig. I-1 shows how well a Gaussian profile centered at $x_0 = 15$ m, with a $\sigma_x = 5.13$ m, fits the experimental curve. Therefore, in order to ensure an accurate fit of model predictions to the experimental data, the diffusive term was 'switched on' during the optimization routine, using the following form of the equation:

$$diffusive(x) = e^{-(x-x_0)^2/(2\sigma_x^2)} \quad \text{(I-2)}$$

where:

x is the distance along the x-axis of the grid; and
σ_x is the full width at half maximum of the Gaussian curve that best fits the experimental profile.

The initial approximation was set to a very low value (91 kBq) compared to the true value (910MBq). The result of the fit for a selected effective deposition velocity, v_d, of 0.01 m/s is shown in Fig. I-2, where the experimental contour plot of surface activity is shown together

with the calculated one. The initial norm of the residual was 40.5; with the optimization, it decreased to 23.6, and after 33 iterations, the resultant optimal source term was (940 MBq), which is comparable to the true source term (910 MBq).

The experimental, initial and optimized profiles in the *x*-axis and *y*-axis directions are shown in Fig. I-3. The initial approximation profiles of the plume in these two directions were very low compared with the measured values. Nevertheless, their shapes are similar to the measured ones. By comparison, the optimized profiles differ only slightly from the measured ones (see Fig. I-3).

In order to account for the large range of variability of the deposition velocity, the optimal source term was calculated for other different plausible effective deposition velocities (range from 5×10^{-5} to 8×10^{-1} m/s; shown in Fig. I-4); an effective deposition velocity can be considered as an 'average' amongst the different unknown deposition velocities associated with different aerosols. The strong linear dependence of the deposition velocity v_d on the value of the source term, Q_r, is shown in Fig. I-4.

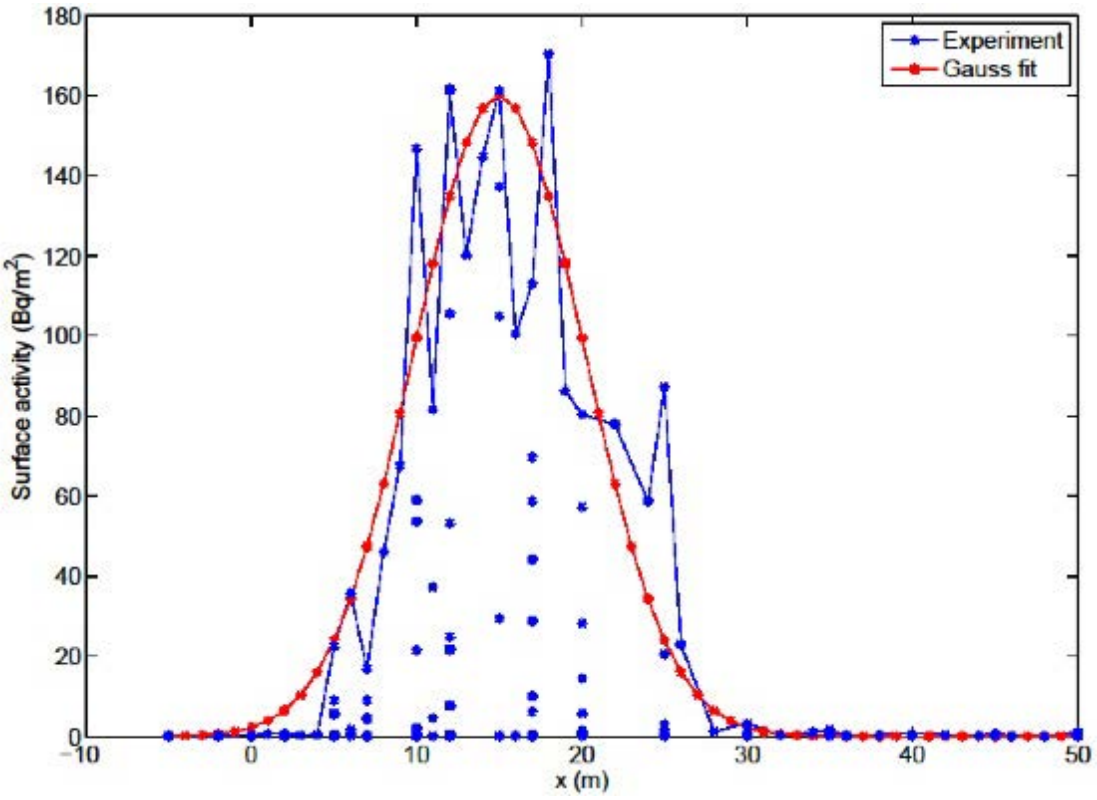

FIG. I-1. Experimental surface activity in the x-direction fitted to a Gaussian profile.

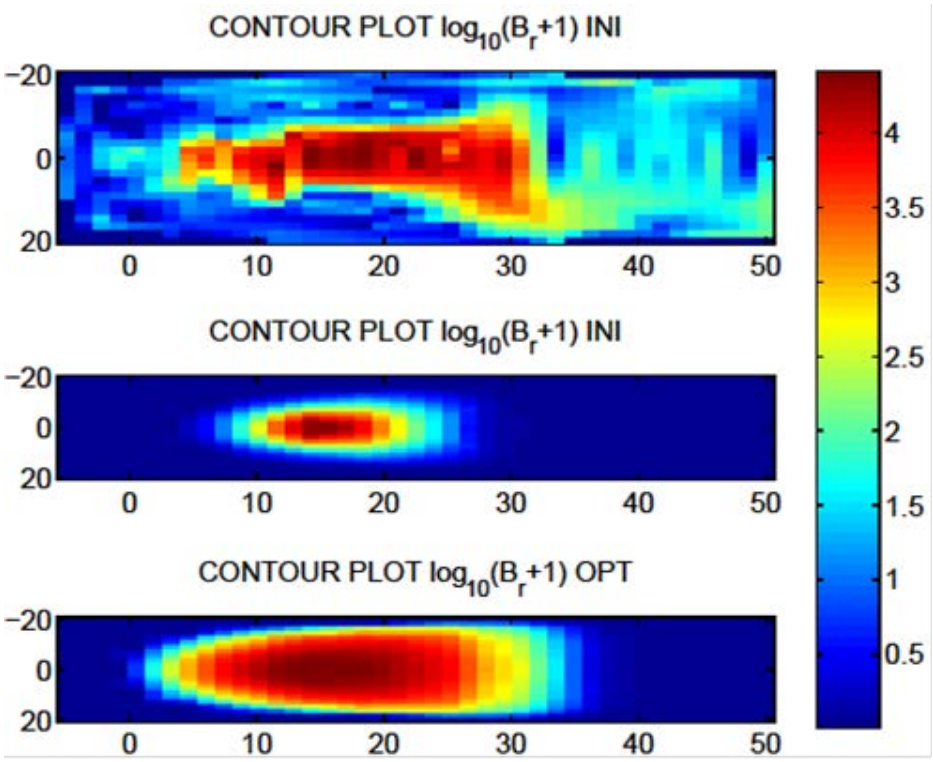

FIG. I-2. Experimental (top), initial approximation (centre) and optimized result (bottom) for the distribution of the surface activity for Test 2.

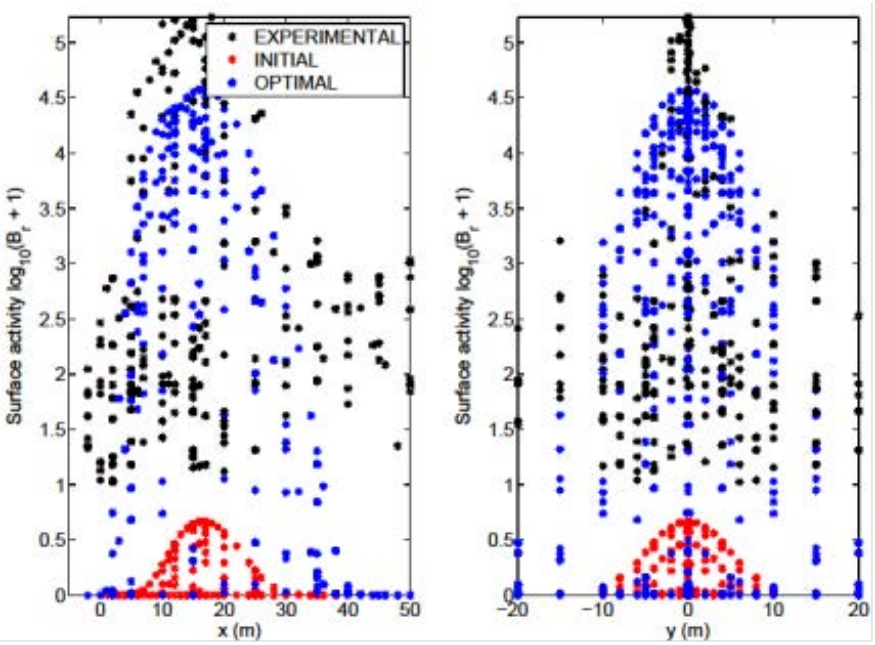

FIG. I-3. Experimental (measured), initial, and optimized profiles of the surface activity in the x and y directions of the plume.

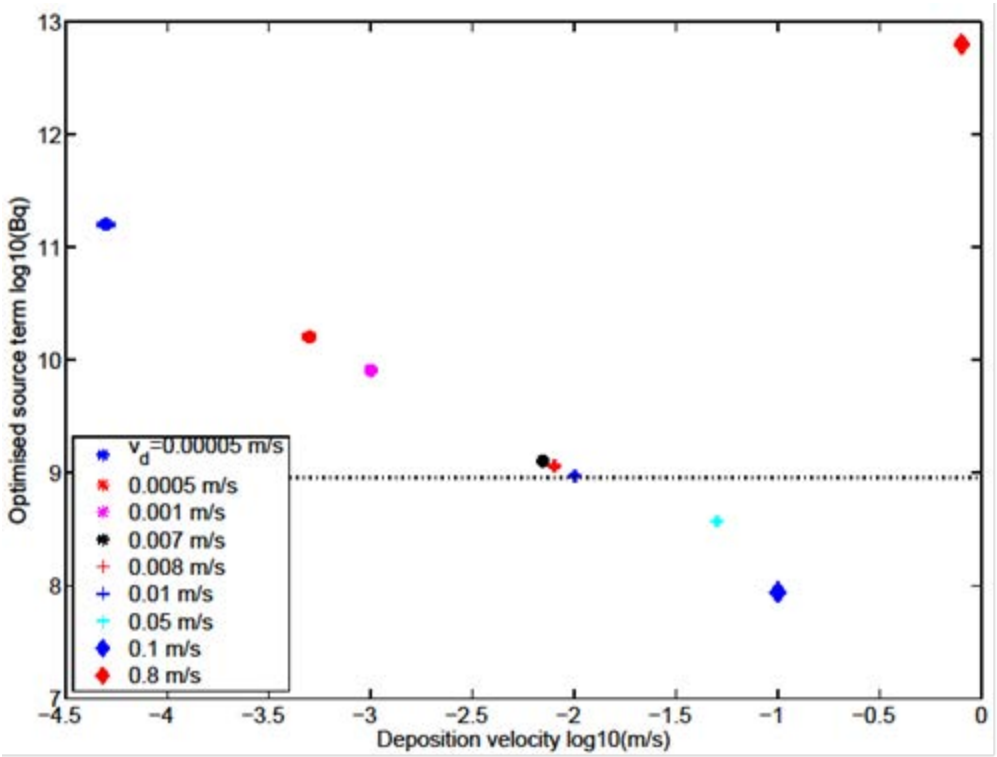

FIG. I-4. Optimized source term for Test 2 with respect to the deposition velocity. The expected value for the source term corresponds to an effective deposition velocity of about 0.01 m/s.

I-1. REFERENCES TO ANNEX I

[I-1] URSO, L., KAISER, J.C., WODA, C., HELEBRANT, J., HULKA, J., KUCA, P., PROUZA, Z., A fast and simple approach for the estimation of a radiological source from localised measurements after the explosion of a radiological dispersal device, Radiation Protection Dosimetry **158** (2014) 453.

[I-2] HOMANN, S.G., HotSpot Health Physics Codes Version 2.07 User's Guide, Rep. LLNL-TM-411345, Lawrence Livermore National Laboratory, CA (2009).

[I-3] MORÉ, J.J., SORENSEN, D.C., HILLSTROM, K.E., GARBOW, B.S., "The MINPACK project", Sources and Development of Mathematical Software (COWELL, W.R., Ed), Prentice-Hall, New Jersey (1984) pp. 88–111.

[I-4] PASQUILL, F., Atmospheric Diffusion: The Dispersion of Windborne Material from Industrial and Other Sources, Second edition, John Wiley and Sons, New York (1974) 429 pp.

CONTRIBUTORS TO DRAFTING AND REVIEW

Andersson, K.G.	Risø-DTU National Laboratory for Sustainable Energy, Denmark
Berkovskyy, V.	Ukrainian Radiation Protection Institute, Ukraine
Brown, J.	International Atomic Energy Agency
Charnock, T.W.	Public Health England, United Kingdom
Chouhan, S.L.	Canadian Nuclear Laboratories, Canada
de With, G.	Nuclear Research and Consultancy Group, Netherlands
Ďúran, J.	VÚJE Inc., Slovakia
Fuka, V.	Charles University, Czech Republic
Helebrant, J.	National Radiation Protection Institute, Czech Republic
Hůlka, J.	National Radiation Protection Institute, Czech Republic
Hwang, W.T.	Korea Atomic Energy Research Institute, Republic of Korea
Kamboj, S.	Argonne National Laboratory, United States of America
Kuča, P.	National Radiation Protection Institute, Czech Republic
Mancini, F.	SOGIN S.p.A., Italy
Navarro, E.	Institute for Radiological Protection and Nuclear Safety, France
Periáñez, R.	University of Seville, Spain
Prouza, Z.	National Radiation Protection Institute, Czech Republic
Sdouz, G.	Austrian Institute of Technology GmbH, Austria
Starinskaia, R.	Burnasyan Federal Medical Biophysical Center of Federal Medical Biological Agency, Russian Federation
Thiessen, K.M.	Oak Ridge Center for Risk Analysis Inc., United States of America
Tomás Zerquera, J.	Center for Protection and Hygiene of Radiation, Cuba
Trifunović, D.	State Office for Radiological and Nuclear Safety, Croatia
Urso, L.	German Research Center for Environmental Health, Germany
Walter, H.	Federal Office for Radiation Protection, Germany
Yankovich, T.L.	International Atomic Energy Agency, Austria
Yu, C.	Argonne National Laboratory, United States of America

LIST OF PARTICIPANTS

Andersson, K.G.	Risø-DTU National Laboratory for Sustainable Energy, Denmark
Baccouche, S.	Centre National des Sciences et Technologies Nucleaires, Tunisia
Berkovskyy, V.	Ukrainian Radiation Protection Institute, Ukraine
Bonchuk, Y.	Ukrainian Radiation Protection Institute, Ukraine
Brechler, J.	Charles University, Czech Republic
Cabral Molina, W.S.	National Regulatory Authority of the Ministry of Industry, Uruguay
Charnock, T.W.	Public Health England, United Kingdom
Chouhan, S.L.	Canadian Nuclear Laboratories, Canada
de With, G.	Nuclear Research & Consultancy Group, Netherlands
Ďúran, J.	VÚJE Inc., Slovakia
Földi, A.	KFKI Atomic Energy Research Institute, Hungary
Fuka, V.	Charles University, Czech Republic
Helebrant, J.	National Radiation Protection Institute, Czech Republic
Horyna, J.	State Office for Nuclear Safety, Czech Republic
Hosseinipanah, M.	Iranian Nuclear Regulatory Authority, Islamic Republic of Iran
Hůlka, J.	National Radiation Protection Institute, Czech Republic
Hwang, W.T.	Korea Atomic Energy Research Institute, Republic of Korea
Ikäheimonen, T.K.	Radiation and Nuclear Safety Authority, Finland
Kaiser, J.C.	German Research Center for Environmental Health, Germany
Kamboj, S.	Argonne National Laboratory, United States of America
Kouts, K.	Republican Scientific-Practical Centre of Hygiene, Belarus
Kuča, P.	National Radiation Protection Institute, Czech Republic
Malátová, I.	National Radiation Protection Institute, Czech Republic
Mancini, F.	SOGIN S.p.A., Italy
Marella, G.	Institute for Environmental Protection and Research, Italy
Miller, C.	Centers for Disease Control and Prevention, United States of America
Navarro, E.	Institute for Radiological Protection and Nuclear Safety, France
Periáñez, R.	University of Seville, Spain

Prouza, Z.	National Radiation Protection Institute, Czech Republic
Rowan, D.	Canadian Nuclear Laboratories, Canada
Sdouz, G.	Austrian Institute of Technology GmbH, Austria
Thiessen, K.M.	Oak Ridge Center for Risk Analysis Inc., United States of America
Tomás Zerquera, J.	Center for Protection and Hygiene of Radiation, Cuba
Tracy, B.L.	Health Canada, Canada
Trifunović, D.	State Office for Radiological and Nuclear Safety, Croatia
Turcanu, C.	Belgian Nuclear Research Centre, Belgium
Urso, L.	German Research Center for Environmental Health, Germany
Walter, H.	Federal Office for Radiation Protection, Germany
Winters, G.	Rensselaer Polytechnic Institute, United States of America
Yu, C.	Argonne National Laboratory, United States of America

EMRAS II Technical Meetings, IAEA Headquarters, Vienna

19–23 January 2009, 25–29 January 2010, 24–28 January 2011

Interim Working Group Meetings, EMRAS II, Working Group 9

Prague, Czech Republic: 13–15 July 2009; Seville, Spain: 8–10 June 2010;
Ontario, Canada: 15–18 June 2011; Vienna, Austria: 17–19 October 2011

IAEA
International Atomic Energy Agency

No. 26

ORDERING LOCALLY

IAEA priced publications may be purchased from the sources listed below or from major local booksellers.

Orders for unpriced publications should be made directly to the IAEA. The contact details are given at the end of this list.

NORTH AMERICA

Bernan / Rowman & Littlefield

15250 NBN Way, Blue Ridge Summit, PA 17214, USA
Telephone: +1 800 462 6420 • Fax: +1 800 338 4550

Email: orders@rowman.com • Web site: www.rowman.com/bernan

REST OF WORLD

Please contact your preferred local supplier, or our lead distributor:

Eurospan Group

Gray's Inn House
127 Clerkenwell Road
London EC1R 5DB
United Kingdom

Trade orders and enquiries:

Telephone: +44 (0)176 760 4972 • Fax: +44 (0)176 760 1640
Email: eurospan@turpin-distribution.com

Individual orders:

www.eurospanbookstore.com/iaea

For further information:

Telephone: +44 (0)207 240 0856 • Fax: +44 (0)207 379 0609
Email: info@eurospangroup.com • Web site: www.eurospangroup.com

Orders for both priced and unpriced publications may be addressed directly to:

Marketing and Sales Unit
International Atomic Energy Agency
Vienna International Centre, PO Box 100, 1400 Vienna, Austria
Telephone: +43 1 2600 22529 or 22530 • Fax: +43 1 26007 22529
Email: sales.publications@iaea.org • Web site: www.iaea.org/publications

21-00057E

International Atomic Energy Agency
Vienna